JOURNAL OF ATMOSPHERIC AND TERRESTRIAL PHYSICS

EDITORIAL ADVISORY BOARD

H. O. G. ALFVÉN-STOCKHOLM · J. BARTELS-GÖTTINGEN · P. M. S. BLACKETT-LONDON · E. G. BOWEN-SYDNEY · SIR DAVID BRUNT-LONDON · R. BUREAU-BAGNEUX · S. CHAPMAN-ALASKA · J. EGEDAL-COPENHAGEN · H. FICKER-VIENNA V. F. HESS-NEW YORK · E. O. HULBURT-WASHINGTON, D.C. · H. ISRAEL-AACHEN D. H. MENZEL-CAMBRIDGE, MASS. · S. K. MITRA-CALCUTTA · M. NICOLET-UCCLE E. H. NORINDER-UPSALA · B. van der POL-GENEVA · J. A. RATCLIFFE-CAMBRIDGE O. E. H. RYDBECK-GOTHENBURG · SIR GEORGE SIMPSON-LONDON · H. SOLBERG-OSLO · C. STØRMER-OSLO · J. VELDKAMP-DE BILT · M. WALDMEIER-ZÜRICH R. v. d. WOOLLEY-HERSTMONCEUX · J. ZENNECK-ALTHEGNENBERG

EDITOR IN CHIEF

SIR EDWARD APPLETON, F.R.S.

EDINBURGH

VOLUME 8

JANUARY—JUNE

1956

PERGAMON PRESS · LONDON & NEW YORK

J. Atmosph. Terr. Phys.

VOL.
8
1956

CONTENTS

Nos. 1/2

SYDNEY CHAPMAN and K. C. WESTFOLD: A comparison of the annual mean solar and lunar atmospheric tides in barometric pressure, as regards their worldwide distribution of amplitude and phase 1

G. V. GROVES: Introductory theory for upper atmosphere wind and sonic velocity determination by sound propagation 24

J. W. DUNGEY: The influence of the geomagnetic field on turbulence in the ionosphere . . 39

G. R. ELLIS: The *Z* propagation hole in the ionosphere 43

J. P. WILD and J. A. ROBERTS: The spectrum of radio-star scintillations and the nature of irregularities in the ionosphere 55

D. W. R. MCKINLEY: Radar-echo duration and height of a Perseid meteor 76

O. BURKARD: Die tages- und jahreszeitlichen Variationen der F_1-Ionisation. Ein Deutungsversuch 83

R. M. SHERIFF: A study of the total electron content of the *F*-region of the ionosphere over Ahmedabad (23 N, 72 38′ E), India 91

E. N. BRAMLEY: Tilts in the ionosphere during the solar eclipse of 30 June 1954 98

J. EGEDAL and N. AMBOLT: The effect on geomagnetism of the solar eclipse of 30 June 1954 (supplementary communication) 105

M. E. SZENDREI and M. W. MCELHINNY: Preliminary results of the ionospheric solar eclipse of 25 December 1954 108

Research Notes:

M. J. SEATON: On the extinction correction used in the determination of airglow emission heights by the van Rhijn method 115

MRINMAYEE GHOSH: Determination of the *F*-region collisional frequency (over Calcutta) 116

G. H. HUXLEY: The interpretation of measurements of radio-wave interaction 118

F. H. HIBBERD: On the observation of ionospheric self-interaction 120

M. J. SEATON: A possible explanation of the drop in *F*-region critical densities accompanying major ionospheric storms 122

J. ALAN CHALMERS: The electrical charge on the earth 124

K-Indices of geomagnetic activity from the observatories at Abinger, Eskdalemuir and Lerwick, from July to September, 1955 126

No. 3

S. A. BOWHILL: The fading of radio waves of frequencies between 16 and 2400 kc/s . . . 129

R. MÜHLEISEN: On the deviations of the course of elements of atmospheric electricity on continents from the worldwide course 146

R. W. PARKINSON: The fading periods of the *E*-region coupling echo at 150 kc/s 158

D. W. G. CHAPPELL and C. L. HENDERSON: The determination of the horizontal velocity of ionospheric movements from fading records from spaced receivers 163

G. W. G. COURT and E. S. GILFILLAN: A determination of ionospheric winds for a 24-hour period 169

B. H. BRIGGS: Observations of short bursts of signal from a distant 50 Mc/s transmitter . . 171

Research Note:

G. A. M. KING: Electron distribution in the ionosphere 184

K-Indices of geomagnetic activity from the observatories at Abinger, Eskdalemuir and Lerwick, from October to December, 1955 186

Nos. 4/5

G. V. GROVES: Theory of the rocket-grenade method of determining upper-atmospheric properties by sound propagation 189

H. G. BOOKER: A theory of scattering by nonisotropic irregularities with application to radar reflections from the aurora 204

H. ELSÄSSER und H. SIEDENTOPF: Mitteilungen aus dem Astronomischen Institut der Universität Tübingen Nr. 20 222

J. S. CHATTERJEE: The crust as the possible seat of earth's magnetism 233

R. W. WRIGHT, J. R. KOSTER, and N. J. SKINNER: Spread *F*-layer echoes and radio-star scintillation 240

DONALD G. YERG: Observations and analysis of ionospheric drift 247

J. A. RATCLIFFE: The formation of the ionospheric layers *F*-1 and *F*-2 260

G. A. M. KING and C. H. CUMMACK: Electron distribution in the ionosphere 270

Research Notes:

T. E. Cranshaw, W. Galbraith, and N. A. Porter: Cosmic-ray observations during the flare of 23 February 1956 . . . 274
M. Lambie and H. Elliot: Cosmic rays and the solar flare of 23 February 1956 . . . 277
P. L. Marsden, J. W. Berry, P. Fieldhouse, and J. G. Wilson: Variation of cosmic-ray nucleon intensity during the disturbance of 23 February 1956 . . . 278
J. S. Belrose, M. H. Devenport, and K. Weekes: Some unusual radio observations made on 23 February 1956 281
T. Gold and D. R. Palmer: The solar outburst, 23 February 1956. Observations by the Royal Greenwich Observatory . . . 287
M. A. Ellison and J. H. Reid: A long-wave anomaly associated with the arrival of cosmic-ray particles of solar origin on 23 February 1956 . . . 291
A. C. B. Lovell: A note on the interpretation of transient echoes from the ionosphere . . . 293

Letters to the Editor:

K. Bibl: Automatic recordings of ionospheric characteristics . . . 295
K. Rawer: Focusing on a "rippled" ionosphere . . . 296

No. 6

D. Lepechinsky: On the existence of a "Q.L."–"Q.T." "transition-level" in the ionosphere and its experimental evidence and effect . . . 297
D. R. Bates and B. L. Moiseiwitsch: Origin of the Meinel hydroxyl system in the night airglow 305
A. J. Lyon and A. J. G. Moorat: Accurate height measurements using an ionospheric recorder 309
N. F. Barber: A correlation treatment of fading signals . . . 318
K. M. Kotadia: Sporadic echoes from the *E* region over Ahmedabad (23° 02′ N, 72° 38′ E) . 331
G. R. Ellis: On the propagation of whistling atmospherics . . . 338
D. M. Hunten, F. E. Roach, and J. W. Chamberlain: A photometric unit for the airglow and aurora . . . 345

Research Notes:

Edward S. Epstein, Charles Osterberg, and Arthur Adel: Note on the variations of atmospheric ozone as a function of height . . . 347
K. Whitham and E. I. Loomer: The diurnal and annual motions of the north magnetic dip pole . . . 349

Book Review:

"Radio Astronomy" by J. L. Pawsey and R. N. Bracewell (reviewed by F. G. Smith) . . . 352

VOL. 8 1956

AUTHOR INDEX TO VOLUME 8

(B) denotes a book review

Adel, A. p. 347
Ambolt, N. p. 105
Barber, N. F. p. 318
Bates, D. R. p. 305
Belrose, J. S. p. 281
Berry, J. W. p. 278
Bibl, K. p. 295
Booker, H. G. p. 204
Bowhill, S. A. p. 129
Bramley, E. N. p. 98
Briggs, B. H. p. 171
Burkard, O. p. 83
Chalmers, J. A. p. 124
Chamberlain, J. W. p. 345
Chapman, S. p. 1
Chappell, D. W. G. p. 163
Chatterjee, J. S. p. 233
Court, G. W. G. p. 169
Cranshaw, T. E. p. 274
Cummack, C. H. p. 270
Devenport, M. H. p. 281
Dungey, J. W. p. 39
Egedal, J. p. 105
Elliot, H. p. 277
Ellis, G. R. pp. 43, 338
Ellison, M.A. p. 291
Elsässer, H. p. 222
Epstein, E. S. p. 347
Fieldhouse, P. p. 278
Galbraith, W. p. 274
Ghosh, M. p. 116
Gilfillan, E. S. p. 169
Gold, T. p. 287
Groves, G. V. pp. 24, 189
Henderson, C. L. p. 163
Hibberd, F. H. p. 120
Hunten, D. M. p. 345
Huxley, L. G. H. p. 118
King, G. A. M. pp. 184, 270
Koster, J. R. p. 240
Kotadia, K. M. p. 331
Lambie, M. p. 277
Lepechinsky, D. p. 297
Loomer, E. I. p. 349
Lovell, A. C. B. p. 293
Lyon, A. J. p. 309
Marsden, P. L. p. 278
McElhinny, M. W. p. 108
McKinley, D. W. R. p. 76
Moiseiwitsch, B. L. p. 305
Moorat, A. J. G. p. 309
Mühleisen, R. p. 146
Osterberg, C. p. 347
Palmer, D. R. p. 287
Parkinson, R. W. p. 158
Porter, N. A. p. 274
Ratcliffe, J. A. p. 260
Rawer, K. p. 296
Reid, J. H. p. 291
Roach, F. E. p. 345
Roberts, J. A. p. 55
Seaton, M. J. pp. 115, 122
Sheriff, R. M. p. 91
Siedentopf, H. p. 222
Skinner, N. J. p. 240
Smith, F. G. p. 352 (B)
Szendrei, M. E. p. 108
Weekes, K. p. 281
Westfold, K. C. p. 1
Whitham, K. p. 349
Wild, J. P. p. 55
Wilson, J. G. p. 278
Wright, R. W. p. 240
Yerg, D. G. p. 247

Journal of Atmospheric and Terrestrial Physics, 1956, Vol. 8, pp. 1 to 23. Pergamon Press Ltd., London

A comparison of the annual mean solar and lunar atmospheric tides in barometric pressure, as regards their worldwide distribution of amplitude and phase

SYDNEY CHAPMAN
Geophysical Institute, University of Alaska, Alaska; also
High Altitude Observatory, Boulder, Colorado*

and

K. C. WESTFOLD
Department of Applied Mathematics, University of Sydney, N.S.W., Australia

Abstract—The solar and lunar semidiurnal atmospheric "tides" are compared as regards their worldwide distribution, on the basis of data from sixty-eight stations. Both these tides decrease with increasing latitude, but not quite symmetrically relative to the equator; there is some indication that in northern latitudes the lunar tide decreases rather more rapidly than the solar. Both tides are abnormally great over east Africa; the solar tide is also large in India, and the lunar tide in the East Indies. The lunar tide is large relative to the solar tide along and near the east coast of Asia, and also in the East Indies; it is small relative to the solar tide over India and western North America. The phase difference between the solar and lunar tides is specially large along and near the east Asiatic coast.

OL.
8
956

1. INTRODUCTION

IN this paper a comparison is made between the solar and lunar semidiurnal variations of barometric pressure, as regards their geographical distribution. These pressure variations are one manifestation of the solar and lunar atmospheric tides; "tide" is here used, as by CHAPMAN (1951), to signify a semidiurnal variation, not necessarily wholly due to tidal forces; these gravitational forces are the sole cause of the lunar atmospheric tide, but the solar "tide" is partly gravitational and partly thermal in origin. It is convenient to use the symbols L_2, S_2 to denote the two atmospheric tides, lunar and solar respectively; each of these symbols will denote the corresponding phenomenon as a whole, including its geographical distribution and seasonal and other time variations of amplitude and phase. The tides are manifested in various meteorological elements, notably in the barometric pressure p, the eastward and northward wind components u, v, and the heights of the ionospheric layers; less notably in the air temperature T, the level of formation of secondary cosmic rays (mesons and neutrons), the upward wind component w, and other elements. The manifestation of L_2 or S_2 in any such element, e.g., pressure, can be denoted by $L_2(p)$ or $S_2(p)$. The solar daily variations of the meteorological elements also include harmonic components that are not semidiurnal. These can be denoted by S_n, where n may denote 1, 3, 4, $\cdots$, as well as 2. The whole solar daily variation can be denoted by S; $S = S_1 + S_2 + \cdots$.

Any such harmonic component S_n can be represented by

$$s_n \sin (nt + \sigma_n), \tag{1}$$

* Now engaged in a joint research programme with the High Altitude Observatory and the National Bureau of Standards, at Boulder, Colorado.

where t denotes local mean solar time, reckoned in angle at the rate 2π or 360° per mean solar day, from mean midnight; s_n is the amplitude, σ_n the phase. Similarly L_2 can be represented by

$$l_2 \sin (2\tau + \lambda_2), \tag{2}$$

where τ denotes mean lunar time reckoned from lower (or upper) transit of the mean moon. If more than one meteorological element is being considered, the one referred to in each case can be indicated in the same way as for S or L_2 as a whole; this paper deals only with $l_2(p)$, $\lambda_2(p)$, $s_2(p)$, $\sigma_2(p)$, so that further reference to p will be unnecessary in the symbols used here.

The unit in which s_2 and l_2 are expressed in this paper is the microbar, or 1 dyne/cm^2; 1 inch of mercury in barometric pressure equals approximately $3{\cdot}386 \times 10^4$ microbars (the number depends on the local value of gravity g); 1 mm of mercury corresponds approximately to 1333 microbars.

This paper deals only with the annual mean values of S_2 and L_2. These tides undergo a variation from month to month throughout the year, in a manner which, especially as regards L_2, is very remarkable and not at all understood. In a later paper we hope to discuss and compare the geographical distributions of S_2 and L_2 at different epochs in the year.

2. THE STATIONS AND THE MATERIAL USED

The values of l_2, λ_2, s_2, σ_2 used in this paper are drawn from sixty-nine stations, for which Table 1 gives the name, geographical co-ordinates, height (in metres), and (where available) the mean barometric pressure* (in millibars); the latter is in several cases taken from the 1930 *Réseau Mondial*. Table 1 also indicates, in the last column, the initials of the surnames of the authors, or the source of the determinations quoted, and the date of the published account (if any) of the determinations, as given in the list of references at the end of this paper. Column (e) indicates the number of years' data used; this is given as the integer nearest to $N/365$, where N is the number of days used. For forty-two of the sixty-nine stations L and S have been determined from the same data, as is desirable for the purpose of a comparison between the two tides, such as is here made; in such cases there is only one reference in the last column. In the remaining cases S_2 was not evaluated in the course of determining L_2, and the data for S_2 have been drawn from various sources, mainly three papers by HANN (1889, 1918a, 1918b); in Table 1 these are referred to as $H1, H2, H3$. In such cases columns (e) and (o) of Table 1 refer separately to L_2 and S_2 (in this order). The data for S_2 obtained in the course of the twenty-seven determinations of L_2 given by CHAPMAN and TSCHU (1948) have not previously been published; for Ocean Island (station 53), S_2 was specially determined for this paper, from unpublished hourly values supplied by the Meteorological Office, by the courtesy of its late Director, Sir N. K. JOHNSON. Data for stations 45–48 were kindly supplied by Dr. S. K. PRAMANIK. We are indebted to Dr. J. BARTELS for the value of σ_2 for Hamburg (station 4), and for other particulars in Table 1.

The stations of Table 1 are also listed in LANDOLT-BÖRNSTEIN (1952), where the

* Values in column (d) marked by an asterisk * refer to mean sea level, *not* station level.

VOL. 8 1956

actual years and the number N of days used in the L_2 determinations are given (but without the values of the mean pressure); the geographical co-ordinates here given have been carefully checked, especially in the few cases where they differ slightly from those there given.

Table 1 also gives for each station the values of s_2 and σ_2, and of l_2 and λ_2. The probable errors (PE) of the determinations of L_2 are given, next after the l_2 column; the corresponding uncertainty in the phases λ_2, taken to be measured by $\sin^{-1}(\mathrm{PE}/l_2)$, is given in column (n), under the heading PE′.

The probable errors given for the determinations of L_2 are taken wherever possible from the sources quoted in Table 1; but in the paper by CHAPMAN and TSCHU (1948) the probable errors given for fourteen of the twenty-seven stations there considered were incorrect, as explained later by CHAPMAN (1952); the correct values are here given; the stations subject to this correction are 23–25, 31, 33, 49, 52, 54–56, 59, 62, 65, and 69. The probable errors for stations 1, 15, 39, 57, and 64 were given by BARTELS (1927). In a few other cases the probable errors are only estimates; these are indicated in Table 2, columns (i) (l), and (n), by an asterisk*. Blank spaces are left in the four columns (k) to (n) where L_2 is ill-determined.

In Table 1 the value of σ_2 for Keitum, and the values of l_2, λ_2 for Paris, though they have been determined, could not be obtained for insertion here.*

3. Harmonic Dial Representation on the World Map

A variation S_n or L_2, specified by (1) or (2), can be represented graphically on a harmonic dial. A vector is drawn, of length corresponding to s_n or l_2, on a suitable scale, in the direction corresponding to the phase angle σ_n or λ_2; this angle is measured counterclockwise from a horizontal line drawn to the right from the origin. The components of the vector along and perpendicular to this line are therefore $s_n \cos \sigma_n$, $s_n \sin \sigma_n$ or $l_2 \cos \lambda_2$, $l_2 \sin \lambda_2$. In the case $n = 2$, the vector has the direction of the hour hand on the dial of a clock that keeps solar or lunar time respectively, at the times of maximum pressure (occurring twice daily) due to S_2 or L_2.

A harmonic dial may be provided with a framework of reference; this may show the origin and initial line, from which the phase angles are measured; it may also include a circle concentric with the origin, on which angles are marked at regular intervals, to aid in estimating at sight the magnitude of the phase angle of the dial vector: this circular scale may also be time-marked (time increasing clockwise—opposite to the direction in which the phase angle increases—from the vertical direction, which represents lower or upper transit of the sun or moon). But this framework may when desirable be omitted, provided that the origin is distinguished from the "free" end of the dial vector, and that the direction of the initial line for phase angles is understood to be horizontal from the origin towards the right.

This simplified dial representation is used to illustrate, in Fig. 1, the world distribution of S_2 and L_2, as given by Table 1. As far as we know, S_2 and L_2 dial vectors have not hitherto been thus represented on the same map, though one of

* Note added in proof: the Paris L_2 data have been obtained and inserted in Table 1, but not in the Figures.

Table 1. *Determinations of the annual mean solar and lunar semidiurnal air-tides S_2 and L_2; particulars of the stations. Amplitudes s_2 and l_2 are expressed in microbars. See Section 2 for detailed explanation.*

Column	(a)	(b)	(c)	(d)	(e)	(f)	(g)	(h)	(i)	(j)	(k)	(l)	(m)	(n)	(o)
Number and name of station	Lat. °	Long. °	Height, metres	Mean press. mb., at station level	No. of years used L_2, S_2	s_2	σ_2 °	l_2	PE	λ_2 °	$\frac{100 l_2}{s_2}$	PE	$\sigma_2 - \lambda_2$ °	PE' °	References
Northern stations															
50°–60°															
1. Aberdeen, Scotland	57·9	2·5 W	14	1006	12, 12	241	145·8	15·1	3·1	98	6·2	1·3	48	12	CF(1922); H3
2. Glasgow, Scotland	55·9	4·2 W	55	1012*	12, 12	283	149·1	4·7	3	83					Robb(1936b); H3
3. Keitum (Frisian I.), Germany	54·9	8·4 E	11	1013	10, 9	221		8·1	3·7	80					B(1927); H3
4. Hamburg, Germany	53·6	10·0 E	26	1008	37, 9	276	170	14·4	3·1	94	5·2	1·1	76	12	B(1927); H3
5. Potsdam, Germany	52·4	13·1 E	85	1004	30, 10	308	140·2	14·0	2·8	92	4·5	0·9	48	12	B(1927); H3
6. Greenwich, England	51·5	0	45	1009	18, 20	319	154	11·7	2·4	114	3·7	0·8	40	12	C(1918); Met. C.
40°–50°															
7. Vancouver, B.C., Canada	49·3	123·1 W	41	1017*	12	242	118	1·9	4·4	58					C(1935b)
8. Paris, France	48·8	2·5 E	50	1008	26, 25	393	150·6	13·4	2·7	105	3·4	0·7	45	12	——; H3
9. Victoria, B.C., Canada	48·4	123·3 W	70	1009	29	208	127	5·3	2·9	107					C(1935b)
10. Portland, Ore., U.S.A.	45·5	122·7 W	47	1013	15	344	133·1	2·8	5·4	54					CTs(1948)
11. Montreal, Canada	45·5	73·6 W	57	1009	28	423	168	27	4·1	72	6·4	1·0	96	9	C(1935b)
12. St. John, N.B., Canada	45·3	66·1 W	36	1010	17	432	166	26	4·7	83	6·0	1·1	83	10	C(1935b)
13. Toronto, Canada	43·7	79·4 W	115	1002	31	428	170	29	4·1	78	6·8	1·0	92	8	C(1935b)
14. Sapporo, Hokkaido, Japan	43·1	141·4 E	17	1013*	40	407	176·7	25·7	2·5	69	6·3	0·6	108	6	C(1937)
15. Tiflis, Georgia, U.S.S.R.	41·6	44·5 E	442	970	25, 22	501	157·9	27	2·4	65	5·4	0·5	93	5	C(1924); H1
16. Rome, Italy	41·9	12·5 E	50	1009	4, 15	416	146·7	27	6·4	98	6·5	1·5	49	14	M(1899); H3
17. Salt Lake City, Utah, U.S.A.	40·8	111·9 W	1329	868	15	408	148·0	7·1	5·0	51	1·7	1·2	97		CTs(1948)
18. Coimbra, Portugal	40·2	8·4 W	141	1018*	61	584	157·9	16·9	1·7	74	2·9	0·3	84	6	CTs(1948)

VOL. 8 1956

30°–40°															
19. Philadelphia, Pa, U.S.A.	40·0	75·2 W	36	1013	12	540	159·4	28·2	4·4	64	5·2	0·8	95	9	CTs(1948)
20. Santa Cruz, Azores	39·4	31·1 W	40	1021*	26	480	154	18·4	2·2	58	3·8	0·4	96	7	C(1936a)
21. Washington, D.C., U.S.A.	38·9	77·0 W	34	1014	12	582	156·9	31·1	4·9	58	5·3	0·8	98	9	CTs(1948)
22. Lisbon, Portugal	38·7	9·2 W	95	1006	54	572	153·2	22·1	1·7	62	3·9	0·3	91	4	CTs(1948)
23. Lick Obs., Calif., U.S.A.	37·9	122·3 W	1285		44	357	116·4	10·9	1·6	68	3·1	0·4	49	8	CTs(1948)
24. San Francisco, Calif., U.S.A.	37·8	122·4 W	47	1011	15	527	143·0	14·7	2·3	58	2·8	0·4	85	9	CTs(1948)
25. Dodge City, Kansas, U.S.A.	37·8	100·0 W	766	928	15	622	152·4	21·8	5·0	73	3·5	0·8	79	13	CTs(1948)
26. Ponta Delgada, Azores	37·7	25·7 W	22	1019	39	527	146	21·7	1·6	55	4·1	0·3	91	4	C(1936a)
27. San Fernando, Spain	36·5	6·2 W	29	1013*	56	565	144·4	27·7	1·5	79	4·9	0·3	65	3	CTs(1948)
28. Tokio, Japan	35·7	139·8 E	21	1014	43	710	168·8	38·6	2·5	60	5·4	0·4	109	4	C(1937)
29. Mt. Wilson Obs., Calif., U.S.A..	34·2	118·2 W	1782		16	485	141·0	15·9	2·4	75	3·3	0·5	66	9	CTs(1948)
30. Kumamotu, Kyushu, Japan	32·8	130·7 E	39	1016*	37	633	163·5	37·4	2·2	48	5·9	0·3	116	3	C(1937)
31. San Diego, Calif., U.S.A.	32·7	117·2 W	26	1012	15	594	145·1	23·2	3·0	69	3·9	0·5	76	7	CTs(1948)
32. Bermuda I., Atlantic Ocean	32·4	64·7 W	49	1015	6	641	156·0	41·5	5·9	67	6·5	0·9	89	8	CTs(1948)
33. Haifa-Jerusalem, Israel	32·3	35·1 E	10 & 826	1013*	5	429	139·9	23·3	4·3	36	5·4	1·0	104	11	CTs(1948)
30°–20°															
34. Cairo-Helwan, Egypt	30·0	31·3 E	35 & 30	1000	9, 3	800	154·2	36	2*	64	4·5	0·2*	90	3*	C(1928); H3
35. New Orleans, La., U.S.A.	30·0	90·1 W	16	1016	12	682	157·5	33·9	3·9	70	5·0	0·6	88	7	CTs(1948)
36. Galveston, Texas, U.S.A.	29·3	94·8 W	16	1016	12	688	149·5	35·7	4·9	71	5·2	0·7	79	8	CTs(1948)
37. Naha, Chusan I., China	26·2	127·6 E	10	1011	33	749	158·2	48·6	2·2	43	6·5	0·3	115	3	C(1937)
38. Taihoku, Formosa	25·0	121·5 E	9	1013	36	857	164·7	55·5	2·1	50	6·5	0·2	115	2	C(1937)
39. Hong Kong, China	22·3	114·2 E	33		27, 9	1081	151·3	60	2·4	60	5·6	0·2	91	2	C(1919); H3
40. Honolulu, Hawaii	21·3	157·9 W	15	1015	20	891	163·7	45	2·6	66	5·1	0·3	98	3	C(1935a)
20°–10°															
41. Mexico City, Mexico	19·4	99·1 W	2280	775	15, 3	1044	157·6	35	3*	74	3·5	0·3*	84	5*	CH(1928); H1
42. Bombay, India	18·9	72·8 E	11	1010	46, 25	1291	156·9	49	2*	81	3·8	0·1*	76	2*	P(1931); H1
43. Manila, Philippine I.	14·6	121·0 E	14		45	1204	158·7	73·2	1·4	59·9	6·1	0·1	99	1	CTs(1948)
44. Madras, S. India	13·1	80·3 E	7	1010	16, 10	1473	158·1	53	2*	56	3·6	0·1*	102	2*	CH(1928); H1
45. Kodaikanal, S. India	10·2	77·5 E	2341	772	7, 11	1078	155	52	12*	68	4·8	1·1*	87	13*	PCJ(1931)
46. Periyakulam, S. India	10·1	77·5 E	288	980	7, 6	1482	158	52	12*	62	3·5	0·8*	96	13*	PCJ(1931)
10°–0°															
47. Agustia, S. India	8·6	77·3 E	1880	816	3, 4	1070	157	49·3	7·2	75·2	4·6	0·7	82	8	P(1951)
48. Trivandrum, S. India	8·5	77·0 E	60	1005	10, 12	1463	167	50·7	6·2	73·1	3·5	0·4	94	7	P(1951)
49. Lagos, Nigeria	6·4	3·4 E	7	1010	6	1207	125·3	69·2	4·9	73·1	5·7	0·4	52	4	CTs(1948)
50. Accra, Gold Coast	5·6	0·2 W	100	1010	3	890	136	45	5·8	72	5·1	0·7	64	7	C(1938)
51. Singapore, Straits Settlements.	1·3	103·8 E	5	1010*	4, 5	1312	156·3	89	22*	76	6·8	1·7*	80	14*	E(1852); H1
52. Kololo Hill, Uganda	0·3	32·6 E	1312	869	6	1371	154·8	91·2	5·3	77·9	6·7	0·4	77	3	CTs(1948)

Table 1—*continued*

Column	(a)	(b)	(c)	(d)	(e)	(f)	(g)	(h)	(i)	(j)	(k)	(l)	(m)	(n)	(o)
Number and name of station	Lat. °	Long. °	Height, metres	Mean press. mb	No. of years used L_2, S_2	s_2	σ_2 °	l_2	PE	λ_2 °	$\frac{100 l_2}{s_2}$	PE	$\sigma_2 - \lambda_2$ °	PE' °	References
Southern stations															
0°–10°															
53. Ocean I., Pacific Ocean	0·9	169·6 E	28	1005	5, 3	1086	155·6	71	8	100	6·5	0·7	56	6	C(1931)
54. Kabete, Kenya	1·3	36·8 E	1820	821	6	1536	145·0	87·4	4·3	72·5	5·7	0·3	73	3	CTs(1948)
55. Kazeh Hill, Tanganyika	5·0	32·9 E	1265	874	6	1556	140·8	86·4	5·6	58·3	5·6	0·4	83	4	CTs(1948)
56. Chukwani Palace, Zanzibar I.	6·2	39·2 E	20	1011	6	1595	164·7	91·5	6·0	65·9	5·7	0·4	99	4	CTs(1948)
57. Batavia, Java	6·2	106·8 E	8	1010	30, 40	1325	159·9	83	2·1	68	6·3	0·2	92	1	C(1919); H2
58. Dar-es-Salaam, Tanganyika	6·8	39·3 E	8	1014*	2, 12	1095	158·3	84	23	63	7·7	2·1	95	16	B(1939); H2
10°–20°															
59. Huancayo, Peru	12·0	75·3 W	3355		15	1387	151·0	39·0	3·9	74	2·8	0·3	58	6	CTs(1948)
60. La Molina, Lima, Peru	12·1	77·0 W	251	988	5	1007	154·5	47·5	4·6	73	4·7	0·5	82	6	CTs(1948)
61. Apia, Samoa I., Pacific Ocean	13·8	171·8 W	3		20, 4	981	158·6	73	7*	59	7·4	0·7*	100	6*	CTh(1932); H2
62. Broken Hill, N. Rhodesia	14·4	28·4 E	1197	883	5	1466	125·8	84·4	5·5	66·7	5·8	0·4	59	4	CTs(1948)
63. St. Helena I., Atlantic Ocean	16·0	5·7 W	538	948	4, 5	989	152·7	59·0	18*	93	6·0	1·8*	60	18*	S(1847); H1
20°–30°															
64. Mauritius I., Indian Ocean	20·1	57·5 E	55	1010	38, 12	985	163·7	51	1·1	98	5·2	0·1	66	1	C(1924); H2
65. Pretoria, Transvaal, S. Africa	25·7	28·2 E	1367	872	10	820	148·8	42·0	3·4	90	5·1	0·4	59	5	CTs(1948)
66. Kimberley, C. Gd. Hope, S. Africa	28·7	24·8 E	1203	882	20, 7	823	158·7	46	1·4	101	5·6	0·2	58	2	C(1932); H2
67. Buenos Aires, Argentina	34·6	58·4 W	25	1012	18, 5	607	156·7	12·8	4·2	87	2·1	0·7	70	19	CA(1934); H2
68. Melbourne, Australia	37·8	145·0 E	28	1014	36	690	166·7	28·5	2·3	84	4·1	0·3	83	5	CHM(1936)
69. Wellington, New Zealand	41·1	174·8 E	3		24	432	167·1	38·9	3·2	69	9·0	0·8	98	5	CTs(1948)

VOL. 8 1956

us has previously given maps of this type for L_2 alone (CHAPMAN 1935c, 1939, 1948, and 1951); these maps successively incorporated more data.

Fig. 1 and the later maps here given are on Mercator projection;* their range of latitude, from 60° N to 40° S, is that over which determinations of L_2 have been made, except that station 69 (Wellington, N.Z.) lies just outside the map, at 41° S. For convenience each map is divided into two equal parts (a) and (b), separated by the meridians 20° W and 160° E; the western part (a), which includes most of the Pacific and Atlantic Oceans and most of North and South America, may be called Oceanamerican; the eastern part (b), which includes Europe, Africa, and most of Asia and Australasia, may be called Eurafricasian.

Fig. 1 shows the location of each station, indicated by its serial number, as given in Table 1; it shows also the dial vectors for S_2 and L_2 for each station, drawn from its map-position as origin. The scales of representation for the amplitude l_2 of L_2 and for the amplitude s_2 of S_2 are shown; the former is twenty times the latter. Probable error circles for L_2 are drawn around the ends of the L_2 vectors, to indicate the reliability of the different determinations; this distinguishes the L_2 from the S_2 vectors: the latter are also distinguished by having an arrowhead at the end.

No probable error circles for S_2 are given, but this does not imply that the values given in Fig. 1 for the S_2 vectors would correspond to S_2 in each and every year. The year-to-year variability of S_2 has been studied to some extent, but, for most of the stations here considered, data are not available to give probable error circles of S_2 in Fig. 1. BARTELS (1927)—see also LANDOLT-BÖRNSTEIN (1952), p. 675—has given some attention to the problem, and finds that for Potsdam the probable error of a 30-year mean determination of S_2 is approximately 4 microbars. This is similar to the probable errors of many of the determinations of L_2 given in Table 1, although, where L_2 has been determined from many years' data, its probable error is usually still less: but the probable error is *proportionately* much greater for L_2 than for S_2. For S_2 the probable error circles could not well be shown on Fig. 1, on the reduced scale for S_2 there used.

The small probable error circles for L_2 at many stations show that in some parts of the globe L_2 is very well determined, and particularly so at Kimberley (65), Mauritius (64), and at several Indian and Japanese (or former Japanese) stations. Three stations, 51 (Singapore), 58, and 63 (St. Helena), have rather large probable errors; 51 and 63 are the stations at which the two earliest determinations were made, from only a few years' data; it is desirable that new determinations be made for these stations. The determination for station 58 (Dar-es-Salaam) was made by BARTELS from barometric readings taken only thrice daily—*a tour de force* of computation, showing that even such unpromising material can be used effectively; his result for station 58 agrees well with the much more accurate determination for Chukwani Palace (Zanzibar), station 56.

* Note regarding Figs. 1–6: These figures have been reproduced by superposing two diagrams to form the printing block; one diagram is the geographic base map, the other is the set of points or arrows and numbers; the latter were drawn on tracing paper which unfortunately shrank after drawing, by amounts different in different cases. This has the result that the station points appear in different figures in slightly different relations to the geographic base, so that a coastal station (such as Bombay, India) in some cases appears slightly inland or offshore. The errors of position are, however, not serious enough to detract from the illustrative value of the maps.

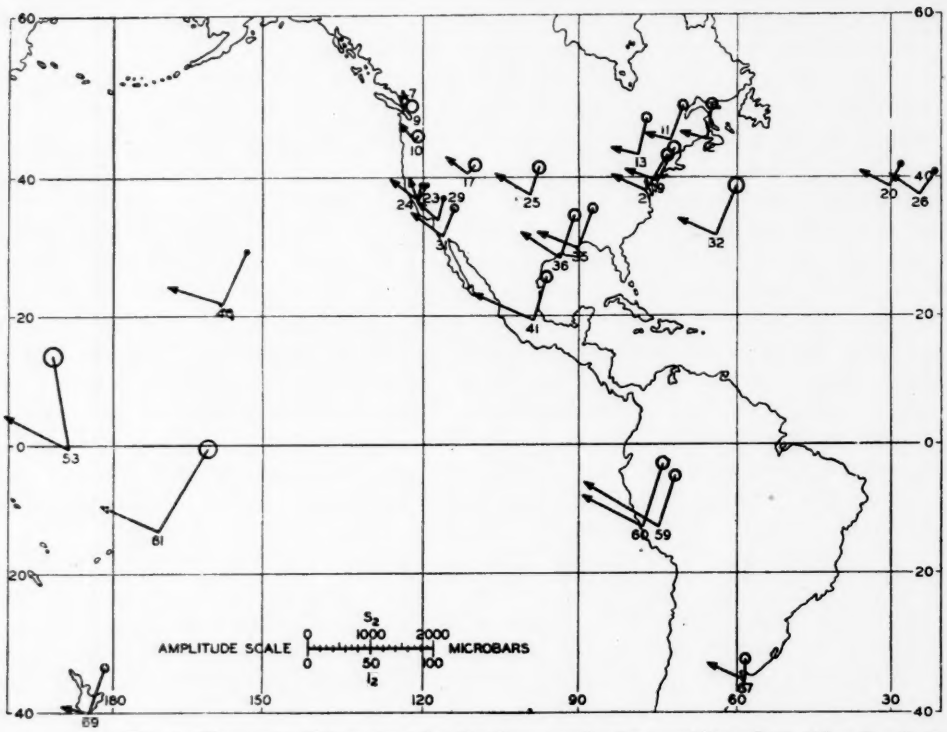

Fig. 1. Harmonic dial vectors for the lunar and solar semidiurnal air-tides L_2, S_2 in barometric pressure at sixty-nine stations (omitting S_2 for station 3 and L_2 for station 8). The lunar amplitudes l_2 are on a scale twenty times that for the solar amplitudes s_2. The circles or dots surrounding the "free" ends of the L_2 vectors indicate the probable error

VOL. 8 1956

4. World Maps Indicating Amplitudes and Amplitude Ratios. Phases and Phase Differences

Fig. 2 shows the distribution of the amplitude s_2 of S_2, and Fig. 3 shows the amplitude l_2 of L_2, by numbers alongside the dots marking the positions of the stations. Fig. 4 shows similarly the ratio $100l_2/s_2$, which is tabulated, with its probable error, in Table 2. Figs. 5 and 6 likewise show the distribution of the phases σ_2 and λ_2. In Fig. 6 the degree of reliability of the value of λ_2 is indicated; where the probable error PE′ (column (n) of Table 1) lies between 5° and 9°, a single dot is placed under the value for λ_2; two dots indicate that the probable errors lies between 10° and 14°; and three dots, that it exceeds 14°; the values with no dot below them are, of course, the most accurate.

In Fig. 7 the phase differences $\sigma_2 - \lambda_2$ are indicated. Instead, one might indicate the opposite differences $\lambda_2 - \sigma_2$ (which are all negative or, if positive, greater than 180°), but it was not thought necessary to do this, although $\lambda_2 - \sigma_2$ is the argument, as $100l_2/s_2$ is the amplitude, of the complex ratio $100\ L_2/S_2$, if S_2 and L_2 are expressed as $s_2 \exp \iota\sigma_2$ and $l_2 \exp \iota\lambda_2$. The differences $\sigma_2 - \lambda_2$ are subject to very nearly the same uncertainty as λ_2, but in Fig. 7 only the least accurate values are identified,

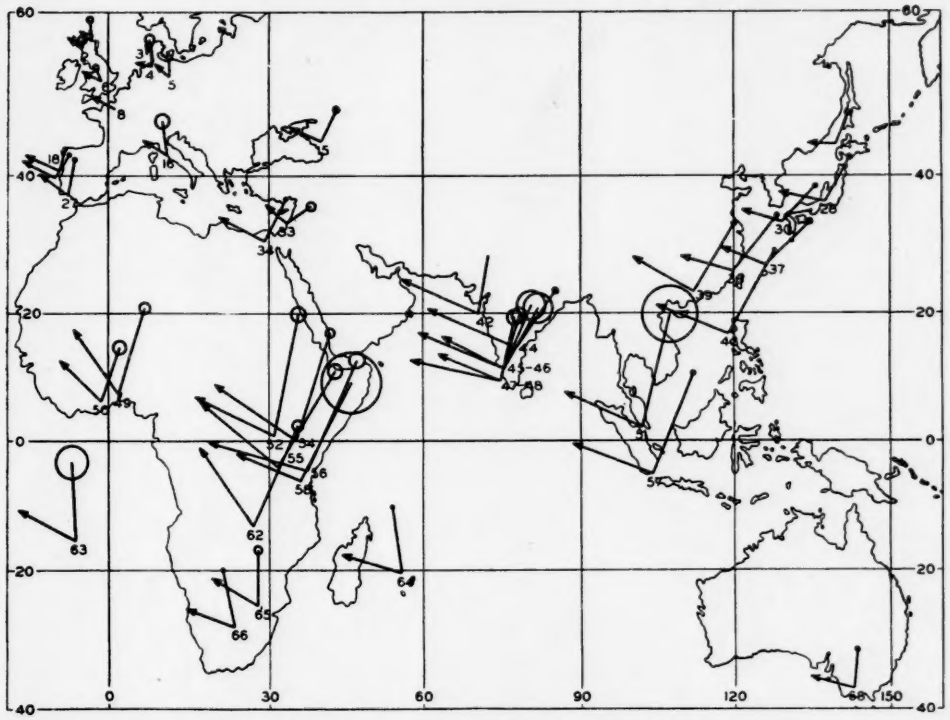

of the L_2 determinations, which are to be reckoned satisfactory if this error does not exceed $(1/3)l_2$. The L_2 and S_2 vectors refer to the station situated, on the map, at the common origin of the two vectors. The number alongside each point is the serial number of the station in Table 1.

using three dots, for the same stations as in Fig. 6. The reliability of the other values of $\sigma_2 - \lambda_2$ can be inferred by reference to Fig. 6.

Figs. 1–7 show that L_2 is now known in many parts of the world; the Oceanamerican Fig. 1(a) includes 27 stations (21 northern, 6 southern); the Eurafricasian Fig. 1(b) includes 42 stations (31 northern, 11 southern).

Figs. 1–7 show also that there are large areas with few or no determinations of L_2. In many areas barometric data are available from which determinations of L_2 (and S_2) could be made—using either hourly or bi-hourly data, or, as in the case of Dar-es-Salaam, series of observations made as few as three times daily. For South America there are only the three determinations for Buenos Aires (67) and the two fairly adjacent Peruvian stations 60 (Lima: at a low level) and 59 (Huancayo: at high level). For Australia there is only one determination, likewise for New Zealand. Large areas in north America, eastern Europe, and Asia are without determinations, though there may be some Russian, Chinese, and other determinations of which we are unaware. Only eight oceanic islands—the Azores (20, 26), Bermuda (32), St. Helena (63), Hawaii (40), Samoa (61), Ocean Island (53), and Mauritius (64)—provide determinations, though there must be many others for which suitable barometric data are available (in low latitudes a few years' data suffice).

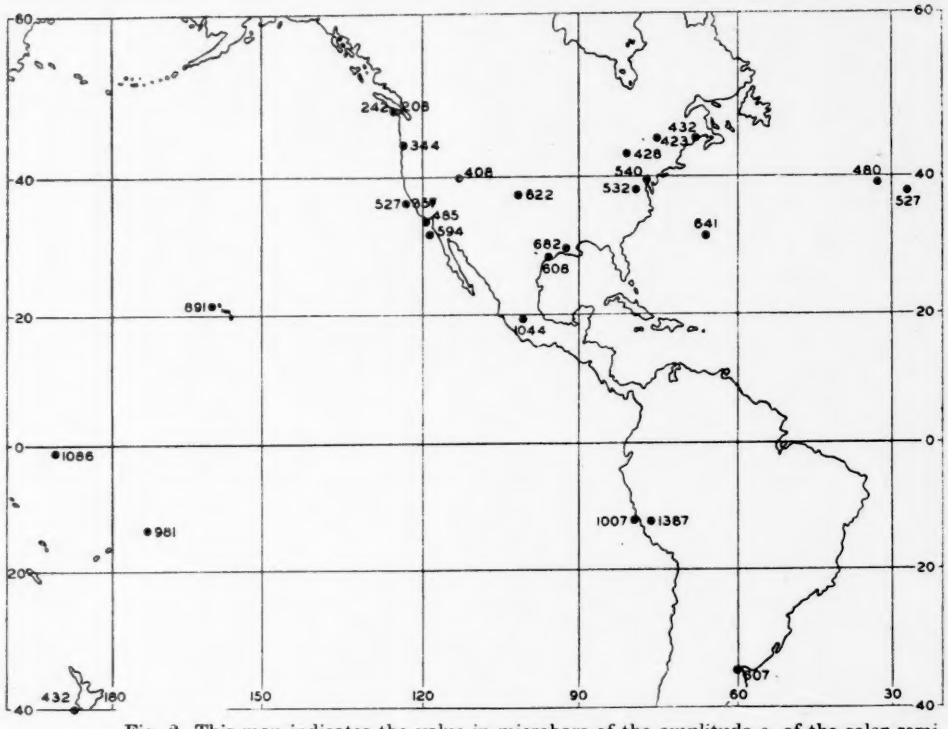

Fig. 2. This map indicates the value in microbars of the amplitude s_2 of the solar semi-diurnal air-tide S_2 in barometric pressure at sixty-seven stations of Table 1. Regions

5. Discussion of the Distribution of the Amplitudes s_2 and l_2

In Fig. 1 some of the L_2 vectors are longer, others are shorter than the corresponding S_2 vectors. The overall means of s_2 and l_2, for the sixty-eight stations for which both s_2 and l_2 are given in Table 1, are 784 and 39·5, of which the ratio is 19·8. Thus the twenty-fold scale ratio used in representing S_2 and L_2 in Fig. 1 is closely appropriate.

Fig. 1 indicates in a general way that s_2 and l_2 are greatest in low latitudes. This is more definitely shown by the following table of mean values of s_2 and l_2 for successive 10° belts of latitude. The ratio of the mean s_2 to the mean l_2 is given for each latitude belt, and also the mean value of $100l_2/s_2$, as given in Table 1 and illustrated in Fig. 4.

The ratios $\bar{s}_2/\bar{l}_2$ and (mean) $100l_2/S_2$ show a generally inverse relation, but their product (given in the last row) is not exactly 100, because the inverse of the harmonic mean is not equal to the arithmetic mean.

Table 2 clearly shows the considerable decline of s_2 and l_2 towards higher latitudes, illustrated graphically in Fig. 8, in which, as in Fig. 1, the scale ratio for s_2 and l_2 is 20. The decline beyond latitude 20° N and S is fairly similar in the two hemispheres, so far as the scanty southern data permit a comparison; but the variation in the tropical belt is *not* symmetrical relative to the equator. The

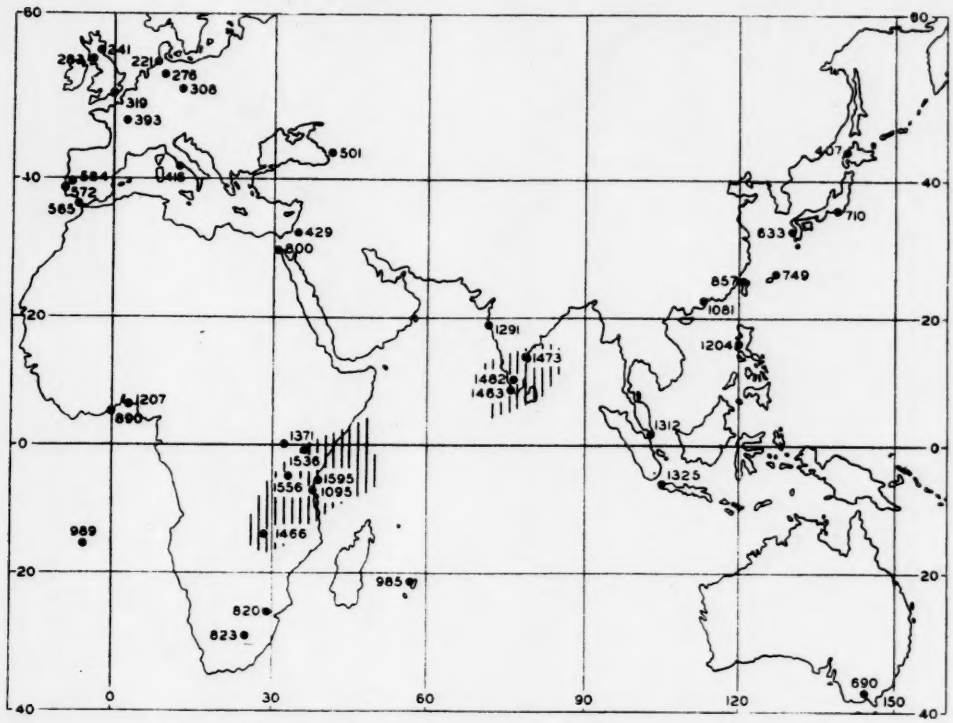

where s_2 is specially large are marked by vertical shading. The values for two high-level Indian stations (45, 47) are omitted.

greatest mean values of both s_2 and l_2 are found in the belt 0°–10° S; the number of stations in this belt is small, but the main cause of the irregularities in the tropical-latitude variations of s_2 and l_2 can be seen from Figs. 2 and 3 to be the existence of some areas of exceptionally high values; these areas (for $s_2 > 1400$. $l_2 > 80$) are indicated on the maps by vertical shading. One of these areas, in east Africa, is common to the two maps; but the other areas are different, namely over India for s_2, and over the East Indies for l_2. India, indeed, has values of l_2 that are rather low for its latitude. It would be of interest to determine whether the large values of s_2 extend over the area between east Africa and India, and

Table 2. Mean amplitudes $\bar{s}_2$ and $\bar{l}_2$ and their ratios, for 10° belts of latitude

Latitude	N60–50°	50–40°	40–30°	30–20°	20–10°	N10–0°	0–10°S	10–20°	20–30°	30–40°S
Number of stations	6	12(11)	15	7	6	6	6	5	3	3
Mean latitude	54·4°	44·5°	36·3°	26·3°	14·4°	5·1°N	4·45°S	13·7°	24·8°	37·8°
Mean s_2	275	399	551	821	1262	1219	1366	1166	876	576
Mean l_2	11·3	17·8	25·1	45·0	52·4	65·7	83·9	60·6	46·3	26·7
Ratio $\bar{s}_2/\bar{l}_2$	24·3	22·4	22·0	18·3	24·1	18·5	16·3	19·2	18·9	21·6
Mean $100l_2/s_2$	4·2	4·2	4·5	5·5	4·2	5·4	6·3	5·3	5·3	5·1
Product	102	94	99	101	101	100	103	102	100	110

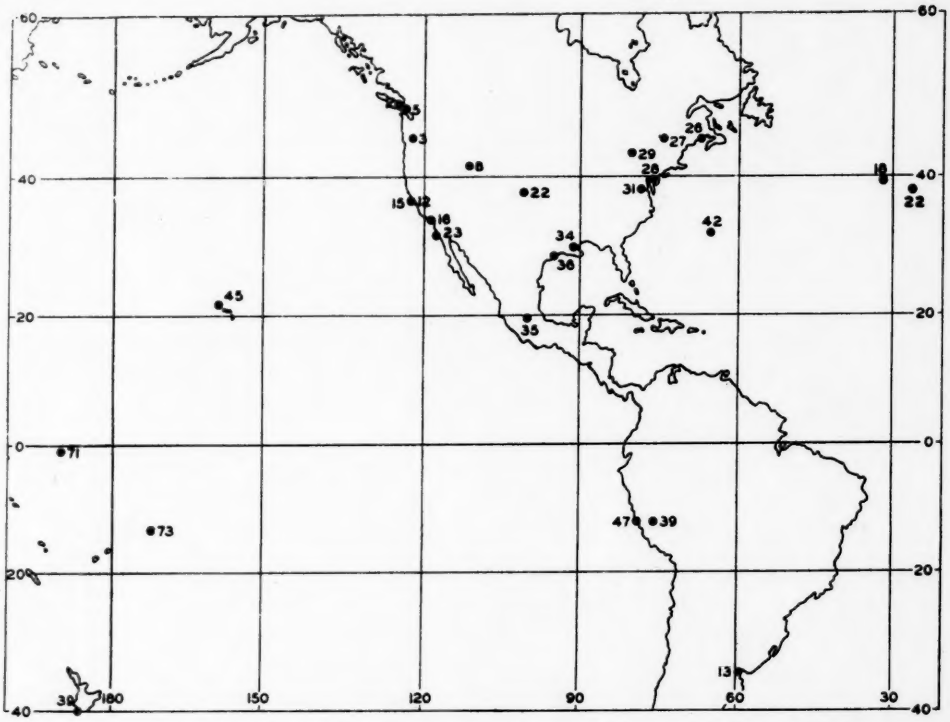

Fig. 3. This map indicates the value in microbars of the amplitude l_2 of the lunar semi-diurnal air-tide L_2 in barometric pressure at each of sixty-six stations (see Table 1).

whether l_2 is large over the region between east Africa and west Indonesia. This might be revealed by studies of the barometric data for the Maldive, Laccadive, and Seychelle islands, the Chagos Archipelago, and the islands in the region of Madagascar and north of Mauritius.

One might attempt to draw isolines on Figs. 2–7, and one of us has tentatively done so for l_2 (CHAPMAN, 1948, 1951); it would not be appropriate to attempt to draw isolines for s_2 and σ_2 on the scanty portion of the whole available material that is here represented. SPAR (1952) has given isolines for s_2 and σ_2 over the U.S.A., on the basis of values from one hundred stations, using material published by the U.S. Weather Bureau. He remarked: "The striking characteristic of the map (for s_2) is the relatively small variation of s_2 with longitude; it is primarily a function of latitude. However, some departures from zonal symmetry are apparent. About 100–200 miles inland from the east coast is found an axis of relatively high amplitudes. The central part of the country is characterized by relatively small longitudinal variation. The next maximum of s_2 lies approximately along the continental divide at almost all latitudes. The amplitude then decreases in the Great Basin and increases again along the Sierras. The smallest values of s_2 are found along the west coast. It appears obvious that s_2 is not free of orographic influences, although they are not large enough to obscure completely the variation with latitude." If values of s_2 were available from a network of stations of equal

VOL. 8 1956

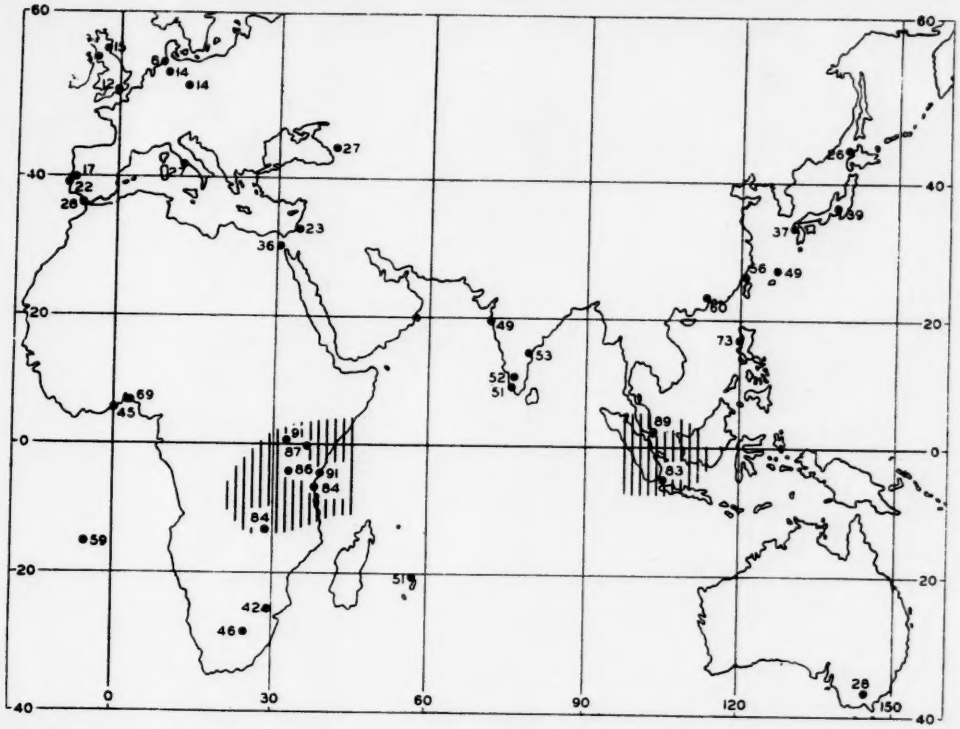

Regions where l_2 is specially large are marked by vertical shading. Values for two high-level Indian stations (45, 47) and for Paris (8) are omitted.

density over other continental regions with considerable mountain areas, departures of comparable magnitude from a distribution varying only with latitude might be expected. Some notable effects that may be ascribed to orographic influences are indicated on Fig. 2. For Huancayo (59), a high-level station with a mean pressure considerably less than that at the not-very-distant coastal station Lima (60), s_2 is much greater than at Lima.

Other anomalies shown by Fig. 2 are the considerable differences between the values of s_2 at the pairs of fairly adjacent stations 49 (Lagos) and 50 (Accra); 33 (Haifa-Jerusalem) and 34 (Cairo-Helwan); and 56 (Chukwani Palace) and 58 (Dar-es-Salaam). Such cases call for further study, using additional data from the two stations themselves, and also data from other stations in the same region. The anomalies of s_2 between stations 49 and 50, and between 33 and 34, are to some extent paralleled in l_2, but this is not the case for the other two pairs mentioned. Buenos Aires (67) seems almost normal as regards s_2, but has an anomalously low value of l_2.

Besides Huancayo and Lima (59, 60) there are four other pairs of adjacent stations in Table 1, one at high level, the other at low—23 and 24 (Lick Observatory and San Francisco); 29 and 31 (Mount Wilson and San Diego); 45 and 46 (Kodaikanal and Periyakulam); 47 and 48 (Agustia and Trivandrum). In these four

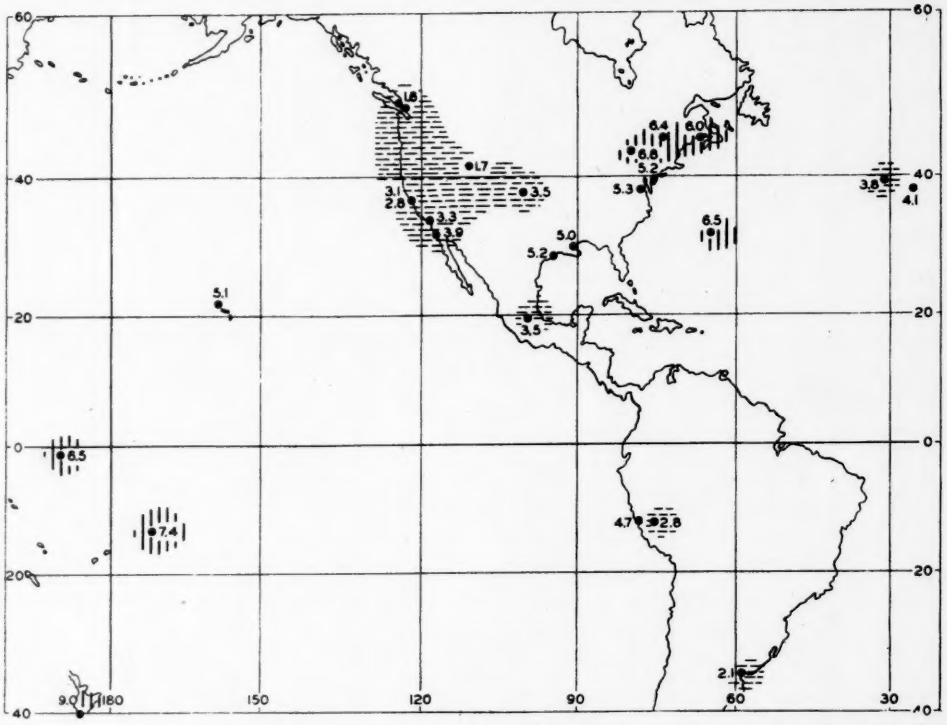

Fig. 4. This map indicates for sixty-eight stations (Table 1) the value of $100l_2/s_2$, the ratio of the amplitude l_2 of the lunar semidiurnal air-tide in barometric pressure to the corresponding solar amplitude s_2, multiplied by 100. A joint value is given for stations 7, 9;

pairs. s_2 for the higher station is decidedly less than for the lower, and so is l_2 for the first two pairs of stations, but not for the two Indian pairs. This is illustrated as follows:

Table 3

	Station No.	s_2	l_2	Station No.	s_2	l_2	Station No.	s_2	l_2
High	23	357	10·9	29	485	15·9	45	1078	52
Low	24	527	14·7	31	594	23·2	46	1482	52
High	47	1070	49·3	59	1387	39·0			
Low	48	1482	50·7	60	1007	47·5			

As SPAR (1952) has shown, the s_2 and l_2 isolines are tortuous when data are available for a close network of stations; the same may be true for l_2 and λ_2. Similarly, isomagnetic charts in many regions are more complex, the more detailed the network of observations—cf. p. 110 of *Geomagnetism* (CHAPMAN and BARTELS, 1940, 1951). The local geomagnetic influence of internal non-uniformities in the

VOL. 8 1956

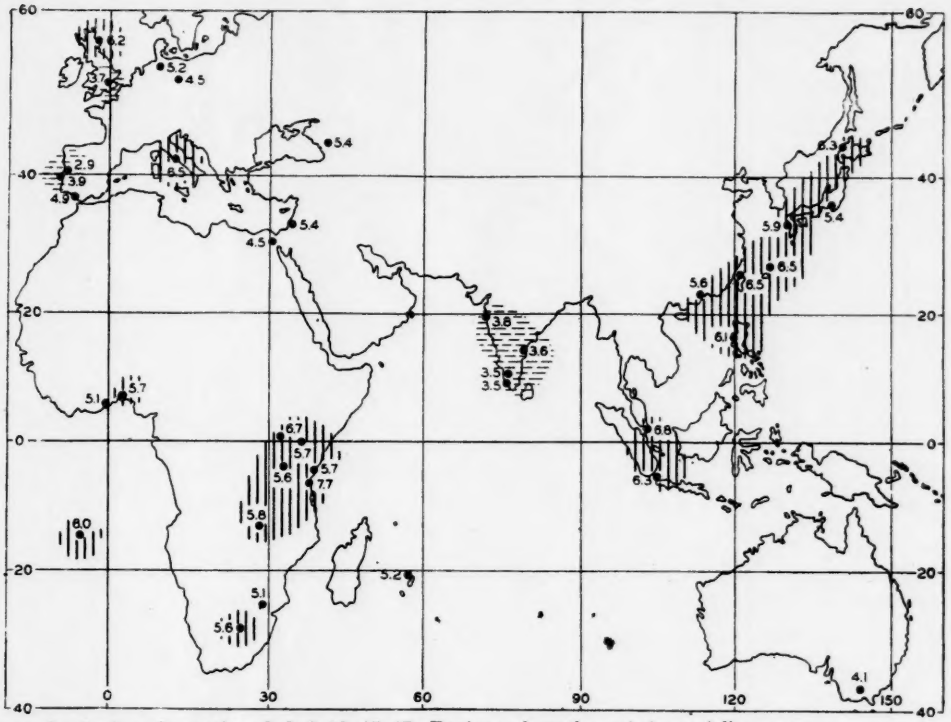

no value is given for stations 2, 3, 8, 10, 45, 47. Regions where the ratio is specially great or small are indicated respectively by vertical or horizontal shading.

earth diminishes with increasing height, and likewise the orographic influence on the air-tides may be expected to decrease in importance as one ascends. But there is no close analogy between the geomagnetic field and the air-tides in this respect, because the region between the ground and the ionosphere may be regarded, magnetically, as merely empty space, whereas it is filled with the air, whose tides must be affected by the thermal and dynamical irregularities of the atmosphere itself. In time we may hope to be able to study the world distribution of the air-tides in three dimensions, by means of the variations of upper air winds, and of the level of formation of cosmic-ray secondary particles, and by means of winds and variations of level in the ionosphere.

On world charts it is only possible to show smoothed isolines, whether geomagnetic or air-tidal, and they give the best general view of the distribution. As yet, however, the determinations of L_2 are too few to permit much accuracy in drawing even smoothed isolines.

Apart from the general decrease of s_2 and l_2 with increasing latitude, the vertical shaded areas of specially high values of s_2 and l_2 are the main features of Figs. 2 and 3.

With more complete data a more refined treatment of the distribution of s_2 and l_2 would be worth while, in which the amplitudes should be corrected to sea-level, or expressed as a fraction of the mean barometric pressure at the station.

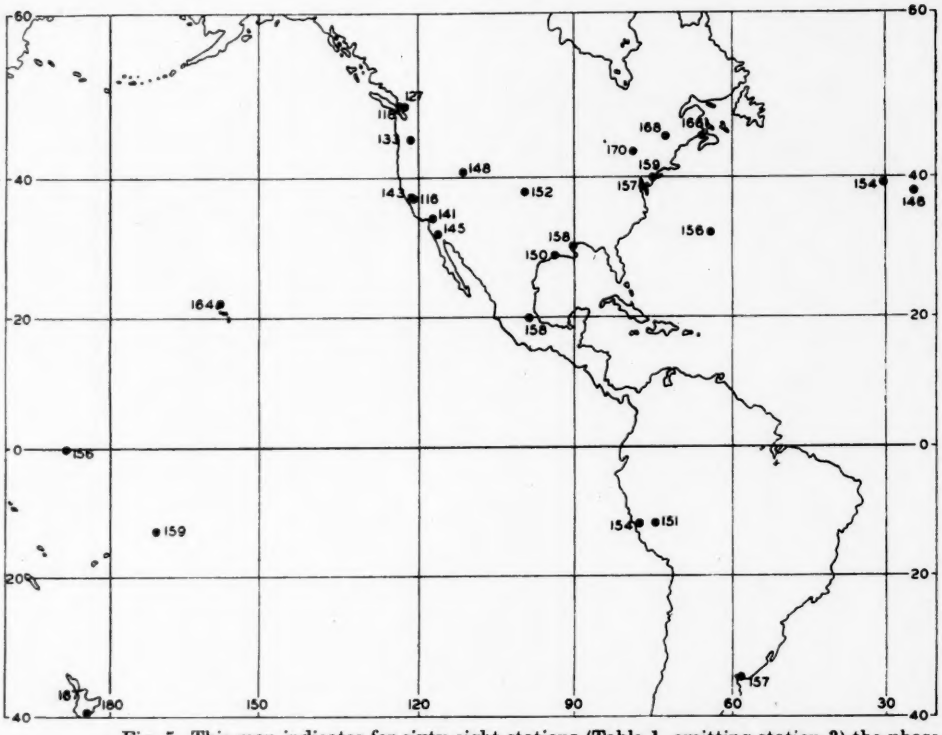

Fig. 5. This map indicates for sixty-eight stations (Table 1, omitting station 3) the phase

The amplitude ratios $100l_2/s_2$, shown in Fig. 3, are free from the direct influence of latitude and of differences of height or mean pressure at different stations. In this figure areas of specially high values (5·5 or more) are indicated by vertical shading, and those of specially low values (4·0 or less) by horizontal shading. The main areas of high ratio are in and near southern Africa, north-eastern America, and eastern Asia; the main regions of low ratio are in north-western America (where the orographic reduction of l_2 is greater than that s_2), and in India.

CHAPMAN and HARDMAN (1928) mention that the (printed) data used for the L_2 determination at station 41 (Mexico City) were corrected to sea-level. In making such a correction, a pressure is added to the actual barometric reading equal to that exerted by a fictitious column of air at temperature T, extending from the level of the station to sea-level; T is in many cases taken to be the current air temperature at the station, but the practice of the U.S. Weather Bureau is to take T to be the mean of the current temperature and that of twelve hours earlier. In either case the correction will contain a semidiurnal component that will affect the determination of S_2 (but not of L_2), and that depends on the semidiurnal temperature variation at the station. Necessary though such a sea-level correction may be when the pressure data are used for synoptic purposes, it is preferable in the study of $S(p)$ and $L_2(p)$ to use data not so corrected. For low-level stations the effect of the correction upon the determination of $S_2(p)$ will be small.

VOL.
8
1956

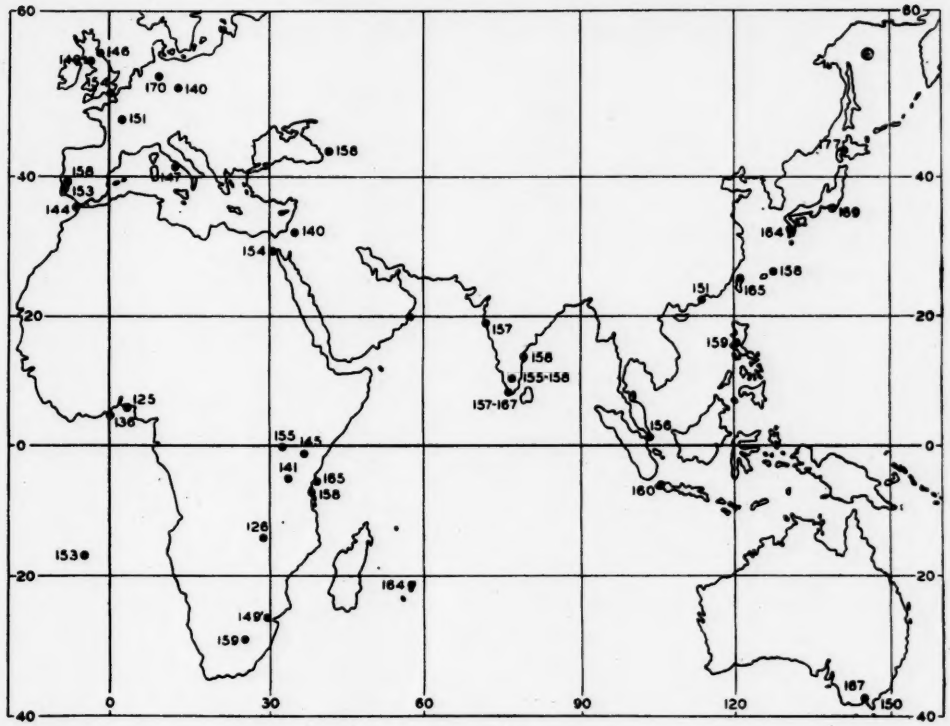

angle σ_2 of the solar semidiurnal air-tide S_2 in barometric pressure.

On enquiry we find that the U.S. Weather Bureau corrects only the synoptic data in the above way, not the hourly data here used (stations 10, 17, 19, 21, 24, 25, 31), which were not corrected to sea-level; nor were the data for stations 23, 29. The Canadian practice is to correct hourly as well as synoptic barometric data to sea-level, by a constant if below 50 ft, or if higher (as in the case of the five stations 7, 9, 11, 12, 13) by the method described by BIGELOW (1902). The data for the six Indian stations 42, 44–48 were not corrected, nor those for Greenwich (6), Haifa-Jerusalem (33), and the East African stations 52, 54, 55, 56, and 62, and Huancayo (59). For British and British overseas stations in general, at levels below 1500 feet, a correction is made to sea-level, using a mean T for the fictitious air column, derived from the screen air T at the time of the barometer reading, and an assumed lapse rate equal to half the dry adiabatic.

Further information will be sought on this matter for the stations not here mentioned, and it is hoped to include such additional information in a later paper, and also to fill the few remaining gaps in column (d) of Table 1. It is to be desired that in all further accounts of determinations of S_n and L_2 clear information will be given as to whether the data had been corrected to sea-level, and if so, how it was done; the station level and the mean barometric pressure should also be stated.

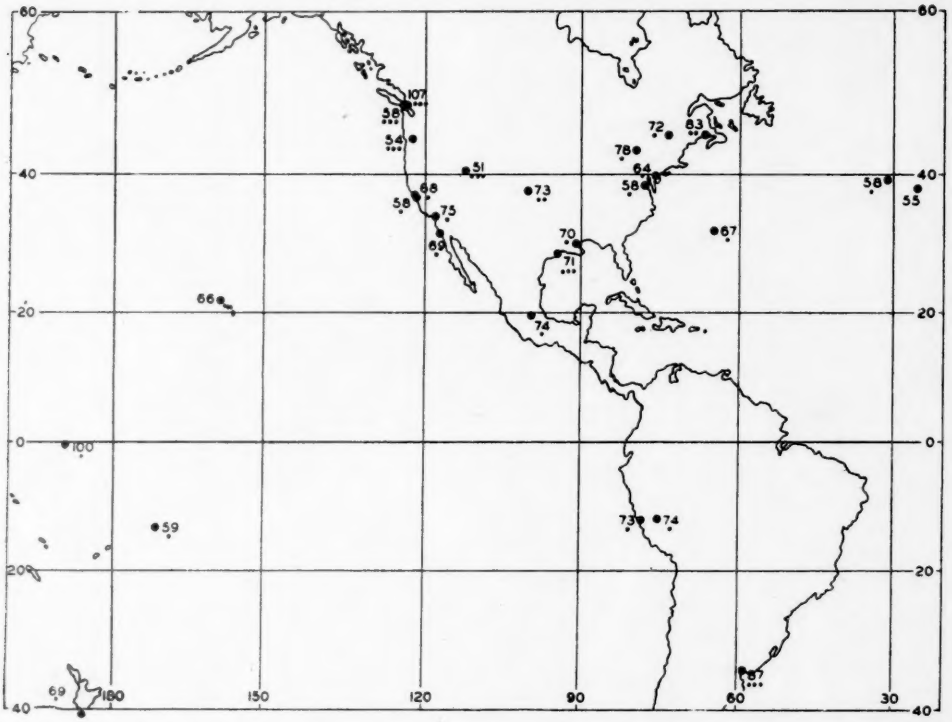

Fig. 6. This map indicates for sixty-eight stations (Table 1, omitting Paris) the phase angle λ_2 of the lunar semidiurnal air-tide L_2 in barometric pressure. Probable errors greater

6. Discussion of the Phases and Phase Differences

It is clear from Fig. 1 that the time of maximum pressure due to S_2 is about two hours before noon, and that at most stations the maximum pressure due to L_2 occurs somewhat after the lunar transits (upper and lower). But the maximum of L_2 undoubtedly precedes lunar transit at some stations, such as Mauritius (64) and Kimberley (66)—for which L_2 is known with special accuracy—and also at Ocean Island (53) and in northern Europe.

The extreme range of the S_2 phase angle σ_2 shown by Table 2 and Fig. 5 is from 177° (at Sapporo, 14, from forty years' observations) to 116° (at the mountain station, Lick Observatory, 23, from forty-four years' observations); San Francisco (24), on the coast near to station 23, does not show any marked anomaly of σ_2. Spar (1952) has given isolines for σ_2 over the U.S.A.; they are more complicated than those for s_2; the range of σ_2 found by him over this area is 30°, from 138° at Marquette, Michigan, to 168° at Tatoosh Island, Washington State, at approximately the same latitude; apart from station 23 (Lick Observatory), the range of σ_2 for the U.S.A. stations here considered is 26° (from 133° for station 10, Portland, Oregon, to 159° for station 19, Philadelphia). The rather low values of σ_2 on the west coast of U.S.A. continue up to British Columbia (stations 7 and 9, Vancouver and Victoria). In Africa, stations 49 (Lagos), 50 (Accra), and 62 (Broken

VOL. 8 1956

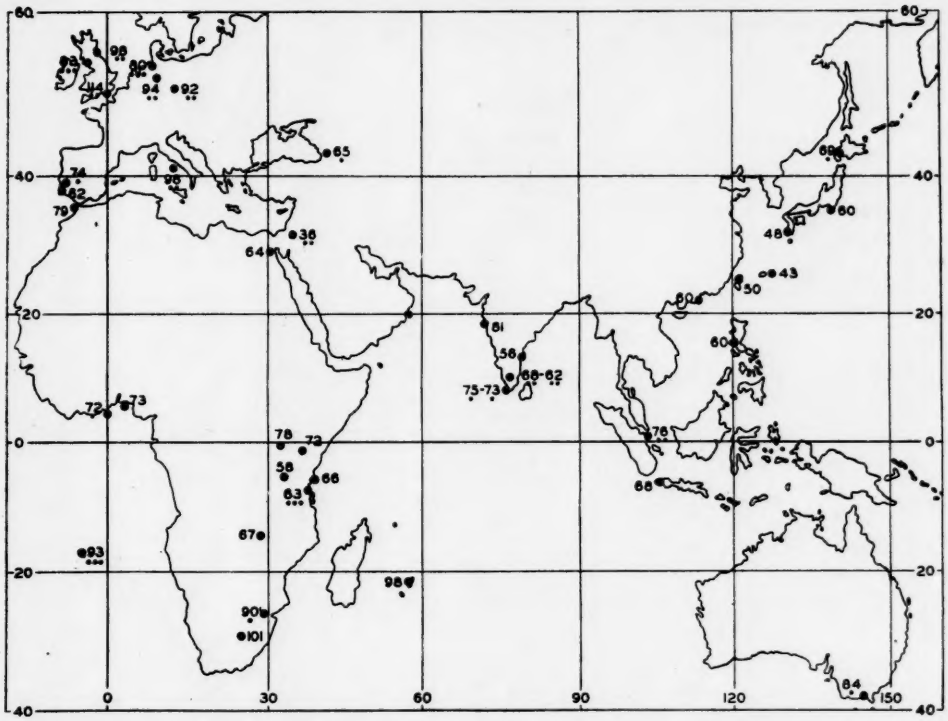

than 4° are indicated by one, two, or three dots under the value of λ_2, indicating probable errors 5°–9°, 10°–14°, and 15° or more, respectively.

Hill) show low values of σ_2. The values of σ_2 for the islands off the east coast of Asia are rather high. SPAR (1952) found that his abundant U.S.A. data for σ_2 showed "no systematic dependence on latitude, and indeed none is to be expected from the tidal theory." The same remarks would be expected to hold for λ_2. The following table shows the means of σ_2 and λ_2 for 10-degree belts of latitude.

Table 4. Mean phases, $\bar{\sigma}_2$ and $\bar{\lambda}_2$, and their differences, for 10-degree belts of latitude

Latitude	60–50	50–40	40–30	30–20	20–10	10N–0	0–10S	10–20	20–30	30–40	All
Number of stations	5(6)	12(11)	15	7	6	6	6	5	3	3	
Mean σ_2	152°	152°	149°	157°	157°	149°	154°	149°	157°	163°	152·75°
Mean λ_2	93°	74°	65°	61°	67°	74°	71°	73°	96°	80°	72°
$\bar{\sigma}_2 - \bar{\lambda}_2$	59°	78°	84°	96°	90°	75°	83°	76°	61°	83°	82°

If the last two belts are combined, so that their "weight" (six stations) becomes not less than that of most of the other belts, the range in the means of σ_2 is 11°; the corresponding range of λ_2 is 32°, of which perhaps less than a quarter can be

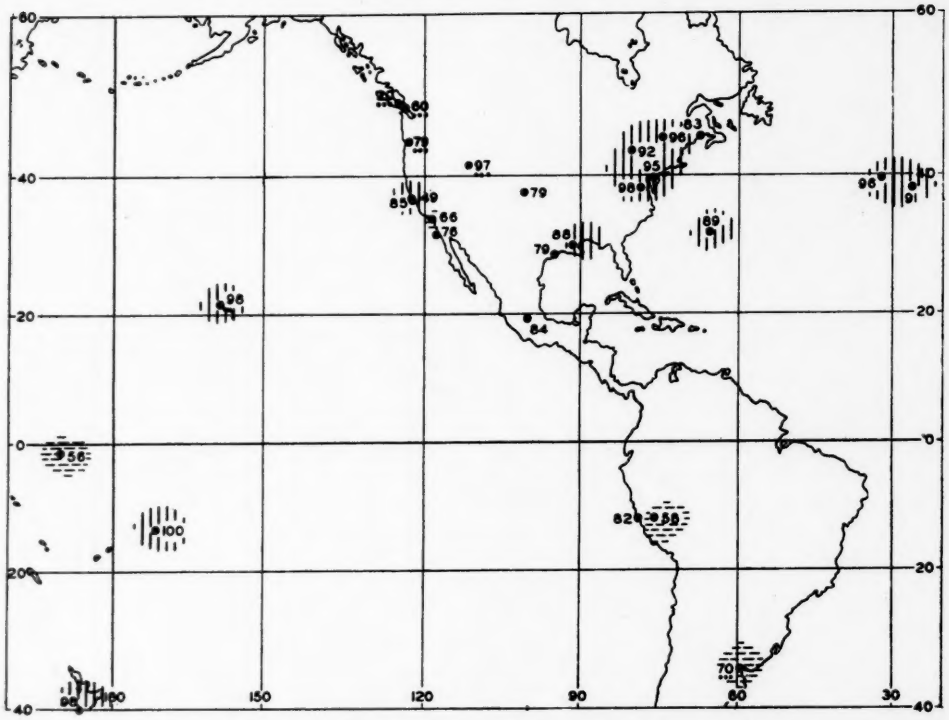

Fig. 7. This map indicates for sixty-seven stations (Table 1, omitting stations 3, 8) the phase difference $\sigma_2 - \lambda_2$ between the solar and lunar semidiurnal air-tides in barometric pressure. The least reliable values are indicated, as in Fig. 6, by three dots under the

ascribed to accidental errors in the individual values. This suggests, as does Fig. 1. that the phase of L_2 is more variable than that of S_2, although as L_2 is purely tidal in origin, and S_2 is partly due also to thermal causes, S_2 might be expected to be the more variable of the two. The regularity of distribution of S_2 is one of the arguments in favour of a considerable degree of resonance magnification in its production; but orographic influences, themselves also associated with temperature irregularities, undoubtedly affect it, in a manner which KERTZ (1951) has attempted to explain theoretically.

The degree of variability of σ_2 is indicated by the following frequency table:

Limits of σ_2	115° –125°	125° –135°	135° –140°	140° –145°	145° –150°	150° –155°	155° –160°	160° –165°	165° –170°	170° –180°
Range of σ_2	10°	10°	5°	5°	5°	5°	5°	5°	5°	10°
Number of cases	2	4	2	6	8	12	20	5	8	1

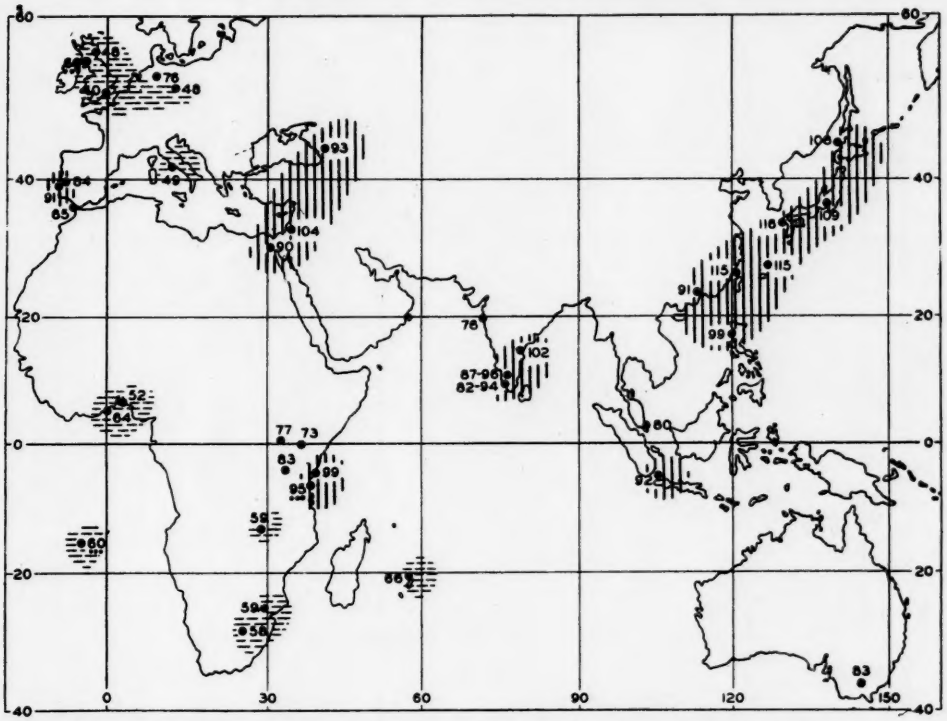

value. Regions where $\sigma_2 - \lambda_2$ is specially great or small are indicated respectively by vertical or horizontal shading.

This distribution is decidedly asymmetrical about the mean value, and different from the Gaussian form. The mean numerical difference of σ_2 from its mean is 9·1°; for λ_2 it is 11·5°, a value enlarged by considerable accidental error, in a minority of the values of λ_2. The mean numerical difference of $\sigma_2 - \lambda_2$ from its mean is 16·2°, indicating that σ_2 and λ_2 do not vary in parallel from their respective mean values.

It is not yet possible to say whether these latitude variations of λ_2 from one belt to another are typical of the whole distribution of L_2 over the earth, because for some of the belts of latitude the determinations cover only a small fraction of the whole range of longitude. As regards σ_2, the existence of the standing-wave part of S_2 (dependent on universal time) implies real variations in the latitude distribution; however, the variations of σ_2 due to this wave will average out round any circle of latitude.

On Fig. 7, regions where $\sigma_2 - \lambda_2$ is decidedly above or below normal are indicated by shading, vertical ($\sigma_2 - \lambda_2 > 85°$) or horizontal ($\sigma_2 - \lambda_2 < 70°$). The main large areas of abnormality are the coastal region of east Asia, and western Canada and U.S.A.; $\sigma_2 - \lambda_2$ is specially large over the east Asian region, mainly because, in general, σ_2 is rather above normal, and λ_2 is still more below normal, in this region; in the region of western Canada the excess of $\sigma_2 - \lambda_2$ above the average is smaller, and seems mainly due to rather large values of σ_2.

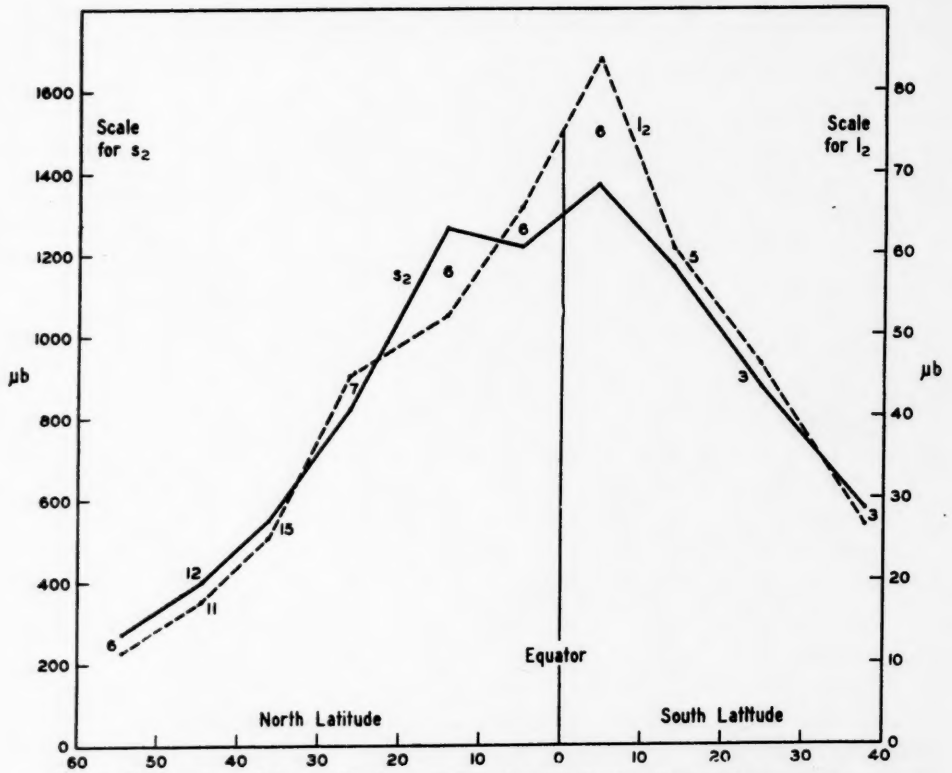

Fig. 8. Mean values of the amplitudes s_2 (full line) and l_2 (broken line) of the annual mean solar and lunar semidiurnal air-tides in barometric pressure, for 10-degree belts of latitude. The numbers against each point indicate from how many stations that point was determined.

Acknowledgements—In addition to the acknowledgements made in the Introduction, thanks are due to Mr. G. A. BULL, Librarian, and Mr. H. H. LAMB, Head of the World Climatology Branch, of the (British) Meteorological Office; Dr. A. A. GIESECKE, JUN., of the Geophysical Institute, Huancayo; Dr. S. K. PRAMANIK, lately of the Meteorological Office, India; Dr. T. SCHUMANN, Director of the S. African Meteorological Service; Dr. A. THOMSON, Director of the Canadian Meteorological Service; and Dr H. WEXLER, of the United States Weather Bureau, for some of the information embodied in Table 1; also to the staff of the Drawing Office and the Publications Section of the Radio Physics Laboratory, C.S.I.R.O., Sydney, for skilled help in the preparation of the tables in this paper, and, together with D. C. WILDER, of the Geophysical Institute, Alaska, in the preparation of the diagrams.

REFERENCES

BARTELS, J. 1927 *Veröff. Preuss. Met. Inst. Abh.* **8**, Nr. 9

BARTELS, J. 1939 *Gerl. Beitr. Geophys.* **54**, 56

BIGELOW, F. H. 1902 Barometry of the United States, Canada, and the West Indies, Report of Chief of Weather Bureau, 1900–1901, vol. 2, Washington, D.C.

VOL. 8 1956

CHAPMAN, S.	1918	*Quart. J. Roy. Met. Soc.* **44,** 271
CHAPMAN, S.	1919	*Quart. J. Roy. Met. Soc.* **45,** 113
CHAPMAN, S., and FALSHAW, E.	1922	*Quart. J. Roy. Met. Soc.* **48,** 246
CHAPMAN, S.	1924	*Quart. J. Roy. Met. Soc.* **50,** 99
BARTELS, J.	1939	*Gerl. Beitr. Geophys.* **54,** 56
CHAPMAN, S., and HARDMAN, M.	1928	*Mem. Roy. Met. Soc.* **2,** 153
CHAPMAN, S., and HARDMAN, M.	1931	*Quart. J. Roy. Met. Soc.* **57,** 163
CHAPMAN, S., and THOMSON, A.	1932	*Mem. Roy. Met. Soc.* **4,** 21
CHAPMAN, S.	1932	*Mem. Roy. Met. Soc.* **4,** 29
CHAPMAN, S., and AUSTIN, M.	1934	*Quart. J. Roy. Met. Soc.* **60,** 23
CHAPMAN, S.	1935a	*Quart. J. Roy. Met. Soc.* **61,** 189
CHAPMAN, S.	1935b	*Quart. J. Roy. Met. Soc.* **61,** 359
CHAPMAN, S.	1935c	*Proc. Roy. Soc.* **A151,** 105
CHAPMAN, S.	1936a	*Quart. J. Roy. Met. Soc.* **62,** 41
CHAPMAN, S.	1936b	*Proc. Roy. Soc. Edinburgh* **56,** 1
CHAPMAN, S., HARDMAN, M., and MILLER, J. C. P.	1936	*Quart. J. Roy. Met. Soc.* **62,** 540
CHAPMAN, S.	1937	*Quart. J. Roy. Met. Soc.* **63,** 457
CHAPMAN, S.	1938	*Quart. J. Roy. Met. Soc.* **64,** 523
CHAPMAN, S.	1939	Pres. Address Met. Assoc. (U.G.G.I.), Washington
CHAPMAN, S., and BARTELS, J.	1940, 1951	*Geomagnetism.* (Oxford, Clarendon Press)
CHAPMAN, S., and MILLER, J. C. P.	1940	*Monthly Not. Roy. Astron. Soc.* Geophys. Suppl. **4,** 649
CHAPMAN, S.	1948	Pres. Address Met. Assoc. (U.G.G.I.), Oslo
CHAPMAN, S., and TSCHU, K. K.	1948	*Proc. Roy. Soc.* **A195,** 310
CHAPMAN, S.	1951	*Compendium of Meteorology,* 510–530, Waverley Press Inc., Baltimore, Md.
CHAPMAN, S.	1952	*Austral. J. Sci. Res.* **A5,** 218
ELLIOT, C. M.	1852	*Phil. Trans.* **142,** 125
HANN, J. v. (H1)	1889	*Denkschr. Akad. Wiss. Wien,* Abt. I, **55,** 49
HANN, J. v. (H2)	1918a	*Denkschr. Akad. Wiss. Wien,* Abt. I, **95,** 1
HANN, J. v. (H3)	1918b	*Sitzungsber. Akad. Wiss. Wien,* Abt. IIA, **127,** 263
KERTZ, W.	1951	*Ann. Meteorol.,* 1951 Beiheft
LANDOLT-BÖRNSTEIN	1952	*Zahlenwerte und Funktionen aus Physik, Chemie, Astronomie, Geophysik und Technik,* III. (Springer, 6th ed.)
Met. Council, London	1891	Harmonic Analysis of hourly observations of Air Temperature and Pressure at the British Observatories
MORANO, F.	1899	*R.C. Accad. Naz. Lincei,* 8(*v*), 521
PRAMANIK, S. K.	1931	*Mem. Indian Meteorol. Dept.* **25,** 279
PRAMANIK, S. K., CHATTERJEE, S. C. and JOSHI, P. P.	1931	*Sci. Notes Meteorol. Dept. India* **4,** 1
PRAMANIK, S. K.	1951	*Indian J. Meteorol. Geophys.* **2,** 57
ROBB, R. A.; see CHAPMAN, S.	1936b	
SABINE, E.	1847	*Phil. Trans.* **137,** 45
SPAR, J.	1952	*Bull. Amer. Meteorol. Soc.* **33,** 438

Journal of Atmospheric and Terrestrial Physics, 1956, Vol. 8, pp. 24 to 38. Pergamon Press Ltd., London

Introductory theory for upper atmosphere wind and sonic velocity determination by sound propagation

G. V. GROVES
Department of Physics, University College, London

(*Received* 13 *June* 1955)

Abstract—The problem is considered of deriving the mean values of the horizontal wind velocity components $u(z)$, $v(z)$ and the velocity of sound $c(z)$, averaged with respect to height z along a sound-ray travelling between two known points in the atmosphere, from measurements of the time of travel of the ray between these points and the co-ordinates of the ray. It is shown that, for a ray which does not suffer total reflection, expressions can be derived for $\overline{u(z)}$, $\overline{v(z)}$, and $\overline{c(z)}$ in terms of the measured quantities, and the mean value of the vertical component of wind velocity $w(z)$, provided the variations in $u(z)$, $v(z)$, $w(z)$, and $c(z)$ with height are sufficiently small.

The theory is carried further by working out in detail the second order contributions to $\overline{u(z)}$, $\overline{v(z)}$, and $\overline{c(z)}$ which arise from the variations in $u(z)$, $v(z)$, $w(z)$, and $c(z)$. Using typical atmospheric data, the more important of these second-order terms are evaluated numerically for the case of a sound-ray received at an observation point on the ground from a source at any height up to 90 km. It is shown that the contributions from these terms to $\overline{u(z)}$, $\overline{v(z)}$, and $\overline{c(z)}$ are less than 0·8 m/sec when the ray lies near the vertical. For a ray which departs appreciably from the vertical (inclination about 45°), the contributions amount to a few metres per second, but are unlikely to exceed about 8 m/sec unless exceptionally large wind velocities are present.

VOL.
8
1956

1. INTRODUCTION

SOUND propagation has been used by several experimenters as a means of studying certain physical properties of the upper atmosphere. WHIPPLE (1931) carried out some of the first systematic observations on abnormal propagation of sound during 1929 and 1930 in England; and from these observations he was able to derive air temperatures in the region from 30- to 60-km altitude. It was realized at the time that these results did not always represent true air temperatures on account of possible wind contributions to the velocity of sound at these heights; and in more recent work attempts to overcome this difficulty have been made by determining the apparent velocity of sound in several different horizontal directions. In this way the contribution due to wind has been separated out and true air temperatures derived (CRARY, 1952; RICHARDSON and KENNEDY, 1952).

Information from abnormal propagation experiments is always limited to heights at which total reflection occurs, and these heights are usually found to be between 40 and 60 km. The use of sound propagation has nevertheless been extended to greater heights by transporting sound grenades in a high-altitude rocket to points above the reflecting layer, where they have been ejected from the rocket and exploded. This was first carried out at White Sands in 1950, using Aerobee rockets, and has been repeated several times since. From observations on the incidence of the resulting sound-waves at an observation point on the ground, wind velocities and air temperatures have been derived up to 80 km (WEISNER, 1954; BRASEFIELD, 1954).

In most sound propagation experiments, it is effectively the same set of quantities that is recorded in connection with the passage of sound from a particular source to

a particular observation point. If $Oxyz$ are reference axes with Oz vertical and Ox, Oy in the horizontal plane, the quantities measured are (Fig. 1)—

(i) the co-ordinates of the source (x_0, y_0, z_0);
(ii) the co-ordinates of the observation point (x_1, y_1, z_1);
(iii) the time interval (t_0, t_1) during which the sound travels between these two points;
(iv) the co-ordinates of the sound-ray received (a, b).*

Each experiment may yield several sets of such quantities, depending on the number of observation points and number of explosions employed. From this collection of data it is required to derive empirical formulae for the velocity of

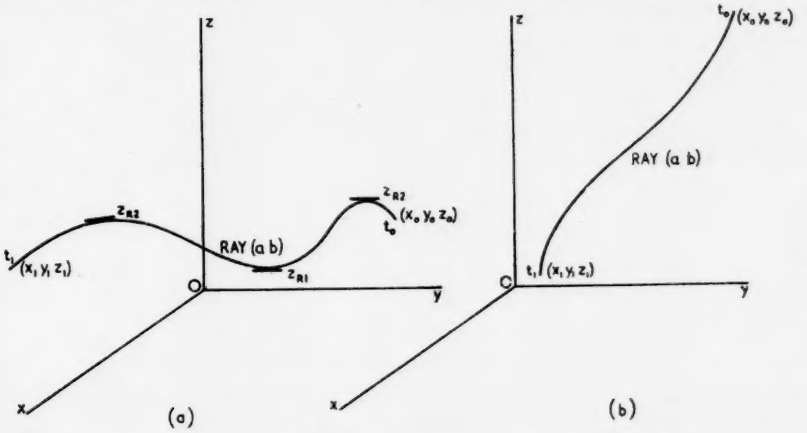

Fig. 1. Paths of (*a*) a totally reflected ray and (*b*) an unreflected ray in the atmosphere.

sound $c(z)$ and the horizontal wind velocity components $u(z)$, $v(z)$ over the interval of height z investigated. In the experiments referred to above, this rather difficult problem has been tackled in each case on certain broad assumptions which preclude the possibility of establishing a rigorous method of analysis. Theoretical errors are therefore introduced into the analysis which, although probably small, cannot be estimated; and this uncertainty reduces the significance that can be attached to the results derived.

The present paper has been undertaken as a first step towards obtaining a rigorous theoretical treatment for the analysis of data from sound propagation experiments. Attention will be confined to the case where the experimental data consists of just one set of the quantities (i) to (iv), i.e., $[(x_0, y_0, z_0), (x_1, y_1, z_1), (t_0, t_1), (a, b)]$. It would be expected that, from such a meagre set of data as this, the most that one could hope to derive would be the average values of $u(z)$, $v(z)$, and $c(z)$ in the interval (z_0, z_1), at least in the case of the rocket-grenade experiment. For the abnormal sound propagation experiment the sound-ray is totally reflected at some unknown height z_R, and it might be expected that the corresponding deductions could be made for the intervals (z_0, z_R) and (z_R, z_1), where z_0, z_1 are

* a and b are the velocities with which the incident sound-wave passes the observation point along two horizontal lines intersecting at this point and parallel to Ox and Oy respectivelv.

now ground-level heights. The problem of the totally reflected ray is however less straightforward, because z_R is not observable and needs to be derived in the analysis. This paper will therefore be confined primarily to the case of an unreflected sound-ray, and the theory developed is applicable to the rocket-grenade experiment. The solution is reached at equations (69) to (71). A treatment applicable to abnormal propagation experiments could probably be undertaken along similar lines.

2. SOUND-RAY EQUATIONS

It has been shown (GROVES, 1955) that the wavefront of a sound propagation in the atmosphere at time t_1 has the parametric equation

$$x_1 = x_0(a, b) + \int_{z_0(a,b)}^{z_1} \frac{u(z) + c(z)\lambda(a, b, z)}{w(z) + c(z)\nu(a, b, z)}\, dz \tag{1}$$

$$y_1 = y_0(a, b) + \int_{z_0(a,b)}^{z_1} \frac{v(z) + c(z)\mu(a, b, z)}{w(z) + c(z)\nu(a, b, z)}\, dz \tag{2}$$

$$t_1 = t_0 + \int_{z_0(a,b)}^{z_1} \frac{dz}{w(z) + c(z)\nu(a, b, z)}; \tag{3}$$

where

$$x_0 = x_0(a, b) \qquad y_0 = y_0(a, b) \qquad z_0 = z_0(a, b)$$

is the equation of the wavefront at time t_0, and $\lambda(a, b, z)$, $\mu(a, b, z)$, $\nu(a, b, z)$ are the direction cosines of the wavefront normal at the point of the ray (a, b) at height z. and satisfy

$$[c(z) + \lambda u(z) + \mu v(z) + \nu w(z)]/\lambda = a \tag{4}$$

$$[c(z) + \lambda u(z) + \mu v(z) + \nu w(z)]/\mu = b \tag{5}$$

$$\lambda^2 + \mu^2 + \nu^2 = 1. \tag{6}$$

$u(z)$, $v(z)$, $w(z)$ are the components of the wind velocity vector, and $c(z)$ is the velocity of sound at height z. The symbol $\int$, in the above equations, denotes integration along the ray (a, b): the range of integration is therefore divided whenever z reaches one of the two heights z_{R1}, z_{R2} at which total reflection of the ray (a, b) occurs. z_{R1}, z_{R2} have been shown to satisfy the relation

$$p^2(z) + w^2(z) - c^2(z) = 0, \tag{7}$$

where

$$p(z) = k[1 - u(z)/a - v(z)/b];$$

and $k(a, b)$ is the characteristic velocity of the ray (a, b) defined by

$$1/k^2 = 1/a^2 + 1/b^2. \tag{8}$$

For fixed values of a and b, equations (1) to (3) are the condition that the ray (a, b) passes through (x_0, y_0, z_0) at time t_0 and $(x_1, y_1, z_1,)$ at time t_1. If $w(z)$ is regarded as a known function, they express a relationship between the set of observed quantities $[(x_0, y_0, z_0), (x_1, y_1 z_1), (t_0, t_1), (a, b)]$ and the functions $u(z)$. $v(z)$, and $c(z)$. In general it is not possible to derive mean values of $u(z)$, $v(z)$, and $c(z)$ averaged over any height interval, and this leads to the considerations of the following section.

VOL.
8
1956

3. The Atmosphere as a Slightly Non-uniform Medium of Propagation

From the summary of atmospheric temperatures prepared by the Upper Atmosphere Rocket Research Panel (1952), Fig. 2 has been drawn to show the corresponding velocity of sound for heights between ground-level and 90 km. Below 30 km these results were taken from radiosonde balloon measurements at White Sands, and above this height are based on data obtained from various rocket experiments. If the velocity of sound is expressed as

$$c(z) = c_0 + c_\varepsilon(z). \tag{9}$$

then Fig. 2 shows that for heights up to at least 90 km it is reasonable to assume that

A.1 a value for c_0 can be chosen so that $c_\varepsilon(z)$ is small compared with c_0.

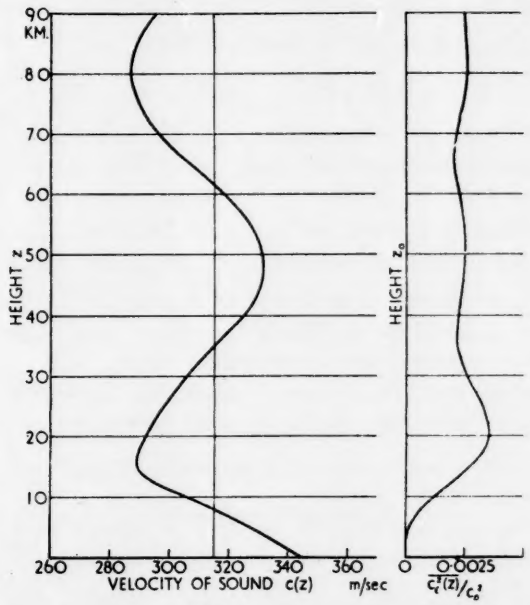

Fig. 2 Fig. 3

Fig. 2. Velocity of sound-versus-height relation based on Rocket Panel summary.
Fig. 3. Relative mean square deviation in velocity of sound $\overline{c_\varepsilon^2}/c_0^2$ between sea-level and height z_0.

The maximum value of $|c_\varepsilon(z)|/c_0$ will be taken to define the magnitude of the first order of smallness. If c_0 is taken to be 315 m/sec, Fig. 2 shows that $|c_\varepsilon(z)|/c_0$ is less than 0·1 for heights below 90 km.

Information on horizontal wind velocities in the upper atmosphere is at present rather fragmentary and not always very reliable. The data available indicates that above 30 km wind velocities may occur which are considerably in excess of those found at lower levels. Information in the 30- to 60-km region comes mainly from abnormal sound propagation experiments, and this work shows that winds are usually easterly in summer and somewhat stronger and westerly in winter. A maximum velocity is often reached at the 50- to 60-km level, and a typical

maximum value is 50 m/sec. In the region from 60 to 110 km, meteor trails have provided the chief source of information, and velocities are of the order of 50m/sec (WHIPPLE, 1954). The overall picture appears rather complicated, and appreciable variations in wind velocity can occur. Little information on vertical wind velocities is available; values derived from radio doppler measurements on meteor ionization trails have been found to be less than 10 m/sec. A summary of wind observations has been made by KELLOGG and SCHILLING (1951), and more recently by WHIPPLE (1954). Write

$$\begin{aligned} u(z) &= u_0 + u_e(z) \\ v(z) &= v_0 + v_e(z), \\ w(z) &= w_0 + w_e(z) \end{aligned} \tag{10}$$

then it seems justified to assume, in view of the foregoing remarks, that

A.2 values for u_0, v_0, and w_0 can be chosen so that

$$|u_e(z)|/c_0, \qquad |v_e(z)|/c_0 \qquad \text{and} \qquad |w_e(z)|/c_0$$

are quantities of the first order of smallness or less. Under assumptions A.1 and A.2, approximate forms of the sound-ray equations of Section 2 will now be derived.

4. APPROXIMATE SOLUTIONS FOR THE DIRECTION COSINES OF THE WAVEFRONT NORMAL ALONG A GIVEN RAY

Let u_0, v_0, w_0, and c_0 be chosen in accord with A.1 and A.2, and consider first a hypothetical uniform atmosphere in which the velocity of sound is everywhere c_0 and the wind velocity components everywhere (u_0, v_0, w_0). For a ray of given co-ordinates (a, b) in this medium, (4) to (6) show that the direction cosines of the wavefront normal have the values λ_0, μ_0, ν_0 at all points of the ray, where

$$c_0 + u_0\lambda_0 + v_0\mu_0 + w_0\nu_0 = a\lambda_0 = b\mu_0 \tag{11}$$

$$\lambda_0^2 + \mu_0^2 + \nu_0^2 = 1. \tag{12}$$

These equations can be solved to give the two sets of solutions

$$\lambda_{01}, \lambda_{02} = (k/a)[c_0p_0 \pm w_0(p_0^2 + w_0^2 - c_0^2)^{\frac{1}{2}}]/(p_0^2 + w_0^2) \tag{13}$$

$$\mu_{01}, \mu_{02} = (k/b)[c_0p_0 \pm w_0(p_0^2 + w_0^2 - c_0^2)^{\frac{1}{2}}]/(p_0^2 + w_0^2) \tag{14}$$

$$\nu_{01}, \nu_{02} = [-c_0w_0 \pm p_0(p_0^2 + w_0^2 - c_0^2)^{\frac{1}{2}}]/(p_0^2 + w_0^2), \tag{15}$$

Where

$$p_0 = k[1 - u_0/a - v_0/b]. \tag{16}$$

and the positive and negative signs are taken with the suffixes 1 and 2 respectively. Now by (1) to (3) the path of this ray is a straight line with direction ratios $u_0 + c_0\lambda_0 : v_0 + c_0\mu_0 : w_0 + c_0\nu_0$. Hence two directions for the ray are possible, corresponding to the two sets of values for λ_0, μ_0, and ν_0. It is easily shown, using (15), that $w_0 + c_0\nu_{01} > 0$ and $w_0 + c_0\nu_{02} < 0$ (provided $w_0 < c_0$. which is of course true in reality); and so λ_{01}, μ_{01}, ν_{01} correspond to an upwards-moving ray (a, b) and λ_{02}, μ_{02}, ν_{02} to a downwards-moving ray (a, b).

VOL. 8 1956

In the case of a non-uniform atmosphere, write for the ray (a, b) under consideration

$$\begin{aligned} \lambda(z) &= \lambda_0 + \lambda_\varepsilon(z) \\ \mu(z) &= \mu_0 + \mu_\varepsilon(z) \\ \nu(z) &= \nu_0 + \nu_\varepsilon(z) \end{aligned} \tag{17}$$

Then, if $u(z)$, $v(z)$, $w(z)$, and $c(z)$ are expressed by (9) and (10) and λ_0, μ_0, ν_0 are chosen to satisfy (11) and (12), it follows from (4) to (6) that $\lambda_\varepsilon(z), \mu_\varepsilon(z), \nu_\varepsilon(z)$ satisfy

$$(u_0 - a)\lambda_\varepsilon + v_0\mu_\varepsilon + w_0\nu_\varepsilon + q_\varepsilon = -(u_\varepsilon\lambda_\varepsilon + v_\varepsilon\mu_\varepsilon + w_\varepsilon\nu_\varepsilon) \tag{18}$$

$$u_0\lambda_\varepsilon + (v_0 - b)\mu_\varepsilon + w_0\nu_\varepsilon + q_\varepsilon = -(u_\varepsilon\lambda_\varepsilon + v_\varepsilon\mu_\varepsilon + w_\varepsilon\nu_\varepsilon) \tag{19}$$

$$\lambda_0\lambda_\varepsilon + \mu_0\mu_\varepsilon + \nu_0\nu_\varepsilon = -\tfrac{1}{2}(\lambda_\varepsilon^2 + \mu_\varepsilon^2 + \nu_\varepsilon^2), \tag{20}$$

where

$$q_\varepsilon = c_\varepsilon + \lambda_0 u_\varepsilon + \mu_0 v_\varepsilon + \nu_0 w_\varepsilon. \tag{21}$$

When assumptions A.1, A.2 are valid and u_0, v_0, w_0, and c_0 have been chosen accordingly, a solution of (18) to (20) can be sought on the assumption that λ_ε, μ_ε, ν_ε are first- or higher-order quantities. Neglecting the second-order terms on the right-hand sides of (18) to (20), the first-order solution for λ_ε, μ_ε, ν_ε is

$$\begin{aligned} a\lambda_\varepsilon = b\mu_\varepsilon &= \nu_0 q_\varepsilon/[p_0\nu_0/k + w_0(\lambda_0/a + \mu_0/b)] \\ \nu_\varepsilon &= -(\lambda_0/a + \mu_0/b)q_\varepsilon/[p_0\nu_0/k + w_0(\lambda_0/a + \mu_0/b)]. \end{aligned}$$

These equations represent two solutions for λ_ε, μ_ε, ν_ε corresponding to the two solutions for λ_0, μ_0, ν_0. By (13) to (15), it is found that

$$\lambda_{\varepsilon 1,2} = \pm(k/a)\nu_{01,2}\, q_\varepsilon/(p_0^2 + w_0^2 - c_0^2)^{\frac{1}{2}} \tag{22}$$

$$\mu_{\varepsilon 1,2} = \pm(k/b)\nu_{01,2}\, q_\varepsilon/(p_0^2 + w_0^2 - c_0^2)^{\frac{1}{2}} \tag{23}$$

$$\nu_{\varepsilon 1,2} = \mp k\,(\lambda_{01,2}/a + \mu_{01,2}/b)\, q_\varepsilon/(p_0^2 + w_0^2 - c_0^2)^{\frac{1}{2}}, \tag{24}$$

where upper signs correspond to suffix 1 and lower signs to suffix 2. These expressions are of the first or higher order of smallness provided $(p_0^2 + w_0^2 - c_0^2)^{\frac{1}{2}}/c_0$ is of order unity or greater. When this condition does not hold, the initial assumption that λ_ε, μ_ε, ν_ε are first- or higher-order quantities is not justified, and equations (22) to (24) are therefore no longer valid. The following modified treatment is then required.

Taking $(p_0^2 + w_0^2 - c_0^2)^{\frac{1}{2}}/c_0$ to be a quantity of the first or higher order of smallness, a solution of (18) to (20) can be sought on the assumption that λ_ε^2, μ_ε^2, ν_ε^2 are first-order quantities. Neglecting the terms on the right-hand sides of (18) and (19), the solution for λ_ε, μ_ε obtained from these equations is

$$a\lambda_\varepsilon = b\mu_\varepsilon = k(q_\varepsilon + w_0\nu_\varepsilon)/p_0.$$

Substituting these values into the right-hand sides of (18) and (19) and solving again, the solution for λ_ε, μ_ε correct to the second order becomes

$$a\lambda_\varepsilon = b\mu_\varepsilon = (k/p_0)\{(1 - p_\varepsilon/p_0)q_\varepsilon + [w_0(1 - p_\varepsilon/p_0) + w_\varepsilon]\nu_\varepsilon\}, \tag{25}$$

where

$$p_\varepsilon = -k(u_\varepsilon/a + v_\varepsilon/b). \tag{26}$$

Hence if second-order terms are neglected, it is found using (13), (14) that

$$\lambda_\varepsilon^2 + \mu_\varepsilon^2 = (2q_\varepsilon + w_0\nu_\varepsilon)w_0\nu_\varepsilon/p_0^2$$

$$\lambda_0\lambda_\varepsilon + \mu_0\mu_\varepsilon = \{c_0q_\varepsilon + [c_0w_0(1 - p_\varepsilon/p_0) + c_0w_\varepsilon \pm (w_0^2/p_0)(p_0^2 + w_0^2 - c_0^2)^{\frac{1}{2}}]\nu_\varepsilon\}/(p_0^2 + w_0^2).$$

Substituting these relations into (20) and using (15), the equation for ν_ε becomes

$$(p_0^2 + w_0^2)^2\nu_\varepsilon^2 + 2[c_0p_0(p_0w_\varepsilon - w_0p_\varepsilon) + w_0(p_0^2 + w_0^2)q_\varepsilon \pm p_0(p_0^2 + w_0^2)(p_0^2 + w_0^2 - c_0^2)^{\frac{1}{2}}]\nu_\varepsilon + 2c_0p_0^2q_\varepsilon = 0.$$

The solution for ν_ε correct to the first order of smallness is therefore

$$\nu_\varepsilon = \{-[c_0p_0(p_0w_\varepsilon - w_0p_\varepsilon) + w_0(p_0^2 + w_0^2)q_\varepsilon \pm p_0(p_0^2 + w_0^2)(p_0^2 + w_0^2 - c_0^2)^{\frac{1}{2}}] \pm [-2(p_0^2 + w_0^2)^2c_0p_0^2q_\varepsilon]^{\frac{1}{2}}\}/(p_0^2 + w_0^2)^2.$$

Now, using (13) to (15) and (26), q_ε is found from (21) correct to the first order to be

$$q_\varepsilon = (c_0c_\varepsilon - p_0p_\varepsilon - w_0w_\varepsilon)/c_0. \tag{27}$$

Hence

$$\nu_\varepsilon = -\{w_0c_\varepsilon + c_0[(p_0^2 - w_0^2)w_\varepsilon - 2p_0w_0p_\varepsilon]/(p_0^2 + w_0^2) \pm p_0(p_0^2 + w_0^2 - c_0^2)^{\frac{1}{2}} \mp p_0(-2c_0q_\varepsilon)^{\frac{1}{2}}\}/(p_0^2 + w_0^2).$$

Combining this with (15), it is found that $\nu(z)$ can be expressed correct to the first order as

$$\nu(z) = -c(z)w(z)/[p^2(z) + w^2(z)] \pm (p_0/c_0^2)[-2\,c_0q_\varepsilon(z)]^{\frac{1}{2}}.$$

The vertical component of velocity of the ray under consideration is then

$$dz/dt = w + c\nu = (-2c_0q_\varepsilon)^{\frac{1}{2}}[w_0(-2c_0q_\varepsilon)^{\frac{1}{2}} \pm p_0\,c_0]/c_0^2$$

to the first order. This means that the ray is confined to lie between two consecutive roots z_{R1}, z_{R2} of the equation

$$q_\varepsilon(z) = 0$$

i.e., by (27), of

$$c_0c_\varepsilon - p_0p_\varepsilon - w_0w_\varepsilon = 0.$$

This condition is seen to be the same as the general condition for total reflection (equation 7) taken correct to the first order, as would be expected.

The results of this section have shown that a given ray (a, b) will belong to one of two physically distinct classes according to whether the co-ordinates (a, b) are such that $(p_0^2 + w_0^2 - c_0^2)^{\frac{1}{2}}/c_0$ is either (i) of order unity or greater, or (ii) of the first order of smallness or less. In the first case the ray will remain unreflected in an atmosphere for which A.1 and A.2 are valid. In the second case, which applies to rays whose paths are more nearly horizontal, total reflection can occur successively at two height levels: z_{R1}, z_{R2}.

VOL. 8 1956

5. Solution for Average Wind and Sonic Velocities Along an Unreflected Sound-ray

It is now given that the ray (a, b) travels from the point (x_0, y_0, z_0) at time t_0 to the point (x_1, y_1, z_1) at time t_1 without being totally reflected in an atmosphere for which A.1 and A.2 are valid. A solution is first required for u_0, v_0, and c_0 in terms of the observed quantities on the assumption that $(p_0^2 + w_0^2 - c_0^2)^{\frac{1}{2}}/c_0$ is of order unity or greater. It is not possible to determine w_0 as well, because only three relations, namely equations (1) to (3), are determined by the ray. w_0 and w_ε will therefore be considered known. Write

$$\begin{aligned} X &= x_1 - x_0 \\ Y &= y_1 - y_0 \\ Z &= z_1 - z_0 \\ T &= t_1 - t_0 \end{aligned} \tag{28}$$

then in view of the identity

$$1/(w + cv) = 1/(w_0 + c_0\nu_0) - (w_\varepsilon + c_0\nu_\varepsilon + \nu_0 c_\varepsilon + \nu_\varepsilon c_\varepsilon)/(w + cv)(w_0 + c_0\nu_0), \tag{29}$$

equations (1) to (3) can be written as

$$X = \int_{z_0}^{z_1} \frac{u_0 + c_0\lambda_0}{w + cv}\,dz + \int_{z_0}^{z_1} \frac{(u_\varepsilon + c_0\lambda_\varepsilon + \lambda_0 c_\varepsilon + \lambda_\varepsilon c_\varepsilon)}{w_0 + c_0\nu_0}\,dz$$
$$- \int_{z_0}^{z_1} \frac{(u_\varepsilon + c_0\lambda_\varepsilon + \lambda_0 c_\varepsilon + \lambda_\varepsilon c_\varepsilon)(w_\varepsilon + c_0\nu_\varepsilon + \nu_0 c_\varepsilon + \nu_\varepsilon c_\varepsilon)}{(w + cv)(w_0 + c_0\nu_0)}\,dz \tag{30}$$

$$Y = \int_{z_0}^{z_1} \frac{v_0 + c_0\mu_0}{w + cv}\,dz + \int_{z_0}^{z_1} \frac{(v_\varepsilon + c_0\mu_\varepsilon + \mu_0 c_\varepsilon + \mu_\varepsilon c_\varepsilon)}{w_0 + c_0\nu_0}\,dz$$
$$- \int_{z_0}^{z_1} \frac{(v_\varepsilon + c_0\mu_\varepsilon + \mu_0 c_\varepsilon + \mu_\varepsilon c_\varepsilon)(w_\varepsilon + c_0\nu_\varepsilon + \nu_0 c_\varepsilon + \nu_\varepsilon c_\varepsilon)}{(w + cv)(w_0 + c_0\nu_0)}\,dz \tag{31}$$

$$T = \int_{z_0}^{z_1} \frac{dz}{w + cv} = \int_{z_0}^{z_1} \frac{dz}{w_0 + c_0\nu_0} - \int_{z_0}^{z_1} \frac{(w_\varepsilon + c_0\nu_\varepsilon + \nu_0 c_\varepsilon + \nu_\varepsilon c_\varepsilon)}{(w + cv)(w_0 + c_0\nu_0)}\,dz \tag{32}$$

and are exact. A solution for u_0, v_0, and c_0 is obtained by taking

$$u_0 + c_0\lambda_0 = X/T \tag{33}$$

$$v_0 + c_0\mu_0 = Y/T \tag{34}$$

$$w_0 + c_0\nu_0 = Z/T, \tag{35}$$

so that only first- and higher-order quantities remain in (30) to (32). Using (11) and (12), equations (33) to (35) give for λ_0, μ_0, ν_0

$$(X - aT)\lambda_0 + Y\mu_0 + Z\nu_0 = 0$$
$$X\lambda_0 + (Y - bT)\mu_0 + Z\nu_0 = 0.$$

Hence

$$a\lambda_0 = b\mu_0 = (Z/\tau)\nu_0, \tag{36}$$

where

$$\tau = T - X/a - Y/b. \tag{37}$$

By (8) and (12), the two solutions for λ_0, μ_0, ν_0 are then found to be

$$\lambda_{01}, \lambda_{02} = \pm(Z/a\tau)/[1 + (Z/k\tau)^2]^{\frac{1}{2}} \tag{38}$$

$$\mu_{01}, \mu_{02} = \pm(Z/b\tau)/[1 + (Z/k\tau)^2]^{\frac{1}{2}} \tag{39}$$

$$\nu_{01}, \nu_{02} = \pm 1/[1 + (Z/k\tau)^2]^{\frac{1}{2}}. \tag{40}$$

From (33) to (35), u_0, v_0, and c_0 are found to be

$$u_0 = [X - (Z - w_0T)Z/a\tau]/T \tag{41}$$

$$v_0 = [Y - (Z - w_0T)Z/b\tau]/T \tag{42}$$

$$c_0 = \pm[1 + (Z/k\tau)^2]^{\frac{1}{2}}(Z - w_0T)/T. \tag{43}$$

The positive sign is taken in (43) if the ray has an upwards path and the negative sign if the path is downward: in both cases a positive value is determined for c_0 since in reality $|w_0| < |Z|/T$. From (16), (41), and (42) it is found that

$$p_0 = [1 + (Z - w_0T)Z/k^2\tau^2]k\tau/T, \tag{44}$$

and hence by (43) that

$$(p_0^2 + w_0^2 - c_0^2)^{\frac{1}{2}}/c_0 = \pm k\tau/(Z - w_0T). \tag{45}$$

The evaluation will now be undertaken of $\overline{u_\varepsilon}$, $\overline{v_\varepsilon}$, $\overline{c_\varepsilon}$, where a bar denotes the average value of a function of z in the interval (z_0, z_1). The first- and second-order terms in (30) to (32) are related by

$$\begin{aligned}
(w_0 + c_0\nu_0)(\bar{u}_\varepsilon + c_0\bar{\lambda}_\varepsilon + \lambda_0\bar{c}_\varepsilon) &= \overline{(u_\varepsilon + c_0\lambda_\varepsilon + \lambda_0 c_\varepsilon)W_\varepsilon} - (w_0 + c_0\nu_0)\overline{\lambda_\varepsilon c_\varepsilon} \\
(w_0 + c_0\nu_0)(\bar{v}_\varepsilon + c_0\bar{\mu}_\varepsilon + \mu_0\bar{c}_\varepsilon) &= \overline{(v_\varepsilon + c_0\mu_\varepsilon + \mu_0 c_\varepsilon)W_\varepsilon} - (w_0 + c_0\nu_0)\overline{\mu_\varepsilon c_\varepsilon} \\
(w_0 + c_0\nu_0)(\bar{w}_\varepsilon + c_0\bar{\nu}_\varepsilon + \nu_0\bar{c}_\varepsilon) &= \overline{(w_\varepsilon + c_0\nu_\varepsilon + \nu_0 c_\varepsilon)W_\varepsilon} - (w_0 + c_0\nu_0)\overline{\nu_\varepsilon c_\varepsilon}.
\end{aligned} \tag{45a}$$

where

$$W_\varepsilon = w_\varepsilon + c_0\nu_\varepsilon + \nu_0 c_\varepsilon. \tag{46}$$

λ_ε, μ_ε, ν_ε can be eliminated from the left-hand side of these equations by linear addition according to (18) to (20). This gives

$$\begin{aligned}
(w_0+c_0\nu_0)[(u_0-a)\bar{u}_\varepsilon+v_0\bar{v}_\varepsilon+w_0\bar{w}_\varepsilon-c_0\bar{q}_\varepsilon-c_0\bar{c}_\varepsilon] &= \overline{[(u_0-a)u_\varepsilon+v_0v_\varepsilon+w_0w_\varepsilon-c_0q_\varepsilon-c_0c_\varepsilon]W_\varepsilon} \\
&+(w_0+c_0\nu_0)[\overline{q_\varepsilon c_\varepsilon}+c_0(\overline{u_\varepsilon\lambda_\varepsilon}+\overline{v_\varepsilon\mu_\varepsilon}+\overline{w_\varepsilon\nu_\varepsilon})]
\end{aligned} \tag{47}$$

$$\begin{aligned}
(w_0+c_0\nu_0)[u_0\bar{u}_\varepsilon+(v_0-b)\bar{v}_\varepsilon+w_0\bar{w}_\varepsilon-c_0\bar{q}_\varepsilon-c_0\bar{c}_\varepsilon] &= \overline{[u_0u_\varepsilon+(v_0-b)v_\varepsilon+w_0w_\varepsilon-c_0q_\varepsilon-c_0c_\varepsilon]W_\varepsilon} \\
&+(w_0+c_0\nu_0)[\overline{q_\varepsilon c_\varepsilon}+c_0(\overline{u_\varepsilon\lambda_\varepsilon}+\overline{v_\varepsilon\mu_\varepsilon}+\overline{w_\varepsilon\nu_\varepsilon})]
\end{aligned} \tag{48}$$

$$(w_0+c_0\nu_0)\bar{q}_\varepsilon=\overline{q_\varepsilon W_\varepsilon}+\tfrac{1}{2}c_0(w_0+c_0\nu_0)(\overline{\lambda_\varepsilon^2}+\overline{\mu_\varepsilon^2}+\overline{\nu_\varepsilon^2}). \tag{49}$$

VOL. 8 1956

Adding $2c_0$ times (49) to (47) and (48), it is seen by (21) that

$$(w_0 + c_0\nu_0)[(u_0 + c_0\lambda_0 - a)\bar{u}_\varepsilon + (v_0 + c_0\mu_0)\bar{v}_\varepsilon + (w_0 + c_0\nu_0)\bar{w}_\varepsilon]$$
$$= \overline{[(u_0+c_0\lambda_0 - a)u_\varepsilon + (v_0 + c_0\mu_0)v_\varepsilon + (w_0+c_0\nu_0)w_\varepsilon]W_\varepsilon} + (w_0 + c_0\nu_0)\overline{q_\varepsilon Q_\varepsilon}$$

$$(w_0 + c_0\nu_0)[(u_0 + c_0\lambda_0)\bar{u}_\varepsilon + (v_0 + c_0\mu_0 - b)\bar{v}_\varepsilon + (w_0 + c_0\nu_0)\bar{w}_\varepsilon]$$
$$= \overline{[(u_0 + c_0\lambda_0)u_\varepsilon + (v_0 + c_0\mu_0 - b)v_\varepsilon + (w_0 + c_0\nu_0)w_\varepsilon]W_\varepsilon} + (w_0 + c_0\nu_0)\overline{q_\varepsilon Q_\varepsilon},$$

where

$$q_\varepsilon Q_\varepsilon = q_\varepsilon c_\varepsilon + c_0\lambda_\varepsilon(u_\varepsilon + c_0\lambda_\varepsilon) + c_0\mu_\varepsilon(v_\varepsilon + c_0\mu_\varepsilon) + c_0\nu_\varepsilon(w_\varepsilon + c_0\nu_\varepsilon). \tag{50}$$

Using (33) to (35), the solution of these two equations for $\bar{u}_\varepsilon$, $\bar{v}_\varepsilon$ can be written

$$\bar{u}_\varepsilon = (Z/a\tau)\bar{w}_\varepsilon + (T/Z)[\overline{u_\varepsilon W_\varepsilon} - (Z/a\tau)(\overline{w_\varepsilon W_\varepsilon} + \overline{q_\varepsilon Q_\varepsilon})] \tag{51}$$

$$\bar{v}_\varepsilon = (Z/b\tau)\bar{w}_\varepsilon + (T/Z)[\overline{v_\varepsilon W_\varepsilon} - (Z/b\tau)(\overline{w_\varepsilon W_\varepsilon} + \overline{q_\varepsilon Q_\varepsilon})]. \tag{52}$$

The solution for $\bar{c}_\varepsilon$ then follows from (49), using (21) and (36)

$$\bar{c}_\varepsilon = -\nu_0[1 + (Z/k\tau)^2]\bar{w}_\varepsilon + (T/Z)[\overline{(c_\varepsilon + \nu_0 w_\varepsilon)W_\varepsilon} + \nu_0(Z/k\tau)^2(\overline{w_\varepsilon W_\varepsilon} + \overline{q_\varepsilon Q_\varepsilon})]$$
$$+ \tfrac{1}{2}c_0(\overline{\lambda_\varepsilon^2} + \overline{\mu_\varepsilon^2} + \overline{\nu_\varepsilon^2}). \tag{53}$$

Now by (38) to (40) and (45), equations (22) to (24) give

$$\left.\begin{aligned} c_0\lambda_\varepsilon &= \nu_0\kappa'\alpha q_\varepsilon \\ c_0\mu_\varepsilon &= \nu_0\kappa'\beta q_\varepsilon, \\ c_0\nu_\varepsilon &= -\nu_0\kappa'\kappa q_\varepsilon \end{aligned}\right\} \tag{54}$$

where

$$\left.\begin{aligned} \alpha &= k/a \\ \beta &= k/b \end{aligned}\right\} \tag{55}$$

$$\left.\begin{aligned} \kappa &= Z/k\tau \\ \kappa' &= \kappa - w_0 T/k\tau. \end{aligned}\right\} \tag{56}$$

Using these relations, (40) gives

$$\nu_0^2 = 1/(1 + \kappa^2); \tag{57}$$

and hence using (8) it is seen that

$$c_0^2(\lambda_\varepsilon^2 + \mu_\varepsilon^2 + \nu_\varepsilon^2) = \kappa'^2 q_\varepsilon^2. \tag{58}$$

Using (36), (21) becomes

$$q_\varepsilon = c_\varepsilon + \nu_0[\kappa(\alpha u_\varepsilon + \beta v_\varepsilon) + w_\varepsilon]: \tag{59}$$

(50) gives

$$Q_\varepsilon = c_\varepsilon + \nu_0\kappa'(\alpha u_\varepsilon + \beta v_\varepsilon - \kappa w_\varepsilon) + \kappa'^2 q_\varepsilon$$
$$= (1 + \kappa'^2)c_\varepsilon + \nu_0\kappa'(1 + \kappa\kappa')(\alpha u_\varepsilon + \beta v_\varepsilon) + \nu_0\kappa'(\kappa' - \kappa)w_\varepsilon \tag{60}$$

by (59); and (46) becomes

$$W_\varepsilon = w_\varepsilon + v_0 c_\varepsilon - v_0\kappa'\kappa q_\varepsilon$$
$$= v_0(1 - \kappa\kappa')c_\varepsilon - v_0^2\kappa'\kappa^2(\alpha u_\varepsilon + \beta v_\varepsilon) + (1 - v_0^2\kappa'\kappa)w_\varepsilon \tag{61}$$

by (59). Substituting (59) to (61) into (51) to (53), it is seen that $\bar{u}_\varepsilon$, $\bar{v}_\varepsilon$, and $\bar{c}$ can be expressed as

$$\bar{u}_\varepsilon = (Z/a\tau)\bar{w}_\varepsilon + c_0\varepsilon_u \tag{62}$$

$$\bar{v}_\varepsilon = (Z/b\tau)\bar{w}_\varepsilon + c_0\varepsilon_v \tag{63}$$

$$\bar{c}_\varepsilon = \mp[1 + (Z/k\tau)^2]^{\frac{1}{2}}\bar{w}_\varepsilon + c_0\varepsilon_c, \tag{64}$$

where ε_u, ε_v, ε_c are second-order quantities of the form

$$\varepsilon_\theta = \sum_{i\le j=1,2,3,4} \theta_{ij}\,\overline{\psi_i\psi_j} \qquad (\theta = u, v, \text{ or } c), \tag{65}$$

where ψ_1, ψ_2, ψ_3 denote u_ε/c_0, v_ε/c_0, c_ε/c_0 respectively, and ψ_4 is taken as $+w_\varepsilon/c_0$ for an upward-moving ray (i.e., $Z > 0$) and $-w_\varepsilon/c_0$ for a downward-moving ray (i.e., $Z < 0$). It is found that the dimensionless factors u_{ij}, v_{ij}, c_{ij} have the following expressions for both upward- and downward-moving rays:

$$\left.\begin{aligned}
u_{11} &= -\alpha[1 + \alpha^2(1 + \kappa'\kappa)]\kappa'^2|\kappa|/(1 + \kappa^2)^{\frac{1}{2}}\\
u_{12} &= -\beta[1 + 2\alpha^2(1 + \kappa'\kappa)]\kappa'^2|\kappa|/(1 + \kappa^2)^{\frac{1}{2}}\\
u_{13} &= [(1 - \kappa'\kappa) - \alpha^2\kappa(\kappa' + 2\kappa'^2\kappa + \kappa)]\kappa'/\kappa\\
u_{14} &= \{1 - \kappa(\kappa' - \kappa) - \alpha^2\kappa'\kappa[1 + 2\kappa(\kappa' - \kappa)]\}\kappa'/\kappa(1 + \kappa^2)^{\frac{1}{2}}\\
u_{22} &= -\alpha\beta^2(1 + \kappa'\kappa)\kappa'^2|\kappa|/(1 + \kappa^2)^{\frac{1}{2}}\\
u_{23} &= -\alpha\beta\kappa'(\kappa' + 2\kappa'^2\kappa + \kappa)\\
u_{24} &= -\alpha\beta[1 + 2\kappa(\kappa' - \kappa)]\kappa'^2/(1 + \kappa^2)^{\frac{1}{2}}\\
u_{33} &= -\alpha(1 + \kappa'^2)(1 + \kappa^2)^{\frac{1}{2}}|\kappa'|\\
u_{34} &= -2\alpha[1 + \kappa'(\kappa' - \kappa)]|\kappa'|\\
u_{44} &= -\alpha[1 + (\kappa' - \kappa)^2]|\kappa'|/(1 + \kappa^2)^{\frac{1}{2}}
\end{aligned}\right\} \tag{66}$$

$$\left.\begin{aligned}
v_{11} &= -\alpha^2\beta(1 + \kappa'\kappa)\kappa'^2|\kappa|/(1 + \kappa^2)^{\frac{1}{2}}\\
v_{12} &= -\alpha[1 + 2\beta^2(1 + \kappa'\kappa)]\kappa'^2|\kappa|/(1 + \kappa^2)^{\frac{1}{2}}\\
v_{13} &= -\alpha\beta\kappa'(\kappa' + 2\kappa'^2\kappa + \kappa)\\
v_{14} &= -\alpha\beta[1 + 2\kappa(\kappa' - \kappa)]\kappa'^2/(1 + \kappa^2)^{\frac{1}{2}}\\
v_{22} &= -\beta[1 + \beta^2(1 + \kappa'\kappa)]\kappa'^2|\kappa|/(1 + \kappa^2)^{\frac{1}{2}}\\
v_{23} &= [(1 - \kappa'\kappa) - \beta^2\kappa(\kappa' + 2\kappa'^2\kappa + \kappa)]\kappa'/\kappa\\
v_{24} &= \{1 - \kappa(\kappa' - \kappa) - \beta^2\kappa'\kappa[1 + 2\kappa(\kappa' - \kappa)]\}\kappa'/\kappa(1 + \kappa^2)^{\frac{1}{2}}\\
v_{33} &= -\beta(1 + \kappa'^2)(1 + \kappa^2)^{\frac{1}{2}}|\kappa'|\\
v_{34} &= -2\beta[1 + \kappa'(\kappa' - \kappa)]|\kappa'|\\
v_{44} &= -\beta[1 + (\kappa' - \kappa)^2]|\kappa'|/(1 + \kappa^2)^{\frac{1}{2}}
\end{aligned}\right\} \tag{67}$$

VOL. 8 1956

$$
\left.\begin{aligned}
c_{11} &= \alpha^2(3 + 2\kappa'\kappa)\kappa'^2\kappa^2/2(1 + \kappa^2)\\
c_{12} &= \alpha\beta(3 + 2\kappa'\kappa)\kappa'^2\kappa^2/(1 + \kappa^2)\\
c_{13} &= \alpha[\kappa'\kappa(1 + 2\kappa'^2) + \kappa'^2]|\kappa|/(1 + \kappa^2)^{\frac{1}{2}}\\
c_{14} &= \alpha[1 + 2\kappa(\kappa' - \kappa)]\kappa'^2|\kappa|/(1 + \kappa^2)\\
c_{22} &= \beta^2(3 + 2\kappa'\kappa)\kappa'^2\kappa^2/2(1 + \kappa^2)\\
c_{23} &= \beta[\kappa'\kappa(1 + 2\kappa'^2) + \kappa'^2]|\kappa|/(1 + \kappa^2)^{\frac{1}{2}}\\
c_{24} &= \beta[1 + 2\kappa(\kappa' - k)]\kappa'^2|\kappa|/(1 + \kappa^2)\\
c_{33} &= [2 + \kappa^2(1 + 2\kappa'^2) - \kappa(\kappa' - \kappa)^2]\kappa'/2\kappa\\
c_{34} &= [2(1 + \kappa^2) - \kappa(1 - 2\kappa'\kappa)(\kappa' - \kappa)]\kappa'/\kappa(1 + \kappa^2)^{\frac{1}{2}}\\
c_{44} &= \{2(1 + \kappa^2)^2 + \kappa'\kappa[2\kappa(\kappa' - \kappa) - (1 + 2\kappa^2)]\}\kappa'/2\kappa(1 + \kappa^2)
\end{aligned}\right\} \qquad (68)
$$

Finally, the average values of $u(z)$, $v(z)$, and $c(z)$ over the interval (z_0, z_1) are readily obtained correct to the second order. From (9), (10), (41) to (43), and (62) to (64) it is seen that

$$\overline{u(z)} = \{X - [Z - \overline{w(z)}\ T]Z/a\tau\}/T + c_0\,\varepsilon_u \qquad (69)$$

$$\overline{v(z)} = \{Y - [Z - \overline{w(z)}\ T]Z/b\tau\}/T + c_0\,\varepsilon_v \qquad (70)$$

$$\overline{c(z)} = \pm[1 + (Z/k\tau)^2]^{\frac{1}{2}}[Z - \overline{w(z)}\ T]/T + c_0\,\varepsilon_c \qquad (71)$$

6. Estimation of Accuracy of Solutions for $\overline{u(z)}$, $\overline{v(z)}$, and $\overline{c(z)}$.

The second order terms ε_u, ε_v, ε_c in the solution for $\overline{u(z)}$, $\overline{v(z)}$, $\overline{c(z)}$ will now be evaluated numerically for certain typical atmospheric and experimental data. In this way an estimate can be made of the accuracy to be expected from these solutions.

The terms $\overline{\psi_i\psi_j}$ will be investigated first; and of these, typical values of $\overline{c_\varepsilon^2}/c_0^2$ can be derived from the velocity of sound versus height relation shown in Fig. 2. From this graph $\bar{c}$ and $\overline{c^2}$ can be readily calculated, and then, since $c_0 = \bar{c}$ to the first order, $\overline{c_\varepsilon^2}/c_0^2$ can be calculated to the second order from

$$\overline{c_\varepsilon^2}/c_0^2 = \overline{(c - \bar{c})^2}/\bar{c}^2 = (\overline{c^2}/\bar{c}^2) - 1.$$

This has been done for a case of practical interest by taking $z_1 = 0$, i.e., the observation point at sea-level, and the height of the source z_0 between 0 and 90 km. Fig. 3 shows $\overline{c_\varepsilon^2}/c_0^2$, and it is seen that this quantity remains remarkably constant for z_0 between 30 and 90 km, not departing by more than 15 per cent from the value 0·0025. For the horizontal wind velocity structure, the hypothetical curve shown in Fig. 4 has been taken as representative of a possible situation.* With Fig. 4 as the Ox-component of wind velocity, $\overline{u_\varepsilon^2}/c_0^2$ has been calculated from

* The most significant feature of this curve as far as it affects the deductions of this section is that the change in wind-speed is 50 m/sec; the choice of 30 and 60 km for the levels between which the change takes place is less important.

the relation $\overline{u_\varepsilon^2}/c_0^2 = (\overline{u^2} - \bar{u}^2)/\bar{c}^2$ for $z_1 = 0$ and z_0 from 0 to 90 km, and is plotted in Fig.5: the greatest value reached by $\overline{u_\varepsilon^2}/c_0^2$ is 0·005 at 90 km. In a similar way $\overline{u_\varepsilon c_\varepsilon}/c_0^2$ has been calculated from Figs. 2 and 4, and is shown in Fig. 6. No reasonable estimate can be made of the terms $\overline{\psi_i \psi_j}$ which contain the variation w_ε in the vertical wind-velocity component; but these would however, be expected to be appreciably smaller than those just considered and will be neglected in the following discussion.

When the ray under consideration has co-ordinates $a = b = \infty$, $\varepsilon_u, \varepsilon_v, \varepsilon_c$ reduce to particularly simple expressions. For this ray, equations (4) and (5) show that

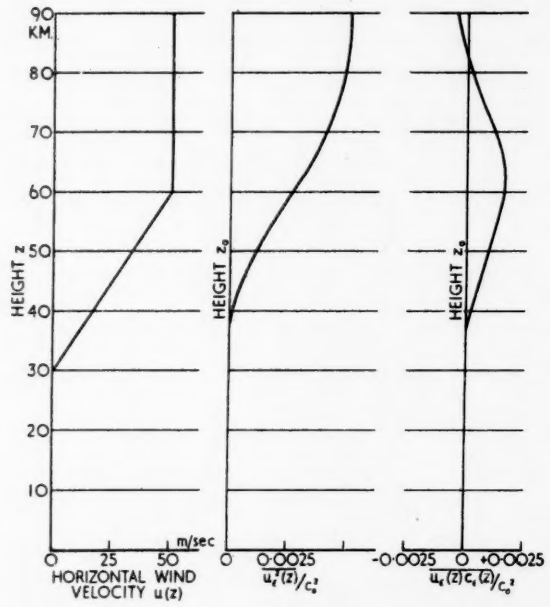

Fig. 4 Fig. 5 Fig. 6

Fig. 4. Hypothetical horizontal wind velocity-versus-height relation.

Fig. 5. Relative mean square deviation in horizontal wind velocity $\overline{u_\varepsilon^2}/c_0^2$ between sea-level and height z_0.

Fig. 6. Relative mean product deviation $\overline{u_\varepsilon c_\varepsilon}/c_0^2$ between sea-level and height z_0.

$\lambda = \mu \equiv 0$, i.e., the wavefront normal is vertical. The ray is typical of one that might be received in the rocket-grenade experiment when the point of explosion of a grenade lies near the vertical through the observation point. Now in this case, $\kappa = \kappa' = 0$ by (8) and (56), and hence all coefficients u_{ij}, v_{ij}, c_{ij} $(i \leqslant j = 1, 2, 3)$ are seen to be zero except u_{13}, v_{23}, and c_{33}, which have the value κ'/κ, i.e., $(Z - w_0 T)/Z$. Taking $w_0 = 0$, u_{13}, v_{23}, and c_{33} are then unity, and hence

$$\varepsilon_u = \overline{u_\varepsilon c_\varepsilon}/c_0^2$$

$$\varepsilon_v = \overline{v_\varepsilon c_\varepsilon}/c_0^2$$

$$\varepsilon_c = \overline{c_\varepsilon^2}/c_0^2.$$

VOL. 8 1956

The fact that ε_u, ε_v do not depend on $\overline{u_\varepsilon^2}/c_0^2$, $\overline{v_\varepsilon^2}/c_0^2$ might seem surprising at first until it is remembered that the wavefront is horizontal along the ray under consideration, and consequently no refraction arises directly from wind gradients. For the atmospheric data of Figs. 2 and 4, ε_c is the function of Fig. 3 and ε_u of Fig. 6; ε_v is zero. It is therefore possible to draw some fairly general conclusions about the effect of neglecting second-order terms in equations (69) to (71). $\overline{c(z)}$ will be underestimated by an amount $c_0(\overline{c_\varepsilon^2}/c_0^2)$, and for heights of the source between 30 and 90 km this will have a value lying within about 15 per cent of 0·8 m/sec. Second-order contributions to $\overline{u(z)}$ and $\overline{v(z)}$ are $c_0(\overline{u_\varepsilon c_\varepsilon}/c_0^2)$ and $c_0(\overline{v_\varepsilon c_\varepsilon}/c_0^2)$, and these quantities can have positive and negative values on account of the oscillatory nature of c_ε: on the data of Fig. 6, $\overline{u(z)}$ would be underestimated by at most about 0·5 m/sec.

As a second example, a ray is considered which departs appreciably from the vertical, but not so much that total reflection occurs. The condition for a ray to be unreflected is that $(p_0^2 + w_0^2 - c_0^2)^{\frac{1}{2}}/c_0$ should not be less than order unity, i.e., by (45) and (56), that $|\kappa'|$ is order unity or less. An extreme ray will therefore be considered such that $|\kappa'| = 1$, and it will be supposed that w_0 has been chosen to be zero, so that $\kappa = \kappa'$.* (66) to (68) then reduce to simple expressions in α and β, and have the following extreme values with respect to α, β, since $|\alpha|$, $|\beta| \leqslant 1$:

$\lvert u_{11}\rvert = 2{\cdot}12$	$\lvert v_{11}\rvert = 0{\cdot}54$	$\lvert c_{11}\rvert = 1{\cdot}25$
$\lvert u_{12}\rvert = 1{\cdot}52$	$\lvert v_{12}\rvert = 1{\cdot}52$	$\lvert c_{12}\rvert = 1{\cdot}25$
$\lvert u_{13}\rvert = 4{\cdot}00$	$\lvert v_{13}\rvert = 2{\cdot}00$	$\lvert c_{13}\rvert = 2{\cdot}83$
$\lvert u_{22}\rvert = 0{\cdot}54$	$\lvert v_{22}\rvert = 2{\cdot}12$	$\lvert c_{22}\rvert = 1{\cdot}25$
$\lvert u_{23}\rvert = 2{\cdot}00$	$\lvert v_{23}\rvert = 4{\cdot}00$	$\lvert c_{23}\rvert = 2{\cdot}83$
$\lvert u_{33}\rvert = 2{\cdot}83$	$\lvert v_{33}\rvert = 2{\cdot}83$	$\lvert c_{33}\rvert = 2{\cdot}50.$

All mean square deviations $\overline{u_\varepsilon^2}/c_0^2$, $\overline{v_\varepsilon^2}/c_0^2$, and $\overline{c_\varepsilon^2}/c_0^2$ will now contribute to each of ε_u, ε_v, and ε_c. Using the data of Figs. 3 and 5, the maximum contributions from $c_0(\overline{u_\varepsilon^2}/c_0^2)$ and $c_0(\overline{c_\varepsilon^2}/c_0^2)$ to $c_0\varepsilon_u$ are 3·2 m/sec and 2·3 m/sec; to $c_0\varepsilon_v$ are 0·8 m/sec and 2·3 m/sec; and to $c_0\varepsilon_c$ are 1·9 m/sec and 2·0 m/sec. Second-order contributions can therefore amount to the order of a few metres per second. The total contribution appears unlikely to exceed about 8 m/sec for altitudes below 90 km, unless the maximum wind velocities are much larger than the nominal figure of 50 m/sec used in these calculations.

7. Conclusions

A theory applicable to the rocket-grenade experiment has been developed, which enables mean values of the horizontal wind velocity and velocity of sound to be deduced from observations on a single grenade explosion. Extension of the theory to the case of a number of grenades should now be straightforward, and will be dealt with in a later paper.

* When $|\kappa| = 1$, equation (57) gives $\nu_0^2 = \frac{1}{2}$, so that the wavefront normal is at about 45° elevation along the ray under consideration..

In the solution for the average horizontal wind velocity and velocity of sound (equations (69) to (71)), second-order contributions arising from the variations in the velocity of sound and wind-velocity field have been derived and, under certain typical conditions, are shown to amount to less than 0·8 m/sec for a nearly vertical sound-ray and less than 8 m/sec for a ray departing appreciably from the vertical (inclination about 45°). Account can be taken of these terms in the analysis of the data of the rocket-grenade experiment without much extra labour, provided the velocity of sound and wind-velocity field are known between ground-level and the point of explosion of the grenade with first-order accuracy. If meteorological information is available for the lower altitudes, this could be done using the results of the first-order analysis of the experimental data: the errors in the solution would then be reduced to the third order of magnitude of smallness. In practice, it would only be worthwile evaluating the solution to this higher order of accuracy if the experimental errors were sufficiently small to justify it.

REFERENCES

BRASEFIELD, C. J.	1954	*J. Geophys. Res.* **59,** 233
CRARY, A. P.	1952	*J. Met.* **9,** 93
GROVES, G. V.	1955	*J. Atmosph. Terr. Phys.* (to be published)
KELLOGG, W. W., and SCHILLING, G. F.	1951	*J. Met.* **8,** 222
RICHARDSON, J. M., and KENNEDY, W. B.	1952	*J. Acoust. Soc. Amer.* **24,** 731
Rocket Panel	1952	*Phys. Rev.* **88,** 1027
WEISNER, A. G.	1954	*Rocket exploration of the upper atmosphere,* Pergamon Press, 133.
WHIPPLE, F. J. W.	1931	*Quart. J. R. Met. Soc.* **57,** 331
WHIPPLE, F. L.	1954	*Proc. Nat. Acad. Sci. U.S.A.,* **10,** 966

Journal of Atmospheric and Terrestrial Physics, 1956, Vol. 8, pp. 39 to 42. Pergamon Press Ltd., London

The influence of the geomagnetic field on turbulence in the ionosphere

J. W. DUNGEY
Cavendish Laboratory, Cambridge

(*Received* 11 *May* 1955)

ABSTRACT

If turbulent motion of the neutral particles occurs in the ionosphere, it may be influenced by the geomagnetic field. It is shown that electromagnetic damping is negligible for the smaller eddies. In the higher regions the electrons are constrained to move nearly parallel to the magnetic field, and this results in variations of electron density, even when the density of neutral molecules does not vary. These variations are probably appreciable above 100 km.

THE suggestion (VILLARS and WEISSKOPF, 1954; MAXWELL, 1954) that some of the irregularities in the ionosphere may be caused by turbulence, raises the question whether the geomagnetic field would have any important effect on turbulent motion there. The magnetic field can have a direct influence only on charged particles, so that its influence on the motion of the neutral molecules can only be felt through collisions with charged particles; of these, collisions with heavy ions are much more important than collisions with electrons. The collision frequency of neutral molecules with heavy ions is believed to be roughly independent of temperature and to have a value of about $10^{-9}\,n$ sec^{-1} (COWLING, 1945), where n is the number density of heavy ions. In the ionosphere n is never many times 10^6 cm^{-3}, so that collisions with charged particles will be unimportant for irregular motions with time scale much less than 10^3 secs; if the velocity $\sim$100 m/sec, this corresponds to an eddy size of 100 km. It follows that the influence of the geomagnetic field on the motion of the neutral constituent is negligible for the small eddies.

The motion of the charged particles is driven by that of the neutral particles, which are much more numerous, but is also affected by the magnetic field in a way which is now discussed.

The effect of the magnetic field may be seen qualitatively as follows. It obstructs any motion of charged particles in directions perpendicular to $\boldsymbol{H}$, and, if we consider the extreme cases in which the field is very strong, the motion of the charged particles is constrained to be parallel to $\boldsymbol{H}$. The neutral particles tend to carry the charged particles with them, so that the component parallel to $\boldsymbol{H}$ of the velocity of the charged particles is the same as that of the neutral particles. Since it is variations in the electron density that are observed, the important result is that large variations in the density of the charged particles can result from a motion in which the density of neutral particles varies very little. An illustration is shown in the figure, in which the sloping lines indicate the direction of the magnetic field; the horizontal arrows represent the velocity of the neutral molecules, and their components parallel to the field represent the velocity of the charged particles. The motion does not alter the density of neutral particles, but the charged particles are being strongly compressed. This effect will now be discussed quantitatively.

The motion of the charged particles is determined by the equation

$$\frac{\partial \boldsymbol{u}}{\partial t} + (\boldsymbol{u} \cdot \nabla)\boldsymbol{u} = -\nu(\boldsymbol{u} - \boldsymbol{V}) + \frac{e}{m}(\boldsymbol{E} + \boldsymbol{u} \wedge \boldsymbol{H}/c) - \nabla p/nm, \tag{1}$$

which refers to one ionic constituent, but is formally the same for each ionic constituent: $\boldsymbol{u}$ and $\boldsymbol{V}$ are the mean velocities of the ionic constituent and the neutral particles respectively, ν the frequency for the ions of collisions with neutral

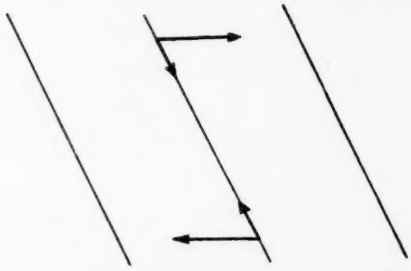

Fig. 1. The sloping lines indicate the direction of $\boldsymbol{H}$, the horizontal arrows represent the velocity of the neutral particles. When the collision frequency is small, the velocity of the charged particles is shown by the sloping arrows.

molecules, and p is the partial pressure of the ions. The quantity eH/mc is the gyrofrequency Ω of the ions in the magnetic field, and at middle latitudes is about $7 \cdot 10^6$ sec^{-1} for electrons and 140 sec^{-1} for N_2^+ ions. It follows that the terms on the left-hand side of (1) are negligible compared with the magnetic term. For heavy ions, comparison of the pressure term with νV gives

$$\frac{|\nabla p|}{nm\nu V} \sim \frac{\delta n}{n} \frac{C^2}{L\nu V}$$

where L is a characteristic length and C is the thermal velocity for the ions. For heavy ions C and ν have the same orders of magnitude as the thermal velocity of the neutral molecules and the collision frequency for neutral molecules colliding with each other. Then $C^2/\nu \sim$ the kinematic viscosity of the neutral molecules, and

$$\frac{|\nabla p|}{nm\nu V} \sim \frac{\delta n}{n} R^{-1}$$

where R is the Reynold's number corresponding to the values L and V. In turbulence $R \gg 1$, and hence the pressure term is small. The electron-pressure term will also be omitted, and discussed later. If (1) is then solved for $\boldsymbol{u}$, the result takes the form

$$u_i - V_i = \frac{e}{m} T_{ij}(E_j + (\boldsymbol{V} \wedge \boldsymbol{H})_j/c) \tag{2}$$

and, taking H in the z-direction,

$$T_{ij} = (\nu^2 + \Omega^2)^{-1} \begin{pmatrix} \nu & \Omega & 0 \\ -\Omega & \nu & 0 \\ 0 & 0 & (\nu^2 + \Omega^2)/\nu \end{pmatrix}$$

VOL. 8 1956

Consider now a model with electrons and only one kind of positive ion, so that there are just two equations (2); quantities referring to electrons and positive ions will be denoted by suffixes e and p. It will be verified later that the densities of electrons and positive ions are very nearly the same; both will be denoted by n with no suffix. It is assumed at first that ν_p is substantially larger than Ω_p, and then, since $m_p\nu_p \gg m_e\nu_e$, the current density is approximately $ne(\boldsymbol{V} - \boldsymbol{u}_e)$. It is now necessary to use MAXWELL'S equations, and for the purpose of estimating orders of magnitude we consider a Fourier component of the disturbance having wave number $\boldsymbol{k}$ and angular frequency ω, with values characteristic of the turbulence. MAXWELL'S equations then give

$$c^2\boldsymbol{k} \wedge \boldsymbol{k} \wedge \boldsymbol{E} + \omega^2\boldsymbol{E} = 4\pi i\omega\boldsymbol{j} \tag{3}$$

Since $\omega/k \sim$ the turbulent velocity, $\omega \ll kc$, and the second term on the left-hand side is small. Next the term $c^2\boldsymbol{k} \wedge \boldsymbol{k} \wedge \boldsymbol{E}$ must be compared with $4\pi\omega ne^2\, m_e^{-1}T'_{ij}E_j$, where T'_{ij} is the tensor determining $\boldsymbol{j}$, but is nearly the same as T_{ij} for electrons. Now $(m_ec^2/ne^2)^{\frac{1}{2}}$ is the plasma wavelength and is $2 \cdot 10^6\, n^{-\frac{1}{2}}$ cm, which is never much less than 20 m. Then, when $T'_{ij} < \Omega_e^{-1}$, we have $wT'_{ij} < 10^{-7}$, and for eddy sizes up to several kilometres

$$c^2k^2 \gg 4\pi\omega ne^2m_e^{-1}T'_{ij}$$

and consequently, from (3)

$$|\boldsymbol{k} \wedge \boldsymbol{k} \wedge \boldsymbol{E}| \ll k^2\,|\boldsymbol{V} \wedge \boldsymbol{H}|\,/c \tag{4}$$

It may be noted that the disturbance in the magnetic field is $-\omega^{-1}c\boldsymbol{k} \wedge \boldsymbol{E}$, which, since $kV \sim \omega$, is much less than H.

When equation (3) for the component parallel to $\boldsymbol{k}$ is considered, ω must be compared with $4\pi ne^2m_e^{-1}T'_{ij}$. The smallest value of T'_{ij} is given by ν_e^{-1} at the lowest height of interest. At 90 km, ν_e is about 10^6 sec^{-1} (NICOLET, 1953), and then $4\pi ne^2m_e^{-1}T'_{ij} \sim 3{,}000\, n$ sec^{-1}, which is very much larger than ω. It then follows that

$$k_iT'_{ij}E_j \approx -k_iT'_{ij}\,(\boldsymbol{V} \wedge \boldsymbol{H})_j/c \tag{5}$$

Put in words, (4) and (5) mean that $\boldsymbol{E}$ is nearly parallel to $\boldsymbol{k}$, and its component in the direction $k_iT'_{ij}$ nearly cancels the component of $\boldsymbol{V} \wedge \boldsymbol{H}/c$ in that direction. The result (4) implies that $\boldsymbol{E}$ is approximately a potential field, and $\boldsymbol{E}$ is then determined approximately by (5). It follows that $|\boldsymbol{E}|$ is generally of the same order of magnitude as $|\boldsymbol{V} \wedge \boldsymbol{H}|/c$. We may now verify that the number densities of electrons and positive ions are nearly the same, for

$$\frac{n_p - n_e}{n} \sim \frac{\text{div } \boldsymbol{E}}{4\pi ne} \sim \frac{VH}{4\pi Lcne} \sim (150\,\pi nt)^{-1}$$

where n is in cm^{-3}, and t is the characteristic time of the turbulence in seconds. We may also now investigate the importance of the pressure gradient term in equation (1) for electrons, by comparing it with eVH/m_ec. Putting $T = 300°$K and $V = 100$ m/s, the ratio $\delta nckT/neHVL$ is $\sim 500\,\delta n/nL$, where L is in cm; the pressure gradient is therefore unimportant.

We now return to the problem of determining the variation of the electron density. We need not here consider a Fourier component, but assume that the

results $n_p \approx n_e$ and div $\boldsymbol{j} \approx 0$ are generally true. Suppose that div $\boldsymbol{V} \approx 0$, so that there is no variation of the density of neutral molecules. Although $\boldsymbol{j} \approx ne(\boldsymbol{V} - \boldsymbol{u}_e)$, it must not be concluded that div $\boldsymbol{u}_e$ is small compared with t^{-1}; it does follow, however, that div $\boldsymbol{u}_e \approx$ div $\boldsymbol{u}_p$, and the problem is then simplified as follows. Eliminating $\boldsymbol{E}$ between the two equations (1) gives

$$nm_p\nu_p(\boldsymbol{U} - \boldsymbol{V}) = \boldsymbol{j} \wedge \boldsymbol{H}/c \tag{6}$$

where

$$\boldsymbol{U} = (m_p\nu_p\boldsymbol{u}_p + m_e\nu_e\boldsymbol{u}_e)/(m_p\nu_p + m_e\nu_e)$$

and $m_e\nu_e$ has been neglected in comparison with $m_p\nu_p$. Then

$$\text{div } \boldsymbol{u}_e \approx \text{div } \boldsymbol{U} = (nm_p\nu_pc)^{-1} \text{ div}(\boldsymbol{j} \wedge \boldsymbol{H}).$$

This involves the component of $\boldsymbol{j}$ perpendicular to $\boldsymbol{H}$ and assuming still that ν_P is substantially greater than Ω_p, so that T'_{ij} is approximately given by T_{ij} for electrons

$$\text{div } \boldsymbol{u}_e \sim (nm_p\nu_pc)^{-1} \frac{ne^2}{m_e} \frac{VH^2}{Lc(\nu_e^2 + \Omega_e^2)^{\frac{1}{2}}}$$

$$\sim \frac{\Omega_e\Omega_p}{\nu_p(\nu_e^2 + \Omega_e^2)^{\frac{1}{2}}t}$$

When $\nu_e > \Omega_e$, this is roughly $\Omega_e\Omega_p/\nu_e\nu_pt$, and, when $\Omega_e > \nu_e$, it is roughly Ω_p/ν_pt. When $\Omega_p > \nu_p$, the motion of the ions across the field is strongly inhibited and the qualitative argument given at the beginning leads us to expect div $\boldsymbol{u}_e \sim t^{-1}$. This may be verified: when $\Omega_p \gg \nu_p$, $|\boldsymbol{u}_p - \boldsymbol{u}_e| \ll |\boldsymbol{u}_e - \boldsymbol{V}|$ and the component of $\boldsymbol{j}$ perpendicular to $\boldsymbol{H}$ is approximately $\frac{ne^2\nu_p}{m_p\Omega_p^2}|\boldsymbol{E} + \boldsymbol{V} \wedge \boldsymbol{H}/c|$.

When div $\boldsymbol{u}_e \sim t^{-1}$, large variations of n_e occur. For smaller values the variations are given roughly by $\delta n/n \sim t$ div $\boldsymbol{u}_e$. When $\nu_e = \Omega_e$, the variations are about 0·4 per cent, which is probably rather smaller than required by the observations. In the atmosphere $\nu_e = \Omega_e$ at about 80 km, and above this level $\Omega_e > \nu_e$. At 110 km, ν_p is about 20 Ω_p, so that the mechanism described here would produce ~5 per cent variations in the electron density.

Acknowledgement—This work has been carried out during the tenure of an I.C.I. Fellowship.

REFERENCES

COWLING, T. G.	1945	*Proc. Roy. Soc.* **A183,** 453
MAXWELL, A.	1954	*Phil. Mag.* **45,** 1247
NICOLET, M.	1953	*J. Atmosph. Terr. Phys.* **3,** 200
VILLARS, F., and WEISSKOPF, V. F.	1954	*Phys. Rev.* **94,** 232

VOL. 8 1956

Journal of Atmospheric and Terrestrial Physics, 1956, Vol. 8, pp. 43 to 54. Pergamon Press Ltd., London

The *Z* propagation hole in the ionosphere

G. R. Ellis
The Commonwealth Observatory Ionospheric Prediction Service, Hobart, Australia

(*Received 7 April* 1955)

ABSTRACT

The occurrence of *F*-region triple-splitting allows us to examine experimentally the properties of an unusual propagation hole in the ionosphere. Two methods of estimating the angular size of the hole are discussed. The first is based on the beam effect of *Z* echoes, according to which *Z* echoes are returned to the ground in a narrow beam. The second follows from an analysis of the distribution of angle of arrival of *Z* echoes. It is found at Hobart that, with a wave frequency of 4·65 Mc/s, the hole is approximately circular with an angular width to half-power points of less than 0·84°.

Under certain circumstances the propagation hole provides a means by which waves can pass completely through an otherwise reflecting ionospheric layer.

List of Symbols.

e = charge of electron

m = mass of electron

c = velocity of electromagnetic waves in free space

H = intensity of the earth's magnetic field

θ_0 = inclination of the earth's magnetic field to the vertical

$p_H = \dfrac{eH}{mc}$ = gyro-frequency of electrons in the ionosphere

N = electron density

p = angular wave frequency

$p_0^2 = \dfrac{4\Pi Ne^2}{m}$

$y = \dfrac{p_H}{p}$

n = refractive index

ϕ_r = angle of refraction

$q = n \cos \phi_r$

1. Introduction

When an electromagnetic wave is incident on an ionospheric layer, in the magnetic meridian vertical plane, and at a certain critical angle of incidence given by

$$\sin \phi_c = \sqrt{\frac{y}{1+y}} \sin \theta_0 \qquad (1)$$

then the complex refractive indices of the ordinary and extraordinary modes become equal at the ordinary level of reflection for which $p_0^2/p^2 = 1$ (see Fig. 1).

It has been pointed out by Poeverlein (1949) and Millington (1954) that there is, therefore, a possibility that the ordinary wave may be transformed to an extraordinary wave at this level, and be propagated to the second extraordinary, or Z, reflection level near $p_0^2/p^2 = 1 + y$. In the case of a smooth

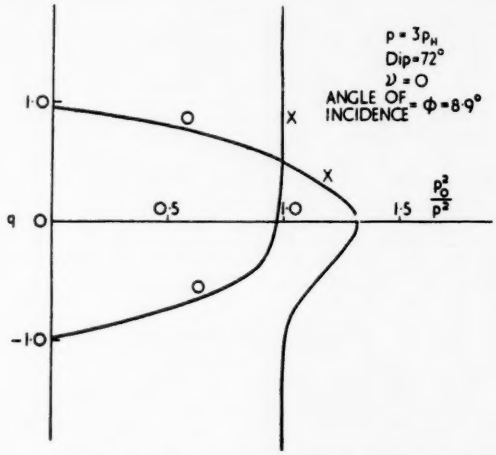

Fig. 1. Refractive index curves at the critical angle of incidence.

layer, such a wave would, after reflection, be highly attenuated on its downward path near the ordinary reflection level and would not be observable at the ground.

However, it is now known that such propagation is associated with the triple splitting of F-region ionospheric echoes, the third or Z echo of a triple occurring

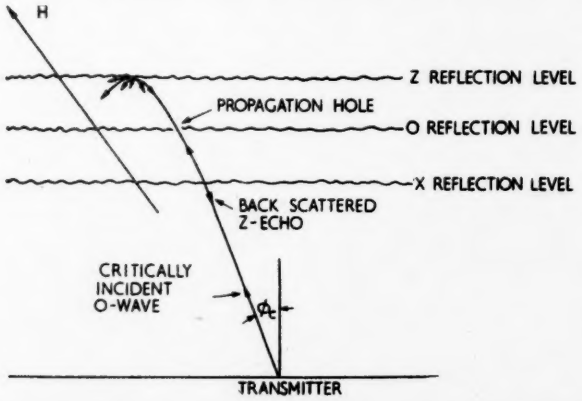

Fig. 2. Illustrating the mechanism of occurrence of F-region Z echoes.

when the reflecting layer is sufficiently rough to produce observable backscattering from the Z reflection level of a critically incident ordinary wave (Ellis, 1953). Triple splitting, therefore, provides a means of investigating this remarkable propagation phenomenon which, in effect, produces a "propagation hole" in the ordinary level of reflection (see Fig. 2).

VOL. 8 1956

The primary properties of the hole are its direction, which is given by ϕ_e, and its "width" or angular attenuation function. The corresponding observable properties of Z echoes are their direction of arrival and their angular power spectrum. Measurements of the direction of arrival of Z echoes have already been reported (ELLIS, 1953), and in this paper we shall discuss the results of measurements of their angular power spectrum which have been made at Hobart. There is a direct way of obtaining information about the angular power spectrum which is based on the unique property of Z echoes, that they must be returned to the ground in a narrow beam. If a receiver is moved in a horizontal

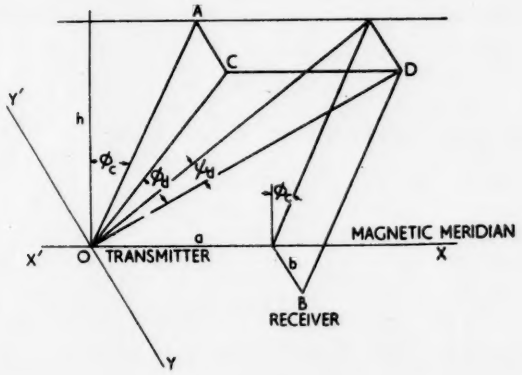

Fig. 3. The co-ordinate system for measurements of Z echo power.

direction away from the transmitter, then the area of the Z reflection level seen by the receiver will cease to coincide with that illuminated by the transmitter. As the distance is increased the Z echo power will decrease in a way which may be related to the form and parameters of the angular power spectrum. This property of Z echoes is due to the fact that the direction of the propagation hole is always relative to the observer.

The parameters of an assumed power spectrum may also be obtained from a statistical analysis of the random fluctuation in direction of arrival. This method, which has been treated by MACDONALD (1949) and BRAMLEY (1951), affords an independent way of checking measurements based on the beam effect of Z echoes.

2. THEORETICAL

2.1. *The theory of the Z beam*

Suppose we have a rectangular co-ordinate system on the ground centred on the transmitter and orientated with the XOX^1 axis along the magnetic meridian. Let the co-ordinates of the receiver be (a, b) and let D be the projection of this point on to a flat ionospheric layer in a direction given by the vertical angle ϕ_e in the plane of the magnetic meridian. Points D, and A, the projection of the origin in the same direction, represent the centres of the propagation hole with respect to the receiver and the transmitter. We also use two angular co-ordinate systems based on the vertical and perpendicular planes through OA and BD (Fig. 3).

As we shall see, most of the power transmitted from O will pass through the propagation hole within a couple of degrees of OA. We may, therefore, write for the angular co-ordinates of D with respect to OA:

$$\phi_d \sim \frac{a \cos^2 \phi_c}{h}$$
$$\psi_d \sim \frac{b \cos \phi_c}{h} \tag{2}$$

and if the angular co-ordinates of an element of area of the reflecting layer with respect to OA are (ϕ, ψ) then its co-ordinates with respect to BD will be approximately

$$(\phi - \phi_d, \psi - \psi_d)$$

Let the angular power spectrum of Z echoes at the transmitting point be

$$P(\phi, \psi)$$

the power incident on an element of area of the reflecting level will then be represented by

$$\propto \sqrt{P(\phi, \psi)}\, d\phi\, d\psi$$

and the power received at point B from this element by

$$\propto \sqrt{P(\phi, \psi) \cdot P(\phi - \phi_d, \psi - \psi_d)}\, d\phi\, d\psi$$

We then have the total power received at B

$$P_B \propto \int_{-\pi}^{\pi}\int_{-\pi}^{\pi} \sqrt{P(\phi, \psi)\, P(\phi - \phi_d, \psi - \psi_d)}\, d\phi\, d\psi$$

It is convenient to normalize the power received at B so that

$$\frac{P_B}{P_0} = \frac{\int_{-\pi}^{\pi}\int_{-\pi}^{\pi} \sqrt{P(\phi, \psi) \cdot P(\phi - \phi_d, \psi - \psi_d)}\, d\phi\, d\psi}{\int_{-\pi}^{\pi}\int_{-\pi}^{\pi} P(\phi, \psi)\, d\phi\, d\psi}$$

To progress further, it is necessary to make a plausible assumption regarding the form of the power spectrum. We will assume that the spectrum of echoes received at the transmitter is gaussian, that is:

$$P(\phi, \psi) \propto \exp\left(-\frac{1}{2}\left(\frac{\phi^2}{{\sigma_1}^2} + \frac{\psi^2}{{\sigma_2}^2}\right)\right) \tag{3}$$

The total power received at B is then

$$P_B \propto \int_{-\pi}^{\pi}\int_{-\pi}^{\pi} \exp\left(-\frac{1}{4}\left(\frac{\phi^2}{{\sigma_1}^2} + \frac{\psi^2}{{\sigma_2}^2}\right) - \frac{1}{4}\left(\frac{(\phi - \phi_d)}{{\sigma_1}^2}\right)^2 + \frac{(\psi - \psi_d)^2}{{\sigma_2}^2}\right) d\phi\, d\psi$$

VOL.
8
1956

For receiving-points in the magnetic meridian of the transmitter we have $\psi_d = 0$, and integrating with respect to ψ, we have

$$\frac{P_B}{P_0} = e^{-\frac{\phi_d^2}{8\sigma_1^2}} \tag{4}$$

A gaussian power spectrum will therefore result in a gaussian variation of Z echo power with distance from the transmitter along the magnetic meridian. By measuring the ratio P_B/P_0, and the true height of reflection h, we can determine the standard deviation of the assumed spectrum. Measurements at different distances from the transmitter would be expected to provide some indication of the validity of the assumed form of the power spectrum.

2.2. *Phase analysis*

In analyzing the distribution of the directions of arrival of Z echoes, it is necessary to assume that the random fluctuations in direction are caused by multiple random scattering from irregularities within the illuminated area of the Z reflection level. This assumption has a certain amount of justification if we use the estimate by Briggs and Phillips (1950) that the average size of lower F-region irregularities is about 200 metres. Since the illuminated area will be several kilometres in extent, a considerable number of scattering centres would be included within it.

Consider two aerials E and F spaced a distance d apart under the influence of a system of co-planar rays of the same frequency $f = p/2\pi$, the plane of the rays is assumed to contain the line EF. Then the voltage produced in the aerials may be written

$$V_1 = A_1 \cos(pt + B_1)$$

$$V_2 = A_2 \cos(pt + B_2)$$

The amplitudes A and the phase angles B will in general be different for the two aerials. It is assumed that the phases of the component waves vary at random and independently of each other, and also that the frequency of variation is small compared with the radio frequency. The quantity observed with the direction finder is the phase difference between the voltages produced in the aerials, that is $(B_1 - B_2)$

The relation between the distribution of phase difference and the angular power spectrum of the waves has been investigated by Bramley (1951) who showed that for a narrow gaussian power spectrum the mean deviation from the mean direction of arrival measured with a direction finder is very nearly equal to the standard deviation of the power spectrum. Using our assumed function of equation (3), we have

$$\sigma_1 \sim \overline{|\phi|}$$

$$\sigma_2 \sim \overline{|\psi|}$$

We, therefore, have two independent methods of estimating the standard deviation of the angular power spectrum of Z echoes.

3. Experimental

3.1. *Z echo power measurements*

Measurements of the average Z echo power were made at four points whose positions relative to the transmitting station are shown in Fig.4. These positions were chosen as near as possible to the magnetic meridian through the transmitter. The technique used was to record photographically the amplitude of all weak echoes simultaneously at all stations. Recordings were made on an automatic basis for two hours every afternoon. On occasions when Z echoes were observed at the transmitting station the transmitter power was subsequently reduced to

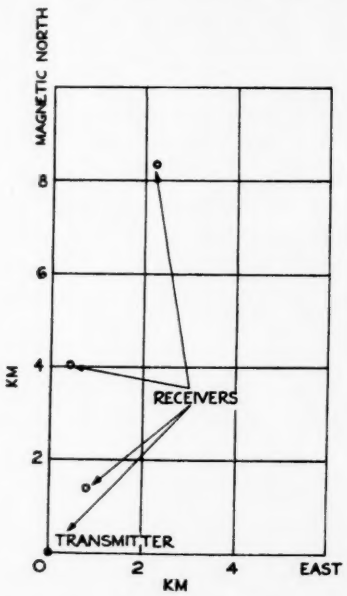

Fig. 4. The relative positions of the transmitting and receiving stations.

allow ordinary echo amplitudes to be recorded at all stations for comparison. This was done to calibrate the receivers, the assumption being that the average power of ordinary echoes was either the same at all stations or that any diversity effects affected the similarly polarized O and Z echoes to the same extent. The average Z echo power was calculated as follows:

$$\frac{Z \text{ echo power at } B}{Z \text{ echo power at } O} = \frac{\overline{(Amp_Z\, B)^2}\ \overline{(Amp_O\, O)^2}}{\overline{(Amp_Z\, O)^2}\ \overline{(Amp_O\, B)^2}}$$

The geographic co-ordinates of the transmitting station were 147·5° E, 42·9° S, the geomagnetic co-ordinates 224·6° E, 51·7° S, and the magnetic dip 72°.

Modified Loran type A/A PN4 receivers were used. The transmitter had a peak power of 4 kW, a pulse width of 100 microsec, and a pulse repetition frequency of 50 per sec. The wave frequency was 4·65 Mc/s.

VOL.
8
1956

The detailed results of all measurements are given in Table 1.

Table 1. *Results of Z echo power measurements*

Time	*Date*	*Number of observations*	*Normalized value of* $\frac{\overline{(Z\ amplitude)^2}}{(O\ amplitude)^2}$			*True height*
			Receiver A	*Receiver B*	*Receiver C*	
						km
1800	30/3/54	54	0·084	0·30	0·77	210
1710	2/4/54	38	0·09	0·29	0·80	220
1735	3/4/54	61	0·195	0·40	0·65	214
1715	4/4/54	52	0·12	0·28	0·9	220
1800	6/4/54	98	0·17	0·45	0·81	220
1701	22/4/54	65	0·13	0·42	0·60	213
1710	25/4/54	80	0·035	0·37	—	210
1703	6/5/54	42	0·07	0·53	0·86	205
1700	9/5/54	110	0·055	0·39	0·68	205
1650	27/5/54	76	0·14	—	0·73	210
1500	5/8/54	81	—	0·45	0·64	202
1530	6/8/54	62	—	0·31	0·97	200
		Average	0·084	0·38	0·75	210
		Standard deviation	0·046	0·067	0·11	

Since from equations (2) and (4), a higher level of reflection would be expected to produce an increase in the Z echo power at each receiving site, it was necessary to calculate the true height of reflection for each series of observations. This was done from simultaneous $P'f$ records by finding the true height at the frequency for which reflection of the O wave occurred at the same electron density level as the Z wave at the operating frequency. It was necessary to use the ordinary wave, as only a small part of the Z trace near the critical frequency was normally visible. To obtain the appropriate O wave frequency we make use of the fact that the reflection at the Z level is nearly independent of azimuth. As a result we may write

$$f_Z(\text{oblique}) \sim f_Z(\text{vertical}) \ . \ \sec \phi_c$$

That is

$$f_O = \sqrt{f_{Z_v}{}^2 \cos^2 \phi_c + f_{Z_v} \cdot f_H \cos \phi_c}$$

The actual method of calculating the true height from the $P'f$ curve was that developed by KELSO (1954), which allows for the effect of the geomagnetic field.

It can be seen from Table 1 that the true height of reflection did not vary much throughout the observations and, because of the much greater variation in the relative Z echo powers observed, it was considered that no serious error would be caused by referring all measurements to the mean height of 210 km. The

mean variation of Z echo power with radial distance from the transmitter is shown in Fig. 5.

It is clear that Z echoes do return to the ground in a narrow beam, as predicted by the theory. The decrease in power with distance is approximately gaussian, and is therefore in reasonable agreement with the assumed gaussian form of the angular power spectrum. A gaussian curve fitted to the experimental points has a standard deviation of 3·3 km, which, with the nominal reflection height of 210 km, gives us 0·37° for the N–S standard deviation of the angular power spectrum. Although a better fit to the observed points may be obtained by considering other angular power functions, it is considered that the number of points and the accuracy of the observations is not sufficient to justify detailed deductions. A gaussian spectrum may be regarded as a good first approximation.

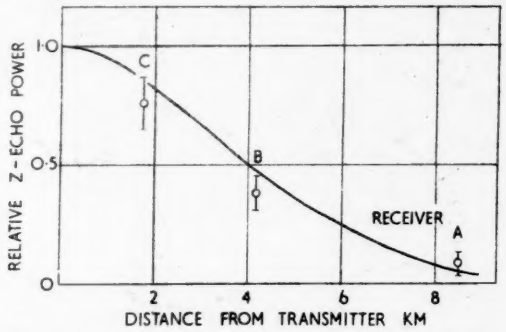

Fig. 5. The variation of Z echo power in the vicinity of the transmitter.

3.2. *The direction of arrival of Z echoes*

Measurements of the direction of arrival of F-region Z echoes were made at Hobart during 1952 and 1953. The technique used was the well-known one of observing the phase difference between the signals induced in two spaced loop-aerials by a selected downcoming echo (Ross *et al.*, 1951). A twin-channel cathode-ray direction-finding receiver was used to amplify the signals. The loop spacing was 120 ft. Altogether four aerials were used, one pair along the magnetic meridian, and one pair along a magnetic east–west line.

Observations were made manually by photographing the phase-difference ellipse on the receiver cathode-ray tube. The quantities measured were the magnetic north–south and east–west components of the angle of arrival, denoted by ϕ_i and ψ_i respectively. A complete observation took about 25 sec. When measurements of only the north–south or the east–west component of direction were made, one photograph was taken every 15 sec.

Since it was necessary to isolate the Z echo from the O and X echoes, only a short time was available for observations on each occasion. At Hobart, F-region Z echoes can normally be resolved over a frequency range of only a few hundred kilocycles below the Z critical frequency and, as a result, the measurement time was limited to that taken by the F-region critical frequency to change through this range. D.F. measurements were generally possible only for about ten minutes,

VOL. 8 1956

although on a few occasions the Z echo could be followed for about half an hour. The usual method of observation was to have the direction finder ready to operate during each afternoon on a frequency below the average maximum daytime critical frequency. The slow decrease in critical frequency during the afternoon would then bring any resolvable Z echoes into the direction-finder operating frequency. The results of all observations are summarized in Table 2.

Table 2. The directions of arrival of Z echoes

Date	*Time*	*Number of observations*	*Average directions*		*Deviations from mean*	
			ϕi *degrees N*	ψi *degrees*	$\overline{\lvert \phi i - \bar{\phi} i \rvert}$ *degrees*	$\overline{\lvert \psi i - \bar{\psi} i \rvert}$ *degrees*
3/9/52	1540	18	9·05	0·35 E	0·54	0·48
10/9/52	1540	22	8·75	0·1 E	0·47	0·44
17/9/52	1530	19	9·0	0·5 E	0·69	0·36
18/9/52	1600	21	9·0	0·2 E	0·74	0·55
26/9/52	1535	20	8·6	0·3 E	0·52	0·4
1/10/52	1550	22	9·3	0·15 W	0·7	0·6
3/11/52	1750	102	8·65	—	0·55	—
22/4/53	1730	21	8·9	—	0·68	—
26/4/53	1710	28	9·1	—	0·6	—
1/5/53	1700	21	8·4	—	0·4	—
2/5/53	1716	114	8·55	—	0·54	—
12/5/53	1600	31	8·5	—	0·65	—
18/5/53	1615	73	8·95	—	0·59	—
22/5/53	1603	150	8·6	—	0·55	—
29/5/33	1600	20	8·25	—	0·75	—
5/6/53	1615	38	9·2	—	0·6	—
Average all observations			8·7	0·2 E	0·56°	0·47°

Wave frequency = 4·65 Mc/s.

From these results we get for the standard deviations of the assumed gaussian power spectrum:

$$\sigma_1 = 0{\cdot}56^\circ$$

$$\sigma_2 = 0{\cdot}47^\circ$$

The north–south result is in reasonable agreement with that obtained from the power measurements, particularly since in the case of angle observations we are using a quantity $\overline{\lvert \phi \rvert}$. the observed value of which will be increased by any random D.F. errors. In the case of the power observations, random errors would be averaged out in the final result. It is considered, therefore, that the result obtained from the power measurements is likely to be nearer the correct value. However, the D.F. results do suggest that the spectrum is not greatly

different in the north–south and east–west directions. Summing up, we may say that, with the conditions of frequency, layer height, and geomagnetic field in which these measurements were conducted, the angular power spectrum of *Z* echoes is nearly symmetrical about the mean direction with a standard deviation of about 0.37°. The corresponding half-power point would lie at 0.42° from the mean direction. Since the distribution of *Z* echo power with angle of arrival will be determined by the angular attenuation function of the propagation hole, together with any scattering of the waves which may occur between the ground and the level of the hole, we may regard these measurements as setting upper limits to the size of the propagation hole.

4. Penetration of an Ionospheric Layer

By choosing the operating frequency above the *Z* critical frequency, waves which have penetrated the *Z* hole in the *O* level will not be reflected at the *Z* level, but will penetrate the electron maximum of the layer. Between the *Z* and *O* critical frequencies neither the *X* or *O* waves will pass through the layer which will form

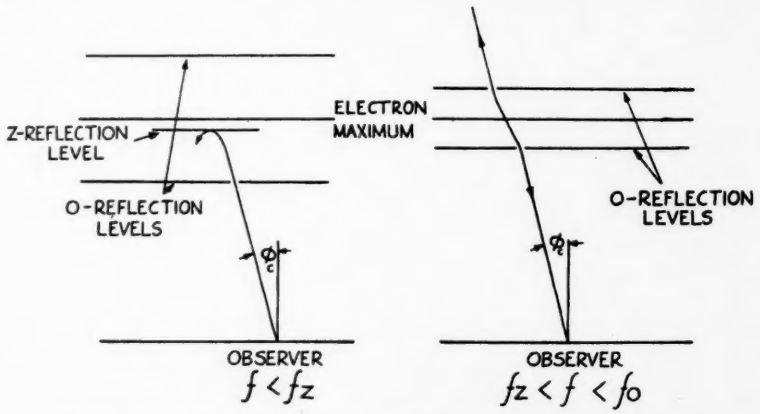

Fig. 6. Approximate ray paths for penetration of an ionospheric layer.

a reflecting screen, except in the direction of the hole. For complete penetration of the layer the upgoing or downcoming *O* wave would have to penetrate a second *Z* hole at the ordinary level of reflection above the electron maximum. The approximate ray paths are shown in Fig. 6.

Since the magnetic field strength and magnetic dip will be different at the two ordinary reflection levels, the direction of the upper hole will in general be different from that of the lower hole. It is necessary, therefore, that for complete penetration of the layer, this difference in direction should be somewhat less than the hole angular diameter.

The actual difference in direction for any set of circumstances may easily be calculated, since the ray path between the holes is very nearly in the direction of the magnetic field. Using a parabolic layer, a dipole field, and magnetic elements

VOL. 8 1956

at the ground appropriate to Hobart, we obtain from equation (1) the curve shown in Fig. 7. For typical values of the scale height, height of electron maximum, and critical frequency, it is seen that the difference in direction decreases from 0·16° at the Z critical frequency to zero at the O critical frequency. Under these conditions a wave will therefore penetrate the layer by means of the propagation holes at all frequencies between these limits.

5. Conclusion

The small angular size of the Z propagation hole can, in certain circumstances, provide a receiver with a very narrow effective aerial beam width. A possible application, for example, lies in which the study of the horizontal irregularities of the ionosphere. Here, existing techniques allow only measurements in which the average effect of all the irregularities over a wide area can be observed. However, by using Z

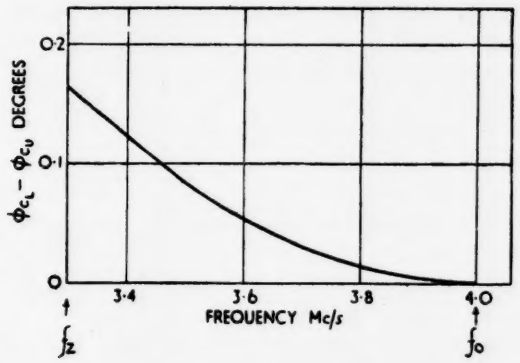

Fig. 7. Curve showing the difference in the direction of the upper and lower holes in the frequency range between the O and Z critical frequencies.

ϕ_{cu} = direction of upper hole
ϕ_{cl} = direction of lower hole
Parabolic layer:
Scale height = 75 km
N max. at 300 km
p_H (300 km) = 1·5 Mc/s
Dip (300 km) = 72°

echoes, we may examine at oblique incidence the properties of a small e ement of the reflecting layer. Another possible application is in the field of radio astronomy, although the necessity of operating close to the critical frequency introduces other factors, the effect of which cannot at present be assessed.

Acknowledgements—This investigation has been carried out in association with the University of Tasmania, and forms part of the research programme of the Ionospheric Prediction Service. Part of the D.F. installation was financed by a grant to the University by the Radio Research Board of the C.S.I.R.O. Thanks are due to Mr. G. Goldstone, who assisted in building and operating the amplitude measuring equipment.

REFERENCES

BRAMLEY, E. N.	1951	*Proc. Inst. Elec. Engrs.* **98,** (Pt. III), 19
BRIGGS, B. H., and PHILLIPS, G. J.	1950	*Proc. Phys. Soc.* **63,** (Pt. II), 907
ELLIS, G. R.	1953	*J. Atmosph. Terr. Phys.* **3,** 263
KELSO, J. M.	1954	*J. Atmosph. Terr. Phys.* **5,** 11
MACDONALD, D. K. C.	1949	*Proc. Camb. Phil. Soc.* **45,** 368
MILLINGTON, G.	1954	*Proc. Inst. Elec. Engrs.* **101,** (Pt. IV), 235
POEVERLEIN, H.	1949	*Z. angew. Phys.* **1,** 517
ROSS, W., BRAMLEY, E. N., and ASHWELL, G. E.	1951	*Proc. Inst. Elec. Engrs.* **98,** (Pt. III), 294

VOL.
8
1956

Journal of Atmospheric and Terrestrial Physics, 1956, Vol. 8, pp. 55 to 75. Pergamon Press Ltd., London

The spectrum of radio-star scintillations and the nature of irregularities in the ionosphere

J. P. WILD and J. A. ROBERTS
Division of Radiophysics, Commonwealth Scientific and Industrial Research Organization, Australia

(*Received* 1 *July* 1955)

ABSTRACT

An observational study of the spectrum of radio-star scintillations has been made with a view to exploring the small-scale structure of the ionosphere. Observations of the intense source in Cygnus were made near transit at an altitude of about 15°. Three instruments were used simultaneously: (1) a swept-frequency spectroscope to record the dynamic spectrum of scintillations, (2) a swept-frequency interferometer to study positional deviations at different frequencies, and (3) a triangular spaced-aerial system for studying the lateral size and motion of the pattern on the ground.

The commonly occurring types of dynamic spectra are described, and their interpretation in terms of ionospheric phenomena is discussed. From the nature of the spectra it is inferred that most of the fluctuations are due to focusing by single lens-like irregularities, rather than to diffraction at a large number of irregularities. The spectra also show that the scintillation patterns are often dispersed across the ground, different frequencies being focused at different points. This is tentatively attributed to ionospheric gradients which act like huge prisms. Such "dispersing regions" may lie at different levels from the "focusing regions."

The degree of fluctuation shows two maxima, one near midnight (winter) and the other near midday (summer). The size, shape, and motion of the pattern on the ground, as well as the dispersion, also vary throughout the year.

In many cases the pattern on the ground is highly elongated, a feature which complicates the determination of the direction and speed of motion. For daytime conditions at least, this elongation indicates marked anisotropy in the ionospheric irregularities.

1. INTRODUCTION

MOST of our knowledge of the terrestrial ionosphere has been obtained with the use of radio waves transmitted from the earth, reflected from the various layers of the ionosphere, and received again at the earth. With this method, investigation is restricted to regions below the layer of maximum electron density. The discovery of extra-terrestrial radio sources now permits the study of the ionosphere by means of radio waves transmitted from outside. This method is of special interest, because it may allow us to study regions above the layer of maximum ionization.

The twinkling of radio stars due to scattering in the ionosphere has been investigated extensively during the past five years at Cambridge (RYLE and HEWISH, 1950; HEWISH 1952) Manchester (LITTLE and MAXWELL, 1951, 1952; MAXWELL and DAGG, 1954), and Sydney (MILLS and THOMAS, 1951; BOLTON, SLEE, and STANLEY, 1953). Observations taken simultaneously at different points on the ground have revealed that the fluctuations in intensity are due predominantly to the motion of a *relatively* stable diffraction pattern over the ground at speeds of the order 100 m/sec. The outstanding problem is the interpretation of this pattern in terms of the ionospheric structure responsible for its formation. Previously this problem has been attacked by statistical methods based on the theory of diffraction at an irregular screen. Using such methods, it has been inferred that the fluctuations result from diffraction at ionospheric irregularities

with lateral sizes of the order of 5 km. Most observers, particularly those in England, have found the fluctuations to occur predominantly at night-time, and have given evidence that the irregularities lie in the F_2-region near or beyond the layer of maximum ionization. However, the series of low-altitude observations in Australia by BOLTON, SLEE, and STANLEY (1953) has revealed the occurrence of intense fluctuations by day as well as by night, and these were attributed to irregularities in the sporadic E-layer.

All previous observations have been made at discrete frequencies. In the present paper we describe observations of the twinkling phenomenon over a continuous range of frequencies. It will be shown that the introduction of spectral data leads to a remarkable simplification in the interpretation of records. It has been found possible to recognize different types of refraction and diffraction phenomena, and even to interpret complex records in which two phenomena appear superposed. In many cases the observed spectra can be used, without recourse to statistical methods, to infer the detailed ionospheric structure responsible for the scintillations.

Preliminary accounts of these investigations were given by Dr. J. L. PAWSEY to the XIth General Assembly of U.R.S.I. in August 1954, and to the ionospheric conference held by the Physical Society at Cambridge in September 1954.

2. THE METHODS OF OBSERVATION

The complete specification of the spectrum of a diffraction pattern on the ground requires measurement of both intensity and phase as functions of frequency and position on the ground. With this consideration in view, apparatus was built to record radio-star scintillations simultaneoulsy in the following three ways:

(1) The recording of intensity at one point as a function of time and frequency, using a 40–70 Mc/s spectroscope.

(2) The recording of the phase gradient along one direction as a function of time and frequency, using a 40–70 Mc/s "swept-frequency interferometer."

(3) The recording of intensity at a fixed frequency (45 Mc/s) as a function of time at three points on the ground, arranged at the corners of an approximate equilateral triangle. Since variations with time are due mainly to the motion of the diffraction pattern across the ground (a result confirmed by the present observations), the temporal variations in (1) and (2) can be expressed in terms of spatial variations by using the drift velocity deduced from (3).

The observations were made entirely on the intense source in Cygnus (R.A. 19h 57·7m, dec. 40·6°) for up to two hours per day centred on the time of transit of the source. The observing station is located at Dapto, N.S.W. (latitude 34°28·5′ S, longitude 150°47·5′ E). Here the altitude of the source is approximately 15° at transit, changing by no more than 1° during the observing period. The restricted period of observation permits the use of fixed aerials.

In describing the apparatus used for taking the three types of record, it is convenient initially to consider the three as separate instruments and subsequently to show how they are operated in combination. The three instruments are shown diagrammatically in Fig. 1.

2.1. *Instrument No.* 1: *The spectroscope*

The spectroscope consists of a broad-band aerial connected to a tunable receiver. The tuning condensers of the latter are mechanically rotated in such a way that the frequency band of acceptance ($\frac{1}{2}$ Mc/s wide) is swept over the range 40–70 Mc/s in $\frac{1}{3}$ second. The receiver output is used to modulate the intensity of the spot of a cathode-ray tube. At the same time the horizontal displacement of the spot is swept in synchronism with the receiver tuning, so that a single spectrum is given in the form of an intensity-modulated line. Spectra are repeated at intervals of one second. The cathode-ray tube display is photographed with a camera in which the film moves continuously at the rate of $\frac{1}{2}$ inch per minute normal to the trace. Thus, the record consists of a series of parallel lines, of variable intensity, spaced on the film at intervals of

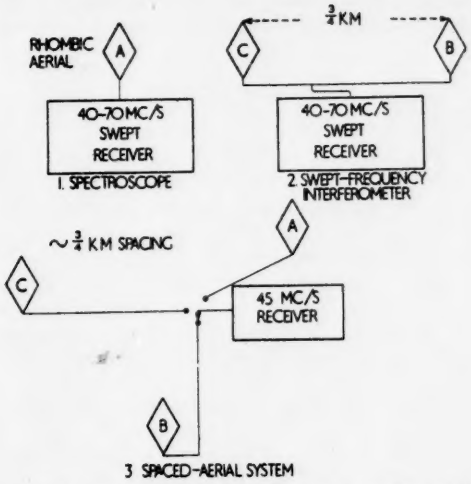

Fig. 1. Principles of the three instruments used for observing radio-star scintillations.

1/120 inch. When viewed broadly, the record gives the *dynamic spectrum* of the observed phenomenon—i.e., the variation of intensity in the frequency-time plane. Time is registered by photographing a clock placed beside the display, and illuminated by a flash at intervals of one minute. Records are calibrated in frequency using a standard signal generator and in intensity using a diode noise generator.

The swept-frequency receiver is part of that used by Wild, Murray, and Rowe (1954) for solar observations, and follows the principles described by Wild and McCready (1950).

The aerial is a fixed horizontal rhombic whose direction of maximum acceptance is due north. The dimensions are as follows:

Length of each side	31·1 m
Angle between wires at side corners	148°
Height above ground	4·2 m

These dimensions give approximately the optimum gain obtainable with a horizontal rhombic aerial for reception at an altitude of 15° (see Bruce, Beck and Lowry, 1935). The horizontal beamwidth between half-power points is 10·3° at 40 Mc/s and 4·6° at 70 Mc/s. The aerial is connected to the receiver by means of 700-ohm open-wire line.

2.2. *Instrument No.* 2: *The swept-frequency interferometer**

The two-aerial interferometer, operated at a single frequency, is an instrument well known in radio astronomy for the accurate location of isolated sources. In its commonest form the two

* Detailed results obtained with this instrument will be described in a subsequent paper.

aerials are connected to a central receiver with two equal lengths of cable, and the position of a source drifting across the interference pattern is determined by the sidereal times at which the maxima and minima occur. However, this method is unsuitable for the location of sources whose intensity or position in the sky changes appreciably in the time-interval between adjacent maxima. One method of tracking variable sources is to sweep the lobes of the interference pattern to and fro across the source by mechanically varying the length of one of the aerial cables (essentially the method used by LITTLE and PAYNE-SCOTT, 1951, for solar observations). In the present case we achieve a similar result by sweeping the frequency rather than the phase. This method has the important advantage that directional data are obtained at a number of frequencies simultaneously.

Consider two broad-band aerials spaced a distance a apart and connected in phase by equal lengths of cable to a central swept-frequency receiver. Maxima of the interference pattern then occur in directions inclined to the normal plane bisecting the line joining the two aerials at angles θ_n given by

$$\sin \theta_n = n\lambda/a$$

for integral values of n.

Thus a maximum occurs at all frequencies when $\theta_n = 0$ (the zero-order fringe), and the spacing of neighbouring maxima varies in direct proportion to the wavelength. Fig. 2(a) shows a typical swept-frequency record of the Cygnus source (under quiet ionospheric conditions) drifting through the central fringes of an interferometer.

At times well before or after transit, the source lies in high-order fringes, and the pattern in the time-frequency plane consists of a series of maxima and minima running nearly parallel to the time axis. When operated in this condition it is possible to trace the minima of visible fringes even in the presence of rapid variations of intensity. From a knowledge of the loci of these minima in the time-frequency plane, a continuous plot of position can be deduced at m equally spaced frequencies, where m is the number of minima simultaneously visible.

In our case we wish to observe the source with high-order fringes at times around transit. To do this we make the two aerial cables of unequal length. A typical record of a twinkling source passing through high-order fringes is shown in Fig. 2(b). Short-period fluctuations in position can be immediately recognized by kinks in the lines of minima.

The interferometer used here consists of two horizontal rhombics of the kind described in Section 2.1, spaced a distance of 780 m along a direction 118·5° E of N. These are connected directly to a 40–70 Mc/s swept-frequency receiver through long lengths of 700-ohm open-wire transmission line.* The aerial spacing is such that the angular separation of adjacent lobes is 33′ at 40 Mc/s and 19′ at 70 Mc/s. Angular deviations corresponding to about one-fifth of a lobe-width can be recognized on the records.

2.3. *Instrument No.* 3: *The spaced-aerial system*

For measuring the scale size and movement of the diffraction pattern on the ground, the intensity is recorded effectively simultaneously at three points on the ground spaced at the corners of and approximately equilateral triangle with sides of about 750 m (see Fig. 1). With the first arrangement tried, the whole *spectrum* was recorded at the three points. The three records usually showed very similar features but with systematic time displacements which were frequency-insensitive. In the final arrangement adopted, the three records were taken only at a single frequency, 45 Mc/s. This allowed the information to be displayed in the form of ordinary charts of intensity *versus* time, and improved the reading accuracy for the measurement of time delays.

The three aerials were of the type described in Section 2.1, and each was connected to the receiving hut by long lengths of open-wire line. Signals received in the three aerials were displayed on a common cathode-ray tube by means of a rapid switching system described below.

* The line consists of copper wires of diameter 0·064 inch spaced 11 inches apart, and has a theoretical attenuation of only 4·6 db per km at 50 Mc/s.

VOL. 8 1956

VOL. 178 1956

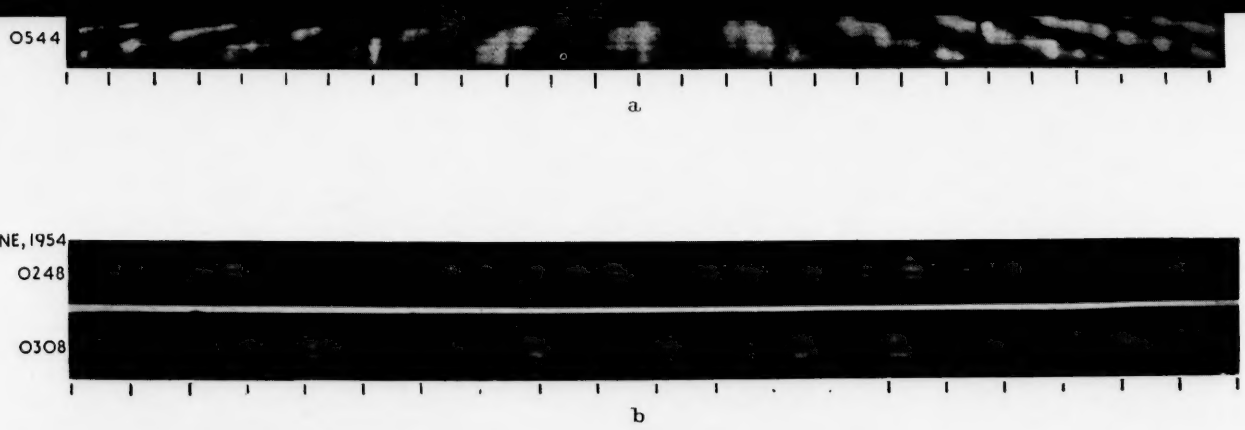

Fig. 2. Swept-frequency interferometer records of the Cygnus source. Frequency increases vertically from 40 to 70 Mc/s, time horizontally (150° E time, one-minute marks shown). In (a) the source is passing through the central fringes of the system, and fluctuations are slight. In (b) the source passes through high-order fringes; pronounced fluctuations are evident, and short-term variations in apparent position are revealed by kinks in the interference pattern.

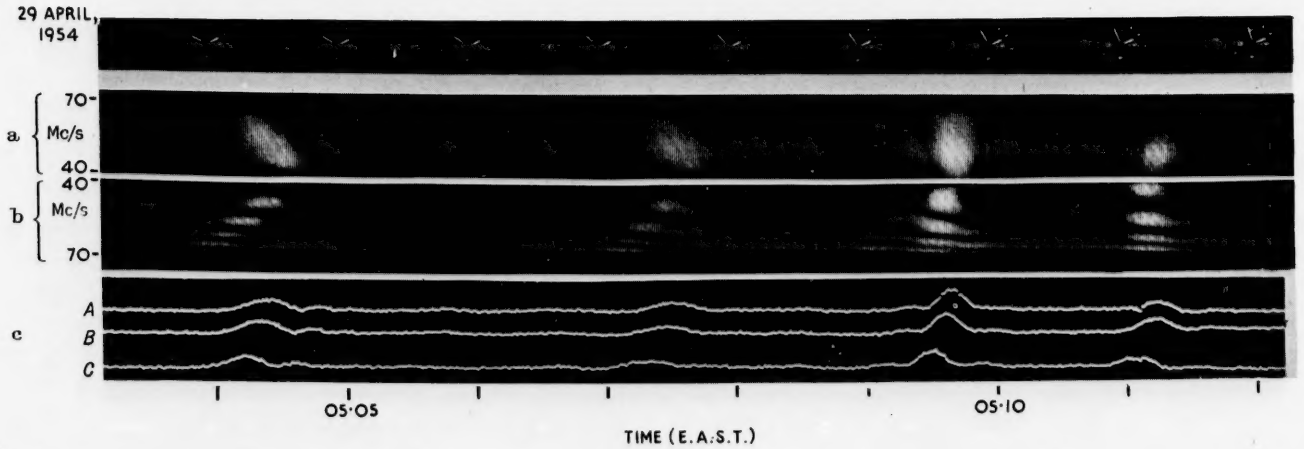

Fig. 3. A complete record of ridge-type scintillations. (a) The dynamic spectrum. (b) The swept-frequency interferometer pattern. (c) 45-Mc/s records taken with the spaced-aerial system and showing systematic time delays. Eastern Australian Standard Time (E.A.S.T.) is referred to longitude 150° E.

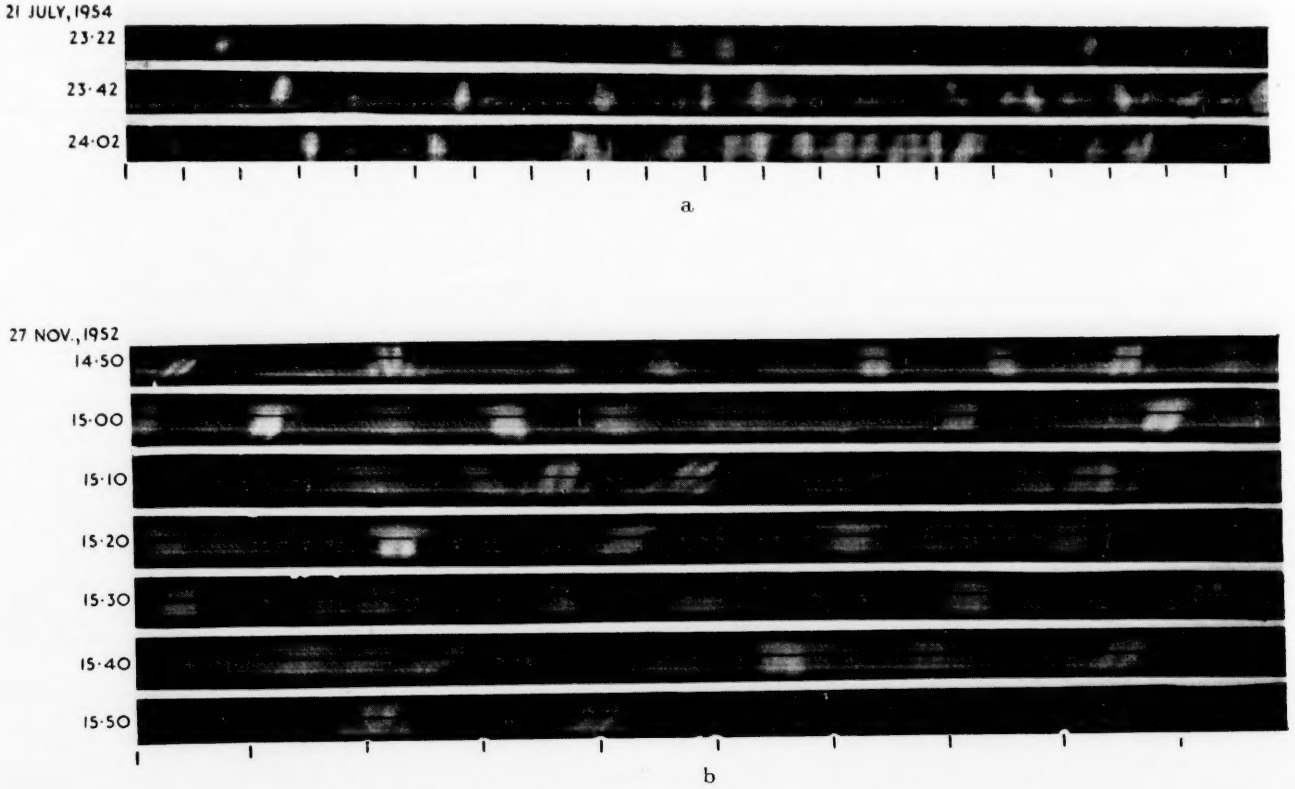

Fig. 5. Dynamic spectra of ridge-type scintillations. (a) is typical of night-time (winter) records. In (b) many of the ridges are seen to show an internal fine structure. Frequency increases vertically from 40 to 70 Mc/s, time horizontally (one-minute marks shown). Times are in E.A.S.T.

VOL.
8
1956

2.4. *The combined operation of the three instruments*

A system of operation was devised in which the three instruments described above were realized with common aerials and receiving equipment. A total of three aerials are used. These are referred to as A, B, and C (see Fig. 1). The aerials are connected in sequence to a swept-frequency receiver (see Section 2.1) through mechanically operated switches.

A complete switching cycle takes 1 second. This cycle is divided into eight sub-periods of $\frac{1}{8}$ second each. Connection to aerials is made during four of these sub-periods as follows:

1. 0–$\frac{1}{8}$ second—aerials B and C in combination to form the interferometer.
2. $\frac{1}{8}$–$\frac{1}{4}$ second—aerial A.
3. $\frac{1}{2}$–$\frac{5}{8}$ second—aerial B.
4. $\frac{5}{8}$–$\frac{3}{4}$ second—aerial C.

The receiver sweeps from 70 to 40 Mc/s during sub-periods 1 and 3, and from 40 to 70 Mc/s during sub-periods 2 and 4.

The information is displayed on two cathode-ray tubes:

(i) An intensity modulated display (as described in Section 2.1), in which the spectra obtained during sub-periods 1 and 2 are displayed side by side displaced in the X direction. This gives records of the swept-frequency interference pattern and the ordinary spectrum respectively.

(ii) A display in which the output obtained during sub-periods 2, 3, and 4 *at the instant when the receiver tuning passes through* 45 *Mc/s* is displayed as an X deflection of the spot. The magnitude of the X displacement of the spot for zero output is changed for each sub-period, giving three approximately equally spaced dots. When a signal is received in a given aerial, the appropriate spot is further deflected in the X direction by an amount proportional to the signal. Both displays are photographed on film continuously moving in the Y direction. Records obtained with the two displays are shown in Fig. 3.

3. Characteristics of the Dynamic Spectra

Spectral records of scintillations were taken between September 1952 and February 1955. As mentioned previously, each record is of one to two hours duration, being taken near the time at which the Cygnus source transits at Sydney (e.g., about midnight on 21 July and noon on 19 January). During the observing period the elevation of the source is $14\frac{1}{2} \pm \frac{1}{2}°$. The degree of fluctuation varied from day to day and showed a marked statistical dependence on the local time (or season) of observation. These and other diurnal variations will be considered in Section 5.

We first attempt to describe the general character of the records of dynamic spectra. Various types of spectra will be illustrated by actual records. Also idealized examples of the principal types are sketched in Fig. 4.

3.1. *The "ridge" pattern*

Figs. 3 and 5(a) are typical of the commonest type of record obtained at times of intense fluctuation. It is seen to consist of a series of bright bands or "ridges" running across the spectral width of the record. At the peak of a ridge the intensity is commonly greater than twice the mean level, and occasionally greater than five times. At any one frequency the duration of a single ridge is normally between 10 seconds and 1 minute, the mean being about 30 seconds. The average spacing between fluctuations is typically two to five times the duration. The ridges do not appear to be distributed randomly in time, but show

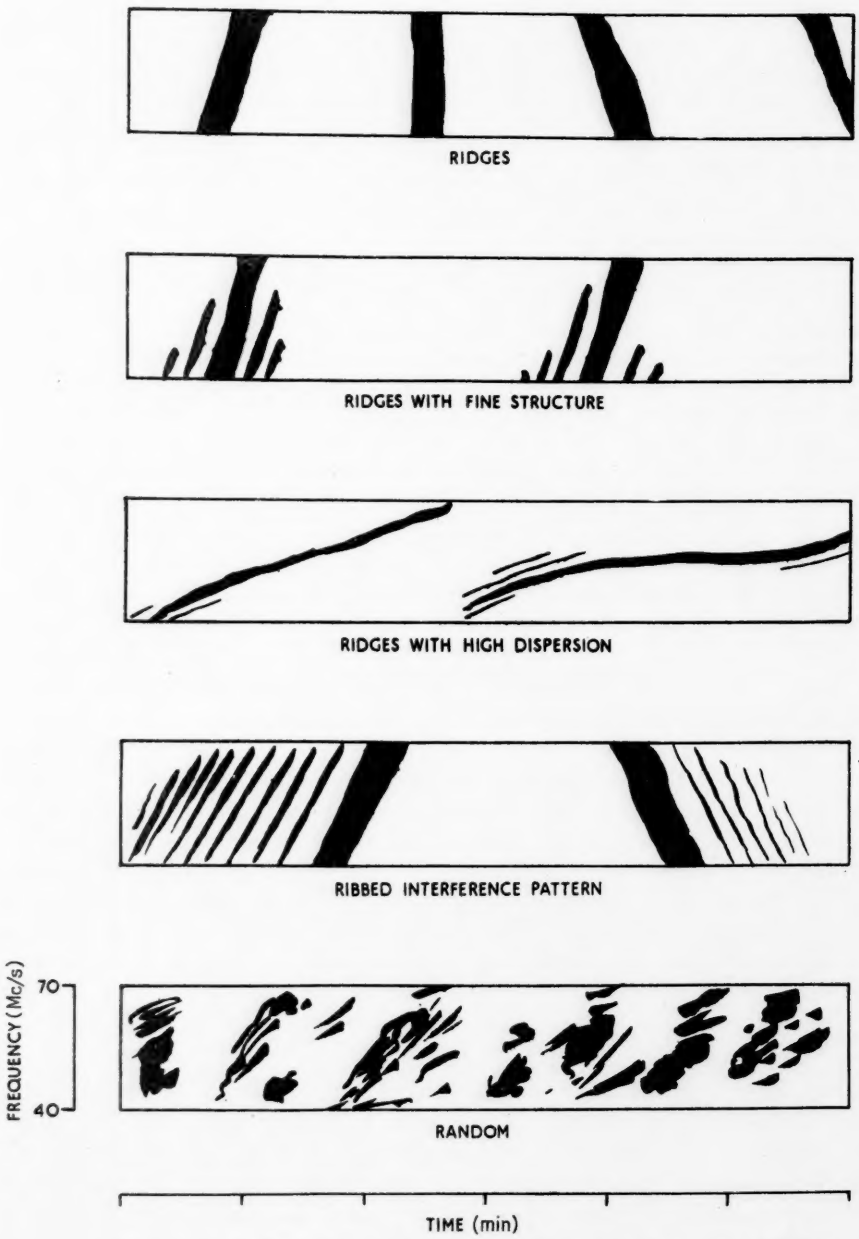

Fig. 4. Sketches showing idealized examples of the principal types of dynamic spectra observed.

VOL.
8
1956

some degree of regularity. This is exemplified in Fig. 5(b), where, between 15h 18m and 15h 31m, seven successive ridges occur at nearly equally spaced intervals of time.

The spaced-receiver observations show that the temporal variations in ridge-type records result from the movement of a spatial pattern of localized illumination along the ground through the aerial position. It will be shown later that these discrete ridges of broad spectral width cannot be explained in terms of diffraction from a large number of irregularities of a random-phase changing screen in the ionosphere. Rather, each ridge appears to result from the focusing effect of a single ionospheric "lens" consisting of a region of relatively low electron density—i.e., relatively high refractive index.

It is of interest that such intense discrete fluctuations have not been reported as a normal occurrence by observers in England. This may be due either to different ionospheric conditions at the different latitudes or to the low altitude of the present observations.

3.2. *Systematic frequency dispersion*

The ridges in the time-frequency plane do not always lie along lines of constant time. In general there are systematic time delays between high and low frequencies causing the ridges to be inclined to the frequency axis. These delays may be in the sense of high frequencies preceding low frequencies, or vice versa. Adjacent ridges sometimes occur with slopes of opposite sign. However, it is common to find periods of up to about one hour in which many successive fluctuations are all inclined in the same sense. Cases are also observed in which the magnitude and sign of the slope in a sequence of ridges appear to change gradually with time. Such changes can show a distinct periodicity of some 5–10 min periods.

It has been found that ridges recorded during the daytime (summer observations) typically show much greater slopes than those recorded during the night (winter observations). Figs. 5(a) and 6 are characteristic of "night" and "day" records respectively. The statistics of this diurnal or seasonal variation will be considered in Section 5.

To investigate the cause of slope in ridge patterns, use was made of the special set of observations in which the *spectrum* was recorded simultaneously at each of the three spaced aerials. It was found that the three spectra were normally similar, the systematic time delays between the same frequency at different positions being independent of the frequency. Evidently the frequencies are dispersed across the ground in the nature of a rainbow, and the whole pattern drifts coherently past the aerials. The phenomenon is attributed to dispersion by horizontal gradients of electron content in the ionosphere which act like huge prisms.

The regions of the ionosphere responsible for the dispersion are not necessarily the same as those responsible for focusing. We shall attempt to resolve this problem in subsequent papers.

3.3. *Fine structure in individual ridges*

At times of intense fluctuation a variety of ridge pattern sometimes occurs in which the time profile is split into a fine structure, showing a small number of

closely spaced maxima. One of the fluctuations in Fig. 3 shows this effect. A more striking example is the 1-hour record reproduced in Fig. 5(b). The multiple bands in any one ridge are seen to be approximately parallel, but with a tendency to converge towards the lower frequencies. The subsidiary bands do not necessarily extend over the whole observed range, and tend to be more numerous at the lower frequencies. It will be shown in a subsequent paper that regular fine structure in the pattern on the ground can be naturally explained in terms of diffraction and refraction by an ionospheric lens whose plane of best focus lies above the ground.

3.4. *Interference effects: the ribbed pattern*

Figs. 7(a–d) show examples of a "ribbed"-type pattern sometimes recorded at times of intense fluctuation. The pattern is characterized by a close group of approximately equally spaced maxima of small amplitude running across the spectral record, approximately parallel to one another but inclined to the frequency axis. The single-frequency profiles appear roughly sinusoidal. Ribbed patterns often seem to occur in pairs, the members of each pair having opposite slopes. Each group may contain as many as thirty ribs and last for several minutes. The ribbed patterns are usually mingled with ordinary ridge-type fluctuations, and it has been noticed that their presence is often accompanied by ridges of high dispersion or by a sudden change in the dispersive slope of successive ridges.

Records containing ribbed patterns may be highly complex. Cases such as Fig. 7(c) occur in which two ribbed patterns of different slopes are superposed.

On two occasions, both during calm periods, a variety of ribbed pattern has been recorded in which the time scale is considerably extended. In the example shown in Fig. 7(e) the ribs are separated by up to 1 minute and the pattern persists for over 10 minutes. In this case the ribs converge acutely towards the low-frequency edge.

Ribbed patterns are believed to arise when rays pass through a region of the ionosphere in which the large-scale horizontal gradient of ionization changes abruptly. Rays passing through the two gradients are bent towards each other and interfere. An optical analogy may be found in the Fresnel Biprism.

3.5. *Systematic and random effects*

An important feature of the spectral observations is their power to distinguish readily between "systematic" effects due to a single refracting element in the ionosphere (or a small number of such elements) and "random" effects due to the resultant of a large number of irregular elements. By a single element we mean an area of the ionosphere over which the refractive index in the line of sight varies in a regular manner (e.g., one having a single maximum value, acting like a single lens). When the received radiation is due predominantly to rays passing through a single element, variation of the frequency causes the phase along all rays to vary in a consistent fashion; hence the resultant pattern on the ground will show a systematic variation with frequency, and the dynamic spectrum will consist of a systematic pattern over the entire spectrum.

VOL.
8
1956

AUST. J. PHYS. 1958 1956

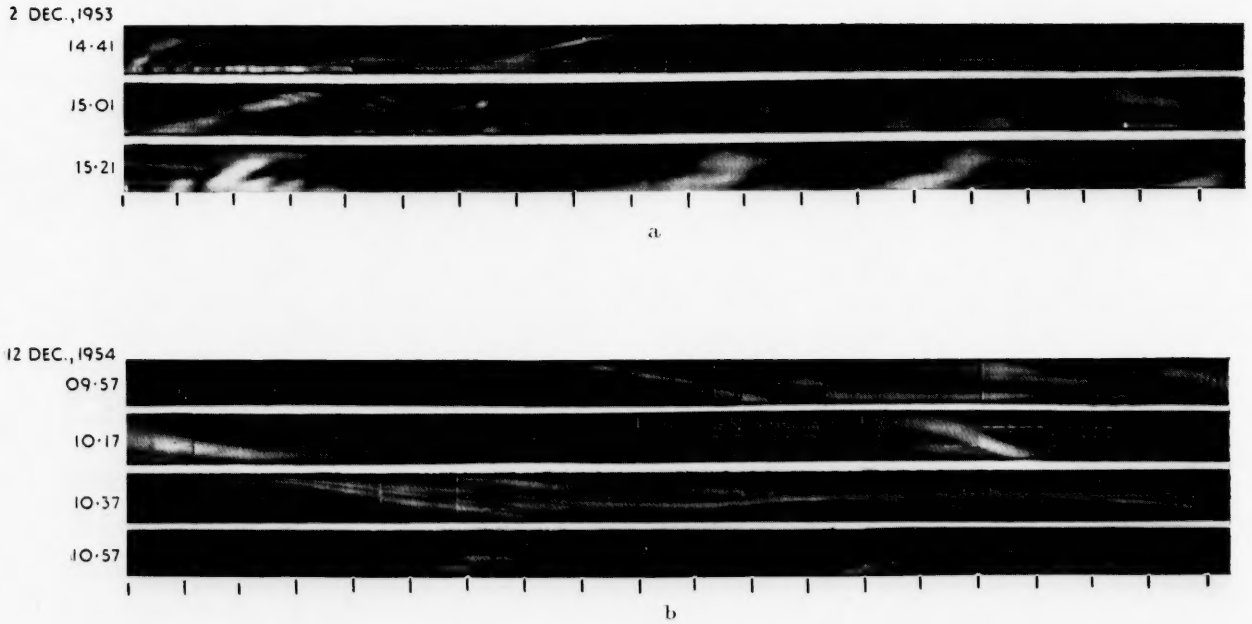

Fig. 6. Dynamic spectra of scintillations showing pronounced frequency dispersion. These are typical of many records obtained during daytime (summer observations). Frequency increases vertically from 40 to 70 Mc/s, time horizontally (one-minute marks shown). Times are in E.A.S.T.

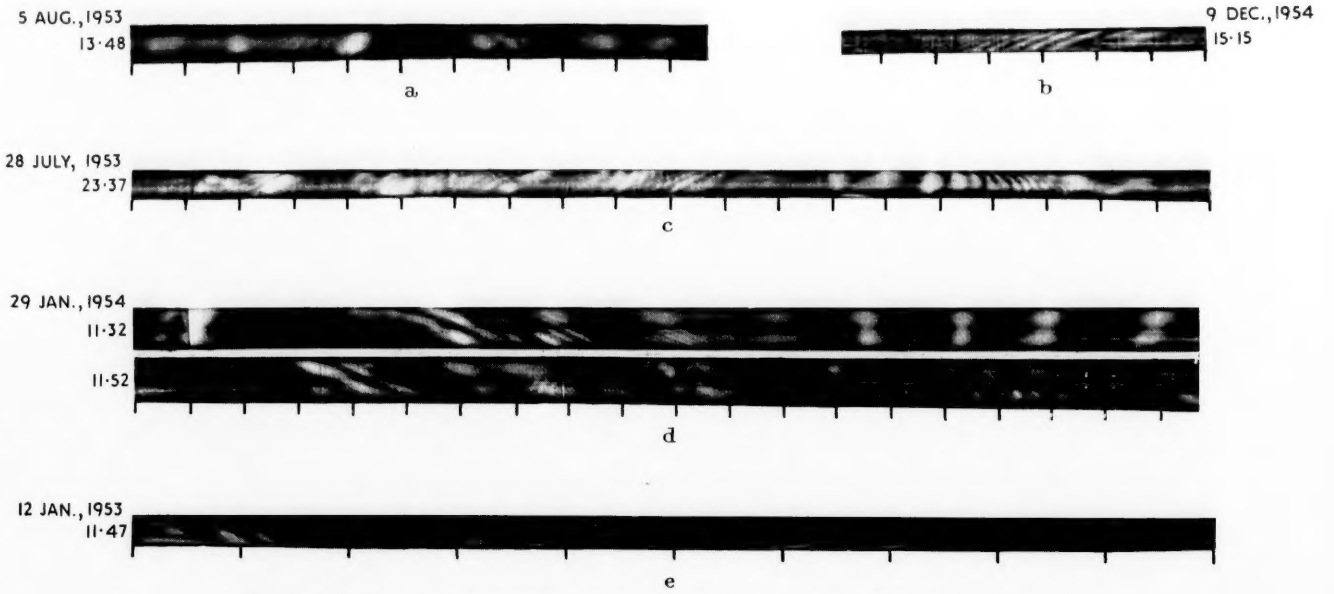

Fig. 7. Dynamic spectra showing examples of "ribbed" patterns, believed due to interference from two waves refracted from different gradients in the ionosphere. See also Fig. 6(a). Frequency increases vertically from 40 to 70 Mc/s, time horizontally (one-minute marks shown. Times are in E.A.S.T.

VOL.
8
1956

AUSTRALIAN J. PHYS. 1956 9

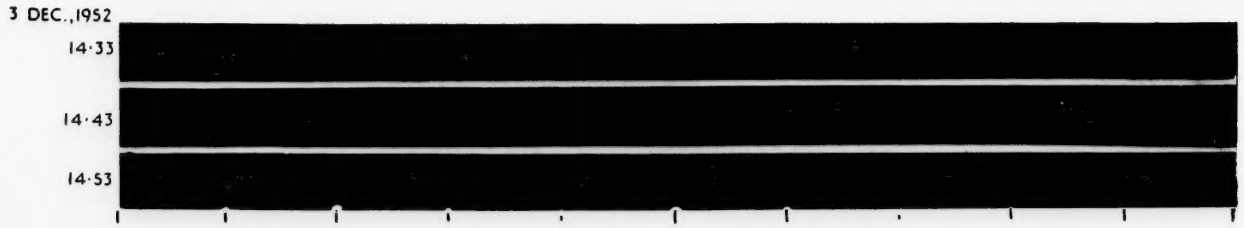

Fig. 8. An example of a dynamic spectrum record in which systematic features are largely obscured by random effects. Frequency increases vertically from 40 to 70 Mc/s, time horizontally (one-minute marks shown). Times are in E.A.S.T.

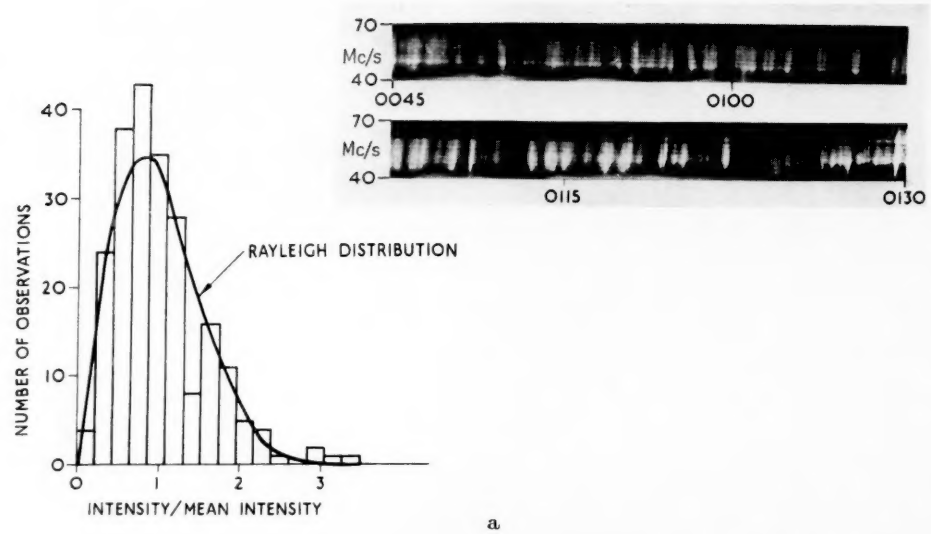

a

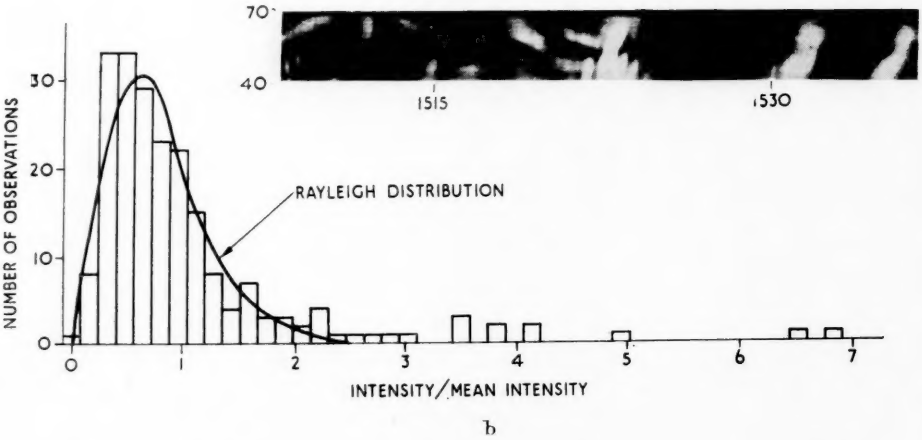

b

Fig. 9. Amplitude distributions of ridge-type records. (a) 7 July 1953: 0045–0130 E.A.S.T. (b) 2 December 1953: 1508–1536 E.A.S.T. The insets show the spectral records on a compressed time-scale.

VOL.
8
1956

Now the condition that an irregular screen will behave like a series of individual lenses is just that the scale-size of the finest structure of the screen exceeds the size of the first Fresnel zone (LITTLE, 1951). Thus, when this condition is satisfied, the pattern in the time-frequency plane will vary systematically from the highest frequencies down to the frequency at which the first Fresnel zone becomes comparable with the finest structure of the refracting regions in the ionosphere. At much lower frequencies, where contributions are received from many refracting elements, the amplitude at each point on the ground results from a large number of waves of random phase; in this case a small fractional change in frequency is sufficient to yield an unrelated pattern on the ground (LITTLE, 1951). The dynamic spectrum then shows a type of pattern containing narrow-band features disposed randomly in the time-frequency plane.

Examination of the actual records shows that the great majority are dominated by systematic features. However, in certain cases, such as Fig. 8, random effects are prominent throughout the observed range, thus indicating the presence of abnormally fine structure in the ionosphere on these occasions.

If the height of the irregular refracting regions is known, it is possible to estimate a lower limit for the scale size of structure responsible for systematic patterns, and an upper limit for random patterns. Thus, assuming a height of 400 km, the slant distance at 15° altitude is about 1200 km, and the diameter of the first Fresnel zone at this distance is 2·3 km at 70 Mc/s and 3 km at 40 Mc/s. This gives a lower limit of 3 km for the scale-size of structure responsible for spectral patterns which are systematic over the observed range, and an upper limit of 2·3 km for the fine structure responsible for random effects.

These arguments bearing on scale-size will be pursued in greater detail in subsequent papers.

While dynamic spectra appear to provide the best available means of distinguishing between random and systematic effects, it is of interest to note that a possible test for randomness is provided by determining the probability distribution of amplitude of a single-frequency record. If the amplitude results from the addition of a large number of waves of approximately equal amplitude and random phase, the distribution of amplitude at equal intervals of time should show a Rayleigh distribution (RAYLEIGH, 1880). This test was performed on two good examples of the systematic ridge-type records. In one case (Fig. 9(a)) the amplitude distribution approximated to a Rayleigh distribution, despite the systematic spectral features; in the second case (Fig. 9(b)) for which the ridges were particularly intense, the distribution approximated to a Rayleigh distribution except that some very high values, several times the mean, occurred with a frequency far beyond the statistical accommodation of the Rayleigh distribution. It is clear that while this test may in some cases indicate the non-random character of a record, a good fit does not necessarily indicate randomness in the sense defined above.

4. The Size, Shape, and Motion of the Pattern on the Ground

In this section we consider the use of spaced-receiver observations at 45 Mc/s to study the size, shape, and motion of the pattern on the ground.

A typical set of spaced-receiver records is shown in Fig. 3. In this case it is seen

that the records for all three aerials are very similar in shape but displaced in time. The time displacement between records A and B is much less than that between B and C, and at any one time the intensities at aerials A and B are approximately equal, while that at aerial C is often quite different. Since the aerials are approximately equidistant, these conditions indicate that the instantaneous pattern on the ground was anisotropic, being elongated approximately along the axis AB. This property of anisotropy appears to be a commonly occurring characteristic, especially for ridge-type records.

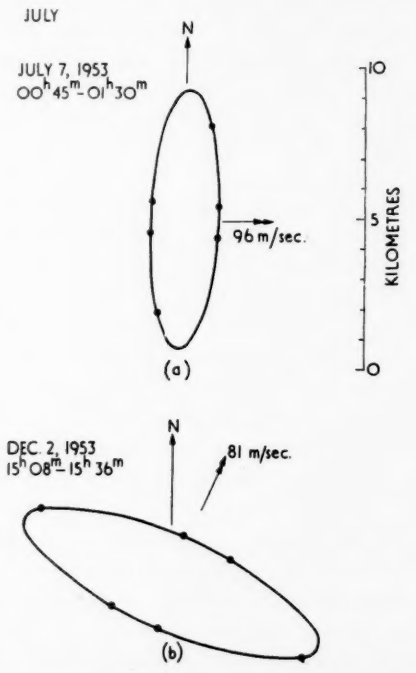

Fig. 10. Showing the size and shape of the pattern on the ground for ridge-type scintillations. These "ellipses of scale-size" are obtained by cross-correlating records taken at the three aerials of the spaced-aerial system.

To obtain a quantitative estimate of the mean shape and scale-size of the pattern on the ground, we first compute the three cross-correlation coefficients between the records, taken in pairs. Then by making plausible assumptions regarding the shape and spacing of isophotes of the pattern on the ground, these coefficients are used to derive uniquely an equivalent ellipse of scale-size. Such an ellipse represents the minimum distance between points on the ground at which the intensity becomes uncorrelated for different directions. The detailed procedure of deriving these ellipses is described in the Appendix.

Fig. 10 shows equivalent ellipses computed for two records, both consisting of a series of intense ridges. In both cases it was established that the records remained statistically constant throughout their length by dividing them into small sections,

VOL. 8 1956

and demonstrating that the cross-correlation coefficients remained approximately constant from section to section.

The ellipses are seen to be highly eccentric, the major and minor axes being about 10 km and 3 km respectively. In case (a), a winter-night record, the major axis runs nearly N–S; in (b) a summer-day record, roughly E–W. In Section 5 it will be shown that the N–S elongation appears to be a normal feature of winter nights, while on summer days the elongation shows no fixed orientation.

It is possible that N–S elongations result merely from oblique projection on the ground of a circular cone of rays: at an altitude of 15° the ratio of major and minor axes would then be nearly 4. Such an effect would occur when the focusing irregularities were quasi-spherical in shape rather than horizontal strata. However, no such effect can explain E–W elongations. The observation of the latter seems to be a definite indication that the irregularities are both stratified and elongated in these cases.

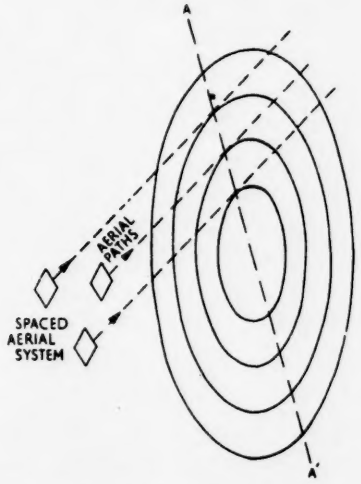

Fig. 11. Showing the relative motion of the spaced-aerial system and a scintillation ground pattern with elliptical contours. The apparent motion deduced from time delays is normal to the *apparent ridge line AA'*. This is seen to differ from the direction of motion.

It is of interest to note that the apparent drift velocities, calculated from the relative time delays, are directed almost exactly along the minor axis in both cases. The significance of this result will be discussed below.

4.1. *The significance of derived velocities*

The result that ridge patterns on the ground may be highly elongated affects the interpretation of the velocity calculated from the time delays between peaks received at the three aerials. This may be demonstrated by considering the simple case (Fig. 11) of a stable elliptical pattern drifting with constant velocity across the spaced aerial system whose spacings are small compared with the overall length of the pattern. It is convenient to use the frame of reference in which the pattern is stationary and the aerials drift along parallel paths (shown dotted in the

figure). The peak intensity at each aerial occurs at the point of contact between this path and the elliptical contour of the pattern which touches it. Such points lie on a straight line AA', referred to as the "apparent ridge line." The velocity component normal to this line is calculated simply from the geometry of the aerial system. However, the velocity component parallel to this line is indeterminate. *Hence for an elongated pattern the velocity calculated from the time delays refers not to the velocity of drift but merely to the component normal to the apparent ridge line.*

When the pattern is highly elongated, the apparent ridge line is only slightly inclined to the axis of elongation for a wide range of directions of motion. Thus the calculated direction of motion usually gives a good indication of the orientation of the pattern. This conclusion is consistent with the results of Fig. 10.

These qualifications appear to have been overlooked by previous investigators of ionospheric "winds" by the scintillation method.*

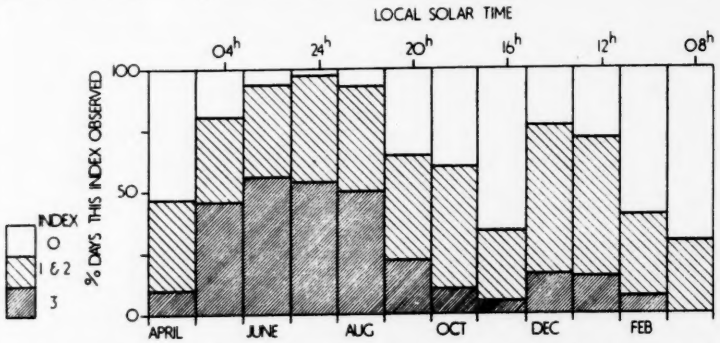

Fig. 12. The annual variation of the fluctuation index. Observing period: September 1952 to February 1955.

5. Quantitative Measurements and Diurnal (or Seasonal) Variations

In previous sections the qualitative features of the fluctuation records have been described, and the methods of measuring the characteristics of the pattern on the ground have been discussed. The present section is devoted to more quantitative aspects, including a discussion of the variation throughout the year of the various properties of the fluctuations.

These observed annual variations may be due to a genuine *seasonal* change in the ionosphere. But, because the solar time of transit of the source varies throughout the year, the changes could be due to a purely *diurnal* variation. With the present series of observations it is not possible to separate these effects, and accordingly we have shown the variations on a scale of local time of transit, as well as a scale of months.

5.1. *The fluctuation index*

The degree of fluctuation was found to change quite abruptly from day to day, or even within one observing period. Besides such short-term variations, there

* The anisotropy of ionospheric diffraction patterns has now been recognized by other workers. See the Report of the Physical Society Conference on the Physics of the Ionosphere held at the Cavendish Laboratory, Cambridge, September 1954 (London: Physical Society, 1955), especially pages 127 and 167.

VOL. 8 1956

was, however, a marked trend throughout the year. To study this variation a (subjective) *fluctuation index* was assigned to each spectral record, the index taking the values 0 (no fluctuations), 1, 2, or 3, according to the intensity and prevalence of fluctuations.

Fig. 12 shows the variation of this index throughout the year. There are two distinct maxima: the larger and broader peak occurs when observations are made near the middle of the night (winter), and the smaller and narrower peak for

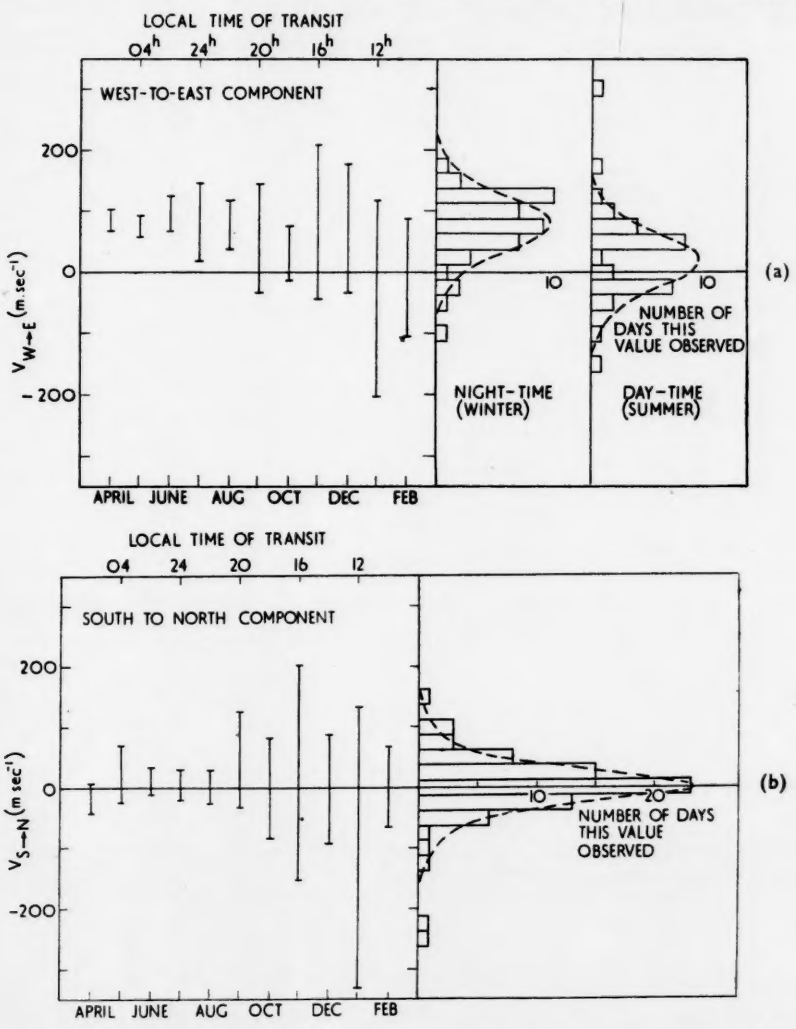

Fig. 13. The annual variation of (a) the west-to-east, and (b) the south-to-north components of the velocity across the ground. For each month a vertical line is centred on the mean of the daily values, the length of the line being twice the standard deviation shown by the daily values. Data: June 1953–February 1955. At the right are shown histograms of the daily values for the same period: the broken curves are symmetric distributions which approximate to the histograms. In the case of the west-to-east component separate histograms are given for the daytime and night-time observations.

observations near midday (summer). The existence of these two maxima is in agreement with other observations at this latitude (BOLTON, SLEE, and STANLEY, 1953). It differs from observations in England (HEWISH, 1952), which reveal the scintillations as a night-time phenomenon having a single (diurnal) maximum near local midnight.

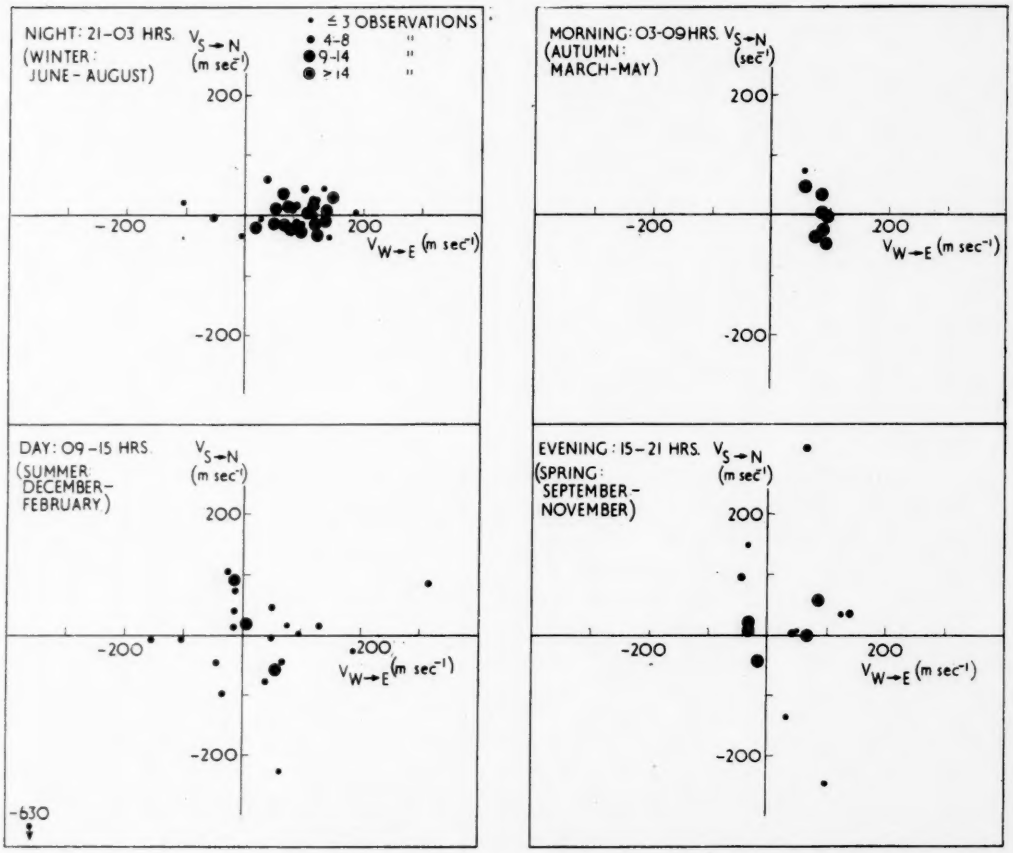

Fig. 14. Vectorial plots showing daily means of the velocity of the pattern across the ground for the four quarters of the year. Data: June 1953–February 1955. The size of the dot indicates the number of fluctuations used in assessing the daily mean velocity.

5.2. *The velocity and orientation of the pattern on the ground*

A daily value for the apparent velocity of the pattern across the ground was determined by averaging the velocities on the day in question for every clear-cut fluctuation having a similar form at each of the three aerials. In Fig. 13 the monthly means of these daily values are indicated by vertical lines, centred on the mean, and of length equal to twice the standard deviation of the daily values. Also included in Fig. 13 are histograms showing the distribution of the daily

values of the west-to-east and south-to-north components. Fig. 14 further illustrates the variation of the velocities throughout the year. Here a vector diagram of the daily values has been plotted for each of the four quarters of the year. On the diurnal scale these quarters correspond to night, morning, day, and evening periods.

Although the figures do not show the regular variation of apparent motion described by observers in England (MAXWELL, and DAGG, 1954), they do reveal significant differences between the daytime (summer) and night-time (winter) velocities. The night-time values have a relatively low dispersion, and are clustered around a prevailing west-to-east motion of about 80 msec^{-1}; in the daytime the values show a very wide dispersion and the mean west-to-east component is considerably lower. There does not appear to be a prevailing south-to-north component at any season: the histogram shows the south-to-north values as distributed symmetrically about zero.

The rotation of the earth contributes a steady west-to-east component of motion whose magnitude depends on the height of the irregularities. Our discussion of the region of origin of the scintillations will be given in a later paper, but we may note here that a strong correlation of night-time scintillations with spread *F* has been found, implying that these irregularities are located in the upper *F*-region. There is weaker evidence suggesting that the daytime scintillations are associated with sporadic *E*.

For irregularities at a height of 400 km (upper *F*-region), the west-to-east component contributed by the earth's rotation amounts to 65 msec^{-1}, and so accounts for most of the observed night-time mean of 80 msec^{-1} (see the histogram of Fig. 13(a)). This implies that the night-time irregularities in the upper *F*-region at these latitudes do not have any prevailing proper motion greater than about 20 msec^{-1}. A similar conclusion applies to the daytime irregularities: if these are located in the *E*-layer, the effect of the earth's rotation would account for the observed mean motion of 20 msec^{-1}, and would imply that any prevailing proper motion of the *E*-region irregularities was small.

Conversely, if the prevailing motions are attributed entirely to the rotation of the earth, then we may use them to estimate the heights of the layers. From the histograms in Fig. 13(a) we infer a (vertical) height of 500 km at night (winter) and about 100 km by day (summer).

5.3. *The size of the pattern on the ground*

The time-scale of variation of fluctuation records has been assessed by measuring the overall duration (at 45 Mc/s) of those fluctuations used for determining the velocity of the pattern. Fig. 15(a) shows a scatter diagram of the duration of fluctuations *versus* the inverse of the speed of the pattern across the ground. These quantities, rather than their reciprocals, were chosen for plotting so as to give weight to the longer durations and time delays which are the more accurately determined values. The correlation between the duration of the fluctuations and the inverse of the speed is in fair agreement with the correlation found by other observers between the *rate* of fluctuations and the speed (LITTLE and MAXWELL, 1952; HEWISH 1952).

For elongated fluctuations the product of the measured speed and the duration is an approximate measure of the *width* of the fluctuation in the direction of its minor axis (cf. Section 4.1). Thus, in the scatter diagram, points corresponding to fluctuations of a given width lie along a straight line through the origin. Fig. 15(a) shows that at 45 Mc/s this width lies between 1·5 and 8 km.

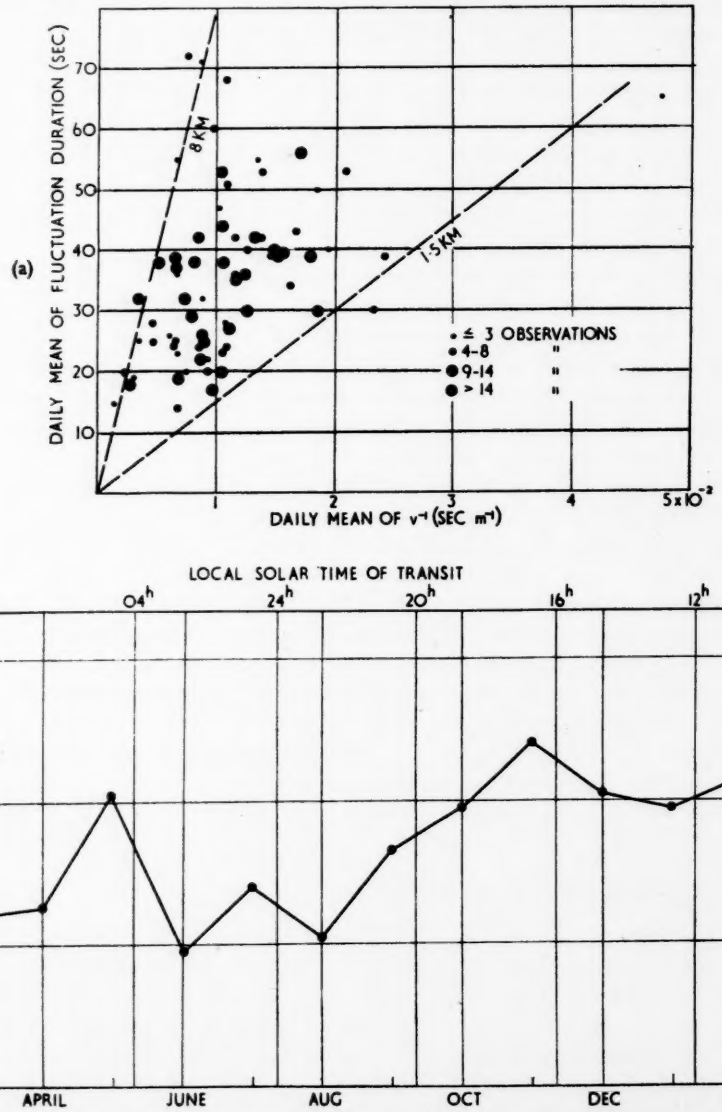

Fig. 15. (a) Correlation of the duration of fluctuations with v^{-1}, the inverse of the speed of the pattern across the ground. Daily mean values. Data: June 1953–February 1955. (b) The annual variation of the width of the pattern on the ground at 45 Mc/s. The ordinate is $\overline{t/v^{-1}}$, where t is the duration of the fluctuation and v the speed across the ground. The bars denote monthly means of daily mean values.

VOL. 8 1956

The annual variation of the size of the pattern on the ground is shown in Fig. 15(b). The daytime (summer) fluctuations appear to be wider than the night-time (winter) fluctuations, the size in daytime being about 4 km compared with 2 km at night. There is a suggestion of a subsiduary maximum of about 4 km near 0400 h (May).

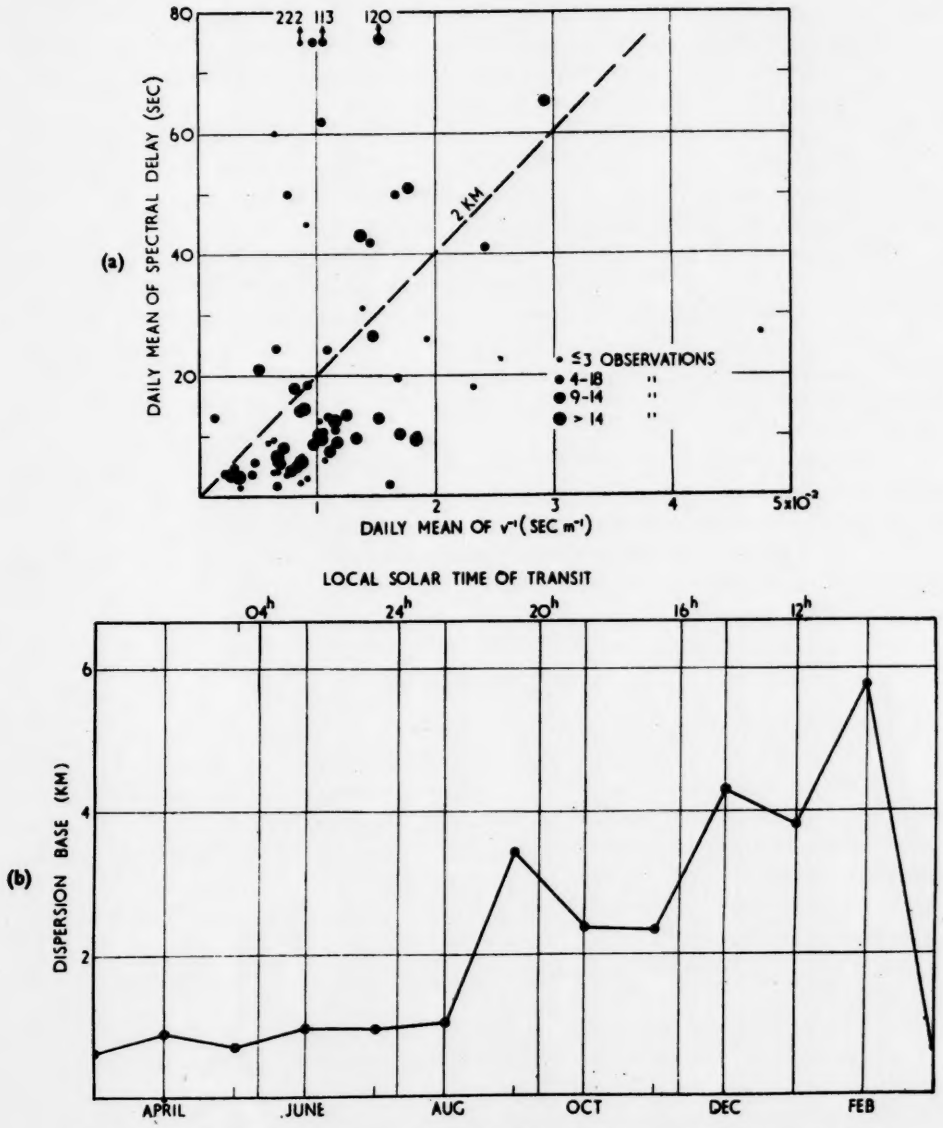

Fig. 16 (a) Correlation of the spectral delay with v^{-1}, the inverse of the speed of the pattern across the ground. Daily mean values. Data: June 1953–February 1955. (b) The annual variation of the dispersion base. Monthly means are defined as for Fig. 15(b)

5.4. *The frequency dispersion*

The dispersion in ridge-type records (Section 3.2) is measured directly by the *spectral delay* of the intensity maximum at 70 Mc/s relative to that at 40 Mc/s. However, a more fundamental measure is provided by the 40–70-*Mc/s dispersion base*, defined as the product of the measured speed and the modulus of the spectral delay. The dispersion base is thus the distance on the ground between the maxima of the 40-Mc/s and 70-Mc/s patterns, the distance being measured along the direction of apparent motion. When the height of the dispersing layer (and of the focusing layer) is known, the magnitude of the ionization gradients responsible for the dispersion may be inferred from this quantity.

Fig. 16(a) is a scatter diagram in which daily means of the modulus of the spectral delay are plotted against the daily mean of the inverse of the speed. As might be anticipated, there is no marked correlation. All that can be said is that the dispersion base (40–70 Mc/s) is usually less than 2 km.

The magnitude of the dispersion changes markedly throughout the year, as is shown in Fig. 16(b). During the night-time (winter months) the dispersion base is small and constant at about 1 km, but it rises sharply to between 4 and 6 km during the daytime (summer). This daytime increase in the dispersion base reflects the incidence of the characteristic type of record in which very long spectral delays are associated with ribbed structure (cf. Section 3.4 and Fig. 6).

A probable explanation of this increase in dispersion is found in the known increase in ionospheric ionization during the daylight hours. For both the *E*- and *F*-regions, the daytime values of the density of ionization, and also of the total electron content, are far in excess of the night-time values (MITRA, 1947; RATCLIFFE, 1951). Under such conditions it seems likely that ionization gradients would also be increased.

VOL. 8 1956

6. CONCLUSIONS

The conclusions of this paper may be summarized as follows.

(1) Observations of dynamic spectra indicate that the commonest type of fluctuation is produced by the focusing effect of a single ionospheric irregularity. Other types, having the appearance of interference phenomena, are believed to result from two irregularities. Occasionally, pronounced random effects indicate contributions from a large number of irregularities.

(2) The "focused" pattern is often dispersed across the ground like a rainbow. This effect is attributed to large-scale gradients in the ionosphere, but it is not yet known whether the focusing and dispersing effects occur in the same part of the ionosphere.

(3) The pattern on the ground is usually highly elongated. This complicates the determination of its motion. In some cases the elongation may be due merely to oblique projection on the ground; in others, it is an unambiguous indication of anistropy in the structure of the focusing region.

(4) The degree of fluctuation shows a marked diurnal or annual variation, exhibiting maxima near midnight (winter observations) and midday (summer

observations). Dynamic spectra and other properties change their character between the night and day observing periods.

Quantitative aspects are summarized in Table 1.

Acknowledgements—The authors are indebted to J. D. MURRAY and W. C. ROWE for valuable contributions in both instrumental and observational phases of this work, and to J. JOISCE, M. KOMESAROFF, and G. SWARUP for assistance in taking the observations. The authors also wish to thank Dr. J. L. PAWSEY, F.R.S., for his interest in this work, and his enthusiasm in presenting preliminary accounts of it at overseas conferences during 1954.

Table 1. *Summary of the characteristics of the pattern on the ground. Brackets are used to indicate less reliable values*

Observing period / *Characteristic*	*Night-time (winter)*	*Daytime (summer)*
Width	1–6 km	2–9 km
Spacing	(3–10 km)	(5–20 km)
Elongation	3 or 4 to 1	3 or 4 to 1
Orientation	Mostly N–S	Variable
Dispersion base (40–70 Mc/s)	0–2 km	0–10 km
Apparent motion	Predominantly west to east Mean speed 80 m sec^{-1}	Variable

APPENDIX

Derivation of equivalent ellipses of scale size (see Section 4)

The complete determination of the spatial distribution of intensity in the scintillation pattern on the ground requires simultaneous observations at a large number of points on the ground. However, if certain assumptions are made, it is possible to specify the mean orientation and degree of elongation of the pattern from observations at only three points. For this purpose we shall assume that the pattern consists of a distribution of discrete "bright" patches whose intensity profiles in any direction conform to a particular idealized shape of a kind suggested by actual single-frequency records of ridge patterns. No restriction is placed on the scale-size of such profiles, which may vary systematically with direction. It will be shown that, when such a pattern moves across the three triangularly spaced aerials A, B, and C, the intensity time records can be used to compute the mean scale size in the three directions $\vec{AB}$, $\vec{BC}$, and $\vec{CA}$. These values allow us to draw an equivalent ellipse of scale-size.

It is convenient to specify scale-size in a given direction in terms of the instantaneous spatial auto-correlation function, defined by

$$\rho_s(x, \theta) = \frac{\overline{I(x')I(x' - x)}}{\{\overline{I(x')}\}^2}$$

where x and x' are independent measures of distance along a line inclined at the azimuth angle θ, $I(x')$ denotes the intensity at x', and the bars indicate averages over all x'. The smallest value of x at which ρ_s falls to zero will be referred to as the *scale-size*, $X(\theta)$.

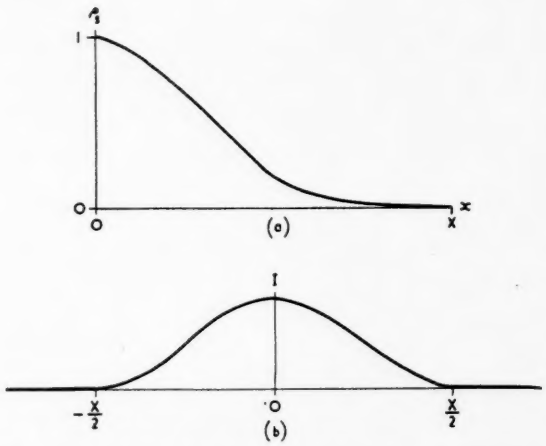

Fig. 17. The autocorrelation function, (a), of the assumed intensity profile, (b).

We shall here assume ρ_s to have the shape shown in Fig. 17(a). This is actually the autocorrelogram of the idealized profile shown in Fig. 17(b), which is merely one cycle of a sine wave.

To determine the value, $X(\overrightarrow{AB})$, of the scale-size in the direction $\overrightarrow{AB}$, we first compute the *temporal* cross-correlation coefficient (for zero-time displacement) of records A and B. This coefficient is defined by

$$\rho_t(x_1, \theta_1) = \frac{\overline{I_A(t)I_B(t)}}{[\{\overline{I_A(t)}\}^2 \{\overline{I_B(t)}\}^2]^{1/2}}$$

where (x_1, θ_1) denotes the vector $\overrightarrow{AB}$, $I_A(t)$ and $I_B(t)$ denote the intensity recorded at time t at aerials A and B respectively, and the bars indicate time averages.

The statistical properties of the moving spatial pattern are taken to be independent of time. It follows that the products $I_A(t)I_B(t)$ of simultaneous intensities at aerials A and B for a large number of times give a representative sample of values of $I(x')I(x' - x_1)$ where x' and x_1 are measured in the direction (θ_1) of $\overrightarrow{AB}$.

VOL. 8 1956

Hence

$$\rho_t(x_1, \theta_1) = \rho_s(x_1, \theta_1).$$

Having thus determined experimentally one point on the spatial autocorrelogram (Fig. 17(a)), the value of the scale size $X(\theta_1)$ is uniquely set.

The above procedure is repeated for the directions of $\overrightarrow{BC}$ and $\overrightarrow{CA}$ and the equivalent ellipse $X(\theta)$ constructed.

References

Bolton, J. G., Slee, O. B., and Stanley, G. J.	1953	*Aust. J. Phys.* **6,** 434
Bruce, E., Beck, A. C., and Lowry, L. R.	1935	*Proc. I.R.E.* **23,** 24
Hewish, A.	1952	*Proc. Roy. Soc.* **A214,** 494
Little, C. G.	1951	*M.N.R.A.S.* **111,** 289
Little, C. G., and Maxwell, A.	1951	*Phil. Mag.* **42,** 267
Little, C. G., and Maxwell, A.	1952	*J. Atmosph. Terr. Phys.* **2,** 356
Little, A. G., and Payne-Scott, Ruby	1951	*Aust. J. Sci. Res.* **A4,** 489
Maxwell, A., and Dagg, M.	1954	*Phil. Mag.* **45,** 551
Mills, B. Y., and Thomas, A. B.	1951	*Aust. J. Sci. Res.* **A4,** 158
Mitra, S. K.	1947	*The Upper Atmosphere* (India: Royal Asiatic Society of Bengal)
Ratcliffe, J. A.	1951	*J. Geophys. Res.* **56,** 487
Rayleigh, Lord	1880	*Phil. Mag.* **10,** 73
Ryle, M., and Hewish, A.	1950	*M.N.R.A.S.* **110,** 381
Wild, J. P., and McCready, L. L.	1950	*Aust. J. Sci. Res.* **A3,** 387
Wild, J. P., Murray, J. D., and Rowe, W. C.	1954	*Aust. J. Phys.* **7,** 439

Journal of Atmospheric and Terrestrial Physics, 1956, Vol. 8, pp. 76 to 82. Pergamon Press Ltd., London

Radar-echo duration and height of a Perseid meteor

D. W. R. McKinley
National Research Council, Ottawa, Canada

(*Received* 27 *June* 1955; *in revised form* 12 *September* 1955)

ABSTRACT

Three-station radar observations of an unusual Perseid meteor echo have yielded a height-duration profile of the echo components, with an overall duration of 549 sec. The main part of the enduring echo, at a mean height of 91 km, drifted in an easterly direction at a rate of 119 m/sec. The meteoric velocity and deceleration are discussed briefly. Of special interest is the appearance of diffuse echo components which have been due either to direct reflections from meteoric ionization created over the height range 130–160 km, or to ground scatter via the main part of the meteoric ionization.

In a recent paper (McKinley, 1955) it was suggested that a useful study might be made of the variation of meteor echo duration as a function of height, using specific examples of echoes from large meteors which have been shown to have little or none of the aspect sensitivity of the usual diffraction echoes obtained from the smaller meteors Fig. 1 shows a portion of the range-time record of a radar echo from a Perseid meteor observed at Ottawa at 18 h 44 m 4·95 s E.S.T., 12 August 1948. This echo was observed also at Arnprior and Carleton Place, hence accurate triangulation data are available. A preliminary analysis of this echo was made some time ago, and the reader may refer to Fig. 6 of Millman (1950) for the three station records of the main part only of the echo. The parameters of the three radar equipments are listed in Table 1 of McKinley and Millman (1949). (In this table there is a typographical error; the longitude of the Ottawa station is 75° 38′ 05″, not 75° 36′ 05″.)

Although it was not observed visually this meteor was unquestionably a very bright one, because the main part of the echo lasted for 549 sec at Ottawa, and for 532 sec at both Arnprior and Carleton Place The weaker and diffuse echoes appearing on Fig. 1 at ranges from 185 to 280 km, and with durations up to 158 sec, were also caused by this meteor, though it is uncertain whether they were direct echoes from actual clouds of ionization created earlier on the meteor trail, or reflections from the ground via the strong meteoric ionization at short range. This point will be discussed in more detail later. For the present it may be noted that these long-range diffuse echoes could not be a consequence of the *F*-type echo which appeared at 18 h 43 m 50 s at a range of 213 km This *F*-type echo was recorded at all three stations, and was shown by triangulation to have occurred about 195 km west of Ottawa and at a height of 86 km. (See Fig. 2,)

Determination of the Meteor Path

Our timing and recording techniques prior to 1949 were not very satisfactory for the measurement of velocity and deceleration along the meteor path. In this particular instance, though, the presence of a local thunderstorm was of considerable benefit inasmuch as the electrical noise from the lightning flashes appeared on the records of all three stations (note the vertical streaks and bands in Fig. 1),

VOL.
8
1956

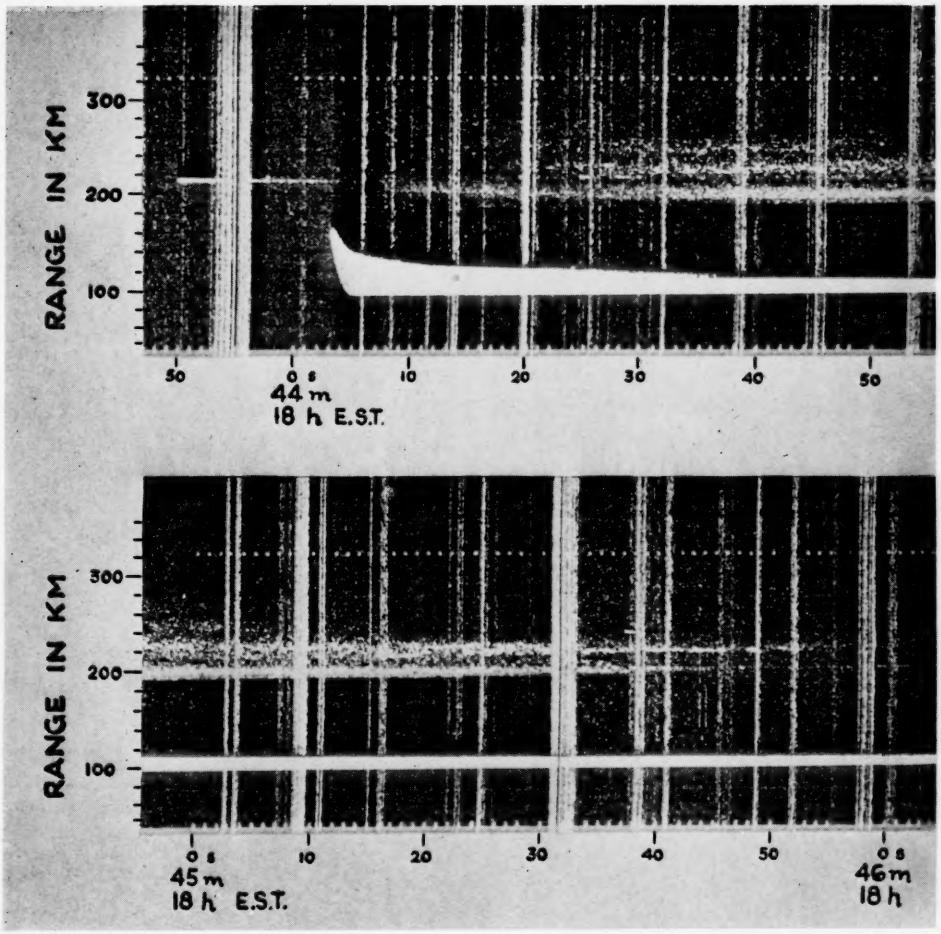

Fig. 1. Ottawa range-time record of a Perseid meteor echo at 18 h 44 m E.S.T. 12 August 1948, showing diffuse ionization at longer ranges than the main part of the echo. The first two minutes only are shown—the echo lasted for 9 m 9 s.

VOL.
8
1956

thus fixing the time on each record with much greater accuracy than could be obtained from the radio time signals, which were jittering considerably. Each station record was reduced independently, following the methods described in McKinley and Millman (1949). For the part of the path that was observed in common at all three stations (between $t = 3{\cdot}9$ s and $t = 5{\cdot}0$ s) the mean velocity was 55 km/s. The computed values of R_0, the nearest distance to the meteor path, and t_0, the corresponding time, are listed in Table 1. The observed meteor path, ended at about $t = 5{\cdot}0$ s, hence the Carleton Place figures were obtained by extrapolating the range-time data for this station.

The mean velocity measured from the Ottawa record over the time interval $t = 2{\cdot}9$ s, when the h characteristic echo first appeared, to $t = 3{\cdot}9$ s was 60 km/s. The mean deceleration over the terminal part of the path was thus of the order of 5 km/s/s, but the record is not good enough to determine this more accurately.

Table 1

	Ottawa	Arnprior	Carleton Place
R_0 (in km)	95·4	128·1	106·1
t_0 (in sec)	4·95	4·95	5·40

OL.
8
956

Using the elements given in Table 1, the meteor path was computed to have a bearing of 9° from true north and an elevation of 15°. At the time of occurrence of this meteor the bearing and elevation of the mean position of the Perseid radiant at Ottawa were respectively 7·8° and 14·6°, hence one may reasonably assume that the meteor was a Perseid. The projection of the path on the plane through the three observing stations is shown in Fig. 2. The solid portion of the path corresponds to the h-characteristic part of the main echo observed at Ottawa, with a path length of 120 km, and the dashed portion to the part that would be presumed to have yielded the diffuse echoes, on the hypothesis that these echoes were received directly and not by ground reflection. The overall path length would then be 280 km. The triangled points refer to parts of the enduring ionization which were triangulated. The h-characteristic echo was also triangulated, of course, at frequent intervals over the time interval 3·9–5·0 s. The time scale placed on the meteor path assumes that the velocity was 60 km/s prior to $t = 3{\cdot}9$ s and 55 km/s thereafter.

Height and Drift Velocity of the Enduring Ionization

A small separated component of the main echo, visible on the Ottawa record at a range of 114 km, at 18 h 44 m 33 s, was triangulated to yield a height of 102·5 km. (See Fig. 3, which is an enlargement of part of Fig. 2.) This echo appeared to move north-west at a rate of 330 m/s.

The long-enduring part of the main echo has provided the most satisfactory data for wind drift measurements. The triangulations were made at intervals of approximately one minute, and as Fig. 3 shows, the direction of drift was roughly

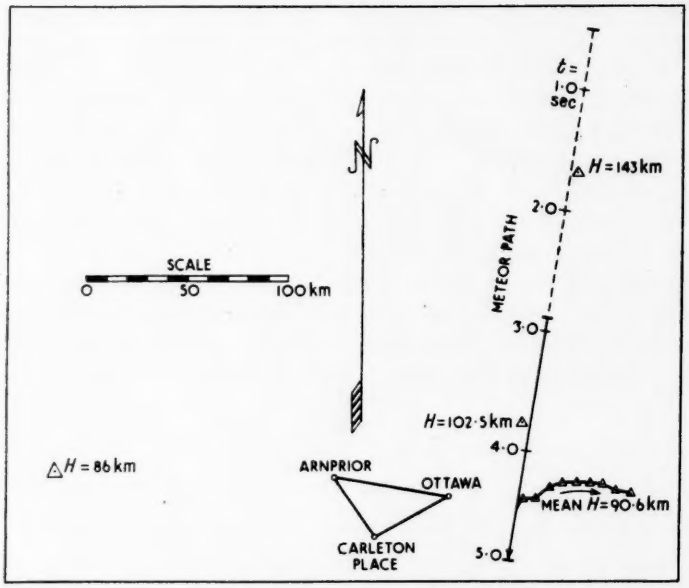

Fig. 2. Projection of the observed meteor path on the plane through the three observing stations. The small triangles indicate triangulated points. The solid line part of the meteor path was observed as a head echo at Ottawa: the latter half of this part was observed at all three stations. The dashed portion is presumed to have yielded the enduring diffuse ionization shown in Fig. 1. A plot of the *F*-type echo (at 18 h 43 m 50 s, Fig. 1) is shown in the lower left-hand corner.

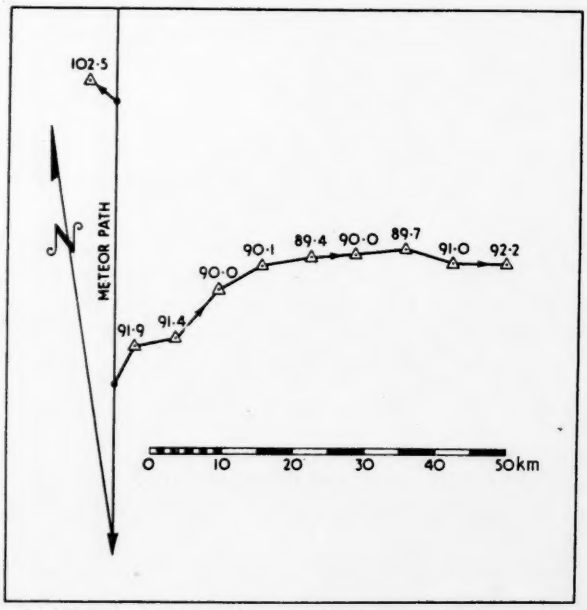

Fig. 3. Details of drifting cloud observations, as projected on the ground plane. Figures are computed heights above sea-level and arrows indicate direction of drift.

VOL. 8 1956

east by north-east for the first four minutes, shifting to almost due east for the remainder of the track. The figures attached to the triangled points are the computed true heights above sea-level. While these figures suggest that the height of the drifting cloud may have varied 1 or 2 km from the mean of 90·6 km, the evidence is inconclusive in view of the average probable height error of ± 1 km at the mean distance of these observations from the centroid of the three-station system. The average horizontal drift velocity, integrated along the path, was 119 m/s.

Fig. 4 shows in outline the true heights of the salient features of the meteoric echo, where each point on the meteor path has been taken as zero reference time for the ionization occurring at that level. The signal strength of the main part of the echo was so great on the Ottawa record that it has completely masked much of the fine detail. However, several components are clearly visible on the Arnprior and Carleton Place records (see Fig. 6 of MILLMAN, 1950) and these have been indicated in cross-hatching on Fig. 4. On the assumption that the long-range echoes of Fig. 1 were due to direct reflection from ionized clouds created by the meteor, the heights of these clouds have been computed from the Ottawa range values and the meteor path position: these heights range from 130 to 160 km, as shown in Fig. 4. The triangled point, with a height of 143 km, represents the one possible three-station height that could be determined. (This point is shown in plan

Table 2

Height spread at zero time	Mean height at half duration time	Duration
86–89 km	90 km	539 s
92–98	93	539
101–104	102	32
109–111	110	6
—	133	158
—	140	137
—	148	70
—	158 (faint)	10

position in Fig. 2.) The true heights, corrected for the earth's curvature, of the more prominent resolvable levels of enhanced ionization, or layers, are given in Table 2. The two lowest components were resolvable on the Carleton Place record for the first half of their durations, but thereafter they were indistinguishable, hence it is not clear which component endured for 539 s, with a terminal height of 92 km. The reality of the last four tabulated heights is in question, of course.

DIRECT ECHO OR GROUND REFLECTION

We have not been able to answer, in an unequivocal manner, the interesting question of whether the long-range diffuse echoes of Fig. 1 are caused by real clouds of ions at the heights indicated in Fig. 4 or by reflections from the terrain transmitted

via the main ionization. The difficulty is that only very faint traces of these diffuse echoes appeared on the Arnprior and Carleton Place records, since for this meteor the effective overall sensitivity of these stations was roughly 15 db below that of the Ottawa station, and therefore the accuracy and validity of three-station triangulations are in considerable doubt. The most likely set of range values has yielded the point shown in Figs. 2 and 4 at a height of 143 km, which would seem to support the direct echo hypothesis. However, because the possible ground reflection points might easily be quite different for the rays traced from each of the stations via the strongly ionized cloud at 91 km, there is no assurance that this triangulated point

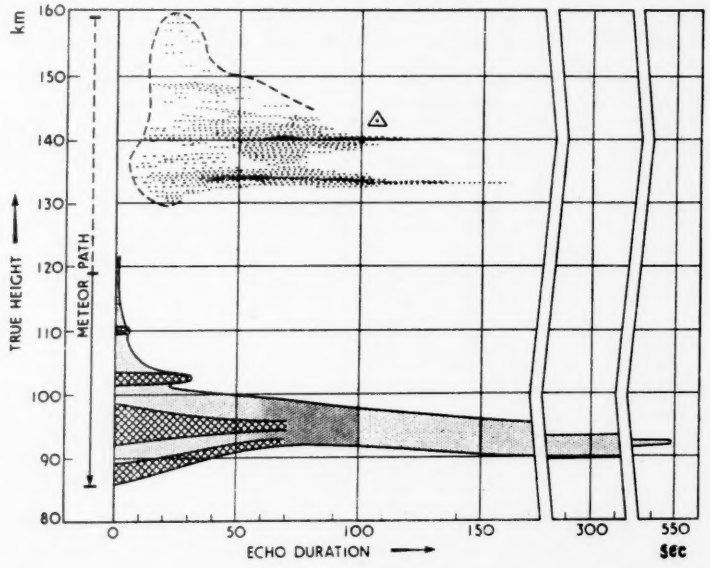

Fig. 4. Profile of echo height versus duration. Cross-hatched portions indicate components which were resolvable only on the Arnprior and Carleton Place records. The components shown above 130 km are plotted on the assumption that these echoes were due to direct reflection.

might not be a virtual image of the ground, although one would tend to expect such images to occur about 150 km south-east of the computed position. From the Ottawa record alone the ranges of the various parts of the diffuse ionization are not inconsistent with the ground reflection hypothesis, provided that oblique scattering from the ground obtains, since normal reflection cannot account for all the observed echo ranges.

We have made an attempt to compute the echo power that would be expected if the diffuse echoes were actually ground reflections. The duration of the main echo was 549 sec, which, when inserted in the theoretical formula for backscatter from a line source of electrons at a height of 91 km (Kaiser, 1953, Greenhow and Neufeld, 1955), yields a line density of 3×10^{17} electrons per metre. The maximum echo power of the main echo may then be computed to be about 10^{-8} watts

VOL.
8
1956

(ESHLEMAN, 1955) which is −80 db relative to 1 watt, or 60 db above the receiver noise level. This is somewhat greater than the observed echo level of 50 db above noise, which cannot be determined directly from the Ottawa record because of the intense receiver saturation, but which may be deduced by noting that the observed power at Arnprior was about 35 db above noise, to which must be added the 15-db difference in effective sensitivity between the Arnprior and Ottawa stations.

For the case where the energy is reflected from the meteor trail to the ground, scattered by the ground, then reflected again by the meteor trail back to the receiver, there will be further attenuation. As a simple model we assume that the trail acts as a coherent line source (though it is hard to believe this will hold true for more than a small fraction of the total time during which the diffuse echoes were observed) and that the heavily-wooded hilly terrain acts as a scatterer rather than as a perfect reflector. Taking 100 km as reasonably appropriate for the meteor-to-ground distance, we find that an additional attenuation of 85 db should occur over the meteor-ground-meteor path. The theoretical value of the received power will then be 25 db below noise, or 40 db below the observed power of the diffuse echoes. This may be regarded as an upper limit to the predicted power. If the meteor trail were not a coherent line source but were more like an irregular cloud, the overall attenuation should be even greater.

On the other hand, the objection that may be raised against the hypothesis that the echoes have been received directly from high-altitude ionized clouds is that the application of current meteor theory to this case predicts the production of unusually high numbers of electrons per metre of path length. For example, we find by extrapolating the adopted diffusion-height curve given by GREENHOW and NEUFELD, 1955, that the diffusion coefficient at 133 km is $2{\cdot}5 \times 10^3$ m²/sec, which, with the observed duration of 158 sec for the component at this height, yields a value of 7×10^{19} electrons/metre for the line density. This is two orders of magnitude greater than the density computed above for the main part of the echo. However, we may compare this with data published on another meteor (Meteor No. 4 of MCKINLEY and MILLMAN, 1953) which had a well documented height of 117 km and a duration of 930 sec. Adopting from GREENHOW and NEUFELD an extrapolated value of 2×10^2 m²/sec for the diffusion coefficient, we find the line density to be 3×10^{19} electrons/metre, which is the same order of magnitude as the present example, and which is equally difficult to accept. It may be that one cannot extrapolate the published diffusion data to heights above 110 km, or that at these heights other factors must be taken into consideration which do not apply in the normal range of meteoric heights,

Whatever the explanation of the diffuse echoes of Fig.1 may be—and we regret we are unable to offer an unassailable one—the observations may possibly be unique in showing either the first published example of ground-scatter received via a meteor trail, or the existence of high-altitude meteoric ionization. We, at least, have found no similar echoes to date in our records. It may require another such rare observation to settle the matter. Both Dr. VON R. ESHLEMAN, of Stanford, and Dr. GERALD S. HAWKINS, of Harvard, have been most helpful in discussions on this meteoric echo, and both lean towards the ground-scatter hypothesis.

References

Eshleman, Von R. (1955) *Trans. I.R.E.* AP-3, 32
Greenhow, J. S., and Neufeld, E. L. (1955) *J. Atmosph. Terr. Phys.*, **6**, 133
Kaiser, T. R. (1953) *Phil. Mag.*, Supp. 2, 495
McKinley, D. W. R. (1955) (The meteoric head echo) *Conference on Meteor Physics*, Pergamon Press (in the press)
McKinley, D. W. R., and Millman, Peter M. (1949) *Canad. J. Res.*, **A27**, 53
McKinley, D. W. R., and Millman, Peter M. (1953) *Canad. J. Phys.*, **31**, 171
Millman, Peter M. (1950) *J. Roy. Astron. Soc. Canada*, **44**, 209

VOL.
8
1956

Journal of Atmospheric and Terrestrial Physics, 1956, Vol. 8, pp. 83 to 90. Pergamon Press Ltd., London

Die tages- und jahreszeitlichen Variationen der F_1-Ionisation Ein Deutungsversuch

The daily and annual variations of F_1-ionisation and their interpretation

O. Burkard
Institut für Meteorologie und Geophysik Universität Graz

(*Received* 13 *June* 1955)

ABSTRACT

The simple relation between the critical frequencies of the F_1-layer and the position of the sun—shown by the formula $(f_0F_1)^2 = C^2 \cdot (\cos\chi)^x$—suggests a rather primitive law for the layer formation. This supposition has been verified. The mentioned relation is easy to explain if a linear increase of temperature with height is assumed for the F_1-layer, and if the recombination-coefficient is—very tentatively—assumed to have the form $\alpha = \alpha_0 \cdot p^k \cdot T^n \cdot N^m$. The constants k, n, and m are partly evaluated from the ionospheric observations, but a study of the possible recombination processes would be necessary to clarify the problem completely.

Research concerning the possible temperature conditions yields a model (Fig. 2) which shows a temperature gradient smaller in summer than in winter. Accordingly, the whole warm layer has a bigger thickness in summer and therefore extends over a greater height-interval than in winter. A model (Fig. 1) where the increase of temperature starts at the same height in winter and in summer (and the gradient in summer is greater than in winter) does not agree with the observations.

ZUSAMMENFASSUNG

Der einfache Zusammenhang zwischen den kritischen Frequenzen der F_1-Schicht und dem Sonnenstand —durch die Formel $(f_0F_1)^2 = C^2 \cdot (\cos\chi)^x$ darstellbar—läßt eine ebenso einfache Gesetzmäßigkeit für den Prozeß der Schichtbildung vermuten. Diese Vermutung wird bestätigt. Die genannte Beziehung findet ihre einfache Deutung, wenn man für die F_1-Schicht einen linearen Temperaturanstieg mit der Höhe voraussetzt und weiters den Wiedervereinigungskoeffizienten—in größter Allgemeinheit zunächst—in der Form $\alpha = \alpha_0 \cdot p^k \cdot T^n \cdot N^m$ ansetzt. Über die hier vorkommenden Konstanten k, n, und m können zum Teil bereits auf Grund des ionosphärischen Beobachtungsmaterials begrenzende Aussagen gemacht werden, zum Teil wird das Studium der möglichen Rekombinationsprozesse diesbezüglich Klarheit schaffen müssen.

Untersuchungen über die möglichen Temperaturverhältnisse führen auf ein Modell (Abb. 2), bei dem der Temperaturgradient im Sommer kleiner ist als im Winter. Man muß sich demnach vorstellen, daß die ganze warme Schicht im Sommer größere Mächtigkeit besitzt und sich daher auch über einen entsprechend größeren Höhenbereich erstreckt als im Winter.—Ein Modell (Abb. 1) bei dem der Temperaturanstieg im Sommer und Winter in der gleichen Höhe beginnt und der Temperaturgradient im Sommer größer ist als im Winter, ist dagegen mit dem Beobachtungsmaterial nicht vereinbar.

Die gegenwärtige Situation hinsichtlich der Erforschung der Ionisationsvorgänge in der Ionosphäre ist dadurch gekennzeichnet, daß zwar auf der einen Seite aus den Echolotungen ein bereits recht umfangreiches Beobachtungsmaterial vorliegt, daß weiters von theoretischer Seite die Ionisations–und Rekombinationsprozesse ziemlich genau untersucht wurden, daß es aber im Gegensatz dazu bisher nicht gelang, eine Brücke von der einen zur anderen Seite zu schlagen. Das ist umso bedauerlicher, als das Beobachtungsmaterial auf sehr einfache Beziehungen hinzudeuten scheint.

Da von der theoretischen Seite her derzeit offenbar keine Fortschritte zu erwarten sind, wird im folgenden versucht, auf Grund des Beobachtungsmaterials zu neuen Erkenntnissen zu gelangen. Es bieten sich uns zu diesem Vorhaben besonders die Beobachtungen der F_1-Schicht an, deren Maximalionisation im Tagesverlauf praktisch symmetrisch zum höchsten Sonnenstand verläuft. Damit kann man in der Gleichung für die Ionisierungsbilanz alle jene Glieder außer

Betracht lassen, die diese Symmetrie stören würden, sodaß man also einfach die übliche Formel für den Gleichgewichtszustand verwenden kann.

Man könnte vielleicht Bedenken haben, die F_1-Schicht für bestimmte Aussagen heranzuziehen, weil sie zu gewissen Zeiten mit der F_2-Schicht verschmilzt und dann natürlich nicht beobachtbar ist. Dem ist entgegen zu halten, daß es, wie BURKARD gezeigt hat, durchaus wahrscheinlich ist, daß die beiden F-Schichten auf ein–und denselben Ionisierungsvorgang zurückgeführt werden können. In einem solchen Fall ist aber die Ionisierung in der F_1-Schicht nur von den dort herrschenden Druck—und Temperaturwerten abhängig. Es ist sehr wesentlich zu beachten, daß also die Verhältnisse in der F_2-Schicht in keiner Weise auf die F_1-Schicht rückwirken können, da keinerlei Größen der F_2-Schicht in die Formeln für die F_1-Schicht eingehen.

Gehen wir nun zum Beobachtungsmaterial der F_1-Schicht über, dann findet man, daß das Quadrat der kritischen Frequenz (f_0F_1) in sehr einfacher Weise mit dem jeweiligen Sonnenstand zusammenhängt, indem eine Beziehung von der Form

$$\lg (f_0)^2 = 2 \lg C + x \cdot \lg (\cos \chi) \qquad (1)$$

recht genau erfüllt wird, wenn mit χ der Zenitwinkel der Sonne bezeichnet wird und wenn man die stündlichen Monatsmittelwerte (medians) für f_0 verwendet. Das Quadrat der kritischen Frequenzen ist bekanntlich ein Maß für die maximale Elektronenkonzentration. Wäre die F_1-Schicht isotherm, so würden die einfachen CHAPMANschen Beziehungen gelten und es müßte $x = \frac{1}{2}$ gesetzt werden, wenn die Elektronenvernichtung dem Quadrat der Elektronenkonzentration proportional angenommen wird, hingegen müßte $x = 1$ sein, wenn zwischen diesen beiden Größen ein linearer Zusammenhang bestünde. (Gleichgewichtszustand vorausgesetzt.)

In Wirklichkeit ergeben jedoch die Beobachtungen recht unterschiedliche Werte für x, die im allgemeinen nicht mit den oben genannten Werten in Einklang zu bringen sind. Die Tabelle I enthält das Zahlenmaterial für x, das nach der Gl. (1) aus den monatlichen Zentralwerten (medians) der in Washington vom CRPL gemessenen stündlichen f_0F_1-Werte der Jahre 1934–1954 errechnet wurde. Man ersieht aus der Tabelle sehr gut den offenbar vorhandenen jahreszeitlichen Gang ebenso wie eine geringe Abhängigkeit vom Sonnenfleckenzyklus. Der Wert von x variiert so etwa zwischen 0,30 und 0,56; ähnliche Zahlen fanden bereits MENZEL und WOLBACH (1950) und SCOTT (1952) auch für andere Stationen.

Eine Deutung dieser Abweichungen von der CHAPMANschen Beziehung ergibt sich aus Überlegungen, die NICOLET-BOSSY (1949), NICOLET (1951) sowie BURKARD (1950, 1952, 1954) anstellten, indem sie die Temperatur (oder allgemeiner die "Skalenhöhe") linear mit der Höhe anwachsen ließen. Ein unmittelbarer Vergleich dieser theoretischen Überlegungen mit den experimentellen Befunden wurde zwar für die E-Schicht von NICOLET (1951), für die F_2-Schicht unter vereinfachenden Annahmen (konstanter Wiedervereinigungskoeffizient) von GLEDHILL und SZENDREI (1950) bzw. SAHA (1953) und in jüngster Zeit bei entsprechender Erweiterung (Annahme einer tageszeitlichen Variation des Temperaturgradienten)

VOL.
8
1956

Tabelle 1. Zusammenstellung der nach Gl. (1) ermittelten x-Werte für Washington, D.C.

	Jan.	*Feb.*	*März*	*Apr.*	*Mai*	*Juni*	*Juli*	*Aug.*	*Sep.*	*Okt.*	*Nov.*	*Dez.*
1934	.	.	.	.	0,36	0,30	0,32	0,30	0,34	.	.	.
1935	.	.	0,28	0,34	0,34	0,36	.	.	.	.	.	.
1936	.	.	.	.	.	.	0,40	0,40	.	.	.	.
1937	.	.	.	0,44	0,52	0,56	0,52	.	.	.	.	.
1938	.	.	.	0,64	0,44	0,38	0,28	0,45	.	.	.	.
1939	.	.	.	.	0,36	0,40	0,38	0,36	.	.	.	.
1940	.	.	.	0,44	0,46	0,36	0,42	0,40	0,50	0,36	.	.
1941	0,40	0,56	0,54	0,46	0,40	0,38	0,40	0,40	0,36	0,44	0,40	.
1942	.	0,40	0,52	0,38	0,36	0,32	0,36	0,34	0,40	0,48	.	.
1943	0,52	0,54	0,50	0,38	0,36	0,36	0,38	0,38	0,44	0,46	.	.
1944	0,56	0,50	0,44	0,38	0,36	0,34	0,30	0,34	0,42	0,48	0,48	.
1945	0,48	0,56	0,42	0,40	0,36	0,38	0,32	0,38	0,42	0,50	.	0,56
1946	.	.	0,52	0,50	0,40	0,42	0,40	0,40	0,44	.	.	.
1947	.	.	.	.	.	0,38	0,42	0,42	.	.	.	.
1948	.	.	.	.	0,42	0,38	0,40	0,44	.	.	.	.
1949	.	.	.	.	0,50	0,40	0,34	0,50	.	.	.	.
1950	.	.	.	0,48	0,42	0,40	0,36	0,37	0,44	0,44	.	.
1951	.	.	0,52	0,36	0,44	0,42	0,34	0,40	0,48	.	.	.
1952	.	.	0,48	0,42	0,34	0,40	0,35	0,45	0,46	0,48	.	.
1953	.	0,48	0,44	0,40	0,36	0,35	0,36	0,37	0,40	0,51	.	.
1954	0,52	0,44	0,44	0,36	0,36	0,35	0,36	0,34	0,36	0,44	0,50	.

Tabelle 2. Zusammenstellung der nach Gl. (1) ermittelten lg *C-Werte für Washington, D.C.*

	Jan.	*Feb.*	*März*	*Apr.*	*Mai*	*Juni*	*Juli*	*Aug.*	*Sep.*	*Okt.*	*Nov.*	*Dez.*
1934	.	.	.	.	1,48	1,46	1,46	1,45	1,49	.	.	.
1935	.	.	1,51	1,49	1,47	1,51	.	.	.	.	.	.
1936	.	.	.	.	.	.	1,63	1,64	.	.	.	.
1937	.	.	.	1,68	1,69	1,73	1,73	.	.	.	.	.
1938	.	.	.	1,71	1,67	1,64	1,70	1,72	.	.	.	.
1939	.	.	.	.	1,68	1,65	1,61	1,62	.	.	.	.
1940	.	.	.	1,61	1,60	1,60	1,60	1,62	1,63	1,62	.	.
1941	1,49	1,58	1,59	1,56	1,54	1,55	1,55	1,57	1,52	1,59	1,59	.
1942	.	1,55	1,60	1,59	1,54	1,48	1,48	1,48	1,52	1,57	.	.
1943	1,57	1,59	1,57	1,51	1,49	1,49	1,49	1,46	1,52	1,53	1,59	.
1944	1,59	1,55	1,53	1,47	1,46	1,46	1,44	1,48	1,49	1,54	1,54	.
1945	1,54	1,58	1,53	1,54	1,52	1,55	1,53	1,54	1,57	1,63	.	1,59
1946	.	.	1,67	1,68	1,64	1,64	1,63	1,68	1,67	.	.	.
1947	.	.	.	.	1,73	1,71	1,72	1,71	.	.	.	.
1948	.	.	.	.	1,75	1,71	1,72	1,71	.	.	.	.
1949	.	.	.	.	1,72	1,68	1,68	1,70	.	.	.	.
1950	.	.	.	1,69	1,66	1,63	1,59	1,59	1,59	.	.	.
1951	.	.	1,60	1,55	1,58	1,58	1,55	1,57	1,60	.	.	.
1952	.	.	1,50	1,48	1,46	1,49	1,49	1,52	1,52	1,55	.	.
1953	.	1,49	1,49	1,48	1,45	1,46	1,46	1,45	1,50	1,52	.	.
1954	1,50	1,45	1,47	1,45	1,44	1,44	1,44	1,45	1,46	1,50	1,51	.

von AKASOFU (1953) gezogen; für die F_1-Schicht bestand bisher in dieser Hinsicht jedoch eine Lücke, die die vorliegende Untersuchung auszufüllen versucht.

Die Aufgabe, die wir uns stellen, ist nun eine zweifache:

(1) Sollen die CHAPMANschen Ansätze für die Schichtbildung so erweitert werden, daß unter Wahrung größtmöglicher Allgemeinheit dem durch Gl. (1) wiedergegebenen experimentellen Befund entsprochen werden kann. Unsere Formeln sollen also den beobachteten Tagesgang der kritischen Frequenz ergeben.

(2) Durch bestimmte Modellvorstellungen über die Temperaturverhältnisse im Gebiet der F_1-Schicht soll versucht werden, auch die jahreszeitlichen Änderungen von x and $\lg C$ zu erklären, bzw. soll aufgezeigt werden, daß manche heute geläufige Vorstellungen über die jahreszeitlichen Temperaturänderungen nicht mit dem Beobachtungsmaterial in Einklang zu bringen sind.

Zur ersten Aufgabe kann leicht eine Lösung angegeben werden, die für sich den Vorzug einfacher physikalischer Deutbarkeit beanspruchen kann. Es läßt sich zwar nicht ohne weiteres beweisen, daß diese Lösung die einzig mögliche ist, wohl aber ist sie unzweifelhaft die naheliegendste und einfachste, um Theorie und Praxis miteinander in Einklang zu bringen. Die zwei Bedingungen, die erfüllt sein müssen, um aus dem CHAPMANschen Ansatz die in Gl. (1) festgehaltene Beziehung zu erhalten lauten:

$$dT/dh = \gamma \tag{2}$$

und

$$\alpha = \alpha_0 \cdot p^k \cdot T^n \cdot N^m \tag{3}$$

Demnach soll die Temperatur linear mit der Höhe variieren und γ sei der zugehörige Temperaturgradient. In einem solchen Fall besteht zwischen Druck und Temperatur ein Zusammenhang von der Form:

$$T \cdot p^{\gamma R} = T_0 \cdot (p_0)^{\gamma R} = M \tag{4}$$

wobei durch M eine ganz bestimmte "Polytrope" gekennzeichnet ist. R ist die Gaskonstante (mit der Dimension km/Grad). Die zweite Bedingung (3) betrifft den Wiedervereinigungskoeffizienten α, der zunächst einer beliebigen Potenz des Druckes (p^k), der Temperatur (T^n), und der Elektronenkonzentration (N^m) proportional gesetzt wird. (Es sei hier vermerkt, daß $m = -1$ einer "Anlagerung", $m = 0$ einer "Wiedervereinigung" entspricht).

Für die Elektronenproduktion q ($\mathrm{cm^{-3} \cdot sec^{-1}}$) erhält man nach der allgemein bekannten Ableitung

$$q = q_0 \cdot \frac{p}{T} \cdot e^{-\frac{Ap}{g \cos \chi}} \tag{5}$$

Hierin sind in q_0 verschiedene Konstante zusammengefaßt, u.a. ist natürlich q_0 der Intensität der ionisierenden Strahlung außerhalb der Erdatmosphäre proportional. Für den Spezialfall der F_1-Schicht darf, wie eingangs bereits erwähnt wurde, der Gleichgewichtszustand ($dN/dt = 0$, $\frac{N}{T} \cdot \frac{dT}{dt} = 0$ u.s.w.) vorausgesetzt werden, sodaß also weiters gilt:

$$q = \alpha \cdot N^2 \tag{6}$$

Da das Beobachtungsmaterial eindeutige Aussagen nur hinsichtlich der kritischen Frequenzen gestattet, muß schließlich noch N^*, die maximale Elektronenkonzentration berechnet werden, die ja durch

$$N^* = \delta' \cdot (f_0)^2 \qquad \delta' = 1{,}24 \cdot 10^{-8} \tag{7}$$

verknüpft ist. Eine einfache Rechnung ($dN/dp = 0$) ergibt so als Endresultat unter Verwendung der Bedingungen (2, 3):

$$\lg {f_0}^2 = \frac{1}{2+m} \lg \frac{q_0}{\alpha_0 \delta} - \frac{1+n}{2+m} \lg M + \frac{z}{2+m} \lg \frac{z \cdot g}{Ae} + \frac{z}{2+m} \lg \cos \chi \tag{8}$$

wobei $\delta = (\delta')^{2+m}$ gesetzt wurde und

$$z = 1 - k + \gamma R(1+n) \tag{9}$$

bedeuten soll. Man findet ferner, daß die maximale Elektronenkonzentration in jener Höhe auftritt, in der der Druck die Gleichung

$$p^* = \frac{z \cdot g \cdot \cos \chi}{A} \tag{10}$$

erfüllt.

Eine Diskussion dieses Ergebnisses führt zunächst zu folgenden Erkenntnissen: Es ist möglich, durch die vorgenommene Erweiterung des CHAPMANschen Ansatzes eine Übereinstimmung mit dem Beobachtungsmaterial zu erzielen. Der beobachtete Tagesverlauf der kritischen Frequenz wird durch Gl. (8) wiedergegeben, indem offenbar $x = z/(2+m)$ zu setzen ist. Der Temperaturgradient γ ändert sich somit im Höhenbereich der F_1-Schicht tagsüber nicht. Die jahreszeitlichen Änderungen in x und $\lg C$ sind jedoch auf eine entsprechende Änderung des Temperaturgradienten zurückzuführen. Wenn ferner die Monatsmittelwerte (f_0) für die einzelnen Tageszeiten der Beziehung Gl. (8) genügen, so heißt dies nichts anderes, als daß die Druckwerte (p^*) und die zugehörigen Temperaturen (T^*), die im Laufe des Tages erreicht werden, sämtlich einer einzigen, ganz bestimmten Polytrope angehören. Bestimmt ist diese jeweilige Polytrope einerseits durch ihre "Ordnung," die bei der hier verwendeten Bezeichnungsweise durch den Quotienten $\frac{1}{1+\gamma R}$ gegeben ist, andrerseits durch den Wert der Konstanten $M = p^{\gamma R} \cdot T = {p_0}^{\gamma R} \cdot T_0$.

In verschiedenen Monaten, also z.B. in je einem Monat im Winter bzw. Sommer liegen die (p^*, T^*)-Wertepaare auf Polytropen verschiedener Ordnung und diese beiden Polytropen besitzen demnach im Endlichen einen Schnittpunkt. (Polytrope gleicher Ordnung schneiden sich im endlichen Bereich nicht.) Dieser Umstand wird von Bedeutung, wenn man zur zweiten Aufgabe übergeht und versucht, die jahreszeitlichen Änderungen in x und $\lg C$ mit Änderungen des Temperaturgradienten zu erklären. Setzt man im Anschluß an die Ergebnisse der Raketenforschung einen positiven Temperaturgradienten voraus, dann sind nur solche Temperaturverhältnisse sinnvoll, bei denen die Schicht im Sommer nicht kälter als im Winter wird. Man gelangt damit zu den zwei einfachen, in Abb. 1 und 2 dargestellten Modellen.

Das einfachere Modell I ist dadurch charakterisiert, daß oberhalb eines bestimmten Ausgangsniveaus (h_0) der Temperaturgradient im Winter kleiner ist als im Sommer; unterhalb des Niveaus herrsche Isothermie.

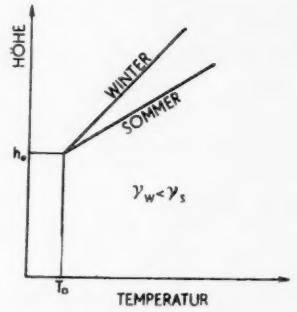

Abb. 1. Prinzipieller Temperaturverlauf mit der Höhe im Modell I.

Modell II dagegen weist im Winter einen größeren Temperaturgradienten auf als im Sommer; dadurch wird die Zusatzforderung notwendig, daß der Temperaturgradient im Winter oberhalb der F_1-Schicht allmählich kleiner wird, wie dies in Abb. 2 strichliert angedeutet ist. Im Winter reicht bei diesem Modell die Isothermie bis zur Höhe h_1, im Sommer aber nur bis h_0.

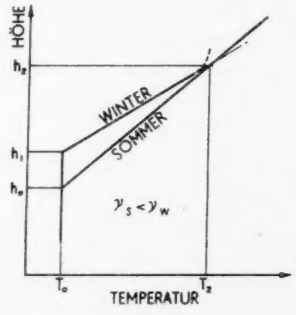

Abb. 2. Prinzipieller Temperaturverlauf mit der Höhe im Modell II.

Es läßt sich nun relativ einfach zeigen, daß das Modell I auf Grund des in den Tabellen I und II niedergelegten Zahlenmaterials unmöglich ist. Wenn dieses Modell nämlich die tatsächlichen Verhältnisse richtig wiedergeben würde, dann müßten die (p^*, T^*)-Wertepaare in einem Wintermonat alle auf einer Polytropen von der Ordnung $\frac{1}{1+\gamma_W R}$ liegen und zwar durchwegs oberhalb h_0. In einem Sommermonat liegen die (p^*, T^*)-Werte natürlich auf einer anderen Polytrope, die zwar auch wieder durch (p_0, T_0) in der Höhe h_0 hindurchgeht, aber nun die Ordnung $\frac{1}{1+\gamma_S R}$ besitzt. Da das Beobachtungsmaterials im Tagesverlauf einen konstanten Temperaturgradienten ergibt, müssen auch im

VOL. 8 1956

letzteren Fall alle (p^*, T^*)-Werte oberhalb h_0 bleiben. Unter Verwendung der Gl. (4, 8, 10) erhält man so für das Verhältnis p^*/p_0 folgenden Ausdruck:

$$\lg p^*/p_0 = 1 + \lg x + \lg \cos \chi + \frac{2(\lg C_W - \lg C_S) - x_W \lg x_W + x_S \lg x_S}{(x_W - x_S)} \qquad (11)$$

worin die Indizes W und S auf Winter und Sommer hindeuten sollen. Die Zahlenwerte können den Tabellen entnommen werden. Als Endergebnis findet man nun, daß p^*/p_0 sowohl im Winter als auch im Sommer nur in den Morgenstunden kleiner als Eins ist, zu Mittag aber größer als Eins wird, sodaß die vorhin erwähnte Bedingung ($h^* > h_0$ bzw. $p^* < p_0$) nicht erfüllt ist. So einfach das Modell I also auch aussieht, es ist unmöglich.

Prüft man nun nach, ob das Modell II mit dem Beobachtungsmaterial in Einklang zu bringen ist, so müssen zunächst analog den früheren Ansätzen die folgenden Voraussetzungen gemacht werden:

(*a*) $h_W^* \geqq h_1$

(*b*) $h_S^* \geqq h_0$

(*c*) $h_W^* < h_2$

(h^* bezeichne die Höhe der maximalen Elektronenkonzentration, p^* ist der in dieser Höhe herrschende Druck, h_0, h_1, und h_2 entnimmt man der Abb. 2). Die Notwendigkeit dieser drei Bedingungen ist leicht einzusehen. Wäre (*a*) oder (*b*) nicht erfüllt, dann würde die maximale Elektronenkonzentration im Tagesverlauf nicht mehr $(\cos \chi)^x$ proportional sein, was dem experimentellen Befund widersprechen würde. Die Forderung (*a*) ergibt aber weiters bei der zahlenmäßigen Durchrechnung die Einschränkung, daß nur jene Fälle möglich sind, bei denen $\gamma_W > \gamma_S$ ist, sodaß die dritte Bedingung (*c*) hinzutreten muß. Sie verhindert, daß oberhalb h_2 die Temperatur im Winter höher ist als im Sommer. Demgemäß wurde auch in der Abb. 2 bereits $\gamma_W > \gamma_S$ eingezeichnet, obwohl diese Ungleichung nicht von vornherein festliegt. Um die Erfüllung der Forderungen (*a*) bis (*c*) zu überprüfen, wird ähnlich wie im vorhergehenden p_W^*/p_0 bzw. p_S^*/p_0 berechnet. Die zwar einfache, aber mühsame Rechnung sei hier nicht angeschrieben. Von Interesse ist lediglich das Resultat, daß das Beobachtungsmaterial dem Modell II nur dann genügt, wenn außer $\gamma_W > \gamma_S$ auch noch die Ungleichung $x_S > \frac{1-k}{2+m}$ erfüllt ist. Damit wird aber die Wahl der bisher ja noch ganz offen gelassenen Konstanten k und n recht weitgehend eingeschränkt, sodaß man in Tabellenform für einige ausgewählte k- und n-Werte die aus dem Beobachtungsmaterial errechneten Temperaturgradienten zusammenstellen kann. Dies ist in der dreiteiligen Tabelle III für $m = -1$ (Anlagerung), $m = 0$ (Wiedervereinigung), und $m = 1$ (Dreierstoß?) geschehen. Als Grundlage für die Berechnung der Tab. III wurde ein Wert $R = 0{,}0416$ km/Grad für die Gaskonstante gewählt, indem die Schwerebeschleunigung mit $g = 900$ cm · sec^{-2} und die Zusammensetzung der Atmosphäre mit 65% N_2 + 35% O angenommen wurde. Für den Winter wurde $x_W = 0{,}50$ und für den Sommer $x_S = 0{,}35$ als Durchschnittswert (bei geringer Sonnenaktivität) angesetzt. Wie man der Tabelle [stark eingerahmter Teil] entnimmt, erhält man für dieses Modell II durchaus plausible Temperaturgradienten und damit kann die

Tabelle 3. Aus den Ionosphärenbeobachtungen ermittelte Temperaturgradienten (Grad/km) für das Modell II. (Winter und Sommer).

$m=-1$	$n=-\frac{1}{2}$	$n=0$	$n=\frac{1}{2}$	$n=1$	$n=\frac{3}{2}$	$n=2$	$n=3$	γ_w/γ_s
$k<0{,}65$		*Im Modell II unmöglich*						
$k=1{,}00$	24,0 16,8	12,0 8,4	8,0 5,6	6,0 4,2	4,8 3,4	4,0 2,8	3,0 2,1	1,43
$k=1{,}50$	48,0 40,8	24,0 20,4	16,0 13,6	12,0 10,2	9,6 8,2	8,0 6,8	6,0 5,1	1,18
$k=2{,}00$	72,0 64,8	36,0 32,4	24,0 21,6	18,0 16,2	14,4 13,0	12,0 10,8	9,0 8,1	1,11

$m=0$	$n=-\frac{1}{2}$	$n=0$	$n=\frac{1}{2}$	$n=1$	$n=\frac{3}{2}$	$n=2$	$n=3$	γ_w/γ_s
$k<0{,}30$		*Im Modell II unmöglich*						
$k=0{,}50$	24,0 9,6	12,0 4,8	8,0 3,2	6,0 2,4	4,8 1,9	4,0 1,6	3,0 1,2	2,50
$k=1{,}00$	48,0 33,6	24,0 16,8	16,0 11,2	12,0 8,4	9,6 6,7	8,0 5,6	6,0 4,2	1,43
$k=1{,}50$	72,0 57,5	36,0 28,8	24,0 19,2	18,0 14,4	14,4 11,5	12,0 9,6	9,0 7,2	1,25

$m=1$	$n=-\frac{1}{2}$	$n=0$	$n=\frac{1}{2}$	$n=1$	$n=\frac{3}{2}$	$n=2$	$n=3$	γ_w/γ_s
$k<-0{,}05$		*Im Modell II unmöglich*						
$k=0$	24,0 2,4	12,0 1,2	8,0 0,8	6,0 0,6	4,8 0,5	4,0 0,4	3,0 0,3	10,00
$k=0{,}50$	48,0 26,4	24,0 13,2	16,0 8,8	12,0 6,6	9,6 5,3	8,0 4,4	6,0 3,3	1,82
$k=1{,}00$	72,0 50,5	36,0 25,2	24,0 16,8	18,0 12,6	14,4 10,1	12,0 8,4	9,0 6,3	1,43
$k=1{,}50$	96,0 74,4	48,0 37,2	32,0 24,8	24,0 18,6	19,2 14,9	16,0 12,4	12,0 8,8	1,29

eingangs gestellte Aufgabe als gelöst angesehen werden, die Aufgabe nämlich, das mittlere Verhalten der kritischen Frequenzen f_0F_1 im Tages- und Jahresverlauf durch ein einfaches Modell wiederzugeben. Es wäre begrüßenswert, wenn die "theoretische Seite" nun ihrerseits die hier aufgezeigten Ansatzpunkte für eine neuerliche Aufrollung des Rekombinationsproblems in der Ionosphäre aufgreifen würde.

Für die Berechnung der Tabellenwerte I und II habe ich Herrn Dr. H. PICHLER zu danken.

LITERATURVERZEICHNIS

AKASOFU, S.	1953	Science Reports, Tohoku University, *Geophysics* **5**, 123
BURKARD, O.	1950	*Arch. f. Met. Geoph. Biokl.* **A2**, 308
	1952	*Geofisica pura e appl.* **22**, 63
	1954	*Arch. f. Met. Geoph. Biokl.* **A7**, 283
GLEDHILL, J. A., und SZENDREI, M. E.	1950	*Proc. Phys. Soc.* **B63**, 427
NICOLET, M.	1951	*J. Atmosph. Terr. Phys.* **1**, 141
NICOLET, M., und BOSSY, L.	1949	*Ann. de Geophys.* **5**, 275
SAHA, A. K.	1953	*Indian J. Phys.* **27**, 431

VOL. 8 1956

Journal of Atmospheric and Terrestrial Physics, 1956, Vol. 8, pp. 91 to 97. Pergamon Press Ltd., London

A study of the total electron content of the *F*-region of the ionosphere over Ahmedabad (23° N, 72° 38′ E), India

R. M. SHERIFF
Physical Research Laboratory, Ahmedabad, India

(*Received* 18 *May* 1955)

ABSTRACT

The total number of electrons in a column of unit cross-section in the F_1- and F_2-regions of the ionosphere up to the heights of maximum electron density has been calculated for three magnetically quiet days and three disturbed days in each month from February 1953 to January 1954. The method of analysis is that suggested by RATCLIFFE, assuming parabolic electron density distribution in the layers. The values of the mean daily variations of n, the total electron content in a vertical column of unit cross-section up to the height of maximum electron density of the F_2-layer, and n_T the corresponding number of F_1- and F_2-layers together, for each of the three seasons (Nov.–Feb., May–Aug., and Mar.–Apr. plus Sept.–Oct.) are given in the form of graphs.

The mean daily variations of the following parameters of the F_2-region, viz., y_m its semi-thickness, h_p the height of maximum electron density, and $h_p - y_m$, or h_o, the base of the layer assuming parabolic electron density distribution, have also been studied. n and n_T show maxima in March and October, with a minimum in summer.

The relation between y_m and h_p of the F_2-layer shows that thick layers are associated with higher values of h_p and that the parabolic electron distribution law does not hold for very thick layers. A histogram, showing the semi-thickness of the F_2-region against the number of occurrences, is given. 1953 being a year of weak solar activity, the disturbed-day values do not differ substantially from those of quiet days.

INTRODUCTION

APPLETON and BEYNON (1940a) have given the following well-known relation between h', the virtual height for the vertical reflection of ordinary waves of frequency f, and the frequency. In this a parabolic distribution of electron density is assumed, and the effect of the earth's magnetic field is neglected.

$$\frac{h' - h_o}{h_p - h_o} = f/2f_c \log_e \left| \frac{f_c + f}{f_c - f} \right| \tag{1}$$

where h_p is the height of maximum electron density or the virtual height corresponding to 0·834 f_c, h_o is the lower height of zero electron density, and f_c the critical frequency for the particular layer. This can also be written as

$$h' = h_p + y_m \phi (f/f_c) \tag{2}$$

where $y_m = h_p - h_o$, semi-thickness of the layer, and

$$\phi(f/f_c) = f/2f_c \log_e \left| \frac{f_c + f}{f_c - f} \right| - 1 \tag{3}$$

This formula is true for a perfect parabolic layer with no ionized region below it. If there exists a lower layer of maximum electron density less than that of the above one, then waves of frequency greater than the critical frequency of the lower layer will get reflected from the upper layer. The virtual height of the

upper layer will be increased due to the retardation in the lower one. The retardation is given by

$$\Delta h' = y_m \phi(f/f_c)$$

where y_m is the semi-thickness of the lower layer and f_c its corresponding critical frequency.

RATCLIFFE (1951a) has suggested a quick method of analysis to get the total electron content in a vertical column of unit cross-section up to the level of maximum electron density, assuming parabolic electron density distribution in the layer. The value of n is given by

$$n = 2/3\ B y_m f_c^2$$

where $B = 1{\cdot}24 \times 10^{-8}$ and y_m and f_c have the usual meaning. Hence what is required for the determination of n is the critical frequency of the layer and its semi-thickness. As the critical frequency is got directly from the h'-f record, RATCLIFFE'S method enables the semi-thickness to be obtained directly from the variation of the virtual height of reflection with frequency using equations (2) and (3).

RATCLIFFE (1951b) has analyzed the data of Watheroo, Huancayo, and College (Alaska), and found that the diurnal variation of n was more regular than that of $N_m F_2$, the maximum electron density in the F_2-layer, and that it was more closely related to the zenith angle χ than $N_m F_2$.

OSBORNE (1952) has analyzed the records of Slough and Singapore, and concluded that the seasonal and diurnal variations of maximum electron density differed from those of n, and that n showed a closer dependence on cos χ.

SKINNER and WRIGHT (1954) have analyzed the data of IBADAN, and have shown that n behaves in a more regular manner than $N_m F_2$.

CHATTERJEE (1953) has claimed that if, instead of the total electron content in the F_2-region up to the height of maximum electron density, the total electron content in the F_1- and F_2-layers together is considered, the regularity in the diurnal variation curve is improved.

ANALYSIS OF AHMEDABAD RECORDS

The ionospheric recorder at Ahmedabad is of the British NPL type and was installed in January 1953. Since then, automatic h'-f records for all the twenty-four hours of the day are being taken. As the data for January 1953 were scanty, that month was omitted, and instead, January 1954 was taken for the purpose of the analysis.

In order to analyze Ahmedabad records, standard curves were drawn by plotting $y_m \phi(f/f_c)$ against (f/f_c) on a logarithmic scale. Stencils of the graph for selected values of semi-thickness, y_m, were prepared. The values of $\phi(f/f_c)$ were taken from BOOKER and SEATON'S (1940b) table. The h'-f traces were translated before analysis on a semi-logarithmic graph paper with the logarithm of frequency as abscissa and virtual height as ordinate. As the plot along the abscissa is on a logarithmic scale, the slope of the graph does not change whether f or f/f_c is plotted, as long as f_c remains constant. Plotting the function against f instead

VOL. 8 1956

of against f/f_c on a logarithmic scale only causes a shift along the x-axis. The advantage of using f/f_c is that the same stencil relating to a particular semi-thickness can be used for any critical frequency.

The analysis was made by selecting the stencil which fits best the h'-f curve drawn on the logarithmic scale. The best fit is judged by making the stencil line $f/f_c = 1$ to coincide with the ordinate corresponding to the critical frequency at the particular hour, with the horizontal line h_p parallel to the frequency axis. The semi-thickness is given by the stencil, and the value of h_p is the ordinate of the point where the h_p line on the stencil meets the h'-f curve.

If the layer is very nearly parabolic, as is usual at night and at some other hours, the whole h'-f curve fits well with a stencil curve. On some occasions, about half of the portion near the critical frequency matches well with the standard curve. The h'-f curves at certain hours of the day cannot be made to fit even approximately with the standard curves. These were not used for analysis. The number of mismatches of the h'-f trace with the standard curves is more during the early morning and evening hours than during midday and night hours.

When an F_1-layer was present, a correction was made for the increase in virtual height of the F_2-layer, and the corrected h'-f trace used for analysis. When F_1- and F_2-layers overlapped, no special consideration was given to this fact, but the two layers were treated as separate.

Diurnal and Seasonal Variation of N_m, n, and n_T

Three magnetically quiet and three disturbed days in each month were taken from February 1953 to January 1954 for the purpose of the analysis. The quietness and disturbedness of a day were judged from the magnetic character K figures for Alibag.

For the purpose of the present paper the months were grouped into three seasons, summer, winter, and equinoxes, and the diurnal variations of n and n_T were studied. Figures 1(a) and (b) give the variation of these quantities for quiet and disturbed days. The average times of ground sunrise and sunset are indicated in the figures.

It will be seen that the variations are smooth, reaching a maximum in the afternoon. The maximum is reached later in summer months compared to winter months. The curves have a single maximum, except the curve for quiet days in the equinoctial months. The addition of the contribution of the F_1-layer to that of F_2 does not change the nature of the curve, and where there are two maxima, they continue to remain so after this addition. This differs from Chatterjee's conclusion.

The curves in Fig. 3 give the graphs of the noon values of n, n_T, and N_mF_2 in each month. n and n_T show two maxima, one in March and another in October, but a primary maximum of N_mF_2 is in April while a secondary maximum remains in October.

Correlation of y_m, h_p, and h_o

Figures 2(a) and (b) give the diurnal variation of y_m, h_p, and h_o of the F_2-layer. The curves of y_m, h_p, and h_o show clearly a semi-diurnal variation with maxima at about noon and about midnight. In addition, however, there is another hump

in the curves of all the three quantities at about the time of sunrise in the layer. As the hump occurs near the time of minimum total electron content, the result is curious. It appears to be that, before sunrise, the existing night-time F_2-layer lowers and sometimes even disappears, while a new F_2-layer forms at a higher level and gradually descends. Thus we are on many days dealing with physically

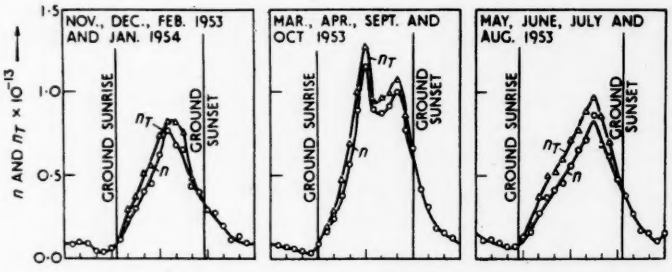

Fig. 1(a) Mean diurnal variation of n and n_T at Ahmedabad on *quiet days*.

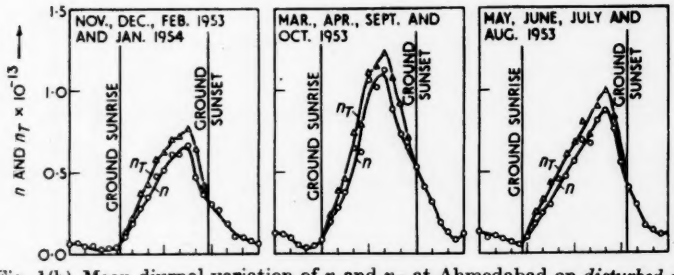

Fig. 1(b) Mean diurnal variation of n and n_T at Ahmedabad on *disturbed days*.

different layers, one before sunrise and another after sunrise. In summer months, the sunrise effect is not prominent and the diurnal variation curve of y_m is also somewhat different from those of h_p and h_o.

RELATIONSHIP OF h_p AND y_m

Fig. 4 gives the relation between h_p and y_m of the F_2-layer. The greater the thickness of the F_2-layer the greater is the height of maximum electron density, and with increasing thickness, the height tends towards a maximum. A histogram of the number of occurrences of different values of the semi-thickness is given below. It can be seen that the most probable value of y_m lies between 75 and 105 km.

CONCLUSION

The hour of maximum total electron content in each month occurs in the afternoon, but the actual hour varies from month to month; n is not just a simple function of cos χ. The bite-out effect in the diurnal variation in certain months is not removed by the inclusion of the electron content of the F_1-layer as reported by CHATTERJEE. The total number of electrons, n and n_T, is a maximum in the equinoctial months and minimum in winter. It is curious that the maximum does not occur in summer. There is no change in the diurnal variation of mean n and

VOL. 8 1956

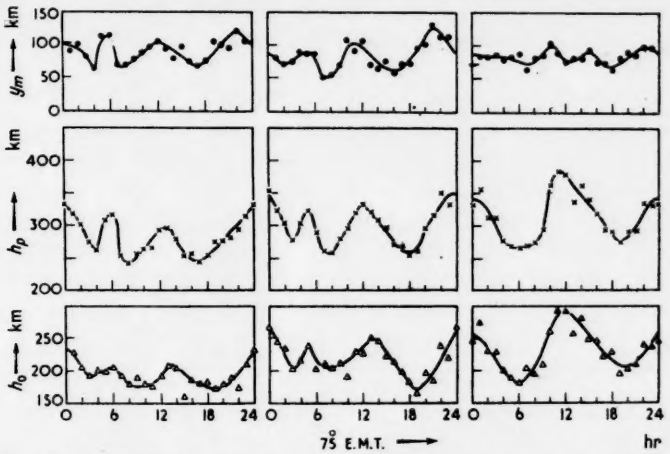

Fig. 2(a) Mean diurnal variation of y_m, h_p, and h_o of the F_2-layer over Ahmedabad on *quiet days*.

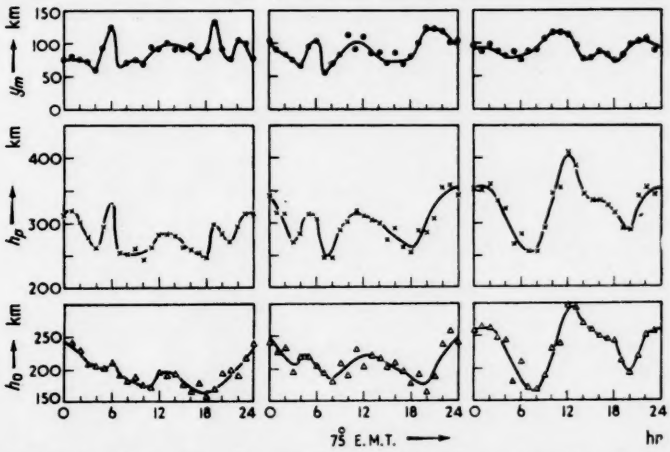

Fig. 2(b) Mean diurnal variation of y_m, h_p, and h_o of the F_2-layer over Ahmedabad on *disturbed days*.

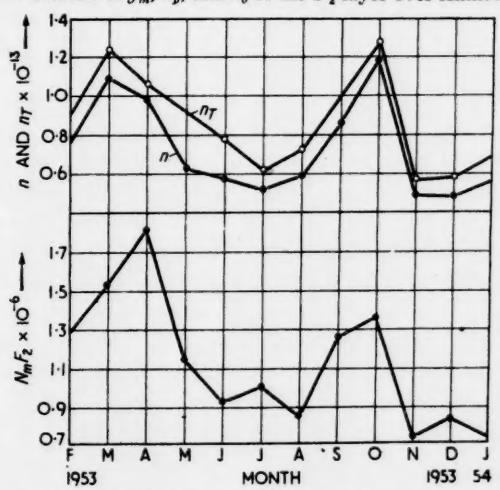

Fig. 3. Seasonal variation of noon values of n, n_T, and N_mF_2.

n_T between magnetically quiet and disturbed days. This conclusion may not hold for years of high solar activity.

The variations of y_m, h_p, and h_o of the F_2-layer are mainly semi-diurnal in character. As reported by MITRA (1951c), the day maximum in the diurnal variation of h_p and h_o occurs shortly after noon in winter and before noon in summer. In the y_m curve of summer months there are two maxima, one at about 10–11 hours and another at about 15–16 hours. The rise in h_p, h_o, and y_m at sunrise is accompanied by a minimum in n, and the probable reason for this has already been stated. The feebleness of the hump in summer may be due to the fact that

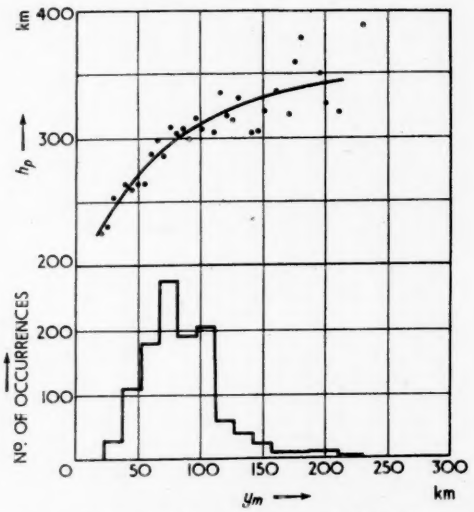

Fig. 4. Relation between h_p and y_m of the F_2-layer and histogram showing the number of occurrences of y_m of the F_2-layer over Ahmedabad.

h_pF_2 is high and the amplitude of variation of y_m is small. The two maxima in the seasonal variation of the noon values of n, n_T, and N_mF_2 show that they are not simple functions of cos χ. The relation between y_m and h_p is not linear. Thick layers are associated with greater heights of maximum electron density. Very thick layers do not obey the law of parabolic electron density distribution.

It may be mentioned that the values of y_m deduced here, using RATCLIFFE'S method, do not take into account the effect of the earth's magnetic field. As Ahmedabad (geomag. lat. = 13.6° N, mag. dip = 34°) is a low magnetic latitude station, the overestimation in the values of y_m as seen from the graphs given by SHINN and WHALE (1952b) does not exceed 10 per cent.

Acknowledgements—The work described is part of the programme of ionospheric research carried out at this laboratory with the financial assistance of the Council of Scientific and Industrial Research (India). The author is indebted to Prof. K. R. RAMANATHAN for his keen interest and guidance.

References

Appleton, E. V., and Beynon, W. S. G.	1940	*Proc. Phys. Soc.* [London] **52,** 518
Booker, H. G., and Seaton, S. L.	1940	*Phys. Rev.* **57,** 87
Chatterjee, B.	1953	*J. Geophys. Res.* **58,** 353
Mitra, A. P.	1951	*J. Atmosph. Terr. Phys.* **1,** 286
Osborne, B. W.	1952	*J. Atmosph. Terr. Phys.* **3,** 58
Ratcliffe, J. A.	1951a	*J. Geophys. Res.* **56,** 463
Ratcliffe, J. A.	1951b	*J. Geophys. Res.* **56,** 487
Skinner, N. J., and Wright, R. W.	1954	*J. Atmosph. Terr. Phys.* **5,** 290
Shinn, D. H., and Whale, H. A.	1952	*J. Atmosph. Terr. Phys.* **2,** 85

OL.
8
956

Journal of Atmospheric and Terrestrial Physics, 1956, Vol. 8, pp. 98 to 104. Pergamon Press Ltd., London

Tilts in the ionosphere during the solar eclipse of 30 June 1954*

E. N. BRAMLEY

Official communication from D.S.I.R. Radio Research Station, Slough

(*Received* 23 *May* 1955)

ABSTRACT

Directional measurements at nearly vertical incidence on the *F* layer during the eclipse showed the existence of a tilt whose direction agreed with that expected from the geometry of the eclipse. The magnitude of the tilt was also of the same order as that calculated from observed changes in the height of reflection.

Oblique-incidence bearing measurements on signals reflected from the normal *E* layer failed to reveal any eclipse effect, and theoretical calculation showed that no detectably large effect would have been expected in this case.

1. Measurements at Nearly Vertical Incidence

As part of the Radio Research Board's programme of ionospheric investigations on the effects of the eclipse, directional measurements were made with a wide-aperture spaced-loop system (Ross, Bramley, and Ashwell, 1951) at Winkfield, Berkshire, using pulse transmission from the Radio Research Station, Slough, 10 km away.

The period of the eclipse at Slough was from 1113 to 1350 U.T. on 30 June 1954, and the maximum obscuration of the sun at a height of 230 km was 0·72 of its area, at 1235 U.T. The period of observations was 0900–1600 on the day of the eclipse, and also, for comparison, on each of the four days 28, 29 June and 1, 2 July. The frequency used for the transmissions was varied from time to time to suit conditions, within the range 3·4–4·7 Mc/s. Where possible, echoes from the *F* and sporadic *E* layers were both studied, measurements being made on each at regular intervals of 30 sec. During the eclipse itself, the fall in *F*-layer critical frequencies involved various components of the *F* reflections being used in turn, namely oF_1, oF_2, xF_2, xF_1, and oF_1, and a selection of results on these components (except xF_2) was obtained on the control days. E_s echoes were also obtained throughout the eclipse.

The directional measurements were supplemented by conventional $h't$ (equivalent height versus time) photographic records on the operating frequency, taken at Slough, and by visual observations, as required from time to time, of the polarization of the received echoes. These latter observations were made at Winkfield, using the c.r.d.f. display of a twin-channel (Type FHB) receiver (de Walden, Rocke, Barrett, and Pitts, 1947) connected to a pair of crossed vertical loops.

2. Analysis of Results

The directional results, consisting of the phase differences on the N–S and E–W pairs of spaced aerials, were examined from two points of view, namely the slowly varying changes due to layer tilts, and the rapid, second-to-second fluctuations

* The material of this paper forms part of a Thesis approved by the University of London for the degree of Doctor of Philosophy.

VOL. 8 1956

believed to be due to small-scale ionospheric irregularities. In order to separate these effects, the results were divided into ten-minute periods, centred on times at five-minute intervals. For each period the mean phase difference was calculated, and the variation of the means with time was taken to represent the changing ionospheric tilts. Also, as an index of the rapid variations, the standard deviation of the individual results within each ten-minute period was estimated from the number of values and their range, using tables quoted by JOSEPHS (1945) (due to TIPPETT).

3. LAYER TILTS

3.1. *F region*

At the start of the eclipse, reflections were being received from the F_1 layer (ordinary ray) on a frequency of 3·8 Mc/s. With the onset of the eclipse, the effective reflection point drifted off to the south-east, while the equivalent height increased rapidly, due to the fall in foF_1, until further measurements on this echo could not be made. At 1208 measurements became possible on the oF_2 reflection, until 1227, when this echo also "ran out" and was replaced by the xF_2 reflection. The eclipse having passed the maximum phase, the critical frequencies began to rise again, and the xF_1 reflection took the place of xF_2 at 1242. This xF_1 echo was observed until 1310, when a reduction of working frequency to 3·4 Mc/s was made, and observations were continued on the oF_1 echo for the rest of the eclipse period.

Fig. 1 shows the ten-minute mean values of the F-layer tilts measured on the eclipse day. The spread of the individual values from which these means were computed was such that the estimated standard deviation of the means is of the order of 0·5° of tilt. The most notable effect is the downward tilt of the F_2 layer towards the south, some 4° in magnitude at the middle of the eclipse. In the east-west component during the eclipse period, there is also an indication, though not very clearly defined, of a tilt downwards to the east, returning to zero at about 1225, and followed by a tilt in the opposite direction before returning to normal conditions.

It will now be shown that on simple ideas of the relation between layer tilts and heights of reflection, the eclipse would be expected to produce tilts corresponding roughly in magnitude and direction to those observed.

Consider a point in the ionosphere at which the sun is partially eclipsed, the fraction of the area of the disc obscured at any time t being M. The major effect of the partial obscuration is that some of the incident radiation producing ionization is cut off, so that the ionization density falls. In general this involves an increase in the height of reflection for waves of a fixed frequency. Since, at a given time, M is a function of horizontal position, the change in height is also a function of position and thus a tilt of the surfaces of constant ionization density is produced. If s represents a distance measured horizontally, then the maximum tilt may be expected to occur in the direction for which $\left|\frac{\partial M}{\partial s}\right|$ is a maximum, the direction of the horizontal component of grad M. The tilt will be upwards in this direction, since the height h increases with increasing M; the reflection point for a ray incident normally on the ionosphere will thus be deflected in the

opposite direction. Values of the horizontal component of grad M, for various heights, were kindly supplied by H.M. Nautical Almanac Office; as will be seen, a range of about 100 km in true height of reflection was involved in the observations, but since the values of M and grad M varied only slightly with height, the figures for a fixed height of 230 km have been used in all calculations. The magnitude of the horizontal component of grad M, i.e., $\left|\frac{\partial M}{\partial s}\right|_{max}$, varied during the eclipse, as shown in Fig. 2, and its direction varied as shown in the full line of Fig. 3.

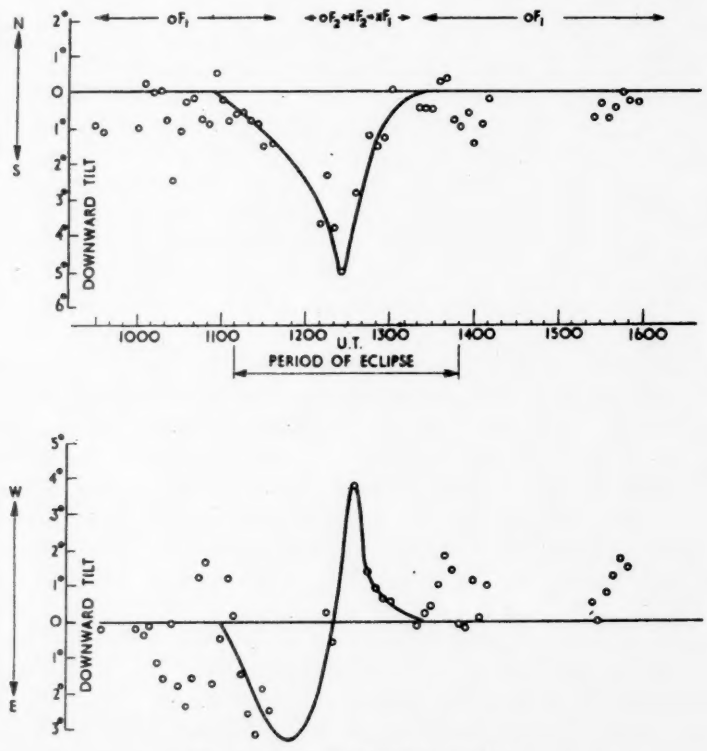

Fig. 1. F layer tilts 30 June 1954.

The changes in direction correspond to the passing of the centre of the moon's shadow from west to east, along a track lying to the north of Slough.

In Fig. 1, smooth curves have been drawn tentatively through the plotted points, assuming that the measured tilt can be regarded as a continuous function of time, although different layers of the ionosphere were sampled in turn during the eclipse. This appears to be a reasonable assumption, since, as will be seen, no very large discontinuities in the true height of reflection are believed to have occurred. The directions of the observed tilt, as represented by these curves, are shown in Fig. 3 as a dotted line. The curves in Fig. 1 could with equal justification be drawn in slightly different ways, which would alter the dotted curve in Fig. 3

VOL. 8 1956

somewhat, but the agreement between the latter and the theoretical curve appears to be not entirely fortuitous, when it is considered that under non-eclipse conditions the whole range of azimuths from 0 to 360° is usually involved in the random ionospheric tilts, with uniform probability.

With regard to the magnitude of the tilts to be expected, these may be taken to be of the same order as $\partial h/\partial s$, where h is the true height of reflection. Without the use of suitably spaced receivers working on the same transmissions, the

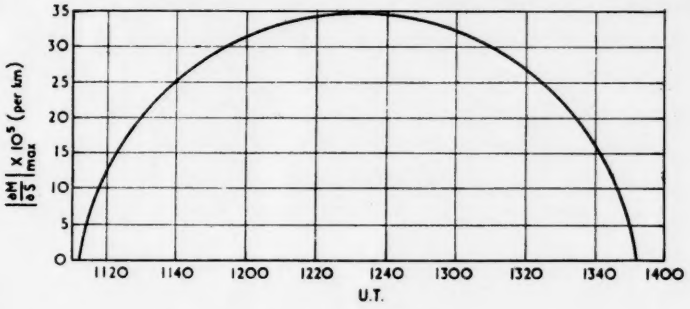

Fig. 2. Variation of $\left|\frac{\partial M}{\partial s}\right|$ during eclipse.

magnitude of $\partial h/\partial s$ must be obtained indirectly. The equivalent height h' was measured in the present observations, and from the sequence of $h'f$ (equivalent height versus frequency) records taken at the Radio Research Station during the eclipse, the corresponding values of true height of reflection h could be deduced. The values of $\frac{\partial M}{\partial t}$ and $\left|\frac{\partial M}{\partial s}\right|_{max}$ were also known; the total magnitude of the expected layer tilt could thus be calculated as $\left|\left(\frac{\partial h}{\partial t}\right)\left(\frac{\partial M}{\partial s}\right)_{max}\Big/\left(\frac{\partial M}{\partial t}\right)\right|$, except near the time of maximum phase of the eclipse when $\partial M/\partial t$ and $\partial h/\partial t$ were both near zero.

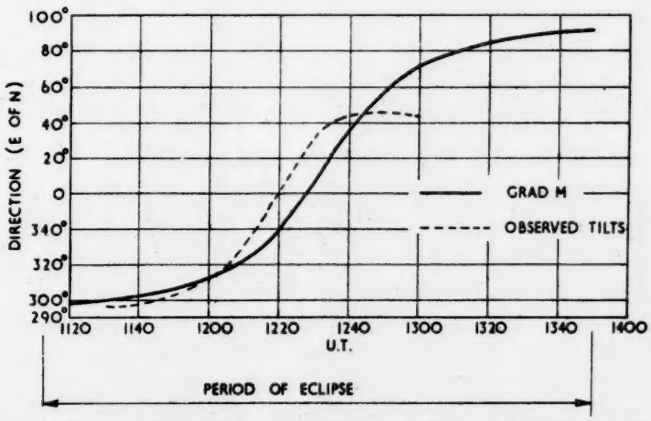

Fig. 3. Horizontal direction of grad M and of observed tilts during eclipse.

The variations of h' observed at the working frequency during the eclipse are shown in Fig. 4, together with the corresponding values of h. The latter were deduced by assuming the F_1 and F_2 layers to have a parabolic ionization distribution, and deducing their parameters from the $h'f$ records. The heights appropriate to the xF_1 and xF_2 reflections were assumed to be the same as for an ordinary ray on a frequency 0·65 Mc/s (half the gyrofrequency) lower than that actually in use. The effect of group retardation in the E layer was ignored in the calculations, and the whole process may be subject to appreciable errors, but it is considered adequate to give the order of magnitude of the actual height changes involved.

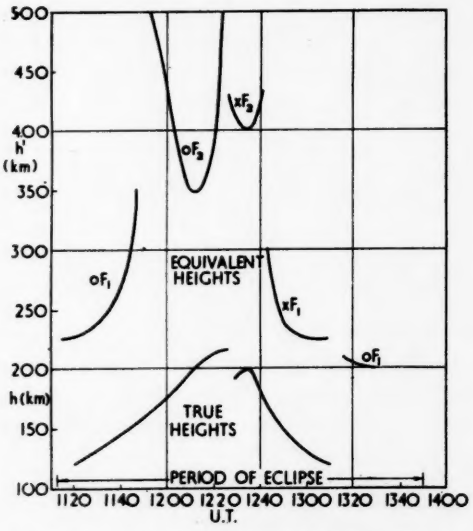

Fig. 4. Variation of h' and h during eclipse.

The variation of M during the eclipse is shown in Fig. 5, and from this and the curve for h in Fig. 4, the variation of the true height of reflection with M has been plotted in Fig. 6. The slope of this curve then enables the magnitude of the tilt to be calculated as $\left|\left(\frac{\partial h}{\partial M}\right)\left(\frac{\partial M}{\partial s}\right)_{\max}\right|$. The value of $\partial h/\partial M$ is seen to be about 140 km, and combining this with the values of $\left|\frac{\partial M}{\partial s}\right|_{\max}$ shown in Fig. 2 gives theoretical tilts up to about $2\frac{1}{2}°$. This is somewhat smaller than the maximum tilt observed, though of the same order of magnitude. To give closer agreement, a larger range of variation of height would be required during the eclipse.

Comparison with results obtained on the control days, and in previous similar experiments, shows that tilts in the F_2 layer as large as those observed during the eclipse are not unknown, but in general occur for only a small proportion of the time. The agreement between the observed and predicted sense of the tilts, and the relatively long period of the effect compared with the usual random tilts, may be taken as evidence that in this case they were a consequence of the eclipse.

VOL. 8 1956

3.2. *E_s layer*

The eclipse period results showed no abnormalities, as compared with the control-day results, which are likely to have been associated with the eclipse itself. From 1246 to 1255, during the eclipse, the results indicated that reflections were being obtained from a drifting cloud of ionization, moving in a direction 115° E of N at a speed of about 70 m/sec, but similar results (Bramley, 1953) have been obtained from time to time under normal ionospheric conditions.

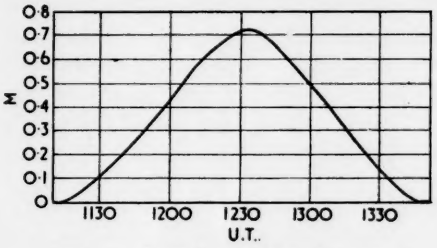

Fig. 5. Variation of M during eclipse.

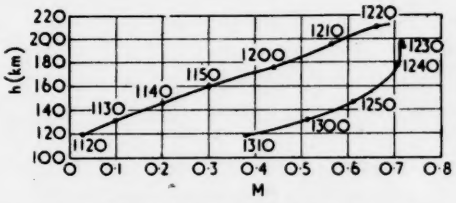

Fig. 6. Variation of h with M during eclipse.

4. Rapid Fluctuations

During the eclipse no very marked abnormality in the magnitude of the rapid fluctuations was observed, except for a few minutes at about 1215, when large and erratic variations occurred on the E_s echo. The F_2-layer echoes showed somewhat greater fluctuations than usual, but this was probably due to the closeness to penetration conditions, the echoes being rather weak and scattered.

A marked increase in the magnitude of the rapid directional fluctuations was observed to occur on both the oF_1 and the E_s echoes on 3·8 Mc/s, from about 1020 to 1045 on the eclipse day. The standard deviation of the individual values was increased by a factor of about 3 during this period, which was marked by deep and rapid fading of the echoes. The directional fluctuations were larger than at any other time during the five days' measurements, and the effect seems worth mentioning since it occurred about two hours before the optical eclipse and so might possibly be associated with a corpuscular eclipse. But no great weight can be attached to this possibility, since similar, though smaller, increases in the fluctuations were observed on several occasions during the measurements on other days. In the case of the F echoes, both on the eclipse and other days, these increases were usually genuine enlargements in the angular spread of a single magnetoionic component, but the E_s echoes sometimes consisted of a mixture of ordinary and extraordinary rays, interference between which would no doubt contribute to the fluctuations. This interference condition was observed on the polarimeter during the pre-eclipse enhancement just described.

5. Oblique-incidence Bearing Measurements

In addition to the directional measurements at vertical incidence, described above, bearing observations were carried out with a U-Adcock direction finder at Slough on a 5-Mc/s pulse transmission from Inverness, 700 km away in a direction 18° W of N. These measurements were made from 1030–1530 U.T. on each day from 28 June to 2 July, on the echo reflected from the normal E layer.

The bearings were read visually from a c.r.d.f. display at 30-sec intervals, and the means for 5-minute periods were calculated. On each day these means varied over a range of at least $2\frac{1}{2}°$, but there were no particularly unusual variations during the eclipse period, as compared with times outside this period.

The magnitude of the bearing deviations to be expected as a result of the eclipse were calculated from the theoretical tilt in the E layer, given by $\left|\left(\frac{\partial h}{\partial M}\right)\left(\frac{\partial M}{\partial s}\right)\right|$, as in Section 3.1. s is here measured normal to the vertical plane of transmission. In this case $\partial h/\partial M$ was calculated by assuming the E layer to be of Chapman form, and the rate of ion production at any time to be proportional to the unobscured area of the sun's disc, i.e., to $(1 - M)$. The bearing deviations so calculated had a maximum value during the eclipse of only 0·15°, which is much too small to show up among the random variations observed with the Adcock.

6. CONCLUSIONS

It is concluded that this solar eclipse, reaching 72 per cent of totality at Slough, produced a tilt in the F layer, which was observed on a particular frequency to be up to about 5° in magnitude; its direction varied with time roughly as expected from the geometry of the eclipse. No normal E-layer tilts attributable to the eclipse were detected in oblique-incidence bearing measurements, nor would any appreciable effect have been expected theoretically under the conditions used.

Acknowledgements—Dr. W. C. BAIN was responsible for the oblique-incidence work described in Section 5, and Mr. R. NAISMITH for the vertical-incidence $h'f$ measurements used in the analysis. The author acknowledges the assistance of a number of other colleagues in the experimental work and reduction of the results and also the benefit derived from discussions with Dr. H. G. HOPKINS and Mr. C. M. MINNIS.

The work described above was carried out as part of the programme of the Radio Research Board. This paper is published by permission of the Director of Radio Research of the Department of Scientific and Industrial Research.

REFERENCES

BRAMLEY, E. N. 1953 Direction Finding Studies of Large-Scale Ionospheric Irregularities. *Proc. Roy. Soc.* **A220,** 39

JOSEPHS, H. J. 1945 The Fixing of Confidence Limits to Measurements. *J.I.E.E.*, Pt. II, **92,** 194

ROSS, W., BRAMLEY, E. N., and ASHWELL, G. E. 1951 A Phase Comparison Method of Measuring the Direction of Arrival of Ionospheric Radio Waves. *Proc. I.E.E.*, Pt. III, **98,** 294

DE WALDEN, S., ROCKE, A. F. L., BARRETT, J. O. G., and PITTS, W. J. 1947 The Development of a High-Frequency Cathode-Ray Direction Finder for Naval Use. *J.I.E.E.*, Pt. IIIA, **94,** 823

VOL. 8 1956

Journal of Atmospheric and Terrestrial Physics, 1956, Vol. 8, pp. 105 to 107. Pergamon Press Ltd., London

The effect on geomagnetism of the solar eclipse of 30 June 1954 (supplementary communication)

J. EGEDAL* and N. AMBOLT†

(*Received* 27 *June* 1955)

Abstract—Beyond observations treated earlier, magnetic observations from 30 June 1954 from five magnetic observatories have been received and examined. The results obtained agree with earlier ones.

1. INTRODUCTION

AFTER the completion of the treatment of magnetic data for the period of the solar eclipse of 30 June 1954 from a series of observatories in northwest Europe (EGEDAL and AMBOLT, 1955), the authors had the pleasure to receive data from east Europe, where the track of totality of the said eclipse crossed the USSR. This enabled the authors to study the phenomenon over a larger part of the track and to study the effect while deviations due to the daily magnetic variation are diminishing.

2. THE OBSERVATIONS

Copies of the magnetograms were received from the magnetic observatory Niemegk, and a film containing copies of the magnetograms from Leningrad (SELTSY), Moscow (KRASNAYA PAKHRA), Odessa (STEPANOVKA), and Tiflis (DUSHETI) were received from the Academy of Science of Moscow.

3. THE TREATMENT

The examination, based on the supposition that the effect should be proportional to the covered part of the sun's disc, has been confined to the magnetic declination, and consists firstly in the determination of the time of passage of the totality, or of the maximal obscuration and of the time of the maximal effect on the declination, and secondly of the maximal diminution in percent of a derived departure of the daily variation for the time of maximal obscuration.

4. OCCURRENCE OF MAXIMAL OBSCURATION AND OF THE MAXIMAL DEVIATION

In U.S.S.R. the axis of the ellipse-formed area of the totality is not perpendicular to the track, and consequently the maximal obscuration at each of the different observatories occurs at times different from that at which it occurs at the point of the track nearest to the observatory. This had to be taken into account at the determination of the time of the occurrence of maximal obscuration. Table 1 gives the names of the stations, their latitude and longitude, time of maximal obscuration, and occurrence of maximal deviation from the normal variation of the day in question.

* The Danish Meterological Institute, Copenhagen, Denmark.
† The Hydrographic Office, Stockholm, Sweden.

Table 1. *Occurrence of maximal obscuration and of maximal deviation of the declination during the solar eclipse of* 30 *June* 1954

Station	φ	λ	*Maximal obscuration GMT*	*Maximal deviation GMT*
Niemegk	52°04′	12°40′	1251	1245
Leningrad (SELTSY)	59°57′	30°42′	1255	1305
Moscow (KRASNAYA PAKHRA)	55°28′	37°19′	1308	1311
Odessa (STEPANOVKA)	47°47′	30°53′	1318	1315
Tiflis (DUSHETI)	42°05′	44°42′	1336	—

The reason why no value for the maximal deviation at Tiflis (DUSHETI) has been given, is that the deviation was too small to be traceable. It will be seen that the maximal deviation in average occurs at the same time as the maximal obscuration, just as for the observations examined earlier.

5. THE DIMINUTION IN PERCENT OF A DERIVED DEPARTURE

EGEDAL and AMBOLT (1955) have used a certain method in order to determine the amount percent of the effect at a considered observatory in relation to the maximal effect.

A new method has now been developed by EGEDAL and, as it was found more appropriate, it has been used for the present examination. However, values found according to this method only differ slightly from values found by means of the method used earlier.

For the new method, a map of the area surrounding the observatory in question is furnished with curves giving the covered part of sun's disc at the different places in percent of the whole disc for the moment of time when the track of totality is nearest to the observatory. On a transparent paper a network of points —a distance apart equal to 100 km on the map—is entered, and furnished with a cipher, giving the magnetic effect on the magnetic declaration at the considered observatory of a certain electric current flowing in the direction of the declination, at a height of 100 km above the point. The network comprises an area of 500 km in radius. Placing the transparent paper on the map with the centre on the observatory and orientated in the magnetic north–south direction, corresponding values of the map and the transparent paper are noted for all points. The two corresponding values are multiplied for all points, and the products are summed up. Next the centre of the transparent paper is placed on the centre of the totality on the map, and the same operation is carried through. From the two obtained sums the desired percent is found.

In Table 2 are given: Station, distance from central line of the totality (to the north +, and to the south −), $0{\cdot}9° \cot h_s \cos d$, where 0·9° is the height of the considered electric currents (100 km) expressed in latitude degrees, h_s the altitude of the sun at totality as observed from the point of the central line nearest to the place of observation in question (the magnetic observatory), and d the difference

Table 2. Position of stations in relation to the track of totality, maximal effect expressed in percent of the derived departure

Station	*Distance from central line*	$0{\cdot}9° \cdot \cot h_s \cdot \cos d$	*Distance from projection of ionospheric central line*	*Derived departure*	*Deviations at maximal obscuration*	*Percent of maximal effect*	*The maximal effect in percent of the derived departure*
Niemegk	−5·4°	+0·5°	−4·9°	−7·0′	2·1′	89	34
Leningrad (SELTSY)	+6·7°	+0·7°	+7·4°	−7·1′	2·0′	83	34
Moscow (KRASNAYA PAKHRA)	+5·9°	+0·8°	+6·7°	−6·0′	1·8′	87	34
Odessa (STEPANOVKA)	−2·5°	+0·8°	−1.7°	−4·8′	0·7′	98	15
Tiflis (DUSHETI)	−0·6°	+1·1°	+0·5°	−2·7′	0·0′	100	0

Weighted mean: 29 ± 6

between the azimuth of the line from the mentioned point to the place of observation and the azimuth of the sun at the above-mentioned moment of time, the distance from the projection upon the earth of the ionospheric central line (E-layer), derived departure, effect at maximal obscuration, percent of maximal effect, and the maximal effect in percent of the derived departure (see EGEDAL and AMBOLT, 1955).

The weighted mean is of the same order of magnitude as the mean for observations examined earlier, but the standard deviation is, for different reasons, greater in the present case. The deviation at Tiflis (DUSHETI) is found to be zero, but on account of the relative small value of the derived departure the influence on the weighted mean is only slight.

6. CONCLUSIONS

The results of the present examination agree with the results of the earlier examination, and the effect for places in U.S.S.R. seems to support the supposition that the effect is proportional to the departure of the daily variation, the effect diminishing through the afternoon, and of the order of magnitude predicted by CHAPMAN (1933).

Acknowledgements—We acknowledge the receipt of reproductions of magnetograms, and express our sincere thanks to the Academy of Sciences, Moscow, for having supplied us with valuable data from four different magnetic observatories in U.S.S.R., and to Geomagnetic Observatory, Niemegk.

REFERENCES

CHAPMAN, S. 1933 *Terr. Mag.* **38**, 175.
EGEDAL, J., and AMBOLT, N. 1955 *J. Atmosph. Terr. Phys.* **7**, 40.

Journal of Atmospheric and Terrestrial Physics, 1956, Vol. 8, pp. 108 to 114. Pergamon Press Ltd., London

Preliminary results of the ionospheric solar eclipse of 25 December 1954

M. E. SZENDREI and M. W. MCELHINNY
Physics Department, Rhodes University, Grahamstown, South Africa

(*Received* 12 *July* 1955)

Abstract—The effects of this solar eclipse on the ionospheric layers may be approximately explained by assuming that the solar radiation responsible for the layers comes uniformly from the sun's disc. Values of the recombination coefficient obtained for each of the three main layers are in good agreement with recent values obtained by independent methods.

1. INTRODUCTION

IONOSPHERIC readings at vertical incidence were taken in Grahamstown during an annular eclipse of the sun which occurred on 25 December 1954. Grahamstown lay practically at the centre of the belt of annularity (Fig.1); the times of the various phases of the eclipse are shown in Table 1. Fig. 2 shows the unobscured fraction, f, of the sun at a height of 200 km above Grahamstown as a function of South African Standard Time.

A specially designed and completely automatic ionosphere sounder was used, covering the range from 1·5 to 15·0 Mc/s. The equipment delivered pulses of 100-μsec duration at an average output of 2 kW. The variation in frequency

VOL. 8 1956

Table 1. *Times of contact, S.A. Standard Time = U.T. + 2h.*

Height (km)	*1st contact*	*2nd contact*	*3rd contact*	*4th contact*
100	06h 16m	08h 00m	08h 07m	09h 35m
200	06 45	07 58	08 05	09 34
300	06 43	07 57	08 03	09 32

was obtained by beating a fixed oscillator at 30 Mc/s with a variable oscillator operating between 31·5 and 45·0 Mc/s. The latter also served as the first oscillator of a double conversion receiver, so that it was automatically tuned to the transmitter at all frequencies. Thus both transmitter and receiver covered the full frequency range by rotation of a single condenser. From the h',f records, frequencies could be read to an accuracy of 0·02 Mc/s, and virtual heights to the nearest 2 km.

2. OBSERVATIONS

Readings were taken over thirty control days centring on the eclipse every quarter of an hour from 0500 to 1000 S.A. Standard Time, and at hourly intervals for the rest of the day. On 25 December for the duration of the eclipse, readings were taken at 2½-min intervals. Owing to the lengthy procedure of converting virtual

heights to true heights (MANNING, 1947; KELSO, 1952), only part of the records taken have been analyzed fully, and the results presented in this paper are deduced only from critical frequencies. True heights evaluated so far indicate that during the eclipse the heights of maximum electron density were not significantly different

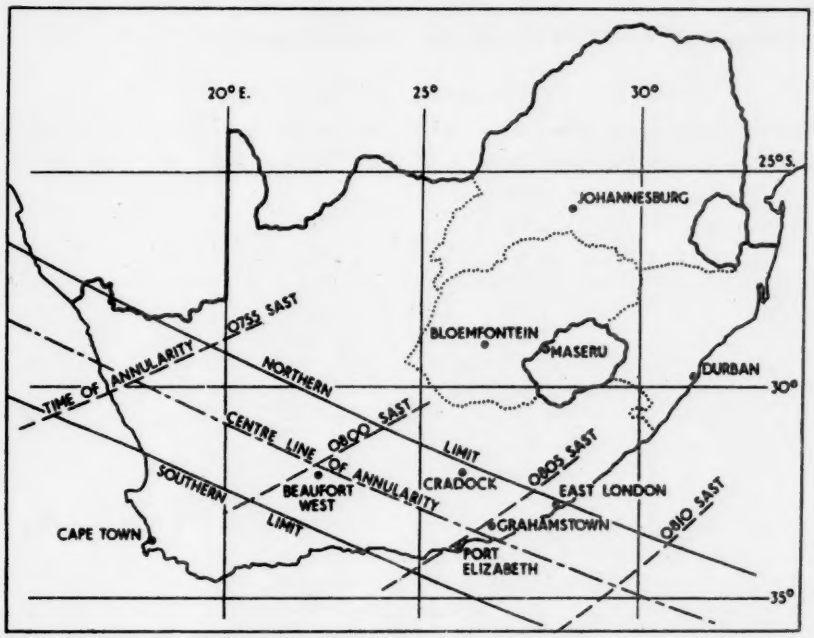

Fig. 1. Path of annular eclipse over South Africa.

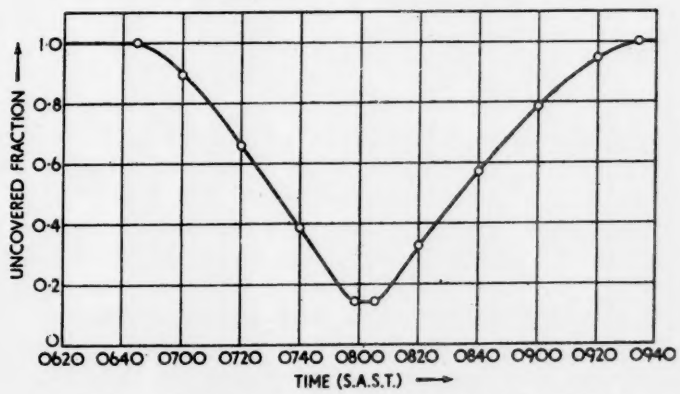

Fig. 2. Unobscured fraction of sun at a height of 200 km.

from those of the control days. It was gratifying to note from data supplied by the Magnetic Observatory, Hermanus, that the period under consideration was magnetically quiet, there being no days with magnetic character figure 2, and the three-hour range magnetic indices never rising above 4.

From the critical frequencies, f_0, for any particular layer, the maximum electron density, N, in that layer was calculated from:

$$N = 1{\cdot}24 \times 10^4 f_0^2 \tag{1}$$

were f_0 is expressed in Mc/s. Mean values of N as a function of time of day were calculated for each of the layers for the thirty control days.

3. INTERPRETATION OF RESULTS

Without making any assumption as to the processes of ion and electron production and recombination, the rate of increase of electron density can be put in the form:

$$\frac{dN}{dt} = q - \alpha N^2 \tag{2}$$

where q is the rate of electron production per cm^3, and α is the effective recombination coefficient.

If we assume that the ionizing radiation responsible for the formation of a particular layer comes uniformly from the sun's disc, at any stage during an eclipse, equation (2) must be modified to:

$$\frac{dN}{dt} = fq - \alpha N^2 \tag{3}$$

in which f represents the uncovered fraction of the sun's disc and may be calculated from astronomical data.

To test equation (3), likely values of α were assumed, and q was then calculated at suitable intervals from equation (2), using the control data. Theoretical curves of N on the eclipse day were then obtained by following the gradient stage by stage, using equation (3). If the assumptions implied in equation (3) are justified, the theoretical curves, obtained by using the correct value of α, should coincide with the experimental data for the eclipse day.

(a) *E-region*

At this laboratory it has been noted that the E-region is frequently split into two layers, referred to as E_1 and E_2; the E_1 corresponds to the normally accepted E-region, while the E_2 is somewhat irregular, mainly due to the fact that at times it cannot be distinguished from E_{sp}. Observations during the eclipse on the E_2 were in fact disturbed by intermittent E_{sp}; in view of the doubt existing on the identity of E_2 and E_{sp}, no further calculations have been carried out on this layer, although the general trend may be interpreted as an eclipse effect.

Fig. 3 shows the effect of the eclipse on the E_1-layer and three theoretical curves for three values of α. While the general shape of the theoretical curves agrees with the experimental data, no perfect fit could be obtained. In all cases the minima occur too late, and none of them accounts for the rapid drop in N observed during the early phases of the eclipse. This early drop has been observed also by MINNIS (1955) and by PIERCE (1948). However, if we take the value of the minimum as a criterion for determining α, it appears that, for the E_1-region, the recombination coefficient is $0{\cdot}7 \times 10^{-8}$ cm^3 s^{-1}. By the same method, MINNIS (1955) has

VOL. 8 1956

recently found that $\alpha = 0{\cdot}8 \times 10^{-8}$, although these values are somewhat lower than the figure of $1{\cdot}5 \times 10^{-8}$ obtained from rocket measurements (HAVENS *et al.*, 1955).

It has been shown (HULBURT, 1939) that q should be directly proportional to the cosine of the solar zenith distance, χ, for a Chapman layer, i.e.,

$$q = q_0 \cos \chi \tag{4}$$

where q_0 should be constant for a given layer, and represents the rate of ion

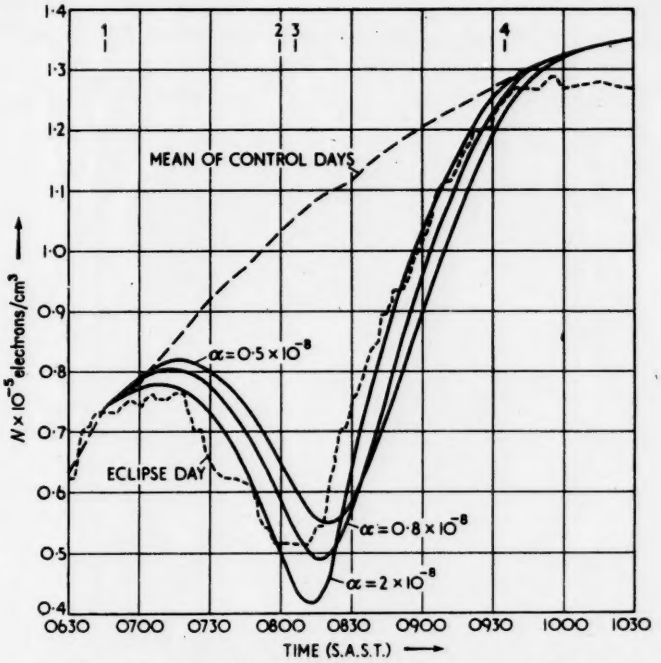

Fig. 3. Experimental and theoretical curves for the E_1-layer.

production at a point where the sun is directly overhead. Combining equations (2) and (4), we have:

$$\frac{dN}{dt} = q_0 \cos \chi - \alpha N^2 \tag{5}$$

Since N and $\frac{dN}{dt}$ are known from the control curve, and $\cos \chi$ may be calculated, a value of α may thus be found from any two points on the control curve. For the E_1-layer, using this method, the recombination coefficient was found to be $0{\cdot}55 \times 10^{-8}$ cm^3 s^{-1}, and this value was constant throughout the morning period; it will be noted that it agrees with the eclipse measurement.

(b) *F_1-region*

Since the F_1-layer occurs only in summer during the middle part of the day, comparatively few eclipse measurements have been carried out on this layer. As

this eclipse occurred very near the summer solstice, the F_1-layer was well defined by a sharp cusp on the *h'f* records, well before the beginning of the optical eclipse.

The effects of the eclipse on the F_1-layer are shown in Fig. 4. During the middle part of the eclipse, the F_1 could not be observed directly on account of the relatively high value of the electron density in the E_2. Retardation caused by the F_1 on the F_2 reflections showed, however, that the F_1 was present throughout the eclipse, and a rough estimate made from this retardation indicates a value of N of $0{\cdot}94 \times 10^5$ cm^{-3} during the annular phase.

Fig. 4 also shows three theoretical curves for three likely values of α. The relation between the experimental and theoretical curves is very similar to that obtained for the E_1-region. For any of the three assumed values of α, the minimum occurs later than in the experimental curve, and the observed early drop in electron

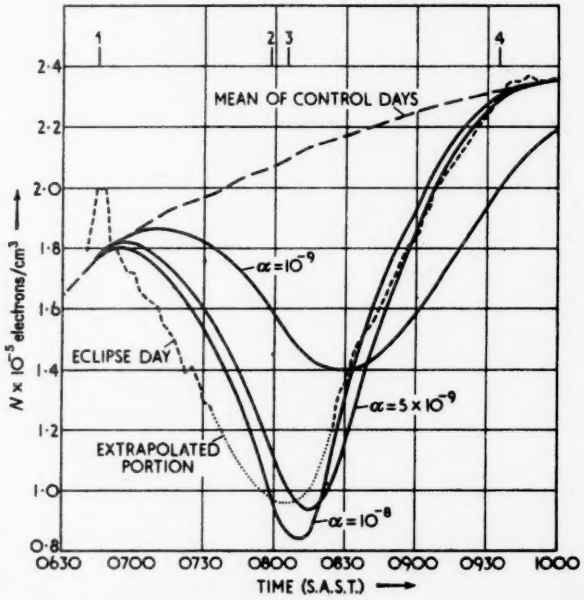

Fig. 4. Experimental and theoretical curves for the F_1-layer.

density could only be accounted for by such a large value of α that the resulting theoretical curve would not fit the experimental data at any other point. Again, taking the minimum as an indication of the recombination coefficient, $\alpha = 5 \times 10^{-9}$ cm^3 s^{-1}. This agrees fairly well with the value of $2{\cdot}0 \times 10^{-9}$ obtained from rocket measurements (HAVENS *et al.*, 1955), and $8{\cdot}2 \times 10^{-9}$ obtained by MINNIS (1955) from similar eclipse measurements.

(c) *F_2-region*

Fig. 5 shows the experimental data for the F_2-region. The effects of the eclipse on this layer are not so noticeable. The eclipse data hardly show any minimum at all, and the probability of the maximum deviation from the control curve occurring

VOL. 8 1956

on any day is 32 per cent. This maximum deviation occurs as late as $1\frac{1}{2}$ hours after the annular phase.

Three theoretical curves are also shown on Fig. 5. Owing to the lower value of α, these curves show a less-marked minimum, and the maximum electron density in the layer takes a much longer time to recover to its average day value. The experimental points are found to agree reasonably well with the theoretical curve for $\alpha = 5 \times 10^{-11}$ cm^3 s^{-1}.

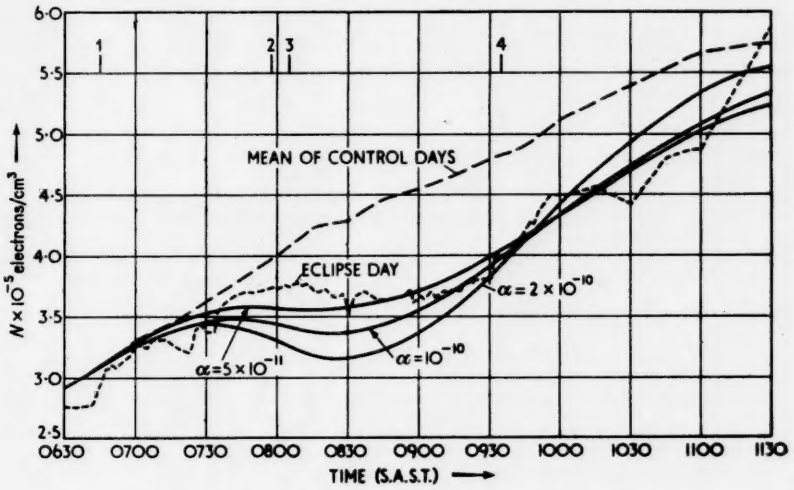

Fig. 5. Experimental and theoretical curves for the F_2-layer.

In dealing with the F_2-region, the recombination coefficient may be estimated by using the fact that $q = 0$ at night, when equation (2) reduces to

$$\alpha = -\frac{1}{N^2} \cdot \frac{dN}{dt} \tag{6}$$

This method gave $\alpha = 1{\cdot}6 \times 10^{-10}$ cm^3 s^{-1}, which does not agree with the eclipse value. The latter, however, is in surprisingly good agreement with the most recent estimates of 6×10^{-11} obtained by MARTYN (1955) from lunar-tides in the ionosphere, and 7×10^{-11}, obtained by HAVENS *et al.* (1955).

Several eclipse observations have been made on the F_2-region. In general it has not been possible to draw any conclusions regarding this layer, because of the high probability of variations during the middle part of the day due to numerous factors such as horizontal movement, temperature variations, diffusion, etc., which are known to affect this region. Furthermore, owing to its low recombination coefficient, an eclipse of the sun should not produce so large a difference from the control data as it does for the lower layers.

It is noteworthy that the only two previous eclipse measurements on this region in cases where the eclipse was already under way at sunrise (GLEDHILL and SZENDREI, 1947; WELLS, 1952) produced results analogous to those presented in

this paper. The values of α found to fit the experimental data were $2{\cdot}8 \times 10^{-10}$ and $3{\cdot}0 \times 10^{-10}$ respectively, obtained from equation (6). It would appear therefore that the recombination coefficient decreases towards the middle part of the day, owing possible to a change in temperature or chemical composition, or simply to a change in height of the maximum electron density in the layer.

4. Conclusions

The above analysis shows that the effect of this eclipse on the E_1-, F_1-, and F_2-layers may be regarded to a first approximation to be due to a geometrical obscuration of a solar disc of uniform intensity. Such analysis has yielded values for the recombination coefficient in the three main layers which are in good agreement with the recombination coefficient in the three main layers which are in good agreement with the most recent estimates obtained in most cases by independent methods.

It suffers from the disadvantage that only maximum electron densities have been considered and, furthermore, it has been assumed that the height and temperature of each of the layers remains unchanged over the duration of the eclipse. Work is in progress to take into account these variable factors.

Acknowledgements—The authors would like to take this opportunity to thank the Council for Scientific and Industrial Research for a substantial grant used in building the automatic ionosphere sounder, and Mr. A. M. van Wijk of the Magnetic Observatory, Hermanus, for supplying the magnetic data.

VOL.
8
1956

References

Gledhill, J. A., and Szendrei, M. E.	1947	*Trans. Roy. Soc. S.A.* **31,** 315
Havens, R. J., Friedman, H., and Hulburt, E. O.	1955	*Physics of the Ionosphere*, ed. Phys. Soc., London, pp. 237ff.
Hulburt, E. O.	1939	*Terrestrial Magnetism and Electricity*, ed. J. A. Fleming, McGraw-Hill, New York, pp. 514ff.
Kelso, J. M.	1952	*J. Geophys. Res.* **57,** 357
Manning, L. A.	1947	*Proc. I.R.E.* **35,** 1203
Martyn, D. F.	1955	*Physics of the Ionosphere*, ed. Phys. Soc. London, pp. 212ff.
Minnis, C. M.	1955	*J. Atmos. Terr. Phys.* **6,** 91
Pierce, J. A.	1948	*Proc. I.R.E.* **36,** 8
Wells, H. W.	1952	*J. Geophys. Res.* **57,** 291

RESEARCH NOTES

On the extinction correction used in the determination of airglow emission heights by the van Rhijn method

(*Received* 23 *June* 1955)

IT has been suggested by ASHBURN (1955) that, in the determination of airglow heights by the van Rhijn method, it may be necessary to correct for a supplementary extinction in addition to that due to Rayleigh scattering and ozone absorption. The purpose of the present note is to emphasize not only the desirability of establishing whether such supplementary extinction exists at the time when zenith-horizon observations are made, but also, if it does exist, the desirability of determining the optical properties of the particles responsible.

We consider an atmosphere containing n particles per unit volume with optical cross-section Q_0; the total light removed from the incident beam of intensity I by the particles in the volume element is then $\delta I = InQ_0\delta v$. We denote by $f(\theta)\delta I$ the fraction of this which is scattered per unit solid angle in the direction making an angle θ with the direction of the incident beam. For pure absorption we have $f(\theta) = 0$ and for pure scattering we have $2\pi \int_0^\pi f(\theta) \sin\theta \, d\theta = 1$. The optical depth τ is related to the path length δx by $\delta\tau = nQ_0\delta x$.

We consider the simple model of a plane atmosphere. The observed intensity of a point source lying above the atmosphere (starlight) will then vary as $\exp(-\tau_1/\cos Z)$, where τ_1 is the zenith optical depth and Z the zenith distance; this provides us with a means of measuring τ_1. However, the observed intensity of an extended source lying above the atmosphere will depend on the form of $f(\theta)$. To illustrate this dependence we consider the intensity above the atmosphere to be independent of direction, and calculate, for various functions $f(\theta)$, the ratio $I(75°)/I(0°)$ which would be observed. For small values of $\tau_1/\cos Z$ we may use the first order approximation

$$I(Z) = \left(1 - \frac{\tau_1}{\cos Z}\right) + \frac{\tau_1}{\cos Z}\int_{\chi=0}^{\pi/2}\int_{\xi=0}^{2\pi} f(\theta)\sin\chi \, d\chi \, d\xi \qquad (1)$$

where the first term gives the transmitted light and the second the scattered light; the intensity above the atmosphere is taken equal to unity. In (1) θ is the angle between the direction Z and the direction specified by the polar angles χ, ξ, i.e. $\cos\theta = \sin Z \sin\chi \cos\xi + \cos Z \cos\chi$. We put

$$f(\theta) = \begin{cases} 1/2\pi(1 - \cos\theta_0) & \text{for} \quad \theta \leqslant \theta_0 \\ 0 & \text{for} \quad \theta > \theta_0 \end{cases} \qquad (2)$$

For $\theta_0 = 180°$ this corresponds to isotropic scattering, for which the solution will differ but little from that for Rayleigh scattering by particles of molecular dimensions (BARBIER, 1952). For $\theta_0 = 30°$ or $45°$ the function (2) gives a schematic representation of the scattering

of light in the visual region by dielectric spheres of radii $r \sim 5 \times 10^{-5}$ or $r \sim 1 \times 10^{-4}$ cm respectively (VAN DE HULST, 1946). Using (1) and (2), it is readily shown that $I(Z) = 1$ for $(90° - Z) \geqslant \theta_0$.

Table 1 gives values of $I(75°)/I(0°)$ for $\tau_1 = 0{\cdot}05$. We consider the following cases: (i) pure absorption (the exact solution $I(Z) = \exp(-\tau_1/\cos Z)$ and the approximation (1) which reduces to $I(Z) = 1 - \tau_1/\cos Z$); (ii) isotropic scattering (the approximation I of BARBIER (1949), which for $\tau_1 = 0{\cdot}05$ does not differ significantly from the exact solution, and the approximation (1)); (iii) the approximation (1) for $\theta_0 = 30°$; and (iv) the approximation (1) for $\theta_0 \leqslant 15°$.

Table 1

	$I(75°)/I(0°)$
(i) Pure absorption — exact solution	0·867
(i) Pure absorption — approximation (1)	0·849
(ii) Isotropic scattering — approximation I of BARBIER (1949)	0·934
(ii) Isotropic scattering — approximation (1)	0·927
(iii) $\theta_0 = 30°$ (dielectric spheres, $r \sim 5 \times 10^{-5}$ cm), approximation (1)	0·962
(iv) $\theta_0 < 15°$ (dielectric spheres, $r \geqslant \sim 1 \times 10^{-4}$ cm), approximation (1)	1·000

It is seen that, for a given extinction of a point source, the greatest correction to the zenith-horizon ratio may be expected for pure absorption, but that cases of pure scattering may arise for which the correction to the ratio is negligible.

The author is indebted to Dr. D. BARBIER for many stimulating discussions.

M. J. SEATON

*Institut d'Astrophysique, Paris**

VOL. 8 1956

REFERENCES

ASBURN, E. V.	1955	*Jour. Atm. and Terr. Phys.* **6**, 67
BARBIER, D.	1949	*Ann. de Géophys.* **5**, 83
BARBIER, D.	1952	*Ann. d'Astr.* **15**, 247
VAN DE HULST, H. C.	1946	*Rech. Astr. de l'Obs. d'Utrecht* **11**, part 1, p. 61

* On leave from the Department of Physics, University College, London.

Determination of the *F*-region collisional frequency (over Calcutta)

(*Received* 24 *June* 1955)

WHEN a radio wave passes through an ionized region in the upper atmosphere the electrons (and also the ions) are set into oscillation by the incoming electromagnetic wave. If in course of this oscillation an electron happens to make an "inelastic collision" with some particle; a portion of the energy is dissipated in the process; i.e., absorption takes place.

Thus the absorption of a radio wave in passing through an ionized medium gives a measure of the number of inelastic collisions, or, in other words, the value of the collisional frequency (ν) in the medium. It is evident that ν will depend on the particle concentration in the medium as well as the kinetic agitation of the particles, i.e., their temperature. In this

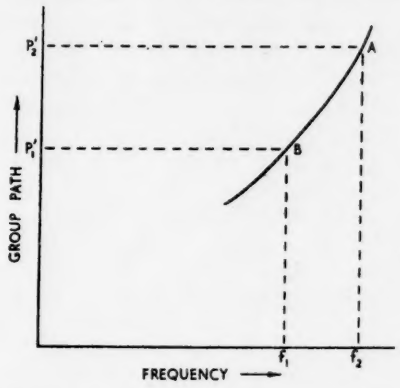

Fig. 1. P'-f curve as used for calculating the collisional frequency.

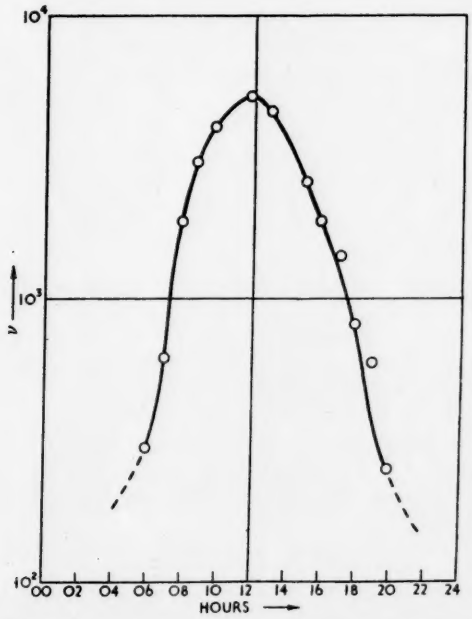

Fig. 2. Diurnal variation curve of the collisional frequency of the F-region over Calcutta.

note we shall describe the result of measurements on collisional frequency carried out at Calcutta (geo. lat. 22° 33′ N, mag. lat. 12° N) during the period 26 May to 3 July 1954. Determination of the collisional frequency at the F-region height was made by the method of APPLETON (1935) from the measurements of the reflection coefficient and the P'-f curve.

If ρ_1 be the reflection coefficient at a frequency f_1, and ρ_2 that at f_2, then the collisional frequency ν is given by

$$\nu = 2c \frac{f_1 \log_e \rho_1 - f_2 \log_e \rho_2}{\text{area } ABP_1'P_2' \text{ as shown in Fig. 1}}$$

when c is the velocity of light in vacuum, and P's represent the group paths.

The reflection coefficients were determined with a manually operated recorder in the Ionosphere Laboratory of the Institute of Radio Physics and Electronics, Calcutta University, and by using the method as given by CHATTERJEE (1952).

The average diurnal variation curve of the collisional frequency is shown in Fig. 2. It is observed that the value of ν is of the order of 10^3/sec, and becomes maximum (about 5×10^3/sec) near about noon, and minimum (about 10^2/sec) near about midnight.

The diurnal variation curve for ν was also plotted against cos χ. But it was not linear. This shows another deviation of the F-region from the Chapman law. Actually, the rate of rise of ν was found to increase with cos χ, and this may be explained in terms of the rapid rise of temperature in the F-region with the approach of noon.

MRINMAYEE GHOSH

Patna Women's College, Patna, India

REFERENCES

APPLETON, E. V. 1935 *Nature* **135**, 618
CHATTERJEE, B. 1952 *Indian J. Phys.* **26**, 585

VOL. 8 1956

The interpretation of measurements of radio-wave interaction

(*Received* 18 *August* 1955)

THE theory of the interaction of radio waves in the ionosphere (BAILEY and MARTYN, 1934, 1937, 1938) is based upon an equation for the time-dependence of the mean agitational energy Q of electrons moving among molecules of the air under the influence of the field of the disturbing radio wave. If $w(t)$ is the power delivered to an electron by the radio wave, and R the rate at which electrons with energy Q lose energy in collisions with the molecules, then the basic equation is

$$dQ/dt + R = w(t). \tag{1}$$

The quantity R, in a given gas, is a function of the agitational energies Q and Q_0 of the electrons and gas molecules, such that R is evanescent as Q approaches Q_0. In the original formulation of the theory it was supposed that

$$R = G\nu(Q - Q_0), \tag{2}$$

where ν is the collisional frequency of the electrons and G a parameter whose value it was hoped could be found from laboratory measurements of electronic motion in air. Measurements of radio-wave interaction, when interpreted in terms of this formulation of the theory,

led to values of the quantity Gv at the seat of the cross-modulation in the ionosphere; consequently it was considered that v could be found if G were known.

When, however, the manner in which the quantity R is measured is considered, as well as the theory of its origin, it becomes evident that the introduction of the collisional frequency at this early stage is artificial, and that the physical quantity that is immediately concerned is the number of molecules in unit volume n, rather than v the collisional frequency of the electrons.

It is suggested therefore that equation (2) should be replaced by

$$R = Bn(Q - Q_0), \tag{3}$$

where B is a function of Q and Q_0 that is effectively constant when $(Q/Q_0 - 1) \ll 1$. Thus the atmospheric parameter that it can be hoped to find directly from measurements of radio-wave interaction is not the collisional frequency v, but the molecular concentration n.

In laboratory experiments, when electrons in a steady state of motion drift at speed W through a gas at pressure p under the action of an electric field Z, the power $w = ZeW$ supplied to an electron is equal to the rate of loss of energy R in collisions. It follows that, if p is expressed in millimetres of mercury and Z in volts per centimetre,

$$\left(\frac{3 \times 10^2 \times 3{\cdot}35 \times 10^{16}}{4{\cdot}8 \times 10^{-10}}\right) R/n = 2{\cdot}09 \times 10^{28} R/n = (Z/p)W.$$

Since both W and Q/Q_0 are functions of Z/p, the latter parameter may be eliminated and the experimental dependence of R/n on Q/Q_0 determined in principle. In order to relate the experimental dependence of R upon Q/Q_0 to the theory of radio-wave interaction, an approximate theoretical investigation was made of the loss of energy by electrons in those collisions that produce changes in the rotational energies of the molecules of diatomic gases. The following dependence of R upon Q and Q_0 was deduced, and was found to describe the experimental results corresponding to the smaller values of Q/Q_0:

$$R/n = \alpha Q^{1/2}[\exp(-\beta/Q) - \exp(-\beta/Q_0)], \quad \text{c.g.s. units.} \tag{4}$$

where α and β are constants. In oxygen at $T = 288°\text{K}$, when $Q/Q_0 < 7$ the experimental results* are closely represented by this formula with $\alpha = 3{\cdot}04 \times 10^{-16}$ and $\beta/Q_0 = 14{\cdot}4$. In nitrogen, the measurements corresponding to small values of Q/Q_0 are not sufficiently extensive for accurate values of α and β/Q_0 to be assigned, although it is evident that $\beta/Q_0 \neq 3$. In air, the quantity R is $R = 0{\cdot}2R_{O_2} + 0{\cdot}8R_{N_2}$, and it proves to be the case that when $Q/Q_0 > 7$ the term $0{\cdot}2R_{O_2}$ is predominant; but as $Q \to Q_0$ the contribution of the oxygen to R in air is negligible. Thus when $Q \to Q_0$, $R_{\text{air}} \to 0{\cdot}8R_{\text{nitrogen}}$. Also, when $(Q - Q_0)/Q_0 \ll 1$, equation (4) assumes the form:

$$R/n \to \alpha\beta[\exp(-\beta/Q_0)/Q_0]\, Q^{-1/2}(Q - Q_0). \tag{5}$$

A comparison of this formula and the extrapolated experimental results in nitrogen at $T = 288°\text{K}$ leads to the following special, but at present approximate, form of equation (5) applicable at any temperature T:

$$(R/n)_{\text{nitrogen}} \doteq 9 \times 10^{-19}\left(\frac{288}{T}\right)[\exp\{-3(1 - T/288)\}]\, Q^{-1/2}(Q - Q_0). \tag{6}$$

* Unpublished measurements by Drs. R. W. Crompton and D. J. Sutton in this department.

If it be supposed that the temperature in the ionosphere at about 85 km above the ground is 200°K, and that in radio-wave interaction $(Q - Q_0)/Q_0 \ll 1$, then

$$(R/n)_{\text{air}} = 0{\cdot}8(R/n)_{\text{nitrogen}} = 8{\cdot}5 \times 10^{-12}\,(Q - Q_0) = B\,(Q - Q_0).$$

In observation of radio-wave interaction at oblique incidence (e.g., RATCLIFFE and SHAW, 1948; HUXLEY, 1952), it was found that Bn (formerly Gv) ranged from 10^3 to $2{\cdot}5 \times 10^3$. The corresponding range of n is therefore $1{\cdot}2 \times 10^{14}$ to 3×10^{14} cm^{-3}. The corresponding range of heights is 83 to 89 km. These heights are consistent with the values determined from the phase of the cross-modulation. The collisional frequency ν can be derived from n through the relationship $\nu = nA\bar{U}$, where A is the mean collisional cross-section and $\bar{U}$ the mean speed of agitation of the electrons, provided the dependence of A upon $\bar{U}$ is known. It is found (CROMPTON, HUXLEY, and SUTTON, 1953) that in air when $Q/Q_0 < 9$, $A = 2{\cdot}48 \times 10^{-23}\bar{U}$. Since $\bar{U} = 4{\cdot}33 \times 10^{13}Q^{1/2}$, it follows that $\nu = 4{\cdot}9 \times 10^4 nQ$. The values of ν that correspond to $n = 1{\cdot}2 \times 10^{14}$ and 3×10^{14} when $T = 200$°K are $\nu = 2{\cdot}4 \times 10^5$ and $6{\cdot}1 \times 10^5$.

In order to determine the value of B more precisely, further laboratory values of R in nitrogen at small values of Q/Q_0 are needed.

These matters will be discussed in greater detail in another paper.

Department of Physics,
The University of Adelaide,
South Australia.

L. G. H. HUXLEY.

VOL. 8 1956

REFERENCES

BAILEY, V. A.	1937	*Phil. Mag.* **23,** 929;
	1938	**26,** 426
BAILEY, V. A., and MARTYN, D. F.	1934	*Nature* **133,** 218;
		Phil. Mag. **18,** 369.
	1935	*Nature,* **135,** 585.
CROMPTON, R. W., HUXLEY, L. G. H., and SUTTON, D. J.	1953	*Proc. Roy. Soc.* **A218,** 507.
HUXLEY, L. G. H.	1952	*Nuovo Cimento Supplement,* vol. IX, ser. IX.
RATCLIFFE, J. A., and SHAW, I. J.	1948	*Proc. Roy. Soc.* **A193,** 311.

On the observation of ionospheric self-interaction

(*Received* 1 *June* 1955)

Abstract—Essential precautions are described that must be taken in experimental studies of ionospheric self-interaction to avoid misleading results caused by interference between various rays and by the band-width of the receiver.

THERE is at present interest in, and some controversy about, the phenomenon of self-interaction. The author has recently published (HIBBERD, 1955) a quantitative theory of the effect in the absence of a magnetic field, which should serve as a guide to experiment. The presence of the magnetic field complicates the situation, and makes a quantitative

analysis near the gyro-frequency particularly complex, so that for this at present the approach must be largely empirical. Self-interaction occurs because absorption of energy from a wave changes the absorption coefficient of the ionosphere for the wave. To produce any detectable effect, the radiation and absorption of considerable power is required. When the transmitted wave is sinoidally modulated, the most obvious effect of self-interaction is a reduction in the depth of the modulation, and this depends in a specified manner on the modulation frequency and is proportional to the power.

It is the purpose of this note to point out simple but essential precautions that must be taken in experiments to observe and study the effect. Self-interaction is obviously to be looked for on a sky-wave, that is, on a wave that has been reflected in the ionosphere. To be able to interpret the measurements of amplitude, and perhaps of phase, of the received modulation, it is necessary that this ray be one that has undergone only a single ionospheric reflection. Further, if other rays reach the receiver, such as a ground-wave or other sky-waves, interference between the received rays will cause the resultant modulation amplitude and phase to vary in a random fashion, and may even result in gross distortion of the original modulation, equivalent to modulation exceeding 100 per cent. It is not feasible at broadcasting frequencies to design an aerial system with sufficient resolution to select one out of a number of downcoming rays. One must therefore make measurements when only the once-reflected sky-wave is present. The simplest way to be certain of the absence of other rays is to superimpose a short pulse on the sinoidally modulated wave at the transmitter. To avoid the ground-wave it is probably best to locate the receiver sufficiently far from the transmitter, rather than to attempt to suppress the ground-wave.

In addition, one must not overlook the effect of the finite band-width of the receiver and the shape of its selectivity curve in decreasing the amplitude of the sidebands of a modulated wave with respect to the carrier amplitude. This obviously reduces the modulation of depth of a modulated signal in passing through the receiver, the reduction being the greater the higher the modulation frequency. Any receiver employing resonant circuits must suffer from this defect to some extent. When the selectivity of the receiver or, better, the reduction in modulation depth produced by it at each modulation frequency, is known, one may easily correct for this effect. Care is needed in tuning the receiver so as to avoid unequal effects on the two sidebands.

It is relevant to report here that in 1952 the author undertook brief experiments with the co-operation of the Australian P.M.G.'s Department. The transmitter was at Brisbane, and radiated a sinoidally modulated continuous wave of 10 kW on 590 kc/s: the receiver was at Sydney, some 700 km distant. Observations were made between 2320 hours and midnight (local time), and between 0530 and 0600 hours, including dawn. When the received signal was strong and steady, as indicated by a signal-strength meter (so that presumably only a single sky-wave was present, though this is not a safe assumption in precise measurements), consistent and reproducible results were obtained. These showed a steady reduction in modulation depth as the modulation frequency increased, typical observed factors of reduction being 0.94 at 100 c/s, 0.60 at 1600 c/s, and 0.11 at 5000 c/s. However, when corrections were applied for the effect of the selectivity of the receiver, the true depth of the received modulation was equal, within the limits of measurement, to that transmitted. Some measurements were made using 5 kW, with the same result. These results were not surprising as, in view of the theory presented elsewhere (Hibberd, 1955), no appreciable self-interaction was to be expected with such low powers as 10 kW.

When severe fading occurred, the modulation depth varied in a random manner, sometimes decreasing and sometimes increasing to over 100 per cent, and the shape of the modulation envelope was at times distorted beyond recognition. Although identifying pulses were not used, previous experience indicated that the fading observed was that

due to interference between various downcoming rays. The general conclusions drawn from the tests were that no appreciable self-interaction occurred under the circumstances of the experiment and that the effects that were observed could be interpreted readily in terms of known phenomena.

In view of the foregoing, it is most desirable that in any experimental investigations of self-interaction the precautions described above be taken to eliminate spurious effects, to establish whether self-interaction involving the physical processes described by the author is occurring, and to see if any hitherto unknown phenomenon is present. It is to be emphasized that the reduction of modulation depth by self-interaction should, in all circumstances, be directly proportional to the emitted power.

University of New England,
Armidale, N.S.W., Australia.

F. H. HIBBERD.

REFERENCE

HIBBERD, F. H. 1955 *J. Atmosph. Terr. Phys.* **6**, 268–279

VOL.
8
1956

A possible explanation of the drop in *F*-region critical densities accompanying major ionospheric storms

(*Received* 28 *July* 1955)

MAJOR ionospheric storms are frequently characterized by decreased *F*-region critical densities and by increased virtual heights. An explanation in terms of thermal expansion of the atmosphere is shown to be insufficient, and an alternative explanation in terms of increased recombination rates is suggested.

According to CHAPMAN'S theory, the maximum electron density in a layer is given by

$$n(e \mid \max) = \left\{\frac{S \cos \chi}{eH\alpha}\right\}^{\frac{1}{2}} \tag{1}$$

where S is the photon flux, χ the solar zenith angle, e the Napierian base, H the scale height (proportional to T), and α the recombination coefficient. It is seen that, if α were constant, $n(e \mid \max)$ would vary as $T^{-\frac{1}{2}}$. Whatever more refined model were considered, we might still expect to find that $n(e \mid \max)$ would be insensitive to thermal expansion effects.

Thermal expansion effects have been discussed in more detail by LEPESHINSKY (1951). Following the severe magnetic storm of 24–26 January 1949, the F_2 vertical height at Poitiers increased by 125 km, which could be explained in terms of a temperature increase of 35 per cent. However, assuming thermal expansion to be the only effect, the corresponding decrease in $n(e \mid \max)_{F_2}$ was calculated to be only 14 per cent compared with an observed decrease by a factor of 4. LEPESHINSKY suggested that it might be necessary to invoke increased recombination coefficients.

For the very greatest ionospheric storms the problem is even more acute; the critical density in F_2 may decrease by a factor of at least 100 (BERKNER, WELLS, and S. L. SEATON, 1939; BERKNER and S. L. SEATON, 1940), and it then appears probable that there is a real decrease in the total electron content of the ionosphere.

The most probable recombination processes appear to be

$$O^+ + O_2 \rightarrow O + O_2^+ \quad (2)$$

$$O_2^+ + e \rightarrow O' + O'' \quad (3)$$

(BATES, 1954). There is some uncertainty in the rate coefficients for these reactions, but until recently the most serious problem was to see how the O_2 molecules destroyed by (2) and (3) could be replenished sufficiently rapidly. However, an important advance has been made by NICOLET (1954), who has shown that the O_2 abundance at great heights is governed, not by photochemical equilibrium, but by vertical transport. The calculated transport rates indicate that the number of molecules reaching the F-regions may be sufficient to explain the observed recombination by (2) and (3).

According to these ideas, the recombination coefficient may depend critically on the vertical transport of a rare constituent in such a way that an increased transport rate would result in increased recombination and decreased density. Support for the suggestion that increased O_2 transport may explain the storm-time fall in density is provided by the observations that violent ionospheric storms are accompanied by a great deal of scatter, particularly in their early stages, which seems to indicate a condition of violent turbulent agitation in and presumably below the F-regions (BERKNER *et al.*, 1939, 1940). There is evidence that the turbulent elements are in rapid motion, and that they tend to become smaller as the storm progresses; thus turbulent transport and subsequent mixing may be very efficient.

The maximum drop in $n(e)$ due to increased O_2 abundance would be by a factor $(\alpha/\alpha')^{\frac{1}{2}}$, where α is the normal recombination coefficient and α' the coefficient for the dissociative recombination reaction (3). The value of α for F_2 is somewhat uncertain, and may show real variations, but its value is almost certainly between 4×10^{-11} and 1×10^{-9} cm^3 sec^{-1} (BATES, 1951). The value of α' is also uncertain, but probably lies between 10^{-8} and 10^{-6} cm^3 sec^{-1} (see BATES, 1950; FAIRE, FUNDINGSLAND, and ADEN, 1954). Thus a sufficient increase in O_2 would decrease $n(e \mid \max)_{F_2}$ by a factor at least as great as 3, and possibly as great as 150.

Such a mechanism would appear capable of explaining the slow recovery of F_2 after a major storm; the density would remain low until the reactions (2) and (3) had reduced the O_2 abundance to its normal value. It appears less certain that it could explain the behaviour of major storms at equatorial stations. Although these may be preceded by some moderate scatter, the phase involving disappearance of F_2 echoes may proceed without any sign of scatter (BERKNER *et al.*, 1939, 1940); it may be noted that in these cases a new and apparently normal F_2 is re-formed quite quickly.

M. J. SEATON.

Institut d'Astrophysique.
Paris.
(On leave from *The Department of Physics, University College, London.*)

REFERENCES

BATES, D. R. 1950 *Phys. Rev.* **78,** 492;
1951 *Proc. Phys. Soc.* **B64,** 805;
1954 *The Earth as a Planet* (ed. G. P. Kuiper), Univ. Chicago Press, p. 576.

Berkner, L. V., Wells, H. W., and Seaton, S. L.	1939	*Terr. Mag.* **44**, 283.
Berkner, L. V., and Seaton, S. L.	1940	*Terr. Mag.* **45**, 393.
Faire, A. C., Fundingsland, O. T. and Aden, A. L.	1954	*Phys. Rev.* **93**, 650.
Lepeshinsky, D.	1951	*J. Atmosph. Terr. Phys.* **1**, 278.
Nicolet, M.	1954	*Rocket Exploration of the Upper Atmosphere* (eds. R. L. F. Boyd and M. J. Seaton), Pergamon Press, London, p. 361.

The electrical charge on the earth

(*Received* 20 *September* 1955)

In a recent research note in this journal, under the above title, Clark and Kraakevik (1955) discuss the effect of the charges induced by thunderclouds upon the total charge on the earth. This matter can be treated more simply; Gish and Wait (1950) have shown that the average thunderstorm conveys about $\frac{1}{2}$ A of negative charge to the earth, and the measurement of the fine-weather current to the earth requires a total of 1800 A, so that there should be about 3600 storms in action at once; this is not inconsistent with the statistical results of Brookes (1925), which give 1800 storms, neglecting cases of two storms in one day at an observing station and also neglecting showers which do not give audible thunder but which, nevertheless, transfer charge to the earth. If the total induced negative charge on the earth from these 3600 storms is to balance the positive charge on the fine-weather portions of the earth, each cloud would have to contribute about 170 c. A similar calculation has been given by the author (Chalmers, 1953b), where the equality of q and $j/4\pi\lambda$ would give a resultant of zero charge on the earth.

The actual charge induced on the earth below a thunderstorm has never been directly measured, but there have been estimates of the total free charges in thunderclouds, giving average values of around 40 c. However, the charge induced on the earth below a storm would be equal to this value only if all the lines of force from the upper pole of the cloud ended on the ionosphere and none on the earth. Now, it is well known that the potential gradient at the earth due to a distant thundercloud is positive, so that some of the lines of force from the upper pole do reach the earth, thereby reducing the total induced charge below the cloud to a value considerably less than the charge on the lower pole. It therefore seems to be very unlikely that the induced charge below storms approaches the value of 170 c per storm which would be necessary to give zero total charge on the earth. A reasonable estimate might be that the positive induced charge below storms is about 10 per cent of the total negative charge on the fine-weather portions of the earth.

There are other points in Clark and Kraakevik's (1955) note which call for comment. In attempting to apply the argument of Chalmers (1953a) to a surface close to the earth, they are surely incorrect in considering space-charge convection to be the only current which is not a true conduction current, since they neglect precipitation currents and lightning currents and they also ignore the fact that point-discharge currents are by no means simple conduction currents, since there is a ratio of current to potential gradient which is far

VOL.
8
1956

different from the normal conductivity and is not even constant for different potential gradients. CHALMERS's (1953a) argument can be applied only over a complete surface of constant conductivity, and this does not exist below storms. CLARK and KRAAKEVIK appear to suggest that if a lightning flash occurs, the potential gradient at the earth's surface must reach the breakdown value; but investigations of lightning show that the breakdown value is only reached over a small volume and the flash is then propagated from this region; certainly the breakdown stress for lightning flashes is quite unrelated to the average potential gradient below the storm.

J. ALAN CHALMERS

Physics Department,
Durham Colleges,
Durham University.

REFERENCES

BROOKES, C. E. P. 1925 *Geophys. Mem. Meteorol. Off.* (*London*), **24**
CHALMERS, J. A. 1953a *J. Atmosph. Terr. Phys.*, **3**, 345
CHALMERS, J. A. 1953b *J. Atmosph. Terr. Phys.*, **4**, 84
CLARK, J. F., and KRAAKEVIK, J. H. 1955 *J. Atmosph. Terr. Phys.*, **6**, 344
GISH, O. H., and WAIT, C. R. 1950 *J. Geophys. Res.*, **55**, 473

OL.
8
956

Journal of Atmospheric and Terrestrial Physics, 1956, Vol. 8, pp. 126 to 128. Pergamon Press Ltd., London

Indices of geomagnetic activity

of the Observatories ABINGER (*Ab*), ESKDALEMUIR (*Es*), and LERWICK (*Le*)

July to September 1955

The figures given on pages 126 and 128 represent the K-indices for three-hour intervals, beginning with 00–03 hrs for the first and ending with 21–24 hrs for the eighth figure.

July 1955

Day	*Ab* Range for $K = 9 : 500\gamma$			*Es* Range for $K = 9 : 750\gamma$			*Le* Range for $K = 9 : 1000\gamma$			Day
	K-Indices		*Sum*	*K-Indices*		*Sum*	*K-Indices*		*Sum*	
1	2122	2211	13	2122	1110	10	1121	1111	9	1
2	2323	3554	27	1312	3554	24	2212	3454	23	2
3	3322	2322	19	3322	2321	18	3322	1221	16	3
4	1221	2211	12	1121	1110	8	1121	1010	7	4
5	2111	2222	13	1111	1211	9	1111	1211	9	5
6	1111	2334	16	1111	1323	13	1111	1223	12	6
7	3322	4322	21	3322	3322	20	4322	2212	18	7
8	1224	3432	21	0123	2431	16	1112	2432	16	8
9	1223	2212	15	1112	2112	11	1112	2112	11	9
10	2223	4323	21	1123	4322	18	1122	3322	16	10
11	3234	4433	26	3234	3432	24	3334	3312	22	11
12	5333	3224	25	4233	3324	24	5223	3234	24	12
13	4221	3321	18	3211	3321	16	3211	3311	15	13
14	2212	3220	14	2221	3210	13	1221	2210	11	14
15	1122	4433	20	1112	4533	20	1112	3433	18	15
16	3222	3233	20	3212	2233	18	4211	2223	17	16
17	1322	1223	16	1321	1122	13	1321	1112	12	17
18	2322	2221	16	2321	1121	13	1322	2110	12	18
19	1113	2211	12	1112	1201	9	1102	2101	8	19
20	2112	2121	12	2012	2221	12	1111	2121	10	20
21	2012	2213	13	1101	0213	9	1101	1113	9	21
22	1112	2213	13	1102	2213	12	1101	1202	8	22
23	3222	2233	19	2112	2123	14	2111	1123	12	23
24	3323	2222	19	2323	2222	18	3222	1211	14	24
25	2222	3222	17	2122	2222	15	1111	1211	9	25
26	2323	4433	24	2223	4333	22	2123	3333	20	26
27	3212	2322	17	3112	1222	14	2111	1121	10	27
28	1122	3312	15	1012	2202	10	1111	2211	10	28
29	2122	2233	17	2121	1133	14	2111	0132	11	29
30	1122	3322	16	0212	2222	13	1112	1213	12	30
31	3121	3321	16	3121	2211	13	2121	2210	11	31

VOL. 8 1956

August 1955

Day	*Ab* Range for $K = 9 : 500\gamma$		Sum	*Es* Range for $K = 9 : 750\gamma$		Sum	*Le* Range for $K = 9 : 1000\gamma$		Sum	Day
	K-Indices			*K-Indices*			*K-Indices*			
1	2122	3321	16	1002	3321	12	1101	2221	10	1
2	2211	2122	13	2200	1122	10	2201	1013	10	2
3	4223	3433	24	4212	2323	19	3321	2323	19	3
4	2434	4444	29	2334	4444	28	3333	4444	28	4
5	2233	3444	25	2233	3444	25	3123	3344	23	5
6	3344	3535	30	3334	3535	29	4344	4435	31	6
7	3333	3343	25	3323	3334	24	3333	3233	23	7
8	2123	3322	18	2113	3222	16	2122	3221	15	8
9	3222	2222	17	2122	2221	14	2111	2121	11	9
10	2322	3222	18	1201	3212	12	1211	2212	12	10
11	1221	2123	14	1110	1122	9	1111	1111	8	11
12	2232	2212	16	2122	2111	12	1111	2111	9	12
13	1213	2323	17	1212	2223	15	1112	1113	11	13
14	3222	3333	21	3212	2333	19	3212	2333	19	14
15	3323	3221	19	3322	3111	16	3311	3111	14	15
16	0231	2221	13	0231	2111	11	0221	2111	10	16
17	1123	3333	19	1012	2323	14	1111	2323	14	17
18	2222	3232	18	1232	2232	17	2222	1122	14	18
19	2222	2232	17	1212	2222	14	2221	1233	16	19
20	1122	2321	14	1002	2220	9	1112	2221	12	20
21	3121	1112	12	3110	1111	9	2121	1111	10	21
22	0122	1111	9	0111	1121	8	0111	1111	7	22
23	1011	1211	8	1101	1111	7	1120	1111	8	23
24	1223	2212	15	0113	2211	11	0112	2111	9	24
25	1122	3221	14	1111	3221	12	1111	2221	11	25
26	2223	3222	18	1113	3322	16	1113	2312	14	26
27	0021	2233	13	0011	2333	13	1111	1222	11	27
28	1353	3222	21	1343	3122	19	0343	2211	16	28
29	3232	2234	21	2222	2233	18	2222	2333	19	29
30	1223	2322	17	1112	1322	13	1111	2211	10	30
31	2122	2123	15	2112	2223	15	1112	1213	12	31

September 1955

1	1133	3342	20	1133	3342	20	2122	2342	18	1
2	3434	3322	24	3423	3322	22	3323	3322	21	2
3	3334	3233	24	3334	3222	22	3323	3122	19	3
4	4333	3434	27	4333	3324	25	4333	3424	26	4
5	4433	3332	25	4333	3332	24	4433	3332	25	5
6	2333	2333	22	2232	1333	19	2222	2333	19	6
7	3133	2211	16	3233	2211	17	3122	2211	14	7
8	1112	3323	16	1103	3313	15	0112	2322	13	8
9	3212	2222	16	3222	2212	16	3311	1112	13	9
10	1122	2221	13	1122	1221	12	1122	1211	11	10
11	2122	2223	16	2111	2222	13	2111	2212	12	11
12	3343	3334	26	3343	3224	24	2232	3214	19	12
13	4333	2421	22	4333	3421	23	4333	3331	23	13
14	1222	2212	14	0222	2212	13	1122	2212	13	14

September 1955 (*contd.*)

Day	*Ab* *Range for* $K = 9 : 500\gamma$		*Es* *Range for* $K = 9 : 750\gamma$		*Le* *Range for* $K = 9 : 1000\gamma$		*Day*
	K-Indices	*Sum*	*K-Indices*	*Sum*	*K-Indices*	*Sum*	
15	2112 2232	15	2101 2232	13	2101 2231	12	15
16	3223 3213	19	3222 2112	15	3221 3102	14	16
17	3332 2222	19	3332 2222	19	3332 2222	19	17
18	2222 2331	17	2222 2321	16	1212 2231	14	18
19	2222 3223	18	2222 2112	14	3221 2112	14	19
20	3233 1223	19	3223 1222	17	3222 1112	14	20
21	1121 1212	11	1112 1113	11	1111 1113	10	21
22	4312 3232	20	4301 2122	15	3311 1122	14	22
23	1233 2233	19	1133 3233	19	1123 2234	18	23
24	4112 2331	17	3112 2230	14	4211 1230	14	24
25	2021 1112	10	1011 1102	7	1111 1102	8	25
26	1111 1112	9	1001 2111	7	1100 1111	6	26
27	2233 3454	26	2233 3454	26	2223 3454	25	27
28	2333 3243	23	2333 3243	23	2332 2243	21	28
29	3222 3444	24	3222 2444	23	3212 2744	25	29
30	4555 4445	36	4554 4444	34	4554 4444	34	30

VOL.
8
1956

Journal of Atmospheric and Terrestrial Physics, 1956, Vol. 8, pp. 129 to 145. Pergamon Press Ltd., London

The fading of radio waves of frequencies between 16 and 2400 kc/s

S. A. Bowhill
Cavendish Laboratory, Cambridge

(*Received* 23 *July* 1955)

ABSTRACT
The lowest ionosphere, which reflects low-frequency radio waves, contains irregularities of ionization which cause fading of these frequencies. The irregularities have been studied by three types of experiment, all of them using c.w. transmissions reflected from the ionosphere at nearly vertical incidence during the night-time. Firstly, fading records over the frequency range 16–200 kc/s show shallow fading, with a substantially constant quasi-period of 7 minutes up to 70 kc/s; above this frequency a rapid fading of quasi-period about 1 minute appears as well, increasing in depth till it dominates the slower fading. Secondly, two receivers tuned to 85 kc/s separated by various distances give fading records whose statistical correlations lead to structure sizes at the ground of 5 km for the slow fading and 1 km for the fast fading. Thirdly, records taken at three receivers at right angles at 70 kc/s show that the slow fading is due mainly to random velocities of about 40 metres/sec at the reflecting layer, together with a smaller drift velocity which is very variable.

These results lead to a suggested model, with small irregularities slightly above the 70 kc/s reflection level, together with large irregularities below this level.

1. Introduction

The purpose of the paper is to discuss the fading of radio waves received at the ground after reflexion from the ionosphere at nearly vertical incidence. In the experiments to be discussed, it was arranged that the downcoming wave consisted essentially of only one reflected wave, multiply reflected waves being removed either by the use of a time-selective pulse arrangement, or because they were strongly absorbed.

Radio frequencies ranging from 16 to 2400 kc/s are considered. It is shown that there are two different types of fading; a slow type which is most marked on frequencies less than 100 kc/s, and a fast type which is most marked on greater frequencies. On frequencies near 100 kc/s both types can be detected.

In order to establish the reality of these two separate types of fading, it is necessary to apply statistical theory. The appropriate theory is given in Section 2, and the experimental results are discussed in Section 3.

It is well known that there is a close relation between the structure size of the random variations of amplitude over the ground, and the speed of fading of a downcoming wave observed at one point. It was therefore of interest to investigate the size of the amplitude irregularities over the ground. This investigation was made at a frequency of 85 kc/s, where two separate sizes of irregularity might be expected, corresponding to the slow and the fast fading. Frequencies of 71 kc/s and 16 kc/s are also considered, and it is shown that there are two sizes of irregularity corresponding to the two fading speeds. This part of the discussion is given in Section 4.

The fading of a wave received at a single point might be related to the radio diffraction pattern at the ground in several different ways. Thus it might be caused by a steady drift of an unchanging diffraction pattern past the receiver, or by random changes taking place in a pattern which was, on the average, stationary,

or by a combination of both of these causes. Briggs, Phillips, and Shinn (1950) showed how the fading curves recorded at three points could be analysed so as to determine the relative importance of the average drift-motion and the changing of the pattern as it moves. Their method is here applied to experimental measurements of the slow fading made with a frequency of 70 kc/s, and it is shown that this fading was caused mainly by the random alterations of the diffraction pattern. The discussion of these matters is in Section 5.

Finally, in Section 6, the results which have been deduced about the nature of the diffraction pattern at the ground are used in speculations about the irregular structure of the lowest ionosphere at different heights.

2. Statistical Analysis of Fading Speed

To investigate how the fading speed depends on the radio-frequency, it is necessary first to define the statistical parameters involved. It was suggested by Ratcliffe (1948) that random fading could be compared to random electrical noise which had passed through a narrow-band filter, centred on the radio-frequency. This means that the results established by Rice (1945) for the amplitude of a noise voltage may be considered as applying to the amplitude of a radio signal.

If we have a signal of amplitude $R(t)$, we can define two measures of fading time:

$$T_1 = \overline{|R(t) - \overline{R(t)}|} \Big/ \overline{|\dot{R}(t)|} = \frac{\text{mean deviation of } R \text{ from its mean}}{\text{mean slope of } R}$$

T_2 = average time difference between maxima of the amplitude

= fading period of the signal.

These two quantities are related statistically: each measures a different aspect of the time variation of the amplitude. The quantity T_1 is similar, but not identical, to the $1/S$ of Briggs, Phillips, and Shinn (1950); it can be found very quickly from a given fading record (see Appendix).

The correlogram of $R(t)$ is defined by

$$\rho_R(\tau) = \frac{\overline{R(t) \times R(t+\tau)} - \overline{R(t)}^2}{\overline{R^2(t)} - \overline{R(t)}^2},$$

and if $R(t)$ has a Gaussian probability distribution, it can be shown that

$$T_1 = \left\{ - \frac{\rho_R(0)}{\rho''_R(0)} \right\}^{\frac{1}{2}}, \tag{1}$$

and Rice shows that

$$T_2 = 2\pi \left\{ - \frac{\rho_R''(0)}{\rho_R''''(0)} \right\}^{\frac{1}{2}}. \tag{2}$$

An important case is where the correlogram of $R(t)$ is Gaussian in form:

$$\rho_R(\tau) = e^{-\tau^2/2b^2} \tag{3}$$

where b is the time displacement for which $\rho_R(\tau) = 0{\cdot}61$. From the relations (1) and (2), we have

$$\left.\begin{aligned} T_1 &= b \\ T_2 &= 3{\cdot}62b = 3{\cdot}62T_1 \end{aligned}\right\}. \tag{4}$$

VOL. 8 1956

If, on the other hand, $R(t)$ has a Rayleigh probability distribution, given by

$$P(R) \times dR = \frac{R}{\psi} \times e^{-\frac{R^2}{2\psi}} \times dR, \tag{5}$$

then it can be shown that

$$\left.\begin{aligned} T_1 &= 0{\cdot}94b \\ \text{and from RICE} \qquad T_2 &= 3{\cdot}52b = 3{\cdot}74T_1 \end{aligned}\right\}. \tag{6}$$

This probability distribution represents an extreme case of those encountered in practice (MCNICOL, 1949). Those values of T_1 and T_2 in (6) are so near to those in (4) that it is justifiable to apply the results of (4) in all practical cases.

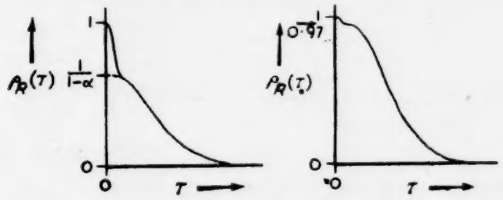

Fig. 1. Correlogram of the sum of a slowly and a quickly fading signal.

If a small amount of a more rapidly varying random function is added to a fading function of this kind, the number of maxima of the function will be affected much more than its mean slope: that is, T_2 will decrease, while T_1 remains virtually unaltered. The quantity T_2 is therefore a more sensitive indicator of the presence of a small amount of rapid fading. Now, the ratio of T_2 to T_1 is 3·62 for a random function with a Gaussian correlogram, so if we define a quantity

$$Q = \frac{3{\cdot}62T_1}{T_2}$$

then a value of Q greater than 1 corresponds to the presence of two fading periods in the function.

If we assume that the correlograms of both fading signals are Gaussian, the correlogram of their sum will be given by

$$\rho_R(\tau) = \frac{1}{1+\alpha} e^{-\frac{1\tau^2}{2b^2}} + \frac{\alpha}{1+\alpha} e^{-\frac{1}{2}\frac{M^2\tau^2}{b^2}}, \tag{7}$$

where α = ratio of mean-square amplitude of the fast fading to that of the slow fading.

M = ratio of the slow to the fast fading period. This function is sketched in Fig. 1. By equations (1) and (2),

$$Q = \frac{\sqrt{(1+\alpha)(1+\alpha M^4)}}{1+\alpha M^2}$$

$$T_1 = b\left\{\frac{1+\alpha}{1+\alpha M^2}\right\}^{\frac{1}{2}}$$

The way in which Q depends on α for various values of M is shown plotted in Fig. 2. For each value of M, Q passes through a maximum value; the left-hand side of a maximum corresponds to the predominance of slow fading over fast, while on the right-hand side of the maximum the reverse is true. Q is in fact a measure

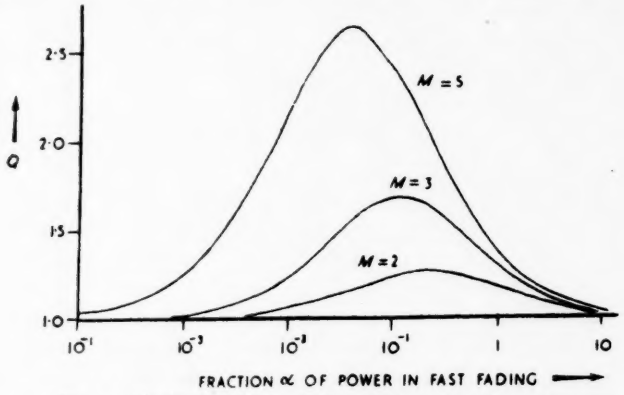

Fig 2. Illustrating the variation of Q over a wide range of α.

of the certainty with which two distinct periods may be distinguished in the record.

An interesting point is that the maximum value of Q for, say, $M = 5$ is reached when the fast fading has only 0·03 of the mean-square value of the slow fading.

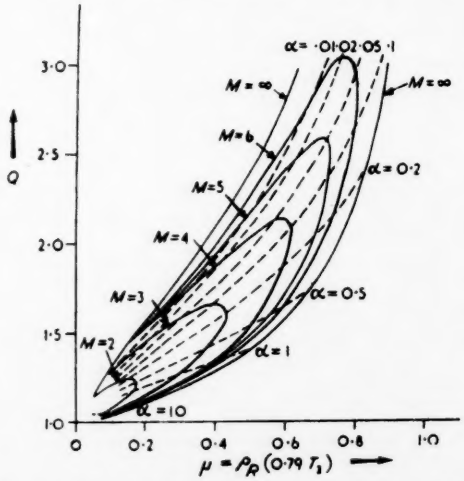

Fig. 3. Diagram for calculating M and α from measured values of Q and μ.

On the correlogram of the original function (Fig. 1), the fast fading would contribute only a small rise superimposed on the correlogram of the slower fading near $\tau = 0$. The correlogram is therefore much less sensitive than either T_1 or T_2 to the presence of a shallow, quickly fading signal.

This fact can be used to calculate α and M from a given record, for in Section 4 an accurate knowledge of α will be needed. One non-dimensional quantity, Q,

VOL. 8 1956

related to α and M, has already been found: one other is needed to complete the determination. We use a quantity μ, one ordinate of the correlogram of the function, which can be found graphically by the method given in the Appendix:

$$\mu = \rho_R(0{\cdot}79T_2)$$

The constant 0·79 has been chosen for reasons of convenience. A simple calculation gives the curves of Fig. 3, which enable M and α to be found from a knowledge of Q and μ.

3. Measurements of Fading Speed

A series of fading curves, made in Cambridge over the past few years on different frequencies, was already available for analysis. To these were added a few more recorded for the purpose of this paper. The transmission paths, and calculated values of T_1, T_2, and Q, are shown in Table 1 for the different frequencies used. The result on 150 kc/s is from a paper by Millman (1952).

Table 1

Frequency kc/s	Transmitter		Receiving site	Path dist. km	Average (min) of		Average Q
	Type	Location			T_2	T_1	
16	GBR	Rugby	Cambridge	90	7	1·9	1
30	CLC	Ongar	Cambridge	54	7	1·9	1
43	GIX	Leafield	Cambridge	122	6	1·9	1
71	Decca	Warwick	Cambridge	102	5	1·9	1·05
113	Decca	Norwich	Cambridge	90	2·5	—	—
127	Decca	Lewes	Malden	143	0·6	0·7	1·5
150	Pulse	Pa., U.S.A.	Pa., U.S.A.	0	0·5	—	—
200	BBC	Droitwich	Cheltenham	56	1·4	—	—
2400	Pulse	Cambridge	Cambridge	0	0·08	—	—

Fig. 4 shows the average values of $1/T_2$ and $1/3{\cdot}62T_1$ plotted logarithmically against frequency. It is clear that T_2 is substantially constant for frequencies from 16 to 71 kc/s, but increases rapidly near 100 kc/s.

The results of Table 1 and Fig. 4 were not all obtained at the same time. It is of interest to consider the results of some special experiments in which fading curves were recorded simultaneously on 16 and 71 kc/s. The fading periods T_2 for the two frequencies are plotted against each other in Fig. 5. Each corresponds to two fading records made during the same period of one hour. It is clear that on about 60 per cent of the occasions the points lie near enough to the line AB for the values of T_2 to be considered equal, but on the other 40 per cent the value of T_2 was less for 71 kc/s than for 16 kc/s. A closer examination of the fading records suggests the following reason for this behaviour.

Fig. 6 is a copy of a fading record on 71 kc/s. The slow fading with a period of about 7 minutes is clearly visible; this fading period is the same as that observed

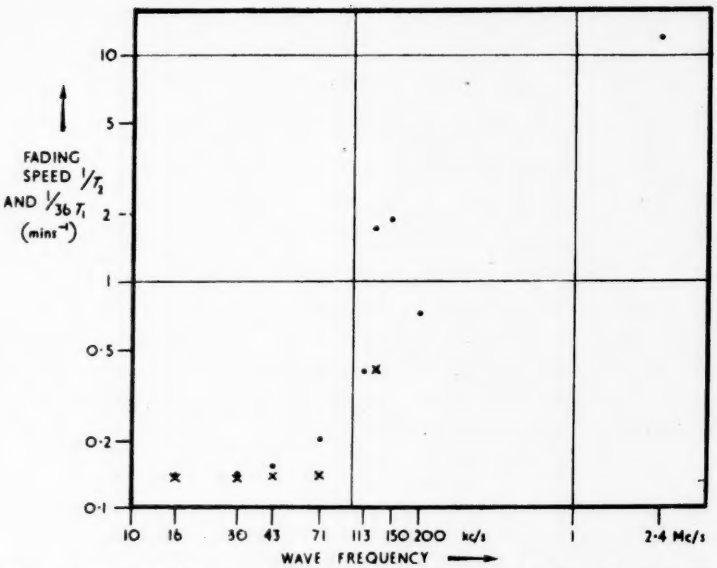

Fig. 4. Average fading speed as a function of frequency. The dots are values of $1/T_2$, and the crosses are values of $1/3{\cdot}6T_1$.

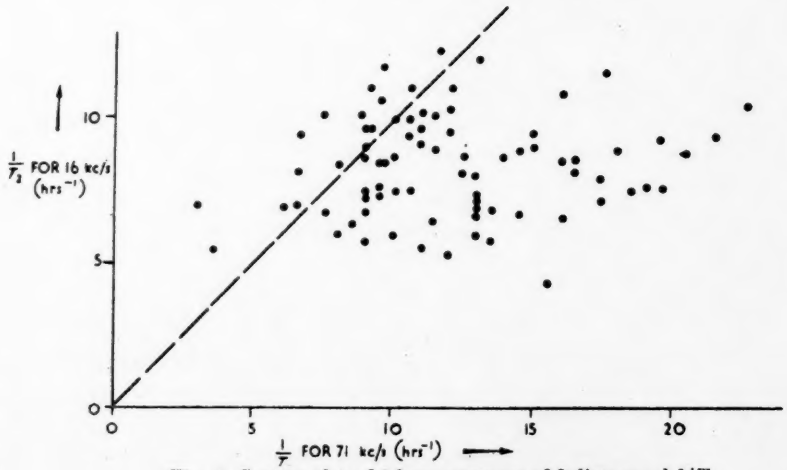

Fig. 5. Scatter plot of 1-hour averages of fading speed $1/T_2$ measured simultaneously at 16 and 71 kc/s.

on 16 kc/s. There is, however, a faster-fading component present, with period about $1\frac{1}{2}$ minutes, but with smaller amplitude. When the amplitude of this is small, the number of maxima, and hence T_2, is determined by the slow fading, but when the amplitude is large, T_2 decreases towards the value of $1\frac{1}{2}$ minutes. It is suggested that this is the explanation of the results shown in Fig. 5; when the fast fading has small amplitude, the points lie near AB, but as its amplitude increases they lie progressively more to the right of AB.

Although the explanation given here seems to be fairly obvious from an

VOL. 8 1956

inspection of records like that of Fig. 6, it is desirable to analyse the records in more detail to make certain that the eye has not been deceived into seeing two separate periods of fading. For the purpose of this analysis the results of Section 2 were used. To illustrate the method, it will be applied to the hour's record of which Fig. 6 is a part.

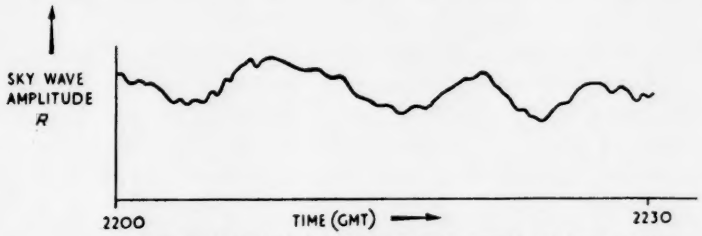

Fig. 6. A typical diturbed 71 kc/s record: 27 April 1952.

For this occasion, selected to show more of the fast fading than is usually present,

$$\left.\begin{aligned} T_1 &= 0{\cdot}960 \text{ minutes} \\ T_2 &= 1{\cdot}82 \text{ minutes} \end{aligned}\right\} \quad Q = 1{\cdot}91.$$

So $0{\cdot}79T_2 = 1{\cdot}42$ minutes, and by graphical methods

$$\mu = \rho_R(1{\cdot}42) = 0{\cdot}670$$

From Figure 6,

$$M = 5{\cdot}1, \quad \alpha = 0{\cdot}28$$

By equation (7),

$$\left.\begin{aligned} b &= 2{\cdot}44 \text{ minutes for slowly fading signal} \\ &= 0{\cdot}48 \text{ minutes for quickly fading signal.} \end{aligned}\right\}$$

These results are obviously reasonable from the appearance of the record.

Table 2

Frequency kc/s	α	b (slow) mins	b (fast) mins
16	0	1·9	—
71 (quiet)	0	1·9	—
71 (disturbed)	0·28	2·0	0·45
127	0·51	1·1	0·17

The values of α may vary very much from night to night; for instance, the average figures for 13 hours on two disturbed nights at 71 kc/s are given in Table 2, together with the figures for 16 kc/s and for quiet nights at 71 kc/s. It is significant that, even on the disturbed nights, the time-scale of the slow fading was unchanged.

As a result of these tests, it seems to be established that on the frequency of 71 kc/s there are two separate fading periods, and that the shorter one predominates when its amplitude is sufficiently large. Inspection of fading curves on higher frequencies suggests that, as the radio-frequency is increased, the amplitude of the short-period fading increases, until finally it swamps the long-period component. Moreover, the fading period of the short-period fading decreases as the radio-frequency increases. This suggestion is supported by detailed calculations made on records of fading on 127 kc/s, which gave the results shown in Table 2.

The results shown in Fig. 4 can now be described as follows. For radio-frequencies below about 70 kc/s there is one, slow, period of fading, independent of radio-frequency. At radio-frequencies near 70 kc/s, another, faster, fading makes its appearance, and as the radio-frequency increases, the amplitude of this fading becomes relatively greater until, for radio-frequencies greater than about 150 kc/s, it, alone, is noticeable. The period of this more rapid fading decreases as the radio-frequency increases. Compared with T_2, the quantity T_1 is relatively insensitive to a small amplitude of rapid fading, and the difference between the plotted values of T_2 and $3{\cdot}62T_1$ (which, as shown in Section 2, would be equal if only one type of fading were present) shows that the short period has only a small amplitude at 70 kc/s, but a much larger one at 127 kc/s.

VOL. 8 1956

4. The Size of the Random Variations at the Ground

Booker, Ratcliffe, and Shinn (1950) have shown that there is a close relation between the size of the random variations of amplitude over the ground, and the size of the irregularities in the ionospheric reflecting layer which cause the fading. The variations in space of the amplitude at a given instant are best described statistically by a spatial correlogram, analogous to the time correlogram defined in Section 2. If two receivers are set up, spaced horizontally by a distance ξ, the correlation between the two fading records is

$$\rho_R(\xi) = \frac{\overline{R(x,t)R(x+\xi,t)} - \overline{R(x,t)^2}}{\overline{R^2(x,t)} - \overline{R(x,t)^2}}$$

Measurements of this quantity were made in the following way.

Simultaneous records of the amplitude of the sky-wave were obtained from two receivers separated by distances of about 1, 2, 5, and 15 km. The frequency chosen was 85 kc/s, as the fading on this frequency was known to consist of both the quickly and the slowly fading signals described in Section 3, and it was anticipated that the two random signal variations might have different sizes at the ground.

Two loop aerials were used, orientated so as to receive only the horizontally polarized component of the sky-wave, and the recording was done at the site of one of them. When the separation was 1 km, the signal from the distant loop was amplified by a portable battery-operated unit and taken to the recording site through a co-axial R.F. feeder. Any small amount of ground-wave in the loops was balanced out by introducing a small amount of signal from a local vertical aerial, in the appropriate phase. This balancing-out operation was performed simultaneously for the two channels in the middle of the day, when the sky-wave was small.

For the larger separations of 2, 5, and 15 km, it was necessary to have a separate receiver and recording instrument at each aerial. The records were synchronized to within a few seconds by using timing marks given out by the Decca Navigator transmitter.

For the purpose of analysis, each pair of records was split up into periods of one hour, which were then analysed separately for correlation by the method described in the Appendix. The resulting spatial correlogram is shown in Fig. 7. Each point represents the average of one night's observations, while the crosses indicate the overall averages for each separation. The broken lines marked *A* and *B* represent

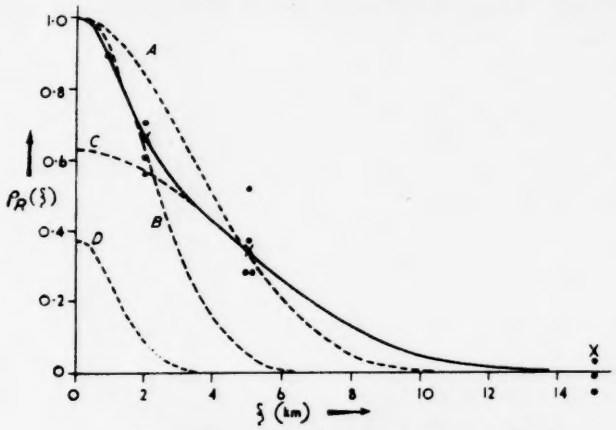

Fig. 7. Observed spatial correlogram at 85 kc/s.
Each dot is the average of one night's observations.

Gaussian functions; it is clear that the correlogram does not resemble this form, which might be expected if the spatial variations were homogeneously random in nature.

An examination of the fading curves shows that the shape of the correlogram is related, as was expected, to the occurrence of two different speeds of fading. To illustrate this, four pairs of typical records are shown in Fig. 8, each pair being one hour's simultaneous record at one of the four separations. On each record the two fading signals described in Section 3 can be seen: the quickly-fading signal with a fading period of about one minute, and the slowly fading signal with a period of about five minutes.

When the separation is 15 km, both components of the fading are completely unrelated, apart from a uniform decrease of amplitude throughout the hour. At a spacing of 5 km, some correlation is evident between the slow fading at the two sites, but the fast fading is quite different. When the spacing is reduced to 2 km the only visible differences in the records are due to the fast fading, but these differences are considerable. At a separation of 1 km, however, the slight differences between the records arise only through differences in the detailed shape of the fast fading.

It therefore appears that there exists a large- and a small-structure size in the random signal variations, associated respectively with the slow and the fast fading.

It seems reasonable to suppose that the spatial variations of large and small size have correlograms of the same Gaussian form as their time variations: this means that the combined spatial correlogram will consist of the sum of two Gaussian curves, as in equation (7) and Fig. 1.

Since the two structures and fading speeds are associated the same value of α will apply to the time and space correlograms, and we can use the value found from the fading curves by the method of Section 2 to reconstruct the spatial correlogram, as follows.

Exactly as in Fig. 1, the Gaussian curve C is drawn intersecting the axis of ρ at $\frac{1}{1+\alpha}$, to fit the correlation points for the greater separations. Another curve D is drawn, intersecting the axis at $\frac{\alpha}{1+\alpha}$, so that when added to C it fits the points corresponding to the smaller separations. The resulting curve, shown as a continuous line, is a reasonable fit to all the points.

The size of the irregularities over the ground can be measured by a correlation distance d, analogous to the fading time b of equation (3):

$$\rho_R(\xi) = e^{-\xi^2/2d^2} \tag{8}$$

and in terms of this quantity, the sizes are:

$$\left.\begin{array}{lll} \text{for slow fading:} & d = 4{\cdot}5 \text{ km} = 1{\cdot}3\lambda, & \theta_0 = 8^\circ \\ \text{for fast fading:} & d = 1{\cdot}1 \text{ km} = 0{\cdot}3\lambda, & \theta_0 = 50^\circ \end{array}\right\}$$

where λ is the wavelength, and θ_0 is the cone angle of the waves arriving at the ground, calculated by the method of Briggs and Phillips (1950). If the reflecting layer were "completely irregular" in the sense used by Booker, Ratcliffe, and Shinn (1950), its irregularities being much smaller than the wavelength, the correlation distance would be $0{\cdot}26\lambda$, in good agreement with the observed value for the fast fading.

No evidence was found of a systematic change in correlation distance through the night.

Some other experimental measures of the size of the irregularities of the signal at the ground are available. They apply to those irregularities related to the slow fading. One set of measurements arises from the work on a frequency of 71 kc/s discussed in Section 5·1, and it is explained there. On most occasions the correlation distance was between 4 and 8 km, with a mean of about 6·5 km. Another set of measurements was reported by Harwood (1954), who measured the size of the irregularities on a frequency of 16 kc/s. He found that the correlation between two aerials about 1·5 wavelengths apart was about 0·6: this led him to a figure of 31 km for the correlation distance, very much larger than the value found at 71 kc/s, although he finds the same value of fading speed as that quoted in Section 3. The disparity between these two values of the correlation distance cannot be explained by the difference in wavelength alone; it must correspond to a real difference in the size of irregularity affecting the reflexion of the two frequencies.

VOL. 8 1956

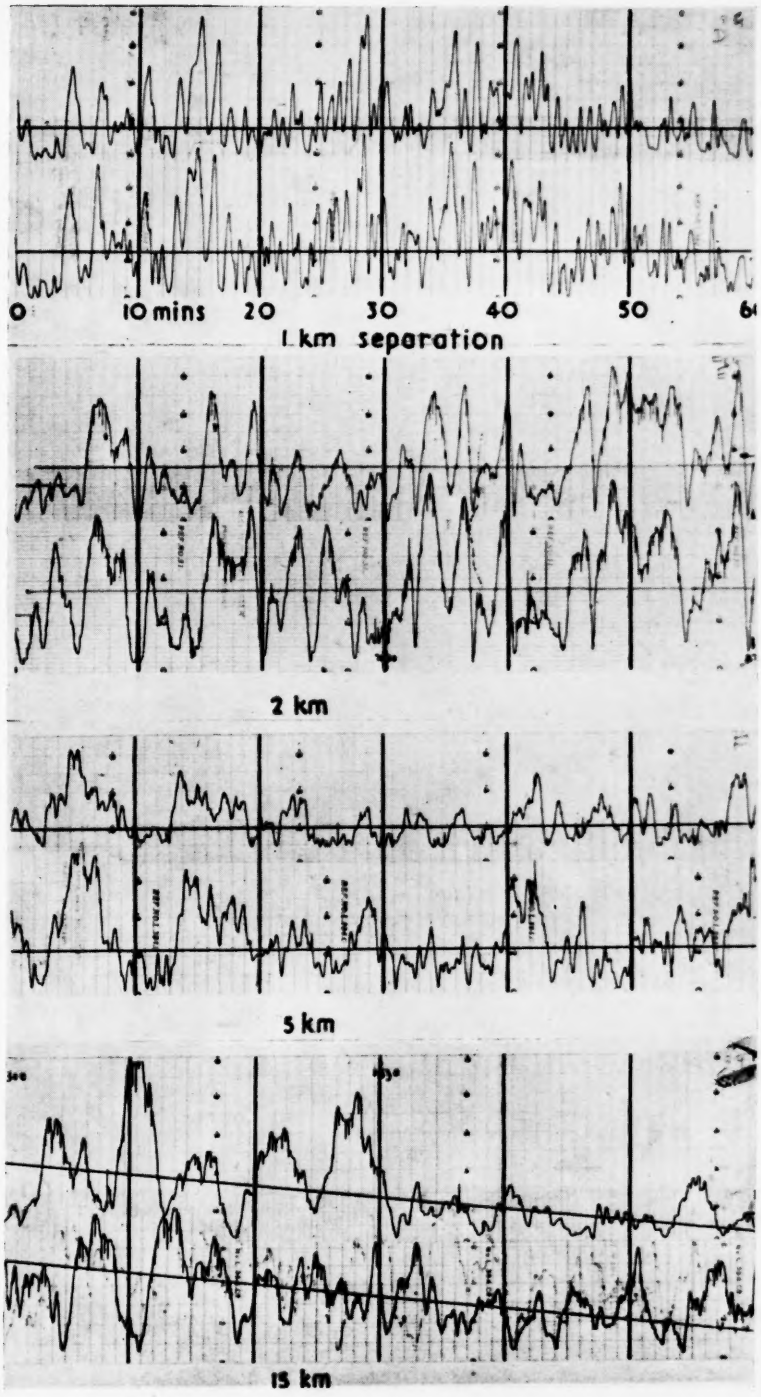

Fig. 8. Typical pairs of fading records at 85 kc/s for various receiver separations, showing the different correlation of the 7-minute and 1-minute period fading on each record.

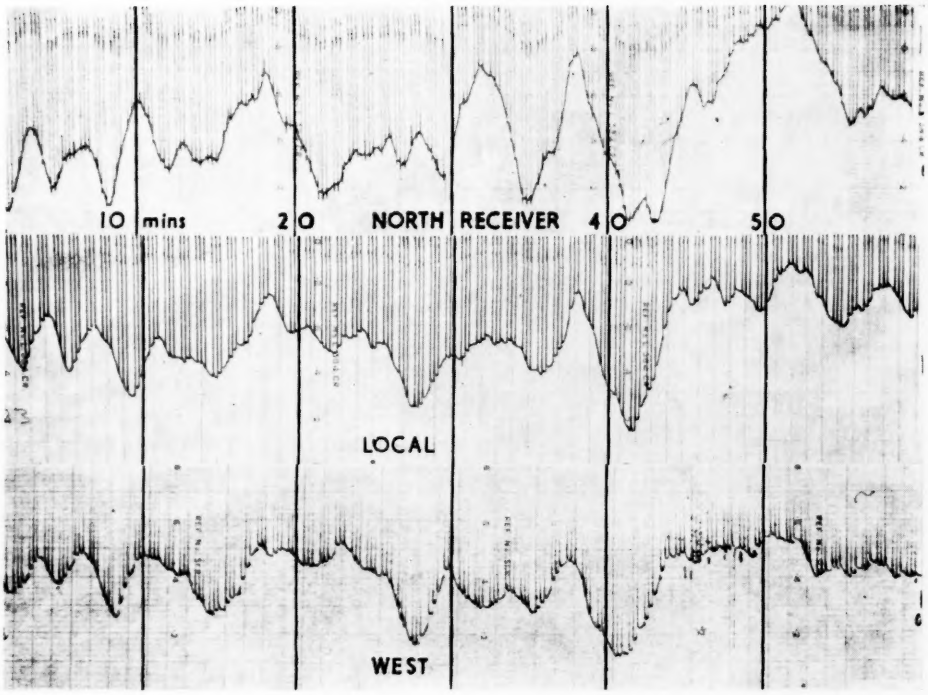

Fig. 9. A typical set of three fading records taken at 71 kc/s with three spaced receivers.

VOL.
8
1956

5. The Relation between the Space and Time Variations

In the previous sections the properties of the space and time variations have been described separately. The next step in the analysis of the fading is to find how these variations are connected. This problem has been studied by Briggs, Phillips, and Shinn (1950), who show that two mechanisms may cause random fading:

(i) A movement of the random amplitude pattern past the receiver without change of form, due to a steady drift of the irregularities in the ionosphere. The amplitude record is then a cross-section of the random variations in space.

(ii) A sequence of random changes in a pattern which is stationary as a whole. To conserve the statistical character of the pattern, the variations must have the same scale as the random pattern itself.

It is also possible to have any condition intermediate between these two. These workers also showed that it is possible, from fading records taken at three receivers at the corners of a right-angled triangle, to find the magnitude and direction of the mean drift velocity, and also whether the fading is due to mechanisms (i) or (ii) above. The details of this analysis are as follows.

The time-scale of the fading is first found, and represented by the fading time b of Section 2. Three spaced receivers are then used to find the extent of the spatial irregularities, represented by the quantity d of Section 4. If it can be assumed that the spatial correlogram is Gaussian, the correlation distance d can be deduced from one suitably chosen spacing of the receivers. A quantity V'_c is then defined by the relation

$$V'_c = d/b$$

It is the velocity with which an amplitude pattern would have to drift over the ground without changing its form, to produce the observed fading.

Next, fading records from a pair of observing points separated by a distance ξ_0 are used to deduce a quantity τ_0, defined as the relative time-shift between the two records which will make the cross-correlation between them the greatest. It was then shown by Briggs, Phillips, and Shinn, that the irregularities drifted along the line joining the receiving points with a velocity V_1, given by

$$V_1 = V'^2_c \tau_0/\xi_0 \tag{9}$$

If V_2 represents the velocity of drift along a perpendicular line, then the total velocity V_T is given by

$$V_T^2 = V_1^2 + V_2^2$$

Briggs, Phillips, and Shinn also showed that a quantity V_c, given by

$$V_c = \sqrt{V_c'^2 - V_1^2 - V_2^2} \tag{10}$$

represents the random velocity of movement of the irregularities.

5.1. *Experimental results on* 71 *kc/s*

It was decided, in view of the results of Section 4, to confine the experiments to a study of the slow variations, of fading period about 7 minutes. A frequency of of 71 kc/s was therefore chosen, and from Fig. 7 it it was clear that the best separation would be about 5 km. Ideally, the two pairs of receiving sites should be equally

separated, and lie in a north–south and east–west direction. Owing to the difficulty of finding suitable sites, neither of the base-lines coincided with a desired geographical direction. The lines will therefore be referred to as "normal" north–south and east–west.

The experimental arrangement was similar to that described for the greater distances in Section 4. As the records were taken near midsummer, when the sky-wave is exceedingly small in the middle of the day, unwanted ground-wave could be removed by balancing the signal at each site to zero at about noon. On some occasions, due to rain on the aerials or some other causes the signal did not decrease to a small value on the day following a night's observations; the record taken on that night was then rejected from the analysis. It may be noted that the presence of a small amount of unwanted ground-wave will not affect a determination of drift velocity, as it introduces no systematic displacement into the fading record.

Simultaneous records were made at the three receiving sites from 17 April to 12 June 1952, with a gap of fourteen days at the beginning of May. A typical set of records, covering a period of one hour, is shown in Fig. 9. All the records are divided into periods of one hour, each of which was analysed separately to find the correlation distance d for both pairs of receivers, the average time-scale b of the three records, and the time displacement τ_1 and τ_2 between the two pairs. Equations (9) and (10) were then used to find for each hour the drift velocity of the random pattern, and its equivalent random velocity. These were finally divided by 2 to give the velocities appropriate to an irregular reflecting layer. The analysis was made on 139 hours' records.

No systematic difference was found between the correlation distances of the random pattern in the N–S and E–W directions: for 80 per cent of the time this quantity, d, lay between 4·0 km and 9·2 km, with an average of 6·4 km. Similarly, the fading time b was between 0·7 minute and 1·7 minutes for 80 per cent of the time, with an average of 1·43 minutes.

The most striking feature of the measurements of drift velocity is the small magnitude of the velocity. Only rarely did either component of it exceed 50 m/s, and 20 m/s is a more typical figure. Although it is very variable, both from night to night and from hour to hour, there is a significant average velocity of drift, with a definite nocturnal variation. Fig. 10 shows the true components V_N and V_E of the overall average velocity at the layer, plotted in vectorial form. These were deduced from the nominal components along the actual base-lines by simple vectorial addition: for the particular geometry of the experiment,

$$\left.\begin{aligned} V_N &= 0{\cdot}953\ V'_N - 0{\cdot}128\ V'_E \\ V_E &= 0{\cdot}455\ V'_N + 1{\cdot}044\ V'_E \end{aligned}\right\}, \qquad (11)$$

the velocities being taken as positive towards the north and towards the east. The vector joining the origin to each point on the diagram therefore represents the direction towards which the drift is occurring. The semi-axes of the ellipses are the standard deviations of the mean velocities, deduced from the spread of the original measurements.

For each hour when observations of both components of drift velocity were

VOL. 8 1956

available, the equivalent random velocity V_e was calculated. The ratio of this to the magnitude of the drift velocity indicates which of the two mechanisms mentioned earlier is predominant as a cause of fading. A histogram of the values of this

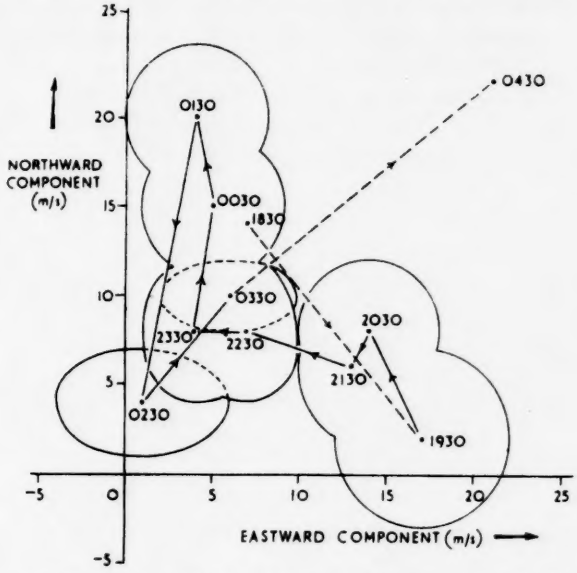

Fig. 10. The hourly variation of the overall average drift-velocity at the layer. The ellipses represent the standard deviations of the average velocities.

ratio is given in Fig. 11. In only 24 per cent of occasions is the drift of the irregularities the principal cause of fading; and on half the occasions, the effect of random changes is more than twice that of drift.

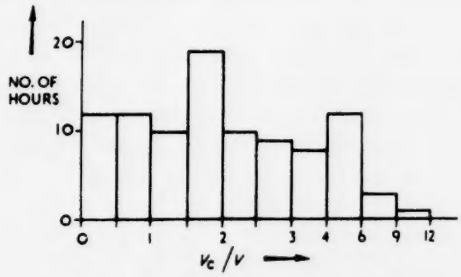

Fig. 11. Histogram for the ratio of the random velocity to the magnitude of the drift-velocity.

This result is the opposite of that found by BRIGGS and PHILLIPS on a frequency of 2·4 Mc/s. They concluded that the main cause of fading was a steady drift of the irregular amplitude pattern past the receiver, and that the effect of changes in the shape of the pattern was secondary.

In addition to the average velocity variation which repeats from night to night, there is a drift velocity of random direction, corresponding to the spread of the

observed velocities. The components of this random velocity average about 15 m/s throughout the night. They contain no lunar tidal component greater than 1 m/s in amplitude. Neither the magnitude nor the direction of the random velocity is correlated with magnetic activity.

The only systematic feature of this random drift is a tendency for its direction to persist from one hour to the next. This is illustrated in Fig. 12, which shows the correlogram of the deviation of the drift velocity from its fourteen-day mean value. The velocities in successive hours have a correlation of about 0·30, but velocities separated by a greater time are not significantly correlated.

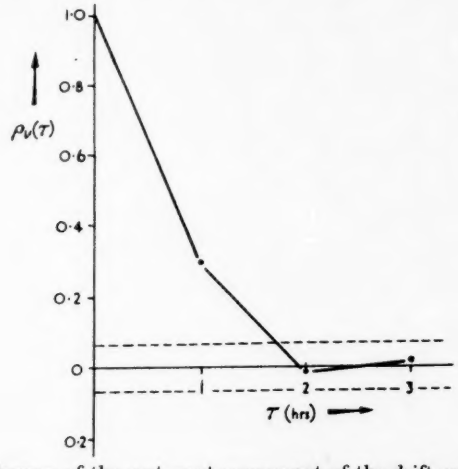

Fig. 12. Correlogram of the east–west component of the drift-velocity. The dotted lines represent the standard deviation of the correlation if its true value is zero.

This persistence of the velocity over about one hour means that several identifiable portions of the random interference pattern have passed over the two receiving points before the drift changes in direction: so the "swirls" in the pattern must be considerably larger than the irregularities themselves. If the changes in swirl velocity are due to the pattern being carried past with the mean drift velocity, this would indicate a swirl size of about 50–100 km at the layer. This could be checked by measuring the drift velocity at two places separated by about 52 km.

It has been established that the fading of 71 kc/s signals is due to

(i) A steady drift of the layer irregularities of about 15 m/s, consistently repeating from night to night, and whose direction always lies between north and east.

(ii) A variable drift velocity of about 20 m/s mean magnitude with random direction, but persisting from one hour to the next.

(iii) An equivalent random velocity of about 40 m/s at the layer.

The last of these is the predominating cause of the fading at 70 kc/s.

5.2. *Results on other frequencies*

Some experiments were made on a frequency of 71 kc/s simultaneously with experiments made by Briggs and Spencer on other frequencies. In one of these,

VOL. 8 1956

they used pulses of frequency 647 kc/s reflected from the *E*-layer. In the course of ten hours' observations on three days, the velocities in the east–west direction were in good agreement, but in every case the north–south components were in opposite senses; the drift at 647 kc/s being from north to south, and that on 71 kc/s in the reverse direction.

On another occasion they used pulses of frequency 2·4 Mc/s reflected from the sporadic *E*-layer. During thirteen hours' simultaneous measurements spread over four nights, there was no obvious relation between the velocities at the two frequencies. A longer series of observations has led Briggs and Spencer (1954) to the conclusion that the average *E*-region velocity, revealed by measurements on a frequency of 2·4 Mc/s, is towards the south-west before midnight, and towards the north-west after midnight.

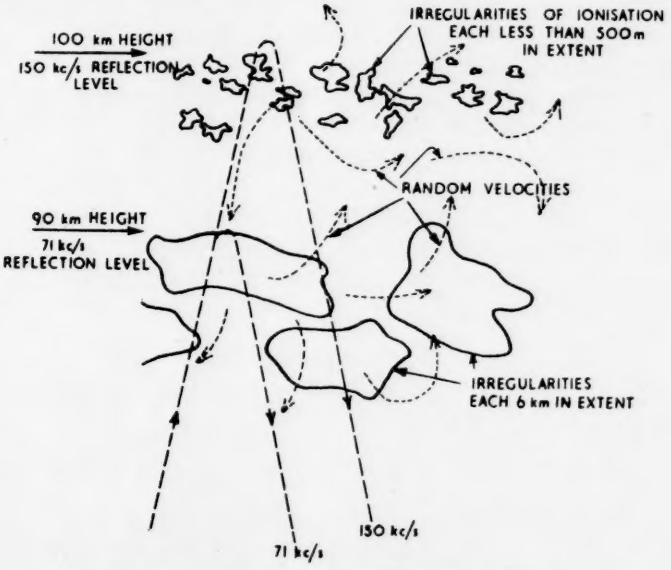

Fig. 13. A suggested model of the irregularities in the *D*-region at night.

The results of Millman (1952) relate only to the winter months. At 150 kc/s in March 1952 he found the velocity to be southwards at 2100 GMT, westwards at 0000, and northwards at 0300, which conflicts with the 71 kc/s results.

The mean directions of drift at 71 kc/s are confined to the north-east quadrant throughout the night; this agrees with the results of Hoffmeister (1946), who observed noctilucent clouds on summer nights.

Manning, Villard, and Peterson (1950) measured the north–south component of drift of meteor trails between 0300 and 0600, using a C.W. radio method. They found an average northward velocity up to 50 m/s, but with considerable random variation.

Harwood (1954), at a frequency of 16 kc/s, was unable to detect a velocity of drift of the random pattern.

6. Discussion

These measurements, made on the random interference pattern at the ground, must be interpreted in terms of the irregularities at the reflecting layer. Previous work by Booker, Ratcliffe, and Shinn (1950), and by Hewish (1951), indicates for the conditions of these experiments that the correlation distance at the layer is half that at the ground, that steady drifts in the ionosphere have a velocity equal to half of those at the ground, and that random changes in the ionosphere have a "correlation time" equal to that of random changes on the ground. With these ideas in mind it is possible to suggest a model which could explain our results.

Fig. 13 is a schematic representation of a tentative model. The irregularities near 90 km have a horizontal extent of the order of 6 km, and they move with a randomly directed velocity, of magnitude about 40 m/s. Waves of frequencies near 70 kc/s are reflected from this level at night. At the 100-km level, which is reached by frequencies of 100 kc/s and above, the irregularities are much smaller than the wavelength, and are moving with random velocities of the same order as that of the lower irregularities. These small irregularities would produce the rapidly fading signal, with correlation distance a fraction of a wavelength at the ground, which is present in increasing amount as the frequency is increased above 100 kc/s.

Acknowledgements—The work described in this paper was carried out in the Cavendish Laboratory, Cambridge, while the author was in receipt of a D.S.I.R. Maintenance Award. The continual advice and encouragement of Mr. J. A. Ratcliffe is acknowledged.

VOL. 8 1956

References

Booker, H. G., Ratcliffe, J. A., and Shinn, D. H.	1950	*Phil. Trans. Roy. Soc.* **A242,** 579.
Briggs, B. H. and Phillips, G. J.	1950	*Proc. Phys. Soc.* **B63,** 907.
Briggs, B. H., Phillips, G. J., and Shinn, D. H.	1950	*Proc. Phys. Soc.* **B63,** 106.
Briggs, B. H. and Spencer, M.	1954	*Rep. Prog. Phys.* **17,** 245.
Harwood, J.	1954	*Proc. Inst. Elect. Engrs.* **IV, 101,** 183.
Hewish, A.	1951	*Proc. Roy. Soc.* **A209,** 81.
Hoffmeister, C.	1946	*Z. Meteorol.* **1,** 33.
Manning, L. A., Villard, O. G., and Peterson, A. M.	1950	*Proc. Instn. Rad. Engrs.* **38,** 877.
McNicol, R. W. E.	1949	*Proc. Inst. Elect. Engrs.* **96,** Part III, 517.
Millman, G. H.	1952	*Ann. de Géophysique,* **8,** 365.
Phillips, G. J.	1952	*J. Atmosph. Terr. Phys.* **2,** 141.
Ratcliffe, J. A.	1948	*Nature* (Lond.) **162,** 886.
Rice, S. O.	1945	*Bell System Tech. J.* **23,** 317, **24,** 73.

Appendix

Rapid statistical analysis

The rapid analysis of fading records can be carried out surprisingly accurately by the use of a distance-integrating instrument such as a pocket map-measurer. By successively running it over equally spaced ordinates of the curve (*a*, *b*, *c*, etc., on

Fig. 14), always in the same direction, the quantity $\overline{|R(t) - \overline{R(t)}|}$ can be found. The mean slope is given by

$$\overline{|\dot{R}(t)|} = \frac{\text{Total vertical distance moved by curve}}{\text{Duration of record}}$$

$$= \frac{PQ + QR + RS + ST + \text{etc.}}{\text{Duration of record.}}$$

The distances PQ, etc., can easily be added with the map measurer.

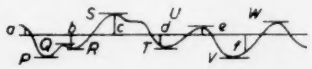

Fig. 14. Showing the distances to be measured on a fading curve to determine the mean slope and the mean deviation.

To find auto- or cross-correlation coefficients, a similar technique is used. If the two quantities to be correlated are $F_1(t)$ and $F_2(t)$, both having mean values of zero,

$$\overline{[F_1(t) - F_2(t)]^2} = \overline{F_1^2} + \overline{F_2^2} - 2\rho\sqrt{\overline{F_1^2}\ \overline{F_2^2}}.$$

Now if F_1 and F_2 have the same form of distribution as $(F_1 - F_2)$,

$$\overline{|F_1 - F_2|}^2 = \overline{|F_1|}^2 + \overline{|F_2|}^2 - 2\rho\,\overline{|F_1|}\ \overline{|F_2|}$$

or

$$\rho = \frac{\overline{|F_1|}^2 + \overline{|F_2|}^2 - \overline{|F_1 - F_2|}^2}{2\,\overline{|F_1|}\ \overline{|F_2|}}$$

so it is only necessary to find the mean moduli of F_1 and F_2 and of their difference. This can easily be done by superposing the graphs of the two functions so that their means coincide, and adding equally spaced ordinates of their difference by means of the map-measurer. It will be noted that the two functions need not be normalized to the same mean-square amplitude.

Journal of Atmospheric and Terrestrial Physics, 1956, Vol. 8, pp. 146 to 157. Pergamon Press Ltd., London

On the deviations of the course of elements of atmospheric electricity on continents from the worldwide course

R. MÜHLEISEN
Max-Planck Institut für Physik der Stratosphäre

(*Received* 27 *July* 1955)

ABSTRACT

We have carried out extensive recordings of atmospheric electricity with transportable instruments in towns, on their borders, and far away from settlements, with the object of ascertaining the causes of the deviations of the diurnal courses of potential gradient and air-earth current from the worldwide course on the oceans. The causes were found to be mainly positive space charges, produced at many places chiefly by urbanization, industry, and traffic. These space charges are carried away many kilometres and distributed by air movements. The results were obtained by measurements made directly at the sources of disturbance, and by laboratory experiments. They preclude further conclusions from most ground measurements of atmospheric electricity. It seems advisable to carry out future measurements only at strictly selected places, possibly on tops of mountains, or to record not only two elements—potential gradient and air-earth current—but (inevitably with rather expensive equipment) also the electrical space charge density, if possible, at various altitudes. This method should enable us better to determine the worldwide functions of the elements of atmospheric electricity.

VOL.
8
1956

INTRODUCTION

IT is in the main clear that a gradient of the atmospheric electrical potential with positive sign can be recorded in fine weather, at nearly all undisturbed and free places of the earth. We can to-day assume with certainty that, whereas the efficiently conducting air-space above approx. 50-km altitude receives positive charges from the surface of thunderclouds, the surface of the earth receives, chiefly by way of point discharges, mostly negative electricity from the bottom of cumulo-nimbus clouds. However, this rather simple picture easily leads one to believe that thunderstorms alone are the cause of the atmospheric electrical field, and there is often the tendency to explain all fluctuations of the elements of atmospheric electricity by changes of atmospheric conductivity alone. This, however, cannot be reconciled with all the established facts. On the contrary, it appears that disturbances are for the most part of such extent, that this simple picture can only be applied in exceptional cases.

The diurnal courses of the potential gradient of atmospheric electricity and air-earth current recorded on the ground are only of value if all their causes and their correlation with atmospheric electrical and meteorological factors are known and can be determined; they will then permit further conclusions. There are various questions and problems, in this respect, waiting for a solution. It would be interesting if we could read the course of worldwide thunderstorm activity from the recording of atmospheric electricity. We know this is possible with recordings on the sea (MAUCHLY, 1923), but not hitherto, with continental recordings. The frequently supposed correlation between the atmospheric electrical field and processes in the lower ionosphere, or the change of air masses and meteorological factors, can only become clear if we have a better knowledge of the local disturbances of atmospheric electrical sizes and their causes; and if we can eliminate these disturbances.

For the above-mentioned reasons, it is the purpose of all our investigations to detect the causes of the courses of electrical elements, particularly of potential gradient and air-earth current. This should be done in detail at every measuring station. After completion of these investigations it should be possible to decide which conclusions we may draw from the recorded sizes and which we may not, and, furthermore, which part of the measuring values of atmospheric electricity is of worldwide origin.

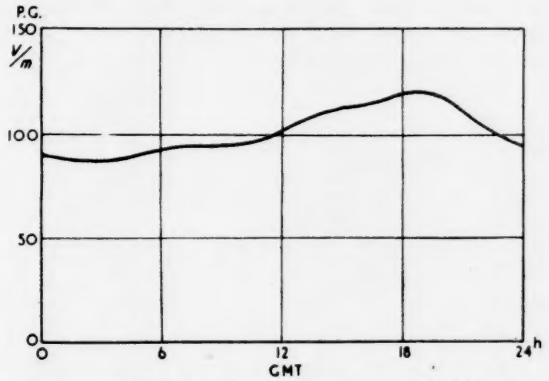

Fig. 1. Mean potential gradient on the oceans with ship *Carnegie*.

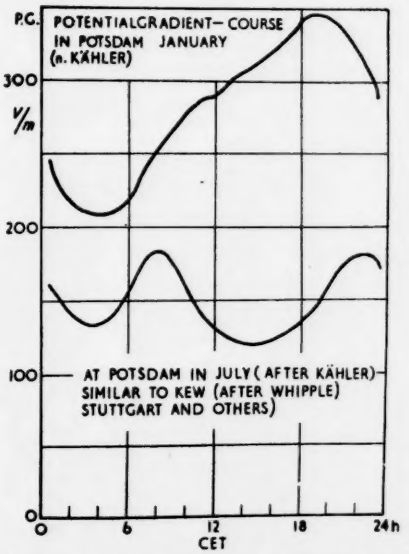

Fig. 2. Typical course of the potential gradient at continental stations, at the top Potsdam in January, at the bottom Potsdam, Kew, Stuttgart, in July.

The Different Diurnal Courses

If we compare the characteristic course of the potential gradient on the oceans in Fig. 1 with the diurnal courses at continental stations in Fig. 2, it is striking that there are single- and double-period courses, in spite of similar conductivity. We

can further see that the measured values of the potential gradient are much higher on the continent than on the ocean. However, if we consider on dry days not only the mean values but also single recordings, we can see still greater deviation, even from the mean-value curves alone. Examples of a measuring station in the city and another at 10-km distance are given in Fig. 3.

PREVIOUS EXPLANATIONS OF THE DIFFERENT DIURNAL COURSES

Many authors have tried to explain the main types of the diurnal variations. ISRAEL (1953) has given a summary of these explanations. It is his opinion that the only reason for the diurnal variations is the "exchange" caused by solar

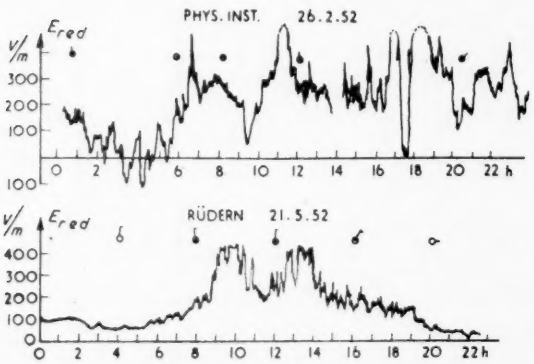

Fig. 3. Typical course of the potential gradient at a large town (top) and at the border of it (bottom).

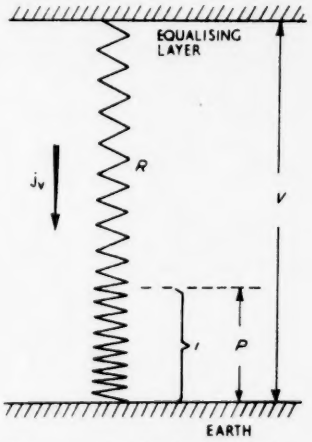

Fig. 4. Atmospheric electrical circuit, after ISRAEL.

radiation and the changes of the contents of the atmospheric condensation nuclei. These factors alter the conductivity, in the course of a day, at various heights. They are believed to cause, thereby, the variation of the potential gradient. This is qualitatively correct, but we shall see that this view is not complete and cannot sufficiently explain the size of the measured values. If we measure the potential gradient in towns and their vicinity, the absolute amounts are higher than can be explained by changes of the columnar resistance and the conductivity caused by the exchange. This will be briefly explained by the known diagrammatic representation for the atmospheric electrical circuit in Fig. 4.

If V stands for the voltage between the lower limit of the efficiently conducting air-space above 50-km altitude and the ground, R for the columnar resistance (surface 1 cm²), and r for the lowest part of it at 1 m height, at which the atmospheric electrical potential on the ground is measured, we apply the known equations:

$$(1)\quad r = \frac{10^2}{\Lambda} \qquad [\Omega m]\ \Lambda = \text{total electrical conductivity } [\Omega^{-1}\,\text{cm}^{-1}];$$

for air-earth current:

$$(2)\quad j = \frac{V}{R}\left[\frac{\text{Amp}}{\text{cm}^2}\right]$$

VOL. 8 1956

and for the potential gradient:

$$(3)\quad PG = r \,.\, j = \frac{10^2}{\Lambda} \cdot \frac{V}{R} \left[\frac{V}{m}\right].$$

As the quasi-stationary equilibrium requires approximately half an hour for its establishment, we can use the simple formula for hourly mean values.

The exchange by vertical mixing by solar radiation in the lower atmosphere carries the condensation nuclei produced on the ground first to the lower, and with increasing radiation to the higher, layers of the atmosphere. The conductivity decreases with increasing nucleus content, and consequently the resistance r of the lowest part of an air column rises from the ground, and its total resistance rises gradually to the equalizing layer R. The potential gradient changes with r ($PG = j \,.\, r$), increasing initially in the morning. When the more intensive exchange has commenced at noon, the resistance r of the lowest part of the columnar resistance decreases, because air masses of smaller nucleus content are brought down from above. The columnar resistance R increases, however, because the air at greater altitudes is enriched with nuclei. The air-earth current should now also diminish in relation to the night values, and the potential gradient should decrease even more. In the evening, the values are again contrary to those in the morning. In this way we try to explain the double-period diurnal course of the potential gradient. At a greater distance from the sources of nuclei the conditions change slowly, because the arriving air masses are already mixed. Here, a single-period diurnal course will gradually be established.

Diurnal Course of the Air-earth Current

If we consider carefully the recorded diurnal courses, it is striking that in the single case not only the potential gradient, but also the air-earth current, rises in the morning, and that the latter is for the most part greater in the daytime than at night. This will be shown by a few examples in Figs. 5–7. The discrepancy in the course of the air-earth current is obviously much greater in large towns. Therefore, our measurements were first carried out in urban areas. The main result of these investigations is as follows: apart from charges in high air layers and on the ground, we have also to consider mostly positive charges in the lowest air layers which enlarge the primary field. These charges are produced on the ground in all populated and cultivated regions, and are brought into the atmosphere together with condensation nuclei and dust particles.

There had already been a great deal of speculation about this additional field increase. Fleming *et al.* (1941) had ascertained that conductivity decreased with the wind during Australian bush-fires, but that the potential gradient *and* air-earth current, however, increased. Brown (1933) found out, by space-charge recordings, that near the ground there are nearly always positive charge densities. He can explain several increases of the potential gradient, but he does not yet state the cause of the positive charges.

The most important indication of the significance of artificial space charges was the negative potential gradient found by Chalmers (1952) and the author (1952) in fine weather.

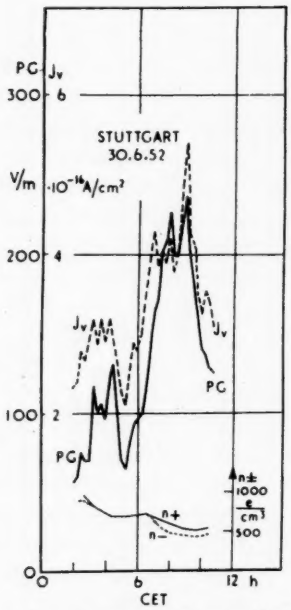

Fig. 5. Course of potential gradient, air-earth current (and the number of small ions), in fine weather at the town of Stuttgart.

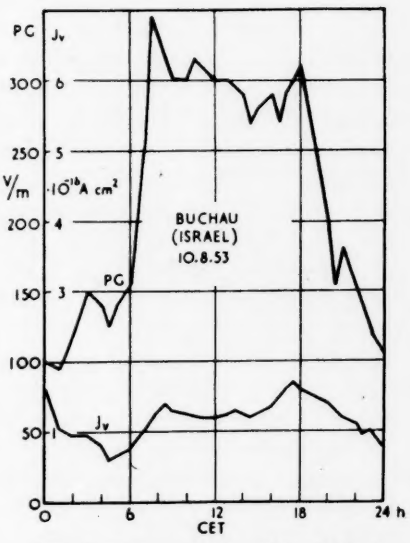

Fig. 6. Course of potential gradient, air-earth current, in fine weather at the country town Buchau, after ISRAEL.

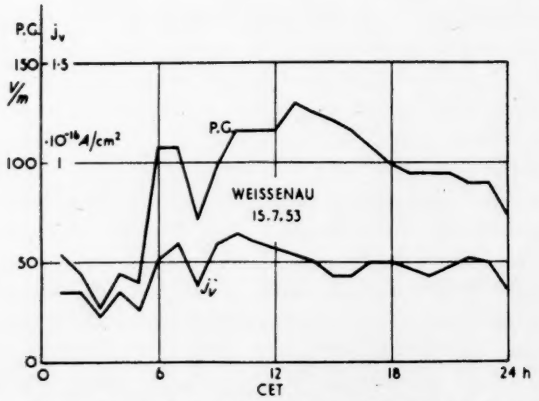

Fig. 7. Course of potential gradient, air-earth current, in fine weather near the village of Weissenau.

VOL. 8 1956

Artificial Space Charges

For our own extensive and systematic investigations (1953) we built quick-indicating transportable instruments for recording, at the outset, the potential gradient (Ehmert and Mühleisen, 1953), the air-earth current, the number of small ions (Mühleisen and Creutzburg, in preparation), the electrical space charge density (Mühleisen and Holl, 1954), and later for recording the number of condensation nuclei (Mühleisen and Holl, 1952). The recording values obtained could be further supplemented by values of wind direction and daylight. They could without exception be recorded by six-channel recorders. Two to four further stations were working simultaneously with minor measuring facilities. These stations were established at many places in the town; at the gas-works, the railway station, and nearby streets, in order to record at the spot the effective charge of smoke, dust, and exhaust gases, and to find out their effect on the potential gradient.

In addition, we carried out extensive experiments in the laboratory, measuring the space charges. Furthermore, we cleared up many single effects and deviations in the recording of potential gradient and air-earth current. This was done either by direct observation of their causes—visible smoke and dust clouds, visible exhaust gases, etc.—or by simultaneous recordings of wind directions when no visible indications were at hand.

Only brief mention of our results will be made here. We found out that the total of nuclei and dust particles on the ground of all populated regions carries a surplus charge from the outset. The signs of the charge clouds depend on the causes of origin, which are given in Table 1. We shall find that processes often taking place in populated regions produce chiefly positive charges. Negative charges, however, are also frequently carried to the atmosphere by gas-works and chemical factories. These charges are carried away by air currents and are gradually distributed, so that "clouds" with mostly positive space-charge density will grow out.

Table 1. *Signs of artificial space charges*

Positive	Negative
Exhaust (benzine motor)	Benzine-fire, open
Exhaust (Diesel motor)	Petroleum-fire, open
Chimney-smoke	Alcohol-fire, open
Coal powder fire	Wood shavings wool—fire, open
Engine steam	Water vapour, pure
Steam cloud (gas-works)	(out of metal jet)

A few examples show very clearly the effect of space charges produced by industry and traffic. Fig. 8 shows the course of the potential gradient on three consecutive days with the same weather conditions, recorded at 10-km distance from the city centre. The second of these three days was a Sunday, a rest day for industry.

If we separate the recorded results of potential gradient and air-earth current according to the wind directions towards and away from the town, we also see the differences of the space-charge production very clearly. Only when there are

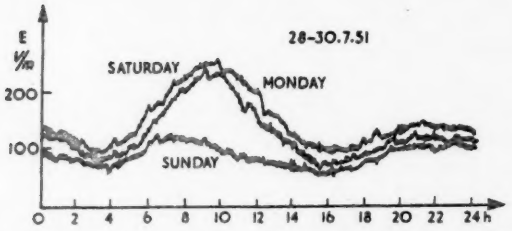

Fig. 8. Differences in the course of the potential gradient on working days and on Sunday under the same weather conditions.

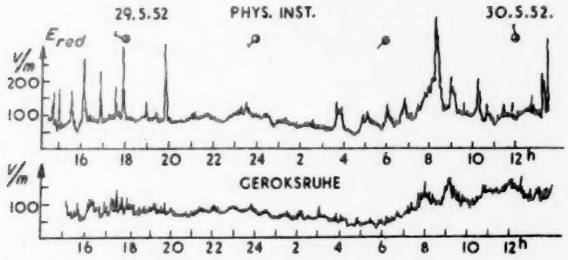

Fig. 9. Examples of simultaneous recordings of potential gradient at two stations with wind speeds above 2 m/sec.

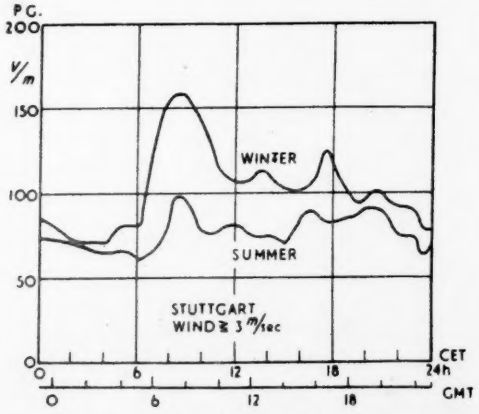

Fig. 10. Mean course of the potential gradient in fine weather at a large town in summer and winter with wind speeds $\geqq$ 3 m/sec.

strong winds, carrying nuclei and space charges rapidly away and leaving very low densities, is a course recorded which, in its way and absolute values is similar to that of thunderstorm activity. Figs. 9 and 10 show this for the town of Stuttgart, where, however, a temporary deviation is caused in the morning by intensive production of nuclei and space charges. This deviation is strong in winter, but very weak in summer. BROWN (1936, 1937) has already pointed out this possibility for rural stations. As far as we know, it has not been mentioned yet for towns.

VOL. 8 1956

There are some other interesting deviations of the atmospheric electrical elements, for instance deviations caused by spraying high-voltage lines (CHALMERS, 1952; MÜHLEISEN, 1952), by intensive radioactivity of the ground, as at Upsala (NORINDER *et al.*, 1954) or by conditions at sea. All these factors are of such a nature that they can cause atmospheric electrical disturbances over large areas. They should therefore be considered as carefully as artificial space charges.

With these results we can answer many questions. We can clear up many anomalies in the daily recordings of potential gradient and air-earth current, and

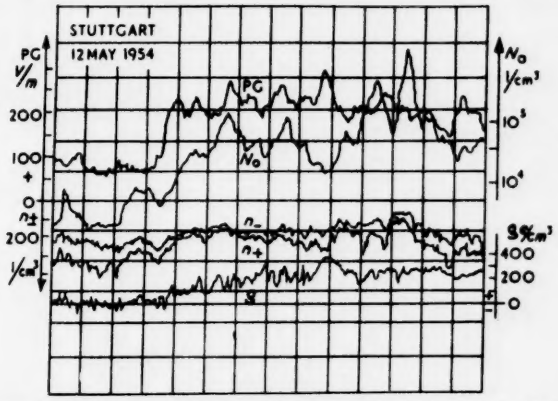

Fig. 11. Example of the course of atmospheric electrical elements in the morning at the town of Stuttgart.

state the active charge sources. The recorded course of the electric space-charge density gives a good explanation of the variations of potential gradient and air-earth current. Fig. 11 shows this for a morning at Stuttgart, where we recorded, besides the potential gradient, the space-charge density at 15-m altitude, and the number of condensation nuclei and positive and negative small ions on the ground. In addition we recorded, with a second instrument, air-earth current, wind direction, and daylight.

A minor calculation will explain the effect of these artificially produced charges. We suppose that early in the morning positive charges are thrust out from chimneys, motor vehicles, etc., and that these charges are homogeneously distributed by horizontal and vertical air movements in a layer with limited upward extention, thereby establishing a constant space-charge density. We can then calculate with these idealized assumptions the altitude of the layer. This is done in Fig. 11 for two cases of the daily recording by means of the schematic Fig. 12. If we assume that the electrical field strength above the layer enriched by artificial charges is E_0, we shall find on the ground the field strength $E_0 + \Delta E$. The increase of the field strength ΔE depends on the space-charge density ρ and the height of the layer h_s. From the Poisson-equation

$$\Delta\rho = -4\pi\rho$$

we obtain for a homogeneous, infinitely extended space-charge layer of the height h_s, as demonstrated in Fig. 12, for the field increase

$$\Delta E = 4\pi\rho \,.\, h_s$$

for ΔE, measured in volt/m, ρ in electrical elementary charges e/cm³ and h_s in m

$$\Delta E = 1{\cdot}81 \,.\, 10^{-2} \,.\, \rho \,.\, h_s$$

For the increase of the potential gradient between 6 and 7 hr of $\Delta E = +130$ V/m and the increase of the electrical charge density there will be a homogeneous altitude of the layer of approx. 70 m, which is quite a plausible value. It is different with the conditions of the field increase at 8 hr 50 min: with a $\Delta E \approx +70$ V/m we find

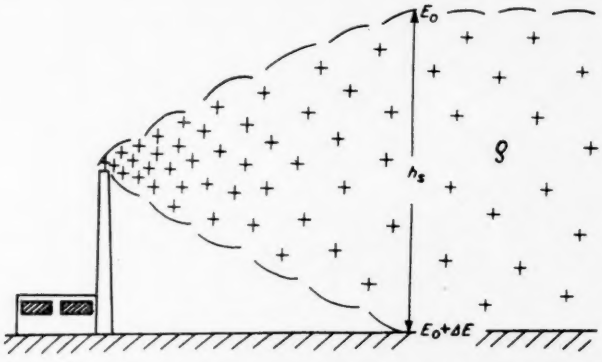

Fig. 12. Illustration to the calculation of the increase of the potential gradient in an extended positive space charge layer caused by chimney smoke.

a $\Delta\rho \approx +200$ e/cm³. From this we get an altitude of the layer of only 18 m, and from the simultaneous decrease of the number of nuclei we can conclude that a "cloud" of greater purity but of positive charge has passed the recording stations. If, instead of a homogeneous, infinitely extended layer, we assume limited clouds, we obtain values of only very little difference.

While further detail would be out of place here, we can see that the recorded diurnal courses are more easily explained by the above results. The positive space charges produced in the morning together with nuclei, not only in towns but at every populated place, increase the potential gradient considerably at the source, and also—even if to a lesser extent—the air-earth current, because the conductivity diminishes simultaneously.

Nuclei and space charges will then be carried away by horizontal and vertical air movements. As the air motions on the ground increase chiefly with the vertical exchange in the morning, the nuclei and space-charge densities will, in the morning, diminish at their source, but increase farther away. The range of such space charges became known from many investigations on their duration of life, which was found to be more than 1 hour. According to the speed of wind they could well be traced at distances of 20 and more km from their source.

As the source of space charges is chiefly found within large settlements, we can well explain the double-period daily course in towns and their vicinity, with the minimum at noon; and farther away the slower rising of potential gradient and air-earth current, their amplitude, and development to the single-period

VOL. 8 1956

diurnal course. The former views, on the explanation of daily fluctuations of the atmospheric electrical elements by exchange, can be maintained if they are supplemented in such a way that the exchange in the lower atmosphere not only distributes nuclei but mainly positive electrical charges as well.

At many places we ascertained that in winter the values of potential gradient are much higher than in summer, at many stations being more than twice the amount. Due to the fact that the air-earth current is also higher (the thunderstorm activity, however, is lower, because of the smaller masses of continents on the southern hemisphere), we consider the cause to be the increased positive charge production in winter by heating processes (see also Fig. 10), and not the decrease of conductivity, as has mostly been assumed.

The problems which arise if we consider permanent recordings of the air-earth current (discussed by ISRAEL, 1954, in a detailed paper) can also be solved if we assume artificial space charges or if in future we also record the space-charge density.

Our investigations are being continued. On one side we are investigating the duration of life of space charges in a closed room, on the other we are tracing their strength from their source during their transportation by air motions.

CONCLUSIONS DRAWN FROM THE LOCAL SPACE-CHARGE PRODUCTION

We shall now draw conclusions from the fact that at most continental places there are atmospheric electrical disturbances, originating mostly from limited sources, and which will therefore—according to the situation and wind direction —more or less influence the atmospheric electrical recordings.

1. One of these conclusions is that the recording of potential gradient and air-earth current is at most places not a picture of worldwide processes, and therefore does not allow any conclusions concerning vast areas. We could, of course, consider the elimination of disturbances on potential gradient and air-earth current by measurements of the space-charge density; if possible, at various heights. But this would require rather extensive measuring facilities and subsequent evaluation. Without these, such measuring results are only of local informatory value. It is necessary to point out that the correlation between atmospheric electrical measurements on the ground and certain meteorological events, such as the change of air masses, is made indistinct by other influences, so that it is impossible to draw any useful conclusions from the result of atmospheric electrical recordings on the other sizes. Therefore, they cannot be used for the calculation of the columnar resistance.

2. Using our knowledge and experience of the sources and effects of disturbing space charges, we can try to choose measuring places at which we can ascertain worldwide atmospheric electrical processes. For this reason, we have started recordings on a 830-m-high mountain in our vicinity, near which there are only small villages. Fig. 13 shows a day's recording of the potential gradient on this mountain. We can see that the morning maximum, known to us from larger places, does not appear at this place before 1200 local time. This displacement in relation to the maximum at the source of disturbance in the early morning is in good agreement with the distance from nucleus and space-charge sources

and the speed of wind. Fig. 14 shows an even more balanced daily course of the potential gradient at Arosa (Switzerland).* This course is nearly parallel to the presumed thunderstorm activity. The simultaneously recorded density of positive and negative small ions was nearly constant during the day. We obtain similar

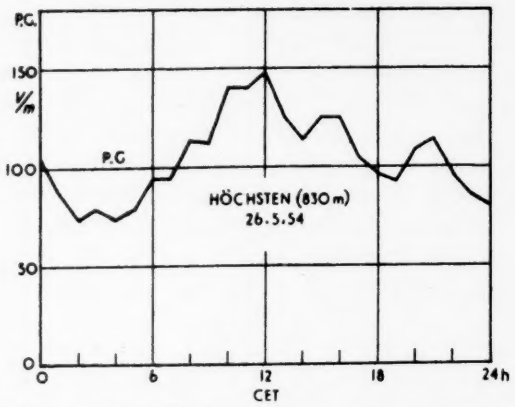

Fig. 13. Course of the potential gradient at a place where the atmosphere is little disturbed.

results by recordings on tops of mountains, as carried out by ISRAEL (1951), ourselves, and others. But there are other factors, such as blizzards and condensation of water vapour, which make these measurements more difficult. Ascents with radiosondes, as taken up by KOENIGSFELD (1953) and others, are

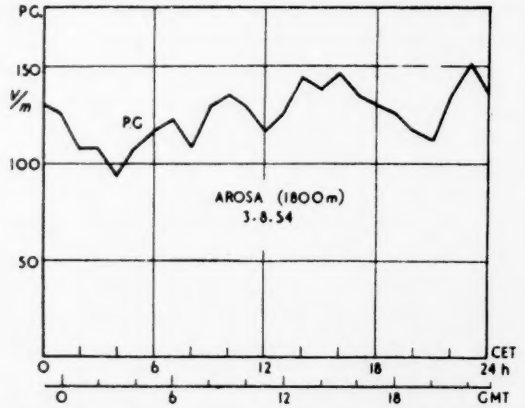

Fig. 14. Course of the potential gradient at Arosa (Switzerland), a place with least disturbances of the atmosphere.

an excellent assistance for some problems. However, these sondes are very expensive and can only give momentary values.

3. In order to detect the local sources of disturbance, we recommend that the wind direction be recorded on the same recording strip as the other atmospheric

* I thank Dr. PERL for having given me the opportunity to carry out the recordings at the Arosa Observatory, and for her energetic support.

VOL. 8 1956

electrical sizes. The correlation of recorded results according to wind directions will easily draw our attention to irregularities, such as artificial space charges.

Furthermore, the values for potential gradient and air-earth current should be published after reduction to the plain field. Experience has proved that this reduction is possible with wind speeds above 3 m/s, even if the distance between measuring station and plain area is several km. The locally caused part of potential gradient and air-earth current can then be separated from the worldwide part. This has already been suggested by BROWN (1935). According to our measurements, this second part is especially caused by space charges. High-potential gradient values nearly always indicate the presence of terrestrial positive space charges; very low values indicate either extremely high conductivity or negative space charges.

4. If the local sources of disturbance in the vicinity of a measuring station are well known, we can carry out special investigations on small spaces, for instance on local air motions and similar factors.

REFERENCES

BROWN, J. G.	1933	*Terrest. Magn.*, **38**, 161
BROWN, J. G.	1935	*Terrest. Magn.*, **40**, 413–424
BROWN, J. G.	1936	*Terrest. Magn.*, **41**, 279
	1937	**42**, 163
CHALMERS, J. A.	1952	*J. Atmosph. Terr. Phys.*, **2**, 155
EHMERT, A., und MÜHLEISEN, R.	1953	*Z. Angew. Phys.*, **5**, 43–47
FLEMING, J. A., WAIT, G. R., and TORRESON, O. W.	1941	*Terrest. Magn.*, **46**, 319
ISRAEL, H.	1953	In BYERS' *Thunderstorm Electricity*, pp. 4–23
ISRAEL, H.	1954	*Ann. Géophys.*, **10**, 93–116
ISRAEL, H., KASEMIR, H. W., and WIENERT, K.	1951	*Arch. Meteorol.*, **3**, 357–381
KOENIGSFELD, L.	1953	In BYERS' *Thunderstorm Electricity*, pp. 24–45
MAUCHLY, S. J.	1923	*Terrest. Magn.*, **28**, 61
MÜHLEISEN, R., Sonderband	1953	*Z. Geophys.*, 142–159
MÜHLEISEN, R., und CREUTZBURG, U.		(In preparation)
MÜHLEISEN, R., und HOLL, W.	1952	*Geofis. pura appl.*, **22**
MÜHLEISEN, R., und HOLL, W.	1954	*Naturwissenschaften*, **41**, 300
MÜHLEISEN, R.	1952	*Naturwissenschaften*, **39**, 376
NORINDER, H., ISRAEL, H., and SIKSNA, R.	1954	*Ark. Geofys.*, **2**, 109–138

Journal of Atmospheric and Terrestrial Physics, 1956, Vol. 8, pp. 158 to 162. Pergamon Press Ltd., London

The fading periods of the *E*-region coupling echo at 150 kc/s*

R. W. PARKINSON†
Ionosphere Research Laboratory, The Pennsylvania State University,
University Park, Pennsylvania

(*Received* 25 *July* 1955)

ABSTRACT

Studies have been made on the fading periods of pulsed 150-kc/s waves returned from the coupling region in the lower ionosphere. Two dominant distributions of the fading periods have been found, centred on two different frequencies, yielding information regarding the diffracting region responsible for the observed fading.

THE distribution of periods of oscillation in amplitude and phase of the main *E*-region echo has been studied by MILLMAN (1952) and JONES (1955). The attempt to interpret the statistical results obtained by these authors has led directly to an investigation of the fading characteristics of the coupling echo. The initial results of such an analysis are presented below, followed by a breakdown of the data into distributions of long and short fades suggested by a comparison of the overall fading characteristics of the coupling echo with those of the main echo. Possible explanations of the experimental observations are suggested in terms of either one or two diffracting screens lying below the main *E*-region.

The coupling echo is observed at the lower frequencies, only at night, apparently reflected from a lower height than, and having substantially different polarization characteristics from, the main echo. The appearance of this echo and its polarization have been discussed by LINDQUIST (1953) and by KELSO *et al.* (1951). The theory and correlation of theoretical and experimental results for this coupling phenomenon have been reported by DAVIDS and PARKINSON (1955) and PARKINSON (1955a), and will not be discussed in detail here. However, a brief review of the points directly applicable to this paper is given below to provide a background for the analysis to follow.

It has been shown (DAVIDS, 1953) that, under certain critical coupling conditions, the coupling terms in the well-known Rydbeck coupled-wave equations go to infinity. This singularity limited the initial investigation of coupling phenomena (GIBBONS and NERTNEY, 1952) to conditions rather far removed from the critical case. DAVIDS and PARKINSON (1955), utilizing a transformation of the wave equations obtained in the principal axis co-ordinate system by DAVIDS (1953), derived coupled-wave equations with coupling factors which did not exhibit the above singularity at critical coupling. Second-order solutions were obtained, and numerical results were calculated for several ionospheric models at critical and near-critical conditions. The analysis showed that high coupling causes appreciable backscatter from the coupling region, which lies below the main reflection level, and thus explains the appearance of split night-time *E*-region echoes at low frequencies. Theoretical

*The research reported in this paper has been sponsored by the Geophysics Research Directorate of the Air Force Cambridge Research Center, Air Research and Development Command, under Contracts AF19(122)-44 and AF19(604)-1304.

† Present affiliation: The Ramo-Wooldridge Corporation, Los Angeles, California.

VOL.
8
1956

backscatter coefficients as high as 0·6 were obtained, with results highly dependent upon the electron-density gradient in the coupling region. PARKINSON (1955a) showed excellent overall agreement between theoretical and experimental results, and was able to propose a provisional model of the lower night-time ionosphere. The analysis of coupling phenomena showed that the overall presence or absence

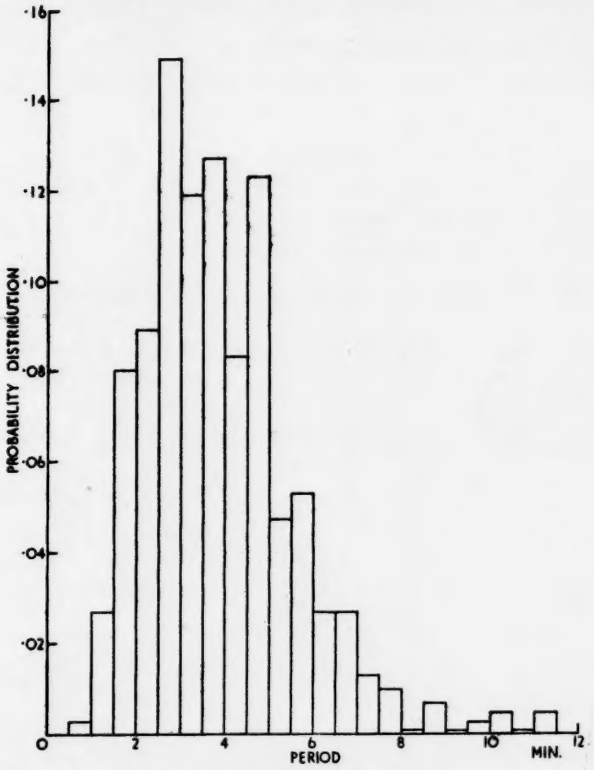

Fig. 1. Distribution of fading-periods, coupling echo, weighted

of the coupling echo depends solely upon the existence of high coupling conditions, that is, upon the proximity of the critical electron-density and collision-frequency levels. This conclusion will be found to be of great importance in the discussion of coupling-echo fading presented below.

The results of the initial determination of coupling-echo fade period are shown in Fig. 1, in which over 2500 observations are represented. The method of data reduction was the same as that used by MILLMAN (1952) and JONES (1955) with the same weighting factor, proportional to the period, as used by the latter. In obtaining this distribution from the raw data, it was noted that the fading pattern for the coupling echo seemed to consist of short-period fades superimposed on long-period overall fades. This tendency was found to be much more apparent for the coupling echo than for the main echo. Fig. 2 shows a tracing of typical main- and coupling-echo amplitude envelopes as functions of time. (A description of the

method of obtaining these data is given by PARKINSON, 1955b.) On the actual record, the amplitude envelopes of Fig. 2 are superimposed. They are shown separately here to facilitate comparison, and it will be noted that the fading pattern described above is rather obvious. With such a situation, it was recognized that

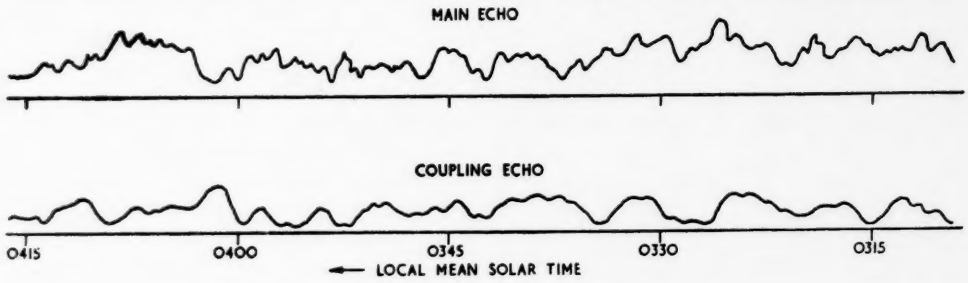

Fig. 2. Typical simultaneous fading records at 150 kc/s

the choice of points at which any given fade begins or ends is an extremely subjective one, in which the human factor may play a large part. For this reason the significance of the data presented in Fig. 1 is considered doubtful.

In order to reduce the subjectivity present in obtaining fade periods for the

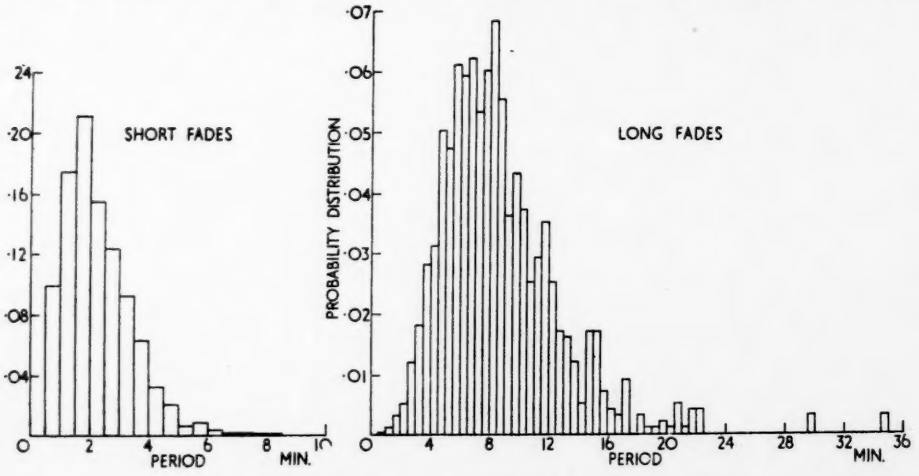

Fig. 3. Distribution of fading-periods, coupling echo, weighted

coupling echo, it was decided to re-examine the experimental records and tabulate long fades separately, while at the same time breaking these down into their component short fades. The results of this analysis are shown in Fig. 3, with over 5000 observations of short fades and 1500 observations of long fades represented. The most probable fading periods thus obtained are about two minutes for short fades and about seven minutes for long fades.

JONES, MILLMAN, and NERTNEY (1953) attributed the fading of the main *E*-region echo to a diffracting screen lying below the main reflection level and at or below

the coupling level, and their subsequent calculations bore out this hypothesis. The evidence for this contention has been strengthened by BANERJI (1955). This is, then, a transmission phenomenon. The presence or absence of the coupling echo, on the other hand, has been shown to be due solely to the proximity of the levels of critical electron density and critical collision frequency, as mentioned above. In addition, the irregular times of appearance of this echo, when combined with polarization data on both main and coupling echoes, have shown that travelling irregularities exist at, or within about one kilometre of, the coupling level (PARKINSON, 1955a).

It appears, then, that we have observed two different fading phenomena, and also two possible mechanisms by which they may be explained. As a first attempt to bring these two ideas together, let us postulate two levels of irregularities or diffracting screens, one at the coupling level and the other below, perhaps 10 km lower. The former will then cause overall fluctuations in coupling-echo amplitude due to the mechanism discussed above. The diffraction screen lying below the coupling region, on the other hand, will have a transmission effect on the coupling echo similar to that previously described for the main echo, causing short-period fades similar to those observed on the latter. The two screens, of course, will have a combined transmission effect on the main echo, with results already discussed.

It must be remembered that we are discussing these heights as though they are fairly localized. The probability is, however, that irregularities and movements exist throughout the whole ionosphere; many workers have observed them at many different heights. Nevertheless, there may be local concentrations for which effective heights can be determined, and it is to such a condition that we refer in speaking of the levels of irregularities.

It should also be noted here that the fact that the long fades on the coupling echo may be attributed to a diffracting screen at 90 km, while the short fades may be attributed to a screen below this level, does not necessarily imply a larger scale of irregularities for the former screen. The mechanisms postulated for the two phenomena are entirely different, and it is entirely possible that the transmission effect of the lower screen may cause short fades, even though its scale of irregularities is the same as or greater than that of the screen at the coupling level.

An alternate, and perhaps more elegant, model by which the observed phenomena may be explained, is that of a *single* diffraction screen situated right at the coupling level. The transmission effect on the main echo will then be the same as before. The effect on the coupling echo, however, is more complicated, since we must now consider both a variation of reflection coefficient due to the changes in both the height of the critical electron density and the value of its gradient, and the effect of a phase-and-amplitude screen varying with the electron density (this latter was neglected in the above discussion of the two-screen possibility). Unfortunately, the theoretical analysis for near-critical coupling conditions is not a simple one (see PARKINSON, 1955a). Lacking a complete theoretical treatment of such a problem, we shall conclude that, while the hypothesis of two diffracting screens presents a simpler picture of the phenomena, the possibility still exists that a single screen may suffice to explain the experimental data.

REFERENCES

BANERJI, R. B.	1955	To be published (Scientific Report No. 71, Ionosphere Research Laboratory, The Pennsylvania State University, 1954)
DAVIDS, N.	1953	*J. Geophys. Res.* **58**, 311–321
DAVIDS, N. and PARKINSON, R. W.	1955	To be published (Scientific Report Nos. 54 and 70, Ionosphere Research Laboratory, The Pennsylvania State University, 1953, 1954)
GIBBONS, J. J. and NERTNEY, R. J.	1952	*J. Geophys. Res.* **57**, 323–338
JONES, R. E.	1955	To be published
JONES, R. E., MILLMAN, C. H., and NERTNEY, R. J.	1953	*J. Atmosph. Terr. Phys.* **3**, 79–91
KELSO, J. M., NEARHOOF, H. J., NERTNEY, R. J., and WAYNICK, A. H.	1951	*Ann. Géophys.* **7**, 215–244
LINDQUIST, R.	1953	*J. Atmos. Terr. Phys.* **4**, 10–27
MILLMAN, G. H.	1952	*Ann. Géophys.* **8**, 365–384
PARKINSON, R. W.	1955a	To be published (Scientific Report No. 73, Ionosphere Research Laboratory, The Pennsylvania State University, 1954)
PARKINSON, R. W.	1955b	*Rev. Sci. Instrum.* **26**, 319–323

VOL.
8
1956

Journal of Atmospheric and Terrestrial Physics, 1956, Vol. 8, pp. 163 to 168. Pergamon Press Ltd., London

The determination of the horizontal velocity of ionospheric movements from fading records from spaced receivers

D. W. G. CHAPPELL and C. L. HENDERSON
Dominion Physical Laboratory, Lower Hutt, New Zealand

(*Received* 9 *August* 1955)

ABSTRACT
RATCLIFFE has shown that, for the Mitra formula for the velocity of ionospheric movements to be valid, a long sample of fading record is necessary. This paper presents a method of deriving the velocity which is not dependent on a long sample of record, and is valid for any arbitrary distribution of orientation of "lines of maximum amplitude." The derived formula is compared with MITRA's formula, and the time delays from a fading record are analysed. The method is not suitable for use with Philips records.

INTRODUCTION

IN MITRA'S (1949) method of determining the horizontal velocity of ionospheric movements, fading records from three spaced receivers are compared. The velocity is deduced from the time delays between corresponding peaks or troughs in the three fading patterns. MITRA considered that a steady drift was indicated by records in which the time delays were essentially constant. RATCLIFFE (1954) demonstrated that in some cases a wide variation of time delays was consistent with a steady motion. He showed that MITRA'S values of speed and direction were correct if

(1) the speed and direction of movement were constant for the duration of a record,
(2) "lines of maximum amplitude" in the interference pattern on the ground were essentially straight relative to the dimensions of the receiver array,
(3) the orientation of these "lines of maximum amplitude" was random.

It can be shown also that the Mitra values are correct for a symmetrical distribution of orientation of the "lines" about a direction normal to the direction of drift.

For a right-angled isosceles triangle of receivers, a simple deduction from RATCLIFFE'S equations is that a dot diagram of pairs of time delays should form a straight line normal to the line from the origin to the mean point of the distribution. Many dot diagrams from fading records at the Dominion Physical Laboratory show straight-line distributions, but these distributions are not in general normal to the lines joining the origin and the respective mean points. This discrepancy is probably due to the short duration (two minutes) of the records, which usually results in an asymmetrical distribution of orientation of the lines of maximum amplitude. In this paper a determination of the velocity is presented in which no assumption is made regarding the distribution of orientation of these lines. The only assumptions are numbers (1) and (2) of RATCLIFFE'S.

THE IDEAL CASE

If a curved line of maximum amplitude passes with linear velocity V, without modification or rotation, across a matrix of n receivers situated at the positions O, r_1, r_2, . . . , r_{n-1} at times O, T_1 , T_2, . . . , T_{n-1} respectively, then at zero time

the points O, $\mathbf{r}_1 - T_1\mathbf{V}$, $\mathbf{r}_2 - T_2\mathbf{V}$, . . ., $\mathbf{r}_{n-1} - T_{n-1}\mathbf{V}$ lie on the line of maximum amplitude. If the velocity of the interference pattern is known, the shape of the line can be deduced, in so far as it can be defined by n points. If on the other hand we wish to deduce the velocity of the line of maximum amplitude, it is necessary to assume that the line has a shape definable by no more than $(n - 2)$ points. However, where several lines cross the receivers in a short interval of time, they can be assumed to have a common velocity. This velocity can be determined, assuming the lines have shapes definable by up to $(n-1)$ points. In the present case we have only three receivers, so the velocity can be determined only by assuming that the lines of maximum amplitude are straight. Thus the join of the points $\mathbf{r}_1 - T_1\mathbf{V}$, $\mathbf{r}_2 - T_2\mathbf{V}$ passes through the origin,

i.e., $$(\mathbf{r}_1 - T_1\mathbf{V}) \times (\mathbf{r}_2 - T_2\mathbf{V}) = 0$$

or $$T_1\,\mathbf{V} \times \mathbf{r}_2 + T_2\mathbf{r}_1 \times \mathbf{V} = \mathbf{r}_1 \times \mathbf{r}_2.$$

If we now put $$\mathbf{V} = \frac{\mathbf{r}_1}{K_1} + \frac{\mathbf{r}_2}{K_2},$$

then $$\frac{T_1}{K_1} + \frac{T_2}{K_2} = 1, \tag{1}$$

and a plot of pairs of values of T_1, T_2 should fall on a straight line whose intercepts on the axis of T_1 and T_2 are K_1 and K_2 respectively.

VOL. 8 1956

THE PRACTICAL CASE

In practice there will be errors in the time measurements from the three received signals, namely τ_0, τ_1, and τ_2, so that if t_{1n}, t_{2n} are the measured time delays for the nth line of maximum amplitude, then from equation (1)

$$t_{1n} = K_1\,(\tfrac{1}{2} + \omega_n) + \tau_{0n} - \tau_{1n}$$

$$t_{2n} = K_2\,(\tfrac{1}{2} - \omega_n) + \tau_{0n} - \tau_{2n},$$

where ω_n is a variable associated with the orientation of the nth line.

The problem is to determine the most probable value of $\mathbf{V}$ (i.e., of K_1 and K_2), and this is arbitrarily decided to be that which results from the "best" linear relationship that can be deduced between the values of t_1 and t_2. Because of the presence of the random variable τ_0 in the values of both t_1 and t_2, methods of deducing this "best" relationship based on the principle of minimum dispersion cannot be used. If, however, we make certain additional assumptions about the statistical properties of the error terms, the problem becomes more tractable. Thus we assume that

$$\bar{\tau}_s = 0,\ \text{cov}\ \tau_s\tau_t = 0,\ \text{cov}\ \tau_s\omega = 0,\ \text{var}\ \tau_s = \text{var}\ \tau,$$

where $$s = 0,\ 1,\ 2$$

$$t = 0,\ 1,\ 2 \neq s.$$

Under these conditions,

$$K_1 = \frac{2\bar{t}_1}{1 + 2\bar{\omega}} \tag{2}$$

$$K_2 = \frac{2\bar{t}_2}{1 - 2\bar{\omega}} \tag{3}$$

$$\text{var } t_1 = K_1^2 \text{ var } \omega + 2 \text{ var } \tau \tag{4}$$

$$\text{var } t_2 = K_2^2 \text{ var } \omega + 2 \text{ var } \tau \tag{5}$$

$$\text{var } (t_1 - t_2) = (K_1 + K_2)^2 \text{ var } \omega + 2 \text{ var } \tau. \tag{6}$$

For convenience let

$$S_1 = \text{var } (t_1 - t_2) - \text{var } t_1 \tag{7}$$

$$S_2 = \text{var } (t_1 - t_2) - \text{var } t_2 \tag{8}$$

$$a^2 = S_1^2 - S_1 S_2 + S_2^2. \tag{9}$$

Substituting for K_1 and K_2 and eliminating the variances of ω and τ, we have

$$\frac{S_1}{S_2} = \frac{2\,\bar{t}_1\bar{t}_2\,(1 - 4\bar{\omega}^2) + \bar{t}_2^2\,(1 + 2\bar{\omega})^2}{2\,\bar{t}_1\bar{t}_2\,(1 - 4\bar{\omega}^2) + \bar{t}_1^2\,(1 - 2\bar{\omega})^2},$$

which leads to

$$2\bar{\omega} = \frac{(S_1\bar{t}_1^2 + S_2\bar{t}_2^2) \pm 2\,\bar{t}_1\bar{t}_2\,a}{(S_1\bar{t}_1^2 - S_2\bar{t}_2^2) - 2\,\bar{t}_1\bar{t}_2\,(S_1 - S_2)};$$

$\therefore$ substituting in (2) and (3),

$$K_1 = \frac{S_1\bar{t}_1 + (S_2 - S_1 \mp a)\,\bar{t}_2}{S_1}$$

$$= \frac{(S_1 - S_2 \mp a)\,\bar{t}_1 + S_2\bar{t}_2}{S_1 - S_2 \mp a},$$

from the identity

$$(S_1 - S_2 + a)(S_2 - S_1 + a) \equiv (S_1 - S_2 - a)(S_2 - S_1 - a) \equiv S_1 S_2.$$

$$K_2 = \frac{(S_1 - S_2 \mp a)\,\bar{t}_1 + S_2\bar{t}_2}{S_2}.$$

To resolve the ambiguity in sign, we note that

$$\frac{K_2}{K_1} = \left(\frac{S_1}{S_2} - 1\right) \mp \frac{a}{S_2}, \tag{10}$$

which leads to

$$\left(\frac{K_2}{K_1} + \frac{1}{2}\right)^2 - 2\left(\frac{S_1}{S_2} - \frac{1}{2}\right)\left(\frac{K_2}{K_1} + \frac{1}{2}\right) - \frac{3}{4} = 0,$$

i.e., the values of $\dfrac{K_2}{K_1}$ lie on either side of $-\frac{1}{2}$.

From (5), (6), and (8)

$$S_2 \gtrless 0 \qquad \text{as} \qquad \frac{K_2}{K_1} \gtrless -\tfrac{1}{2},$$

whence from (10), when $S_2 \gtrless 0$ we require the greater (lesser) value of K_2/K_1, which in both cases requires that the lower sign of the radicle be taken. Thus

$$K_1 = \frac{(S_1 - S_2 + a)\,\bar{t}_1 + S_2\bar{t}_2}{S_1 - S_2 + a} \tag{11}$$

$$K_2 = \frac{(S_1 - S_2 + a)\,\bar{t}_1 + S_2\bar{t}_2}{S_2}; \tag{12}$$

i.e., the most probable value of the velocity is

$$V = \frac{1}{(S_1 - S_2 + a)\,\bar{t}_1 + S_2\bar{t}_2}\,[(S_1 - S_2 + a)\mathbf{r}_1 + S_2\mathbf{r}_2]. \tag{13}$$

THE RIGHT-ANGLED TRIANGLE OF RECEIVERS

For the particular case when $\mathbf{r}_1 = r\mathbf{i}$, $\mathbf{r}_2 = r\mathbf{j}$ where $\mathbf{i}$ and $\mathbf{j}$ are unit vectors to the east and north,

$$\mathbf{V} = r\left(\frac{\mathbf{i}}{K_1} + \frac{\mathbf{j}}{K_2}\right) \tag{14}$$

If α is the direction of drift measured clockwise from the north, then from (11), (12), and (14)

$$\tan\alpha = \frac{K_2}{K_1} = \frac{S_1 - S_2 + a}{S_2}. \tag{15}$$

If V is the scalar value of $\mathbf{V}$, then from (13), (14), and (15)

$$V = \frac{r}{\bar{t}_1 \sin\alpha + \bar{t}_2 \cos\alpha}. \tag{16}$$

Substituting in (16) the Mitra formulae

$$\bar{t}_1 = \frac{r}{V_M}\sin\beta, \qquad \bar{t}_2 = \frac{r}{V_M}\cos\beta,$$

where V_M and β are the Mitra values of speed and direction, we have

$$V = V_M \sec(\alpha - \beta). \tag{17}$$

Thus V is either equal to or greater than the Mitra speed V_M. The difference between the directions α and β is less than $\pi/2$, and usually less than $\pi/4$. Equation (17) is easily established also for a general triangle of receivers.

Fig. 1 shows the distribution of points (t_1, t_2) for a record made in July 1954. From the Mitra formulae it is evident that the line OP is of length r/V_M and direction β. Equations (1), (14), and (15) define ON, the normal from the origin

VOL. 8 1956

to the straight line of equation (1), as having a length $(K_1^{-2} + K_2^{-2})^{-\frac{1}{2}} = r/V$, and direction $\tan^{-1} K_2/K_1 = \alpha$.

Thus the lines OP and ON define the velocities as determined from MITRA's formulae and from equations (15) and (16). The relationship of equation (17) is

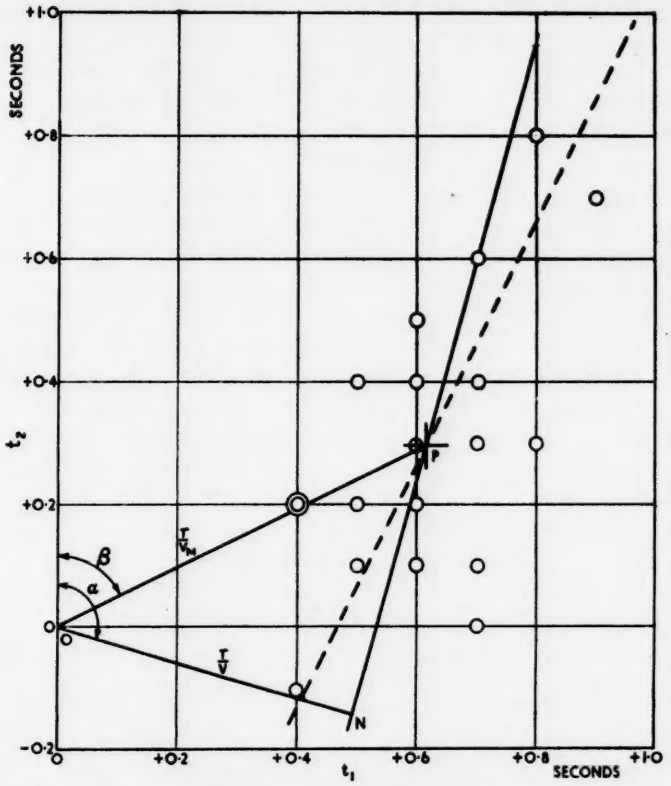

Fig. 1. Dot diagram of (t_1, t_2)
\+ Mean point.
—— Line fitted from equations (1), (11), and (12)
--- Line fitted from least squares

illustrated in the triangle ONP. Similar relationships have been deduced by PÜTTER (1954).

The numerical results for the example of Fig. 1 are

$\bar{t}_1 = +0{\cdot}62$ sec — var $t_1 = 0{\cdot}021$ sec^2

$\bar{t}_2 = +0{\cdot}32$ sec — var $t_2 = 0{\cdot}054$ sec^2

var $(t_1 - t_2) = 0{\cdot}036$ sec^2

$r = 91{\cdot}4$ metre — $\therefore a = 0{\cdot}029$ sec^2

$V = 180$ metre/sec — $\alpha = 106°$ E of N

$V_M = 134$ metre/sec — $\beta = 64°$ E of N

For a straight line fitted to the observations by least-squares, the calculated speed and direction are 220 metre/sec and 117° E of N. This discrepancy illustrates the bias due to the common error term τ_0.

The above results give some indication of the effect of an asymmetrical distribution of the orientation of lines of maximum amplitude on the calculation of velocity.

Acknowledgements—The authors wish to acknowledge the assistance and constructive criticism of their colleagues, in particular Messrs. G. J. BURTT and J. E. DRUMMOND.

REFERENCES

MITRA, S. N. 1949 *Proc. Instn. Elect. Engrs.*, 96 **3**, 441.
PÜTTER, P. St. 1954 Phys. Soc. Conf., "Phys. of the Ionos.," **191**.
RATCLIFFE, J. A. 1954 *J. Atmosph. Terr. Phys.*, **5**, 173.

VOL.
8
1956

Journal of Atmospheric and Terrestrial Physics, 1956, Vol. 8, pp 169 and 170. Pergamon Press Ltd., London

A determination of ionospheric winds for a 24-hour period

G. W. G. COURT* and E. S. GILFILLAN
Dominion Physical Laboratory, Lower Hutt, New Zealand

(*Received* 23 *August* 1955)

ABSTRACT

Results are given of an analysis, by the method proposed in a recent paper (COURT, 1955), of the radio field strength fading records obtained from the Mitra experiment (MITRA, 1949) during the 24-hour period on 17 January 1953. The date chosen was arbitrary, and the results indicate a possible diurnal effect in the variation of wind direction during that period.

GENERAL

IN a recent paper (COURT, 1955), a method of analysis of the field strength fading records obtained from the three spaced aerials suggested by MITRA was proposed. A number of isolated results were given.

This method of analysis has now been applied to the records for an arbitrarily chosen 24-hour period from midnight to midnight, 17 January 1953. The result is given in Figs. 1 and 2, showing variations of direction and magnitude of the winds respectively.

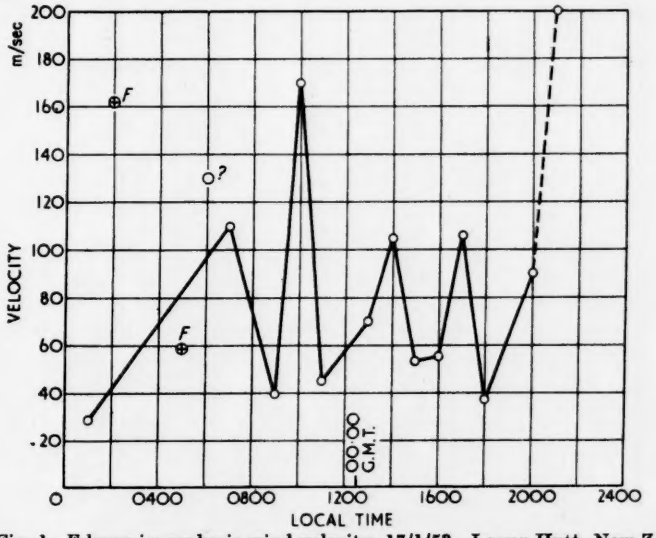

Fig. 1. *E*-layer-ionospheric-wind velocity, 17/1/53. Lower Hutt, New Zealand.

Records had been taken for approximately two-minute periods, on the hour, throughout the period, and sixteen records were analysed. Of these, 0200 and 0500 were from a height of 250 km, and the remainder from the 120-km region. However, the record for 0600 is noted as consisting of a mixture of both layers, and is not admissible. Records for 0300, 0400, 1200, and 1900, could not be analysed to give

* Now at Civil Aviation Administration, Air Department, Wellington

a result, and the result for 2100 is doubtful. Records for 2200, 2300, and 2400 were unsuitable, due to local interference or recording faults.

From Fig. 1 it can be seen that a considerable variation of the magnitude of the wind in indicated, about a mean value throughout the period of about 80 m/s.

Fig. 2 is of interest in that, although there is a considerable scatter in the results, a definite trend can be seen. The wind would appear to have swung from a southerly direction through west and north to the south-east by midday approximately, and returned through north towards the west during the afternoon and evening. The times given are local time, 1230 being equivalent to 0000 G.M.T.

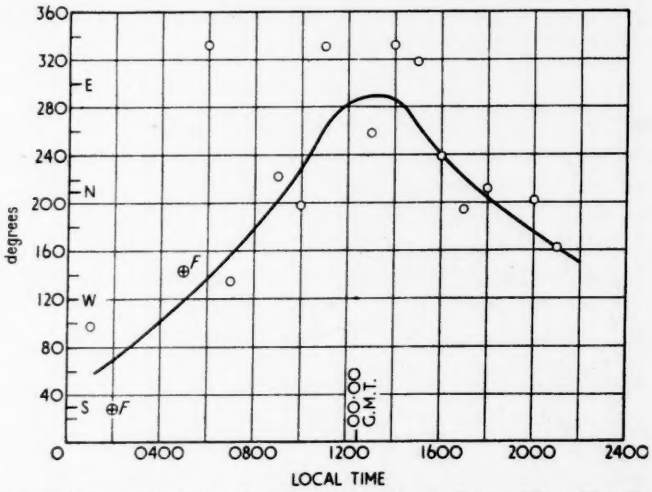

Fig. 2. *E*-layer-ionospheric-wind direction, 17/1/53. Lower Hutt, New Zealand.

Conclusion

This analysis was carried out as a test of the method which had been proposed, and the results obtained are some indication of its usefulness. There is found to be difficulty with certain records, in that insufficient points can be obtained to firmly establish the appropriate construction, and it is considered that records of two or three times the length of those used would be beneficial. Before any large-scale application of the method of analysis is attempted, the construction of some form of optical-mechanical aid, removing the need for tracing, etc., is highly desirable.

References

Court, G. W. G. 1955 *J. Atmosph. Terr. Phys.* **7**, 333.
Mitra, S. N. 1949 *Proc. Instn. Elect. Engrs.* **96** (*Part IV*), 441.

VOL. 8 1956

Journal of Atmospheric and Terrestrial Physics, 1956, Vol. 8, pp. 171 to 183. Pergamon Press Ltd., London

Observations of short bursts of signal from a distant 50 Mc/s transmitter

B. H. Briggs
Cavendish Laboratory, Cambridge

(*Received* 17 *November* 1955)

ABSTRACT
The paper describes observations of short bursts of signal received at Cambridge from the Kirk o' Shotts television transmitter at a distance of about 500 km. The following characteristics are studied: (i) the statistics of the time-intervals between bursts, (ii) the waveforms and durations of the bursts, and (iii) the irregular fluctuations or "fading" during the bursts. It is concluded that the majority, if not all, of the bursts are reflections from ionized trails produced by meteors, and that many of the trails which produce bursts are situated near to the receiving point, rather than near the midpoint of the transmission path.

1. Introduction

Isted (1954, 1955) observed short bursts of signal from television transmitters operating on frequencies near 50 Mc/s and at distances of several hundred kilometres. Most of his observations referred to the reception at Chelmsford of the Kirk o' Shotts television station at a distance of 530 km. Villard, Peterson, Manning, and Eshleman (1953), and Forsyth and Vogan (1955) observed bursts at various distances from transmitters in the same frequency range. The latter groups of workers assumed that the signal bursts were due to reflections from ionized trails produced by meteors, but Isted concluded that the majority he observed were not produced by this mechanism. He proposed instead that the main cause of the bursts was the presence in the *E* region of transient patches of ionization produced by upwardly-directed electrical discharges from clouds. One of the main reasons for advancing this theory was that the bursts seemed to occur in groups or "trains" of three or more bursts, with equal time-intervals between the members of a train. Isted gave an explanation of this on the discharge theory. The records reproduced in his papers did show such trains of bursts, but no statistics were given to show whether they occurred more often than would be expected by chance.

In the present work, signal bursts from the Kirk o' Shotts television station were recorded at Cambridge. The distance is 480 km, and the conditions should be closely similar to those of Isted's experiments. In Section 2 we shall consider some statistical results relating to the time-intervals between successive bursts, in order to see if there is evidence for the presence of "trains." For the purpose of this analysis, the bursts were recorded on a pen recorder. Then in Section 3 we shall describe some further work in which the waveforms and durations of the individual bursts were examined by the use of high-speed photographic recording. These results will be interpreted on the assumption that the bursts are reflections from meteor trails.

The receiving apparatus consisted of a crystal-controlled converter working into an AR-88 receiver used as an intermediate-frequency amplifier. The

intermediate frequency was 10 Mc/s, and the band-width was about 1 kc/s. The converter used a "cascode" first stage, in order to obtain a good noise factor. A voltage proportional to the received signal was taken from the second detector of the AR-88 and amplified with a single-stage d.c. amplifier. The output of this amplifier was used to deflect the pen recorder and the spot of the oscilloscope. The receiving aerial consisted of two vertical half-wave dipoles spaced half a wavelength apart, and connected in parallel. The polar diagram therefore had a zero in the plane of the dipoles and a maximum perpendicular to the plane. It was erected at a height of about fifteen feet, with the plane directed towards the Norwich television station, which operates on the same frequency as Kirk o' Shotts. When set to reject Norwich, the maximum of the polar diagram was very nearly directed towards Kirk o' Shotts. The discrimination between the two stations was further assisted by the fact that Kirk o' Shotts transmits vertically polarized waves, and Norwich horizontally polarized waves. A very weak continuous signal was usually received, and this was sufficient to enable the apparatus to be tuned to the sound carrier, which is on a frequency of 53·25 Mc/s (wavelength 5·7 m).

2. Statistical Results concerning the Time-intervals between Bursts

On the pen recorder, the bursts usually showed a sharp rise, followed by a slower recovery, the duration of which was determined mainly by the inertia of the instrument. By making use of the sharp rise, the time of start of a burst could be measured to $\pm 0{\cdot}05$ sec, with a paper speed of 1 ft per min. In the analysis, only bursts exceeding a pre-determined amplitude (about three times the receiver noise-level) were used.

Three pen records, each of about 1-h duration, were analysed in detail. Each record contained about two hundred signal bursts, and the time-intervals between the starts of successive bursts were measured.

The first test was to see whether the distribution of the time-intervals was consistent with that expected if the bursts occurred at random. It can be shown that, if the bursts occurred at random, the expected number of intervals with durations between t and $t + dt$ would be given by

$$n(t)\,dt = \frac{N}{T}\,e^{-t/T}\,dt \qquad (1)$$

where N is the total number, and T is the mean duration. It may be noted that the high probability of short intervals given by this exponential distribution is, in itself, sufficient to produce an *apparent* grouping of the bursts. This point has been discussed by Marsden and Barratt (1911) for α-particle disintegrations, and by Shain and Kerr (1955) for meteor echoes.

A histogram showing the distribution of time-intervals for one of the three records examined is given in Fig. 1. The dotted curve shows the theoretical distribution calculated from equation (1). It will be seen that there is good agreement between the observed distribution and the theoretical distribution, based on the assumption that the bursts occurred at random. The other records analysed

VOL. 8 1956

gave similar results. An application of the "χ^2 test" showed that in all cases the departures from the theoretical curves were no greater than would be expected from statistical fluctuations.

This result does not exclude the possibility that the bursts may be grouped. It would be possible, for example, to have a number of short intervals followed by a number of long intervals, and so on. This would not necessarily affect the overall distribution for a long sample.

Two methods were used to test directly for the presence of grouping. In the first method, the correlation between one interval and the next was calculated. If the bursts occurred at random, this correlation would be zero. In the second

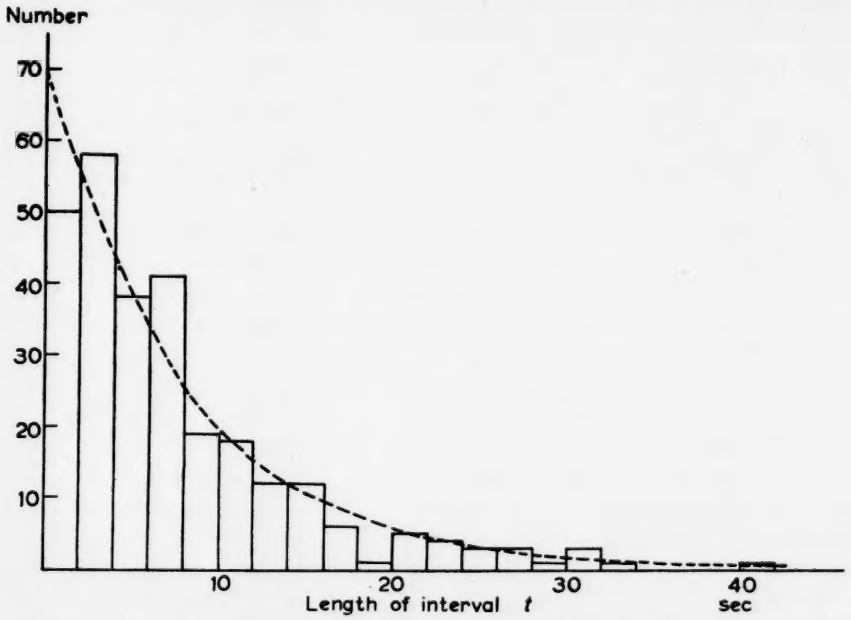

Fig. 1. Distribution of time-intervals for 280 bursts observed between 1010 and 1110 G.M.T. (approx.) on 27.7.55. The dotted curve is the function 69·3 exp (−t/8·05), which is the expected distribution if the bursts occurred at random.

method the number of groups of three equally spaced bursts was counted in a long record, and compared with that expected on the assumption that the bursts occurred at random.

The correlation between successive intervals was calculated for the three records previously analysed. The formulae used for the calculation of the correlation coefficient ρ and its standard error σ were the following:

$$\rho = \frac{\Sigma t_n t_{n+1} - NT^2}{\Sigma t_n^2 - NT^2} \tag{2}$$

$$\sigma = \frac{1}{\sqrt{N}} \tag{3}$$

where t_n is the length of the nth interval, and N and T have the same meanings as in equation (1). The results obtained are given in the table below.

Record	Date	G.M.T. (approx.)	Number of intervals	Correlation
I	8.6.55	1400–1500	239	$0{\cdot}13 \pm 0{\cdot}06$
II	9.6.55	1035–1135	182	$0{\cdot}13 \pm 0{\cdot}07$
III	27.7.55	1010–1110	280	$0{\cdot}11 \pm 0{\cdot}06$

These results taken together provide some evidence for a significant though small correlation between successive intervals. They do not indicate, however, any marked grouping of the bursts.

The second method was a direct test for the presence of trains of bursts. We shall first obtain an expression for the number of trains of three expected if the bursts occurred at random. From equation (1), the probability of an interval between t and $t + dt$ is $e^{-t/T}\,dt/T$, and the probability that this should be followed by an interval of equal length within a certain accuracy of measurement $\delta t'$ is

$$\frac{1}{T}e^{-t/T}\,dt \,.\, \frac{1}{T}e^{-t/T}\,\delta t' \qquad (4)$$

The probability that two successive intervals should be equal, without regard to the length chosen for the first interval, is obtained by integrating the expression (4) over all values of t from zero to infinity. In this way we find for the expected number of equal pairs of intervals in a large number N the expression $\frac{1}{2}N\,\delta t'/T$. If two successive intervals are equal, this gives, of course, an apparent train of three bursts.

The same three records I, II, III, were used in this test, and two successive intervals were taken to be equal if they differed by less than 0·2 sec, so that $\delta t' = 0{\cdot}2$. The expected number of pairs of equal intervals are then found to be: Record I, 2·1; record II, 2·2; record III, 3·5. The observed numbers of pairs were: Record I, 5; record II, 5; record III, 7. Again we find no evidence for any marked grouping into trains, but the number of trains of three is somewhat greater than that expected if the bursts occurred completely at random.

Further work is needed before any firm conclusions can be drawn. The figures for the correlation between successive intervals might be influenced by any long-term trend in the mean rate of occurrence of the bursts, if such a trend existed for the records analysed. The second method, which is a direct test for the presence of trains, is free from this objection, but the expected number of trains is very small, so that it is difficult to obtain statistically significant results with a sample of reasonable size. Provisionally, all that can be said is that the majority of the bursts seem to occur at random, but that a very small proportion may be grouped into trains.

VOL. 8 1956

VOL.
956

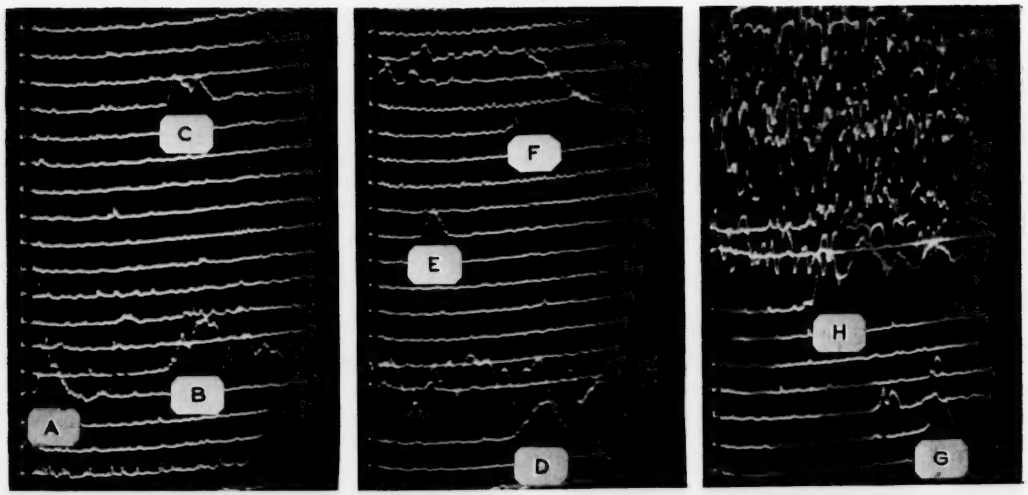

Fig. 2. Photographic records showing various types of signal burst. Each sweep of the time base occupies 1·8 seconds. Time advances from left to right along each sweep, and upwards from one sweep to the next.

VOL.
8
1956

It would be interesting to know whether the meteoric echoes observed in back-scatter experiments occur completely at random. SHAIN and KERR (1955) appear to be the only workers who have considered this point. They stated that their results were consistent with the assumption that the echoes occurred at random. They did not, however, give any details of the tests they employed.

3. OBSERVATIONS OF THE WAVEFORMS OF THE BURSTS

For an investigation of the detailed waveforms and durations of the bursts, photographic recording was used. In order to obtain a high effective film-speed, together with a reasonable economy in the use of film, a linear time-base was combined with a uniform movement of the film to produce records of the type shown in Fig. 2. In these records, time advances from left to right along the time-base, and successive sweeps of the time-base are displaced along the film in such a way that time advances from the bottom of the film to the top. One sweep of the time-base occupies 1·8 sec.

Examination of records of this type showed that the bursts were very variable in waveform and in duration. A description of some of the bursts which appear on the records reproduced in Fig. 2 is given below.

A A burst with a rapid rise and an approximately exponential decay, more or less free from irregular fluctuations.

B A burst with a slow rise, and fluctuations (or "fading") present all the time.

C Probably a close pair of bursts, each with a rapid rise and an exponential decay.

D A burst of longer duration, which lasted for one and a half sweeps of the time-base. The rise is slow, and fading is present almost from the start.

E A small burst of unusual shape.

F A burst with a rapid rise and an exponential decay.

G An unusual burst with a rapid rise and an equally rapid fall.

H The start of a very long-duration burst which lasted for several minutes. Violent fading is present.

In spite of the great variability of the shapes of the bursts, a large proportion could be assigned to one or other of two classes, as follows:–

Type (*i*) *bursts*—These have a rapid rise, usually completed in less than 0·05 sec, followed by an approximately exponential decay. There may be irregular fluctuations or "fading" superimposed on the exponential decay, particularly for the longer-duration bursts of this type. Bursts *A*, *C*, and *F* in Fig. 2 are of type (*i*).

Type (*ii*) *bursts*—These have either a rapid or a slow rise, followed by a period during which the amplitude is approximately constant, apart from random fluctuations or "fading." They are usually of longer duration than the type (*i*) bursts, and the fading is nearly always present. Bursts *B*, *D*, and *H* in Fig. 2 are of type (*ii*).

To begin with, we shall ignore the fading which may occur, and consider only the durations of the bursts. The division of the bursts into type (*i*) and type (*ii*) in

terms of the total duration is shown in Fig. 3. These results were obtained by measuring the durations of the bursts observed in a film record lasting about one hour, which contained 182 bursts which could be classified into type (*i*) or type (*ii*). It will be seen that the majority of the bursts with duration less than 0·4 sec were

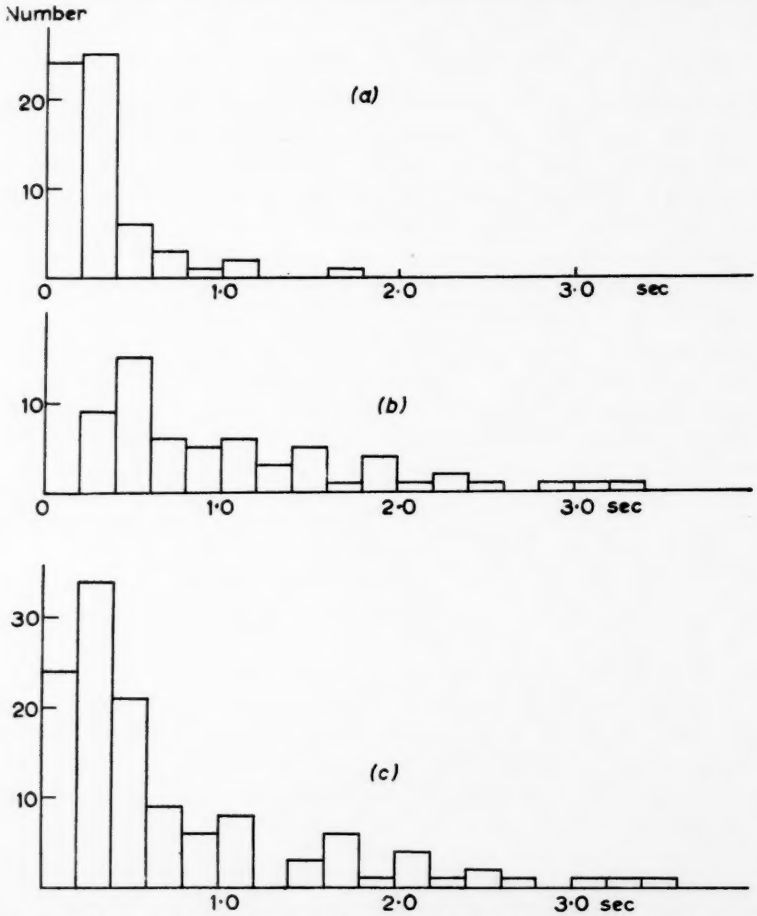

Fig. 3. Distribution of total durations for bursts observed by photographic recording between 1035 and 1135 G.M.T. (approx.) on 9.6.55.
(a) type-(i) bursts; (b) type-(ii) bursts; (c) total. Additional bursts of type (ii) (not plotted) had durations of 4, 5, 6 (4 cases), 7, 12, and 16 seconds.

of type (*i*), and the majority with durations greater than 0·4 sec were of type (*ii*). There is, however, considerable overlapping of the two groups.

The total time for which a burst is observed depends upon the receiver noise-level, and is therefore of no absolute significance. For the type (*i*) bursts, however, it is possible to determine the time ($t_{\frac{1}{2}}$) taken for the amplitude to fall to one-half of its maximum value. This is independent of the receiver noise-level, and determined only by the time-constant of the exponential decay. The values of $t_{\frac{1}{2}}$ were measured for 110 bursts of type (*i*) observed on various occasions, and the results

VOL. 8 1956

are shown as a histogram in Fig. 4. The values range from 0·01 sec to 0·3 sec, and there is a marked peak in the histogram at 0·05 sec.

Qualitatively, these results are very similar to those obtained for the transient "echoes" observed on similar frequencies when the transmitter and receiver are close together. We shall refer to such experiments as "back-scattering" experiments, as distinct from the present experiments which are "forward-scattering" experiments. It is normally assumed that all the echoes observed in back-scattering experiments are reflections from ionized meteor trails, though the coincidence of the echoes with visual meteors has only been demonstrated for the

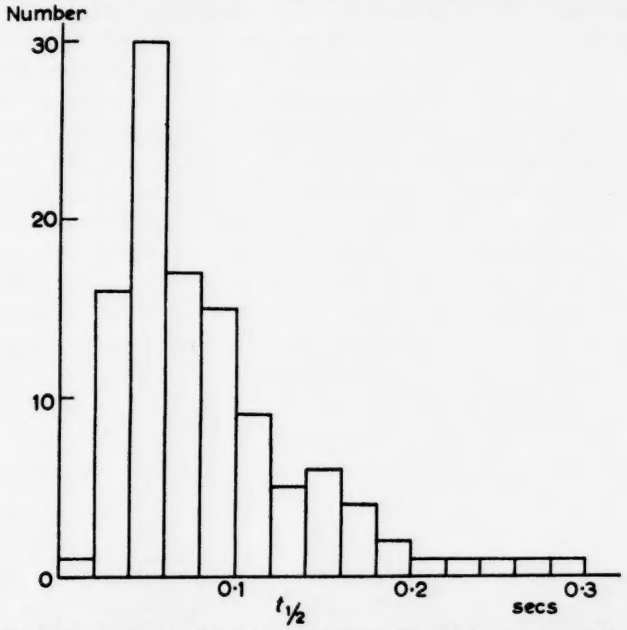

Fig. 4. Distribution of durations of type (i) bursts, for 110 bursts observed on various occasions. The values are measurements of the quantity $t_{\frac{1}{2}}$, the time of fall to half-amplitude.

echoes of longer duration. There is a large amount of circumstantial evidence to suggest that the rest are due to small meteors which cannot be seen visually, and a satisfactory theory has been developed to explain the main characteristics of the echoes. We shall first give a brief account of this theory, and then compare the present results in more detail with the corresponding results obtained in back-scattering experiments.

A survey of the present theory of meteor ionization has been given by KAISER (1953). Echoes with characteristics similar to the type (*i*) bursts described above are believed to be due to meteor trails in which the ionization density is never high enough to make the trail over-dense, so that the incident wave can penetrate to the centre of the column. The exponential decay of the amplitude is due to diffusion of the column, and the time-constant depends only on the diffusion coefficient and the wavelength, and not on the initial line density. Echoes with characteristics similar to the type (*ii*) bursts are believed to be due to trails which

are initially over-dense. In this case the echo amplitude remains more or less constant until the trail has diffused to the point at which it ceases to be over-dense. The amplitude then falls rapidly to zero. The total duration of this type depends on the diffusion coefficient, the wavelength, and the initial line-density. In all cases an echo can normally be observed only if the trail satisfies the condition for specular reflection, which, for back-scattering experiments, requires that a perpendicular should exist from the observing station to the trail. The random fading which is often observed, particularly for the echoes of longer duration, is explained by the distortion of the trails caused by winds and turbulence in the atmosphere. Because of this distortion, the condition for specular reflection in due course breaks down, and the trail is able to return a signal from various "scattering centres" distributed along its length. The random movement of these centres, or a uniform drift of the column as a whole, produces the observed fluctuations. Small periodic fluctuations just after the appearance of an echo are explained as due to Fresnel diffraction from the extending column of ionization; they are similar to the diffraction fringes produced at a straight edge. The Fresnel oscillations have been used to determine the meteoric velocities, but only a small proportion of the echoes show the oscillations clearly. Some long-duration echoes build up gradually in amplitude, and without Fresnel oscillations. These are believed to be due to trails which do not satisfy the specular reflection condition, but which nevertheless can produce an echo when they have become sufficiently distorted to have scattering centres distributed along their length.

The theory of scattering from trails which are not initially over-dense, and which may account for the type (*i*) bursts, has been extended to forward scattering by ESHLEMAN and MANNING (1954). They give the following expression for the power received from a meteor trail of this type:

$$P_R = \frac{P_T}{32\pi^4}\left[\frac{\mu_0 e^2}{4m}\right]^2 \frac{2\lambda^3}{R_1 R_2(R_1+R_2)} \frac{G_T G_R q^2 \sin^2\alpha}{(1-\cos^2\beta\sin^2\phi)} \exp\left[-\frac{32\pi^2 Dt\cos^2\phi}{\lambda^2}\right] \quad (5)$$

where P_T = transmitted power,
μ_0 = permeability of free space,
e = electronic charge,
m = electronic mass,
λ = wavelength,
R_1 = range from transmitter to meteor trail,
R_2 = range from receiver to meteor trail,
G_T = transmitting-aerial gain,
G_R = receiving-aerial gain,
q = number of electrons per metre of trail,
α = angle between the electric vector of transmitted wave and a line along R_2,
ϕ = one-half of the interior angle formed by the two lines along R_1 and R_2,
β = angle between the axis of the meteor trail and the plane containing R_1 and R_2,
D = diffusion coefficient,
t = time.

VOL. 8 1956

The condition for specular reflection in this case is that the trail must be a tangent to an ellipsoid having the transmitter and receiver as foci.

It will be seen that the time-constant of the exponential decay now depends on the value of ϕ as well as on the diffusion coefficient and the wavelength. We shall now attempt to estimate what values the angle ϕ is likely to take in the present experiments.

The conditions of the experiments are shown in Fig. 5, which is drawn roughly to scale, on the assumption that the meteor trails are at a height of 90 km. The transmitting aerial is such that the radiation is greatest for angles within 20° of the horizontal. The receiving aerial has not such a restricted polar diagram, but it has a zero vertically upwards. For these reasons, few bursts can be expected

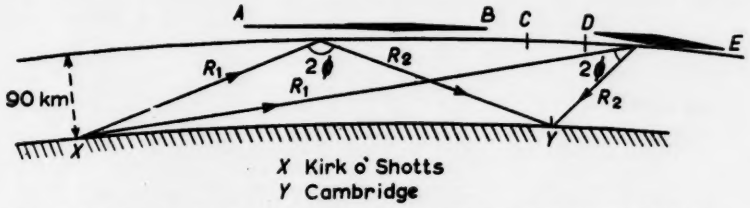

Fig. 5. Diagram of the transmission path from Kirk o' Shotts to Cambridge, drawn approximately to scale.

to come from points to the left of A or from points between C and D. Also, at some point near C, the lines R_1 and R_2 are at right angles, and the polarization factor α in equation (5) is then zero. Thus no bursts can be expected from points near to C. The regions from which bursts may be expected are therefore AB and DE. The reflections will not be confined to the vertical plane, as in Fig. 5, so that the regions AB and DE should be regarded as horizontal areas extending at right angles to the plane of the paper, and they will ultimately join up. If we consider, first of all, propagation in the vertical plane, we find that, for region AB, ϕ takes values from about 60° to 70°, and for DE, values from about 10° to 15°. When the polar diagrams of the aerials are considered, together with the values of R_1 and R_2, it is found that the amplitudes of the bursts from trails in the region DE will be greater than from trails in the region AB. Also, assuming the trails to be oriented randomly in space, the number of trails which satisfy the specular-reflection condition for the region AB will be smaller than for DE, because in AB the trails must be almost horizontal. Hence we conclude that the majority of the bursts will come from the region DE, and will have values of ϕ in the range 10° to 15°. For trails which do not lie in the vertical plane through the transmitter and receiver, values of ϕ intermediate between those characteristic of the region AB and the region DE are possible. The restricted radiation pattern of the transmitting aerial will favour the smaller angles in this range. It is difficult to estimate what the resulting mean value of ϕ will be, but it seems likely that it will be of the order of 15°.

We are now in a position to compare the results for the durations of the type (i) bursts with those obtained in back-scattering experiments. GREENHOW and NEUFELD (1955) analysed 147 decay-type echoes observed by back-scattering on

a wavelength of 4·35 metres. They gave a histogram to show the numbers of echoes of different durations, measured as the times for decay to half-amplitude. To compare the present results with those of Greenhow and Neufeld, their histogram was modified, in accordance with equation (5), by supposing that the durations were proportional to the square of the wavelength and inversely proportional to $\cos^2 \phi$. Values of ϕ of 10° and 70° were used, and the resulting histograms are shown in Fig. 6(a). These histograms show what would be the expected

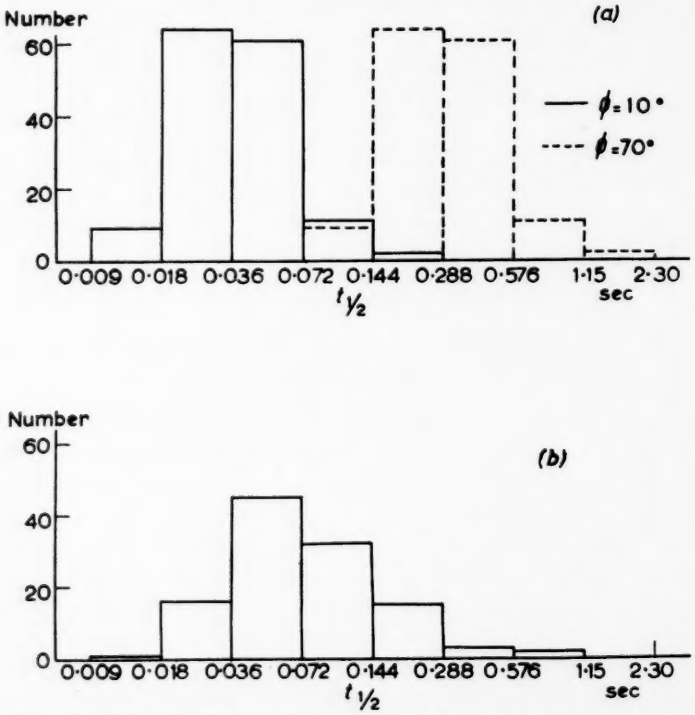

Fig. 6. (a) Predicted distribution of the times of fall to half-amplitude ($t_{\frac{1}{2}}$) if ϕ had the values of 10° and 70°. Based on the measurements of Greenhow and Neufeld (1955).
b) Observed distribution of $t_{\frac{1}{2}}$.

durations of the bursts from the Kirk o' Shotts television transmitter, as received at Cambridge, if ϕ had the stated values, which are the extreme values possible. The results of the present experiments, already shown in Fig. 4, are replotted in Fig. 6(b) for comparison with Fig. 6(a). It will be seen that there is reasonable agreement if we assume that ϕ has values around 10° to 20°, as would be expected if the majority of the bursts come from the region labelled *DE* in Fig. 5.

It is possible that some of the bursts from the region *AB* in Fig. 5 may have been missed because their durations were so long that large fluctuations would develop. This may have prevented the bursts from being recognized as the decay type. It must be remembered that in the above analysis we have been concerned only with those bursts which showed a well-defined exponential decay.

VOL. 8 1956

If we assume a value for the angle ϕ, it is possible to obtain a value for the diffusion coefficient. From equation (5), the time of decay to half-amplitude is given by

$$t_{\frac{1}{2}} = 4{\cdot}4 \times 10^{-3} \times \frac{\lambda^2}{D \cos^2 \phi} \qquad (6)$$

The most frequent value of $t_{\frac{1}{2}}$ observed in the present experiments was 0·05 sec. If we take $\phi = 20°$, we find from equation (6) that $D = 3 \times 10^4$ cm²/sec. The results of GREENHOW and NEUFELD (1955) show that this value would be expected at a height in the atmosphere of 95 km. If we take $\phi = 70°$, we find $D = 2{\cdot}5 \times 10^5$ cm²/sec, and the mean height of the trails would then be 105 km.

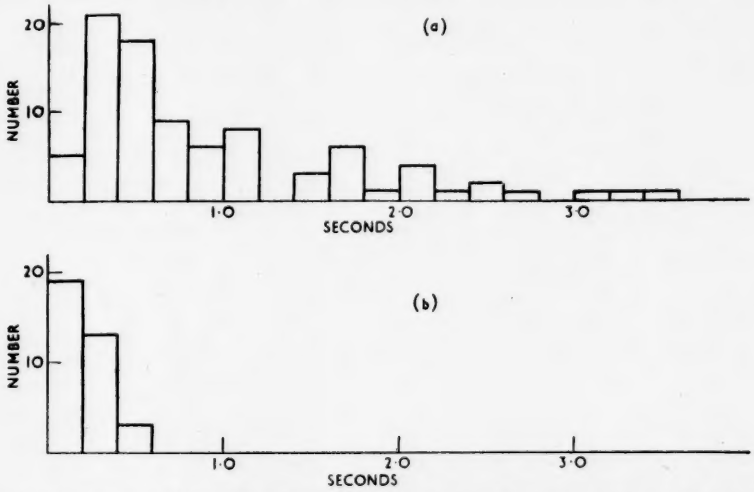

Fig. 7. Distribution of total durations of bursts observed between 1035 and 1135 G.M.T. (approx.) on 9.6.55.
(a) bursts which showed fluctuations
(b) bursts which showed no fluctuations
(total as in Fig. 3c)
Additional bursts, showing fluctuations (not plotted) had durations of 4, 5, 6 (4 cases), 7, 12, and 16 seconds.

We shall now consider the fluctuations of amplitude during the bursts. Only a very small percentage of the bursts observed in the present experiments showed Fresnel oscillations at the start. Thus of 135 bursts observed between 1035 and 1135 G.M.T. on 9.6.55, only 8 showed oscillations which may have been of this type. As the distance of the trail was not known, it was not possible to make use of the Fresnel pattern for the determination of the meteoric velocity. Of the same 135 bursts, 37 showed no random fluctuations, and the remaining 98 showed fluctuations or "fading." Fig. 7 shows the division into the two types according to the total duration. It will be seen that nearly all bursts with durations exceeding 0·5 sec showed fluctuations. The histograms of Fig. 7 may be compared with those of Fig. 3, which are for the same data. In Fig. 3 the division was into bursts which did and did not show an exponential decay.

The 98 bursts which showed random fluctuations were further analysed by

counting for each burst the number of maxima per second. A histogram showing the distribution of this quantity is given in Fig. 8. The average number of maxima per second was 14·2.

We have already given a brief outline of the theoretical explanation of these fluctuations, which are believed to be caused by the random movement of scattering centres situated along the trails. The rate of the fluctuation depends on the root-mean-square velocity of the scattering centres, and on the wavelength,

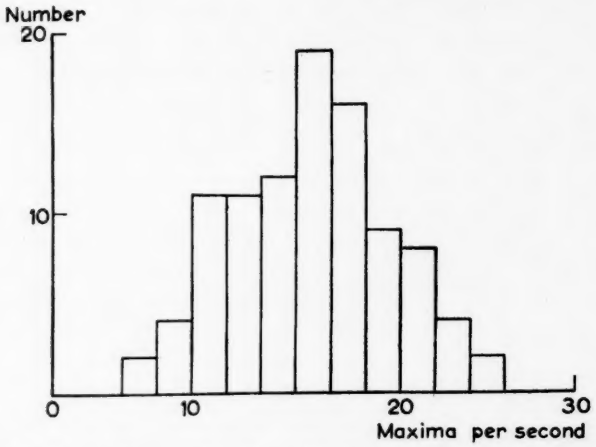

Fig. 8. Distribution of the number of maxima per second for bursts observed between 1035 and 1135 G.M.T. (approx.) on 9.6.55.

as shown by Ratcliffe (1948). We shall assume that the component of the velocity along any line has a Gaussian distribution with a root-mean-square value v_0, so that the probability of a velocity v is given by

$$P(v)\,dv \propto \exp -\{v^2/2v_0^2\}\,.\,dv \tag{7}$$

A simple extension of the argument used by Ratcliffe shows that the power-spectrum of a wave returned from an assembly of such scatterers with a scattering angle ϕ is given by

$$W(f)\,df \propto \exp -\left\{\frac{(f-f_0)^2\lambda^2}{8v_0^2\cos^2\phi}\right\} df \tag{8}$$

The angle ϕ has the same meaning as in equation (5).

Rice (1945) has given an expression for the number of maxima per second of the envelope of a random-noise fluctuation having a narrow Gaussian power-spectrum as in (8). Applied to the present case, his result gives

$$n = 5{\cdot}05\,\frac{v_0}{\lambda}\cos\phi \tag{9}$$

where n is the number of maxima per second.

If we substitute the mean value of n obtained from the present experiments, we find for $v_0 \cos\phi$ the value 16·5 m/sec. With $\phi = 70°$, this gives $v_0 = 48$ m/sec,

VOL. 8 1956

and with $\phi = 20°$ it gives $v_0 = 17{\cdot}5$ m/sec. The angle ϕ must lie within this range, but it is not possible at present to say what its mean value will be. The results for the type (*i*) bursts suggested that the mean value of ϕ was around 20°. The present results, however, are mainly for the longer-duration bursts of type (*ii*), and it is possible that more of these come from points near the mid-point of the transmission path, so that the mean value of ϕ might be greater than 20°.

From back-scattering experiments, GREENHOW (1952) obtained a value for v_0 of 20 m/sec. This was based on the analysis of only one fluctuating meteor echo, and was obtained by a different method of analysis.

CONCLUSIONS

The results of Section 2 concerning the statistical distribution of the time-intervals between bursts are not yet conclusive, but there is no evidence against the hypothesis that the majority of the bursts are reflections from meteor trails. The results of Section 3 provide strong confirmation that this is the case. It seems probable that, for the conditions of the present experiments, many of the meteor trails causing the bursts are not near the mid-point of the transmission path, but are quite close to the receiver. The possibility that a small proportion of the bursts may be due to some cause other than meteors cannot be entirely ruled out.

REFERENCES

ESHLEMAN, V. R. and MANNING, L. A.	1954	*Proc. Inst. Radio Engs.* **42,** 530.
FORSYTH, P. A. and VOGAN, E. L.	1955	*Canad. J. Phys.* **33,** 176.
GREENHOW, J. S.	1952	*Proc. Phys. Soc.* **B65,** 169.
GREENHOW, J. S. and NEUFELD, E. L.	1955	*J. Atmosph. Terr. Phys.* **6,** 133.
ISTED, G. A.	1954	*Marconi Rev.* **17,** 37.
	1955	Phys. Soc. Report of Cambridge Conf. on the Physics of the Ionosphere, page 150.
KAISER, T. R.	1953	*Advances in Phys.* **2,** 495.
MARSDEN, E. and BARRATT, T.	1911	*Proc. Phys. Soc.* **23,** 367.
RATCLIFFE, J. A.	1948	*Nature* **162,** 9.
RICE, S. O.	1945	*Bell Sys. Tech. J.* **24,** 46.
SHAIN, C. A. and KERR, F. J.	1955	*J. Atmosph. Terr. Phys.* **6,** 280.
VILLARD, O. G. JR., PETERSON, A. M. MANNING, L. A., and ESHLEMAN, V. R.	1953	*J. Geophys. Res.* **58,** 83.

RESEARCH NOTE

Electron distribution in the ionosphere

(*Received* 9 *November* 1955)

THIS note is an addition to KING (1954) under the same title. The result given earlier was:—

$$h'_i = \sum_i a_{ij} \cdot D_j$$

where $D = \dfrac{\Delta h(N)}{\Delta \phi(N)}$, ϕ a single-valued function.

$$a = \int_{\Delta\varphi(N)} \mu' \cdot d\phi(N)$$

To include the earth's magnetic field it is necessary to proceed as follows:

Put $G = \dfrac{1}{1-\mu^2}$, $\quad l = f^2/f_N{}^2$, $\quad \gamma_{L,T} = f \cdot f_{L,T}/f_N{}^2$,

where μ is the phase refractive index.

The Appleton-Hartree formula can be written (neglecting collisions),

$$(G-l)^2 + \frac{\gamma_T{}^2}{l-1}(G-l) - \gamma_L{}^2 = 0$$

If $$\tan\phi = 2\,\frac{(l-1)\gamma_L}{\gamma_T{}^2}$$

Then $$(G-l) = \frac{\gamma_T{}^2}{2(l-1)}(\sec\phi - 1)$$

From f and f_N, compute $\gamma_{L,T}$, l, $\tan\phi$, G, and then μ, the last most easily from $\sqrt{G} = \sec\psi$, $\mu = \sin\psi$.

If intervals of $\log f$ and $\log f_N$ are chosen at spacings of 0·1 and 0·01 respectively (frequencies in Mc/s), the calculations can easily be made using only a good set of tables (e.g., COMRIES). Now the group refractive index is given by

$$\mu' = \frac{d}{df}(\mu f)$$

$$= \mu + \frac{1}{2{\cdot}303} \cdot \frac{d\mu}{d\log f}$$

$\mu = \mu\left(\dfrac{f}{f_N}, f_N\right)$ varies only slowly with f_N but rapidly with $\dfrac{f}{f_N}$; approximately, then, we can replace $[d\log f]_{f_N}$ by $[-d\log f_N]_f$ giving

$$a \doteqdot \bar{\mu} \cdot \Delta\log f_N - \frac{1}{2{\cdot}303}\left[\frac{\Delta\mu}{\Delta\log f_N}\right]_f$$

VOL.
8
1956

The first term, the mean value of μ, can be estimated, provided the intervals of $\log f_N$ are small—say 0·01.

The easiest way to use the relation

$$h' = \sum a \,.\, D$$

is to build up a picture of the layer from the bottom. It is not necessary to change the sets of values for each new value of f—each 0·1 in $\log f$ is quite sufficient, and for rough work a single set can be used for a whole record.

Likewise, one need not sample the record at every 0·01 in $\log f$—intervals of 0·02 and 0·04 can be used by lumping together adjacent values of a; the work in a reduction depends on the square of the number of sampling points. An average record can be done on a desk machine in a little over an hour, another hour being needed for preparation and for plotting results.

A reduction done in this way is only strictly applicable if there be no infinite values of h' in the range. Otherwise, it gives a lower limit to the heights obtained from above the infinity. To get an upper limit to these heights, it is a simple matter, from the ratios of the a values, to insert a rectangular valley starting at the top of the lower layer and having a minimum electron density and width such that the D obtained just beyond the infinity is zero.

This work was done at the Geophysical Observatory of the New Zealand Department of Scientific and Industrial Research.

The help given by the Director, Mr. J. W. Beagley, and by members of the staff, especially Mr. C. H. Cummack, is gratefully acknowledged.

G. A. M. King.

Geophysical Observatory,
Christchurch, New Zealand

OL.
8
956

Reference

King, G. A. M. 1954 *J. Atmosph. Terr. Phys.* **5**, 245.

Journal of Atmospheric and Terrestrial Physics, 1956, Vol. 8, pp. 186 to 188. Pergamon Press Ltd., London

Indices of geomagnetic activity

of the Observatories ABINGER (*Ab*), ESKDALEMUIR (*Es*), and LERWICK (*Le*)

October to December 1955

The figures given on pages 186 to 188 represent the *K*-indices for three-hour intervals, beginning with 00–03 hrs for the first and ending with 21–24 hrs for the eighth figure.

October 1955

Day	*Ab* Range for $K = 9 : 500\gamma$		*Sum*	*Es* Range for $K = 9 : 750\gamma$		*Sum*	*Le* Range for $K = 9 : 1000\gamma$		*Sum*	*Day*
	K-Indices			*K-Indices*			*K-Indices*			
1	4224	3232	22	3124	3232	20	4113	2132	17	1
2	3122	3442	21	3122	3442	21	3122	3441	20	2
3	2333	2421	20	2333	2321	19	3322	2321	18	3
4	2333	1222	18	1333	1111	14	2323	1112	15	4
5	2223	3465	27	2223	3365	26	2212	3466	26	5
6	4343	3421	24	4333	3422	24	4432	2422	23	6
7	2222	3213	17	2121	2213	14	1111	2213	12	7
8	3232	2223	19	3222	2222	17	2122	1211	12	8
9	2222	2214	17	1111	1214	12	1111	0213	10	9
10	3333	3431	23	3233	3330	20	3222	3321	18	10
11	0232	3330	16	0232	3220	14	0132	3221	14	11
12	0022	2011	8	0011	1001	4	0010	1001	3	12
13	1022	1122	11	1011	1022	8	0011	1122	8	13
14	2122	2221	14	2111	2112	11	2112	2111	11	14
15	1111	2103	10	1101	1003	7	0101	1003	6	15
16	3112	2212	14	3221	2211	14	3110	1101	8	16
17	2121	1122	12	1111	1022	9	1111	1011	7	17
18	2011	0111	7	1002	1100	5	1001	1101	5	18
19	0112	2211	10	0011	2211	8	0001	1101	4	19
20	2132	2321	16	2112	2221	13	1112	2221	12	20
21	0112	1223	12	1011	1113	9	0011	1113	8	21
22	1113	3231	15	0011	3231	11	0011	2231	10	22
23	2222	2121	14	2112	2221	13	2111	1110	8	23
24	0122	1112	10	0011	2112	8	0011	1101	5	24
25	4444	5554	35	4344	4554	33	4344	5565	36	25
26	4434	4553	32	4433	3453	29	5533	3453	31	26
27	2222	3333	20	2222	3333	20	3222	2333	20	27
28	1222	2312	15	1212	3202	13	1111	3302	12	28
29	1222	1333	17	1222	1333	17	0221	1333	15	29
30	1111	2442	16	1011	2432	14	1111	2442	16	30
31	3322	3455	27	2323	3355	26	3332	3356	28	31

VOL. 8 1956

November 1955

Day	*Ab* Range for $K = 9 : 500\gamma$		*Sum*	*Es* Range for $K = 9 : 750\gamma$		*Sum*	*Le* Range for $K = 9 : 1000\gamma$		*Sum*	*Day*
	K-Indices			*K-Indices*			*K-Indices*			
1	3322	1343	21	3322	1343	21	3431	1242	20	1
2	2113	3232	17	2123	3232	18	1112	3221	13	2
3	1012	2112	10	1112	2111	10	0011	1111	6	3
4	3443	2244	26	3443	2134	24	3443	1134	23	4
5	3332	2112	17	3332	2111	16	3322	1112	15	5
6	2112	1122	12	2010	1022	8	2001	0022	7	6
7	1122	1110	9	1011	1110	6	1001	0011	4	7
8	1222	3445	23	1212	2435	20	1111	2445	19	8
9	5223	2111	17	4222	2111	15	4212	1011	12	9
10	2113	2232	16	1111	1232	12	1011	1132	10	10
11	3122	1323	17	2101	1223	12	2111	1223	13	11
12	1144	3442	23	1044	3432	21	1033	2552	21	12
13	1212	1221	12	1222	1111	11	1102	1111	8	13
14	1112	2232	14	1011	2222	11	0001	1231	8	14
15	2234	3343	24	2134	3343	23	1123	2344	20	15
16	4432	3344	27	3432	3344	26	4532	3444	29	16
17	2412	2222	17	2421	1112	14	2421	1102	13	17
18	1333	3553	26	1332	2553	24	1332	2674	28	18
19	3134	6655	33	2124	8754	33	2123	9854	34	19
20	6443	4655	37	5342	4654	33	5333	4654	33	20
21	4221	2110	13	3221	1010	10	4311	0001	10	21
22	0012	2110	7	0012	2110	7	0011	1101	5	22
23	0113	2122	12	0112	1012	8	0012	1013	8	23
24	2122	2222	15	2022	2222	14	1011	2233	13	24
25	4222	2412	19	4121	2312	16	4211	2302	15	25
26	2122	1203	13	2122	1103	12	2111	0003	8	26
27	3012	2112	12	3012	2102	11	3001	1102	8	27
28	0013	2225	15	1002	2224	13	1002	1115	11	28
29	1112	1232	13	2112	0222	12	1111	1122	10	29
30	0211	2131	11	0211	2121	10	0201	1121	8	30

OL.
8
956

K-indices

December 1955

Day	*Ab* *Range for K = 9 : 500γ*			*Es* *Range for K = 9 : 750γ*			*Le* *Range for K = 9 : 1000γ*			*Day*
	K-Indices		*Sum*	*K-Indices*		*Sum*	*K-Indices*		*Sum*	
1	3023	3455	25	2112	3354	21	2112	3476	26	1
2	3432	2111	17	3432	1001	14	4432	1101	16	2
3	1013	3343	18	1013	2343	17	0011	2243	13	3
4	3112	1011	10	2111	0001	6	2111	1001	7	4
5	1212	2224	16	1101	2124	12	1000	1113	7	5
6	2232	2034	18	2232	1034	17	2231	1034	16	6
7	3311	1111	12	3311	0001	9	3311	1001	10	7
8	1221	2343	18	2221	2243	18	1111	1243	14	8
9	3323	3321	20	3222	3311	17	3222	3311	17	9
10	1112	2231	13	1102	2231	12	1101	2221	10	10
11	1112	2212	12	1102	2112	10	1111	1112	9	11
12	2112	1132	13	1101	1122	9	2110	1122	10	12
13	1011	1211	8	0001	1210	5	0000	1111	4	13
14	0022	1011	7	0002	1000	3	0011	0001	3	14
15	1112	1133	13	1001	1123	9	1110	0123	9	15
16	2223	3221	17	2222	2211	14	2212	2221	14	16
17	1112	1221	11	1102	0121	8	0101	1111	6	17
18	1012	1111	8	1001	1100	4	1111	0000	4	18
19	0022	2332	14	0011	2332	12	0011	2333	13	19
20	3332	3312	20	3322	2312	18	3321	3312	18	20
21	2222	3322	18	2211	3322	16	2111	2322	14	21
22	2212	2211	13	1221	1111	10	1211	1011	8	22
23	1111	1111	8	1101	1011	6	1000	0001	2	23
24	1112	2313	14	0011	2213	10	0010	0213	7	24
25	3432	4342	25	4332	3341	23	3331	3442	23	25
26	0213	3445	22	0123	3446	23	0112	3446	21	26
27	5423	2323	24	4422	2313	21	5431	2313	22	27
28	0022	2231	12	1012	1231	11	0011	1231	9	28
29	0012	1111	7	0000	0010	1	0000	0011	2	29
30	1111	2211	10	1000	1201	5	1000	1101	4	30
31	1223	2332	18	1122	2332	16	1111	1232	12	31

VOL.
8
1956

Journal of Atmospheric and Terrestrial Physics, 1956, Vol. 8, pp. 189 to 203. Pergamon Press Ltd., London

Theory of the rocket-grenade method of determining upper-atmospheric properties by sound propagation

G. V. Groves
Department of Physics, University College, London

(*Received 5 November* 1955)

Abstract—The problem is considered of determining the wind field and velocity of sound in the upper atmosphere as a function of height by means of sound propagation from grenades exploded at these heights. Observations made are taken to be the location and time of each explosion, and the times of arrival of each resulting sound-wave at a number of microphones at known points on the ground. The distribution of microphones is taken to be quite general, within a region of the earth's surface over which horizontal variations in the wind and sonic velocities can be neglected. Differences in the heights of the microphones, which would arise from topographical features and the curvature of the earth, are taken into account. The wavefront from each explosion is taken to be propagated at a known Mach number at any time, so that account can be taken of the departure of the Mach number from unity along any ray.

The nature of the problem requires the solution to proceed by successive approximation in terms of the variations in the wind components and speed of sound. The theory is developed as far as the second-order solution, and this is thought to be adequate for practical needs. It is shown that four microphones are, in general, sufficient for the determination of the three components of the wind-velocity and the speed of sound. By using more than four microphones, a least-squares determination is possible, and this would allow a check to be made on the consistency of the observations and the adequacy of the theory. Finally, it is shown how atmospheric pressure, density, and temperature can be deduced from these determinations, assuming the composition of the atmosphere to be known.

1. Introduction

In the rocket-grenade experiment (Weisner, 1954; Stroud *et al.*, 1955), grenades are ejected one at a time from a high-altitude rocket in flight and exploded at roughly equally spaced points along the trajectory of the rocket. Measurements are made of the location and time of each explosion, and of the time of arrival of the resulting sound-waves at a number of microphones on the ground. From these observations, the wind velocity and temperature structure of the upper atmosphere have then been deduced.

A previous paper (Groves, 1956) considers the passage of a sound-ray between two given points in the atmosphere, and shows how mean values for the speed of sound and wind-velocity components can be deduced, knowing the time of travel and co-ordinates of the ray. These results will now be applied to the problem of the rocket-grenade experiment, and a new method developed for analysing the data of this type of experiment.

2. Ray Equations for an Explosive Source of Sound

Let O be a fixed point on the earth's surface and $Oxyz$ mutually perpendicular axes with Oz in the vertical direction (Fig. 1). R is defined as the region of the Oxy-plane above which the horizontal variations in the wind-velocity components $u(z)$, $v(z)$, $w(z)$ and the speed of sound $c(z)$ at any height z can be neglected. One of the factors limiting the size of R is the curvature of the earth, which restricts R to a circle of a certain radius, depending on the limits within which the horizontal variations in $u(z)$, $v(z)$, $w(z)$, $c(z)$ can be considered negligible. At 50 km from 0, a point on the earth's surface is 200 m below the Oxy-plane, and the corresponding variation in $c(0)$ is about 0·7 m/sec.

Let G be a point (x', y', z') above R at which a grenade explodes at time t'. In the vicinity of G, the disturbance produced by the explosion is propagated as a strong shock-wave with a velocity several times that of the speed of sound. Let $c(x, y, z)$ denote the velocity of propagation of the element of the shock-front at P; then its Mach number is

$$M = c(x, y, z)/c(z). \tag{1}$$

In order to take account of the variation in M, it is assumed that, at any time t, M is the same at all points of the shock-front, i.e., $M = M(t)$. On account of the change in atmospheric pressure with height, this assumption is valid for the

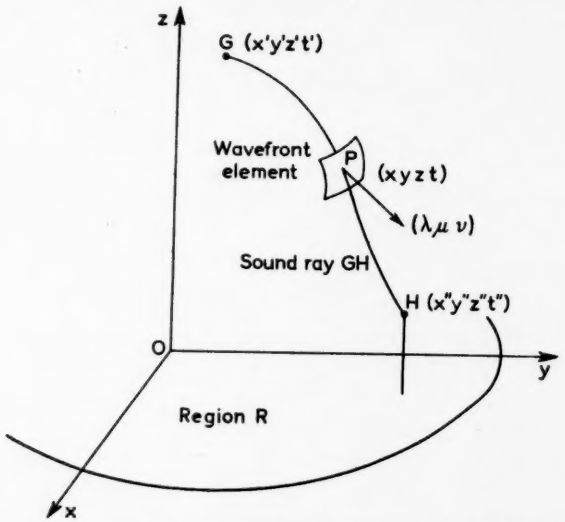

Fig. 1. Diagram showing the passage of a sound-ray from a grenade explosion at G to a microphone at H.

complete shock-front only within small vertical distances from G, i.e., distances small compared with the scale-height. At greater distances from G, it is valid for segments of the shock-front lying within height-intervals that are small compared with the scale-height. At sufficiently large distances below G, M is approximately unity within the accuracy of the analysis, and the above assumption is then valid over height-intervals for which the change in atmospheric pressure is significant. The assumption is favoured by the fact that the approach of M towards unity is more rapid for a wave propagated into air of increasing density than it would be for a medium of uniform density, otherwise the energy of the wave would be increasing.*

Let H be a microphone at the point (x'', y'', z'') within R, and GH the path travelled by the wavefront element received at H. The direction cosines (λ, μ, ν) of the wavefront normal at any point P of the ray will now be derived. The solution

* For the portion of the wave propagated upwards, M is expected to increase eventually, causing the energy of the wave to be dissipated by viscosity and heat-conduction in the upper regions of the atmosphere, unless total reflection returns the wave to earth.

VOL. 8 1956

is most readily obtained in terms of the trace velocities (v_X, v_Y, v_Z) defined by

$$\lambda v_X = \mu v_Y = \nu v_Z = c(x, y, z) + \lambda u(z) + \mu v(z) + \nu w(z). \tag{2}$$

The equations satisfied by (v_X, v_Y, v_Z) have been previously derived for the general case of a moving heterogeneous medium (GROVES, 1955), and in the present problem reduce to

$$\begin{aligned} \frac{\partial}{\partial t}\left(\frac{1}{v_X}\right) + c_x(x, y, z)\left(\frac{1}{v_X^2} + \frac{1}{v_Y^2} + \frac{1}{v_Z^2}\right)^{\frac{1}{2}} &= 0 \\ \frac{\partial}{\partial t}\left(\frac{1}{v_Y}\right) + c_y(x, y, z)\left(\frac{1}{v_X^2} + \frac{1}{v_Y^2} + \frac{1}{v_Z^2}\right)^{\frac{1}{2}} &= 0 \end{aligned}, \tag{3}$$

where $\partial/\partial t$ denotes differentiation with respect to time along the ray GH, and the suffices x, y denote partial differentiation with respect to these quantities. From (1)

$$\begin{aligned} c_x(x, y, z) &= c(z)M_x = c(z)M'(t)/v_X \\ c_y(x, y, z) &= c(z)M_y = c(z)M'(t)/v_Y \end{aligned};$$

and hence equations (3) become, on using (1), (2), and the relation $\lambda^2 + \mu^2 + \nu^2 = 1$,

$$\begin{aligned} v_X\partial(1/v_X)/\partial t + M'(t)/[M(t) + (\lambda u + \mu v + \nu w)/c] &= 0 \\ v_Y\partial(1/v_Y)/\partial t + M'(t)/[M(t) + (\lambda u + \mu v + \nu w)/c] &= 0 \end{aligned}. \tag{4}$$

An approximate integration of the second term in these equations can be carried out by neglecting $(\lambda u + \mu v + \nu w)/c$ in comparison with M. The maximum value of $\lambda u + \mu v + \nu w$ with respect to λ, μ, ν is $(u^2 + v^2 + w^2)^{\frac{1}{2}}$, and so this approximation is justified when the wind-speed is small compared with the speed of sound. Also, as M approaches unity, $M'(t)$ tends to zero and the approximation becomes valid in general. Integration of (4) along the ray GH therefore gives

$$v_X/M = a \qquad v_Y/M = b, \tag{5}$$

where a, b are constants of integration which can be taken as co-ordinates for the ray GH. By (1), (2), and (5), (λ, μ, ν) are found to satisfy

$$c(z) + [\lambda u(z) + \mu v(z) + \nu w(z)]/M = a\lambda = b\mu. \tag{6}$$

The equations of a sound-ray have been given previously (GROVES, 1955, equations 45 to 47). Replacing $c(z)$ by $c(x, y, z)$ in these equations, the equation of the ray GH is obtained, on using (1), as

$$x \equiv x(z) = x' + \int_{z'}^{z} \frac{u(\zeta)/M + \lambda c(\zeta)}{w(\zeta)/M + \nu c(\zeta)}\, d\zeta \tag{7}$$

$$y \equiv y(z) = y' + \int_{z'}^{z} \frac{v(\zeta)/M + \mu c(\zeta)}{w(\zeta)/M + \nu c(\zeta)}\, d\zeta \tag{8}$$

$$t \equiv t(z) = t' + \int_{z'}^{z} \frac{d\zeta/M}{w(\zeta)/M + \nu c(\zeta)} \tag{9}$$

Write (9) as

$$t \equiv t(z) = (t' - \tau) + \int_{z'}^{z} d\zeta/[w(\zeta)/M + vc(\zeta)], \tag{10}$$

where

$$\tau \equiv \tau(t) = \int_{t'}^{t} [M(t) - 1]\, dt. \tag{11}$$

An important result now follows from (6), (7), (8), and (10): these equations are seen to be the same as those obtained previously for a sound-ray with

(1) $u(z)$, $v(z)$, $w(z)$ replaced by $u(z)/M$, $v(z)/M$, $w(z)/M$, and

(2) the time of travel increased by amount τ.

$M(t)$ and $\tau(t)$ depend mainly on the explosive content of the grenade, the height at which it explodes, and the general direction of the ray GH: their calculation is at present being given consideration.

3. Application of Previous Theory on Determination of Wind and Sonic Velocities to the Ray GH

A method of deriving mean values for the wind and sonic velocities along a sound-ray travelling between two points in the atmosphere has already been developed (GROVES, 1956). These results will now be applied to the ray GH by introducing the modifications (1), (2) above, and the theory formulated so that account can be taken of the departure of the Mach number of the wavefront from unity. For the ray GH, write

$$\begin{aligned} u(z)/M &= u_0 + u_\varepsilon(z) \qquad & v(z)/M &= v_0 + v_\varepsilon(z) \\ w(z)/M &= w_0 + w_\varepsilon(z) \qquad & c(z) &= c_0 + c_\varepsilon(z) \\ \lambda(z) &= \lambda_0 + \lambda_\varepsilon(z) \qquad & \mu(z) &= \mu_0 + \mu_\varepsilon(z) \qquad & \nu(z) &= \nu_0 + \nu_\varepsilon(z), \end{aligned} \tag{12}$$

and choose u_0, v_0, w_0, λ_0, μ_0, ν_0 to satisfy the six equations

$$\begin{aligned} u_0 + c_0\lambda_0 &= -X/T \\ v_0 + c_0\mu_0 &= -Y/T \\ w_0 + c_0\nu_0 &= -Z/T \end{aligned} \tag{13}$$

$$c_0 + u_0\lambda_0 + v_0\mu_0 + w_0\nu_0 = a\lambda_0 = b\mu_0 \tag{14}$$

$$\lambda_0^2 + \mu_0^2 + \nu_0^2 = 1, \tag{15}$$

where

$$X = x' - x'', \qquad Y = y' - y'', \qquad Z = z' - z'', \qquad T = (t'' - t') + \tau(t''). \tag{16}$$

c_0 is supposed known with an unspecified value: and in this respect the following treatment differs from that given previously, where w_0 was taken as known and the solution obtained for u_0, v_0, c_0. It is assumed, however, that the value of c_0 is such that $|\, c_\varepsilon(z)\,|/c_0$ is small for $z'' \leq z \leq z'$. A suitable choice for c_0, supposing $c(z)$ to be known, would be

$$c_0 = \int_{z''}^{z'} c(z)\, dz/Z. \tag{17}$$

VOL. 8 1956

The maximum value of $|c_\varepsilon(z)|/c_0$ in (z'', z') is taken to define the first order of smallness. It is further assumed that for the values of $u_0, v_0, w_0, \lambda_0, \mu_0, \nu_0$ determined by (13) to (15), the corresponding maximum values of $|u_\varepsilon(z)|/c_0$, $|v_\varepsilon(z)|/c_0$, $|w_\varepsilon(z)|/c_0$, $|\lambda_\varepsilon(z)|$, $|\mu_\varepsilon(z)|$, $|\nu_0(z)|$ are first- or higher-order quantities. This assumption appears essential in order to determine wind and sonic velocities by observations at the end-points of sound-rays, and enables the solution to proceed by successive approximation.

Integrating (12) over the interval (z'', z'), it is seen that

$$\begin{aligned} \int_{z''}^{z'} u(z)/M\, dz &= U_0 + U_\varepsilon & \int_{z''}^{z'} v(z)/M\, dz &= V_0 + V_\varepsilon \\ \int_{z''}^{z'} w(z)/M\, dz &= W_0 + W_\varepsilon & \int_{z''}^{z'} c(z)\, dz &= C_0 + C_\varepsilon \end{aligned}, \tag{18}$$

where

$$U_0 = u_0 Z, \qquad V_0 = v_0 Z, \qquad W_0 = w_0 Z, \qquad C_0 = c_0 Z \tag{19}$$

and

$$\begin{aligned} U_\varepsilon &= \int_{z''}^{z'} u_\varepsilon(z)\, dz & V_\varepsilon &= \int_{z''}^{z'} v_\varepsilon(z)\, dz \\ W_\varepsilon &= \int_{z''}^{z'} w_\varepsilon(z)\, dz & C_\varepsilon &= \int_{z''}^{z'} c_\varepsilon(z)\, dz \end{aligned} \tag{20}$$

By the method of the previous paper (GROVES, 1956), U_ε, V_ε, W_ε can be expressed in terms of C_ε and integrals of products of the variations $u_\varepsilon(z)$, $v_\varepsilon(z)$, $w_\varepsilon(z)$, $c_\varepsilon(z)$. The form of these relations is (see equations 38–40 and 62–68)

$$\begin{aligned} U_\varepsilon + \lambda_0 C_\varepsilon &= U_2 + U_3 + \ldots \\ V_\varepsilon + \mu_0 C_\varepsilon &= V_2 + V_3 + \ldots, \\ W_\varepsilon + \nu_0 C_\varepsilon &= W_2 + W_3 + \ldots \end{aligned} \tag{21}$$

where $U_2, U_3, \ldots$ are integrals containing second-, third-, ...-order variations. C_ε depends on the value of c_0: when c_0 is determined by (17), $C_\varepsilon = 0$. Expressions for U_2, V_2, W_2 are obtainable from the results of the above paper. In the next section, however, U_ε, V_ε, W_ε, C_ε occur together in the term $C_\varepsilon + \lambda_0 U_\varepsilon + \mu_0 V_\varepsilon + \nu_0 W_\varepsilon$, and this is most readily evaluated from equations (20) and (45a) of the above paper, which give

$$C_\varepsilon + \lambda_0 U_\varepsilon + \mu_0 V_\varepsilon + \nu_0 W_\varepsilon = \int_{z''}^{z'} [\tfrac{1}{2} c_0(\lambda_\varepsilon^2 + \mu_\varepsilon^2 + \nu_\varepsilon^2) - (T/Z)(w_\varepsilon + c_0 \nu_\varepsilon + \nu_0 c_\varepsilon) q_\varepsilon]\, dz + \text{third- and higher-order terms}, \tag{22}$$

where

$$q_\varepsilon = c_\varepsilon + \lambda_0 u_\varepsilon + \mu_0 v_\varepsilon + \nu_0 w_\varepsilon. \tag{23}$$

Now

$$c_0 \nu_\varepsilon = -\nu_0 \kappa' \kappa q_\varepsilon + \text{etc.} \qquad \text{(equation 54)}$$

$$c_0^2(\lambda_\varepsilon^2 + \mu_\varepsilon^2 + \nu_\varepsilon^2) = \kappa'^2 q_\varepsilon^2 + \text{etc.} \qquad \text{(equation 58),}$$

where (from equations 40 and 56),

$$\kappa = (1 - \nu_0^2)^{\frac{1}{2}}/\nu_0 \qquad \kappa' = \omega\kappa$$
$$\omega = (Z + w_0 T)/Z = -(c_0 T/Z)\nu_0. \tag{24}$$

Hence, (22) becomes

$$C_s + \lambda_0 U_s + \mu_0 V_s + \nu_0 W_s = (\omega/c_0\nu_0)\int_{z'}^{z'} [w_s + \nu_0 c_s - \tfrac{1}{2}(\omega/\nu_0)(1 - \nu_0^2)q_s]q_s\, dz + \text{etc.} \tag{25}$$

In practice, the value of ω would be expected to lie near unity.

4. Determination of $U(0, z')$, $V(0, z')$, $W(0, z')$, $C(0, z')$ from Measurements with m Microphones

The co-ordinates (a, b) of the ray GH can be measured directly by positioning microphones along two perpendicular lines in the horizontal plane through H, and then timing the arrival of the wavefront at each microphone. From the distance v. time relation for the passage of the sound-wave along each of these directions, v_X and v_Y can then be derived, and by (5) these are a and b respectively, since M is unity at ground-level. On account of the curvature of the incident wavefront, the region of the horizontal plane about H over which the two lines of microphones can be usefully extended is limited to the region within which the wavefront can be considered plane. The greater the accuracy required for a and b, the smaller this region becomes; and increasingly greater becomes the accuracy with which time measurements need to be made. In view of this difficulty, consideration will be given to the more general problem, where the microphones are not necessarily closely spaced, and consequently the co-ordinates of the rays received by them are significantly different.

Let m be the number of microphones in R, the co-ordinates of the ith microphone at the point H_i being (x''_i, y''_i, z''_i), and t''_i the time of arrival of the wavefront. Define

$$U(\zeta_1, \zeta_2) = \int_{\zeta_1}^{\zeta_2} u(z)\, dz \qquad V(\zeta_1, \zeta_2) = \int_{\zeta_1}^{\zeta_2} v(z)\, dz$$
$$W(\zeta_1, \zeta_2) = \int_{\zeta_1}^{\zeta_2} w(z)\, dz \qquad C(\zeta_1, \zeta_2) = \int_{\zeta_1}^{\zeta_2} c(z)\, dz \tag{26}$$

A solution will be found for $U(0, z')$, $V(0, z')$, $W(0, z')$, $C(0, z')$ in terms of the measurements (x', y', z', t') and $(x''_i, y''_i, z''_i, t''_i)$, $i = 1, \ldots, m$. From (13), (15), and (19), it is seen that

$$(U_{0i} + X_i Z_i/T_i)^2 + (V_{0i} + Y_i Z_i/T_i)^2 + (W_{0i} + Z_i^2/T_i)^2 = C_{0i}^2, \tag{27}$$

where the suffix i is introduced to denote values appropriate to the ray GH_i. Now from (18), (20) and (26),

$$U_{0i} = U(0, z') - (U_{si} + U'_{si}) \qquad V_{0i} = V(0, z') - (V_{si} + V'_{si})$$
$$W_{0i} = W(0, z') - (W_{si} + W'_{si}) \qquad C_{0i} = C(0, z') - (C_{si} + C'_{si}) \tag{28}$$

where

$$\left.\begin{aligned} U'_{si} &= U(0, z''_i) + \int_{z''_i}^{z'} (1 - M^{-1})u(z)\,dz \\ V'_{si} &= V(0, z''_i) + \int_{z''_i}^{z'} (1 - M^{-1})v(z)\,dz \\ W'_{si} &= W(0, z''_i) + \int_{z''_i}^{z'} (1 - M^{-1})w(z)\,dz \\ C'_{si} &= C(0, z''_i) \end{aligned}\right\} \tag{29}$$

Hence (27) can be written

$$(U + X_iZ_i/T_i)^2 + (V + Y_iZ_i/T_i)^2 + (W + Z_i^2/T_i)^2 - C^2 = 2(Z_i/T_i)(g_{si} + h_{si}), \tag{30}$$

where $U \equiv U(0, z')$, $V \equiv V(0, z')$, $W \equiv W(0, z')$, $C \equiv C(0, z')$, and

$$g_{si} = (T_i/Z_i)[U_{si}(U_{0i} + X_iZ_i/T_i) + V_{si}(V_{0i} + Y_iZ_i/T_i) + W_{si}(W_{0i} + Z_i^2/T_i) - C_{si}C_{0i} + \tfrac{1}{2}(U_{si}^2 + V_{si}^2 + W_{si}^2 - C_{si}^2)] \tag{31}$$

$$h_{si} = (T_i/Z_i)[U'_{si}(U + X_iZ_i/T_i) + V'_{si}(V + Y_iZ_i/T_i) + W'_{si}(W + Z_i^2/T_i) - C'_{si}C - \tfrac{1}{2}(U'^2_{si} + V'^2_{si} + W'^2_{si} - C'^2_{si})]. \tag{32}$$

By (13) and (19), (31) can be written

$$g_{si} = -(T_i/Z_i)\{C_{0i}[C_{si} + \lambda_{0i}U_{si} + \mu_{0i}V_{si} + \nu_{0i}W_{si}] - \tfrac{1}{2}(U_{si}^2 + V_{si}^2 + W_{si}^2 - C_{si}^2)\}.$$

In view of (21), though, $U_{si}^2 + V_{si}^2 + W_{si}^2 - C_{si}^2$ is of the third order, and hence by (24), (25), and (23)

$$g_{si} = C_{0i} \sum_{k \le l = 1, 2, 3, 4} g_{kli} \int_{z''_i}^{z'} \phi_{ki}(z)\phi_{li}(z)\,dz + \text{etc.}, \tag{33}$$

where $\phi_{1i}(z), \ldots \phi_{4i}(z)$ denote $u_{si}(z)/c_{0i}$, $v_{si}(z)/c_{0i}$, $w_{si}(z)/c_{0i}$, $c_{si}(z)/c_{0i}$ respectively, and (omitting suffix i)

$$\left.\begin{aligned} g_{11} &= -\tfrac{1}{2}\lambda_0^2(1 - \nu_0^2)\omega^3/\nu_0^3 & g_{23} &= \mu_0[1 - \omega(1 - \nu_0^2)]\omega^2/\nu_0^2 \\ g_{12} &= -\lambda_0\mu_0(1 - \nu_0^2)\omega^3/\nu_0^3 & g_{24} &= \mu_0[\nu_0^2 - \omega(1 - \nu_0^2)]\omega^2/\nu_0^3 \\ g_{13} &= \lambda_0[1 - \omega(1 - \nu_0^2)]\omega^2/\nu_0^2 & g_{33} &= [1 - \tfrac{1}{2}\omega(1 - \nu_0^2)]\omega^2/\nu_0 \\ g_{14} &= \lambda_0[\nu_0^2 - \omega(1 - \nu_0^2)]\omega^2/\nu_0^3 & g_{34} &= [(1 + \nu_0^2) - \omega(1 - \nu_0^2)]\omega^2/\nu_0^2 \\ g_{22} &= -\tfrac{1}{2}\mu_0^2(1 - \nu_0^2)\omega^3/\nu_0^3 & g_{44} &= [\nu_0^2 - \tfrac{1}{2}\omega(1 - \nu_0^2)]\omega^2/\nu_0^3 \end{aligned}\right\} \tag{34}$$

The set of equations (30) can be written

$$[U\ V\ W\ \tfrac{1}{2}(U^2 + V^2 + W^2 - C^2)]\boldsymbol{P} = \boldsymbol{g} + \boldsymbol{g}_s + \boldsymbol{h}_s, \tag{35}$$

where

$$\boldsymbol{P} = \begin{bmatrix} X_1 & \ldots & X_m \\ Y_1 & \ldots & Y_m \\ Z_1 & \ldots & Z_m \\ T_1/Z_1 & \ldots & T_m/Z_m \end{bmatrix} \tag{36}$$

$$\boldsymbol{g} = -\tfrac{1}{2}[(X_1^2 + Y_1^2 + Z_1^2)Z_1/T_1 \ldots (X_m^2 + Y_m^2 + Z_m^2)Z_m/T_m] \quad (37)$$

$$\boldsymbol{g}_\varepsilon = [g_{\varepsilon 1} \ldots g_{\varepsilon m}] \quad (38)$$

$$\boldsymbol{h}_\varepsilon = [h_{\varepsilon 1} \ldots h_{\varepsilon m}]. \quad (39)$$

When $m = 4$, (35) can be solved uniquely for U, V, W, and $\frac{1}{2}(U^2 + V^2 + W^2 - C^2)$, provided $|\boldsymbol{P}| \neq 0$. When $m > 4$, U, V, W, and $\frac{1}{2}(U^2 + V^2 + W^2 - C^2)$ can be chosen to minimize the magnitude $(\boldsymbol{ee}')^{\frac{1}{2}}$ of the residuals

$$\boldsymbol{e} \equiv [e_1 \ldots e_m] = [U\ V\ W\ \tfrac{1}{2}(U^2 + V^2 + W^2 - C^2)]\boldsymbol{P} - (\boldsymbol{g} + \boldsymbol{g}_\varepsilon + \boldsymbol{h}_\varepsilon). \quad (40)$$

This condition is satisfied when

$$\{[U\ V\ W\ \tfrac{1}{2}(U^2 + V^2 + W^2 - C^2)]\boldsymbol{P} - (\boldsymbol{g} + \boldsymbol{g}_\varepsilon + \boldsymbol{h}_\varepsilon)\}\boldsymbol{P}' = 0,$$

where P' is the transpose of P. The solution for U, V, W, and $\frac{1}{2}(U^2 + V^2 + W^2 - C^2)$ is then obtained as

$$[U\ V\ W\ \tfrac{1}{2}(U^2 + V^2 + W^2 - C^2)] = (\boldsymbol{g} + \boldsymbol{g}_\varepsilon + \boldsymbol{h}_\varepsilon)\boldsymbol{Q}, \quad (41)$$

provided $|\boldsymbol{PP}'| \neq 0$, where

$$\boldsymbol{Q} = \boldsymbol{P}'(\boldsymbol{PP}')^{-1}. \quad (42)$$

Since $\boldsymbol{g}_\varepsilon$ is a second-order term, (41) gives the first-order solution for U, V, W, C, provided $\boldsymbol{h}_\varepsilon$ can be estimated with first-order accuracy. From (32), $h_{\varepsilon i}$ is seen to be of the same order as $U'_{\varepsilon i}$, $V'_{\varepsilon i}$, $W'_{\varepsilon i}$, $C'_{\varepsilon i}$: in practice, these quantities would be expected to be second-order or less, in which case $\boldsymbol{h}_\varepsilon$ could be neglected in the first-order solution for U, V, W, C.

VOL. 8 1956

5. Procedure for Deriving $u(z)$, $v(z)$, $w(z)$, $c(z)$

Let N be the number of grenade explosions observed in the experiment, then the first-order solution of (41) for each grenade explosion yields values $U_1, \ldots, U_N$ for $U(0, z')$ at $z' = z_1, \ldots, z_N$, and likewise for $V(0, z')$, $W(0, z')$, $C(0, z')$. The set of points $(z_1, U_1), \ldots, (z_N, U_N)$ gives an empirical determination of the function $U = U(0, z)$ in the range $z_1 \leq z \leq z_N$; and a corresponding empirical determination of $u = u(z)$ is obtained as the derivative of a curve through these points.

For equally-spaced points, a variety of simple formulae for numerical differentiation is available (Milne, 1949, p. 96), and these could be used to derive values $u_1, \ldots, u_N$ of $u(z)$ at $z = z_1, \ldots, z_N$. In general, $z_1, \ldots, z_N$ are not equally-spaced values, and in this case $u_1, \ldots, u_N$ could be determined by differentiation of the Lagrange interpolation formula (Milne, p. 93). An alternative, and possibly shorter, method of obtaining $u = u(z)$ would be to first interpolate values $U'_1, \ldots, U'_N$ of $U(0, z)$ at equally-spaced points $z = z'_1, \ldots, z'_N$, either by evaluating Lagrangian coefficients or by the method of divided differences (Milne, p. 207). Values $u'_1, \ldots, u'_N$ of $u(z)$ at $z = z'_1, \ldots, z'_N$ could then be readily derived, using the differentiation formulae for equally-spaced points. This alternative method is particularly suitable if the altitude spacing of the grenades has been arranged to be nearly constant.

The accuracy of values derived for $u(z)$ is not necessarily of the first order, but depends on the nature of $u(z)$ and the number of grenades used. If, for example, $u(z)$ can be represented correct to the first order in (z_1, z_N) by a polynomial of degree at least α, $U(0, z)$ would need to be represented by a polynomial of degree at least $\alpha + 1$, and at least $\alpha + 2$ grenades would be required for first-order accuracy.

In order to solve (41) for U, V, W, C to second-order accuracy, it is necessary to know $u(z), v(z), w(z), c(z)$ with first-order accuracy for heights below z_N, so that g_{si} can be evaluated by (33). This information is available for the interval (z_1, z_N) from the first-order analysis, while for heights below z_1 it could possibly be obtained with adequate accuracy by extrapolation of these values down to ground-level, or to the level reached by other experimental methods, e.g., balloon measurements. The ten integrals $\int_0^z u^2(\zeta)\,d\zeta$, $\int_0^z u(\zeta)v(\zeta)\,d\zeta$, etc., can then be calculated numerically for $z \leq z_N$. The evaluation of the integrals $\int_{z''_i}^{z'} \phi_{ki}(z)\phi_{li}(z)\,dz$ occurring in g_{si} is shortened by writing them, with the use of (12), (18), (19), and (28), as (omitting suffix i)

$$c_0^2 \int_{z''}^{z'} \phi_1^2(z)\,dz = \int_{z''}^{z'} [u(z)/M - u_0]^2\,dz$$

$$= \int_{z''}^{z'} u^2(z)/M^2\,dz - [(U - U'_\varepsilon)^2 - U_\varepsilon^2]/Z \text{ etc.}$$

$$c_0^2 \int_{z''}^{z'} \phi_3(z)\phi_4(z)\,dz = \int_{z''}^{z'} [w(z)/M - w_0][c(z) - c_0]\,dz$$

$$= \int_{z''}^{z'} w(z)c(z)/M\,dz - [(W - W'_\varepsilon)(C - C'_\varepsilon) - W_\varepsilon C_\varepsilon]/Z$$

$$c_0^2 \int_{z''}^{z'} \phi_4^2(z)\,dz = \int_{z''}^{z'} [c(z) - c_0]^2\,dz = \int_{z''}^{z'} c^2(z)\,dz - [(C - C_\varepsilon')^2 - C_\varepsilon^2]/Z.$$

The terms U_ε^2, $U_\varepsilon V_\varepsilon$, etc., may be omitted in the calculation of these integrals, since by (21) and (34) the sum $g_{11}U_\varepsilon^2 + \ldots + g_{44}C_\varepsilon^2$ vanishes to the second order Hence

$$\left.\begin{aligned} c_0^2 \int_{z''}^{z'} \phi_1^2(z)\,dz &= \int_{z''}^{z'} u^2(z)\,dz - \int_{z''}^{z'} (1 - M^{-2})u^2(z)\,dz \\ &\quad - (U - U'_\varepsilon)^2/Z \text{ etc.} \\ c_0^2 \int_{z''}^{z'} \phi_3(z)\phi_4(z)\,dz &= \int_{z''}^{z'} w(z)c(z)\,dz - \int_{z''}^{z'} (1 - M^{-1})w(z)c(z)\,dz \\ &\quad - (W - W'_\varepsilon)(C - C'_\varepsilon)/Z. \\ c_0^2 \int_{z''}^{z'} \phi_4^2(z)\,dz &= \int_{z''}^{z'} c^2(z)\,dz - (C - C'_\varepsilon)^2/Z. \end{aligned}\right\} \quad (43)$$

The integrals $\int_{z''}^{z'} (1 - M^{-2})u^2(z)\,dz$, etc., which arise from the departure of the

Mach number of the wavefront from unity, would be expected to converge rapidly near to G, and in this case could be evaluated approximately as

$$\int_{z''}^{z'}(1 - M^{-2})u^2(z)\,dz \fallingdotseq u^2(z')\int_{t''}^{t'}(1 - M^{-2})(dz/dt)\,dt$$

$$\fallingdotseq u^2(z')(Z/T)\int_{t''}^{t'}(M^2 - 1)/M\,dt \text{ etc.},$$

and

$$\int_{z''}^{z'}(1 - M^{-1})u(z)\,dz \fallingdotseq u(z')(Z/T)\int_{t''}^{t'}(M - 1)\,dt \text{ etc.}$$

From (43), $\int_{z''}^{z'}\phi_{ki}(z)\phi_{li}(z)\,dz$ can now be evaluated without requiring numerical integration for each individual ray.

From (13), (19), and (28), λ_{0i}, μ_{0i}, ν_{0i} can be expressed correct to the first order, in view of (21), as (omitting suffix i)

$$\begin{aligned}\lambda_0 &= -[(U - U'_\epsilon) + XZ/T]/(C - C'_\epsilon)\\ \mu_0 &= -[(V - V'_\epsilon) + YZ/T]/(C - C'_\epsilon)\,,\\ \nu_0 &= -[(W - W'_\epsilon) + Z^2/T]/(C - C'_\epsilon)\end{aligned} \tag{44}$$

and from (24)

$$\omega = 1 + (W - W'_\epsilon)T/Z^2. \tag{45}$$

g_{kl} can now be evaluated by (34), and $g_{\epsilon i}$ obtained to the second order from (33).

Finally, when $h_{\epsilon i}$ has been calculated from (32), the second-order solution for U, V, W, C can be determined from (41). By repeating the process of numerical differentiation for the new sets of values $(U_1, \ldots, U_N)$, etc., the second approximation to $u(z)$, $v(z)$, $w(z)$, $c(z)$ is obtained. The accuracy of this determination is of the second order, only if the number of grenades observed is sufficiently large; the number required depending on the nature of $u(z)$, $v(z)$, $w(z)$, $c(z)$.

From (40) and (41), the residuals in the least-squares solution for U, V, W and $\frac{1}{2}(U^2 + V^2 + W^2 - C^2)$ are seen to be

$$\boldsymbol{e} = (\boldsymbol{g} + \boldsymbol{g}_\epsilon + \boldsymbol{h}_\epsilon)(\boldsymbol{QP} - \boldsymbol{I}), \tag{46}$$

where $\boldsymbol{I}$ is the $(m \times m)$ unit matrix. By using more than four microphones and solving for $\boldsymbol{e}$ in this way, a check on the consistency of the experimental data is possible. If e_i, for instance, is significantly large, the measurements for the ith microphone could be rejected as being in error, and the determinations thereby improved. On the other hand, any relationship between $[e_1 \ldots e_m]$ and the co-ordinates of the microphones could be attributed to neglecting third-order terms and horizontal variations in the wind and sonic velocities. Standard methods of statistical analysis and inference would, no doubt, help to decide these matters.

6. Determination of Atmospheric Pressure

The problem will now be considered of using the determinations of the wind and sonic velocities to deduce atmospheric pressure. The vertical equation of motion of the atmosphere can be written

$$\frac{1}{\rho(z)}\frac{dp(z)}{dz} = -\left[g(z) + \frac{1}{2}\frac{dw^2(z)}{dz}\right], \tag{47}$$

VOL. 8 1956

where $p(z)$, $\rho(z)$ denote atmospheric pressure and density, and $g(z)$ is the acceleration due to gravity at height z. The contribution to this equation from the earth's rotation is neglected, since it amounts to at most 1·5 cm/sec² for a horizontal wind-velocity of 100 m/sec (BRUNT, 1941). Now, $c(z)$ is, by definition, the velocity of propagation of small adiabatic compressions and rarefactions and, for a perfect gas, is given by

$$c^2(z) = \gamma(z)p(z)/\rho(z), \tag{48}$$

where $\gamma(z)$ is the ratio of the specific heats of air at height z. Hence (47) can be written

$$\frac{1}{p(z)}\frac{dp(z)}{dz} = -\gamma(z)\left[g(z) + \frac{1}{2}\frac{dw^2(z)}{dz}\right]\Big/c^2(z). \tag{49}$$

Integration then gives

$$p(z)/p(z_1) = \exp\left\{-\int_{z_1}^{z}\gamma(\zeta)\left[g(\zeta) + \frac{1}{2}\frac{dw^2(\zeta)}{d\zeta}\right]\Big/c^2(\zeta)\,d\zeta\right\}. \tag{50}$$

Knowing $c(\zeta)$ and $w(\zeta)$ for the interval (z_1, z_N), $p(z)$ can be evaluated by (50) for $z_1 \leq z \leq z_N$, provided $\gamma(\zeta)$ and $p(z_1)$ are known. $\gamma(\zeta)$ depends on the composition of the atmosphere and can be calculated in terms of the specific heats of the constituent gases.* A method of calculating $p(z_1)$, or more generally $p(z)$, $z_1 \leq z \leq z_N$, from the data of the rocket-grenade experiment, is given by the following theory.

For a given interval $(0, z)$, it is assumed that the functions $\gamma(\zeta)$, $g(\zeta)$ can be written

$$\gamma(\zeta) = \gamma_0 + \gamma_\varepsilon(\zeta) \qquad g(\zeta) = g_0 + g_\varepsilon(\zeta), \tag{51}$$

where $|\gamma_\varepsilon(\zeta)|/\gamma_0$ and $|g_\varepsilon(\zeta)|/g_0$ are of the second order of smallness (e.g., of the order 1 per cent) for $0 \leq \zeta \leq z$. In the case of $g(\zeta)$ this assumption is valid up to at least 100 km, as the acceleration due to gravity at this height is only 3 per cent less than at sea-level. Write

$$c(\zeta) = c_0 + c_\varepsilon(\zeta) \qquad (0 \leq \zeta \leq z), \tag{52}$$

and choose

$$c_0 = C(0, z)/z; \tag{53}$$

then

$$\int_0^z c_\varepsilon(\zeta)\,d\zeta = 0. \tag{54}$$

By (51) and (52), equation (49) can be written

$$\begin{aligned}(1/p)dp/d\zeta &= -[\gamma_0 + \gamma_\varepsilon(\zeta)][g_0 + g_\varepsilon(\zeta) + \tfrac{1}{2}dw^2/d\zeta][1 - 2c_\varepsilon(\zeta)/c_0 \\ &\qquad + 3c_\varepsilon^2(\zeta)/c_0^2 - \ldots]/c_0^2 \\ &= -\{\gamma_0 g_0[1 - 2c_\varepsilon(\zeta)/c_0 + 3c_\varepsilon^2(\zeta)/c_0^2] + \gamma_0[g_\varepsilon(\zeta) + \tfrac{1}{2}dw^2/d\zeta] \\ &\qquad + g_0\gamma_\varepsilon(\zeta)\}/c_0^2\end{aligned}$$

* For an ideal gas-mixture containing a fraction μ_i by weight of molecules of kind i, the specific heats are $\sum_i \mu_i c_{vi}$, $\sum_i \mu_i c_{pi}$, where c_{vi}, c_{pi} are the two specific heats of the molecules of kind i (KENNARD, 1938). Hence

$$\gamma = \textstyle\sum_i \mu_i c_{pi} / \sum_i \mu_i c_{vi}. \tag{48a}$$

on neglecting third- and higher-order terms, provided $(\frac{1}{2}dw^2/d\zeta)/g_0$ can be assumed to be a second- or higher-order quantity. Integration now gives, in view of (54),

$$\log[p(z)/p(0)] = -\Big\{\gamma_0 g_0\Big[z + 3\int_0^z c_\varepsilon^2(\zeta)/c_0^2\,d\zeta\Big] + \gamma_0\Big[\int_0^z g_\varepsilon(\zeta)\,d\zeta + \tfrac{1}{2}w^2(z)\Big] + g_0\int_0^z \gamma_\varepsilon(\zeta)\,d\zeta\Big\}\Big/c_0^2, \tag{55}$$

since $w(0) = 0$, i.e., by (53)

$$\log[p(z)/p(0)] = -\Big\{\int_0^z \gamma(\zeta)g(\zeta)\,d\zeta + \gamma_0\Big[3g_0\int_0^z c_\varepsilon^2(\zeta)/c_0^2\,d\zeta + \tfrac{1}{2}w^2(z)\Big]\Big\}z^2/C^2(0, z), \tag{56}$$

since

$$\int_0^z \gamma(\zeta)g(\zeta)\,d\zeta = \gamma_0 g_0 z + \gamma_0\int_0^z g_\varepsilon(\zeta)\,d\zeta + g_0\int_0^z \gamma_\varepsilon(\zeta)\,d\zeta \tag{57}$$

to the second order. Now

$$g(z) = g(0)a^2/(a + z)^2$$

where a is the earth's radius; and so a suitable choice for g_0 would be

$$g_0 = \int_0^z g(\zeta)\,d\zeta/z = g(0)a/(a + z).$$

By (51) it is then seen that $\int_0^z g_\varepsilon(\zeta)\,d\zeta = 0$. If γ_0 is taken as

$$\gamma_0 = \int_0^z \gamma(\zeta)\,d\zeta/z,$$

then $\int_0^z \gamma_\varepsilon(\zeta)\,d\zeta = 0$; and from (57)

$$\int_0^z \gamma(\zeta)g(\zeta)\,d\zeta = \gamma_0 g_0 z. \tag{58}$$

An estimate is readily made of the expected accuracy with which $p(z)$ would be determined by (56). The contribution from $\frac{1}{2}w^2(z)$ is found to amount to 1 per cent (on taking $\gamma_0 = 1{\cdot}40$, $c_0 = 320$ m/sec) when $w(z)$ equals 35 m/sec, and so this term is never likely to be appreciable in practice. The integral $\int_0^z c_\varepsilon^2(\zeta)/c_0^2\,d\zeta$ has already been evaluated, using typical atmospheric data (GROVES, 1956), and its value has been found to be approximately $0{\cdot}0025z$ for z between 30 and 90 km. The contribution from this term to $p(z)$ is therefore 9 per cent at 90 km, and is proportionally less at lower altitudes. An error $\delta\gamma_0$ in γ_0 is seen from (55) to produce a relative error in $p(z)$ of $\delta\gamma_0 g_0 z/c_0^2$. This amounts to 15 per cent at 90 km for $\delta\gamma_0/\gamma_0 = 1$ per cent and varies proportionally with altitude. When $C(0, z)$ is correct to first-order accuracy, the error in $C^2(0, z)$ is of the order 2 per cent $C^2(0, z)$, and this gives rise to an error in $p(z)$ of the order of 25 per cent at 90 km. When $C(0, z)$ is correct to the second order, this error is reduced by a factor of 10, i.e., is of order 2·5 per cent at 90 km.

VOL. 8 1956

7. Determination of Atmospheric Density and Temperature

When $c(z)$ and $p(z)$ have been determined, $\rho(z)$ can be calculated directly from (48). The accuracy with which $\rho(z)$ is obtained is approximately the same as that of $p(z)$.

Absolute temperature θ can be derived from the equation of state. For pressures of 1 atm and less, the ideal gas law

$$p/\rho = R\theta/m \tag{59}$$

holds very accurately (to within 0·1 per cent). This gives, using (48),

$$\theta(z) = [m(z)/\gamma(z)R]c^2(z). \tag{60}$$

With $\gamma = 1{\cdot}402$, $R = 8{\cdot}314 \times 10^7$ erg/deg/mole, and $m = 28{\cdot}97$, corresponding to dry air of ground-level composition, this relation becomes

$$\theta(z) = [c(z)/20{\cdot}06]^2 \text{ °K}, \tag{61}$$

when $c(z)$ is measured in m/sec.

8. Discussion and Conclusions

A theory has been formulated in this paper which, it is hoped, will prove to be adequate for analysing the data of the rocket-grenade experiment. This experiment is to be carried out as part of the British programme of upper-atmosphere rocket experiments. The theory is presented here in advance of the experimental work, in the belief that it may be of value to other workers in this field, particularly as no complete theory has yet been published. Certain features of the theory together with their implications are discussed in the following paragraphs.

With increasing height, the atmospheric disturbance produced by a grenade explosion takes place on a greater and greater scale. The scale-factor can be shown to vary inversely as the cube root of the atmospheric pressure. At 100 km., for instance, where the pressure is 10^{-6} atm, the wavefront of the disturbance travels 10^2 times the distance that it would at ground-level before its Mach number decreases to a certain value. In view of the increasing importance of this effect with height, it has been assumed in this paper that the Mach number M of the wavefront is a known function of time along any ray, and the theory has been formulated in terms of $M - 1$. The convergence of M towards unity arises mainly from (i) the spherical expansion of the wavefront, and (ii) its propagation into air of increasing density. For (i), $M - 1$ decreases asymptotically like r^{-1} on sound-wave theory; but with this form it can be shown that the integrals of $M - 1$ in (11), (29), and (43) do not converge within distances r from the explosion point over which the changes in density are small; and consequently account must be taken of (ii) in their evaluation. Consideration is at present being given to the theoretical evaluation of M and these associated correction terms. M may possibly be determined experimentally in the vicinity of the explosion if sufficient ionization is produced in the shock-front to reflect radio-doppler signals. On account of the differentiation process involved in the determination of wind and sonic velocities, it is largely the variation in the Mach-number correction terms with height which influences these

determinations. For the derivation of atmospheric pressure, this is not the case, on account of the integration that is introduced, and the absolute determination of the Mach-number corrections is required.

It has been seen that four microphones are sufficient for the determination of the three wind-velocity components and the speed of sound, provided $|\boldsymbol{P}| \neq 0$. This condition becomes, on taking the microphones to lie in a horizontal plane so that $Z_1 = \ldots = Z_4$,

$$\begin{vmatrix} X_1 \ldots X_4 \\ Y_1 \ldots Y_4 \\ 1 \ldots 1 \\ T_1 \ldots T_4 \end{vmatrix} \neq 0.$$

Two cases may be noted for which this condition does not hold: they are (i) when the microphones lie in a straight line, and (ii) when $T_1 = \ldots = T_4$, which could arise if the microphones were roughly in a circle centred below the explosion.

By using more than four microphones and deriving a least-squares solution, the accuracy of the experiment can be increased. From the closeness of fit of this solution, it should be possible to estimate the accuracy achieved and possibly to discover the limiting source of error. This may arise, for instance, from horizontal gradients in the wind and sonic velocities or from random horizontal variations due to turbulence; or, if these effects are small, the limit may be set by the accuracy of the measurements, or by neglecting third-order terms in the analysis. When grenades are exploded over a large altitude range, more than four microphones would help to ensure adequate coverage over different ray inclinations.

When second-order terms have been taken into account in the solution for U, V, W, C, remaining errors are expected to be of order $10^{-3}C$. The errors in the wind and sonic velocities, though, are of the corresponding magnitude, i.e., 0·3 m/sec, only if a sufficiently large number of grenades is used; the number required depending on the nature of the wind and speed-of-sound structure under investigation. In practice, experimental errors also set a limit to the accuracy of the determinations, and only if these are sufficiently small would it be worth while carrying through the second-order solution. An investigation into the effect of experimental errors on the accuracy of the wind and sonic determinations is to be undertaken in a later paper.

A method of deriving pressure, density, and temperature has been developed in Sections 6 and 7. It is shown that the second-order solution offers the possibility of evaluating pressures to within a few per cent at heights up to at least 90 km. This determination depends, though, on the mean value γ_0 of the ratio of specific heats of air between ground-level and the height of the determination; and to achieve an accuracy of 3 per cent at 90 km, γ_0 would have to be correct to within 0·2 per cent, which is about the accuracy to which it has been determined at ground-level. Above 90 km, γ_0 first increases on account of dissociation of O_2, and then of N_2, and may be affected by diffusive separation. The uncertainty in atmospheric composition at these heights would reduce the accuracy with which pressures could be deduced, although worth-while values may still be obtainable.

VOL.
8
1956

Acknowledgements—Acknowledgement is made to Professor H. S. W. MASSEY, F.R.S., for supporting this work, and to Dr. R. L. F. BOYD for many helpful discussions in connection with the rocket-grenade experiment.

REFERENCES

BRUNT, D.	1941	*Physical and Dynamical Meteorology*, Cambridge University Press, p. 276.
GROVES, G. V.	1955	*J. Atmosph. Terr. Physics*, **7**, 113.
	1956	*J. Atmosph. Terr. Physics*, **8**, 24.
KENNARD, E. H.	1938	*Kinetic Theory of Gases*, McGraw-Hill Book Company, p. 265.
MILNE, W. E.	1949	*Numerical Calculus*, Princeton University Press.
STROUD, W. G., *et al.*	1955	*Rev. Sci. Instrum.* **26**, 427.
WEISNER, A. G.	1954	*Rocket Exploration of the Upper Atmosphere*, Pergamon Press, p. 133.

OL.
8
956

Journal of Atmospheric and Terrestrial Physics, 1956, Vol. 8, pp. 204 to 221. Pergamon Press Ltd., London

A theory of scattering by nonisotropic irregularities with application to radar reflections from the aurora

H. G. BOOKER
School of Electrical Engineering, Cornell University, Ithaca, New York

(*Received* 15 *November* 1955)

Abstract—A model of the distribution of ionization in an aurora is developed that can explain the aspect sensitivity of radar echoes obtained at VHF during auroral activity. Even when the radar is in the midst of a zone of auroral activity, echoes are obtained only from low angles of elevation in roughly the northern quadrant. However, both the horizontal and vertical angles over which echoes are obtained increase significantly as frequency is decreased from 100 to 25 Mc/s. These observations can be explained in terms of columns of ionization parallel to the earth's magnetic field. The size of the columns must, however, be much smaller than suggested by CHAPMAN (1952) or by BOOKER, GARTLEIN, and NICHOLS (1955). The column size required is of the order of 40 m in length and 1 m in diameter, smoothed so as to avoid discontinuities at the surfaces. It is quite doubtful whether the formation of such short columns of ionization can be associated directly with the formation of visual rays, even though the same axis of symmetry is involved in both cases. The size of irregularities required to explain the observations is in fact of the order of magnitude likely to be involved in atmospheric turbulence, and it is quite likely that the earth's magnetic field could create substantial nonisotropy in the associated irregularities of electron density. Thus the strength of auroral echoes and their aspect sensitivity could be entirely explained as back-scatter arising from nonisotropic atmospheric turbulence in an *E* region having a maximum electron density about a hundred times the normal value. Simple turbulence cannot, however, explain the remarkable fading phenomena associated with auroral reflections (BOWLES, 1954).

VOL.
8
1956

INTRODUCTION

MOST experimenters who have obtained radar reflections from the aurora at VHF have found that their echoes come from low angles of elevation in a generally northerly direction. Some observers have attached no particular importance to this on the grounds that the auroral activity under observation was mainly to the north of them. Others, however, have been able to make frequent observations under conditions when auroral activity was occurring more or less in all directions from the radar, and have found that the echoes were still confined to comparatively low angles of elevation in roughly the northern quadrant. Since the paper by BOOKER *et al.* (1955) was written, another year of observations has been made at the Geophysical Institute of Alaska on frequencies of approximately 25, 50, and 100 Mc/s, and these fully confirm the earlier conclusion concerning the aspect sensitivity of auroral echoes. For a few weeks, DYCE (1955) even operated radar equipment on approximately 50 Mc/s at Point Barrow (magnetic dip 80°), well north of the centre of the auroral zone. Here most of the visual auroral activity was to the south of the station, but 93·6 per cent of the radio echoes came from locations north of the station. The existence of aspect sensitivity in auroral reflections is therefore regarded as completely established, and it is the object of this paper to find a model of the ionosphere capable of explaining the phenomenon.

It has occurred to several authors that such aspect sensitivity could be explained in terms of columns of ionization parallel to the earth's magnetic field giving maximum echo when viewed perpendicular to the earth's magnetic field. The geometry of this explanation has been worked out in detail by CHAPMAN (1952),

who, on certain assumptions about the height of the aurora, has calculated the horizontal and vertical angles over which auroral reflection should be possible for radars in different latitudes. Unfortunately, CHAPMAN'S theory provides too much aspect sensitivity to fit the observations.

At a location such as Ithaca, New York, CHAPMAN'S theory explains the aspect-sensitivity observations made with a 100-Mc/s radar quite satisfactorily. But CHAPMAN predicted on the theory that College (Alaska) and Tromso (Norway) would be poor locations for obtaining auroral echoes, whereas in fact they are very good. Furthermore, numerous individual auroral echoes have been obtained which would involve departure from the condition of perpendicularity between the radius vector from the radar and the earth's magnetic field by angles of the order of 15 or 20°. In fact, there is an important variation with wavelength in the degree of aspect sensitivity. Whereas at 100 Mc/s echoes can be obtained over an angle of roughly $\pm 45°$ from magnetic north, at 50 Mc/s the permitted quadrant is more like $\pm 60°$, and at 30 Mc/s it is around $\pm 90°$, with echoes sometimes occurring south of the east–west line. Likewise, there is a progressive change with wavelength in the angle of elevation up to which echoes can be obtained. The frequency of occurrence of echoes at 100 Mc/s drops rapidly at ranges less than about 500 km. At 50 Mc/s the cut-off in range occurs at more like 400 km, and at 30 Mc/s it is something like 300 km. We may say therefore that, while the condition of perpendicularity assumed by CHAPMAN seems to contain an important element of truth, it is too drastic to explain the lower-frequency observations and too drastic to explain even the 100 Mc/s observations at places such as College and Tromso.

In these circumstances one's mind turns to columns of ionization that are fairly restricted in length. Columns of length S would give satisfactory echoing properties at wavelength λ over angles up to $\lambda/(2S)$ from a normal to the columns. This would permit some deviation from the normality condition to exist, and would make it possible for these deviations to be greater at longer wavelengths. We therefore conceive the idea that the aspect sensitivity of auroral echoes is to be explained in terms of columns of ionization parallel to the earth's magnetic field that are restricted in length. Even without detailed calculation one can see that, in order to explain the observations, this length must be a few wavelengths at a frequency of 30 Mc/s, but many wavelengths at a frequency of 100 Mc/s. Column lengths of the order of a few tens of metres are therefore indicated, with column diameters that are small compared with this.

The columns required to explain the radar echoes from aurorae are thus of a completely different order of magnitude from the visual rays frequently seen in the sky during auroral activity. They are even of a different order of magnitude from the raylets observed by GARTLEIN and reported by BOOKER *et al.* (1955). Even the correlation between the occurrence of radar echoes and the occurrence of visual-ray structure is now weaker than was reported by BOOKER *et al.* While radar echoes at Ithaca, New York, were hardly ever obtained except when ray structure was seen in the sky, numerous examples have occurred in Alaska of radar echoes from homogeneous auroral forms prior to their break-up into rays (BOWLES, 1954). Both visual rays and auroral echoes are undoubtedly associated

with the most active phase of an aurora, but their frequent simultaneous occurrence may not indicate any direct connection. Thus, although we shall be considering columns of the order of a few tens of metres in length with axes parallel to the earth's magnetic field, we shall not be supposing that there is necessarily any relation between these and visual auroral rays.

We shall not be supposing that the aurora involves overdense ionization at VHF wavelengths. Incoming auroral particles are expected to produce ionization densities of the order of 10^6 per cubic centimetre, corresponding to overdense ionization at frequencies up to about 10 Mc/s. Some authors have contemplated the possibility of overdense ionization in the aurora at frequencies as high as 70 and 100 Mc/s. This would involve ionization densities about one-hundred times greater than are likely to occur in auroras. Even the strongest auroral echoes at 100 Mc/s are some 40 db below what would be produced by an overdense layer perpendicular to the line of sight. Overdense ionization at a frequency of 100 Mc/s is not therefore necessary in order to explain auroral echoes of the magnitude observed, and would be embarrassing so far as the physics of the aurora is concerned. We shall therefore assume that overdense ionization does not occur in aurorae at VHF wavelengths, that an incident VHF radio wave is not subject to any appreciable mean refraction in an aurora, and that only a small part of the energy is scattered out of the incident wave by irregularities in the ionization density.

The model of ionization density in an aurora that we shall consider, therefore, is one in which the electron density is of the order of ten times the noon equatorial value for the E region and is insufficient to create overdense ionization in the VHF band. In this ionization we shall suppose that there are irregularities that are non-isotropic, with an axis of symmetry parallel to the earth's magnetic field. The correlation distance L along the earth's magnetic field will be supposed to be large compared to the correlation distance T transverse to the earth's magnetic field, and we are interested in ascertaining what values of L and T are required to explain the known facts concerning auroral echoes.

VOL.
8
1956

2. Scattering by Nonisotropic Irregularities

A theory of scattering of radio waves by an atmosphere containing irregularities in dielectric constant has been given by Booker and Gordon (1950), following a similar treatment for sound-waves by Pekeris (1947). The specific scattering formula derived by Booker and Gordon is appropriate to an atmosphere containing isotropic irregularities described by an exponential autocorrelation function. However, the assumption of an exponential autocorrelation function was introduced only at the end of the derivation (equation 2s), and even the assumption of isotropic irregularities was introduced only at equation 2q. There is consequently no serious difficulty in extending the treatment of Booker and Gordon to cover nonisotropic irregularities. The following derivation was made by the author during a visit from Cornell University to Cambridge University,* and was simultaneously made by G. K. Batchelor during a visit from Cambridge University to Cornell University.†

* As a Guggenheim Foundation Fellow.
† See also H. Staras (1955).

Suppose that linearly polarized radiation from an isotropic transmitter of power P located at T falls on a volume v of the medium where there are irregularities (see Fig. 1), and let us calculate the scattered power received at a point R. We shall suppose that the distances from T to v and from R to v are large compared with the linear dimensions of the portion of the medium from which scattering is important. We shall also assume that the irregularities make no first-order change

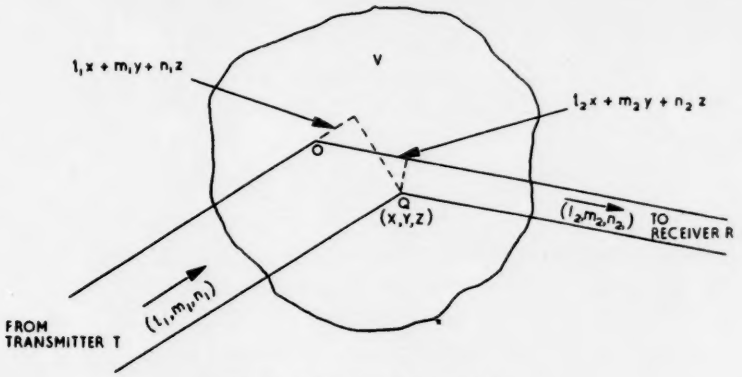

Fig. 1. Geometry of scattering.

in the field strength of the incident wave at any point (BORN's approximation).

The field strength at a point Q of v distance r_1 from T is

$$E_0 = \left(\frac{\zeta P}{2\pi}\right)^{\frac{1}{2}} \frac{\exp(-jkr_1)}{r_1}, \tag{1}$$

where k and ζ are the propagation constant and characteristic impedance of the medium in the absence of irregularities. An increment $\Delta\varepsilon$ in the capacitivity ε of the medium at Q produces an additional electric moment per unit volume

$$\Delta P = E_0 \Delta\varepsilon. \tag{2}$$

At the point R at a distance r_2, this increase in electric moment in an element of volume dv causes a field whose polarization potential is

$$\frac{1}{4\pi\varepsilon}\Delta P \frac{\exp(-jkr_2)}{r_2}\,dv = \frac{1}{4\pi}E_0\frac{\Delta\varepsilon}{\varepsilon}\frac{\exp(-jkr_2)}{r_2}\,dv$$

from (2). Hence the total polarization potential produced at R by irregularities $\Delta\varepsilon/\varepsilon$ at the various points of v is

$$\begin{aligned}\Pi &= \frac{1}{4\pi}\int_v E_0 \frac{\Delta\varepsilon}{\varepsilon}\frac{\exp(jkr_2)}{r_2}\,dv \\ &= \frac{1}{4\pi}\left(\frac{\zeta P}{2\pi}\right)^{\frac{1}{2}}\int_v \frac{\Delta\varepsilon}{\varepsilon}\frac{\exp\{-jk(r_1+r_2)\}}{r_1 r_2}\,dv \end{aligned} \tag{3}$$

from (1). To handle the quantity

$$\frac{\exp\{-jk(r_1 + r_2)\}}{r_1 r_2}$$

it is convenient to choose a reference point O in the volume v. Let O be distant r_1° from T and r_2° from R. Since it is assumed that the linear dimensions of the important part of v are small compared to r_1° and r_2°, the product $r_1 r_2$ in the denominator may be replaced by $r_1^\circ r_2^\circ$. We may now write

$$\Pi = \frac{1}{4\pi}\left(\frac{\zeta P}{2\pi}\right)^{\frac{1}{2}} \frac{\exp\{-jk(r_1^\circ + r_2^\circ)\}}{r_1^\circ r_2^\circ} I, \tag{4}$$

where

$$I = \int_v \frac{\Delta\varepsilon}{\varepsilon} \exp\left[-jk\{(r_1 - r_1^\circ) + (r_2 - r_2^\circ)\}\right] dv. \tag{5}$$

To transform the integral I, let $(l_1, m_1, n_1,)$ be a unit vector in the direction of incidence and (l_2, m_2, n_2) a unit vector in the direction of scattering. Let the co-ordinates of the element of volume dv at Q be (x, y, z). On the assumption that T and R are at a great distance (see Fig. 1), we have

$$\begin{cases} r_1 - r_1^\circ = l_1 x + m_1 y + n_1 z & (6) \\ r_2 - r_2^\circ = -(l_2 x + m_2 y + n_2 z), & (7) \end{cases}$$

so that

$$(r_1 - r_1^\circ) + (r_2 - r_2^\circ) = (l_1 - l_2)x + (m_1 - m_2)y + (n_1 - n_2)z \tag{8}$$

Hence

$$I = \int_v \frac{\Delta\varepsilon}{\varepsilon} \exp\left[\{jk(l_2 - l_1)x + (m_2 - m_1)y + (n_2 - n_1)z\}\right] dx\, dy\, dz \tag{9}$$

$$= p\{k(l_2 - l_1), k(m_2 - m_1), k(n_2 - n_1)\}, \tag{10}$$

where $p(l, m, n)$ is the Fourier transform of $\Delta\varepsilon/\varepsilon\ (x, y, z)$.

We shall actually require $|I|^2$. Now, by KINCHINE's theorem, $|p|^2$ is the Fourier transform of

$$\int_v \frac{\Delta\varepsilon^*}{\varepsilon}(X, Y, Z) \frac{\Delta\varepsilon}{\varepsilon}(X + x, Y + y, Z + z)\, dX\, dY\, dZ\,, \tag{12}$$

and this is equal to

$$v\overline{\left|\frac{\Delta\varepsilon}{\varepsilon}\right|^2} \rho\,(x, y, z)\,, \tag{13}$$

where ρ is the autocorrelation function of $\Delta\varepsilon/\varepsilon$ defined by

$$\rho(x, y, z) = \frac{\displaystyle\int_v \frac{\Delta\varepsilon^*}{\varepsilon}(X, Y, Z) \frac{\Delta\varepsilon}{\varepsilon}(X + x, Y + y, Z + z)\, dX\, dY\, dZ}{\displaystyle\int_v \left|\frac{\Delta\varepsilon}{\varepsilon}(X, Y, Z)\right|^2 dX\, dY\, dZ} \tag{14}$$

VOL. 8 1956

and $\overline{\left|\frac{\Delta\varepsilon}{\varepsilon}\right|^2}$ is the mean square fractional deviation of ε given by

$$\overline{\left|\frac{\Delta\varepsilon}{\varepsilon}\right|^2} = \frac{1}{v}\int_v \left|\frac{\Delta\varepsilon}{\varepsilon}\right|^2 dv. \tag{15}$$

Let $P(l, m, n)$ be the Fourier transform of $\rho(x, y, z)$, the autocorrelation function of $\frac{\Delta\varepsilon}{\varepsilon}(x, y, z)$. Then it follows from (10) and (13) that

$$|I|^2 = v\overline{\left|\frac{\Delta\varepsilon}{\varepsilon}\right|^2} P\{k(l_2 - l_1), k(m_2 - m_1), k(n_2 - n_1)\}. \tag{16}$$

If χ is the angle between the direction of scattering and the direction of E_0, the scattered field at R is

$$\begin{aligned} E &= k^2 \sin\chi\, \Pi \\ &= \frac{1}{4\pi}\left(\frac{\zeta P}{2\pi}\right)^{\frac{1}{2}} k^2 \sin\chi \frac{\exp\{-jk(r_1^\circ + r_2^\circ)\}}{r_1^\circ r_2^\circ} I \end{aligned}$$

from (4). The scattered power-density at R is therefore

$$\frac{|E|^2}{2\zeta} = \frac{P}{(4\pi)^3} k^4 \sin^2\chi \frac{1}{(r_1^\circ)^2(r_2^\circ)^2}|I|^2 .$$

The power scattered per unit solid angle in the direction of R is therefore

$$(r_2^\circ)^2 \frac{|E|^2}{2\zeta} = \frac{P}{4\pi(r_1^\circ)^2} \frac{\pi^2 \sin^2\chi}{\lambda^4}|I|^2 .$$

Hence the power scattered in the direction of R per unit solid angle, per unit incident power-density, is

$$\frac{\pi^2 \sin^2\chi}{\lambda^4}|I|^2.$$

The power scattered per unit solid angle, per unit incident power-density, per unit volume, is therefore

$$\begin{aligned} \sigma &= \frac{1}{v}\frac{\pi^2 \sin^2\chi}{\lambda^4}|I|^2 \\ &= \overline{\left|\frac{\Delta\varepsilon}{\varepsilon}\right|^2} \frac{\pi^2 \sin^2\chi}{\lambda^4} P\{k(l_2 - l_1), k(m_2 - m_1), k(n_2 - n_1)\} \end{aligned} \tag{17}$$

from (16).

The direction of the vector

$$(l_2 - l_1, m_2 - m_1, n_2 - n_1) \tag{18}$$

is the external bisector of the angle between the direction of incidence and the direction of scattering. This defines what may be called the "mirror direction" for the directions of incidence and scattering. Planes perpendicular to the vector (18) are able to "mirror" the direction of incidence into the direction of scattering.

Now the irregularities $\frac{\Delta\varepsilon}{\varepsilon}(x, y, z)$ in the medium may be Fourier-analysed into plane-stratified fractional deviations of ε having sinusoidal profiles, and these are continuously distributed both with regard to direction and corrugation-wavelength. It is this Fourier analysis of $\frac{\Delta\varepsilon}{\varepsilon}(x, y, z)$ that is described by the functions $p(l, m, n)$ and $P(l, m, n)$. What the result (17) implies therefore is that scattering in a particular direction depends on the Fourier content of the irregularities in the associated mirror direction. It also depends on the presence in the mirror direction of corrugation-wavelengths such as to produce constructive interference in the direction of scattering. For a scattering angle θ, there must be important Fourier content of corrugation-wavelength $\lambda/\{2 \sin(\theta/2)\}$ in the mirror direction associated with the directions of incidence and scattering.

To derive the Booker and Gordon scattering formula, we put

$$\rho = \exp\left\{-\frac{1}{L}(x^2 + y^2 + z^2)^{\frac{1}{2}}\right\},$$

and obtain, after Fourier transformation,

$$P = \frac{8\pi L^3}{\{1 + L^2(l^2 + m^2 + n^2)\}}.$$

On substitution into (17), this leads to their formula. In this paper, however, we are interested in nonisotropic scattering.

VOL. 8 1956

3. Back-scattering for Axially Symmetrical Scatters

For radar echoes we are interested only in back-scattering, for which $\chi = \pi/2$ and $(l_1, m_1, n_1) = -(l_2, m_2, n_2) = (l, m, n)$, say. Hence the back-scattering coefficient is

$$\sigma_B = \overline{\left|\frac{\Delta\varepsilon}{\varepsilon}\right|^2} \frac{\pi^2}{\lambda^4} P(2kl, 2km, 2kn), \tag{19}$$

where (l, m, n) is a unit vector in the direction of incidence.

In the application to the aurora we do not know what causes the irregularities that produce scattering, and so we do not know what form to assume for an autocorrelation function of $\Delta\varepsilon/\varepsilon$. In the circumstances we will tentatively assume a Gaussian autocorrelation function. If

$$\rho(x, y, z) = \exp\left\{-\frac{1}{2}\left(\frac{x^2}{a^2} + \frac{y^2}{b^2} + \frac{z^2}{c^2}\right)\right\}. \tag{20}$$

it follows by Fourier transformation that

$$P(l, m, n) = (2\pi)^{3/2} abc \exp\{-\tfrac{1}{2}(a^2l^2 + b^2m^2 + c^2n^2)\}. \tag{21}$$

For an axially symmetrical case in which the z axis is the axis of symmetry, we put

$$a = b = T, \quad c = L,$$

so that T is the correlation distance transverse to the axis of symmetry, and L is the correlation distance along the axis of symmetry. The back-scattering coefficient then becomes

$$\sigma_B = (2\pi)^{3/2}\,\pi^2 \left|\frac{\Delta\varepsilon}{\varepsilon}\right|^2 \frac{T^2 L}{\lambda^4} \exp\left[-2k^2\{T^2(l^2+m^2)+L^2n^2\}\right].$$

Let ψ be the complement of the angle between the direction of incidence and the axis of symmetry. Then

$$n = \sin\psi$$

$$l^2 + m^2 = \cos^2\psi.$$

Hence

$$\sigma_B = (2\pi)^{3/2}\pi^2 \left|\frac{\Delta\varepsilon}{\varepsilon}\right|^2 \frac{T^2 L}{\lambda^4} \exp\left\{-\frac{8\pi^2}{\lambda^2}\,(T^2\cos^2\psi + L^2\sin^2\psi)\right\}. \tag{22}$$

For an ionized medium we have

$$\frac{\varepsilon}{\varepsilon_0} = 1 - \left(\frac{\lambda_0}{\lambda_N}\right)^4, \tag{23}$$

where λ_0 is the free-space wavelength and λ_N is the plasma wavelength corresponding to the electron density. It follows that

$$\overline{\left|\frac{\Delta\varepsilon}{\varepsilon}\right|^2} = \left(\frac{\lambda}{\lambda_N}\right)^4 \overline{\left(\frac{\Delta N}{N}\right)^2}. \tag{24}$$

Hence the formula for back-scattering from axially symmetrical irregularities of electron-density is

$$\sigma_B = (2\pi)^{3/2}\frac{\pi^2}{\lambda_N^4}\,\overline{\left(\frac{\Delta N}{N}\right)^2}\,T^2 L \exp\left\{-\frac{8\pi^2}{\lambda}\,(T^2\cos^2\psi + L^2\sin^2\psi)\right\}. \tag{25}$$

This may be written as

$$\sigma_B = (2\pi)^{3/2}\frac{\pi^2}{\lambda_N^4}\,\overline{\left(\frac{\Delta N}{N}\right)^2}\,T^2 L \exp\left(-\frac{8\pi^2\,T^2}{\lambda^2}\right)\exp\left\{-\frac{8\pi^2}{\lambda^2}\,(L^2 - T^2)\sin^2\psi\right\}, \tag{26}$$

showing that, for isotropic scattering ($L = T$), the dependence on the direction ψ of the incident wave disappears, as it should. We, however, will be interested in the case when $L \gg T$. Moreover, we will be seriously interested only in fairly small values of ψ. In these circumstances we have approximately

$$\sigma_B = (2\pi)^{3/2}\,\pi^2\,\frac{1}{\lambda_N^4}\,\overline{\left(\frac{\Delta N}{N}\right)^2}\,T^2 L \exp\left(-\frac{8\pi^2 T^2}{\lambda^2}\right)\exp\left(-\frac{8\pi^2 L^2}{\lambda^2}\,\psi^2\right). \tag{27}$$

This gives the back-scattering per unit solid angle, per unit incident power-density, per unit volume, from an ionized medium having elongated irregularities, provided that the direction of incidence is not nearly parallel to the axis of symmetry.

4. A Radio Model of the Aurora

We shall assume that the mean ionization-density in an aurora corresponds to a plasma wavelength λ_N appreciably longer than the free-space wavelength λ_0 of the radar in use. It will not therefore be necessary to draw distinction between the local wavelength λ occurring in the aurora and the free-space wavelength λ_0. In particular, we shall neglect refraction of the incidence wave (except, of course, refraction by the irregularities). It has been pointed out by workers at the Chalmers Technical University (private communication) that even slight refraction of the incident wave may be important, because it may decide whether the incident wave is almost exactly normal to the axis of the scatterers or merely roughly normal. While this is true, we shall nevertheless neglect refraction of the incident wave.

We shall assume that the irregularities of ionization density in the aurora are axially symmetrical about the earth's magnetic field and have a back-scattering coefficient described by equation (27). We shall assume that $\frac{1}{\lambda_N^4}\left(\frac{\Delta N}{N}\right)^2$ is uniform throughout the relevant scattering volume, and zero elsewhere. We shall also neglect any variation throughout the scattering volume of the correlation distance T transverse to the earth's magnetic field, and the correlation distance L along the earth's magnetic field.

We now have to decide what assumption it is appropriate to make about scattering volume. For a typical VHF radar, the scattering volume is normally limited in range by the pulse-length p of the equipment, and in azimuth by the width w of the auroral radio phenomenon. It is of course possible for the scattering volume to be limited in range by the dimensions of the aurora and in azimuth by the beam-width of the radar. In any case, a horizontal section through the relevant scattering volume gives an area A, and normally we have

$$A = pw \tag{28}$$

approximately. In height we shall assume that the scattering volume is limited on the underside by a horizontal surface at height h_0 above the earth, and take h_0 to be 100 km. What to assume for the upper limit of the scattering volume is less clear. In practice, we are interested in situations in which the radius vector from the radar is nearly perpendicular to the earth's magnetic field at the bottom of the scattering volume (ψ small in 27). As we go up through the scattering volume, the angle ψ increases, and on account of the increase in ψ the back-scattering decreases with increase in height. It is possible that the height up to which scattering is important may be determined more by the aspect-sensitivity of the scattering irregularities than by the disappearance of the irregularities themselves. We shall simply assume therefore that the irregularities exist from the minimum height h_0 indefinitely upwards, but this assumption could easily be changed.

It may well be that the scattering volume should be regarded as limited, not by vertical lines through the perimeter of the area A involved in equation (28), but rather by the lines of the earth's magnetic field through the perimeter of A. Since,

VOL.
8
1956

however, we are interested in values of magnetic dip in excess of 70°, the difference is unimportant.

To obtain the magnitude of the echo received by a radar, it will be necessary to integrate the back-scattering coefficient σ_B throughout the scattering volume V. On the assumptions stated above

$$\int_V \sigma_B \, dV = A \int_{h_0}^{\infty} \sigma_B \, dh$$
$$= A(2\pi)^{3/2} \pi^2 \frac{1}{\lambda_N^4} \left(\frac{\Delta N}{N}\right)^2 T^2 L \exp\left(-\frac{8\pi^2 T^2}{\lambda^2}\right) \int_{h_0}^{\infty} \exp\left(-\frac{8\pi^2 L^2}{\lambda^2} \psi^2\right) dh$$

from (27). For an echo at range r we have approximately

$$dh = r \, d\psi,$$

and, if ψ_0 is the value of ψ at the bottom of the scattering volume where $h = h_0$, we obtain

$$\int_V \sigma_B \, dv = A(2\pi)^{3/2} \pi^2 \frac{1}{\lambda_N^4} \left(\frac{\Delta N}{N}\right)^2 T^2 L \exp\left(-\frac{8\pi^2 T^2}{\lambda^2}\right) r \int_{\psi_0}^{\infty} \exp\left(-\frac{8\pi^2 L^2}{\lambda^2} \psi^2\right) d\psi. \tag{29}$$

This integral may now be evaluated in terms of the error function, giving

$$\int_V \sigma_B \, dv = \frac{A\pi^3}{2} \frac{1}{\lambda_N^4} \left(\frac{\Delta N}{N}\right)^2 T^2 \lambda \exp\left(-\frac{8\pi^2 T^2}{\lambda^2}\right) r \left\{1 - \operatorname{erf}\left(\sqrt{2}\, \frac{2\pi L}{\lambda} \psi_0\right)\right\}. \tag{30}$$

5. Calculation of Auroral Radar Echo Strength

Let us consider a radar whose antenna has a vertical aperture-width a and horizontal aperture-width b. Suppose that the centre of the antenna is at a height h above level ground and that the axis of the beam is directed horizontally. Consider a direction of radiation in the vertical plane containing the axis of the beam. Let θ be its angle of elevation at the radar and θ_0 the corresponding angle of elevation at the height h_0, allowing for the finite radius of the earth. The vertical amplitude polar diagram of the antenna will be taken as

$$2 \sin\left(\frac{2\pi h}{\lambda_0} \sin\theta\right) \frac{\sin\left(\frac{\pi a}{\lambda_0} \sin\theta\right)}{\frac{\pi a}{\lambda_0} \sin\theta}.$$

Let dV be an element of volume in the aurora at slant range r, and let σ_B be the back-scattering coefficient at this point. A standard radar calculation gives for the ratio of the power P_R received back to the power P_T transmitted by the radar

$$\frac{P_R}{P_T} = 16 \sin^4\left(\frac{2\pi h}{\lambda_0} \sin\theta\right) \frac{\sin^4\left(\frac{\pi a}{\lambda_0} \sin\theta\right)}{\left(\frac{\pi a}{\lambda_0} \sin\theta\right)^4} \frac{(ab)^2}{\lambda_0^2} \int_V \frac{\sigma_B \, dV}{r^4}. \tag{31}$$

If we assume that the scattering volume V is sufficiently restricted for the variation of r within it to be neglected, the integral in (31) reduces to

$$\frac{1}{r^4}\int_V \sigma_B \, dV,$$

the value of which is given by (30). Dropping the distinction between the wavelength λ in the aurora and wavelength λ_0 in free space, we derive for the ratio of the power received to the power transmitted

$$\frac{P_R}{P_T} = 16 \sin^4\left(\frac{2\pi h}{\lambda}\sin\theta\right) \frac{\sin^4\left(\frac{\pi a}{\lambda}\sin\theta\right)}{\left(\frac{\pi a}{\lambda}\sin\theta\right)^4} (ab)^2 \frac{\pi^3}{2}\frac{1}{\lambda_N^4}\left(\overline{\frac{\Delta N}{N}}\right)^2 \frac{T^2}{\lambda}\exp\left(\frac{-8\pi^2 T^2}{\lambda^2}\right)$$

$$A\,\frac{1}{r^3}\left\{1 - \operatorname{erf}\left(\sqrt{2}\,\frac{2\pi L}{\lambda}\psi_0\right)\right\}. \tag{32}$$

To apply this formula, certain geometrical calculations are necessary, making allowance for the finite radius R of the earth. For a target at slant range r and height h_0 we can calculate the angle of elevation θ of the radial from the radar at ground-level. It is convenient to calculate first the corresponding angle of elevation θ_0 at height h_0 by means of the formula

$$\sin\theta_0 = \frac{r^2 + 2Rh_0 + h_0^2}{2r(R + h_0)}, \tag{33}$$

and then deduce θ from the formula

$$\cos\theta = \left(1 + \frac{h_0}{R}\right)\cos\theta_0. \tag{34}$$

We also need to calculate the angle ψ_0 in (32) as a function of the range r of the target and its azimuth ϕ from magnetic north. To do this, we first calculate θ_0 from (33) and then use the formula

$$\sin\psi_0 = \cos I\cos\theta_0\cos\phi - \sin I\sin\theta_0, \tag{35}$$

where I denotes magnetic dip. In this calculation it is necessary to allow for the variation of magnetic dip with range. When these geometrical calculations have been done and the necessary substitutions made into (32), this formula gives P_R/P_T as a function of range r. As parameters in the formula we have the wavelength λ; the antenna dimensions a, b, and h; and the ionospheric quantities h_0, L, T, and $\frac{1}{\lambda_N^4}\left(\overline{\frac{\Delta N}{N}}\right)^2$.

6. Numerical Calculations

The factor in (32) that depends on the aspect sensitivity of the ionospheric irregularities is

$$1 - \operatorname{erf}\left(\sqrt{2}\,\frac{2\pi L}{\lambda}\psi_0\right), \tag{36}$$

VOL. 8 1956

where ψ_0 is given by (35) and related formulae. This factor depends on the correlation distance L along the earth's magnetic field, but not on the correlation distance T transverse to the earth's magnetic field (because $T \ll L$). Now, it is upon the factor (36) that we must primarily depend in explaining the auroral radio observations concerning aspect sensitivity. Only one unknown parameter L is involved in (36). If the theory we have developed is roughly right, choice of the value of L must reproduce the range cut-off in auroral echoes, not merely at one wavelength, but as a function of wavelength. The same value of L must

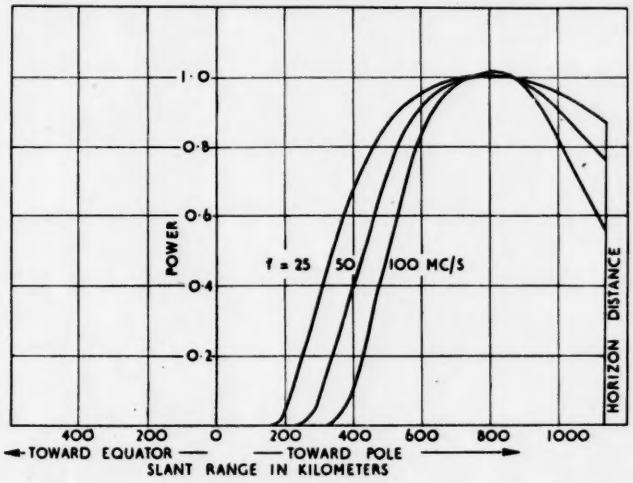

Fig. 2. Aspect-sensitivity factor as a function of slant-range in magnetic meridian for radar at magnetic dip $\pm 75°$.

reproduce the azimuth cut-off in auroral echoes, and again this must be true as a function of wavelength. In short, the whole aspect-sensitivity phenomenon in range and azimuth must be more or less correctly reproduced as a function of wavelength by the factor (36) merely by appropriate choice of the single parameter L.

Calculations have been carried out for a radar located where the magnetic dip is 75°, intermediate between Ithaca, New York (74°) and College, Alaska (77°). At 100 Mc/s it is known that the strength and frequency of occurrence of auroral echoes drops fairly quickly at ranges below about 500 km. This fact has been used to fix a value for L, namely

$$L = 6{\cdot}8 \text{ metres.} \tag{37}$$

The value quoted in the summary is $2\pi L$, and is more appropriate to the statement there made.

Fig. 2 shows the aspect-sensitivity factor plotted as a function of slant range for auroral echoes in the magnetic meridian ($\phi = 0°$ or 180°). Curves are shown for 100, 50, and 25 Mc/s. The 100-Mc/s curve has been chosen so that (36) has the

value 0·5 at a range of 500 km, and this is how the value (37) of L was determined. The two ranges (730 and 870 km) where the aspect-sensitivity factor has the value unity are the ranges at which $\psi_0 = 0$, that is, the ranges at which the radius vector from the radar is perpendicular to the earth's magnetic field at a height of 100 km. In Fig. 3 a fixed slant-range of 700 km has been selected, and the aspect-sensitivity factor has been plotted as a function of the azimuth ϕ of the auroral echo, using the same three frequencies. It will be observed from Figs. 2 and 3 that, with the value (37) of L, the factor (36) in fact reproduces reasonably well the observations concerning aspect sensitivity of auroral echoes described

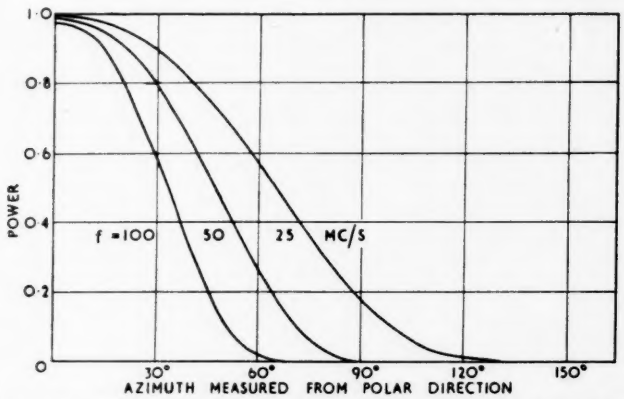

Fig. 3. Aspect-sensitivity factor at slant-range 700 km, as a function of azimuth, for radar at magnetic dip $\pm 75°$.

in Section 1. There is, at a frequency of 100 Mc/s, a marked tendency to suppress short-range echoes, and this decreases with decrease of frequency in about the right way. Moreover, in azimuth, echoes are confined to the northern quadrant at 100 Mc/s, and the cut-off in azimuth increases with decrease of frequency in about the right way. Comparison may be made with the following published observations:

Hellgren and Meos (1952), Figs. 13, 14, 15, and 16.
Currie, Forsyth, and Vawter (1953), Fig. 8.
Harang and Landmark (1954), Figs. 1, 2, 4, and 6.
Booker, Gartlein, and Nichols (1955), Figs. 2, 3, 4, and 5.
Dyce (1955), Fig. 2.

Since the aspect-sensitivity factor (36), with the value (37) for L, appears to have roughly the right behaviour, let us now substitute into the complete formula (32). In this way we include in the range dependence not only the effects of aspect sensitivity, but also the inverse distance factor and the effects of antenna polar diagram. For auroral echoes magnetically due north in the northern hemisphere or due south in the southern hemisphere, we obtain the curves marked A in Fig. 4. The left-hand set of curves refers to an antenna having a vertical aperture a of 12 m

VOL. 8 1956

with its centre at a height h above ground of 9 m. The right-hand set of curves refers to $a = 6$ m, $h = 6$ m. The right-hand set of curves corresponds approximately to antenna arrangements that have been commonly used. However, the 100-Mc/s antenna at Ithaca, New York, corresponds to the left-hand column. By comparison with the observations quoted, it will be seen that the theory places the range-interval in which echoes should be observable in approximately the right place

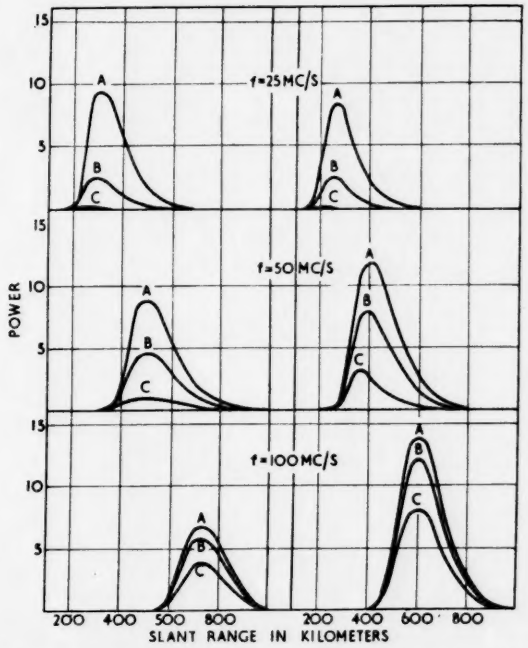

Fig. 4. Auroral response vs. range towards pole for radar at magnetic dip $\pm 75°$. (A) No attenuation, (B) moderate attenuation, (C) heavy attenuation. L.H.S. antenna—centre height 9 m, vertical aperture 12 m. R.H.S. antenna—centre height 6 m, vertical aperture 6 m. The aperture area is same in all cases.

at all three frequencies. The long-range cut-off in auroral response is due to the polar diagram of the antenna. The short-range cut-off is due to the aspect-sensitivity factor at 25 and 50 Mc/s. At 100 Mc/s the short-range cut-off is due principally to the aspect-sensitivity factor, though it is modified somewhat by the antenna polar diagram, as may be seen by comparing results in the left-hand and right-hand columns.

The curves B and C in Fig. 4 show the effect of introducing ionospheric attenuation into the calculations. Curve B assumes that the attenuation suffered in going one way through the relevant portion of ionosphere at vertical incidence at 25 Mc/s would be 1 db. Curve C assumes that the attenuation is four times greater than this. Judging from observations of cosmic noise during aurorae (McKinley and Millman, 1953), it would seem that curve B might correspond

to typical attenuation in an aurora, and curve C to heavy attenuation. The effect of auroral attenuation, although severe in the HF band, is not likely to be of great importance in the VHF band.

The factors of (32) included in preparing Fig. 4 were

$$16 \sin^4\left(\frac{2\pi h}{\lambda} \sin\theta\right) \frac{\sin^4\left(\frac{\pi a}{\lambda} \sin\theta\right)}{\left(\frac{\pi a}{\lambda} \sin\theta\right)^4} \frac{1}{\lambda r^3} \left\{1 - \operatorname{erf}\left(\sqrt{2}\, \frac{2\pi L}{\lambda}\, \psi_0\right)\right\}, \tag{38}$$

and this has to be multiplied by 10^{18} in m.k.s. units to give the ordinates in Fig. 4. To obtain the ratio of the power received to the power transmitted, we have to multiply the ordinates in Fig. 4 by 10^{-18} and also by

$$\frac{\pi^3}{2} \frac{1}{\lambda_N^4} \overline{\left(\frac{\Delta N}{N}\right)^2} T^2 \exp\left(-\frac{8\pi^2 T^2}{\lambda^2}\right) (ab)^2 A. \tag{39}$$

The effect of wavelength dependence is completely included in Fig. 4, except for the factor

$$\exp\left(-\frac{8\pi^2 T^2}{\lambda^2}\right) \tag{40}$$

occurring in (39). Now, this factor would virtually suppress echoes at wavelengths less than about

$$2\pi T. \tag{41}$$

So far as the factors (38) are concerned, auroral echoes could persist into the UHF band, but it would then be more necessary to direct the radar beam perpendicular to the earth's magnetic field. There have so far been no reports of auroral activity affecting transmissions in the UHF band, although there are plenty of reports from amateurs working in the 144-Mc/s band. We therefore assume tentatively that the effect of the aurora upon radio transmission cuts off at a wavelength of around 1 m. This means that (41) has a value of about 1 m, giving

$$T = 0{\cdot}16 \text{ m}. \tag{42}$$

This value is small compared with L, as it should be. In fact, the ratio of L to T is about 40.

If the value (42) for T is accepted, the only remaining unknown in (39) is

$$\frac{1}{\lambda_N^4} \overline{\left(\frac{\Delta N}{N}\right)^2} A, \tag{43}$$

and this can then be determined from measurements of the ratio of power received in an auroral echo to the power transmitted. For fairly strong auroral echoes, with a radar of pulse-length 30 km, (43) has been found experimentally to have a value of the order of

$$10^{-3} \text{ m}^{-2}. \tag{44}$$

VOL. 8 1956

Since we are not assuming overdense ionization in the VHF band, a suitable value for the plasma wavelength is

$$\lambda_N = 30 \text{ m}, \tag{45}$$

corresponding to an electron density of about 10^6 per cm^3. Hence

$$\overline{\left(\frac{\Delta N}{N}\right)^2} A = 10^3 \text{ m}^2. \tag{46}$$

Taking A as given by (28), we deduce that

$$\overline{\left(\frac{\Delta N}{N}\right)^2} w = 3 \times 10^{-2} \text{ m}, \tag{47}$$

where w is a measure of the linear dimensions of the auroral scattering region. Whatever reasonable assumption one may make about w, it is clear that $\overline{\left(\frac{\Delta N}{N}\right)^2}$ is small. A likely value for w, judged from radar observations, is of the order of 100 km, giving

$$\overline{\left(\frac{\Delta N}{N}\right)^2} = 3 \times 10^{-7}. \tag{48}$$

The upshot of our calculations is that the strength and aspect-sensitivity of auroral echoes can be explained if:

(i) the mean electron density corresponds to a plasma wavelength of around (45);
(ii) there are irregularities in electron density axially symmetrical about the earth's magnetic field and having a Gaussian autocorrelation function;
(iii) the correlation distance along the earth's magnetic field is given by (37);
(iv) the correlation distance transverse to the earth's magnetic field is given by (42); and
(v) the mean square fractional deviation of electron density is of the order of (48).

The extremely small value required for $\overline{\left(\frac{\Delta N}{N}\right)^2}$ underlines how unnecessary it is to invoke overdense ionization in the VHF band in order to explain auroral echoes.

7. Discussion

We can now speculate upon what significance these results may have in auroral and ionospheric physics. Booker *et al.* (1955) contemplated the possibility that the elongation of the irregularities of electron density along the earth's magnetic field might be associated with the fact that the auroral ionization is probably produced by ions entering the atmosphere along the lines of force of the earth's magnetic field. This might have been plausible if the correlation distance L along the earth's magnetic field had turned out to be of the same order of magnitude as the scale height of the atmosphere. But in fact L is about a thousand times

less than this, and so some completely different explanation of the elongation of the irregularities along the lines of force of the earth's magnetic field seems to be required.

One's mind turns to irregularities of electron density associated with turbulence. These irregularities are likely to be elongated along the earth's magnetic field at E-region levels and above. At E-region levels the largest irregularities associated with turbulence are likely to be of the order of 100 m in size (Ratcliffe, 1954) and the smallest irregularities of the order of 1 m (Batchelor, 1953). We are interested in explaining irregularities of the order of (37) along the earth's magnetic field and (42) transverse to the field. The geometric mean of these is roughly the size expected for the smallest irregularities due to turbulence. Moreover, it is the smallest irregularities that are important in back-scattering (except at wavelengths large compared with 2π-times the size of the smallest irregularities). We are thus led to formulate the following hypotheses concerning the ionosphere at E-region levels:

(i) Irregularities due to turbulence, or at least the smaller irregularities due to turbulence, are always elongated along the earth's magnetic field whether there is auroral activity or not.

(ii) The smallest irregularities involve correlation distances along the earth's magnetic field of the order of 5–10 m, and transverse to the earth's magnetic field less than 1 m.

(iii) The intensity of the irregularities is insufficient to give an observable echo in the VHF band, except in the most active regions of an aurora.

These hypotheses would explain the existence and aspect-sensitivity of auroral echoes, and we now have to consider what objections there may be to them.

One objection to the above line of reasoning could be that nonauroral sporadic E involves ionization densities as high as those occurring in the aurora, and so should given echoes having auroral-type aspect-sensitivity. This objection is probably not serious, since echoes have recently been identified at Stanford University (magnetic dip 61°) which appear to be of just this type, but which had previously been attributed to back-scattering from the ground (Peterson, 1955).

An objection could also be raised to the value (48) for $\overline{\left(\frac{\Delta N}{N}\right)^2}$, which is between two and three powers of 10 less than the value usually considered appropriate to turbulence at E-region levels. It must be noted, however, that, if the irregularities are in fact due to turbulence, the Gaussian autocorrelation function that we have tentatively assumed must be seriously modified. These modifications have little effect on the conclusions that we have drawn, except that they raise the estimate of $\overline{\left(\frac{\Delta N}{N}\right)^2}$ by about two powers of ten, thereby bringing it into reasonable agreement with other estimates of this quantity.

The most serious objection to regarding turbulence as the cause of the irregularities required to explain auroral echoes is that the fading phenomena of auroral echoes cannot possibly be explained in terms of wind-speed and turbulence.

VOL. 8 1956

The fading rates are too fast by at least a power of 10. Moreover, the Doppler shifts in the echoes do not fit in with the observed rates of change of range, sometimes not even as regards sign (BOWLES, 1954). These facts do not prevent turbulence from being involved in the explanation of the features of auroral echoes with which we have been concerned in this paper, but they do mean that there must be other important features of auroral ionization that we have not attempted to elucidate.

Whatever may be the cause of the irregularities of electron density in the aurora, there seems to be no doubt that the irregularities are elongated along the earth's magnetic field, and that the ones important for back-scattering have a correlation distance along the earth's magnetic field of the order of 5–10 m.

REFERENCES

BATCHELOR, G. K.	1953	*Homogeneous Turbulence*, Cambridge University Press.
BOOKER, H. G. and GORDON, W. E.	1950	*Proc. Inst. Radio Eng.* **38**, 401.
BOOKER, H. G., GARTLEIN, C. W., and NICHOLS, B.	1955	*J. Geophys. Res.* **60**, 1.
BOWLES, K. L.	1954	*J. Geophys. Res.* **59**, 553.
Chalmers Technical University, Gothenburg, Sweden.		Private communication from workers associated with Prof. O. RYDBECK.
CHAPMAN, S.	1952	*J. Atmosph. Terr. Phys.* **3**, 1.
CURRIE, B. W., FORSYTH, P. A., and VAWTER, F. E.	1953	*J. Geophys. Res.* **58**, 179.
DYCE, R. B.	1955	*J. Geophys. Res.* **60**, 317.
HARANG, L. and LANDMARK, B.	1954	*J. Atmosph. Terr. Phys.* **4**, 322.
HELLGREN, A. and MEOS, J.	1952	*Tellus* **4**, 249.
MCKINLEY, D. W. R. and MILLMAN, P. M.	1953	*Canad. J. Phys.* **31**, 171.
PEKERIS, C. L.	1947	*Phys. Rev.* **71**, 268
PETERSON, A. M.	1955	*J. Geophys. Res.* **60**, 497.
RATCLIFFE, J. A.	1954	*The Physics of the Ionosphere*, Physical Society of London, September. (Note: RATCLIFFE'S "size" is 2π-times that used here.)
STARAS, H.	1955	*Proc. Inst. Radio Eng.* **43**, 1374.

Journal of Atmospheric and Terrestrial Physics, 1956, Vol. 8, pp. 222 to 232. Pergamon Press Ltd., London

Mitteilungen aus dem Astronomischen Institut der Universität Tübingen Nr. 20

Die Emissionshöhe der 5577 AE-Linie des Nachthimmelsleuchtens nach Messungen am Jungfraujoch

(The height of emission of the 5577 line of the air-glow as observed on the Jungfraujoch)

H. Elsässer u. H. Siedentopf
Astronomisches Institut der Universität Tübingen, Tübingen Gmelinstr. 6

(*Received* 23 *August* 1955)

ABSTRACT

Observations of the intensity-variation of [O I] 5577 between zenith and horizon at Jungfraujoch in winter 1954/55 with a photoelectric photometer, using the method of V. Rhijn, are discussed. Reduced with individual values of the extinction-coefficient for each observing night, they give a mean altitude of 90 ± 10 km for the luminous layer.

Während unserer Arbeiten zur Photometrie des Zodiakallichts am Jungfraujoch im Winter 1955, über die an anderer Stelle berichtet wird, wurden auch verschiedene Registrierungen der Helligkeitsverteilung der grünen Nordlichtlinie zwischen Zenit und Horizont ausgeführt. Die Registrierungen hatten das Ziel, einen Beitrag zu der noch umstrittenen Frage der Emissionshöhe dieser Linie zu geben.

1. Photometer, Verstärker und Registriereinrichtung

Das benutzte Multiplier-Photometer ist in Abb. 1 dargestellt. Das Photometer bestand aus einem horizontal gelagerten Fernrohr von 75 mm Öffnung und 220 mm Brennweite, vor dessen Objektiv ein rechtwinkliges Prisma angebracht war, das durch einen Synchronmotor mit Getriebe um die optische Achse des Fernrohrs gedreht werden konnte und damit eine Abtastung des Himmels in Grosskreisen durch den Zenit ermöglichte. Im Brennpunkt befand sich ein Diaphragma 5 mm × 20 mm = 1,3° × 5,2°, hinter dem eine Feldlinse die Eintrittspupille auf die Photokathode eines Multipliers 1P21 abbildete. Zwischen Feldlinse und Multiplier konnten mit Hilfe eines Filterrevolvers verschiedene Interferenz- und Farbfilter eingeschaltet werden. Die Durchlässigkeitskurven der benutzten Interferenzfilter für 5577 AE und eine Vergleichswellenlänge (von der Firma Schott/Mainz) sind in Abb. 2 dargestellt; die Halbwertsbreiten der Durchlassgebiete betragen 100 bzw. 90 AE, die maximalen Durchlässigkeiten 34,0% bei 5590 AE und 39,0% bei 5340 AE. Die Spannungsversorgung des Multipliers geschah durch ein Netzgerät, das durch eine Glimmlampenstrecke und eine elektronische Regelschaltung doppelt stabilisiert war und die Betriebsspannung von 950 Volt auf ±0,05% konstant hielt. Der mit einer Doppeltriode 12 AT7 destückte Gleichspannungsverstärker, der der Anpassung des hochohmigen Multiplierausgangs an den niederohmigen Schreiber diente, besass einen Netzteil mit elektronischer Stabilisierung. Die Heizung erfolgte wegen der starken Netzschwankungen aus einem 6 V-Akku. Der Schreiber war zwischen die beiden

METEOROL.
8
956

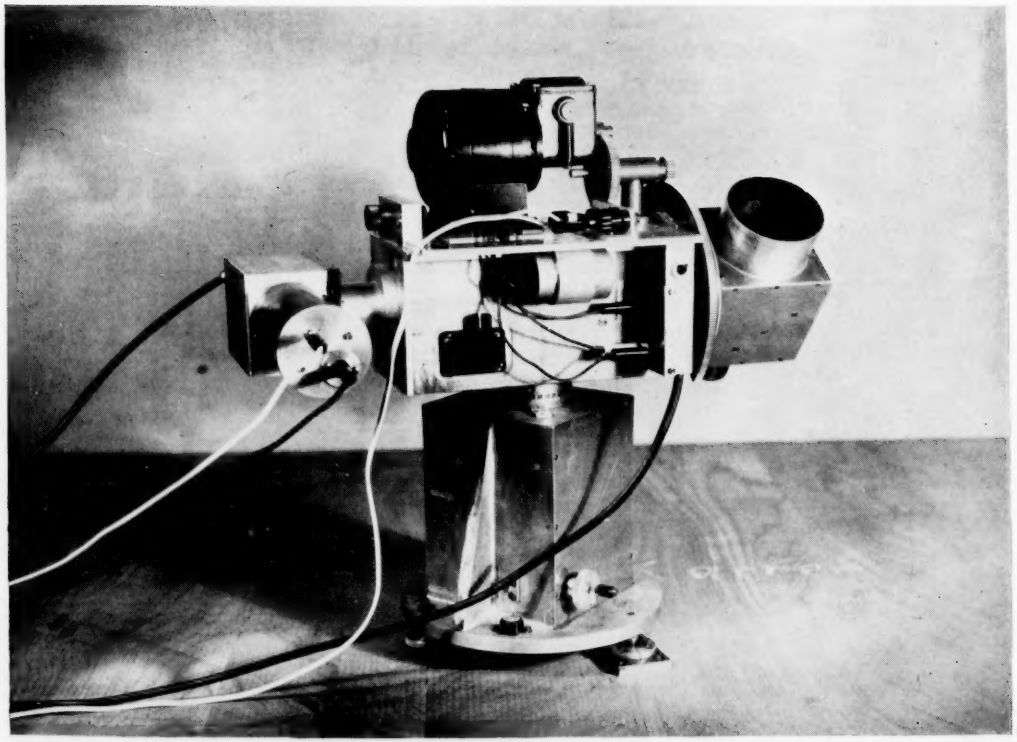

Abb. 1. Photographie des Multiplier-Photometers mit horizontaler optischer Achse. Rechts Gehäuse für das drehbare, vom Motor über eine Zahnraduntersetzung mit Kontaktrad für Höhenmarken angetriebene 90°-Prisma; links Gehäuse für Multiplier mit Spannungsteiler.

VOL.
8
1956

Kathoden der 12 AT7 geschaltet und auf der einen Seite geerdet. Die Arbeitswiderstände betrugen 10 oder 30 MΩ; sie wurden so gewählt, dass am Gitter der einen Triodenstrecke eine Spannung von 0,5–1 Volt lag; das Gitter der anderen

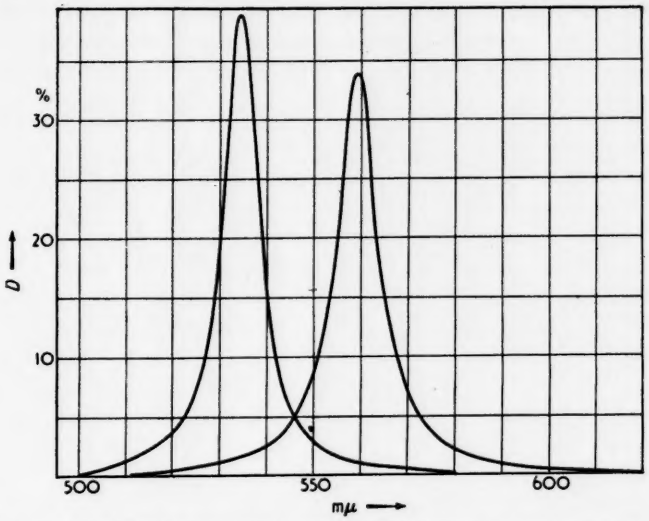

Abb. 2. Durchlässigkeitskurven der benutzten Schott'schen Interferenzfilter für 5577 AE und die Vergleichswellenlänge.

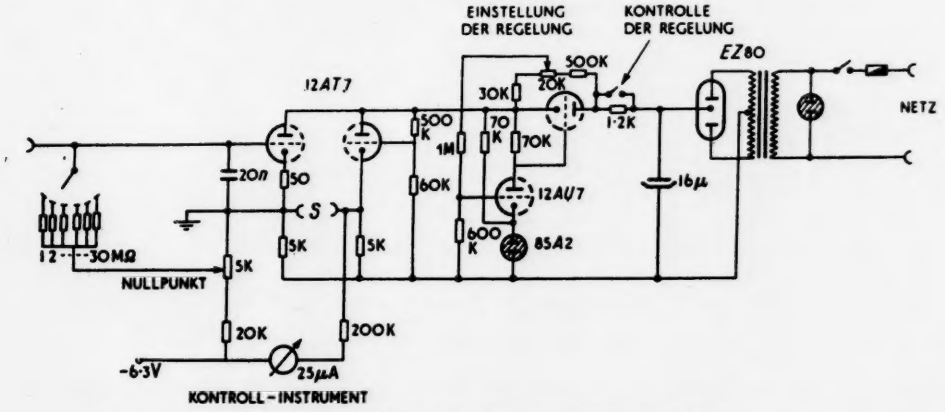

Abb. 3. Schaltskizze des Gleichspannungsverstärkers.

Triode befand sich auf festem Potential. Das Schaltbild ist in Abb. 3 wiedergegeben. Die Konstanz der Apparatur wurde durch Registrierungen einer auf die Eintrittsöffnung des Photometers aufsteckbaren radioaktiven Leuchtfolie vor und nach jedem Beobachtungssatz geprüft.

Als Schreiber diente ein Tintenschreiber von Siemens u. Halske mit einem Drehspulmesswerk von 1000 Ω Innenwiderstand, 2,4 Volt = 2,4 mA Endausschlag und einer Einstellzeit von 0,5 s. Der Schreiber war ausserdem mit einer elektromagnetischen Markiervorrichtung versehen, die dazu benutzt wurde, mit Hilfe

einer Kontaktvorrichtung an der Prismendrehung des Photometers Zenitdistanzmarken von 10° zu 10° auf die Registrierung zu geben. Die Dauer einer Registrierung vom Süd-Horizont über den Zenit bis zum Nord-Horizont betrug 4,5 Minuten. In Abb. 4 ist ein Beispiel einer Registrierkurve bei 5577 AE und der Vergleichswellenlänge 5340 AE gezeigt. Als ein gewisser Nachteil unserer Anordnung gegenüber der von ROACH und PETTIT (1951) beschriebenen könnte angesehen werden, dass die Registrierungen bei 5577 AE und der Vergleichswellenlänge

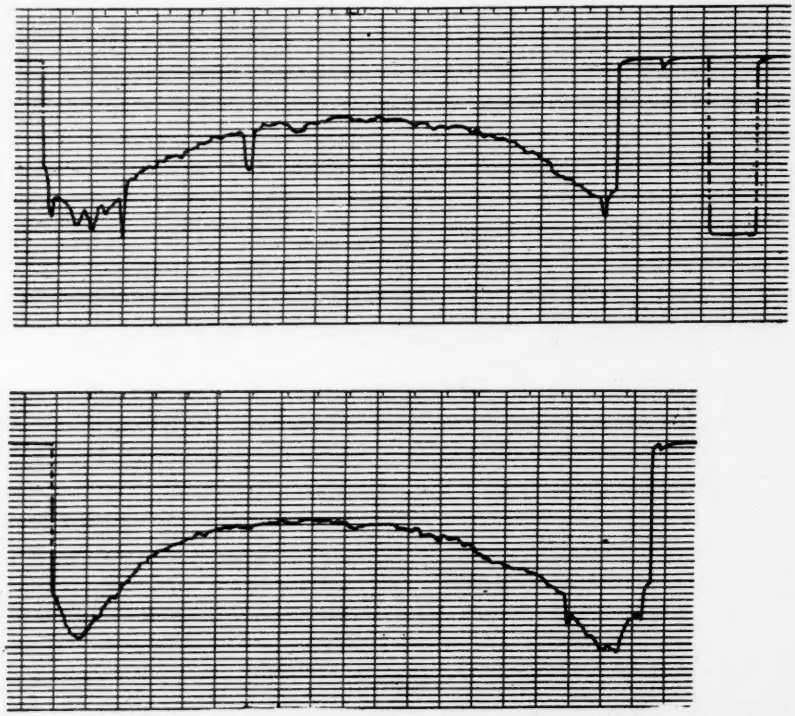

Abb. 4. Beispiel einer Registrierung 1955 März 2430 hr WZ. Obere Kurve 5577-Filter, Süd links, Nord rechts. Untere Kurve Vergleichsfilter, Nord links, Süd rechts; auf der linken Seite Radiumpräparat. Höhenmarken am unteren Rande der Registrierungen. Die stärkeren Schwankungen in der Nähe des Südhorizonts rühren von der Milchstrasse her.

nicht gleichzeitig geschehen, doch erfolgen die Helligkeitsschwankungen des Nachthimmelsleuchtens so langsam, dass die Zeitdifferenz von im Mittel 5 min zwischen den beiden Registrierungen keine merklichen Fehler bewirkt. Ein Vorteil unserer Anordnung ist das bessere Auflösungsvermögen in Zenitdistanz von ca 1,3° gegenüber ca 5° bei der Apparatur von ROACH und PETTIT.

2. DAS BEOBACHTUNGSMATERIAL UND SEINE AUSWERTUNG

Die Beobachtungen erfolgten in 10 Nächten zwischen dem 19.XI.54 und dem 13.III.55. Das Photometer stand auf der obersten Terrasse des Sphinx-Observatoriums (3575 m über N.N) neben der Kuppel; Netzgerät, Verstärker und Schreiber befanden sich in der Kuppel. Die Temperaturen in der Kuppel lagen zwischen

VOL.
8
1956

−10°C und −21°C, die Temperaturen am Photometer waren durchweg etwas niedriger.

Vor der Ausmessung der Registrierkurven wurde zunächst die untere Einhüllende gezeichnet, um die von den Sternen herrührenden Zacken der Kurven zu eliminieren. Die Ordinaten wurden für Zenitdistanzen $z = 0°$ bis 70° in Abständen von je 10°, von 70° bis 85° in Abständen von je 5° ausgemessen und durch Anbringung einer Korrektur, die die Linearitätsabweichungen von Schreiber und Verstärker berücksichtigt, in relative Intensitäten verwandelt. Bezeichnet man diese Intensitäten mit $I_1(z)$ für das 5577 AE-Filter und mit $I_2(z)$ für die Vergleichswellenlänge, so gilt, wenn $D_1(\lambda)$ und $D_2(\lambda)$ die aus den Durchlasskurven der beiden Filter und der Multiplierempfindlichkeit in den beiden Bereichen folgenden Gewichtsfunktionen sind:

$$\begin{aligned} I_1(z) &= I_0(z)\int D_1(\lambda)\, d\lambda + I_{5577}(z) \cdot D_1(5577) \\ I_2(z) &= I_0(z)\int D_2(\lambda)\, d\lambda \end{aligned} \tag{1}$$

Dabei ist vorausgesetzt, dass die Helligkeit des Himmelsuntergrundes $I_0(z)$ innerhalb des von den beiden Filtern überdeckten Spektralbereichs wellenlängenunabhängig ist. Damit folgt für die gesuchte Intensität der grünen Nordlichtlinie

$$I_{5577}(z) = \frac{1}{\beta}\left\{I_1(z) - \frac{\alpha}{\gamma} I_2(z)\right\} \tag{2}$$

wobei nach den Durchlass-Kurven Abb. 3 und dem bekannten Gange der Multiplierempfindlichkeit mit der Wellenlänge:

$$\begin{aligned} \beta &= D_1(5577) = 0{,}14 \\ \frac{\alpha}{\gamma} &= \frac{\int D_1(\lambda)\, d\lambda}{\int D_2(\lambda)\, d\lambda} = 0{,}753 \end{aligned} \tag{3}$$

Es ist nun zu untersuchen, wie 1. die Annahme eines wellenlängenunabhängigen I_0 und 2. die Messfehler in $I_1(z)$ und $I_2(z)$ die Genauigkeit der aus (2) resultierenden Werte für die Intensität der grünen Linie beeinflussen.

Setzen wir

$$I_0(\lambda_1) = I_0(\lambda_2) + \varepsilon \tag{4}$$

wobei λ_1 und λ_2 die effektiven Wellenlängen der beiden Filter sind, so ist der durch die Vernachlässigung der Differenz ε begangene Fehler in I_{5577}

$$\Delta I_{5577} = \frac{\alpha}{\beta}\,\varepsilon. \tag{5}$$

Zur Abschätzung von ε zerlegen wir die Untergrundshelligkeit I_0 in ihre drei Bestandteile Sternhintergrund I_S, in der Atmosphäre gestreutes Stern- und Zodiakallicht I_R und Zodiakallicht I_Z:

$$I_0(\lambda) = I_S(\lambda) + I_R(\lambda) + I_Z(\lambda) \tag{6}$$

und setzen entsprechend

$$\varepsilon = \varepsilon_S + \varepsilon_R + \varepsilon_Z. \tag{7}$$

Für ε_S folgt aus den Berechnungen des mittleren interstellaren Strahlungsfeldes

(Lambrecht 1955) eine Differenz der extraterrestrischen Intensitäten $I_S^*(\lambda_1) - I_S^*(\lambda_2) = -0{,}02 I_S^*(\lambda_2)$. Alle Registrierungen wurden bei dunstfreier Atmosphäre durchgeführt, so dass die Extinktion sich aus dem Rayleigh-Anteil (für den mittleren Luftdruck auf dem Jungfraujoch $b = 490$ mm Hg) mit den Schwächungskoeffizienten

$$a_R(\lambda_1) = 0{,}060 \qquad \text{und} \qquad a_R(\lambda_2) = 0{,}071$$

und dem Ozonanteil (bei 2,0 mm Dicke der Ozonschicht) mit

$$a_{O_3}(\lambda_1) = 0{,}024 \qquad \text{und} \qquad a_{O_3}(\lambda_2) = 0{,}017$$

zusammensetzt. Insgesamt ist also

$$a(\lambda_1) = 0{,}084 \qquad \text{und} \qquad a(\lambda_2) = 0{,}088,$$

und wir erhalten für die Zenitdistanzen 0° und 80°

$$\varepsilon_S(0°) = -0{,}004 I_S(\lambda_2)$$
$$\varepsilon_S(80°) = +0{,}005 I_S(\lambda_2)$$

Die bei einer extraterrestrischen Intensität I^* in der Atmosphäre durch Rayleighstreuung insgesamt gestreute Intensität ist in einer für unsere Zwecke hinreichenden Näherung

$$2 I_R(\lambda) = I^*(\lambda)\,(1 - e^{-a_R(\lambda)\cdot M(z)}). \tag{8}$$

Daraus folgt, wenn man berücksichtigt, dass $I^*(\lambda)$ sich aus Sternlicht und Zodiakallicht zusammensetzt und dass beide Anteile von gleicher Grössenordnung und in dem hier interessierenden Spektralbereich von gleicher Wellenlängenabhängigkeit sind:

$$\varepsilon_R(0°) = -0{,}012 I_S(\lambda_2)$$
$$\varepsilon_R(80°) = -0{,}046 I_S(\lambda_2)$$

Für ε_Z endlich erhalten wir aus den erwähnten Gründen die gleichen Werte wie für ε_S. Die Addition ergibt

$$\varepsilon(0°) = -0{,}020 I_S(\lambda_2)$$
$$\varepsilon(80°) = -0{,}036 I_S(\lambda_2)$$

Daraus folgt weiter, da $I_0 \approx 2 I_S$ (I_R kann gegen $I_S \approx I_Z$ vernachlässigt werden) und da nach (1) $I_0 = I_2/\gamma$,

$$\Delta I_{5577}(0°) = -0{,}010 \frac{\alpha}{\gamma} \cdot \frac{1}{\beta} I_2(0°)$$

$$\Delta I_{5577}(80°) = -0{,}018 \frac{\alpha}{\gamma} \frac{1}{\beta} I_2(80°)$$

Nun zeigen die Registrierungen, dass näherungsweise $I_2(0°) \approx 2\beta I_{5577}(0°)$ und $I_2(80°) \approx \beta I_{5577}(80°)$. Damit wird

$$\frac{\Delta I_{5577}(0°)}{I_{5577}(0°)} = -0{,}0151$$

$$\frac{\Delta I_{5577}(80°)}{I_{5577}(80°)} = -0{,}0135.$$

VOL. 8 1956

In das zur Bestimmung der Höhe der emittierenden Schicht benutzte Verhältnis der Intensitäten der grünen Nordlichtlinie in Zenit- und Horizontnähe geht also die Vernachlässigung von ε kaum ein. Andererseits ist zu bedenken, dass die ungleichmässige Verteilung der Sternhelligkeit und der Zodiakallichthelligkeit über den Himmel kleine zufällige Fehler bei der Bestimmung von I_{5577} bewirkt, deren Betrag nach den vorstehenden Abschätzungen aber unter 1% bleibt.

Die Genauigkeit der Werte für I_{5577} ist in der Hauptsache durch die Messfehler bei den Registrierkurven für $I_1(z)$ und $I_2(z)$ bestimmt. Bezeichnen wir mit σ^2 das Quadrat des mittleren Fehlers, so folgt aus (2)

$$\frac{\sigma^2(I_{5577})}{I^2{}_{5577}} = \frac{\sigma^2(I_1)}{I_1{}^2}\left(\frac{I_1}{I_1 - \frac{\alpha}{\gamma} I_2}\right)^2 + \frac{\sigma^2(I_2)}{I_2{}^2}\left(\frac{\frac{\alpha}{\gamma} I_2}{I_1 - \frac{\alpha}{\gamma} I_2}\right)^2 \tag{9}$$

Die mittleren Fehler $\sigma(I_1)$ und $\sigma(I_2)$ rühren her von der Einstellgenauigkeit des Schreibers ($\pm 1\%$ vom Vollausschlag) und von der Unsicherheit bei der Festlegung der unteren Einhüllenden, durch die der Einfluss einzelner hellerer Sterne ausgeschaltet werden soll. Diese Unsicherheit liegt im Mittel bei $\pm 1\%$ des Ausschlags. Der von der Einstellgenauigkeit herrührende Fehleranteil hängt von der Grösse des Ausschlages ab, insgesamt erhalten wir die folgenden mittleren relativen Fehler für I_1 und I_2:

$$\frac{\sigma(I_1)}{I_1} = \begin{cases} \pm 3{,}2\% & \text{für} \quad z = 0^\circ \\ \pm 1{,}8\% & \text{für} \quad z = 80^\circ \end{cases}$$

$$\frac{\sigma(I_2)}{I_2} = \begin{cases} \pm 3{,}8\% & \text{für} \quad z = 0^\circ \\ \pm 2{,}4\% & \text{für} \quad z = 80^\circ \end{cases}$$

Aus diesen Werten folgt mit $I_1 \approx 1{,}25 I_2$ für $z = 0^\circ$ und $I_1 \approx 1{,}5 I_2$ für $z = 80^\circ$ aus der Gleichung (9)

$$\frac{\sigma(I_{5577})}{I_{5577}} = \pm 9{,}8\% \quad \text{für} \quad z = 0^\circ$$

$$\frac{\sigma(I_{5577})}{I_{5577}} = \pm 4{,}3\% \quad \text{für} \quad z = 80^\circ$$

Zur Bestimmung der Emissionshöhen nach dem im folgenden Abschnitt geschilderten Verfahren wurden die Verhältnisse

$$\bar{q} = \frac{I_{5577}(70^\circ) + I_{5577}(75^\circ) + I_{5577}(80^\circ)}{I_{5577}(10^\circ) + I_{5577}(0^\circ) + I_{5577}(-10^\circ)} \tag{10}$$

für die Nord- und Südseite gebildet. Für den mittleren relativen Fehler eines solchen $\bar{q}$-Wertes ergibt sich dann

$$\frac{\sigma(\bar{q})}{\bar{q}} = \pm 6{,}2\%.$$

In Tabelle 1 ist das Beobachtungsmaterial zusammengestellt.

Tabelle 1. *Das Beobachtungsmaterial*

Datum	Uhrzeit WZ	$I_{5577}(0)$	$\bar{q}_N$	$\bar{q}_S$	Zenitextinktion
	h m				
1954 Nov. 19/20	22 46	20,7	3,55	2,44	
	23 25	27,0	2,58	1,78	
	0 04	27,7	2,48	2,10	0^m095
	0 42	24,8	2,45	2,50	
	1 16	21,8	3,04	2,49	
Nov. 21/22	19 56	13,3	2,76	2,24	
	21 05	12,0	2,31	2,41	
	22 06	13,6	2,59	2,56	0,095
	23 03	15,7	2,16	2,40	
	0 06	13,5	3,38	3,02	
	1 07	12,4	3,48	2,42	
Dez. 16	18 52	9,9	3,10	2,44	
	19 43	12,1	2,06	2,30	
	19 53	12,9	2,26	2,21	0,098
	21 57	11,0	2,46	2,34	
	22 38	11,0	2,58	2,49	
	22 49	11,6	2,24	2,72	
Dez. 17	18 35	9,1	2,52	2,23	
	19 16	8,5	2,52	—	0,098
	19 26	9,1	2,80	2,13	
	23 13	10,1	2,94	—	
Dez. 19/20	18 04	5,4	2,58	2,56	
	19 05	4,8	2,58	2,55	
	21 10	4,2	2,72	2,67	
	22 45	4,7	2,34	2,32	0,098
	0 15	5,4	2,72	3,28	
	1 09	5,9	2,72	2,17	
	1 20	6,0	3,16	2,76	
1955 Febr. 18/19	21 56	9,4	2,62	3,04	0,105
	1 15	12,3	2,22	2,81	
Febr. 26/27	23 34	12,5	2,80	2,60	
	0 28	17,6	2,56	—	0,101
März 2	2 30	16,3	1,94	2,69	0,090
	4 30	12,7	2,64	2,71	
März 3	3 15	20,4	2,87	2,14	0,090
März 13	22 45	17,2	2,82	2,07	0,098

VOL. 8 1956

Die zweite Spalte gibt die Zenithelligkeit der grünen Nordlichtlinie zur Zeit der Beobachtung, die beiden nächsten Spalten die $\bar{q}$-Werte für Nord- und Südhimmel und die letzte Spalte die aus gleichzeitigen Sternbeobachtungen mit einem Multiplierphotometer bei $\lambda_{\text{eff}} = 542$ mμ erhaltenen Zenitextinktionen für die betreffende Beobachtungsnacht in Grössenklassen.

Die mittleren Fehler der Extinktionen betragen $\pm 0^{\text{m}}004$. Die Zenitextinktion einer reinen Rayleigh-Atmosphäre beträgt bei $\lambda_{\text{eff}} = 542$ mμ für den mittleren Luftdruck auf Jungfraujoch 0,073 m, die Absorption für 2 mm Ozon 0,020 m und für 3 mm Ozon 0,030 m. Die festgestellten Extinktionsbeträge, die zwischen 0,090 m und 0,105 m liegen, lassen sich also durch das Zusammenwirken von Rayleighstreuung und Ozonabsorption für 2–3 mm Schichtdicke verstehen, eine nachweisbare Dunstextinktion war in den Beobachtungsnächten nicht vorhanden.

3. Höhenbestimmung der Emissionsschicht

Das Van Rhijn'sche Verfahren wurde unter Benutzung der von E. V. Ashburn (1954) berechneten Tabellen für den Einfluss der Rayleighstreuung und der Bodenreflektion angewandt. Den Ausgangspunkt bildet die Formel

$$q(z) = \frac{I_{5577}(z)}{I_{5577}(0)} = \frac{\dfrac{e^{-aM(z)}}{\sqrt{1-(R/R+H)^2 \sin^2 z}} + S(z) + A(z)}{e^{-a} + S(0) + A(0)} \tag{11}$$

Darin ist a der Schwächungskoeffizient, R der Erdradius, H die Höhe der emittierenden Schicht, $S(z)$ der in der Atmosphäre gestreute Bruchteil der Intensität $I_{5577}(z)$ und $A(z)$ der Einfluss der Bodenreflektion. Die Funktionen $S(z)$ und $A(z)$ sind von Ashburn unter Voraussetzung reiner Rayleigh-Streuung für mehrere Werte von a, für verschiedene Albedos des Bodens und für Emissionshöhen $H = 100$, 200, 300 km und ∞ berechnet worden. Seine Werte wurden für unsere Zwecke in a und H interpoliert (vgl. Abb. 5). Dabei wurde berücksichtigt, dass das a in der Formel (11) den gesamten Schwächungskoeffizienten (also einschliesslich der Ozanabsorption) bedeutet, wie er sich aus den Werten in Tab. 1 unter Umrechnung auf die Wellenlänge 5577 AE ergibt, während in den Termen $S(z)$ und $A(z)$ nur der Rayleigh'sche Streukoeffizient für 5577 AE eingeht. Für die Bodenalbedo wurde der Wert 0,5 angenommen, da zur Zeit der Beobachtungen die Umgebung des Beobachtungsorts grösstenteils mit Schnee bedeckt war; der Einfluss des Albedogliedes ist aber fast zu vernachlässigen.

Die Hauptschwierigkeit der Anwendung von Formel (11) zur Höhenbestimmung liegt darin, dass die Emissionsschicht nicht homogen ist. Die Helligkeitsverteilung in der Schicht und ihre zeitlichen Änderungen sind in verschiedenen Arbeiten von F. E. Roach und H. B. Pettit (1951, 1952), D. Barbier, J. Dufay und D. Williams (1951), und F. E. Roach, D. R. Williams und H. B. Pettit (1953) untersucht worden. Bei unseren Messungen zeigt sich der Einfluss der Helligkeitsschwankungen in den Werten $I_{5577}(0)$, die in den einzelnen Beobachtungsnächten im Mittel um $\pm 10\%$ streuen, während die Unterschiede von Nacht zu Nacht sehr viel grösser sind. Die Streuung in den Werten von $\bar{q}$ beträgt $\pm 11\%$, wobei aber keine systematischen Unterschiede zwischen den verschiedenen

Beobachtungsnächten und keine Korrelation zur Helligkeit der grünen Nordlichtlinie im Zenit festzustellen sind. Diese Streuung ist wesentlich grösser als die durch die Beobachtungsfehler verursachte. Zieht man den Anteil der Beobachtungsfehler ab, so verbleiben $\pm 9\%$ Streuung in $\bar{q}$, die von reellen Helligkeitsschwankungen herrühren. Die von uns während einer Nacht gefundenen zeitlichen

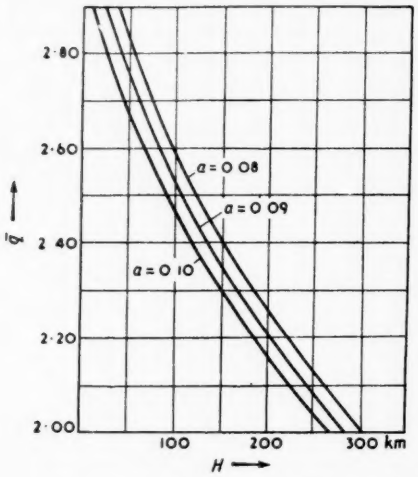

Abb. 5. Abhängigigkeit der Emissionshöhe vom Verhältnis $\bar{q}$ (Gleichung 10) für verschiedene Werte des Extinktionskoeffizienten a_{5577}.

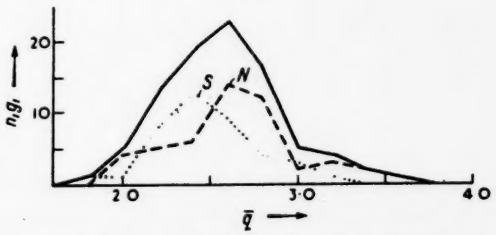

Abb. 6. Verteilungsfunktionen der gewichteten $\bar{q}$-Werte. Ausgezogen Gesamtmaterial, gestrichelt Nordseite, punktiert Südseite.

Helligkeitsschwankungen sind wesentlich kleiner als die von Roach und Pettit beobachteten. Die Ursache dafür könnte darin liegen, dass wir zu einer Zeit sehr geringer Sonnenaktivität gemessen haben, während die Beobachtungen von Roach und Pettit kurz nach dem letzten Aktivitätsmaximum erfolgten.

Die Helligkeitsunterschiede in der emittierenden Schicht machen die Bestimmung der Emissionshöhe aus Einzelbeobachtungen illusorisch; man kann aber erwarten, dass im Mittel über eine grössere Zahl von Beobachtungen die Schwankungen hinreichend ausgeglichen werden. Um von dem Augenblickszustand der leuchtenden Schicht möglichst frei zu kommen, wurden für die Höhenbestimmung die Werte $\bar{q}$ nach (10) benutzt. Innerhalb der erreichbaren Genauigkeitsgrenze ist die Mittelbildung der $q(z)$ und der $H(q)$ nach (11) vertauschbar.

Um die mittlere Emissionshöhe zu erhalten, wurden die beobachteten Werte $\bar{q}_N$ und $\bar{q}_S$ in Tabelle 1 mit Gewichten 0,5(2), 1(46), und 2(21) je nach der im Beobachtungsbuch vermerkten Güte der Beobachtungsbedingungen (Vorhandensein lokaler Wolkenfetzen, Eintrübungen am Horizont usw.) versehen. Die resultierenden Verteilungsfunktionen der $\bar{q}$ sind in Abb. 6 dargestellt. Es ergeben sich die folgenden gewichteten Mittel

$$\bar{q}_N = 2{,}64 \pm 0{,}052$$
$$\bar{q}_S = 2{,}48 \pm 0{,}044$$
$$\bar{q} = 2{,}57 \pm 0{,}038$$

Mit den auf gleiche Weise gemittelten Werten für die Zenitextinktionen folgen daraus nach Abb. 5 die mittleren Emissionshöhen

$$\bar{H}_N = 72 \pm 10 \text{ km}$$

$$\bar{H}_S = 112 \pm 13 \text{ km}$$

$$\bar{H} = 90 \pm 10 \text{ km}$$

Der Höhenunterschied zwischen Nord- und Südseite, der für das mittlere $z = 75°$ einer horizontalen Distanz von rund 1000 km entspricht, braucht nicht reell zu sein; er kann auch durch einen mittleren Helligkeitsanstieg von 6,2% auf 1000 km nach Norden in der Beobachtungsrichtung erklärt werden, der durch Nordlichteinflüsse hervorgerufen sein mag. Die Beobachtungsrichtung fiel angenähert mit einer Normalen auf den Kurven gleicher Nordlichthäufigkeit zusammen. Der Wert auf der Südseite verdient daher mehr Vertrauen als der Wert auf der Nordseite.

Die hier durchgeführte Höhenbestimmung aus dem Mittel der Einzelwerte von $\bar{q}$ ist angemessen, wenn man voraussetzt, dass die Streuung der $\bar{q}$ durch die räumlichen Helligkeitsunterschiede in der Emissionsschicht hervorgerufen wird. Will man stattdessen die Streuung in $\bar{q}$ auf Höhenunterschiede in der Emissionsschicht zurückführen, so müsste man zu jedem beobachteten $\bar{q}$ die Höhe ermitteln und dann aus der Verteilungsfunktion der Höhen die mittlere Emissionshöhe bestimmen. Wegen des Anstiegs von $dH/d\bar{q}$ mit abnehmenden q kommt man dabei zu einer stark unsymmetrischen Verteilungskurve der Höhen, auch müssen die $\bar{q} > 3{,}0$ ausgeschlossen werden, da sie zu Höhen $H < 0$ führen. Man erhält bei diesem Verfahren, bei dem Höhenbestimmung und Mittelbildung gegenüber dem ersten vertauscht sind, eine mittlere Höhe $\overline{H^*} = 130 \pm 9$ km, die ebenfalls noch der E-Schicht der Ionosphäre angehört.

4. Diskussion

Trotz der starken Streuung der Einzelwerte, die wegen der Wolkenstruktur der leuchtenden Schicht unvermeidlich ist, sprechen unsere Ergebnisse ganz eindeutig dafür, dass die Emission der grünen Nordlichtlinie im Nachthimmelsleuchten in oder knapp unter der E-Schicht der Ionosphäre stattfindet. Die nach der gleichen Methode gewonnenen Ergebnisse anderer Autoren, die von Bates und Dalgarno (1953) zusammengestellt sind, schwanken zwischen 100 km und 400–1000 km Höhe; Barbier (1952) nimmt 250 ± 30 km als die plausibelste Emissionshöhe an. Dagegen finden Amand, Pettit, Roach, und Williams (1955) durch Vorwärtseinschnitt der Wolkenstrukturen von zwei Stationen aus eine Emissionshöhe von 80–100 km, die mit unseren Werten übereinstimmt. Eine Emissionshöhe um 100 mk ist auch theoretisch zu erwarten, da (vgl. Bates und Dalgarno, 1953) nur in dieser Höhe die Konzentration der O-Atome gross genug ist, um die beobachteten absoluten Intensitäten der grünen Linie zu liefern. Die abweichenden Ergebnisse der früheren Höhenbestimmungen nach der V. Rhijn-Methode müssen im wesentlichen darauf zurückgeführt werden, dass keine individuellen Extinktionswerte für jede Beobachtungsnacht ermittelt, sondern hypothetische Extinktionskoeffizienten angenommen wurden. Amand,

Pettit, Roach, und Williams (1955) haben am Schluss ihrer Arbeit bereits darauf hingewiesen, dass eine kleine Vergrösserung des Extinktionskoeffizienten die nach der V. Rhijn-Methode bestimmte Emissionshöhe von 200 km auf 93 km zu reduzieren vermag. Mit dem Vorhandensein zusätzlicher Dunsttrübungen, die den Extinktionskoeffizienten über den Wert einer reinen Rayleigh-Atmosphäre vergrössern, muss man aber, ausser im Winter im Hochgebirge, stets rechnen.

Der Deutschen Forschungsgemeinschaft danken wir für die Bewilligung der Mittel für die Durchführung der Messungen am Jungfraujoch und für die Gewährung eines Assistentenstipendiums; der Verwaltung der Hochalpinen Forschungsstation sind wir für die Überlassung von Arbeitsplätzen und für die freundliche Unterstützung unserer Arbeiten ebenfalls sehr zu Dank verpflichtet.

Literatur

Amand, P. St., Pettit, H. B., Roach, F. E., u. Williams, D. R.	1955	*J. Atmosph. Terr. Phys.* **6**, 189.
Ashburn, E. V.	1954	*J. Atmosph. Terr. Phys.* **5**, 83.
Barbier, D.	1952	*Mém. Soc. Roy. Sci. Liège* **12**, 43.
Barbier, D., Dufay, J., u. Williams, D.	1951	*Ann. d'Astrophys.* **14**, 399.
Bates, D. R., u. Dalgarno, A.	1953	*J. Atmosph. Terr. Phys.* **4**, 112.
Lambrecht, H., u. Zimmermann, H.	1953	*Mitt. Univ.-Sternwark Jena Nr.* 13.
Roach, F. E., u. Pettit, H. B.	1955	*Mém. Soc. Roy. Sci. Liège* **15**, 562.
	1951	*J. Geophys. Res.* **56**, 325.
Roach, F. E., Williams, D. R., u. Pettit, H. B.	1952	*Mem. Soc. Roy. Sci. Liège* **12**, 13.
	1953	*J. Geophys. Res.* **58**, 73.

VOL. 8 1956

Journal of Atmospheric and Terrestrial Physics, 1956, Vol. 8, pp. 233 to 239. Pergamon Press Ltd., London

The crust as the possible seat of earth's magnetism

J. S. CHATTERJEE
Institute of Radio Physics and Electronics, Calcutta University, India

(*Received* 10 *November* 1955)

Abstract—The crust of the earth is discussed as a possible seat of the magnetization of the earth. It is shown that the temperature and pressure to which the crust (a thickness of about 20 km) of the earth is subjected, will make its magnetic mineral contents (e.g., magnetite) highly permeable. The shell can thus be magnetically saturated by a field of very low intensity of the order of 0·01 gauss. It is suggested that the magnetizing field is provided by the "ring current" formed in the space round the earth, during worldwide magnetic storms, as a result of the encounter of the solar neutral corpuscular beams (consisting of an equal number of positive and negative charges) with the earth-magnet. It is shown that an initially existing field of even one-hundredth of the present field is enough to build up the magnetization of the crust to saturation.

An explanation of the secular variation is also suggested as caused by the ring current trying to follow (with a lag) the wobbling motion of the magnetic axis round the geographical axis due to the diurnal rotation of the earth.

1. INTRODUCTION

THE origin of the magnetization of the earth is still imperfectly understood. It is not even known if the seat of magnetization is in the "core" or in the "crust" of the earth. Various theories have been proposed about the origin, but none appears to be satisfactory. The latest theories are those due to ELSASSER (1946–47) and to BULLARD (1949), according to which the seat is in the metallic fluid core of the earth, where electric currents are maintained by induction effects caused by the motion of the fluid in the magnetic field. The process resembles that occurring in a self-exciting dynamo, there being initially a feeble magnetization due to some cause. The fluid motion is ascribed to thermal convection caused by localized production of heat by radioactivity. However, the theory is still in an unsatisfactory stage, as is evident from the remark of BULLARD (1949) that "the arguments used still fall short of a proof that the mechanism postulated will produce a field."

In the present paper it is shown that the physical state of the crust of the earth—a thickness of about 20 km—is such that it provides a medium of very easy magnetization, and that as such the crust, rather than the core, may be regarded as the seat of the magnetization of the earth. It is assumed that, to start with, as in the induction theory, the earth by some process had been very feebly magnetized north–south. (A magnetization of the order 1/100th only—or even less—of the present value of magnetization will suffice.) It is then shown that the growth and decay of the magnetic field of the external "ring current" system, that is produced by the encounter of the neutral solar corpuscular streams with this very feebly-magnetized earth, will magnetize the highly-permeable crust to saturation after a few such encounters. The present state of magnetization of the earth may thus be satisfactorily explained.

2. MAGNETIC STATE OF THE CRUST

The crust of the earth is known to contain many magnetic materials such as magnetite, serpentine, basaltic rock, and other materials in sintered form. Iron

occurs in traces. Analysis of many samples of igneous rocks shows that magnetite—which is the most strongly ferromagnetic of the minerals present—accounts for 5% by weight (GUTENBERG, 1939). The crust is subjected to high pressure and is at a high temperature. We shall now show that, due to this high temperature (temperature below the Curie point) and pressure, the magnetic materials in the crust—in a shell some 20 km thick—will acquire very high permeability.

Near the surface of the earth the temperature increases by about 30°C per km. With this temperature gradient, the temperature at depths of 25 km will be near the Curie point of iron, 770°C. It may thus be assumed that, between 5 km and 25 km, there is a 20-km-thick shell in which temperature varies roughly from 180°C to the Curie point, with a mean temperature of about 500°C at the middle. At such temperature, for a ferromagnetic material, the magnetic crystal anisotropy will be small, though the specific magnetization will be a large fraction of that at 0°C. In this respect the hot shell will behave as being made of a material of low-anisotropy constant like permalloy. Again, it is known that, if a material having positive magnetostriction coefficient is compressed, all the domains in it are oriented in a direction normal to the direction of the stress, provided $\frac{3}{2}\lambda_s\sigma > K$, where λ_s is the saturation magnetostriction coefficient, σ is the stress, and K is the anisotropy constant (BOZORTH, 1951a). Now, in the middle of the 20-km-thick hot shell, $\sigma \doteqdot 37 \cdot 10^8$ dyne/cm^2 ($\doteqdot 37$ kg/mm^2) and λ_s (magnetite) $\doteqdot 10^{-6}$. The value of $\frac{3}{2}\lambda_s\sigma$ is therefore about $55{\cdot}5 \times 10^2$ dyne/cm^2. Hence, as K may be taken to be about 10 ergs/cm^3 or less, the above inequality is well satisfied in the hot shell. Thus, due to the effects of high pressure and temperature, the 20-km shell will behave as a material of high permeability being saturated at a very low field of the order of 0·1 to 0·01 gauss. Comparison may be made with the 68-permalloy which is saturated at about 0·1 gauss with a tensile stress of 2 kg/mm^2 (BOZORTH, 1951b).

Considering the direction of easy magnetization with regard to that of the stress, we note that, for materials having positive λ_s (iron, magnetite, etc.), the two are parallel for tensile stress and are at right angles for compression (pressure). Since λ_s for magnetite is positive, the direction of easy magnetization will be at right angles to the direction of applied pressure.

Further, the great pressure to which the shell is subjected will have an effect on the hysteresis loop, which becomes a rectangle. The remnant magnetization I_r will, therefore, be very nearly equal to the saturation magnetization I_s, i.e., $I_r \doteqdot I_s$. The case of 68-permalloy may be cited as an example. With a tensile stress of 2 kg/mm^2, the hysteresis loop becomes a rectangle, with $I_r = I_s$, measurement being made along the direction of the tension. The ferromagnetic compound magnetite has $I_s \doteqdot 490$ gauss. If it is subjected to such pressure as prevails at a depth of a few kilometres, the remnant magnetization will thus be close to I_s, and we may put $I_r \doteqdot I_s$. It is to be noted in this connection, that when the material is in the sintered form, the relation between I_r and I_s depends to a marked extent on the shape and size of the particle. For example, for randomly oriented ellipsoids, STONER and WOHLFARTH (1948) obtain $I_r = \frac{1}{2}I_s$. However, since in the shell the domains are not distributed randomly, but are all oriented normal to the radial direction, I_r will be very nearly equal to I_s, even in the sintered form. Regarding

VOL. 8 1956

the dependence on size, it has been shown by NEEL (1949) that, if the particles are smaller than a certain critical size, the coercive force decreases and stable magnetization is not possible. Large coercive force in the eruptive rocks (CHAPMAN and BARTELS, 1940) indicates that the particle size is such that permanent magnetization is possible. The exact value of I_r will depend, of course, on composition, temperature, pressure, and heat treatment, as well as on the particle size.

We now calculate the total magnetic moment of the 20-km shell due to the presence of magnetite alone, when a field is applied in a specified direction. With average density of 3 g/cm^3 of the shell, magnetite is 2·85% of the volume of the shell (the density of magnetite is taken as 5·25 g/cm^3). The remnant magnetization I_r per unit volume will therefore be 14·0 gauss. Since the domains are held firmly in the planes normal to the radial direction, the easiest direction of magnetization in the shell will be perpendicular to the radial direction. Hence, if a magnetic field directed north–south (the possible source of a magnetic field so directed is discussed in Section 3) is applied to the earth as a whole, the magnetization will not be uniform throughout the shell. For example, near the equator the shell will be saturated in the north–south direction, whereas near the pole the magnetization will be almost zero along the same direction. Taking this non-uniformity of the magnetization into account, the average magnetic moment per unit volume is found to be $14{\cdot}0 \times \pi/4 \doteqdot 11{\cdot}0$ gauss. (The factor $\pi/4$ is due to the averaging of the intensity of magnetization in the shell from equator to the pole.) We note that, if the total magnetization of the earth is confined to a 20-km-thick shell, the moment is 8 gauss per unit volume. Therefore, the estimated moment of the shell due to the presence of the observed quantity of magnetite can explain the observed magnetic moment of the earth. This non-uniform magnetization of the shell also easily explains the fact that, at high latitudes, the field deviates from the dipole-field.

It is to be remarked that, according to the assumed temperature gradient, the Curie point of magnetite (578°C) is reached at a depth of approximately 18 km. Hence it may be argued that the region of the shell beyond this depth would not contribute to the magnetization. It is, however, to be noted that, as calculated above, a shell-thickness of 14 km only is needed to explain the observed magnetic moment of the earth. It is also very likely that the assumed rate of increase of temperature does not persist below the depth of a few kilometres from the surface.

3. MAGNETIZING FIELD OF THE "RING CURRENT"

The problem now remains as to the nature and origin of the magnetizing field that would produce so uniform a magnetization of the crust in one direction. As mentioned in Section 1, this field, according to the author, is provided by the external current system in space (at a distance of 5 to 10 earth-radii from the centre of the earth) formed during worldwide magnetic storms. As is well known, such magnetic storms are associated with the encounter of beams of fast-moving charged particles emanated from the sun. The beam as a whole is electrically neutral, consisting of equal numbers of positively- and negatively-charged particles, but the particles become differentiated as the beam enters the magnetic field of the earth. Detailed study of the phenomenon of the encounter shows that, as the

beam sweeps across the earth, the electrodynamic forces developed produce a toroidal hollow round the earth-magnet. Charged particles cannot enter this hollow, and a sort of ring current is formed round the earth in the equatorial plane. This ring current may last for several days. Typical changes produced in the magnetic field on the surface of the earth during a storm (that is, during the period of the encounter of the beam with the earth and the formation of the ring current) are as follows: The storm begins with a sudden rise of the H value in the course of a few hours. The H value then falls rapidly to a value less than normal. It then gradually recovers to the normal value, taking a few days to do so. Fig. 1 shows the typical variation of the H field during the storm-time.

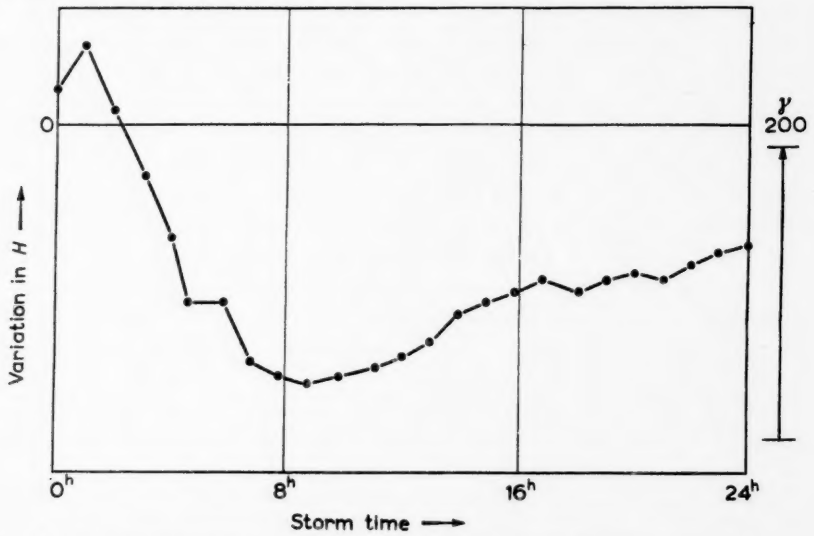

Fig. 1. Typical variation of magnetic intensity (averaged) during magnetic storm.
[From *Geomagnetism*, Vol. I, by CHAPMAN and BARTELS, page 277,
published by Oxford University Press (1940)]

Let us now consider the magnetizing effect on the crust of this varying magnetic field during the storm-period. The rapidly increasing and decreasing field during the earlier part of the storm will have little effect, because the shell will be shielded by the induced earth-currents flowing in the opposite sense immediately below the surface. After this sudden increase and decrease, however, during the slow recovery process the induced earth-current will be very small, and the shell will be acted upon by the field of the ring current, tending to magnetize it in the existing direction. Due to the high permeability of the 20-km shell, the flux passing through the earth will be short-circuited through this shell and for great storms producing 1500-γ change in field, the magnetizing field in the shell will be 2·55 gauss. (The field in the shell will be reduced, due to the demagnetization factor of the thin 20-km shell.) Hence the cumulative effect of the successive storms will magnetize the shell to saturation, even if it were not magnetized in the beginning. It may be noted that the field of 1500 γ associated with great storms is large enough to saturate the shell, as the field necessary to saturate may be as low as 0·01 gauss.

VOL. 8 1956

We are, however, to remember that the ring current is produced only because the earth is already a magnet. But the discussion below shows that, even if the earth were initially magnetized even to one-hundredth of its present intensity, the field of this feeble earth-magnet will have sufficient intensity to produce the ring current as a result of its encounter with the solar neutral corpuscular stream. To explain the present state of magnetization of the earth as the effect of the ring-current field, we may, therefore, assume that the earth by some process had been very feebly magnetized in the existing direction. The cumulative effect of the field of the magnetic storms will then soon magnetize the highly-permeable shell to saturation, resulting in the present observed magnetization.

We now discuss the possibility of a ring current being produced when the intensity of magnetization of the earth is a very small fraction (say 1/100) of the present value. For the present magnetic moment of the earth M_E, CHAPMAN (1954) concludes from cosmic-ray data that

$$M_r < M_E \ (\leq 0{\cdot}1) \tag{1}$$

where M_r is the moment of the ring.

Condition (1) implies

$$\left(\frac{R}{a}\right)^3 \leq \frac{H_0}{5H_\gamma} \tag{2}$$

where R = radius of the ring,

a = radius of the earth,

H_0 = geomagnetic field at the equator,

H_r = field of the ring at the centre of the earth.

When the magnetization of the earth is being built up, a similar relation is expected to hold, and hence

$$\left(\frac{R'}{a}\right)^3 \leq \frac{H'_0}{5H_r} \tag{3}$$

where the dashed symbols refer to quantities when the magnetization of the earth is being built up.

For $H'_0 = 0{\cdot}01 \times H_0$ and $H'_r = 10\,\gamma$

$$R' \leq 1{\cdot}72a.$$

If we assume $\dfrac{M_r}{M_E} \leq 0{\cdot}5$, for $H'_0 = 0{\cdot}01\ H_0$ and $H'_r = 100\,\gamma$, R will be $1{\cdot}44a$.

The cross-section of the ring will in this case be about one-hundredth of earth radius. Above considerations show that, even when the magnetic moment of the earth is one-hundredth of the present value, the ring current characteristic of the magnetic storm will be produced.

It may be noted that CHAPMAN (1932) has also suggested that magnetic storms should have some effect on the magnetization of the earth. However, an investigation on the results of many storms has not revealed any such effect. According to the present hypothesis, this is to be expected, because the crust is already magnetically saturated.

4. DISCUSSION

The theory as sketched above shows that the observed magnetic moment of the earth can be satisfactorily explained as due to the magnetization of the crust. There remains, however, the question of the inclination of the magnetic axis to the geographical axis. The origin of this may be due to the inhomogeneous distribution of magnetic matter in the crust. Let, for example, the initial field be along the geographical axis. The ring current produced by the effect of magnetic storm will then be in the equatorial plane. The magnetizing field due to this will tend to magnetize the crust along the geographical axis, but will actually magnetize it in the direction of the easiest susceptibility that may exist due to inhomogeneous distribution of magnetic matter in the crust.

The crust theory also offers a simple explanation of the secular variation. In the secular variation, it is only the non-dipole part of the earth's magnetic field that varies. The regular dipole field is not affected in any way. The general pattern of the variation is a rotation of the non-dipole field with varying speed (about 0·18° per year) in the westward direction (INGLIS, 1955). A possible explanation of the rotation may be as follows: due to the tilt of the magnetic dipole axis to the geographic axis, the former rotates in a conical path round the latter, west to east. Electromagnetic forces are thus set up between the rotating magnetic axis and the ring current in the equatorial plane. The ring current tends to follow the motion of the dipole axis, but it does so with a certain amount of lag. As a result, the magnetic axis of the ring current wobbles round the earth's magnetic axis, the axis of the ring current being inclined westward with respect to the dipole axis. Thus the magnetic matter in the crust, particularly in high latitudes, is subjected to a magnetic force which tends to rotate the direction of existing magnetization to the west. The integrated effect of all the storms during a year may therefore shift the general pattern of non-dipole field in the observed direction.

It is to be noted that, according to the above theory, the crust will be magnetized to saturation irrespective of any magnetization that may originate in the core, according to the induction theory. Further, since the highly-susceptible crust is saturated in the direction of the magnetic axis of the earth, core magnetization will have no effect in this direction, though the radial component of core magnetization may have some effect on crust magnetization. So it is possible that the core magnetization, if it exists, will thus contribute partly to the secular variation.

Acknowledgements—I take this opportunity of thanking Professor S. CHAPMAN and Professor L. F. BATES for going through the paper and offering a number of helpful criticisms. My sincere thanks are also due to Professor S. K. MITRA for many clarifying discussions during the preparation of the paper.

REFERENCES

BOZORTH, R. M. 1951a *Ferromagnetism*, D. Van Nostrand Co. Inc., p. 636.
1951b *Ferromagnetism*, D. Van Nostrand Co. Inc., p. 596.
BULLARD, E. C. 1949 *Proc. Roy. Soc.* **A197**, 433.
1949 *Proc. Roy. Soc.* **A199**, 413.

VOL.
8
1956

CHAPMAN, S.	1932	*Terrest. Mag.* **37,** 269.
	1954	*Proceedings of the Conference on Auroral Physics*, p. 367.
CHAPMAN, S. and BARTELS, J.	1940	*Geomagnetism*, Oxford University Press, Vol. I, p. 145.
ELSASSER, W. M.	1946	*Phys. Rev.* **69,** 106.
	1946	*Phys. Rev.* **70,** 202.
	1947	*Phys. Rev.* **72,** 821.
GUTENBERG, B.	1939	*Internal Constitution of Earth*, McGraw-Hill Book Co., p. 96.
INGLIS, D. R.	1955	*Rev. Mod. Phys.* **27,** 212.
NEEL, L.	1949	*Compt. rend.* **228,** 664–666.
STONER, E. C. and WOHLFARTH, E. P.	1948	*Phil. Trans. Roy. Soc.* (London), **A240,** 599–644.

OL.
8
956

Journal of Atmospheric and Terrestrial Physics, 1956, Vol. 8, pp. 240 to 246. Pergamon Press Ltd., London

Spread *F*-layer echoes and radio-star scintillation

R. W. WRIGHT,* J. R. KOSTER,† and N. J. SKINNER*

(*Received* 6 *September* 1955)

Abstract—Observations of radio-star scintillations made at University College of the Gold Coast, Achimota, and spread *F*-layers made at University College, Ibadan, Nigeria, have been compared. Considerable correlation is found, although there is 510 km between the two stations, and the ionospheric observations are made entirely at vertical incidence. The diurnal and seasonal variations of the presence of spread *F*-layers are examined. It is found that these depend considerably on the degree of magnetic disturbance. In particular, at Ibadan in winter on disturbed days there is only a quarter of the scatter that occurs on quiet days.

1. INTRODUCTION

CONSIDERABLE attention has recently been drawn to the study of irregularities of the ionosphere. In common with other equatorial stations (BOOKER and WELLS, 1938; WELLS, 1954; REBER, 1954), Ibadan experiences intense *F*-scatter at night throughout most of the year. In view of the results of RYLE and HEWISH (1950), establishing a correlation between the scintillation of radio stars and the occurrence of spread *F*-layers in temperate climates, a preliminary investigation has been made into the correlation between these parameters for two equatorial stations.

In view of the much longer sequence of ionospheric observations compared to that for the scintillation measurements, a detailed analysis of the occurrence of spread *F*-layers at Ibadan has also been included.

S	*Definition*	*Normal routine f_0F_2 designation*
3	No trace of group retardation. Much spread *F*	*F*
2	Slight trace of group retardation. Much spread *F*	e.g., (8·9)*F*
1	f_0F_2 easily measurable. Some spread *F*	e.g., 8·9*F*
0	No trace of scatter	e.g., 8·9

2. CORRELATION OF SPREAD *F* AND SCINTILLATION OF RADIO STARS

Routine *h'f* measurements have been made hourly at University College, Ibadan, Nigeria (lat. 7° 26′ N, long. 3° 54′ E, mag. latitude 2½° S), since December 1951. A special reduction of the records obtained has been made for occurrence of scatter.

* University College, Ibadan, Nigeria.
† University College of the Gold Coast, Achimota.

Each hourly record has been examined and assigned a number from 0 to 3 called the degree of scatter *S*. Such a scale of 3 is convenient, because certain fairly rigid definitions can be attached to each integral value. These are shown in the Table above, together with examples of the normal f_0F_2 designation in each case.

The separate reduction for *S* only was performed to ensure that no inconsistencies due to different observers and passage of time were present.

It is important to point out that no separation into *types* of scatter was attempted. In general, as will be discussed later, two types are observed regularly; namely, in DIEMINGER'S (1950) classification, 1*F* scatter and *G* scatter.

The corresponding hourly-fluctuation index for the scintillations of radio stars at Achimota, Gold Coast, (lat. 5° 32′ N, long. 0° 20′ W, mag. latitude 2½° S), was found from the radio astronomical records in the usual way.

Over the initial period from November 1953 to February 1954 the correlation coefficients between scintillation and scatter were very high—about 0·70 for one hundred pairs of values for the two variables. This is very highly significant, indicating a close relationship between the two phenomena, although the stations are separated by 510 km. Since both phenomena are confined to hours of darkness, values were taken only in the period 1900 hr to 0500 hr.

One would expect many different types of variations in such data, especially diurnal, seasonal, and solar (i.e., sunspot cycle). It seemed, therefore, that a closer comparison of all simultaneous records would be worth while, since the results might throw further light on the variations. The results of the comparison, including in addition the most recent records available, are summarized below.

Radio Star	*No.*	*Observations*		
		Date	*Time*	*Correlation coefficient*
Taurus	24	Nov. 1953–Dec. 1953	2400–0200	0·60
Taurus	35	Jan. 1954–Mar. 1954	1900–2200	0·17
Virgo	27	Jan. 1954–Feb. 1954	0200–0500	0·72
Virgo	32	Feb. 1954–Apl. 1954	2300–0200	0·33
Virgo	37	Apl. 1954–Jun. 1954	2000–2300	0·56
Cassiopeia	25	Nov. 1953–Dec. 1953	1900–2000	0·33
Cygnus	23	Jun. 1953–Jul. 1953	2300–0200	−0·13

Using the method outlined by FISHER (1948) for testing the significance of differences between observed correlation coefficients, one comes to the conclusion that, except for the last value tabulated (which will be considered further below) there is not sufficient evidence to conclude that all the samples are not drawn from equally correlated populations. If one makes the assumption that all the samples in the above data are drawn from equally correlated populations, the value of the correlation coefficient for that population is found to be 0·46 for 165 pairs of values, a result which is highly significant, even on the 0·1 per cent level.

There is, therefore, no significant variation of the observed correlations with

time or season, but some general observations can still be made. Firstly, one can expect comparatively low correlation coefficients for early evening hours, since scintillation sets in very abruptly and is often very violent at this time, lasting for several hours. One would expect the time of onset to differ for two such widely separated points, and hence the correlation coefficient to be comparatively low for the evening hours.

Secondly, one might expect to find seasonal fluctuations in the correlation coefficient. Any seasonal change in the occurrence of the ionospheric irregularities, as well as any change in the general direction of their drift, would have a pronounced effect on the correlation coefficient between two widely separated points.

Thirdly, it should be pointed out that the ionospheric sounding equipment gives information about the lower half of the *F*-layer at the zenith, whereas radio waves from a star must pass completely through the *F*-region, and possibly at a point very far from the zenith. Thus, waves from Cassiopeia pass through the *F*-region some 400 km to the north of the zenith point.

It should be finally noted that there are different kinds of spread *F*-layers, and in this study no account was taken of this fact. It seems quite probable that the different kinds would correlate quite differently with scintillation. The results obtained in June and July on Cygnus are believed to be rather dubious, due to a period of insensitive action of the ionospheric recorder. Spread *F*-layers invariably reduce the strength of the echo received. In this period many night-time records were obtained with no *F*-layer echo visible and had, therefore, to be disregarded, although normally sensitive equipment would probably have revealed spread *F*-layers.

The most significant result of these comparisons is the fact that the correlation coefficient remains as high as it does, in spite of the numerous factors which would tend to reduce it. This can only serve to emphasize the close connection between scintillation and spread *F*-layers at the equator, and would indicate that in Africa, at least, the disturbances are very widespread and uniform. It is in view of this strong correlation that the following more detailed analysis of a much longer series of spread *F*-layer observations was made. This should give a strong indication of the variations to be expected in radio-star scintillations when more measurements become available.

3. Diurnal and Seasonal Variations of Spread *F*

The occurrence of spread *F*-layers at Ibadan has been analysed over the period December 1951–December 1954, and Fig. 1 shows the average diurnal, or rather nocturnal, variation of scatter *S* for the three seasons. The seasonal variation is illustrated better in Fig. 2, where the average values of *S* between the hours of 2100 and 0300 hr inclusive are plotted for each month.

It will be seen that the diurnal variation is somewhat similar to that observed at Hawaii (Reber, 1954) and Huancayo (Wells, 1954) with a main maximum around midnight and slight signs of a pre-sunrise secondary maximum. Both these are slightly modified by the seasons. The seasonal variation shows a maximum of spread *F*-layers in local summer. This is also observed at Huancayo, but only in some stages of the sunspot cycle at Hawaii. It should be remembered, however, that at Ibadan measurements have only been made for three years.

VOL. 8 1956

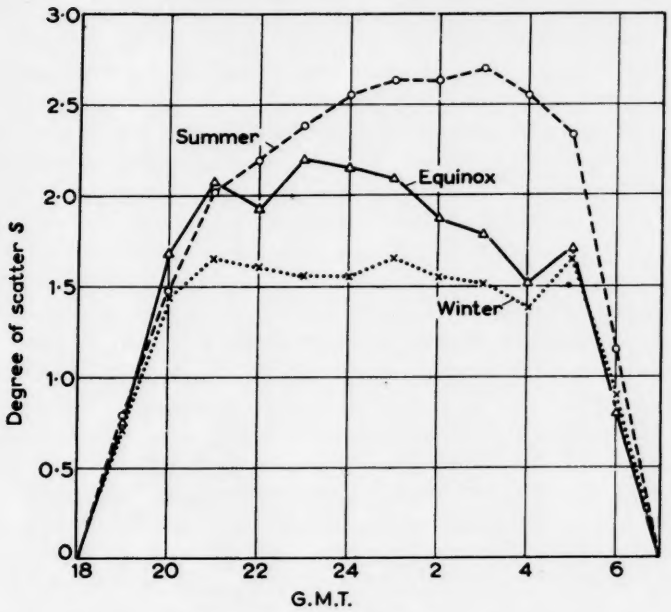

Fig. 1. Graphs of the nocturnal variations of presence of scatter for the three seasons at Ibadan.

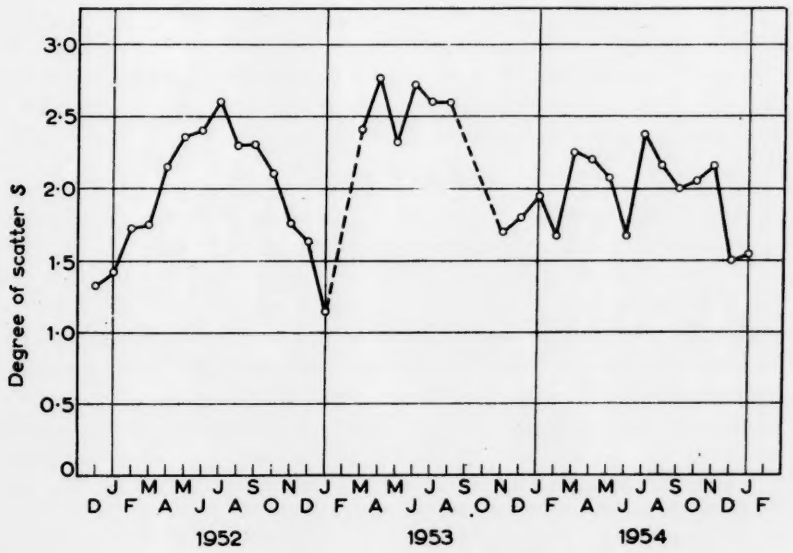

Fig. 2. Graph of mean monthly values of the degree of scatter *S* during the hours 2100–0300 inclusive.

4. Relationship with Magnetic Activity

Since magnetic disturbances have already been found to exert a considerable influence on ionospheric parameters of the F_2-layer at Ibadan (Skinner and Wright, 1955), a relationship was sought between S and the sum of the geomagnetic three-hour planetary indices K_p. For this purpose, the nights were divided into three groups according to whether K_p for the previous day had been $\leqslant 15$ (quiet), $16 \leqslant K_p \leqslant 30$ (moderately disturbed), or $\geqslant 31$ (disturbed).

Fig. 3 shows the nocturnal variation of scatter S for quiet days and disturbed days divided into three seasons. It will be seen in winter that for *increased* magnetic activity there is *decreased* scatter; a surprising result, since one normally associates spread F-layers with irregular or disturbed conditions. It implies that a spread F-layer is the normal state in winter, and that disturbed magnetic conditions cause the scatter to disappear.

In summer at Ibadan it will be noticed there is a slight suggestion of increasing S with increasing K_p, whilst during the equinoxes there is no significant difference.

Very little has previously been reported on a correlation of magnetic activity and scatter. Appleton, Naismith, and Ingram (1937) have commented briefly that in auroral regions the incidence of a magnetic storm causes the F-layer to rise, decrease in electron density, and become scattered. Hence, to this degree the dependence observed at Ibadan of S on K_p is in accord with the other properties of the F-layer, which show a reversal between temperate and equatorial places. In order to obtain some evidence on the phenomena in temperate regions more in line with that presented here, we have examined the occurrence of scatter S at Slough during the year 1952, as given in the Bulletin B published by the Radio Research Station. This year was chosen since there are roughly an equal number of quiet and disturbed days on the definition which we have used. The results are shown graphically in Fig. 4, where the nocturnal variation of S is plotted for the whole year on quiet and disturbed days. The separate seasonal graphs have been examined but show little departure from those of Fig. 4. There is consistently greater scatter on disturbed days than on quiet days.

5. Lunar Effects on Spread F

Tidal effects have been looked for in the data on a basis of division of the hourly values into lunar days, and also of daily values of scatter S with lunar age. No really significant result was obtained. There were signs of a diurnal lunar period of small amplitude giving maximum scatter at new moon, or with the moon at its nadir. This led to an analysis of the K_p figures with lunar age, and over the period concerned a most significant lunar diurnal variation was found with pronounced minimum at new moon. Hence, even if the variation of spread F-layers is significant, it still might be explained as a secondary effect following from the change of magnetic activity. The periodicity of the K_p figures with lunar age over the period used is presumably spurious, being due to the close similarity between the sun's rotation period and the lunar month.

6. Type of Scattering

Dieminger (1950) has distinguished four main types of scattering, of which two, the $1F$ and the G types, are regularly observed at Ibadan. G-scatter differs in

VOL. 8 1956

appearance from 1F-scatter in that reflections are received at higher frequencies than the normal penetration frequency for the layer. Frequently, the same ionospheric record shows 1F-scatter with the usual group retardation near the critical frequency together with G-scatter at higher frequencies. The G-scatter is apparently due to reflections from a disturbed zone not immediately overhead, whilst the

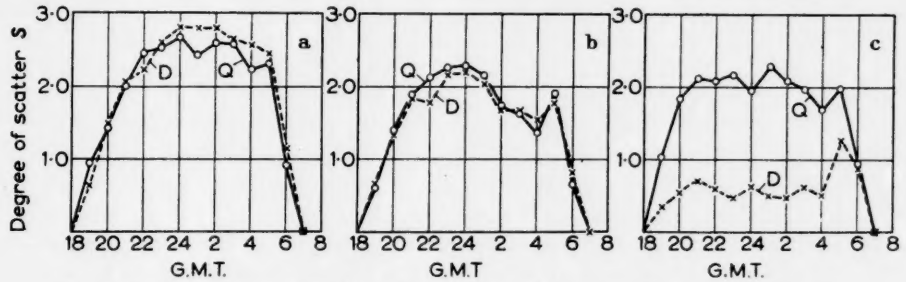

Fig. 3. Graphs to show the nocturnal variations of presence of spread F-layers on magnetically quiet (Q) and disturbed (D) days, for the three seasons.
(3) (a) Summer, (3) (b) Equinox, (3) (c) Winter.

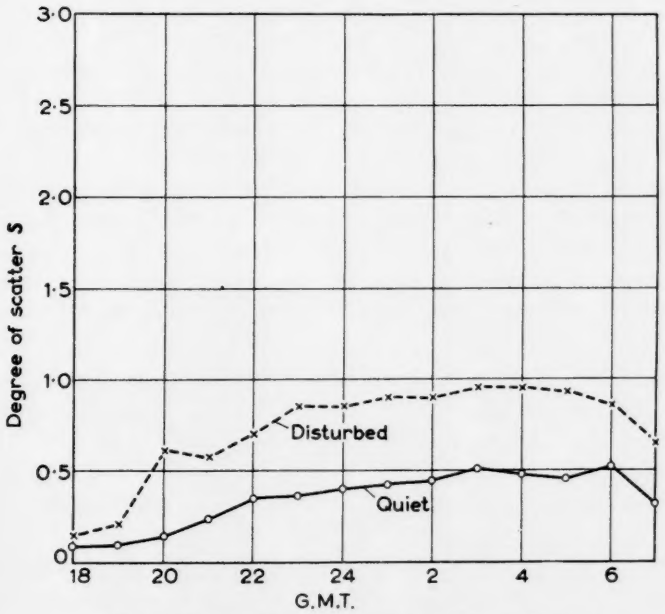

Fig. 4. Degree of scatter observed at Slough, England, on magnetically quiet and disturbed days in 1952.

1F-scatter has been attributed by NETZER (1940) to scattering of the wave by the E_s-layer.

We would suggest, however, that although the latter theory may explain the 1F-scatter to a small extent, the predominating scattering sources at Ibadan are irregularities in the F-layer. It follows that both types of scatter, 1F and G, are

probably manifestations of a single scattering process in the F-layer, G-scatter being followed by $1F$-scatter as the irregularities pass overhead. The suggestion by Netzer that a large proportion of $1F$-scatter is due to irregularities in the E-region is thought to be unlikely. Thus, although the presence of scatter is markedly correlated to magnetic activity, there is very little evidence of geomagnetic control of sporadic E in either temperate or equatorial latitudes. The reversal in sign of the correlation of scatter with magnetic activity from Ibadan to Slough further supports the theory that the scatter originates in the F-layer. It is well known that such an opposite correlation exists between the ionization density in the F-region and magnetic activity for equatorial and temperate regions.

Booker and Wells (1938) have suggested that there is a state of perpetual scatter in the upper regions of the F-layer, and that the variations of scatter actually observed with a vertical-incidence ionospheric recorder are due to changes in the amount of shielding by the F-layer. At Ibadan, we frequently observe a doubling of the normal F-layer echo on all frequencies immediately prior to the occurrence of spread echoes. The fact that this layer tilt or horizontal gradient of ionization immediately precedes scatter would suggest that the scattering sources are coming in laterally, and are not being unmasked, as Booker and Wells suggest.

7. Conclusion

From our observations on (a) the close correlation of scatter S with scintillation of radio stars, and (b) the high degree of dependence of S on magnetic activity (in winter at least), we suggest that it would be interesting to attempt a correlation of radio-star scintillation with magnetic activity. So far there are insufficient results for Achimota to analyse properly, but a preliminary attempt shows negligible correlation. Past investigations have been confined to temperate stations, and have also yielded negative results. If no correlation is found between scintillation of radio stars and magnetic activity at equatorial stations, this may indicate that spread F-layers may be divided into two types—one which is independent of magnetic activity and causes scintillation, and the other dependent on magnetic activity, but not producing scintillation.

Acknowledgements—We are most grateful to W. R. Piggott for much helpful discussion and advice on the subjects herein.

VOL.
8
1956

References

Appleton, E. V., Naismith, R., and Ingram, L. J.	1937	*Phil. Trans. Roy. Soc.* **236,** 191.
Booker, H. G. and Wells, H. W.	1938	*Terrest. Mag.* **43,** 249.
Brown, R. A.	1955	Private communication.
Dieminger, W.	1950	Proc. Conf. on Ionospheric Physics at Penn. State College. Part A, 175.
Fisher, R. A.	1948	*Statistical Methods for Research Workers.* (10th ed.). (Oliver and Boyd).
Netzer, T.	1940	*Hochfrequenztech. Elektroakerst.* **55,** 86.
Reber, G.	1954	*J. Geophys. Res.* **59,** 257.
Ryle, M. and Hewish, A.	1950	*Monthly Not. Roy. Astron. Soc.* **110,** 381.
Skinner, N. J. and Wright, R. W.	1955	*J. Atmosph. Terr. Phys.* **7,** 105.
Wells, H. W.	1954	*J. Geophys. Res.* **59,** 273.

Journal of Atmospheric and Terrestrial Physics, 1956, Vol. 8, pp. 247 to 259. Pergamon Press Ltd., London

Observations and analysis of ionospheric drift*

DONALD G. YERG
College of Agriculture and Mechanic Arts, University of Puerto Rico,
Mayaguez, Puerto Rico†

(*Received* 21 *November* 1955)

Abstract—Observations of radio fading at spaced receivers for 2·33 Mc/s and 4·57 Mc/s indicate that the ionospheric drift is more variable in winter than summer. Average speeds are 19 m/sec for 2·33-Mc/s records and 12 m/sec for 4·57-Mc/s records. Fading resulting from random changes is always significant. Random changes appear to be anisotropic and tend to rotate the correlation ellipse to a position along the magnetic field. The ellipse almost invariably is oriented with the major axis in the SW quadrant. The method of similar fades is less reliable than the correlation method in evaluating drift velocities and directions.

1. INTRODUCTION

RADIO fading records at three spaced receivers have been obtained at Mayaguez, Puerto Rico, on a routine basis for 2·33 Mc/s since February 1954 and for 4·57 Mc/s since April 1954. The observations have been made at two-hour intervals from 0800 to 1800 L.M.T. It is believed that the data for 2·33 Mc/s refer to the *E* region and for 4·57 Mc/s to the *F1* region at a height of approximately 200 km.

All records prior to June 1955 have been examined for similarity of maxima and minima, and 448 records for 2·33 Mc/s and 271 for 4·57 Mc/s were selected for analysis. Since a preliminary study indicated that the method of similar fades was always affected by random changes, so that the velocities were large when compared with the results of the correlation method (YERG, 1955), these records were used to determine only directions as a regular procedure.

The six-point correlation method has been employed on eighty-six records corresponding to 2·33 Mc/s and sixty-eight records for 4·57 Mc/s. Since the statistical burden is considerable and was performed with the assistance of a desk calculator, only a fraction of the total number of records available were analysed. The effort was concentrated on February and June records, so that examples of winter and summer data could be compared.

The purposes of this paper are to present a summary of the data, to compare the results of the method of similar fades with those of the correlation method, and to extend the concepts and applications of the methodology.

2. OBSERVATIONS OF IONOSPHERIC DRIFT

Vector diagrams for the ionospheric drift velocities are given in Figs. 1–4. The directions are given as the directions towards which the motion occurs. The velocities are in m/sec and are half the velocity of the moving ground pattern.

In winter, at 2·33 Mc/s, the drift tends to be toward W and SW, with a scattering of directions between NW and NE. At 4·57 Mc/s the drift is more or less

* The research reported in this paper has been sponsored by the Geophysics Research Division of the Air Force Cambridge Research Center, Air Research and Development Command under Contract No. AF 19(122)-476.

† Now with the Michigan College of Mining and Technology, Houghton, Mich.

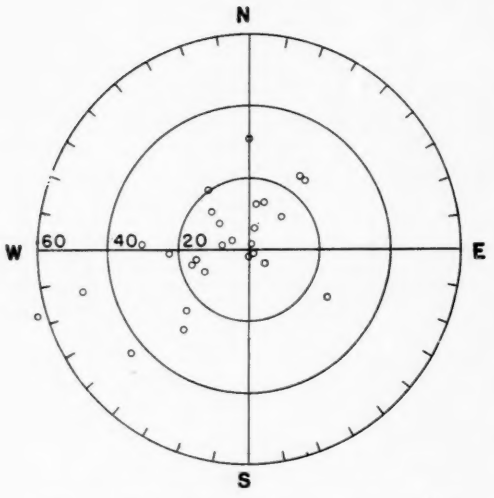

Fig. 1. Vector diagram for ionospheric drift velocities, m/sec, February 1954, obtained from 2·33-Mc/s records. (Drift is towards direction measured counter-clockwise from north.)

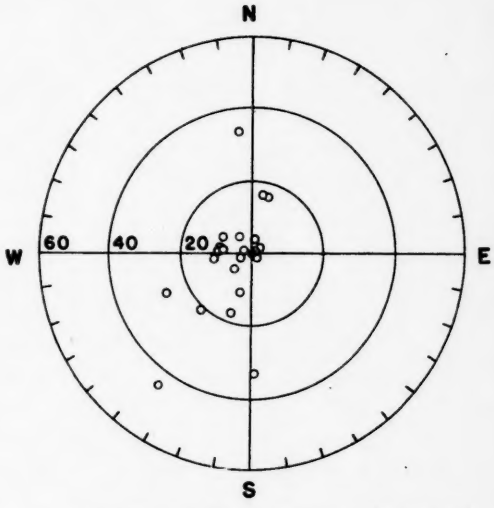

Fig. 2. Vector diagram for ionospheric drift velocities, m/sec, February 1955, obtained from 4·57-Mc/s records. (Drift is towards direction measured counter-clockwise from north.)

VOL.
8
1956

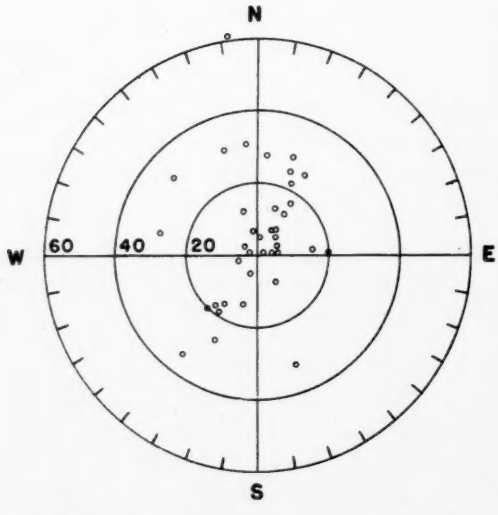

Fig. 3. Vector diagram for ionospheric drift velocities, m/sec, June 1954, obtained from 2·33-Mc/s records. (Drift is towards direction measured counter-clockwise from north.)

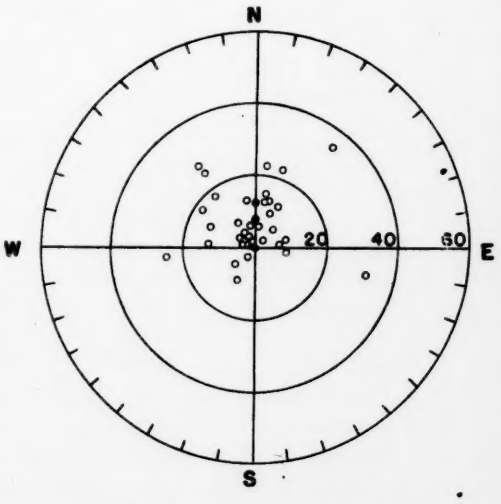

Fig. 4. Vector diagram for ionospheric drift velocities, m/sec, June 1954, obtained from 4·57-Mc/s records. (Drift is towards direction measured counter-clockwise from north.)

to SW, with a scattering of directions toward W to N. In summer the drift shows more definite tendencies at each frequency. At 2·33 Mc/s the drift is predominantly toward NNE, with a secondary trend toward SW. At 4·57 Mc/s only three of the twenty-six observations with speeds greater than 6 m/sec fall between WSW and ESE. The direction of drift is most predominantly between WNW and NNE.

Thus, the direction of drift seems to be more variable in winter than in summer at both levels. In season, the drift is in the same general direction for both frequencies, with the exception that a secondary preference toward SW exists for 2·33 Mc/s, and is nonexistent for 4·57 Mc/s.

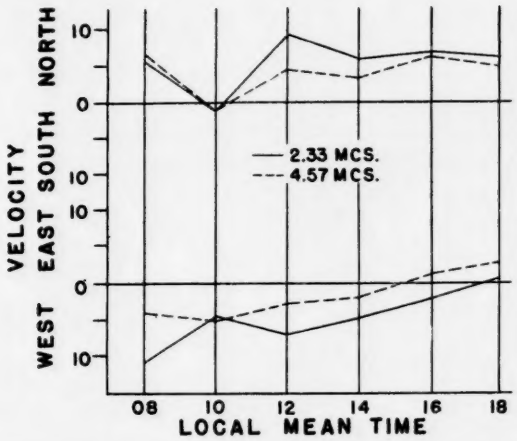

Fig. 5. Hourly mean values of ionospheric drift components, m/sec, obtained from 2·33-Mc/s and 4·57-Mc/s records. (Components are given for N–S and E–W directions.)

The mean speeds for 2·33 Mc/s are 20 m/sec in February, and 17 m/sec in June. For 4·57 Mc/s the mean speeds are 13 m/sec in February, and 12 m/sec in June. No seasonal variation in mean speed is evident, and the speed of drift in the *F1* region is somewhat smaller than in the *E* region.

Six observations in March and twelve in April were analysed for 2·33 Mc/s, and seven observations in April were analysed for 4·57 Mc/s. The results indicate that March data are associated with the winter pattern and April data with the summer pattern.

A plot of the hourly drift components shows a very wide scatter at all hours. No trend is clearly discernible by visual inspection. However, a plot of the hourly mean values does show a trend. The hourly means of the N–S and E–W components are shown for both frequencies in Fig. 5. The similarity of the curves for 2·33 Mc/s and 4·57 Mc/s is remarkable, and suggests that the mean drift corresponding to each frequency results from the same cause.

At 2·33 Mc/s the drift is 11·9 m/sec toward 63° W of N at 0800, becoming 4·6 m/sec towards 15° S of W at 1000. At 1200 the drift is 11·1 m/sec towards 37° W of N, becoming 7·5 m/sec towards 40° W of N at 1400, and shifting to 7·3 m/sec towards 17° W of N at 1600. The drift is 6·0 m/sec towards 5° E of N at 1800.

At 4·57 Mc/s the drift is 7·5 m/sec toward 33° W of N at 0800, becoming 5·2 m/sec toward 12° S of W at 1000. At 1200 the drift is 5·2 m/sec toward 33° W of N, becoming 3·8 m/sec toward 32° W of N at 1400, and shifting to 6·4 m/sec at 10° E of N at 1600. The drift is 5·6 m/sec toward 27° E of N at 1800.

The trend indicates that the mean wind is in the NW quadrant in the morning and shifts through N to the NE quadrant by late afternoon.

3. RANDOM CHANGES AND CORRELATION PATTERNS

The individual velocity V_i (YERG, 1955), or characteristic velocity (BRIGGS, PHILLIPS, and SHINN, 1950), is a measure of the fading due to random changes. The ratio V_i/V is a measure of the fading due to random changes relative to fading resulting from a drifting pattern. The correlation pattern is related to the mean signal intensity pattern on the ground, but may include the effects of anisotropic changes (YERG, 1955). The ratio a/b is the ratio of the major axis to minor axis of an elliptical correlation pattern. If the distance required for the spatial cross-correlation to decrease to 0·5 in a given direction is determined, the lengths of the major and minor axes may be found in metres, and are measures of the size of the ground pattern. Mean values of these quantities are given in Table 1.

Table 1. Data for random changes and correlation pattern
(V_i is in m/sec and a, the major axis, is in metres)

	2·33 Mc/s		4·57 Mc/s	
	February 1954	June 1954	June 1954	February 1955
V_i	70	92	55	73
V_i/V	2·0	3·3	2·5	3·7
a	371	325	155	219
a/b	2·2	1·8	1·8	1·8

The values of the individual velocity are somewhat larger for 2·33 Mc/s than for 4·57 Mc/s. The ratios for both frequencies show that random changes are dominant. The ratios are approximately the same, but the values are larger in summer for 2·33 Mc/s and larger in winter for 4·57 Mc/s. The ratio of major to minor axis is essentially constant in the mean and is somewhat larger in winter at both frequencies. Statistical significance tests with larger samples would be desirable.

The possibility of an association between the correlation pattern and random changes has been considered. For this purpose, frequency tabulations relating the individual velocity and the orientation of the elliptical correlation pattern to the ratio a/b are given in Tables 2 and 3. The orientation of the ellipse is given by the angle measured counterclockwise from N to the major axis. Values of $a/b \leq 1{\cdot}3$ are indicated by 0. Values such that $1{\cdot}4 \leq a/b \leq 1{\cdot}7$ are shown as a $-$, and values such that $a/b \geq 1{\cdot}8$ are shown by a $+$.

In the preparation of Table 2, five observations not shown had orientation angles less than 80 degrees, and two observations of this type were not shown in Table 3. Of these seven observations, four show $a/b \leq 1{\cdot}3$, and only one shows

VOL. 8 1956

Table 2. Frequency tabulation for elliptical correlation pattern as related to orientation and random changes. Data obtained from 2·33-Mc/s records. (θ is the angle measured counter-clockwise from north to the major axis of the ellipse. V_i is the individual velocity in m/sec, 0 refers to $a/b \leq 1{\cdot}3$, − refers to $1{\cdot}4 \leq a/b \leq 1{\cdot}7$, and + refers to $a/b \geq 1{\cdot}8$)

θ \ V_i	0–25	26–50	51–75	76–100	101–125	126–150	>150	Totals	
80–90		+ 0	−				−	1 2 1	4
91–100		+						1 0 0	1
101–110			+				++	3 0 0	3
111–120	0		+	+				2 0 1	3
121–130		+ −	+		+			3 1 0	4
131–140	−	+	− 0	+	0			2 2 2	6
141–150	+ −	+ 0	−	++ −		+	−	5 4 1	10
151–160		+ − − 00	++	+++ −	++ − −		0	8 5 3	16
161–170		+++ −	− 0	+ 0000	−	+ 0	+	6 3 6	15
171–180		+++	+ − 00	++	++	++ 0	++	12 1 3	16
181–190	0							0 0 1	1
Totals +	1	12	6	10	5	4	5	43	
Totals −	2	4	5	2	3	0	2	18	
Totals 0	2	4	4	4	1	2	1	18	
	5	20	15	16	9	6	8		79

Table 3. Frequency tabulation for elliptical correlation pattern as related to orientation and random changes. Data obtained from 4·57-Mc/s records. (θ is the angle measured counter-clockwise from north to the major axis of the ellipse, V_i is the individual velocity in m/sec, 0 refers to $a/b \leq 1{\cdot}3$, − refers to $1{\cdot}4 \leq a/b \leq 1{\cdot}7$, and + refers to $a/b \geq 1{\cdot}8$)

θ \ V_i	0–20	21–40	41–60	61–80	81–100	101–120	>120	Totals	
80–90	+ 0	 0			 0			1 0 2	3
91–100	+	++++	++ −					7 1 0	8
101–110	+ −−	−− 0	−−		+	 0		2 6 2	10
111–120	++	−		+	−			3 2 0	5
121–130		+ −−	+++ −	−	−			4 5 0	9
131–140	+	+ −	+ − 0	+	+			5 2 1	8
141–150		+	+ −	+				3 1 0	4
151–160	−			++				2 1 0	3
161–170	 0	−	 00	−	−−	 0	+ −	1 5 4	10
171–180							+ − 0	1 1 1	3
181–190	−							0 1 0	1
Totals +	6	7	7	5	2	0	2		
Totals −	4	7	6	2	4	0	2		
Totals 0	1	2	3	0	1	2	1		
	11	16	16	7	7	2	5		64

VOL. 8 1956

the angle between the major axis and either an E–W line or a N–S line to be greater than 18 degrees. In both tables a total of nine observations show the major axis to be within 10 degrees of one of the cardinal directions when oriented in the NW–SE quadrants. All the remaining observations fall within the SW quadrant. This tendency of the elliptical pattern for a preferred orientation is outstanding, and has no explanation.

Inspection of the two tables shows that the major axis tends to be near the N–S line for 2·33 Mc/s and near the E–W line for 4·57 Mc/s. At 2·33 Mc/s 61% of the + observations are within 30 degrees of a N–S line, and 16% are within 30 degrees of an E–W line. At 4·57 Mc/s, 45% of the + observations are within 30 degrees of an E–W line and 14% are within 30 degrees of a N–S line. These trends also hold for the — observations.

At 2·33 Mc/s, 22% of the 0 observations, 28% of the —, and 32% of the + observations are associated with values of $V_i > 100$ m/sec. At 4·57 Mc/s, 40% of the 0 observations, 32% of the —, and 31% of the + observations are associated with values of $V_i > 60$ m/sec. Either the data are insufficient to show a simple relation between elliptical contours and random changes at both frequencies, or the drift pattern and turbulence effects combine in varying proportions at the two levels to result in opposite trends.

At both frequencies there is a tendency for + observations associated with large values of V_i to fall near a N–S line. At 2·33 Mc/s the median value of the orientation angle for + observations associated with $V_i > 100$ m/sec is 165 degrees. The median value for all + observations is 153 degrees. At 4·57 Mc/s, the median value of the orientation angle for + observations associated with $V_i > 60$ m/sec is 145 degrees. The median is 121 degrees for all + observations.

These results suggest that large random changes are anisotropic, and tend to cause the correlation pattern to be oriented along the magnetic field.

4. Comparison of the Correlation Method and the Method of Similar Fades

It may be shown from the equations developed by Briggs, Phillips, and Shinn (1950) that the method of similar fades and the correlation method give similar results when the ratio V_i/V is small compared to unity. When this ratio is not small, the fading resulting from random changes is pronounced and the comparison of maxima leads to very large velocities.

The effect of random variations on the method of similar fades may be visualized by considering a simplified illustration. Let there be $m + n$ pairs of maxima for comparison. Suppose that m of these are associated with maxima in the mean signal pattern and have an average time difference $\overline{\delta t} = m^{-1}\Sigma\delta t$, and that n pairs are spurious maxima associated with random changes of sufficiently large scale to appear similar at the two receivers with an average time difference $\overline{\delta t'} = n^{-1}\Sigma\delta t' = 0$. The method of similar fades assumes that the average time difference appropriate for a velocity computation is $\overline{\delta t}$. However, the m pairs of maxima and the n pairs of maxima cannot be distinguished in any given set of records, so that the average time difference is $(m + n)^{-1}\ \Sigma(\delta t + \delta t') = (m + n)^{-1}\ \Sigma\delta t$. This time difference is smaller than $\overline{\delta t}$, and leads to larger velocities.

A total of sixty-five observations have been analysed simultaneously by the correlation method and by the method of similar fades. Of these, thirty-seven are for 2·33 Mc/s and twenty-eight are for 4·57 Mc/s. The results are summarized in Table 4. The method of similar fades shows much larger mean velocities and a much wider range of velocities. These results can be expected, since the ratio V_i/V is usually larger than unity.

A comparison of mean values by the two methods at the two levels indicates that the drift velocity decreases with height in summer. A similar comparison for winter shows that the correlation method again indicates that the drift velocity decreases with height, but that the method of similar fades results in a drift velocity increasing with height. This conclusion by the method of similar fades is a result of the increased importance of the ratio V_i/V, and is an example of an erroneous conclusion based on the incorrect assumption of negligible contributions of random changes.

Table 4. Comparison of ionospheric drift velocities, m/sec, obtained by the correlation method and the method of similar fades from 2·33- and 4·57-Mc/s records.

Month	Number obs.	Correlation method		Method of similar fades		Turbulence ratio	
		Range	Average	Range	Average	Range	Average
			2·33 Mc/s				
January, February, March, 1954	21	6–103	28	25–215	102	0·2–6·3	2·2
April, June, 1954	16	6–65	31	50–179	106	0·3–7·2	2·3
			4·57 Mc/s				
April, June, 1954	14	2–32	13	23–139	67	0·2–5·8	2·7
February, 1955	14	1–44	13	11–188	126	0·7–9·8	4·0

A comparison of all available data shows that the general conclusions regarding directions in winter and summer are essentially similar by both methods. However, differences in detail appear. For example, the polar frequency diagram at 2·33 Mc/s shows that the drift obtained by correlation analysis tends to NNE, and that the drift obtained by comparison of similar maxima is towards E or ENE.

At least two factors may effect small systematic differences between the two methods. The first of these is the shape of the mean signal pattern. RATCLIFFE (1954) and NEWSTEAD (1954) have shown that the line connecting points in the pattern where maximum signal intensity is to be observed by particular stations is determined by lines drawn in the direction of drift and tangent to the isopleths of signal intensity, and that this line is not at right angles to the direction of drift for particular pairs of similar fades. Correlation analysis shows that the mean pattern is elliptical and that the direction of drift is not at right angles to either axis or to

VOL. 8 1956

a line of maxima obtained by drawing tangents. Since the method of similar fades assumes the motion to be at right angles to this line of maxima, and since the ellipse tends to have a preferred orientation, systematic errors in the method of similar fades may be expected to occur.

It has been suggested that the effect of large random changes is anisotropic and tends to rotate the mean ellipse towards a N–S line. A line drawn at right angles to the line of maxima, in general, tends to be rotated towards an E–W line. Then large random changes may be expected to cause analysis by the method of similar fades to show a tendency to be directed towards E and W rather than N and S.

Mean velocity vectors have been obtained from observations evaluated simultaneously by both methods. The correlation method was taken as the standard, and the data were sorted by quadrant. The average components were found, and the resultant was determined. Records with velocities less than 6 m/sec were rejected as unreliable for a comparison of directions. The results are shown in Table 5. The angles are measured counterclockwise from N.

Table 5. Comparison of directions of ionospheric drift obtained by the correlation method and the method of similar fades from 2·33- and 4·57-Mc/s records. (Drift is towards direction measured counterclockwise from north)

Quadrant	Number obs.	Correlation method	Method of similar fades
	2·33 Mc/s		
NW	13	29	65
SW	11	121	111
SE	2	220	247
NE	8	338	290
	4·57 Mc/s		
NW	3	48	62
SW	8	153	149
SE	1	256	202
NE	9	346	345

Of the eight pairs of mean values, one was based on a single observation and one shows a negligible difference of one degree. Each of the remaining six pairs shows that the method of similar fades is associated with the smaller angle with an E–W line. The average difference is 23 degrees, 1 point of a 16-point compass. This difference may be regarded tentatively as systematic.

The effect of the ground pattern or random changes on particular observations may be considerable. If the mean ground pattern is a pronounced ellipse with major axis oriented N and S, a shift in the direction of drift from NNE to NNW might appear as a shift from ENE to WNW when analysed by the method of similar fades. The presence of large random changes make analysis based on a small sample, say fewer than thirty pairs of maxima, to be unreliable for any single observation.

5. DERIVATION OF DRIFT VELOCITIES

The time variation of signal intensity $\delta R/\delta t$ observed in a co-ordinate system moving with velocity components V_x and V_y is given by

$$\delta R/\delta t = \partial R/\partial t + V_x\, \partial R/\partial x + V_y\, \partial R/\partial y \tag{1}$$

where $\partial R/\partial t$, $\partial R/\partial x$, and $\partial R/\partial y$ refer to a stationary system. Multiply this equation by $\partial R/\partial x$ and take a time-average. There results

$$\overline{(\partial R/\partial x)(\delta R/\delta t)} = \overline{(\partial R/\partial x)(\partial R/\partial t)} + V_x\, \overline{(\partial R/\partial x)^2} + V_y\, \overline{(\partial R/\partial x)(\partial R/\partial y)} \tag{2}$$

A similar operation involving $\partial R/\partial y$ yields

$$\overline{(\partial R/\partial y)(\delta R/\delta t)} = \overline{(\partial R/\partial y)(\partial R/\partial t)} + V_x\, \overline{(\partial R/\partial x)(\partial R/\partial y)} + V_y\, \overline{(\partial R/\partial y)^2} \tag{3}$$

Assume that

$$\overline{(\partial R/\partial x)(\delta R/\delta t)} = \overline{(\partial R/\partial y)(\delta R/\delta t)} = 0 \tag{4}$$

Then equations (2) and (3) can be solved for V_x and V_y in terms of quantities measured in a stationary co-ordinate system.

Let the signal pattern be represented by

$$R(x, y, t + \tau) = R(0, 0, t) + (\partial R/\partial x)x + (\partial R/\partial y)y + (\partial R/\partial t)\tau \tag{5}$$

Assume that the mean value and standard deviation are observed to be the same at every fixed position. Add and subtract the mean value from the left and transfer $R(0, 0, t)$ to the left of (5). Square both sides and divide by the square of the standard deviation. Take a time average. The left side can be arranged to form three terms which are correlation coefficients. Two of these terms equal unity and the third is $\rho\,(x, y, \tau)$, the correlation of a record obtained at x, y with respect to a record at the origin after a relative time-shift τ has been effected. Solving for $\rho\,(x, y, \tau)$ gives

$$\rho(x, y, \tau) = 1 + Ax^2 + B\tau^2 + Cy^2 + 2Hx\tau + 2My\tau + 2Nxy \tag{6}$$

where

$$\begin{aligned} A &= -\overline{(\partial R/\partial x)^2}/2\sigma^2 & H &= -\overline{(\partial R/\partial x)(\partial R/\partial t)}/2\sigma^2 \\ B &= -\overline{(\partial R/\partial t)^2}/2\sigma^2 & M &= -\overline{(\partial R/\partial y)(\partial R/\partial t)}/2\sigma^2 \\ C &= -\overline{(\partial R/\partial y)^2}/2\sigma^2 & N &= -\overline{(\partial R/\partial x)(\partial R/\partial y)}/2\sigma^2 \end{aligned} \tag{7}$$

After substitution of (7) into (2) and (3), it can be shown that

$$\begin{aligned} V_x &= (CH - MN)(AC - N^2)^{-1} \\ V_y &= (AM - HN)\,(AC - N^2)^{-1} \end{aligned} \tag{8}$$

Equation (8) is identical with the equations found for the drift velocity in the previous discussion of the six-point correlation method (YERG, 1955).

The purpose of correlation analysis in this development is to determine the mean values of products of derivatives. The definition of the velocity components

VOL.
8
1956

is not the result of correlation terminology, nor is the linear assumption of (5) an inherent requirement. Higher-order terms could be included in (5) and would lead to a more accurate evaluation of (7). Equations (2) and (3) are very general, and the physical interpretation of the velocity components is determined through relations such as (4) involving the variations observed in the moving co-ordinate system. The particular significance of (4) can be seen with the aid of correlation surfaces.

If $\rho(x, y, \tau)$ is held constant, equation (6) represents an ellipsoid. The relation of the average values of products of first derivatives to the coefficients determining this surface should be noted. Let

$$\partial R/\partial x = \Delta R/\Delta x + \delta R/\delta x \tag{9}$$

where $\Delta R/\Delta x$ is the space variation of the mean signal pattern, and $\delta R/\delta x$ is the space variation of a superimposed turbulence pattern. Let similar relations hold for the other derivatives. The correlation surface for the turbulence pattern would be of the form of (6), where quantities related to turbulence may be designated with a prime mark. The coefficients for the correlation surface related to the turbulence pattern would be given by (7), where the partial derivatives would be replaced by $\delta R/\delta x$, etc.

If the mean turbulence pattern is isotropic, the correlation surface must be a sphere, and $H' = M' = N' = 0$. If the mean turbulence pattern is anisotropic in the x, y plane, so that fluctuations progress more in one direction than another but have the same time duration, $N' \neq 0$, and the correlation contour in the x, y plane is an ellipse. Also, $H' = M' = 0$. From (7) it is seen that the condition $H' = M' = 0$, which may be expected in isotropic or anisotropic turbulence of the type described, implies that

$$\overline{(\delta R/\delta x)(\delta R/\delta t)} = \overline{(\delta R/\delta y)(\delta R/\delta t)} = 0; \tag{10}$$

if the turbulence fluctuations are independent of the mean signal pattern

$$\overline{\left(\frac{\Delta R}{\Delta t}\right)\left(\frac{\delta R}{\delta t}\right)} = 0,$$

and similar results hold for other combinations of derivatives. There follows, from results comparable to (9) and (10), that

$$\begin{aligned} \overline{(\partial R/\partial x)(\delta R/\delta t)} &= \overline{(\delta R/\delta x)(\delta R/\delta t)} = 0 \\ \overline{(\partial R/\partial y)(\delta R/\delta t)} &= \overline{(\delta R/\delta y)(\delta R/\delta t)} = 0. \end{aligned} \tag{11}$$

These equations are the assumption of (4).

Thus V_x and V_y, as given by (8), represent the velocity components of a moving co-ordinate system selected, so that observed changes in signal intensity are those representative of a random turbulence pattern. This turbulence pattern may be anisotropic in space. If the mean signal pattern is assumed to be unchanging, the velocity components are those of a steady drift. The magnitude of this drift,

evaluated by correlation analysis, is not affected by isotropic turbulence or anisotropic turbulence of the type assumed.

This discussion shows that the results of the correlation analysis are more reliable in magnitude and direction than the results of the method of similar fades when large random changes are present.

6. THE MOTION OF FOURIER COMPONENTS

If a Fourier analysis is made for each record obtained at several receivers close to the origin, each component is given by

$$R_n(x, y, t) = \alpha_n(x, y) \sin [2\pi nt/\tau + \phi_n(x, y)] \tag{12}$$

where τ is the length of record examined, and α_n and ϕ_n are the amplitude and phase, and may vary from receiver to receiver. The nature of the analysis precludes a time variation during the interval. The average values of the products of derivatives of R_n may be evaluated by assuming linear variations of amplitude and phase. After substitution in (2) and (3), the vector velocities of a pattern associated with each Fourier component with a given frequency can be found.

This procedure was performed for four sets of observations. The Fourier analysis was done with the aid of a desk calculator using forty eight ordinates spaced approximately $1\frac{1}{2}$ sec apart. The velocity vectors plotted on a polar diagram showed considerable scatter for all four sets of observations. However, a tendency for the tips of the vectors to fall on or about a straight line was noted for the observation of 9 June 1954 at 0800. A similar tendency, though not so evident, was noted for the record of 11 June 1954 at 1400. No trends could be identified for the records of 8 June 1954 at 1400 or 10 June 1954 at 1000.

The average time between successive maxima was 7 sec for the record of 9 June and 10 sec for 11 June. The mean period was 15 sec for 8 June and 39 sec for 10 June. The individual velocity and turbulence ratio were 90 m/sec and 3·2 for 9 June, 90 m/sec and 2·6 for 11 June, 59 m/sec and 0·9 for 8 June, and 36 m/sec and 2·8 for 10 June. The drift velocity for 10 June was 6 m/sec, so that the ratio is fairly large even though the individual velocity is smaller than average. The four records are for 2·33 Mc/s.

It is interesting to note that the two records showing the greatest scatter of velocity vectors are associated with the longer mean periods and the smaller values related to random changes.

7. CONCLUSIONS

The ionospheric drift evaluated by the correlation method is more variable in winter than in summer. In winter the drift tends toward SW at both levels associated with 2·33-Mc/s and 4·57-Mc/s records. In summer the drift is almost invariably towards northerly directions for 4·57 Mc/s, and for 2·33 Mc/s is towards NNE with a secondary trend towards SW. The velocities show no seasonal variation of mean values, and average 12 m/sec for 4·57 Mc/s and 19 m/sec for 2·33 Mc/s.

Hourly values of the drift components show a wide scatter at any given hour, but the mean values show an almost identical trend at both frequencies. The

VOL.
8
1956

average drift is towards NW in the morning, shifting through N to NE in the late afternoon.

The ratio of the major axis of the correlation ellipse to the minor axis averages about 1·8 for both 2·33 Mc/s and 4·57 Mc/s, indicating that the correlation pattern is frequently elliptical. The major axis of the ellipse is almost invariably in the SW quadrant. At 2·33 Mc/s the major axis tends to be near a N–S line and at 4·57 Mc/s it tends to be near an E–W line. The median position measured counter-clockwise from north is 153 degrees for 2·33 Mc/s and 121 degrees for 4·57 Mc/s. Ellipses associated with large random changes tend to be rotated toward a N–S line for both frequencies, indicating that the effects of turbulence are anisotropic.

Fading resulting from random changes is always significant. As a result, the method of similar fades yields velocities that are too large. Since the mean signal pattern, as represented by the correlation ellipse, is frequently elliptical and shows a preferred orientation, and since the effects of random changes appear to be anisotropic, systematic errors in mean directions given by the method of similar fades are probable. The shape of the signal pattern and the presence of turbulence may cause individual observations resulting from a comparison of maxima to be very unreliable.

Correlation analysis is a convenient way of determining mean values of products of derivatives used in finding the velocity of a moving co-ordinate system selected, so that the observed changes in signal intensity are random fluctuations. The evaluation of this velocity is not affected by the magnitude or anisotropy of the random changes. The correlation method is more reliable than the method of similar fades.

An example of the application of the general derivation of drift velocity is given by an analysis of the motion of patterns associated with each component of a Fourier expansion of the signal intensity-time records. This analysis suggests that records associated with short mean fading periods and large random changes may exhibit a recognizable trend in the motion of the components, but that records associated with longer mean fading periods and smaller random changes may show no regular pattern of the vector velocities.

Acknowledgements—Sincere appreciation is extended to Dr. MIGUEL WIEWALL, JR., Dean of the Faculty of Science, under whose direction the observational records were obtained. The author's gratitude also is expressed to Mr. WILLIE OCASIO and to Mr. LUIS ESCABI for their considerable assistance in the evaluation of the experimental records. The computational assistance of Mrs. ANNA LEBRON DE SOTO is greatly appreciated.

REFERENCES

BRIGGS B. H., PHILLIPS G. J., and SHINN D. H.	1950	*Proc. Roy. Soc.* **B63,** 106
NEWSTEAD G.	1954	*J. Atmosph. Terr. Phys.* **5,** 182
RATCLIFFE J. A.	1954	*J. Atmosph. Terr. Phys.* **5,** 173
YERG D. G.	1955	*J. Geophys. Res.* **60,** 173

Journal of Atmospheric and Terrestrial Physics, 1956, Vol. 8, pp. 260 to 269. Pergamon Press Ltd., London

The formation of the ionospheric layers *F-1* and *F-2*

J. A. RATCLIFFE
Cavendish Laboratory, Cambridge

(*Received* 26 *November* 1955)

Abstract—Detailed investigations of the electron distribution in the *F-2* region have recently shown (RATCLIFFE *et al.*, 1956) that the *F-2* layer could be formed by the ionizing agency which has its peak of electron production in the *F-1* layer, if the loss-coefficient varies with height in a certain way, explained in the paper referred to. The implications of a loss-coefficient varying in this way are examined in detail in the present paper, and it is shown that it would explain the known facts about the splitting of the *F* layer into separate *F-1* and *F-2* layers. The question of what determines the height of the *F-2* electron peak is also discussed.

1. INTRODUCTION

IN a recent paper (RATCLIFFE *et al.* (1956), subsequently referred to as R.S.S.T.) my colleagues and I examined the height distributions of electron density observed in the *F-2* layer at a series of different places, seasons, and epochs of the solar cycle. We showed that they are consistent with the hypothesis, first advanced by BRADBURY (1938), that the *F-1* and *F-2* layers are formed by the same ionizing agency acting on a single ionizable constituent, and that the rate of electron loss between heights of about 250 and 350 km is proportional to N (attachment-like), with the loss-coefficient decreasing upwards. It is the purpose of this paper to examine this suggestion in more detail.

VOL. 8 1956

Table 1. Time-constants of electrons against recombination at different heights, on the assumption of R.S.S.T. that the loss-coefficient is given by

$$dN/dt = kN, \text{ where } k = 10^{-4} \exp\left\{\frac{300 - h\ (\text{km})}{50}\right\} \text{sec}^{-1}.$$

Height (km)	200	250	300	350	400	450
Time (h)	0·38	1·0	2·8	7·5	21	56

In R.S.S.T. our knowledge of the *F-1* layer was used only in so far as it led to an estimate of the level at which the rate of electron production was a maximum, and of the magnitude of that rate at different solar epochs. The circumstances which would lead to the separate formation of the *F-1* and *F-2* layers were not discussed. These circumstances will be discussed in Section 5.

The problem of the *F-2* layer is complicated by the fact that there the electron loss-rate is small and the electron time-constant* correspondingly large (see Table 1), so that there is no longer approximate equality between the rate of production and the rate of loss as in the lower ionospheric regions. Also in the

* In this paper the term "electron time-constant" will be used to denote that time in which the electron density would decrease to e^{-1} of its original value in the absence of ionizing agencies or of movements.

F-2 layer it is thought that movements of electrons play an important part. Before a full explanation of its formation can be given, it is of use to see what sort of *F-2* layer would be formed if equilibrium were set up between processes of production and loss, and if there were no movements. An attempt is made to do this in Section 6, and the probable results of excluding the complicating factors are discussed.

2. The Electron-loss Coefficient

In R.S.S.T. it was suggested that, at heights above about 150 km electrons of number density N disappear at a rate given by

$$dN/dt = -kN$$

where the loss-coefficient k is as follows:

(a) Low down $k \fallingdotseq 10^{-8}N$ sec^{-1}.

(b) At intermediate levels

$$k \fallingdotseq 10^{-4} \exp\left\{\frac{300 - h(km)}{50}\right\} \text{sec}^{-1} \qquad (1)$$

(c) High up $k \fallingdotseq 10^{-12}N$ sec^{-1}.

(a) represents a process equivalent to recombination with recombination coefficient 10^{-8} cm^3 sec^{-1}; it is supposed to be appropriate to the peak of the *F-1* layer.

(b) represents a process equivalent to attachment; it is deduced from observations made on the *F* layer at night.

(c) represents a process equivalent to recombination with recombination coefficient 10^{-12} cm^3 sec^{-1}, which is the theoretical value for radiative recombination.

These suggestions are consistent with those of Bates and Massey (1946), who supposed that electron-loss processes of the types (a) and (b) could occur in the following way. In the *F* region the ionizable constituent was supposed to be atomic oxygen O, and there were supposed to be molecules XY to which positive charges could be transferred from O^+ ions. The processes operating were then

$$\text{Production} \qquad O + h\nu \rightarrow O^+ + e \qquad \text{(i)}$$

$$\text{Loss} \quad \begin{cases} O^+ + XY \rightarrow O + XY^+ & \text{(ii)} \\ XY^+ + e \rightarrow X + Y & \text{(iii)} \end{cases}$$

On the basis of this explanation it is possible to show, as is done below, how the electron-loss process mentioned at (a) changes into the process (b) near a certain height.* Let us consider a layer which has been irradiated by a constant ionizing radiation for so long that complete equilibrium has been established and the number densities $n(e)$ and $n(O^+)$ of the electrons and oxygen ions are constant. Then let q represent the rate of production of electrons and positive ions by the photo-ionizing process (i); $\lambda_1 n(O^+) n(XY)$ represent the

* A calculation similar to this is given in Massey and Burhop (1952).

rate of the change-transfer process (ii); and $\lambda_2 n(XY^+)n(e)$ represent the rate of the dissociative recombination process (iii), so that we have

$$dn(O^+)/dt = 0 = q - \lambda_1 n(O^+)n(XY) \tag{2}$$

$$dn(e)/dt = 0 = q - \lambda_2 n(e)n(XY^+) \tag{3}$$

and, since the numbers of positively and negatively charged particles are equal,

$$n(O^+) + n(XY^+) = n(e) \tag{4}$$

Elimination of $n(O^+)$ and $n(XY^+)$ from equations 2, 3, and 4 yields

$$q = \frac{\lambda_1\lambda_2 n(XY)n^2(e)}{\lambda_1 n(XY) + \lambda_2 n(e)} \tag{5}$$

We now distinguish two cases

(i) $\lambda_1 n(XY) \gg \lambda_2 n(e)$,

then $$q \fallingdotseq \lambda_2 n^2(e) \tag{6}$$

and the electron-loss process has a rate proportional to $n^2(e)$ and the loss-coefficient (λ_2) is independent of height. This corresponds to the process, listed at (a) above, which occurs low down:

(ii) $\lambda_1 n(XY) \ll \lambda_2 n(e)$,

then $$q \fallingdotseq \lambda_1 n(XY)n(e) \tag{7}$$

and the electron-loss process has a rate proportional to $n(e)$ and the loss-coefficient $\lambda_1 n(XY)$ would be expected to decrease upwards as $n(XY)$ decreased. This corresponds to the process, listed at (b) above, which occurs at intermediate levels.

The change from case (i) to case (ii) will occur near the level where

$$\lambda_1 n(XY) = \lambda_2 n(e). \tag{8}$$

If the distribution of $n(XY)$ is supposed to remain constant, the level at which this change takes place will change as $n(e)$ changes; an increase of $n(e)$ will cause the level to move downwards if, as is reasonable, $n(XY)$ is supposed to increase downwards. A change of $n(e)$ by a factor of 10 would correspond to a change of height of the transition level by 2·3 scale heights of $n(XY)$, since $10 = \exp(2{\cdot}3)$.

Fig. 1 shows the loss-coefficient k plotted as a function of height. The changes between the regions (a), (b), and (c) are shown as fairly sharp; they might, in practice, take place over a distance of about 50 km (one scale height).

If, near any level, k is represented by the expression

$$k = A \exp(-h/a) \tag{9}$$

then we shall call a the local scale height for k. At intermediate levels k is represented by equation (1), and the local scale height is $a = 50$ km. We shall denote this value of a, appropriate to these levels, by the symbol H_k, and in this region we shall rewrite equation (1) as

$$k = k_0 \exp\{-(h - h_0)/H_k\} \tag{10}$$

where h_0 represents a reference level which will be used later, and k_0 represents

VOL. 8 1956

the value k would have if equation (10) continued to hold right down to the reference level. In the upper and lower parts of the ionosphere k is approximately* constant and $a \fallingdotseq \infty$. The local scale height a is plotted as a function of height in Fig. 2, which corresponds to Fig. 1. The levels at which a changes from ∞ to 50 km depend on the electron densities N.

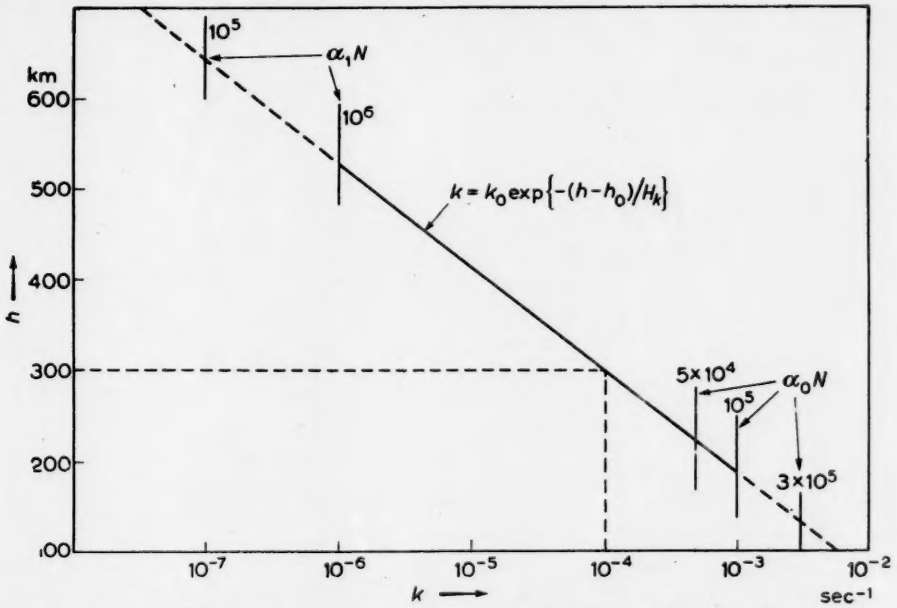

Fig. 1. Values of k at different heights. k is the effective loss-coefficient in the equation $dN/dt = -kN$. Its value at great and small heights is proportional to N.

3. The Rate of Production of Electrons

The rate q of production of electrons is supposed to have its peak in the *F-1* layer and to vary above that height as given by the Chapman expression.

$$q = q_0 \exp\{1 - z - e^{-z} \sec \chi\} \tag{11}$$

in which χ = the sun's zenith distance,

$z = (h - h_0)/H_i$ = the reduced height,

h = height,

h_0 = height of the peak of electron production when $\chi = 0$,

H_i = scale height of the ionizable constituent,

q_0 = rate of production at the peak when $\chi = 0$.

In R.S.S.T. it was suggested that the following numerical values agreed with experiment:

$$h_0 = 180 \text{ km}$$
$$H_i = 45 \text{ km}.$$

* In these regions k is proportional to N, and its approximate independence of height depends on the approximate independence of N on height at these levels.

4. THE EQUILIBRIUM ELECTRON DISTRIBUTION

If equilibrium were established between the rates of production and loss of electrons, the number density N would be given by

$$N = (q_0/k) \exp (1 - z - e^{-z} \sec \chi). \tag{12}$$

By equating dN/dz to zero it can be shown that a peak or a trough of this distribution occurs when z has a value given by

$$\exp (-z) \sec \chi = 1 + (dk/dz)/k \tag{13}$$

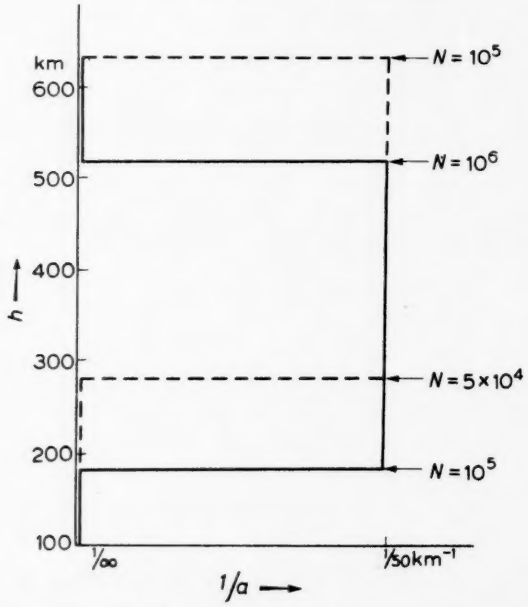

Fig. 2. If the magnitude of k at any level in Fig. 1 is represented locally by $k = A \exp (-h/a)$, the quantity a varies with height, as shown here.

If k is represented by equation (9), then

$$(dk/dz)/k = -H_i/a \tag{14}$$

so that equation (13) takes the form

$$\exp (-z) \sec \chi = 1 - H_i/a. \tag{15}$$

To investigate the levels at which troughs or peaks of N are formed, it is convenient to solve equation (15) graphically, as in Fig. 3(a) or (b). The curves

$$\exp (-z) \sec \chi = x \tag{16}$$

and

$$1 - H_i/a = x \tag{17}$$

are plotted on a set of $z - x$ axes, and their intersections give values of z which satisfy equation (16). The curve of equation (17) (which we will call the k curve)

VOL. 8 1956

is derived from the curve of Fig. 2, which shows how a varies with height. It is represented by $ABCDEF$ in Fig. 3(a) and (b). The vertical portion CD is represented by $x = 1 - H_i/H_k$, and corresponds to positive values of x if $H_k > H_i$, as in Fig. 3(a), and to negative values, as in Fig. 3(b), if $H_k < H_i$. The height of the horizontal part BC depends on the magnitude of N at these heights (see Figs. 1 and 2). Curves are drawn through BC and through $B'C'$ to represent two different values of N.

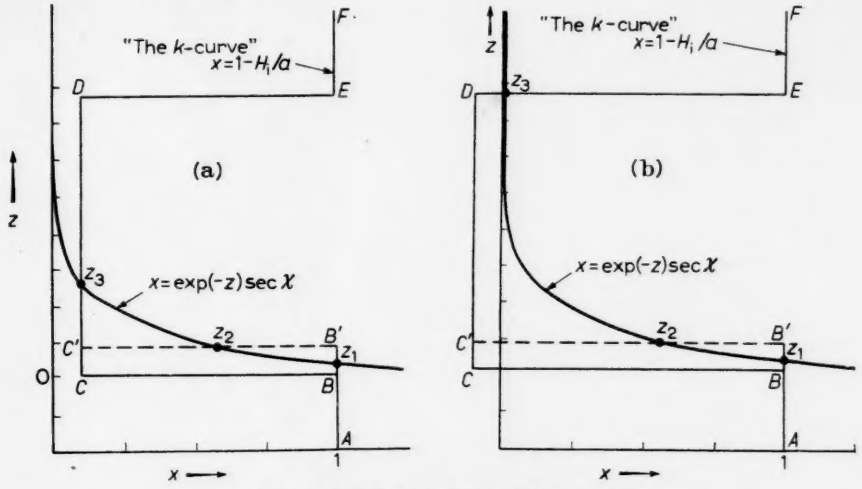

Fig. 3. Graphical solution of the equation

$$\exp(-z)\sec\chi = 1 - H_i/a$$

a is taken from Fig. 2.

(a) represents the case when $H_k > H_i$

(b) represents the case when $H_k < H_i$.

The points z_1, z_2, and z_3, at which the curves intersect, represent peaks or troughs of N. The following consequences are apparent:

(a) There will, in general, be three points (z_1, z_2, and z_3) of intersection.

(b) It can be shown that z_1 and z_3 represent peaks of N (i.e., $d^2N/dz^2 < 1$), and that z_2 represents the trough between the two peaks ($d^2N/dz^2 > 1$), as indicated in the $N(z)$ curve of Fig. 4.

(c) The upper peak, corresponding to z_3, will always occur; it may fall on the vertical part CD of the k curve or on the horizontal part DE. The corresponding peak in the $N(h)$ curve represents the peak of the *F-2* layer. It will be considered in detail in Section 6.

(d) The lower peak, corresponding to z_1, will only occur if the turning-point B (or B') lies above the curve $x = \exp(-z)\sec\chi$. It represents the *F-1* layer. Its behaviour, and in particular the question of whether or not it occurs, will be discussed in Section 5.

5. The *F-1* Layer

The *F-1* layer peak is formed if, in Fig. 3(a) or (b) the point B (or B') lies above the curve $x = \exp(-z)\sec\chi$. Now, the position of this curve depends on the solar zenith distance χ, and the height of B depends on the magnitude

of N at the level concerned. The magnitudes of both χ and N will therefore determine whether or not an *F-1* electron peak is formed.

First, let us consider a fixed value of χ and investigate the effect of changing N. This change could occur, for example, through a change in the epoch of the solar cycle, or through the occurrence of an eclipse. It will be seen, by comparing Figs. 1, 2, and 3, that a decrease of N raises the horizontal part BC of the k curve in Fig. 3 and therefore increases the likelihood that the curves will intersect at z_1

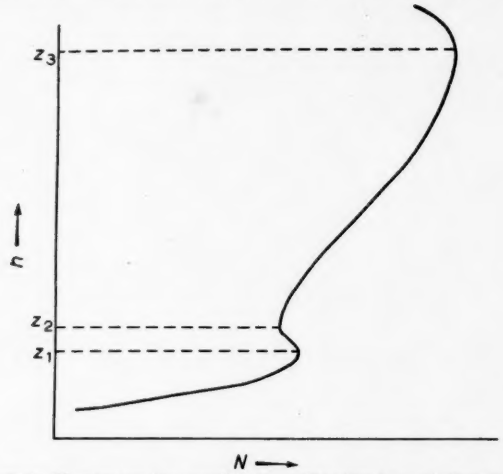

Fig. 4. This illustrates the equilibrium distribution of electron density corresponding to Fig. 3 when the curves intersect.

and that an *F-1* electron peak will be formed. We might therefore expect the *F-1* peak to be more easily formed (a) during an eclipse, and (b) near sunspot minimum.

It is well known that the *F-1* peak often occurs, during eclipses, for values of χ for which it would not normally be seen. It is also clear, from an inspection of the $h'(f)$ curves which were analysed in detail in R.S.S.T., that the *F-1* peak is more clearly in evidence at sunspot minimum than at sunspot maximum. I believe this fact is well known to those who study $h'(f)$ curves, but I cannot find a reference to it in print. Both these facts seem to be explained on our hypothesis.

We now turn to consider the effect of a change in χ. This is a little more complicated, because it is also accompanied by a change in N, and we have to consider the joint effect of altering the two curves in Fig. 3(a) or (b). The height h_B of the point B is given by the intersection of the sloping and vertical lines near the bottom of Fig. 1, and equation (10) shows that it occurs where

$$k_0 \exp\{-(h_B - h_0)/H_k\} = \alpha_0 N \tag{18}$$

Now, in the *F-1* layer it is known that $N = N_0 (\cos\chi)^{\frac{1}{2}}$ fairly closely, so that equation (18) may be written

$$k_0 \exp\{-(h_B - h_0)/H_k\} = \alpha_0 N_0 (\cos\chi)^{\frac{1}{2}} \tag{19}$$

or

$$h_B - h_0 = \tfrac{1}{2} H_k \log(\sec\chi) + H_k \log(k_0/\alpha_0 N_0). \tag{20}$$

VOL. 8 1956

The height h_1 at which the curve $x = \exp(-z) \sec \chi$ cuts the line $x = 1$ is given by

$$1 = \exp\{-(h_1 - h_0)/H_i\} \sec \chi$$

or

$$h_1 - h_0 = H_i \log (\sec \chi) \tag{21}$$

From equations (20) and (21) we find

$$(h_B - h_1) = H_k \log (k_0/\alpha_0 N_0) + (\tfrac{1}{2}H_k - H_i) \log (\sec \chi) \tag{22}$$

If this difference is positive the intersection at z_1 will occur and an *F-1* peak will be formed. Provided $H_i > \frac{1}{2}H_k$, the chance that the layer will be formed is greater for smaller values of sec χ, i.e., when the sun's radiation is incident more steeply. This seems to provide an explanation of the well-known phenomenon that the *F-1* peak is more commonly formed near midday and in summer.

The discussion of this section provides an explanation of the fact that a reduction of ionization during an eclipse leads to enhancement of the *F-1* peak, whereas on ordinary days the opposite happens, and a decrease of radiation makes the *F-1* peak become less obvious.

On the hypothesis here suggested, if the *F-1* peak is formed at all it will behave, below the maximum, like an ordinary Chapman layer formed in a place where the rate of loss of electrons is given by $dN/dt = -10^{-8} N^2$. It is known that the *F-1* layer does behave approximately like this. Movements, or changes of the loss-coefficient with height, seem to be of small importance *at these levels*.

6. The *F-2* Layer

Electron-loss rates given by the sloping line of Fig. 1 correspond to the electron time-constants given in Table 1, from which it is clear that equilibrium between production and loss is far from being established during the course of a day at heights above about 320 km. Since, however, the peak of the *F-2* layer is sometimes formed at (or below) this height, it seems worth enquiring, as a first step, what sort of *F-2* layer would be formed if there were time for equilibrium to be established. In estimating the effects of movements on the *F-2* layer, it is also of value to know what sort of equilibrium layer would be produced without them. In this section, therefore, we shall consider the quite artificial problem of determining the shape of the *F-2* layer which would be produced under equilibrium conditions in an ionosphere described by our previous hypotheses. We shall first outline several considerations which might determine the height of the *F-2* electron peak, and shall then discuss the experimental facts in the light of these considerations.

The height of the *F-2* electron peak would be at the level of the point of intersection z_3 in Fig. 3(a) or (b). There are two possibilities: z_3 can fall either on the vertical part CD of the k curve, as in Fig. 3(a), or at the level of the horizontal part DE, as in Fig. 3(b). If it falls on CD, its reduced height z_3 is given by

$$\exp(-z_3) \cdot \sec \chi = 1 - H_i/H_k. \tag{23}$$

A possibility of this kind can only occur if $H_k > H_i$. This is the well-known result that if the rate of electron production is given by equation (11), and if the

loss-coefficient falls off like exp $(-h/H_k)$, there will be no peak of electron-density if $H_k < H_i$. The reduced heights z_3 of the peak when the sun's radiation is vertical ($\chi = 0$), as calculated from equation (23), for a series of values of H_k/H_i are listed in Table 2, together with the corresponding real heights h_3 for the case where $H_i = 45$ km, $h_0 = 180$ km, as suggested by R.S.S.T.

Table 2. Height of peak of equilibrium *F-2* layer for different values of H_k/H_i.

$\exp(-z_m) = 1 - H_i/H_k$ $\quad h_0 = 180$ km

$h_m = h_0 + H_i z_m$ $\quad H_i = 50$ km

$1 - H_k/H_i$	<1	1	1·05	1·1	1·4	2
z_m	—	—	3	2·3	1·2	0·8
h_m (km)	600	600	315	284	234	216

If $H_k < H_i$, there would be no intersection of the curves on the vertical part CD, and h_3 would be at the height of the horizontal part, as shown in Fig. 3(b). This occurs where $10^{-12}N = k_0 \exp\{-(h_3 - h_0)/H_k\}$ (see Fig. 1), and depends on N. If we give N the value 5×10^5, representative of the electron density at the peak of the *F-2* layer, and $Hk = 50$ km, we find $h_3 = 600$ km. The values obtained for other values of N are not very different, and only the one is listed in Table 2.

In R.S.S.T. it was not suggested that the estimates of H_i and H_k were very accurate, but it did appear that they were of the same order, and the best values appeared to be those previously listed, which give $H_k/H_i = 1{\cdot}1$. Reference to the table shows that the electron peak of an equilibrium layer would then be expected in the region of 285 km.

In their discussion of the electron-loss process, BATES and MASSEY (1946) suggested that the molecule XY (see Section 2) might be molecular oxygen (O_2), so that H_k would have the corresponding scale height.* They supposed that the ionizable gas was atomic oxygen (O). Under these circumstances $H_k < H_i$ and the equilibrium electron peak would be expected near 600 km (see Table 2).

In R.S.S.T. (Section 15(d)) the possibility was considered that the height of the peak might be determined by diffusion. It was pointed out that, if production and loss processes tended to form an electron peak above about 350 km, then in middle latitudes diffusion would rapidly cause it to fall to a level around 350 km. At the equator no such fall would occur, because the horizontal magnetic field of the earth would stop vertical diffusion.

On still another hypothesis the height of the electron peak could be determined primarily by movements having their origin in electric and magnetic fields. Their nature is largely speculative, and there is a temptation to make *ad hoc* suggestions to explain particular phenomena. It therefore seems best at this stage of the

* See also NICOLET and MANGE (1954), who showed that O_2 would be distributed with its normal scale height even above the level where it is considerably dissociated.

VOL. 8 1956

investigation to enquire what the position would be if movements played only a secondary role in determining the height of the peak.

With the above possibilities in mind, let us now consider the facts. By day the *F-2* electron peak is at a height of about 250–350 km in middle latitudes and about 400–500 km near the equator.

The most obvious explanation is that $H_k \fallingdotseq H_i$ or $H_k < H_i$, so that, as shown in Table 2, the peak would be formed, under equilibrium conditions, somewhere between 300 and 600 km. This could well be the primary cause of the high peak near the equator, its precise height being determined, very sensitively, by movements, or by small changes in a ratio H_k/H_i just greater than 1. There is indeed evidence (McNish and Gautier, 1949) that the height and shape of the peak near the equator is much influenced by movements. In middle latitudes the height of the peak would then be determined primarily by diffusion, and would be lower.

An alternative (but less plausible) explanation would require that $H_k \fallingdotseq 1{\cdot}1\, H_i$, as indicated by the rough estimates of R.S.S.T., so that under equilibrium conditions the peak would be near 280 km. The *ad hoc* hypothesis would then have to be made that near the equator there were large electro-magnetic movements which caused the peak to occur much higher.

7. Conclusions

A loss-coefficient varying with height, as discussed in Section 2 and illustrated in Fig. 1, would explain in general when the *F-1* layer does and does not occur separately, and would account for changes with the epoch in the solar cycle, with the solar zenith angle, and during eclipses.

It would lead to the conclusion that, if the peak of electron density were formed near where the production and loss processes balance, then it would be at a height of the order of 600 km. The high peak near the equator may be primarily determined by this balance. The lower peak in middle latitudes would then be formed by a process of diffusion.

References

Bates, D. R. and Massey, H. S. W.	1946	*Proc. Roy. Soc.* **A187,** 261.
Bradbury, N. E.	1938	*J. Terrest. Mag. Atmos. Elect.* **43,** 55.
Massey, H. S. W. and Burhop, E. H. S.	1952	*Electronic and ionic impact phenomena.* (Oxford University Press) p. 645.
McNish, A. G. and Gautier, T. N.	1949	*J. Geophys. Res.* **54,** 181.
Nicolet, M. and Mange, P.	1954	*J. Geophys. Res.* **59,** 1.
Ratcliffe, J. A., Schmerling, E. R., Setty, C. S. G., and Thomas, J. O.	1956	*Phil. Trans.* **A248,** 621. This paper is referred to as R.S.S.T.

Journal of Atmospheric and Terrestrial Physics, 1956, Vol. 8, pp. 270 to 273 Pergamon Press Ltd., London

Electron distribution in the ionosphere

G. A. M. KING and C. H. CUMMACK
Geophysical Observatory, Christchurch, New Zealand

(*Received* 24 *August* 1955)

Abstract—Analysis of h',f records to give true heights suggests that the ionosphere consists of three Chapman layers, *E*, *F1*, and *F2* and that the temperature is uniform.

METHOD OF ANALYSIS

THE basic procedure has been described (1954). The effect of the earth's magnetic field was included. Three separate sets of records were analysed to compile a picture of a representative day. They were selected from magnetically quiet days, and are relatively free from confusion by sporadic *E*.

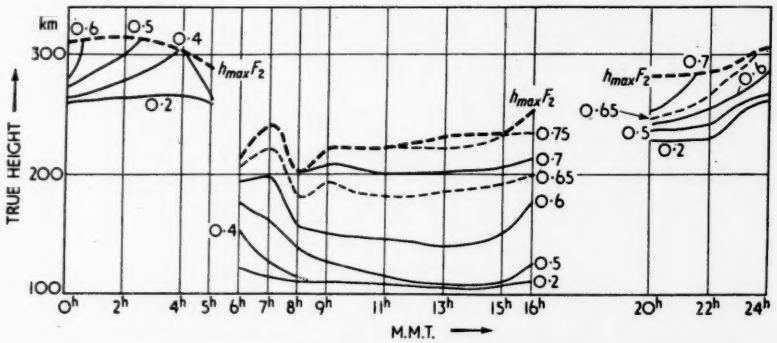

Fig. 1. Contours of ionization in units of log f—26/1/54—based on reductions at the times indicated.

Direct reduction gives, for heights beyond a layer maximum, the lowest values that agree with the h',f curve; it assumes that the space between layers is filled with electrons at least to the value of the lower maximum.

The sunrise records were reduced directly, and also reduced to include the greatest gap consistent with the descending part of the *F*-layer trace. This was not done for the remaining records, as it was felt that the errors would not affect our conclusions greatly.

Errors from second-order effects, neglected in the process of reduction, cause heights just above the *E* and *F1* critical frequencies to be slightly too low and the heights of layer maxima to be too high, perhaps by two or three kilometres.

DISCUSSION

In Fig. 5, we show a model abstracted from the experimental results given in the first four figures.

It shows clearly that the daytime layers form when the sun's rays strike the

VOL. 8 1956

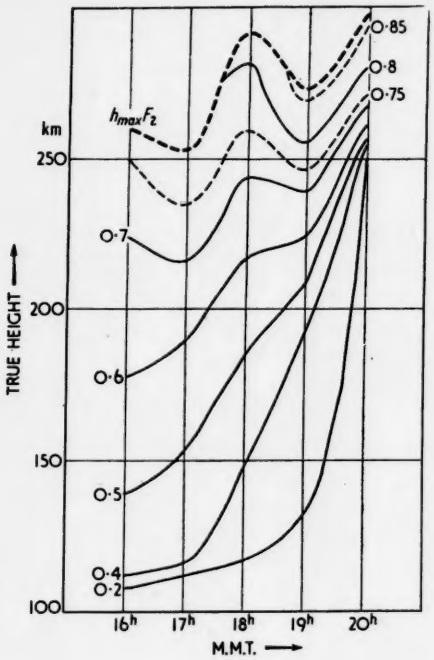

Fig. 2. Contours of ionization—1/2/54.

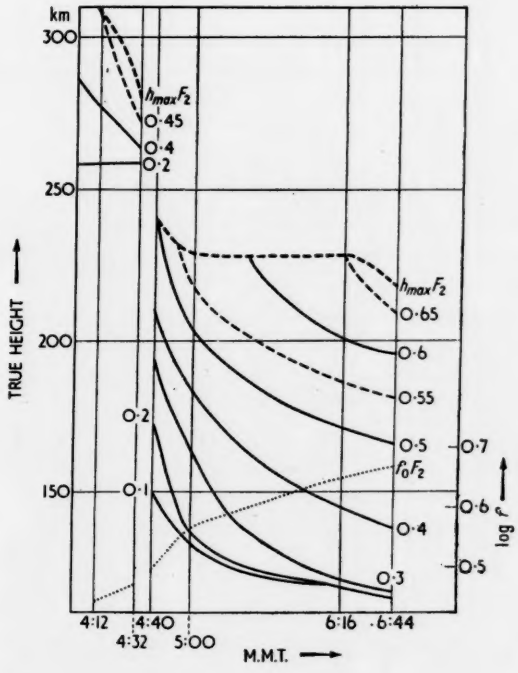

Fig. 3. Contours of ionization and values of f_0F2—18/1/54.

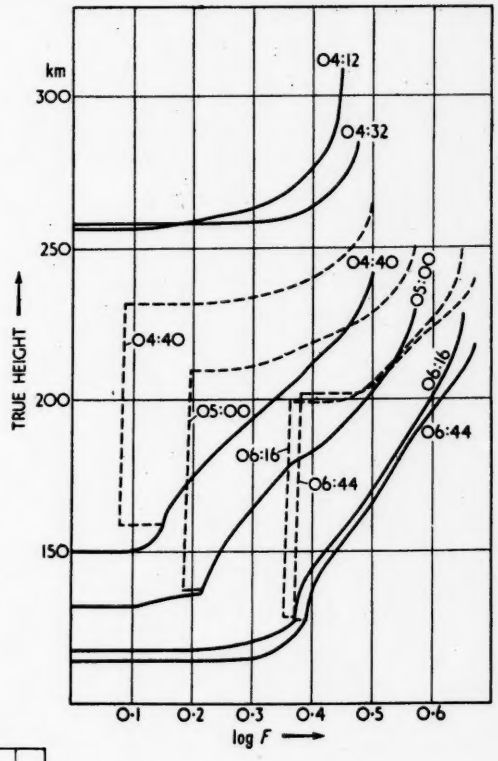

Fig. 4. Full lines show shape of ion distribution given by direct reduction; dotted lines show shape when the greatest gap is put between the *E* and *F* layers—18/1/54.

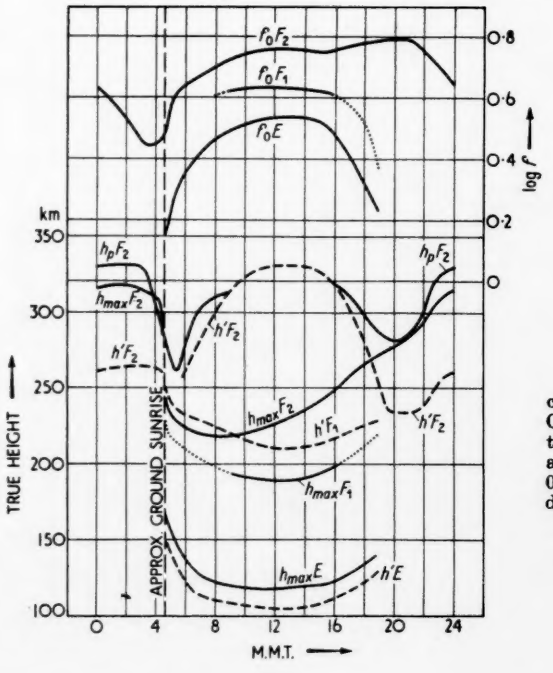

Fig. 5. Model assumed for the discussion—summer, sunspot minimum at Christchurch. This was compiled from the previous figures by making slight allowance for valleys between layers after 0800h and by neglecting effects obviously due to temporary disturbances.

VOL. 8 1956

appropriate level tangentially. The *E* layer seems to come from a gaseous component that is not present at the higher levels; *F1* and *F2* are probably due to the action of different bands of radiation acting on the same component. All three layers appear to be formed in a nearly isothermal atmosphere at 250°–280°K. As recombination lags behind ionization, and as the levels of formation and the shapes of the layers alter with the zenith angle of the sun, the gap between the *F1* and *F2* layers is completely filled until nearly midday, and that between *E* and *F1* largely filled.

In the afternoon, some influence causes the electrons to separate from the positive ions and to move up into a region of low gas-density, making the night-time *F* layer. Recombination takes place only at its lower boundary, as the layer is not in charge equilibrium.

There is an indication, from the slight decrease in height and increase in density in the early morning, that the influence causing the transport of the electrons has a diurnal period.

This picture is consistent with the measurements of ionospheric temperatures from auroral band spectra, and also agrees with the theoretical conclusion that the thermal conductivity of the upper layers is very high.

Acknowledgements—This work is part of the research programme of the Geophysical Observatory of the New Zealand Department of Scientific and Industrial Research. The help given by the superintendent, Mr. J. W. Beagley, and by members of the staff, is gratefully acknowledged.

DL.
3
956

Reference

King, G. A. M. 1954 *J. Atmosph. Terr. Phys.* **5**, 245

RESEARCH NOTES

Cosmic-ray observations during the flare of 23 February 1956

(*Received* 28 *March* 1956)

In this laboratory an air-shower experiment is in progress, and two ratemeters are in continuous use to check the functioning of the apparatus. Ratemeter *A* (Fig. 1) records the rate from 91 units, each of which makes a pulse when two counters 60 cm × 3·3 cm separated by 20 cm are triggered in coincidence. The normal rate is 240 counts/min. Ratemeter *B* (Fig. 2) records the rate from sets of three 60 × 3·3 cm counters under 20 cm Pb. This ratemeter is switched from one set to another at $\frac{1}{2}$-h intervals.

The diagrams are tracings from the records obtained on 23 February, during the occurrence of the solar flare. It will be seen that the coincidence rate increased to about three times its normal value. This can be understood if we suppose that about 5% of the coincidences recorded are produced by the nucleonic component, for instance through local stars in the atmosphere. Then, since this component was observed to increase by a factor of nearly 50, our increase of a factor of 2 is easily accounted for.

The ratemeter *B* unfortunately ran off scale, and moreover at 0400 was switched to a position to which no counters were connected. The observed increase is at least 100%. Both ratemeters return to normal after about 3 h.

The start of the increase in ratemeter *A* appears to be at 0345, and in ratemeter *B* at 0343. As these ratemeters are normally only used for checking purposes, no special care is taken to set the time accurately. The settings were checked about 9 h after the event, and both found to be accurate to within 1 min. However, it is possible when examining the charts to upset the setting by about 1 min, and we cannot be sure that such a disturbance did not occur in this case. Thus the apparent discrepancy in the starting-time of the increase between the two recorders may not be real.

The integrating time-constant on recorder *A* is 160 sec. This is a time comparable to the times involved in the event. Accordingly, we have tried in Fig. 3 to reconstruct the shape of the incoming pulse of cosmic rays from the curve in Fig. 1. This involves differentiating curve *A*, and large errors may arise. The vertical line shows a conservative estimate of what the errors may be.

It appears that the beginning of the pulse was rapid, an increase of 70% taking place in less than 1 min. The rate then rose more slowly to a maximum of about 220% at about 9 min after the start. The increase had fallen to half the maximum 24 min after the start. The tail of the *B* ratemeter curve appears to be about the same as that of the *A* ratemeter.

Another unit checks the rates of single counters of area 15 cm^2, and each half-hour four counters are recorded individually on a recorder. A mark is made on the chart every 20 counts, and we were able in two of the counters to compare their rates just prior to the flare 0330–0340 to that during the period 0350–0400, which includes the maximum. The average rates of the two counters including the counter background are given in the table.

If we assume that half the normal count-rate is due to the counter background, then the cosmic-ray effect increases approximately from 15 c.p.m. to 58 c.p.m., i.e. by nearly 300%.

VOL. 8 1956

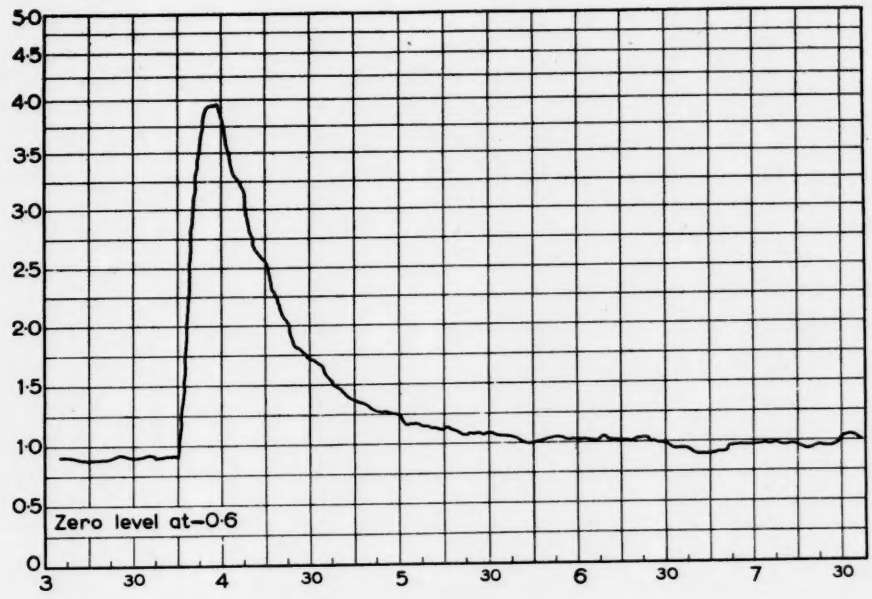
5·0
4·5
4·0
3·5
3·0
2·5
2·0
1·5
1·0
0·5
0
Zero level at−0·6
3
30
4
30
5
30
6
30
7
30

Fig. 1

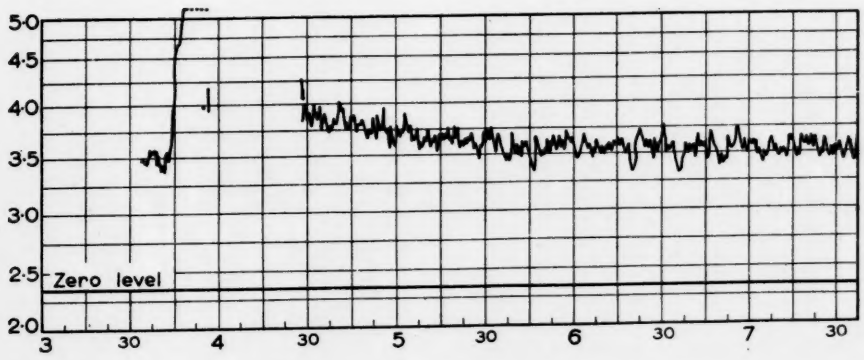
5·0
4·5
4·0
3·5
3·0
2·5
2·0
Zero level
3
30
4
30
5
30
6
30
7
30

Fig. 2

The mean rates of the counters in the half-hour periods following 0400, compared with the "normal" rates of the counters, show that the tail of the curve is similar to that of Fig. 3,

Time	0330–0340	0350–0400
Rate m^{-1}	29 ± 1·7	73 ± 2·7

the increase having dropped to half the peak value in about 25 min from the onset, and down to 10% of the peak 1 h after the onset.

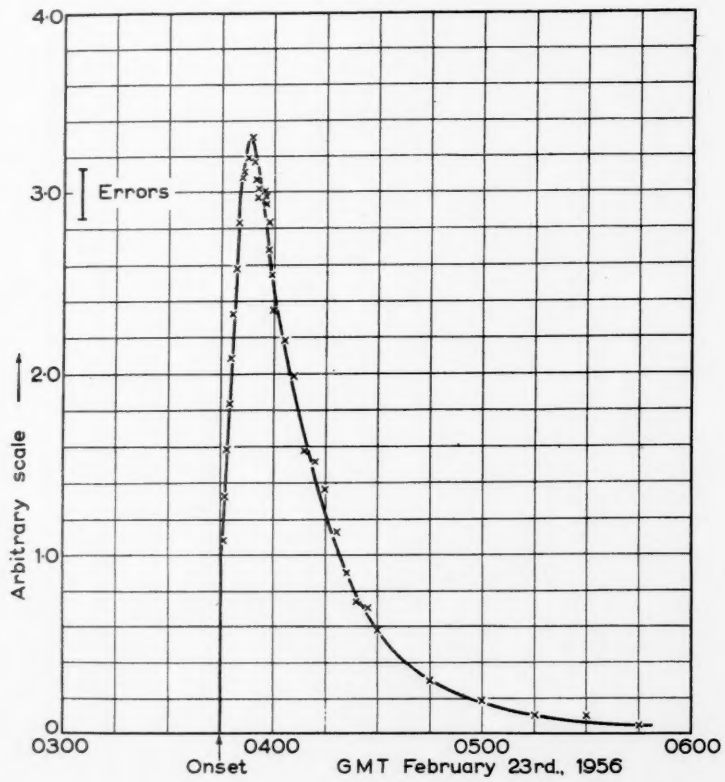

Fig. 3

Acknowledgement—We are grateful to Mr. E. B. Fossey for some computation done in deriving Fig. 3.

Atomic Energy Research Establishment
Harwell, near Didcot,
Berkshire.

T. E. Cranshaw
W. Galbraith
N. A. Porter

VOL. 8 1956

Cosmic rays and the solar flare of 23 February 1956

(*Received* 28 *March* 1956)

A LARGE increase in the sea-level cosmic-ray intensity associated with the solar flare of 23 February was observed in London, using G.M. counter arrays with a wide angle of acceptance. Five independent counter sets were in operation, each consisting of two trays of counters placed one above the other so as to record twofold coincidences. Three of the sets had trays 41·5 cm × 100 cm, separated by 13·5 cm, whilst the other two had trays 58·5 cm × 60 cm, with a separation of 6·2 cm. The twofold coincidence pulses were fed through scalers (÷ 100 in each case) to message registers, which were photographed at half-hourly intervals. Allowing for dead space between the counters, the total effective sensitive area for the five sets is estimated to be 15,000 cm^2. All the recorders were shielded by a concrete roof of 40 gm cm^{-2}. The mean half-hourly counting rate for all five recorders together is ~330,000.

The half-hourly counting rates during the period of increased intensity are given in the accompanying table. CRANSHAW, GALBRAITH, and PORTER find that the increase began at 0345 and, using this information, we have deduced that during the interval 0345–0400 our sets counted 3643 × 100 particles, corresponding to an increase of ~120% during this period.

In comparing the results for different stations and for different types of recorder, it is necessary to consider the additional flux of particles due to the flare rather than percentage changes, since the latter depend on the background against which the extra particles are counted. An extreme example of this is the relative increase recorded by the neutron monitors in Leeds (~46 times normal) compared with the wide angle G.M. counter arrays in London (~2 times normal). This large difference in percentage change can be understood if we suppose that the additional particles are mostly nucleons. The number of nucleons present in the normal cosmic radiation at sea-level is only a few per cent of the total ionizing flux. Consequently, a given increase in the nucleon flux appears as a much larger percentage change for a neutron monitor, which counts nucleons only, than for a G.M. counter array, which counts both nucleons and mesons.

Table 1.

UT 23/2/56	0045	0115	0145	0215	0245	0315	0345	0415	0445
Number of counts scaled by 100	3278	3268	3284	3274	3301	3281	5293	4513	3728
UT 23/2/56	0515	0545	0615	0645	0715	0745	0815	0845	
Number of counts scaled by 100	3494	3412	3367	3374	3338	3333	3301	3306	

In London the total number of additional particles observed was 434,300, that is to say 28 particles/cm^2. During the quarter-hour of peak intensity (0345–0400) the flux of additional particles was 0·015/cm^2/sec. We can compare this latter figure with the accompanying data for the neutron monitors in Leeds. During the period 0345–0400, 143,000 additional particles were counted. The total area of lead was 4050 cm^2, and the additional flux was therefore 0·039/cm^2/sec. The neutron monitor responds to both neutrons and protons,

whereas the G.M. counter sets record only the protons, and a correction must therefore be applied for this. A rough estimate of the factor involved can be obtained from data at 3500-m altitude (CONVERSI, MARTELLI, and ROTHWELL, 1953), which show that the ratio of numbers of neutrons to protons of energy >400 MeV is ~1·5. The value of 0·039 must therefore be multiplied by 1/2·5, giving 0·016 as the flux of protons. This is very close to the value of 0·015/cm²/sec for the G.M. counter array.

The close agreement must be to some extent fortuitous, for although both types of recorder have wide angles of acceptance, we have not taken into account the differences in geometry which undoubtedly exist nor the efficiency of detection for the neutron monitor. This approximate calculation serves to show, however, that despite the very large differences in percentage increase for the two types of recorder, the flux of additional particles involved is about the same.

There is now a large number of stations in operation throughout the world, so that a fairly detailed study of the latitude and longitude dependence should be possible for this event. In view of the results given above, we feel that comparison of data would be easier if the observational results were expressed in terms of the total number of additional particles received per cm² during the period of increased intensity. Failing this, sufficient details of geometry and efficiency of detection should be given to enable this quantity to be estimated.

M. LAMBIE
H. ELLIOT

Imperial College of Science and Technology, London.

VOL. 8 1956

REFERENCE

CONVERSI M., MARTELLI G., and ROTHWELL P. 1953 *Nuovo Cimento* **10**, 898.

Variation of cosmic-ray nucleon intensity during the disturbance of 23 February 1956

(*Received* 28 *March* 1956)

A LARGE increase in the intensity of the nucleonic component of cosmic rays was observed in two recorders at this laboratory (altitude 150 m, geomagnetic latitude 57°N, longitude 1½° W) at the time of the solar disturbance of 23 February 1956.

Nucleons are detected in each instrument through the evaporation neutrons produced in a cube of lead of about 45-cm side; within the cubes the evaporation neutrons are moderated by a 2·5-cm layer of paraffin-wax before capture in $B^{10}F_3$ proportional counters. Each unit is shielded against local slow neutrons by a paraffin-wax shell surrounding the lead cube, 10 cm thick on unit No. 1 and 20 cm thick on unit No. 2. Both units are therefore insensitive to nucleons of energy less than about 10 MeV, unit No. 1 being marginally more sensitive to nucleons of this order of energy. Apart from a common H.T. supply to the

counters, the circuits of the two units are independent. The barometric coefficients for the normal cosmic-ray nucleon flux are respectively $-10{\cdot}4$ and $-10{\cdot}0\%$ cm^{-1} Hg.

The integrated count in each unit is recorded every 15 min, and over six hours before the disturbance was at a rate 209 min^{-1} for the two units taken together. The interval 0330–0345 UT showed a count about 30% above normal, and the peak rate was recorded in the following 15 min. The operating clock was running 0·8 min slow, and the onset of the disturbance, for any reasonable form of rise, is likely to have become detectable within about 1 min of 0345 UT.

Table 1. Initial phase of the disturbance

Time (UT)		Counts per 15 min		
		N_1	N_2	$N_1 + N_2$
22.2.56	1630–2000	1613	1533	3146
	2000–2400	1616	1536	3152
23.2.56	0000–0330	1615	1512	3127
	0330–0345	2106	1969	4075
	0345–0400	77086	69277	146363
	0400–0415	60607	55258	115965
	0415–0430	35567	33123	68690
	0430–0445	24030	21881	45911
	0445–0500	17841	16264	34105

The recorded counts in the two units during the early part of the disturbance are given in Table 1; over the peak 15 min the average counting rate was 46·7 times the normal rate, but there can be no doubt that the actual peak rate was even higher. An estimate of the true height of the peak may be made, noting that for the later phases of the disturbance the form observed by Cranshaw and Galbraith (1956) follows closely that reported here, if we assume that for the peak period also the true time-variation for our apparatus was the same as that of Cranshaw and Galbraith. The maximum counting rate is estimated in this way to have been between $1{\cdot}26 \times 10^4$ and $1{\cdot}31 \times 10^4$ min^{-1}, about sixty times normal.

We have pointed out that unit No. 1 is more sensitive to rather slower nucleons ($\sim$10 MeV) than No. 2, and accordingly the difference of counts between the units in Table 1 is a measure of the behaviour of these slow nucleons. Although these differences are statistically rather poorly defined, they establish that, at least over the period 0345–0430 UT, the increase of intensity of the slow nucleons was relatively greater than that of the total flux. The statistical accuracy is not high enough, nor is the energy discrimination of the two units sufficiently well known, for any numerical estimate of this effect to be useful.

The great magnitude of the increase of counting rate observed in our apparatus allows the time-variation of the disturbance to be followed in detail until the excess in the counting rate has fallen to less than 1% of the maximum value. The variation with time of the excess counting rate for the first nine hours of the event is shown on a logarithmic scale in Fig. 1. The recorded counts of our instruments are shown in the full histogram line, the form and true magnitude of the maximum as suggested by the results of Cranshaw and Galbraith is indicated by a broken line in the immediate neighbourhood of the peak.

In Table 2 the time-scale of the disturbance is illustrated by figures derived from this graph. The time at which the excess count has fallen respectively to 10% and 1% of the peak value is given, in the first place as derived directly from our recorded observations, and relative to the average counting rate over the peak 15 min, and secondly referred to the form of maximum described by CRANSHAW and GALBRAITH and to the peak counting rate

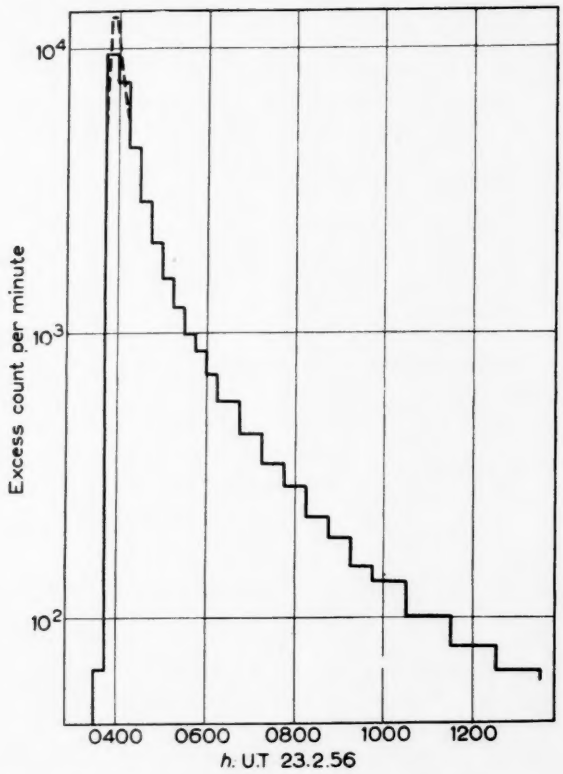

Fig. 1. Variation of cosmic-ray nucleon intensity during the disturbance of 23 February 1956

Table 2. Time-variation of the excess counting rate

Intensity as fraction of peak intensity	Time in minutes after 0345 UT	
	Relative to average intensity, 0345–0400	Relative to assumed form following CRANSHAW and GALBRAITH
1·0	—	9–13
0·1	115	95
0·01	445	380

VOL. 8 1956

derived from this form. The latter figures, although essentially based upon an assumed form of distribution, must be regarded as the more significant. The present disturbance has clearly been of very much shorter duration than that of 19 November 1949, as recorded by ADAMS and BRADDICK (1950). The time-variation of the 1949 event also appears to have been much more closely exponential.

The counting rate fell to within 10% of normal (the excess rate then being 0·2% of the maximum) at about 1900 UT, fifteen hours after the onset of the event. Observations, corrected for barometric pressure, show larger fluctuations than usual, continuing for several days, but it has not yet been possible to connect these with the main event.

P. L. MARSDEN
J. W. BERRY
P. FIELDHOUSE
J. G. WILSON

The University,
Leeds.

REFERENCES

ADAMS N. 1950 *Phil. Mag.* **41**, 503.
ADAMS N. and BRADDICK H. J. J. 1950 *Phil. Mag.* **41**, 505.
CRANSHAW T. E. and GALBRAITH W. 1956 *J. Atmosph. Terr. Phys.*

Some unusual radio observations made on 23 February 1956

(*Received* 29 *March* 1956)

1. INTRODUCTION

THE intense solar eruption of 23 February 1956 produced marked effects on the propagation of radio waves. Some of these were recorded in a series of experiments which has been in progress for some time at Cambridge for the purpose of studying the lower ionosphere by means of the propagation of long and very long waves. It is the purpose of this paper to give (in Section 2) an outline of the experimental results and (in Section 3) a tentative interpretation of them. The detailed deductions from the observed results depend on much accumulated information acquired in the main study relating to the propagation of the waves. This is not the place to discuss this evidence, which, it is hoped, will be published separately in the near future.

The detailed explanation of the results in terms of a distribution of electron (and ion) density with height in the *D* region involves the full theory of reflection of long radio waves in a rapidly varying ionosphere, which is extremely difficult. The necessary calculations are being carried out by BUDDEN (1955), but no results are yet available for the conditions obtaining during this solar event.

2. THE OBSERVED EFFECTS

(a) *Very low frequencies* (16 *kc/s*)

Waves of frequency 16 kc/s were received at Cambridge from the sender G.B.R. at Rugby, distant 92 km. The abnormal component of the sky-wave was isolated by a suitable aerial system (STRAKER, 1955) and its phase and amplitude were recorded automatically. The apparent height of reflection has been determined previously, and the changes of the "phase height" are determined from the record of the phase.

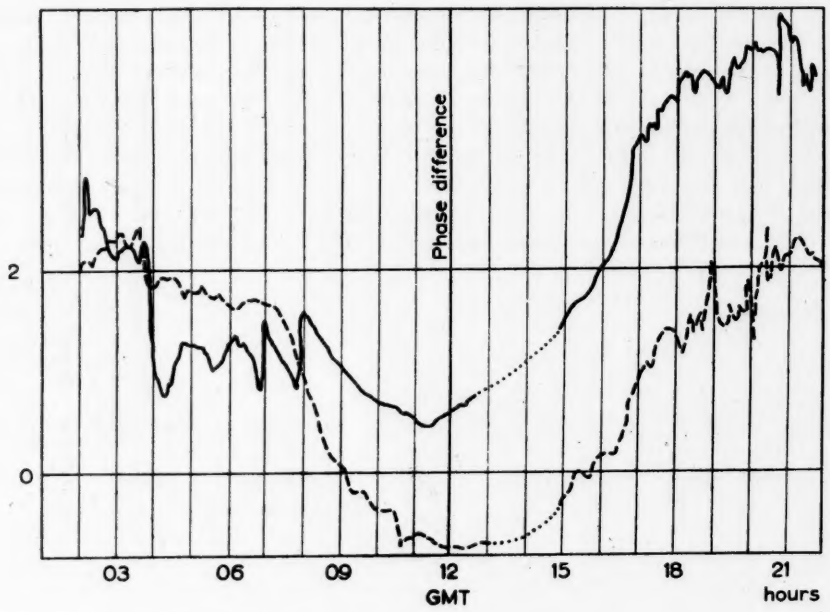

Fig. 1. The phase of the abnormal component of the sky-wave relative to the ground-wave on 16 kc/s at a distance of 90 km.
23 February ——— 21 February – – –
The sender is off from 1300 to 1500 every day for maintenance.

VOL. 8 1956

The changes of phase and amplitude of the abnormal component of the sky-wave on 23 February are shown in Figs. 1 and 2. The records for 21 February are also given as representing a typical "normal" day. (22 February was a rather abnormal day, showing an unusual variation of phase during the early morning and an unusually low reflection height at midday.)

On a few occasions sudden large changes of phase have been observed previously (STRAKER, 1955). A few of these have the same general form, as in this event.

At Newcastle, distant 293 km from the sender, records were being made of the amplitude of waves from G.B.R. received on a loop aerial which was oscillating about the true bearing of the sender.

At 0345 these records showed a sudden departure from their normal behaviour, as judged by the neighbouring days, and the departure reached a maximum at 0420, after which there was some recovery towards normal up to the time of sunrise.

MR. STOFFREGEN is engaged in recording the strength of the waves from G.B.R. as received on a vertical aerial at Upsala, 1350 km distant. He has kindly agreed to our publishing his records made during this period; they are shown in Fig. 3. Important changes took place at 0345 GMT on 23 February. Other evidence (WEEKES, 1950; BUDDEN, 1953) shows that at Upsala the ground-wave is very small in comparison to the total sky-wave.

(b) *Low Frequencies* (70–300 *kc/s*)

A record of the strength of a wave of frequency 71 kc/s transmitted over a distance of 860 km is shown in Fig. 4, with a similar record made on 21 February for comparison. At 0345 on 23 February the amplitude fell suddenly to a value which is known from other

evidence to be that due to the ground-wave alone. It appears that the sky-wave was, temporarily, almost completely removed. The form of the amplitude variation throughout the day was abnormal, but returned to normal the following night.

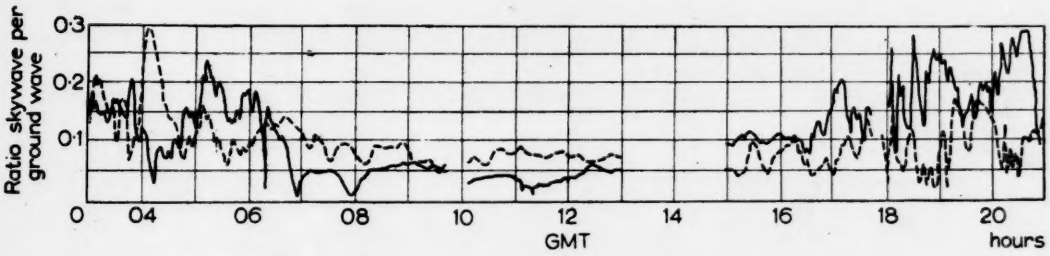

Fig. 2. The ratio of the amplitude of the abnormal component of the sky-wave at 16 kc/s to the ground-wave.
23 February ——— 21 February – – –

Other records with waves of frequency in the range 70–300 kc/s from senders at distances of 700–1500 km showed similar results, starting suddenly at 0345 GMT. All these waves were strongly absorbed from 0345 to 0430.

(c) *Intensity of Atmospherics on* 22 kc/s

Records were being made of the average intensity of atmospherics on a frequency of 22 kc/s. The apparatus was designed to give a true average of the intensity of atmospherics over a period of 2 min. The average is obtained with a storage condenser for which the charging and discharging time-constants are the same.

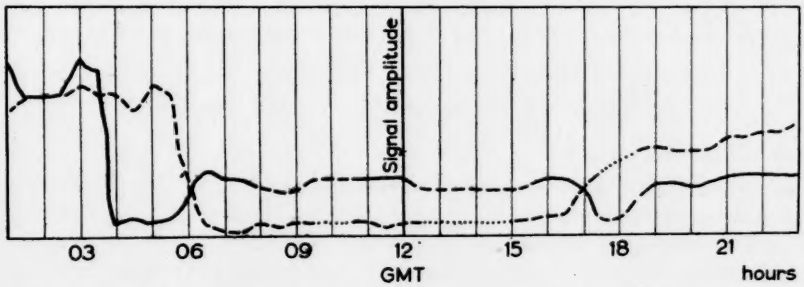

Fig. 3. Signal amplitude on 16 kc/s received on a vertical aerial at Upsala (1350 km).
23 February ——— 21 February – – –

The usual record of atmospherics is somewhat variable from day to day, but on the morning of 23 February there was a sudden drop of about 2/1 in the average intensity at 0345. The subsequent record showed rather large increases in intensity which have been attributed to a local source of interference which makes it impossible to determine the exact variation in the intensity of atmospherics. After the initial drop, the intensity appears to decrease slowly by a further 40% to the normal day-time value at almost ground sunrise.

(d) *High Frequencies* (1·5– 17 *Mc/s*)

Mr. STOFFREGEN has very kindly sent us the records taken on 23 February with the *P'f* equipment (sweeping from 1·5 to 17 Mc/s) at Upsala. These appear to show no effect at all at 0345, but at 0700 MET (just before ground sunrise) almost complete absorption occurred on frequencies below 8 Mc/s. This abnormal absorption persisted all day, although it appeared to be decreasing towards the late afternoon.* It seems likely that this effect was associated with the solar outburst.

Records taken by our colleagues in Cambridge during the day 23 February showed no unusual effects.

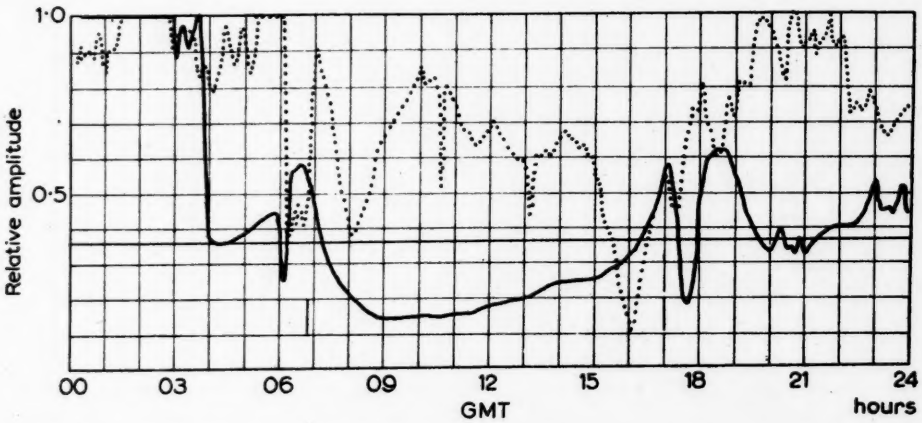

Fig. 4. Signal amplitude on 71 kc/s observed at Cambridge 860 km from the sender
23 February ——— 21 February . . . .
The horizontal line represents the estimated amplitude of the ground-wave. The short vertical lines represent the times of ground sunrise and sunset at the midpoint of the path. The disturbances at 1036 and 1308 GMT on 21 February are due to two small solar flares.

3. TENTATIVE INTERPRETATION OF THE RECORDS

(a) *Height of Reflection*

The records of the phase of waves of 16 kc/s between 0345 and 0700 may be interpreted unambiguously as showing a decrease in phase height of about 8 km; the maximum effect was reached at 0415, after which the height rose 2 km by 0620. If the same change occurs in the actual height of reflection, this would imply that at the peak of the event the reflection height was 79 km. The height appeared to decrease again at about 0625, somewhat earlier than usual.

The rapid changes of phase and amplitude at about 0700 and 0800 are most unusual, and appear to be due to interference effects between two waves of equal amplitude reflected at different heights. BUDDEN (1955) has shown that such effects may occur in the reflection of very long waves. Whenever the amplitude decreases to zero in this way, there is an ambiguity of 2π in the subsequent phase path.

Our interpretation of the true variation of phase height is given in Fig. 5, in which we

* This result is confirmed by the records taken at the Radio Research Substation at Inverness, where the routine *P'-f* records show markedly increased absorption at or about sunrise on 23 February and throughout the day. We are indebted to Mr. H. BEVAN and the Director of Radio for this data.

VOL.
8
1956

have used the increase of phase height in the evening to resolve the ambiguity in the morning phase, but of course the phase heights between 0700 and 0800 remain ambiguous. The results for 21 February are included for comparison.

The apparent height at midday on 23 February was 67 km, compared with 71–72 km at midday on a normal day.

The observations made at 300 km also suggested that the midday phase had a value approximately 180° different from that normally observed at midday. This would suggest that the midday reflection height was about 10 km lower than usual. There are indications that similar lower reflection heights would explain the results observed at Upsala.

Records of the amplitude of low-frequency waves received over distances of 700–1500 km, show characteristic maxima and minima during the time of sunrise and sunset on

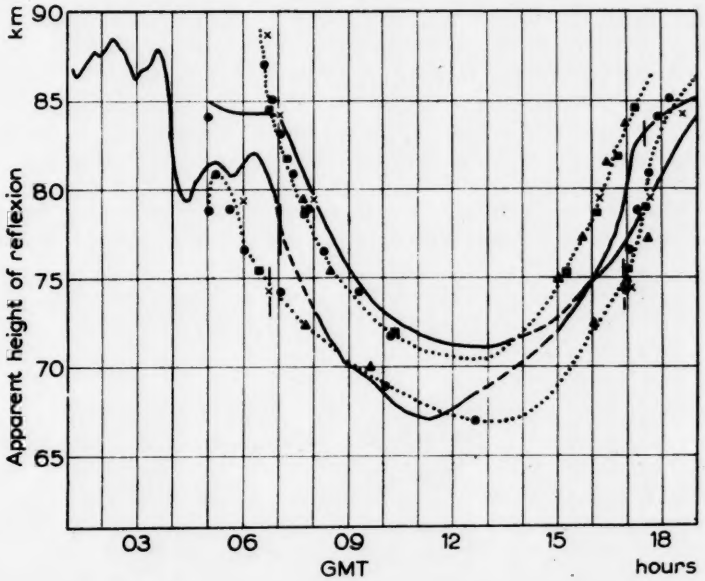

Fig. 5. The changes of apparent height of reflection on 23 February and 21 February on 16 kc/s were at steep incidence (full line), and on higher frequencies at oblique incidence (dotted line)

71 kc/s 860 km ×
113·8 kc/s 870 km ■
128 kc/s 649 km ▲
191 kc/s 1173 km ●

The short vertical lines represent the times of ground sunrise and sunset at the midpoints of the paths.

ordinary days. It has proved possible to decide which of these turning points correspond to in-phase and out-phase relations between a sky-wave and a ground-wave, and to use the results to make deductions about the heights from which the waves are reflected. We hope to publish an account of this work soon.

The knowledge obtained from the records made on ordinary days has been applied to the records made on 23 February to provide the interpretation shown in Fig. 5. Each actual point on the figure corresponds to a turning-point on the record of amplitude. There is some ambiguity at the beginning of the curve, which is indicated by the alternative points.

The height of reflection at midday agrees with that observed on 16 kc/s at steep incidence. The decrease in apparent height appears to start much earlier than usual.

(b) *The Amplitudes of the Reflected Waves*

The most striking feature shown by the amplitudes of the reflected waves is the great decrease in the long-wave oblique-incidence reflection coefficients at 0345. This was followed by an increase after 0430. On a normal day there is near sunrise a characteristic decrease of amplitude; on 23 February this decrease did not take place, so that we may conclude that the conditions of reflection for these waves were considerably different from normal at sunrise.

The amplitude of the abnormal component of the sky-wave at 16 kc/s does not show any marked decrease. At 0345 it increased somewhat, and even at the peak of the disturbance (0415) the amplitude was greater than on a normal summer day.

During the day the amplitude of the sky-wave on 16 kc/s at 90 km from the sender seemed to be rather less than normal, and when received at a distance of 300 km had a reflection coefficient which was about half the normal daytime value. At very oblique incidence (Upsala) the total sky-wave signal was greater than usual.

The midday amplitude of the sky-waves on the low frequencies (70–300 kc/s) was less than normal (although the normal is very variable), but had recovered to the normal value by the night.

On high frequencies in high latitudes (Upsala) the amplitudes of the reflected waves were very much less than normal on all frequencies between 1·5 and 17 Mc/s from sunrise to sunset.

On all frequencies the amplitudes recovered to their normal values during the night of 23 February, and were normal again in the day of 24 February.

VOL.
8
1956

SUMMARY

All the records of sky-wave signals observed by us showed remarkable effects at 0345 $\pm$ 2 min. On low frequencies (70 – 300 kc/s) the effect appeared as very strong absorption which started decreasing at about 0420. On 16 kc/s the main effect was a decrease of 7 to 8 km in the reflection height, with little significant change of amplitude.

Conditions were still markedly abnormal at sunrise and continued so throughout the day but recovered to normal during the following night.

There was some evidence that sunrise effects began rather earlier than usual.

Acknowledgements—We are very much indebted to Dr. F. T. FARMER for operating the recording apparatus on 16 kc/s at Newcastle, and to Mr. W. STOFFREGEN for allowing us to use his 16-kc/s records and $P'f$ curves taken at Upsala.

The 16-kc/s investigations, of which these records form part, were undertaken as part of a contract from the Department of Scientific and Industrial Research.

Cavendish Laboratory,
Free School Lane,
Cambridge.

J. S. BELROSE
M. H. DEVENPORT
K. WEEKES

REFERENCES

BUDDEN K. G.	1953	*Phil. Mag.* **44,** 504.
BUDDEN K. G.	1955	*Phil Trans. A* **248,** 45.
STRAKER T. W.	1955	*I.E.E. Monograph No.* 114.
WEEKES K.	1950	*P.I.E.E.* 97 III, 100.

The solar outburst, 23 February 1956. Observations by the Royal Greenwich Observatory

(*Received* 29 *March* 1956)

Abstract—Cosmic-ray observations, solar photographic observations, magnetic records, and low-frequency radio observations were carried out by the Royal Greenwich Observatory on a routine basis during the period of interest for the investigation of the solar flare that occurred at 0330 UT on 23 February, 1956. The data obtained and relevant instrumental details are presented.

1. *The Cosmic-ray Data*

A STANDARD meson monitor of cubical geometry and incorporating 10 cm of lead-shielding gave the count in 10-min intervals. The equipment is composed of two independent units each with a sensitive area measuring 60 × 60 cm and each having a normal counting rate of approximately 40,000 counts per hour. The table gives the recorded figures in 10-min intervals during the period midnight to midday on 23 February. No barometric correction is included, and correction with the usual total barometric coefficient

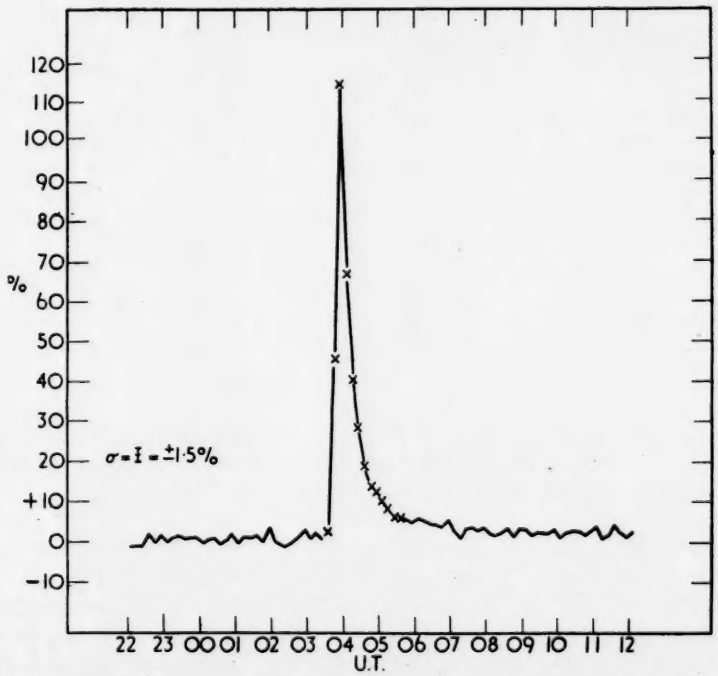

Fig. 1. Cosmic radiation monitor. Herstmonceux sea-level. Cubical geometry 10 cm Pb. Intensity in counts/10 min intervals. Percentage deviation from monthly 10-min mean of 13,440 counts.

of 0·16% per mB would be insignificant during this period. Fig. 1 is a plot of this table, with the two outputs added together.

Fig. 2 represents the total count in two-hour periods from 17 February to 1 March. These data are corrected with the total barometric coefficient of 0·16% per mB. No other atmospheric correction is made. Through smoothing the data by taking them in two-hour intervals, the peak amplitude appears on this graph as only about 17% above normal, whilst this is about 115% above normal when broken up into 10-min intervals.

Table 1. Meson monitor record. Uncorrected counts ÷ 80. (10-min periods.) for each half of monitor and hourly mean barometer readings for period midnight to midday UT 23 February 1956.

UT	1	2	Bar	UT	1	2	Bar	UT	1	2	Bar
0000–0010	83	84		0400–0410	136	140		0800–0810	84	85	
20	83	84		20	116	117		20	84	84	
30	83	85		30	106	107		30	83	86	
40	83	83	1015·8	40	97	99	1016·4	40	86	85	1017·6
50	82	85		50	94	95		50	83	84	
0100	85	84		0500	94	94		0900	85	86	
10	82	84		10	93	90		10	85	85	
20	85	83		20	88	90		20	84	84	
30	84	84	1015·9	30	87	88	1016·7	30	85	84	1017·6
40	84	85		40	88	88		40	83	86	
50	82	84		50	87	88		50	85	84	
6200	86	86		0600	87	87		1000	85	85	
10	83	85		10	86	89		10	84	83	
20	84	85		20	86	87		20	85	84	
30	82	84	1016·0	30	86	88	1017·0	30	85	85	1017·6
40	82	84		40	86	86		40	84	85	
50	83	85		50	85	86		50	85	83	
0300	84	87		0700	87	88		1100	84	85	
10	83	86		10	84	86		10	85	86	
20	85	85		20	82	85		20	83	83	
30	81	85	1016·1	30	85	86	1017·3	30	84	84	1017·5
40	86	83		40	85	86		40	85	87	
50	121	122		50	84	86		50	84	85	
0400	178	178		0800	85	86		1200	83	83	

A decrease occurred at midday on 25 February at which time a magnetic storm following the flare was in progress. The decrease is, however, small, and would by itself not have been regarded as a significant event.

2. *Solar Observations*

Fig. 3 shows the sun as it appeared on the previous day, 22 February. Spots had developed in two well-defined latitude belts, and the method of growth of spots, during which a considerable amount of linking up was observed, had been commented on by solar observers before the great outburst. The flare, which was reported by Kodaikanal Observatory, occurred over the region of spots indicated by the white arrows. Fig. 4 shows the sun on 23 February in the light of Hα; it is taken with the aid of a Lyot birefringent filter. The clear tendency for latitude belts of disturbance is also in evidence there (the sun's axis was inclined by 7° to the line of sight, which accounts for the apparent curvature of the belt).

3. *The Magnetic Records*

Fig. 5 gives the Abinger magnetograms for the three elements H, the horizontal field of strength, D, the declination, and Z, the vertical field of strength. On 23 and 24 February there were only minor disturbances, and a magnetic storm beginning with a sudden commencement of about 40 γ occurred on 25 February. No other substantial

VOL. 8 1956

flare having been recorded in the interval, it appears not unreasonable to relate this storm to the flare under discussion. The interval between the first observation of the flare at 0330 UT on 23 February and the sudden commencement at 0310 UT on 25 February would thus be nearly 48 hours. Although this is rather a long interval, it is not so long as to preclude a connection between the two events.

4. *Low-frequency Radio Observations*

"Atmospherics" (M. WALDMEIER, 1949; M. A. ELLISON, 1950) at a frequency of 27 k/c per second are recorded at Herstmonceux on a routine basis to serve as a flare warning.

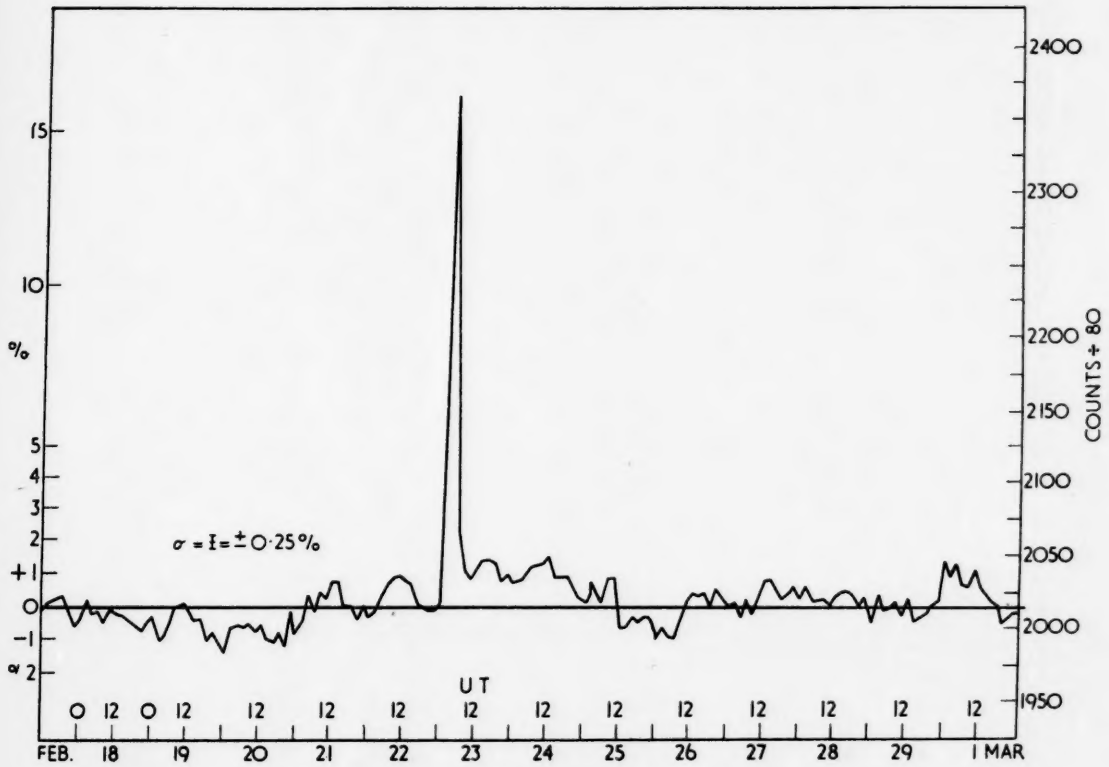

Fig. 2. Herstmonceux. Intensity counts/2-hr period. Corrected for total barometer coefficient 2·15 % cm. Percentage deviation from monthly 2-hr mean of 161,280 counts.

Under normal conditions during the daylight hours the occurrence of a flare improves the reception of atmospherics which mainly arise from thunderstorms in the tropics. It is known that this type of recording is of no value in giving warning of ordinary flares at nighttime. At night the record is usually steady and the level high, indicating that the nighttime reception is principally due to signals transmitted over a nighttime path. Fig. 6 gives the comparison between an ordinary 24-hour record and the record obtained on 23 February. It will be seen that a very substantial decrease occurred at 0345 UT in a time very much shorter than the normal sunrise effect. This phenomenon cannot be attributed to any change in the propagation characteristics in the sunlit hemisphere, for even the

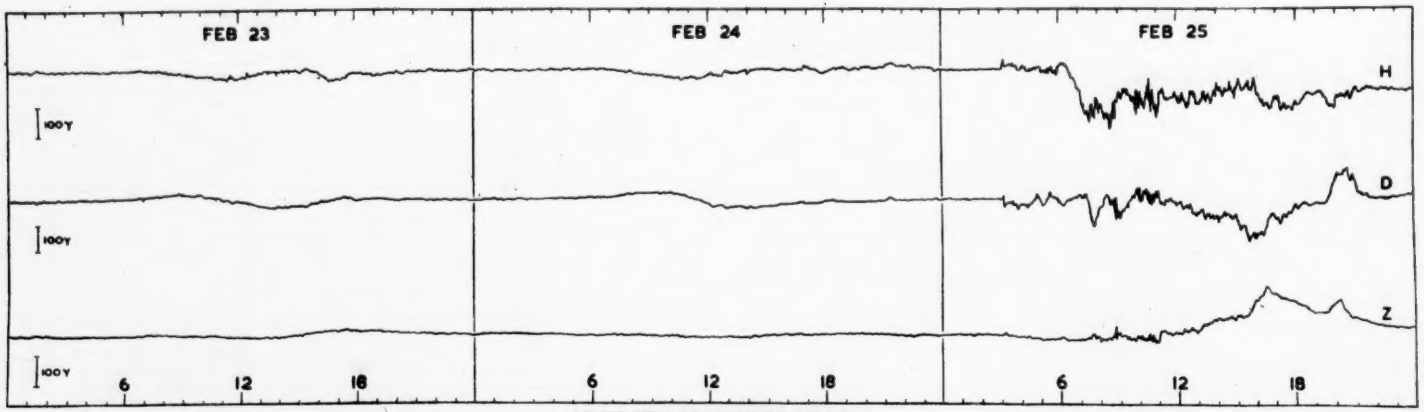

ABINGER MAGNETOGRAM

Fig. 5. Abinger magnetograms, 23–25 February.

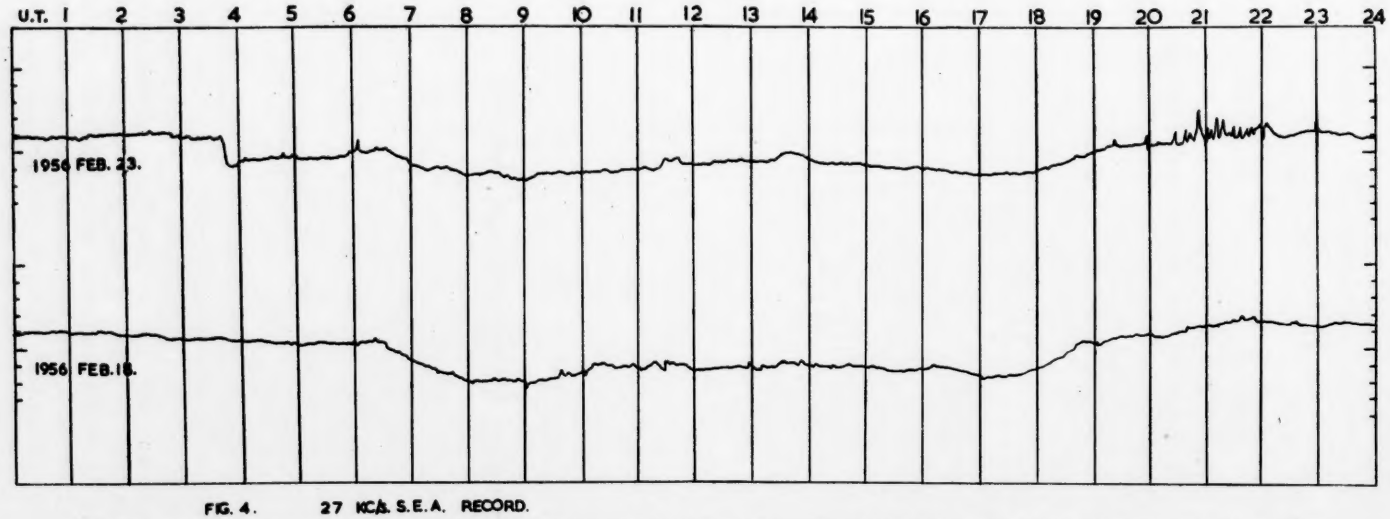

Fig. 6. The upper trace shows the sudden decrease at about 0345 UT. The lower trace shows the usual type of record, with the steady nighttime signal and the gradual decrease after sunrise.

VOL. 8 1956

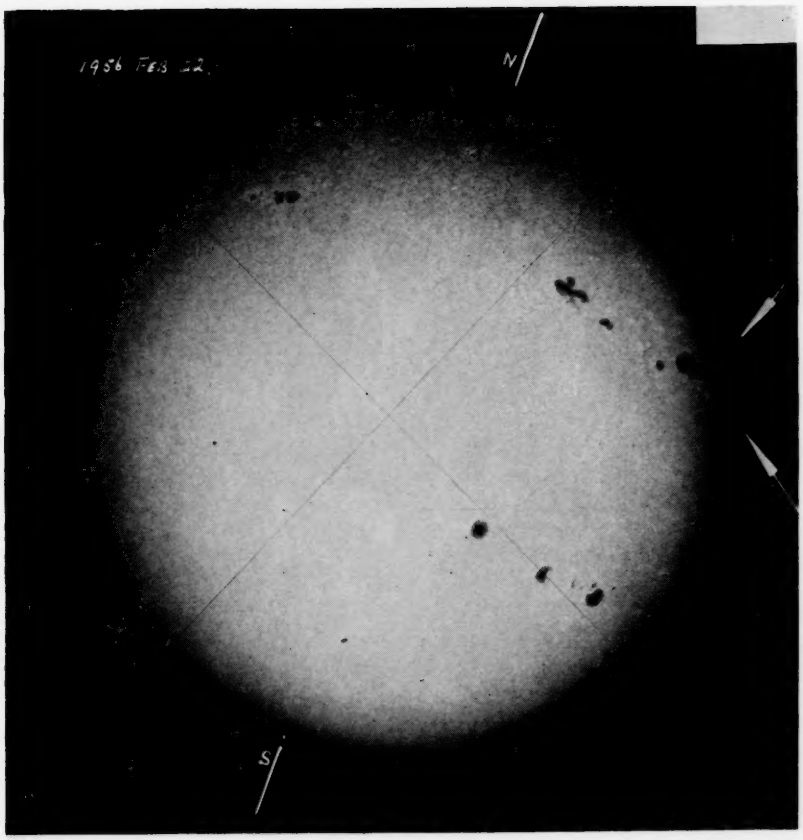

FIG. 3

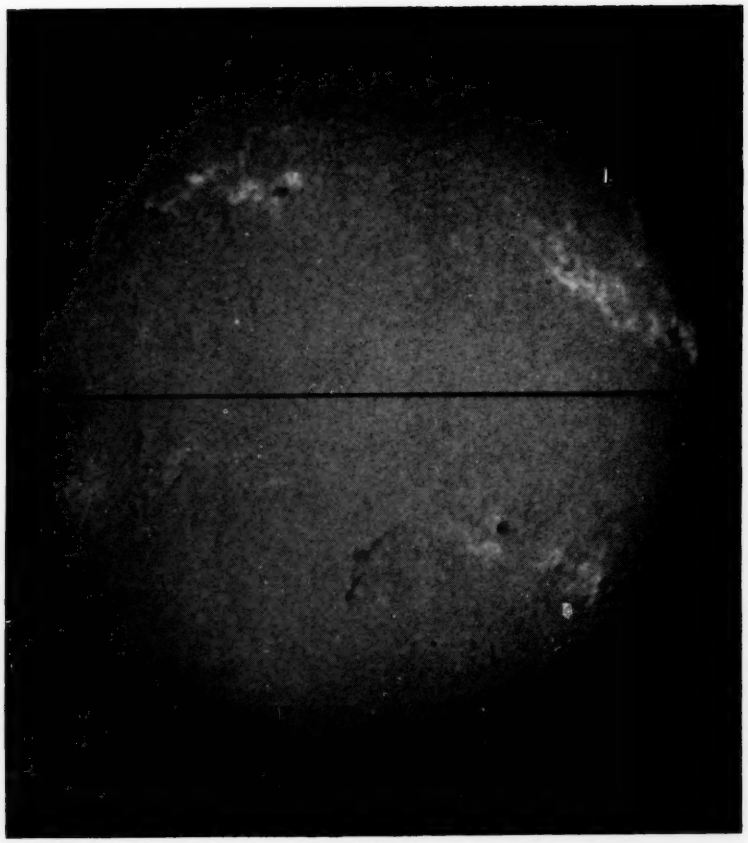

FIG. 4

VOL.
8
1956

complete interruption of the transmission over that side could not have resulted in as great a reduction of the signal. It is therefore necessary to attribute this effect to ionization caused by the stream of particles, and indeed the timing agrees with the cosmic-ray increase rather than with the ultra-violet-light effect on the ionosphere on the daylight side of the earth.

No effect of this sort seems to have been recorded before, and the implications are not at present clear to us. The measurement contains information regarding the cosmic-ray flux at high levels in the atmosphere before it can have been subjected to significant atmospheric attenuation, and it may therefore be of importance in determining the primary spectrum associated with the event.

Acknowledgement—We are indebted to Dr. M. A. ELLISON for drawing our attention to this anomalous record, which is similar to the one obtained by him in Edinburgh. He is in agreement with the interpretation as a particle effect.

T. GOLD
D. R. PALMER

Royal Greenwich Observatory,
Herstmonceux Castle,
Hailsham, Sussex.

REFERENCES

WALDMEIER M. 1949 *Z. Astrophys*, **26**, 205
ELLISON M. A. 1950 *Pubs. Royal Observatory Edinburgh* Vol. 1. No. 4, 54

A long-wave anomaly associated with the arrival of cosmic-ray particles of solar origin on 23 February 1956

(*Received* 19 *March* 1956)

A SOLAR flare of importance 2–3 was observed at the Astrophysical Observatory, Kodaikanal (S. India), on 23 February 1956, lasting from 0335 to 0510 UT. We owe these particulars, as well as much information relating to the Kodaikanal ionospheric observations, to the kindness of the Director, Dr. A. K. DAS, who has placed them at our disposal in advance of publication.

A magnetic crochet in H was recorded at Kodaikanal, beginning at 0335, amplitude 68 γ, with a duration of 79 min; also a short-wave fade-out beginning about 0332 and lasting till 0700. Fade-outs on short waves were reported by Cable and Wireless Limited on far-eastern channels at their stations of Hongkong and Singapore, beginning at 0335 and recovering to normal about 0600 (Singapore).* The long duration of the fade-outs, together with the great amplitude and duration of the crochet, indicate that a particularly intense burst of ultra-violet radiation from this flare must have affected the daylight hemisphere of the earth.

The flare itself is illustrated in the fine $H\alpha$ spectroheliogram (Fig. 1) taken by the Kodaikanal observers at 0400 UT.† The solar co-ordinates (80° W, 20° N) place this flare within the great sunspot group of central meridian passage, 18 February. From past experience, the crochet and fade-out data enable us to fix the time of peak intensity of the flare with some confidence as having occurred between 0335 and 0340.

* Information kindly supplied by the Engineer-in-Chief, Cable and Wireless Limited.

† The area of the flare emission, as measured from the photograph and corrected for foreshortening, is >2000 millionths of the visible hemisphere. On the basis of area, therefore, this flare should perhaps be rated Class 3 or 3+, but the classification is always in some doubt when a flare is so close to the limb.

The long-wave anomaly recorded at the Royal Observatory, Edinburgh, is shown in Fig. 2(b). This is a record of the integrated intensity of atmospherics on a frequency of 24 kc/s (12,500-m wavelength). The unique feature of this record is the sudden diminution in the received signal-strength, beginning at 0345 and coinciding in time with the arrival of the solar cosmic-ray particles in the dark hemisphere. During six years of continuous recording, no similar effect has been found.

For comparison, Fig. 2(a) illustrates the normal behaviour between night and day at this time of year. The integrated intensity is high and fluctuating during the night hours, and this is followed by a drop of intensity to the steadier daylight level which takes place at the time of *D*-layer sunrise (0700). From Fig. 2(b) we can see that the influence of the

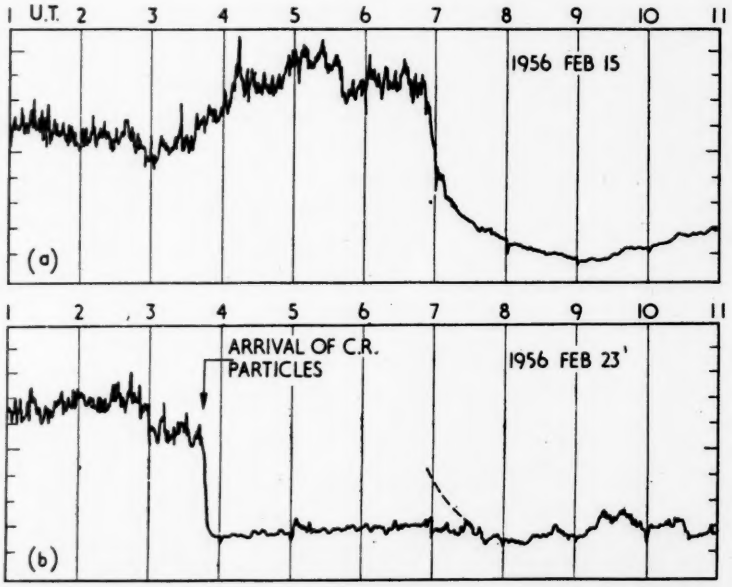

Fig. 2. (a) Normal record of integrated intensity of atmospherics at a frequency of 24 kc/s, showing sunrise effect at 0700. (b) Sudden diminution in received signal strength at 0345 on 23 February 1956, coinciding with the arrival of cosmic-ray particles from the sun.

cosmic-ray particles upon the *D* layer, for reflections occurring at frequency 24 kc/s, was to produce an "artificial sunrise" effect which was completed within the space of 10 min. If the interpretation of extra ionization occurring in *D* is correct, the reflecting ceiling must have fallen suddenly by some 10–15 km. There is evidence of a slight recovery during the next three hours before the normal sunrise effect began to take control.

It may be noted that the main transmitting centres were probably located far to the *south* of the British Isles, in the tropical thunderstorm belts; the records for the days immediately preceding and following 23 February showed a marked absence of local centres of transmission.

Our record of galactic radio noise being received through the *D*, *E*, and *F* layers on a frequency of 18 Mc/s, was perfectly steady at 0345, and showed no increase of absorption.

Four previous examples are known of sudden increases in the high-energy component of cosmic radiation. The time-intervals (cosmic-ray maximum *minus* flare maximum)

VOL. 8 1956

COL.
956

FIG. 1. $H\alpha$ spectroheliogram (23 February 1956, 0400 UT.) taken at Kodaikanal Astrophysical Observatory and reproduced by kind permission of DR. A. K. DAS. Flare shown at *F*.

VOL.
8
1956

were as follows: 28 February 1942, 1 h; 7 March 1942, 1 h; 25 July 1946, 2·5 h; 19 November 1949, 0·5 h.* In the present instance the observed increase appears to have been greater and the time-interval shorter (~0·3 h) than in any of the earlier cases.

M. A. Ellison
J. H. Reid

Royal Observatory,
Edinburgh, 9.

A note on the interpretation of transient echoes from the ionosphere

(*Received* 8 *February* 1956)

In a recent research note, Shain and Kerr (1955) refer to the pronounced midday maximum in the rate of occurrence of transient echoes from meteor trails in the 100-km region of the ionosphere. They mention that this maximum was not satisfactorily explained by the early studies of the diurnal and seasonal variations of these echoes (Appleton and Naismith, 1947; Eastwood and Mercer, 1948), and proceed to demonstrate that the midday maximum disappears if the observed diurnal rate curve is corrected for the effect of cosmic noise on the sensitivity of the apparatus. This is undoubtedly an important effect when observations are made on low frequencies (~18 mc/s) with broad-beam aerial systems, as in the experiments of Shain and Kerr. However, in view of the current interest in meteor ionization as a possible influence on long-distance scatter communication, it is necessary to emphasize that the rate of occurrence of meteors often does show a pronounced midday maximum. The prevalent idea that meteoric activity has a maximum at 0600 and a minimum at 1800 local time, arises from the belief that meteoric effects are due to a uniform distribution of sporadic meteors. The recent radio-echo work on meteors has shown the falsity of this assumption, and has also emphasized the significant influence of daytime meteor streams on the diurnal distributions.

As an example, reference may be made to two radio-echo surveys carried out at Jodrell Bank which have now continued without interruption for several years. The first of these uses two narrow-beam aerials on 70 mc/s (Aspinall, Clegg, and Hawkins, 1951). The effect of cosmic noise on sensitivity variations is small and can easily be included in the analysis. An extensive analysis involving over a quarter of a million meteor echoes has been made by Hawkins (1956) for the years 1949–50, 1950–51, and the results as far as they concern the diurnal distributions have been given by Lovell (1954). The tendency during the months of October to March for the main peak to occur at 0600 is completely reversed during the months of April to September, when the peak at 0600 is small compared with the major peak of activity during the daytime.

The second survey, also on 70 mc/s, uses a beamed aerial rotating twice per minute about a vertical axis. Thus the total meteor activity in the sky is sampled at this rate, and furthermore any residual influences of cosmic noise on the sensitivity will be eliminated in this sampling. The results, which are unpublished, show the same diurnal characteristics as the fixed-beam surveys. Typical examples are shown in Figs. 1(a) and 1(b), where the curve of variation for 18 January 1955 shows a maximum at 0400, whereas that for 14 June 1954 shows a much larger maximum from 0800 to 1200.

---

* See, for example, M. A. Ellison: *The Sun and Its Influence* (Routledge and Kegan Paul, 1955), Table IX, p. 207.

The explanation of these midday maxima is that in the region of longitude 20° to 150° the earth passes through a dense concentration of meteoric debris, made up of the intense summer daytime meteor streams together with a great enhancement of sporadic activity. The cosmological reason for this asymmetry in the distribution of meteoric matter around

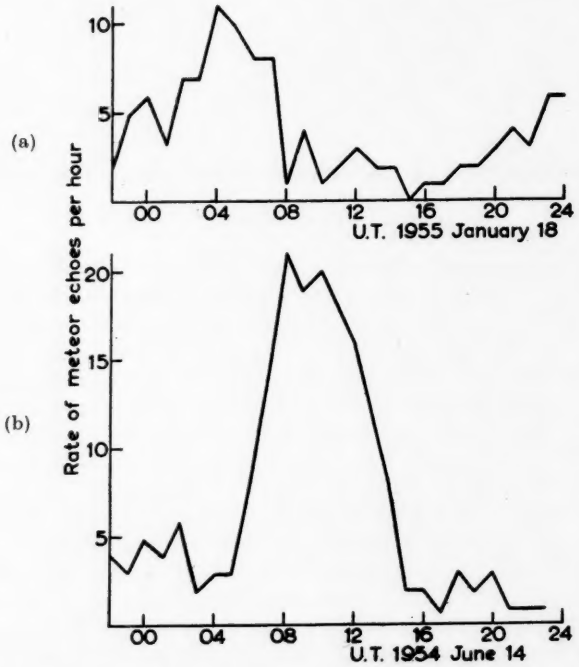

Fig. 1. Diurnal variation of rate of occurrence of radio echoes from meteor trails observed on 70 mc/s with a rotating aerial beam. (a) 18 January 1955, (b) 14 June 1954.

the earth's orbit is unknown, although HAWKINS (1956) has shown that a close correlation exists between this seasonal variation and the variation of the cometary index with solar longitude.

A. C. B. LOVELL

University of Manchester,
Jodrell Bank Experimental Station.

VOL.
8
1956

REFERENCES

APPLETON E. V. and NAISMITH, R.	1947	*Proc. Phys. Soc.* **59,** 461.
ASPINALL A., CLEGG J. A., and HAWKINS G. S.	1951	*Phil. Mag.* **42,** 504.
EASTWOOD E. and MERCER K. A.	1948	*Proc. Phys. Soc.* **61,** 122.
HAWKINS G. S.	1956	*Monthly Not. Roy. Ast. Soc.* (in publication).
LOVELL A. C. B.	1954	*Meteor Astronomy*, Chapter 6.
SHAIN C. A. and KERR F. J.	1955	*J. Atmosph. Terr. Phys.* **6,** 280.

LETTERS TO THE EDITOR

Automatic recording of ionospheric characteristics

RECENTLY, Japanese workers (NAKATA *et al.*, 1953) have proposed a simple device in order to obtain direct records of the minimum virtual height of the ionospheric layers: a normal panoramic ionosonde is connected with a c.r. tube with only one deflection (the virtual height). In another device, after gating a certain echo-trace, only the frequency deflection is applied. One thus obtains a direct record of critical frequencies; blanketing frequencies and absorption limits are also recorded. In the future, most ionospheric characteristics may be directly recorded in this way. Another important characteristic is the MUF, or the M factor, which

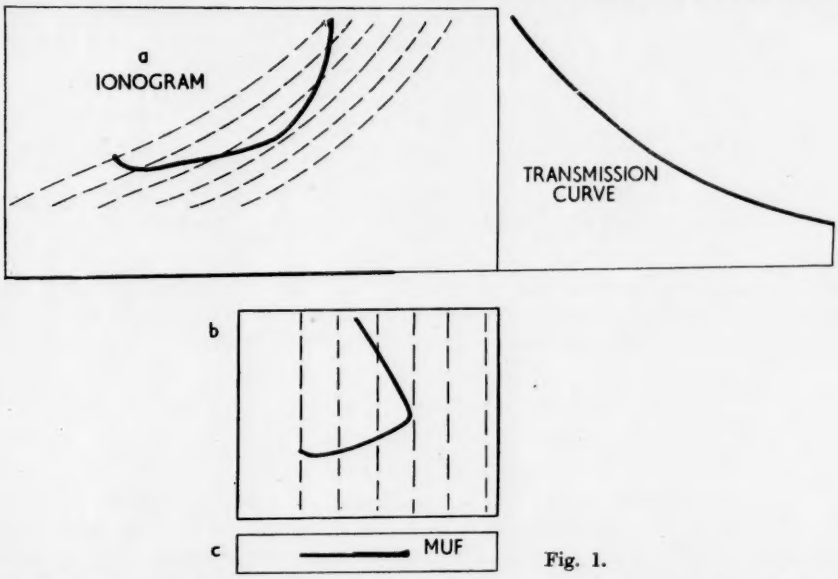

Fig. 1.

is of special importance for transmission application. It is normally determined for a (fictive) distance of 3000 km by applying a set of "transmission curves" to the ionogram. We propose here a device with which one may obtain a direct record of the MUF.

The normal record of an ionogram (Fig. 1a) can be transformed into a "synthetic" oblique-incidence-ionogram (Fig. 1b) by applying to the (slow) frequency deflection an additional tension synchronized with the pulse-recurrence frequency and having the form of the reciprocal "transmission curve" (Fig. 1a). Thus the transmission curves (curves of constant transmission frequency), which are curved in Fig. 1a, are transformed into vertical straight lines (dotted in Figs. 1a and 1b). The transmission curve is independent of the absolute frequency value, provided that the frequency axis itself is logarithmic. This is the case with our ionosondes (BIBL, 1951). The form of the transmission curve can easily be approximated with a waveform given by the discharge of a condenser and a suitable amplification stage. When the virtual height-deflection is suppressed (we then obtain [Fig. 1c] the projection on the MUF axis shown in Fig. 1b), we have a direct record of the MUF.

K. BIBL.

S.P.I.M. (France),
Ionospheric Station Neuershausen (Germany)

REFERENCES

BIBL, K.	1951	*Ann. Geophys.* **7**, 265–267.
NAKATA, Y., KAN, M., and UYEDA, H.	1953	*Rep. Ionosphere Res.*, Japan, **VII**, 129–135.
NAKATA, Y.	1954	*J. Radio Res. Lab. Tokyo* **1**, No. 2.

Focusing on a "rippled" ionosphere

At the Cambridge Conference on the Physics of the Ionosphere, I discussed the influence of geometrical optics on the field strength of waves reflected from the ionosphere (Bibl *et al.*, 1954). Formulae are given for the case of a curved ionosphere and a flat earth. (The expressions corresponding to higher-order echoes are not exact.) The correct system of equations (which is also valuable for the case of strong focusing) is the following, the "photometric decrement" δ_1 (Rawer, 1947, 1948, 1952) corresponds to the logarithm of the brackets [. . .]:

$$E_1 = E_0 \cdot \rho \Big/ \left[2H\left(1 - \frac{H}{r}\right)\right]$$

$$E_2 = E_0\, \rho^2 \rho_T \Big/ \left[4H\left(1 - \frac{H}{r}\right)\left(1 - 2\frac{H}{r}\right)\right]$$

$$E_3 = E_0\, \rho^3 \rho_T{}^2 \Big/ \left[6H\left(1 - \frac{H}{r}\right)\left(1 - \frac{4}{3}\frac{H}{r}\right)\left(1 - 4\frac{H}{r}\right)\right]$$

$$E_4 = E_0\, \rho^4 \rho_T{}^2 \Big/ \left[8H\left(1 - \frac{H}{r}\right)\left(1 - 2\frac{H}{r}\right)\left(1 - \frac{4}{2+\sqrt{2}}\frac{H}{r}\right)\cdot\left(1 - \frac{4}{2-\sqrt{2}}\frac{H}{r}\right)\right]$$

(E field strength, E_0 reference field, ρ reflection coefficient of the ionosphere, ρ_T reflection coefficient of the earth, H altitude of reflection, r radius of curvature of the reflecting surface.)

With this system, focusing exists for the following values of H/r

1st echo: 1
2nd echo: 1, 0·5
3rd echo: 1, 0·75, 0·25
4th echo: 1, 0·5, 0·853, 0·147

Some regularities of this system are easily understood. Focusing exists for all orders if the centre of curvature lies on the surface of the earth ($H/r = 1$). If focusing is obtained with a certain value of H/r for the order n, it must exist for the same values of H/r for every order being an integer multiple of n.

The formulae given here are valuable for "ripples" of a spherical form. In the case of cylindrical-ripples, the focusing effect is less pronounced, and the square roots of all parentheses (. . .) must be taken.

Finally, it is the author's opinion that the "ripples" of the ionosphere are not always present in the same form. Not all variations of the reflected amplitude can be explained with the model used here. On the other hand, there are fairly frequent typical cases which can be explained by ripples. The problem of echo amplitude is very complex, as different influences may often be effective at the same time.

K. Rawer.

S.P.I.M., Neuf-Brisach Ht. Rh. (France)

References

Bibl K., Harnischmacher E., and Rawer, K. 1954 *The Physics of the Ionosphere*, Cambridge Conference, 113–118.
Rawer K. 1947 *Rev. Sci.* **85**, 361.
1948 *Rev. Sci.* **86**, 585.
1952 *Wireless Engr.* **29**, 287–301.

VOL. 8 1956

Journal of Atmospheric and Terrestrial Physics, 1956, Vol. 8, pp. 297 to 304. Pergamon Press Ltd., London

On the existence of a "Q.L."–"Q.T." "transition-level" in the ionosphere and its experimental evidence and effect

D. LEPECHINSKY
Laboratoire National de Radioélectricité, Bagneux (Seine), France

(*Received* 6 *December* 1955)

Abstract—The magneto-ionic theory shows that when the effects of collisions and of the earth's magnetic field are taken into consideration, the propagation is "quasi-longitudinal" in the lower part of the ionosphere, where the collision frequency is high and "quasi-transverse" in its upper part, where the collision frequency is low. For vertical incidence, the altitude at which the transition between the Q.L. and Q.T. regions occurs is that corresponding to the critical collision frequency ν_c which is a function of the gyrofrequency and of the magnetic dip angle only. For France, where this angle is 64° to 65°, the transition level is located at about 95 km, i.e. within the E region. At midday, when the maximum electron density of the E layer occurs at the lowest heights, it may happen that this maximum penetrates the Q.L. region. The evaluation of N_{max} should therefore be made with caution, for in the latter case, the critical frequency observed (corresponding to the ordinary trace vertical tangent), when used in the classical formula, only valid in the Q.T. region, leads to a serious underestimate of N_{max}. When N_{max} is located somewhat lower than the transition level, or exactly at this altitude, the $h'f$ record should show either a crochet (in the first case), or a hollow, i.e. a complete absence of trace (in the second case). Crochets and hollows of this sort are indeed quite often found in the $h'f$ records of the Poitiers and Domont stations. It is shown how these hollows and crochets can be fully explained on the basis of the magneto-ionic theory and that they are in fact an excellent evidence of the existence in the E region of the Q.L.–Q.T. transition level. Finally, attention is drawn to the criteria now in use to determine the f_0E, which often leads to an apparent flattening of the N_{max} diurnal curve, and appropriate formulas and methods are suggested to find the correct values of N_{max}.

1. The Magneto-ionic Theory Consequences

It is generally recognized now that the propagation of an electro magnetic wave in the ionosphere is governed by the fundamental Appleton-Hartree formula (Appleton, 1932) at least to a first approximation. After quite a controversy regarding the validity of the so-called "Lorentz term," it appears now that this term can be disregarded (Darwin, 1943). More recently, a careful study has shown that the collisional frequency ν required a slight adjustment by a factor of 4/3 in order that the formula be in line with that derived independently by Huxley (Pfister, 1954). Attention has also been drawn since 1933, by Appleton and Builder, to the fact that the formula implied the existence of two quite different types of ionospheric propagation, namely the "quasi-transverse" ("Q.T.") and the "quasi-longitudinal" ("Q.L."), according to the value of the ratio:

$$|y_T^2/2zy_L|.$$

But, to our knowledge, the precise picture of the actual change-over from the "Q.L." to the "Q.T." propagation condition that occurs during the upward journey of an electromagnetic wave in the ionosphere, needs some further clarification.

H. G. Booker (1934) has shown in an extensive study how different are these two types of propagation and how essential it is therefore to know the value of the collision frequency ν and also that of the angle of the earth's magnetic field

with the direction of travel of the wave, which both determine the value of the above-mentioned ratio, and thus the propagation type in the medium.

It is quite regrettable that in order to avoid time-consuming calculations required by the complete Appleton-Hartree formula, it has been usual practice up to now to neglect completely the effect of collisions, for it has led to the wrong feeling that ionospheric propagation is always "Q.T.," and thus to inadequate results regarding the reflexion conditions in cases when the propagation is in fact "Q.L."

In order to make this clear, let us put down the complete formula

$$\left(\mu - j\frac{ck}{p}\right)^2 = 1 - \frac{x}{1 - jz - \dfrac{1/2\, y_T^2}{1 - x - jz} \pm \sqrt{y_L^2 + \left(\dfrac{1/2 y_T^2}{1 - x - jz}\right)^2}}, \qquad (1)$$

where μ is the refractive index which governs the phase velocity;

k is the absorption coefficient per unit path-length;

$p = 2\pi f$ is the pulsation of the wave under consideration, whose frequency is f;

$x = \dfrac{4\pi N e^2}{mp^2}$, where N is the electron density per cm^3, e and m are respectively the charge and the mass of an electron;

$y_T = y \sin\varphi$ and $y_L = y \cos\varphi$, where $y = f_H/f$, f_H being the gyrofrequency;

$z = \nu/p$, where ν is the collision frequency per sec; φ is the angle between the direction of propagation and that of the geomagnetic field;

$j = \sqrt{-1.}$

In a recent work (LEPECHINSKY, 1955), the author has shown how the variation of μ or k as a function of x (i.e., of the electron density N, when a fixed frequency f is considered) can be easily derived, and how completely different it is for both magneto-ionic components, according as

$$\nu \gtrless \left| p_H \frac{\sin^2\varphi}{2\cos\varphi} \right|, \qquad (2)$$

the value of ν corresponding to this ratio being called "critical," and represented by ν_c.

Now if ν is actually smaller than ν_c, the propagation is "Q.T." and the variation of μ with N for both the ordinary and extraordinary rays resembles closely that of the $\nu = 0$ case, when $\hat{\varphi} \neq 0°$.

On the contrary, if $\nu > \nu_c$ the propagation is "Q.L." and the variation of μ for both rays resembles closely that of the $\nu = 0$ case, with $\hat{\varphi} = 0°$.

Let us remember that in the former case ($\nu = 0$, $\hat{\varphi} \neq 0°$), μ_0 falls to zero for $x = 1$ and μ_e becomes nil for $x = 1 - y$ (if $f > f_H$), whereas in the latter case, μ_0 falls to zero for $x = 1 + y$, while μ_e still becomes nil for $x = 1 - y$, and that

VOL. 8 1956

these are precisely the classical reflexion conditions for the ordinary and extra-ordinary rays at vertical incidence.

It follows that disregarding the effect of collisions on propagation may lead to a substantial error in the evaluation of the electron density required to reflect the ordinary component of the wave.

2. The Transition Level

It is quite remarkable that condition (2) is *independent of the frequency* of the wave under consideration and that ν_c is a function of the gyrofrequency and

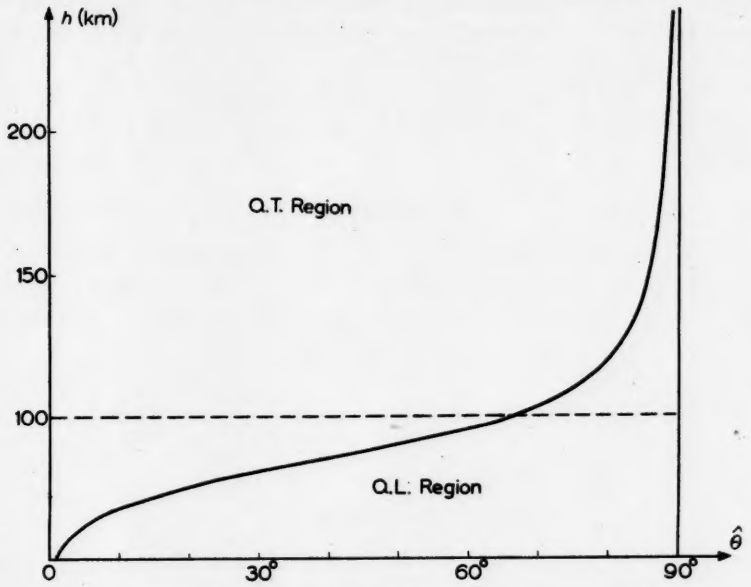

Fig. 1.

of the angle $\hat{\varphi}$ only. In fact, (2) corresponds to the classical "change-over" condition

$$z \gtrless \left| \frac{y_T^2}{2y_L} \right|, \tag{2'}$$

which may be written

$$\frac{\nu}{2\pi f} \gtrless \left| y \frac{\sin^2 \varphi}{2 \cos \varphi} \right|, \qquad \text{where } y = f_H/f.$$

(2′) thus becomes

$$\nu \gtrless \left| p_H \frac{\sin^2 \varphi}{2 \cos \varphi} \right|. \tag{2}$$

For vertical incidence: $\hat{\varphi} = 90° - \hat{\theta}$, if $\hat{\theta}$ is the dip angle of the earth's magnetic field, so (2) in this case reads

$$\nu \gtrless \left| p_H \frac{\cos^2 \theta}{2 \sin \theta} \right|. \tag{2''}$$

Now the gyrofrequency f_H may be considered constant over a considerable range in altitude. It follows that there exists a quite definite "transition level" from the "Q.L." to the "Q.T." propagation region. located at an altitude where $\nu = \nu_c$ and which can be easily determined if the distribution of ν against height is known.

Fig. 1 shows the altitude above ground of this transition level for vertical incidence as a function of the dip angle θ, assuming that ν decreases with height according to the data given in Circular No. 462 of the National Bureau of Standards (U.S.A.), and that $f_H = 1{\cdot}2$ Mc/s. It is quite striking that the "Q.L." region reaches the 100-km level for dip angles θ as low as 65°. According to more recent conservative assumptions regarding the distribution of ν with height (WAYNICK, 1954), this dip angle would correspond to a "Q.L." region extending up to 90 km only.

Taking 95 km as a representative figure, we see that the E layer at midday in our latitudes is most certainly plunged in the "Q.L." region up to its maximum electron density.

3. THE EFFECT ON PROPAPAGATION OF THE TRANSITION LEVEL

In order to ascertain what exactly happens to a wave reaching the "Q.L."–"Q.T." transition level, let us consider in Fig. 2 the curves representing the variation of the refractive indexes μ_0^2 and μ_e^2 with the electron density when $f > f_H$.

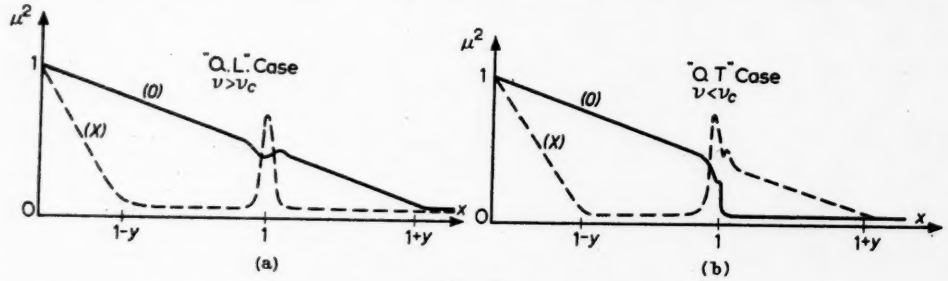

Fig. 2.

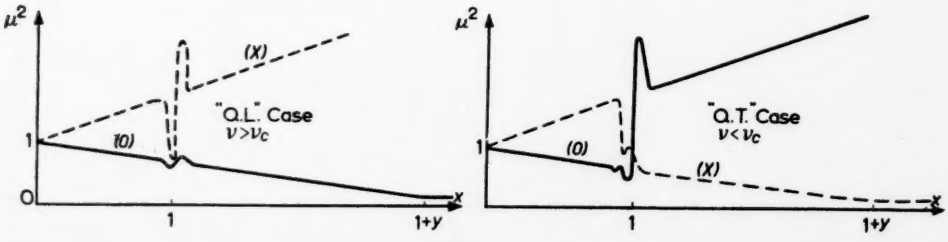

Fig. 3.

Up to $x \doteqdot 1$, corresponding to $N \doteqdot mp^2/4\pi e^2$, there is no significant difference in either μ_0 or μ_e values between the "Q.L." and the "Q.T." cases. Near $x = 1$, there is an abrupt decrease of μ_0 in the "Q.T." case but not in the "Q.L." case. Obviously the major difference occurs for the μ_0 values, when x is greater than 1 and smaller than $1 + y$.

VOL. 8 1956

Thus if the transition level coincides with an electron density corresponding to a value of x within these limits, and if the wave travels vertically upwards, traversing first the "Q.L." region, its ordinary component will suffer an abrupt fall of its refractive index at the transition lever; in other words, this level will actually reflect the wave downwards because of the steep gradient of μ_0 occurring there.

When $f < f_H$, the μ^2 curves are as shown in Fig. 3, and the discontinuity of the refractive index may occur in both the ordinary and extraordinary waves, when at the transition level the value of N corresponds to an x greater than 1. It thus appears that for $f < f_H$, the transition level may also become reflecting.

4. Experimental Evidence of the Existence of the Transition Level.

We have seen that the E layer in our latitudes ($\theta \doteq 65°$) most probably crosses the "Q.L."–"Q.T." transition level for vertical incidence (95 km) during its diurnal forenoon descent.

Let us suppose that the N distribution of the E layer is symmetrical about the level of N_{max}, and consider the following cases:

(a) N_{max} of the E layer is above the transition level XY, where $N = N_L$. In this case the highest frequency f_L ordinary wave reflected according to the pure "Q.L." mode corresponds to

$$x = 1 + y \qquad \text{(see Fig. 2a)}$$

i e., to

$$\frac{4\pi N_L e^2}{m p_L^2} = 1 + \frac{f_H}{f_L}.$$

It is thus given by

$$f_L = \frac{1}{2}\left(-f_H + \sqrt{f_H^2 + \frac{4N_L}{1{\cdot}24\,.\,10^4}}\right), \tag{3}$$

if f_L is expressed in Mc/s and N in electrons per cm^3.

Ordinary wave frequencies higher than f_L are reflected at the XY transition level, because of the discontinuity of μ_0, up to the frequency f_T corresponding to the "Q.T." reflexion condition

$$x = 1$$

i.e., to

$$\frac{4\pi N_L e^2}{m p_T^2} = 1,$$

whereby it follows that

$$f_T = \sqrt{\frac{N_L}{1{\cdot}24\,.\,10^4}}, \tag{4}$$

if f_T is in Mc/s and N_L in electrons per cm^3. f_L and f_T, p_L and p_T should not be confused with the longitudinal and transverse components of the gyrofrequency and their pulsations. An $h'f$ record should thus exhibit in this case an almost constant reflexion height for all frequencies between f_T and f_L, the former being the higher limit of the band.

(b) N_{max} of the E layer coincides with XY transition level. In this case again all frequencies between f_T and f_L are reflected at the transition level XY, but, this level being that of N_{max}, high retardation is suffered by all frequencies and the corresponding $h'f$ record should exhibit a complete absence of trace (hollow) between f_T and f_L.

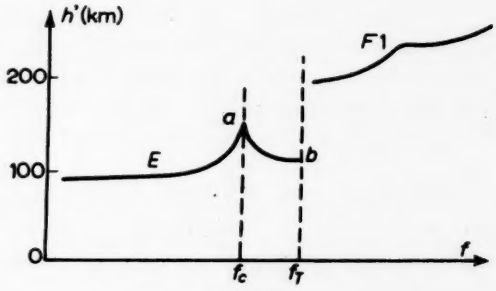

Fig. 4.

(c) N_{max} of the layer is below the transition level in the "Q.L." region. This time, if XY is not too high above N_{max}, frequencies higher than f_c traverse the N_{max} level according to the "Q.L." mode, but suffer an abrupt fall of their "ordinary" refractive index μ_0 at the transition level and are thus reflected downwards.

An additional trace should therefore appear on the $h'f$ record after the f_c's critical frequency vertical tangent (see Fig. 4).

This additional trace ab corresponds to all the frequencies reflected by the XY transition level.

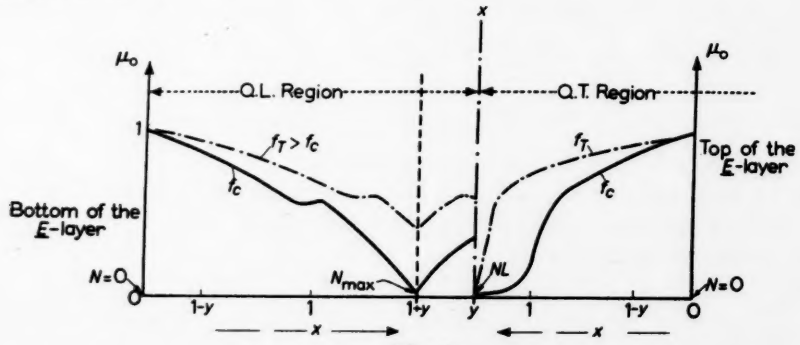

Fig. 5.

The highest of them, f_T, is obviously the frequency whose μ_0 drops to a very small value just at the transition level (where $N = N_L$) according to the "Q.T." mode (see Fig. 5).

It is thus given by

$$f_T = \sqrt{\frac{N_L}{1{\cdot}24\,.\,10^4}},$$

while

$$f_c = \frac{1}{2}\left(-f_H + \sqrt{f_H{}^2 + \frac{4\,N_{max}}{1{\cdot}24\,.\,10^4}}\right).$$

VOL. 8 1956

The crochet *ab* of Fig. 4 may of course be more or less extended in frequency according to the actual distance between the N_{max} and the XY transition levels. It has the longest extent in frequency when XY is just over the N_{max} level, for then:

$$f_T = \sqrt{\frac{N_{max}}{1{\cdot}24 \,.\, 10^4}} \text{ Mc/s.}$$

It is easy to see that if $f_T = 3{\cdot}6$ Mc/s, f_c may be as low as 3·06 Mc/s. Figs. 6 and 7 are $h'f$ records obtained at the Poitiers station (France). They clearly exhibit case (b) and the additional crochet of case (c). This type of record is quite usual at many other middle-latitude stations.

5. Practical Consequences

One of the immediate consequences of the existence of the XY transition level is its bearing on the evaluation of the maximum electron density N_{max} of the E layer. According to present practice, the "critical frequency" f_c of the ordinary wave is used in the classical "Q.T." formula

$$N_{max} = 1{\cdot}24 \,.\, 10^4 \,.\, f_c^2. \tag{5}$$

But, as shown above, one has first to ascertain:

(1) In what region ("Q.L." or "Q.T.") the maximum electron density N_{max} of the E layer is located, for if it is in the "Q.L." region, one should apply, instead of (5), the corresponding ("Q.L.") formula

$$N_{max} = 1{\cdot}24 \,.\, 10^4 \,(f_c^2 + f_c f_H), \tag{6}$$

where f_c is the frequency corresponding to the vertical tangent on the $h'f$ record;

(2) How the f_c value has been scaled on the record, for if it corresponds to the frequency f_T of Fig. 4, i.e., to the "lowest frequency of the upper layer (E-2 or F-1) trace," the use of formula (5) leads to a serious underestimate of N_{max} (as shown above, it gives the value of N_L, i.e., of the electron density at the transition level located above that of N_{max}).

It thus appears that present scaling procedures of f_0E should be revised in order to avoid confusion, and also that the "vertical tangent" criterion seems to be the best, provided that the region ("Q.L." or "Q.T.") where the corresponding N_{max} of the E layer is located, is specified.

This can be done:

(a) By checking the frequency difference $f_xE - f_0E$, which should be approximately equal to the gyrofrequency f_H when the type is "Q.L.," and to half the gyrofrequency ($\frac{1}{2}f_H$) when the type is "Q.T.";

(b) by careful inspection of the diurnal sequence of $h'f$ records and of the occurrence of crochets in the E layer's ordinary trace (as in Fig. 4), which are indicative of the "Q.L." type; high deviative absorption near the f_0E seems also to be indicative of the "Q.L." type.

But this specification seems to be superfluous:

(a) For stations where the value of the dip angle of the earth's magnetic field is greater than 70° and where the evaluation of N_{max} should always be "Q.L.," i.e., according to formula (6);
(b) for stations where $\hat{\theta} < 60°$ and where the evaluation of N_{max} should be "Q.T.," according to the classical formula (5).

Let us also point out that the well-known "flattening" of the f_0E diurnal curve near midday, so frequent at middle-latitude stations, may well serve as an indication of the change-over near midday of the propagation type at the N_{max} level from "Q.T." to "Q.L." because of the E-layer's plunging into the "Q.L." region during these midday hours.

Another important consequence of the existence of the "Q.L."–"Q.T." transition level seems to be its ability to reflect low frequencies at oblique incidence, because of the sharp discontinuity of their refractive indexes at this level.

An alternative explanation of the whistling atmospherics propagation, to that proposed by L. R. O. STOREY, and also of the constant height of reflection exhibited by a wide frequency band of long-wave atmospherics, seems to be open to investigation on these lines.

REFERENCES

APPLETON E. V.	1932	*J. Inst. Elect. Eng.* **71,** No. 430.
DARWIN C. G.	1943	*Proc. Roy. Soc.* **A182,** 152.
PFISTER W.	1954	*Rep. Ph. Soc. Conf. on Ionosph. Cambridge.*
LEPECHINSKY D.	1955	*La Théorie Magneto-ionique et ses résultats,* Note Prélimnaire No 185 du Lab. Nat. de Radioélectricité
BOOKER H. G.	1934	*Proc. Roy. Soc.* **147,** 352.
WAYNICK A. H.	1954	*Rep. Ph. Soc. Conf. on Ionosph,* Cambridge.

VOL. 8 1956

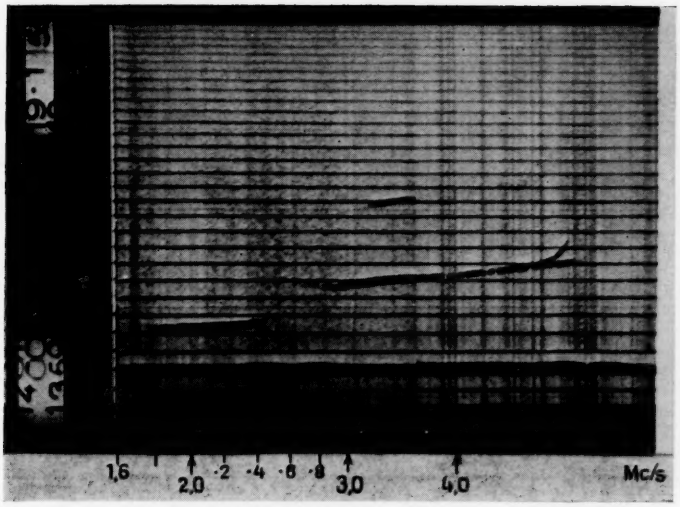

Fig. 6

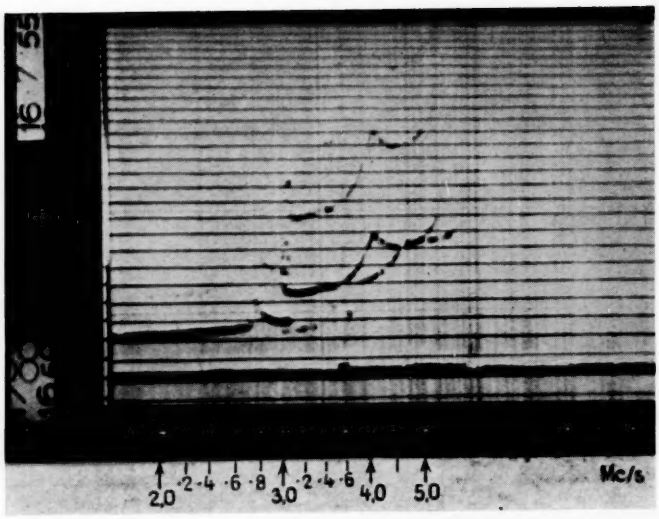

Fig. 7

VOL.
8
1956

Journal of Atmospheric and Terrestrial Physics, 1956, Vol. 8, pp. 305 to 308. Pergamon Press Ltd., London

Origin of the Meinel hydroxyl system in the night airglow

D. R. Bates and B. L. Moiseiwitsch
Department of Applied Mathematics, Queen's University, Belfast

(*Received 7 January* 1956)

Abstract—It is contended that the arguments which have been advanced against the ozone hypothesis are invalid, and that the vibrationally excited oxygen hypothesis, which has been advocated as an alternative, is unacceptable.

1. Introduction

Bates and Nicolet (1950) and Herzberg (1951) have independently suggested that the nocturnal emission of the Meinel hydroxyl system by the upper atmosphere is due to

$$H + O_3 \rightarrow OH^* + O_2, \qquad (1)\dagger$$

the atomic hydrogen being freed again by

$$OH + O \rightarrow O_2 + H. \qquad (2)$$

The suggestion receives some support from the laboratory work of McKinley, Garvin, and Boudart (1955), but has been criticized by Krassovsky (1952, 1954, 1956) who, while accepting the replenishment process (2), considers that (1) should be replaced by

$$H + O_2^* \rightarrow OH^* + O. \qquad (3)$$

We shall first examine the objections raised to the original O_3 hypothesis, and then discuss the new O_2^* hypothesis.

As usual, we shall denote the concentration of a constituent X by $n(X)$ and, except where otherwise stated, shall denote the rate coefficient describing a given process by the symbol k, with the appropriate equation number affixed as an identifying subscript.

2. O_3 Hypothesis

In criticism of the O_3 hypothesis, Krassovsky asserts that (i) the energy available from (1), that is the sum of the reaction and activation energies, is great enough to yield OH^* ($v = 10$); (ii) the process

$$O + O_2 + M \rightarrow O_3 + M \qquad (4)$$

causes $n(O)$ to fall to half the day equilibrium value within 5 sec of sunset at an altitude of 70 km and within 10 min of sunset at an altitude of 80 km so that (2) cannot proceed throughout the night at these altitudes; (iii) the abundance of hydroxyl that would ensue is greater than the limit set by the seeming absence of telluric absorption by the resonance system in stellar spectra, this limit being, according to Shklovsky (1951), 10^{12} OH radicles/cm^2 column; (iv) the rate of

† An asterisk (*) is affixed to the chemical symbol for a molecule when it is desired to draw attention to the presence of vibrational excitation.

photo-dissociation of molecular oxygen in the 70- to 80-km region is less than is required. We offer the following comments.

Claim (i) appears to arise from a computational slip. As may be seen from Table 1, the reaction energy of the process under consideration is 76 kcal/mole. The supposed value of the activation energy is about 3 kcal/mole. Addition of these gives 79 kcal/mole, whereas 81 kcal/mole are needed to excite OH to the 10-level.

Table 1.†

Substance	Heat of formation from atoms (kcal/mole)
O_2	118·0
OH	100·8
O_3	142·4

The fact that (1) does not cause unwanted excitations should not, however, be used as evidence favouring the view that it is the process actually operative, for, as KRASSOVSKY points out, if OH* ($v \geqslant 10$) were formed at low or moderate altitudes, it would be rapidly removed by

$$OH^* \ (v \geqslant 10) + O_2 \rightarrow H + O_3. \qquad (5)$$

Measurements by EUCKEN and PATAT (1936) indicate that the rate coefficient k_4 is only of the order of $5 \times 10^{-36} T^{\frac{1}{2}}$ cm^6/sec, where T is the absolute temperature (cf. BATES and NICOLET, 1950). If this is the case, n(O), in contradiction to claim (ii), would decay extremely slowly: for example, at 75 km n(M) is about 1×10^{15}/cm^3 and $n(O_2)$ is about 2×10^{14}/cm^3, so that the time to decay to half the initial value would be many hours.

The upper limit to the abundance of hydroxyl cited in claim (iii) is much too small. Taking the wavelength to be 3080 Å and the oscillator strength to be $1{\cdot}2 \times 10^{-3}$ (DWYER and OLDENBERG, 1944), we find on substituting in the standard formula relating to the linear part of the curve of growth (cf. ALLER, 1953) that the sum of the equivalent widths of the rotational lines of the X $^2\Pi \rightarrow$ A $^2\Sigma^+$ system of OH is

$$\Sigma w = \{1 \times 10^{-16} \mathcal{N}\} \text{ Å} \qquad (6)$$

where $\mathcal{N}$ is the number of OH radicles/cm^2 column. Thus if $\mathcal{N}$ were at most 10^{12}, as stated, Σw would be at most 10^{-4} Å. Even a single line of this equivalent width could not be detected in stellar spectra; and of course many lines contribute appreciably to the summation. The failure to detect telluric absorption is consistent with $\mathcal{N}$ being 10^{14} or indeed rather higher. Hence the O_3 hypothesis is not in difficulty.

As regards claim (iv), BATES and NICOLET calculated the rate of photo-dissociation of molecular oxygen in the 70- to 80-km region, and found it to be adequate. There seems to be no reason to suspect that their calculations are incorrect. JOHNSON, PURCELL, TOUSEY, and WATANABE (1952), on repeating them, obtained

† In computing this table, account was taken of the recent work of BRIX and HERZBERG (1954) on oxygen.

VOL. 8 1956

essentially the same results. According to these authors, the rate of liberation of oxygen atoms by photo-dissociation averages about $1 \times 10^6/\text{cm}^3$ sec at 75 km. As far as can be judged, this suffices.

3. O_2^* Hypothesis

The basic assumptions of Krassovsky are that (i) the O_2^* molecules involved in (3) are formed through three-body association

$$O + O + M \rightarrow O_2^* + M \tag{7}$$

the mean yield, $F(O_2^*)$, being $10^7/\text{cm}^3$ sec in the region of the 100-km level; (ii) deactivation to levels with v less than 4 occurs in collisions with other molecules, but is very slow, the effective rate coefficient κ describing the process being only some 2×10^{-14} cm^3/sec; (iii) the process

$$O_2^* \ (v \geqslant 26) + O_2 \rightarrow O + O_3 \tag{8}$$

is so rapid that it prevents any appreciable accumulation in levels with v more than 25, and thus renders

$$O_2^* \ (v \geqslant 26) + H \rightarrow OH^* \ (v \geqslant 10) + O \tag{9}$$

negligible.

If $F(O_2^*)$ and κ are taken to have the values cited, and $n(M)$ is taken to be $1 \times 10^{13}/\text{cm}^3$, the approximate equilibrium equation

$$F(O_2^*) = \kappa n(O_2^*) n(M) \tag{10}$$

gives that $n(O_2^*)$ is $5 \times 10^7/\text{cm}^3$. The yield of hydroxyl radicles from (3) is

$$F(OH^*) = k_3 n(O_2^*) n(H). \tag{11}$$

For k_3, Krassovsky, following Nalbandjan and Voevodsky (1949), adopts the value 7×10^{-11} cm^3/sec, and supposing that $n(H)$ is $3 \times 10^8/\text{cm}^3$ (which is in accord with the crude estimate of Bates and Nicolet), he hence finds that $F(OH^*)$ is about $10^6/\text{cm}^3$ sec. As he states, such a yield would suffice for the nightglow.

The O_2^* hypothesis is an interesting one, but certain of the assumptions made in the quantitative development are scarcely acceptable. Thus, recent rocket research (cf. Friedman, 1955) indicates that the intensity of the solar emission in the Schumann-Runge region corresponds to a temperature of only about 4500°K, from which it follows that the mean total yield of O_2^* molecules is unlikely to exceed $5 \times 10^{11}/\text{cm}^2$ sec, and (supposing that this total is distributed over a 10-km-thick layer) that $F(O_2^*)$ is unlikely to exceed $5 \times 10^5/\text{cm}^3$ sec. Again, because of the strong chemical attraction, oxygen atoms must remove the vibrational energy rapidly through the direct process

$$O + O_2^* \ (v = v_1) \rightarrow O + O_2^* \ (v < v_1) \tag{12}$$

and through the interchange process

$$O + O_2^* (v = v_1) \rightarrow O_2^* (v < v_1) + O. \tag{13}$$

The sum of the rate coefficients for (12) and (13) would be expected to be of the

order of 10^{-10} cm^3/sec. Taking $n(O)$ near the 100-km level to be 2×10^{12}/cm^3 (NICOLET, 1954), we find that the equilibrium value of $n(M)$ is probably at most about 3×10^3/cm^3. The corresponding value of $F(OH^*)$ is only 60/cm^3 sec, which is far below what is required.

Moreover, (8) must in fact be relatively slow due to activation energy and perhaps steric hindrance.† It cannot cause the population distribution amongst the vibrational levels of oxygen to fall abruptly when v reaches 26, and therefore cannot prevent (9) from proceeding. The absence from the nightglow spectrum of hydroxyl bands with v greater than 9 (MEINEL, 1950, JONES, 1955) is therefore not an immediate consequence of the O_2^* hypothesis. It might be suggested that (5) is responsible. But k_5 would have to be as high as 3×10^{-10} cm^3/sec to make the collisional life of OH^* ($v > 9$) as low as 10^{-3} sec near 100 km, where $n(O_2)$ is about 3×10^{12}/cm^3 (cf. NICOLET, 1954); and according to HEAPS and HERZBERG (1952), the radiative life is of the order of 10^{-2} sec. There is thus at least some doubt as to whether the process results in a sufficiently pronounced suppression of the bands in question.

REFERENCES

ALLER L. H.	1953	*Astrophysics*, Ronald, New York
BATES D. R. and NICOLET M.	1950	*J. Geophys. Res.* **55**, 301.
BRIX P. and HERZBERG G.	1954	*Canad. J. Phys.* **32**, 110.
DWYER R. J. and OLDENBERG O.	1944	*J. Chem. Phys.* **12**, 351.
EUCKEN A. and PATAT F.	1936	*Z. Phys. Chem.* **33**, 459.
FRIEDMAN H.	1955	*Ann. Geophys.* **11**, 174.
HEAPS H. S. and HERZBERG G.	1952	*Z. Phys.* **133**, 48.
HERZBERG G.	1951	*J. Roy. Astron. Soc. Canada* **45**, 100.
JOHNSON F. S., PURCELL J. D., TOUSEY R., and WATANABE, K.	1952	*J. Geophys. Res.* **57**, 157.
JONES A. VALLANCE	1955	*Nature* **175**, 950.
KRASSOVSKY V. I.	1952	*Prog. Phys. Sci.* **47**, 493 and 503;
	1954	*ibid.* **54**, 469 and 481.
	1956	*The Aurorae and the Airglow*, (ed. E. B. Armstrong and A. Dalgarno), Pergamon Press, London.
MCKINLEY J. D., GARVIN D., and BOUDART, M. J.	1955	*J. Chem. Phys.* **23**, 284.
MEINEL A. B.	1950	*Astrophys. J.* **111**, 433.
NALBANDJAN A. B. and VOEVODSKY V. V.	1949	*Mechanism of Hydrogen Oxidization and Burning*, Publishing House of the Acad. of Sci. of U.S.S.R.
NICOLET M.	1954	*J. Atmosph. Terr. Phys.* **5**, 132.
SHKLOVSKY I. S.	1951	*Publ. Crim. Obs.* **7**, 34.

† Attention is drawn in this connection to the investigation by EUCKEN and PATAT (1936).

Journal of Atmospheric and Terrestrial Physics, 1956, Vol. 8, pp. 309 to 317. Pergamon Press Ltd., London

Accurate height measurements using an ionospheric recorder

A. J. LYON* and A. J. G. MOORAT†

Official communication from D.S.I.R. Radio Research Station, Slough

(*Received* 2 *November* 1955)

Abstract—A method for the calibration of an ionospheric recorder is described, which corrects errors in height measurement arising from the distortion of the echo-pulse in its passage through the receiver. The amount of this error depends on the echo-amplitude, and is shown to vary in an approximately linear manner with the width of the recorded echo-trace. Several methods of checking the calibration confirm that it is reliable to within ± 2 km. Using a calibrated recorder and an expanded time-base, it is possible to measure E-region equivalent heights to this order of accuracy. The systematic error due to pulse distortion will, in general, cause the heights recorded in routine ionospheric measurements to be from 5 to 15 km too high. Some consequences of this, e.g., for MUF predictions, are mentioned.

1. INTRODUCTION

THE necessary conditions for accurate height measurement have been well known for many years and are fully exploited in pulse navigational aids. Conventional automatic ionospheric recorders, however, do not conform with these conditions, and some errors are therefore to be expected in their measurements (NAISMITH, 1949). In this paper we discuss a technique for correcting the error in height measurement due either to the distortion of the pulse during its passage through the receiver, or to any slight asynchronism between the transmitted pulse and the height-calibration markers.

An attempt has recently been made to provide more accurate h'-f curves for the E layer than are required in normal practice. The equipment used was a D.S.I.R. automatic ionospheric height recorder (CLARKE and SHEARMAN, 1953) of the type widely used, but with the time-base sweep adjusted to record about 300 km of equivalent height instead of about 1000 km. Examples of records, showing the considerable expansion of E-region traces compared with normal, are given in Fig. 1. By this means the nominal reading accuracy for reflections from layers below about 300 km can be improved from ± 5 km to ± 1 km.

Inspection of these and similar records shows, however, that the bottom of the trace, corresponding to the leading edge of the echo-pulse, fluctuates as the width of the trace varies. Thus, the lower edge of the trace cannot be used without correction even for a relative measure of equivalent height, and it is essential to determine the necessary corrections.

2. MEASUREMENT OF THE HEIGHT ERRORS OF AN IONOSPHERIC RECORDER

The D.S.I.R. automatic ionospheric height recorder, in accordance with internationally accepted practice, is so arranged that the pulse in the modulator of the transmitter is synchronized to one of the height calibration markers. Hence,

* University of Edinburgh: Now at University College, Ibadan, Nigeria.
† Radio Research Station.

under normal operating conditions, the start of the large ground-wave signal coincides with this marker, which forms a natural origin from which to measure the heights of reflection.

The total error in the observed height, measured to this origin, and its variation with echo-amplitude, can be very simply determined by using the transmitted pulse (or "ground-wave") as an artificial echo. To do this, the receiver aerial is replaced by a probe small enough to ensure that the r.f. stages of the receiver are not overloaded. In this way the transmitter pulse input to the receiver is reduced to the amplitude of a normal echo, and by varying the receiver attenuation a sequence of signal amplitudes may be obtained, corresponding to the normal range of echo-amplitudes.

An example of the photographic records obtained by this procedure is shown in Fig. 2. The required total error (whether due to receiver or transmitter) is the distance from the bottom of the zero height-marker to the bottom of the signal trace. Clearly the error decreases steadily as the width of the trace increases —from some 10 km for a weak signal to 2 or 3 km for strong signals.

A series of records similar to the one in Fig. 2 were made for ten frequencies ranging from 0·8 Mc/s to 6·0 Mc/s, using the normal transmitter pulse-width of 150 microseconds. In each case the error Δ, measured as above, was plotted as a function of the width of the trace w. For any single frequency, the error closely follows a linear law of the form

$$\Delta = a - bw. \tag{1}$$

With the equipment in use, it is convenient to divide the frequency band into two parts. For the range 0·8 to 2 Mc/s the best straight line is

$$\Delta = 17{\cdot}5 - 0{\cdot}25w \tag{1a}$$

and for the range 2·5 to 6·0 Mc/s

$$\Delta = 14{\cdot}5 - 0{\cdot}25w \tag{1b}$$

The true equivalent height of an actual echo may now be obtained by subtracting the error as given by these equations from the observed height. With this instrument, as will be seen from Fig. 3, the observed heights will be too high by amounts ranging mostly between 5 and 10 km.

3. The Origin of the Height Errors and Their Variation with Echo-amplitude

As is usual with ionospheric pulse-transmitters, the delay between the modulator pulse and the r.f. pulse radiated from the aerials is found to be very small—certainly less than 2 km (13 μsec). It follows that the major part of the observed errors must arise in the receiver circuits. The character of the distortion is shown diagrammatically in Fig. 4, which gives the equivalent shapes of an originally square pulse, after passage through the receiver, for two particular amplitude levels, assuming that the rise-time and decay-time remain constant. Now, in practice there is a threshold level, OA, below which no signal appears on the record; consequently, the width of the pulse recorded is that of a section across

VOL. 8 1956

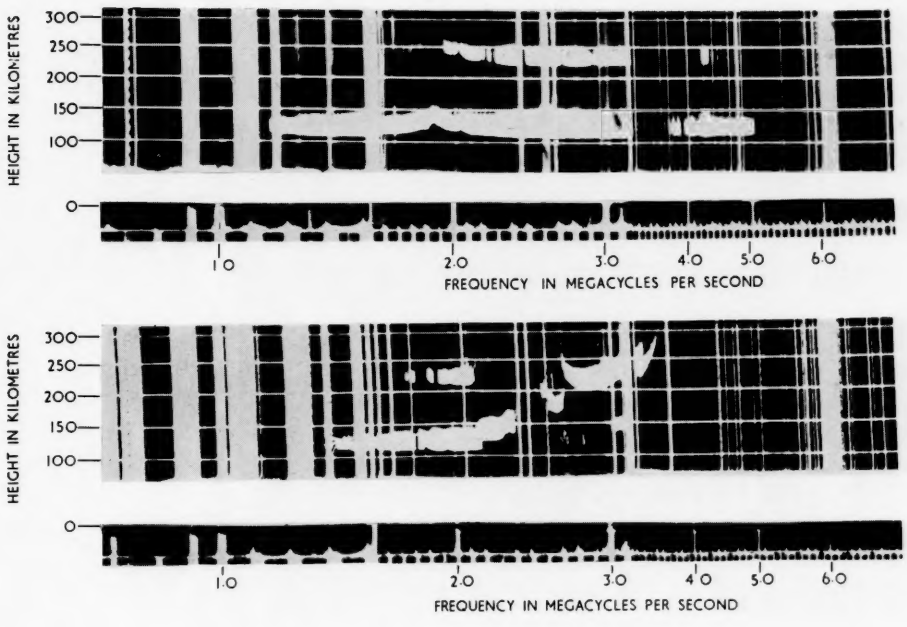

Fig. 1. *h'f* records made using a D.S.I.R. ionospheric height recorder, with the time-base sweep adjusted to 300 km instead of about 1000 km. (The thin horizontal lines are the 50-km height markers; and the irregular vertical streaks are due to broadcast and other interference.)

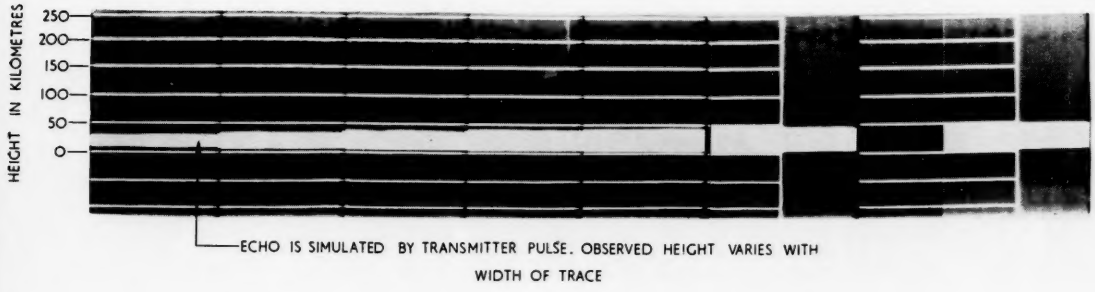

Fig. 2. A calibration record. The observed delay from the zero height-marker varies with the width of the trace, and hence the amplitude of the signal.

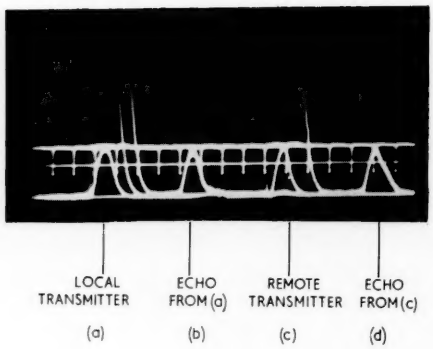

Fig. 6. Ground-wave and E echoes using local and remote transmitters seen on the display of the absorption equipment. The frequency is 1·6 Mc/s, the height markers are at 25 km intervals, and the reading accuracy is $\pm$ 1 km.

VOL.
8
1956

the pulse at height OA, i.e., for the smaller pulse the section BC. When the amplitude of the pulse increases, the width of the section BC increases, and the error in the observed height decreases. To give $b = 0{\cdot}25$, the slope of the leading edge is three times that of the trailing edge, so that when the recorded trace-width increases by 4 km, the bottom of the trace will fall by 1 km and the top will rise by 3 km.

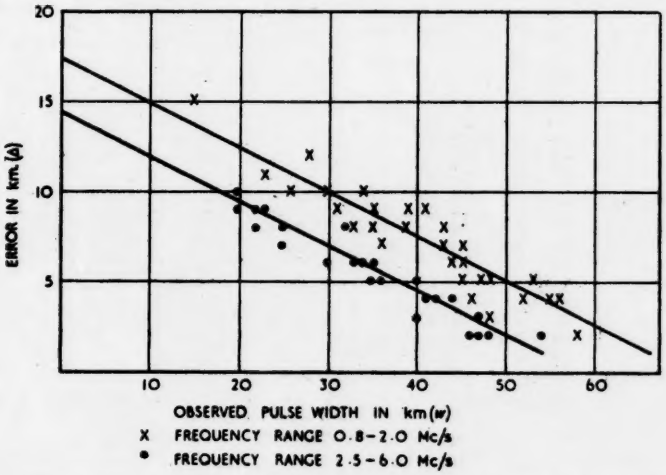

Fig. 3. Recorder height error as a function of observed pulse-width, constructed from calibration records of the type shown on Fig. 2.

Expressing delay-times in kilometres of equivalent height (so that 1 km = 6·6 μsec), the time of rise of the leading edge of the pulse, as measured from Fig. 4, is 7·5 km, which would be the theoretical rise-time for an ideal rectangular band-pass of 20 kc/s. Now, the actual band-pass of the receiver, measured to points 6 db below the peak, is 15 kc/s, and since of course the response curve is not ideal, this may be considered very reasonable agreement. The delay-time measured to the centre of the time of rise is 6 km (40 μsec): but the observed delay may be greater or less than this, depending on the pulse-amplitude.

The quantity a is determined solely by the shape of the pulse after passage through the receiver (it can be measured from the intersection of the lines EK and GL in the figure); hence it does not vary with the threshold level or with the position of the C.R.T. "brightness" control. It will vary, however, with the transmitter pulse-width used, being a little less if the pulse-width is shorter; recalibration is therefore advisable when the pulse-width is changed. The small variation of a with frequency in the instrument under test appears to indicate a slight difference in the receiver characteristics at low and high frequencies: this would not be unreasonable.

4. Checks of the Calibration Procedure

It is desirable to check first that the linear law for the variation of apparent height with trace-width—and particularly the gradient of 0·25—are still true for actual echoes. This can be tested by taking $h' - t$ records at constant frequency, and the echo trace-width can be varied by altering the receiver attenuation

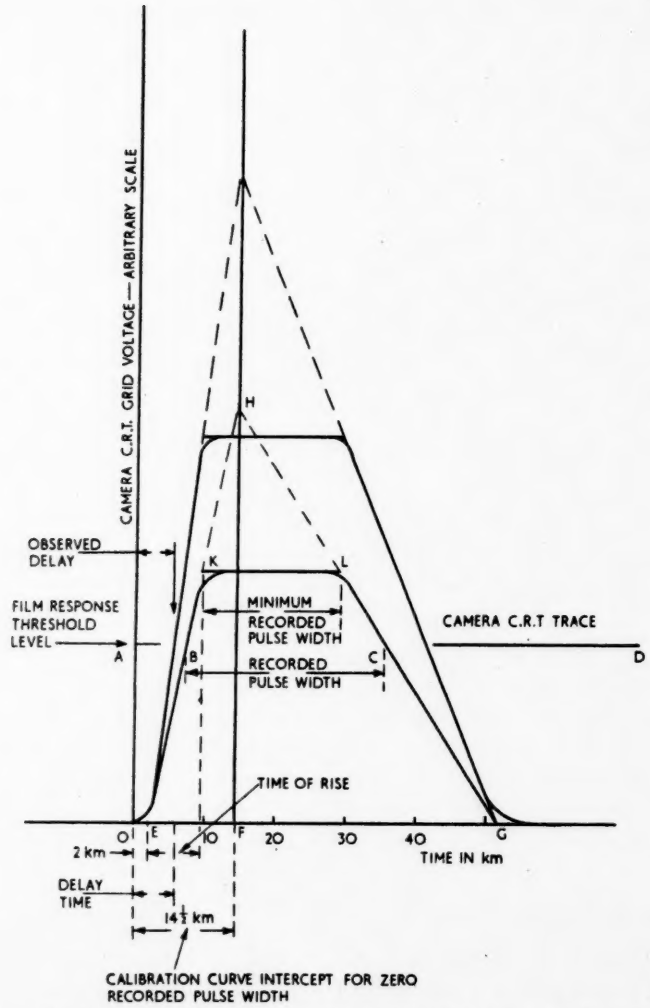

Fig. 4. Equivalent pulse-shape plotted from the position of the recorded trace (Figs. 2 and 3). It is *not* the shape of the receiver output-pulse, but reproduces the essential delay characteristics of that pulse.

VOL. 8 1956

or by using natural fading. It will be seen from Fig. 5, plotted from such records, that the gradient $d\Delta/dw$ is again very near to 0·25. This test verifies that our correction equation (1) with $b = 0{\cdot}25$ is satisfactory at least for relative heights.

We may test the accuracy of the correction equations for absolute heights with the aid of multiple echoes. Let the true equivalent height of reflection be

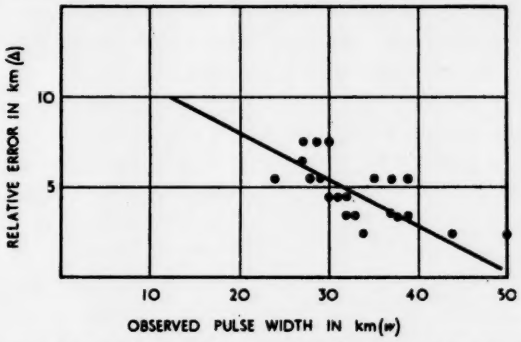

Fig. 5. Recorded relative height error as a function of observed pulse-width constructed from $h' - t$ records.

h'_0, then by equation (1) the observed equivalent height of the rth order echo will be

$$h'_r = rh'_0 + a - bw_r$$

where w_r is the width of the rth echo and b $(= 0{\cdot}25)$ is known. Hence the true height and the constant a may be expressed in terms of the apparent heights, say of the 1st and rth echoes, by the equations

$$h'_0 = \frac{1}{r-1}\left\{(h'_r + bw_r) - (h'_1 + bw_1)\right\} \tag{2}$$

and

$$a = \frac{1}{r-1}\left\{r(h'_1 + bw_1) - (h'_r + bw_r)\right\} \tag{3}$$

Using equation (3), we have determined a in ten cases where a second echo was present (this being the highest multiple echo that can be recorded with our expanded time base). For eight of these cases (mostly for frequencies greater than 2 Mc/s) the average value of a was 15 km, in good agreement with (1b). The two remaining cases gave much lower values (2 km and 7 km respectively); these anomalous results are probably due to the presence of composite echoes whose lower component is not visible in the second echo.

Overlapping echoes from different apparent heights are not uncommon in E-region reflections. Though not always visible in the records, such composite echoes may be clearly seen on the monitor display, which, unlike the photographic record, shows the variation of signal-amplitude with equivalent height. In such a case, if the lower component is the weaker it may not be visible after a second reflection, so that the observed h'_1 would be too small in relation to the observed h'_2, and by equation (3) the derived value of a would then be too small.

It is worth noting that the crude test of comparing the observed heights from ground-wave to first echo and from first to second echo, without applying any width correction, usually underestimates the real error. When, however, eight or nine multiple echoes are visible, the presence of the error is unmistakable even without width corrections.

A further method of checking the correction formula (1) is to compare the corrected heights with heights measured simultaneously, using the type of manual equipment employed for absorption measurements (PIGGOTT, 1955). With this instrument, the ground-pulse is attenuated at i.f. to a standard amplitude and a height-marker is set to a point on its leading edge. The attenuation is then reduced until the echo reaches the standard amplitude, and the equivalent height is read to the corresponding point on the echo-pulse. Thus the ground-wave and echo signals are distorted equally by the receiver, and no error in height measurement is involved, provided overloading of the r.f. stages does not occur.

Normally the heights are read directly, but, for the present tests, photographs of the tube face were taken. This technique made possible a reading accuracy of about ± 1 km, the same as with the expanded time-base method. In several tests at various frequencies, the heights determined by the two methods agreed to within 2 or 3 km in all cases.

To show that the very intense field from the adjacent transmitter did not cause errors due to alteration of pulse-shape by overloading or leakage, the same technique was used with a transmitter sufficiently remote from the receiver not to overload it. The gain of the absorption receiver was adjusted so as to bring to a standard amplitude in quick succession:

(a) the ground-wave from the local transmitter,
(b) the echo from the local transmitter,
(c) the ground-wave from the distant transmitter, and
(d) the echo from the distant transmitter,

the output at each setting being photographed. A typical example, using a frequency of 1·6 Mc/s, is reproduced in Fig. 6. In this case, the apparent height measured between (a) and (b) is 105 km, and that between (c) and (d) is 106 km; and simultaneous measurements on the D.S.I.R. automatic height recorder gave 105 km when corrected. Other results, using local and remote transmitters, also agreed within the accuracy of the measurements.

These various checks confirm the general soundness of the primary method of calibration described in Section 2, and indicate that expansion of the time-base enables one to achieve, for *E*-region equivalent heights, an accuracy of the order of ± 2 km in cases where the echo observed is simple. The corrections are of course equally applicable, and necessary, when a normal time-base sweep is in use.

Increasing the time-base-sweep velocity is not the only method of improving the reading accuracy. We have found that optical magnification is almost equally effective, though less convenient, even when the records are made on paper.

5. HEIGHT CORRECTIONS IN ROUTINE MEASUREMENTS

It has been recommended internationally (C.C.I.R., 1948) that routine height measurements should normally be made with an accuracy of ± 10 km, and most stations attempt to reach this accuracy. For many purposes, irregular errors of this magnitude are comparatively unimportant. Systematic deviations of the type discussed above, however, introduce discrepancies which can prove significant both in the prediction of maximum usable frequencies and in the study of the

VOL. 8 1956

physics of the ionosphere. For example, a systematic error causing the observed heights to be 10 km too high, which is probable using existing techniques, will make the MUF factors for the E and F layers (respectively) about 6% and 3% too low at medium or long distances. This is an appreciable fraction of the discrepancy known to occur (C.C.I.R., 1953).

Our analysis shows that the correction needed with the type of recorder used at all D.S.I.R. out-stations should vary between about 5 and 10 km. This is confirmed by analysis of a few typical night-time records having a large number of

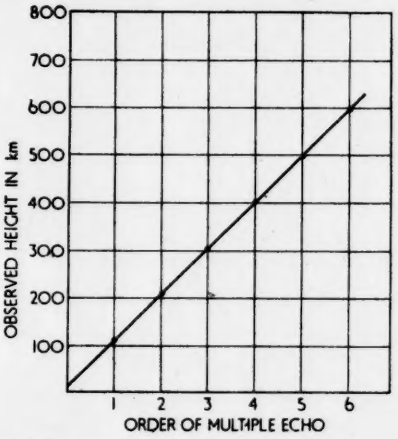

Fig. 7. Heights of multiple echoes from a routine record taken with the prototype recorder at Slough after small corrections (<5 km) have been made for observed pulse-width. The error of the first echo, in this case 13 km, is the intercept on the observed height axis.

multiple echoes, made by the D.S.I.R. recorders at Singapore and Khartoum. These records give values of a, derived by equation (3), of about 13 km, and the corresponding errors in the apparent heights of first-order echoes are between 6 and 8 km. (Since the pulse-width used is shorter than that used in our tests, a smaller value of a is to be expected.) Records from the prototype recorder (Naismith and Bailey, 1951) used at Slough for routine measurements, give an average value for the systematic error of between 10 and 15 km. For example, Fig. 7 shows the heights of six successive multiple echoes from a routine record, after small corrections have been made for pulse-width. In this case the error in the apparent height of the first echo was 13 km; and the average error from seven similar examples was about 12 km.

This result can be checked by comparing the monthly mean values of $h'E$, measured using the same instrument, with the equivalent heights at 2·0 Mc/s obtained during routine absorption measurements at Slough. These two parameters are plotted in Fig. 8 for the years 1951–53. In winter a 2-Mc/s signal is often reflected from heights considerably below the normal E layer, but most of these observations can be removed by omitting heights at or below 105 km in winter months, as shown by the dashed curve. The mean difference between the heights obtained on the two instruments, after allowing for the abnormal winter reflections, is 13 km—in excellent agreement with the figure of 12 km quoted above.

Since the band-widths used in other routine recorders cannot differ greatly from those employed at Slough, and since a considerable part of the delay must be ascribed to the time of rise of the signal, which is determined by the band-width, similar errors are probably present at all stations. It is desirable that these errors should be estimated elsewhere before commencing the intensive observational programme of the International Geophysical Year. For reasons of continuity, however, it would be inadvisable to circulate corrected heights or corrected MUF factors unless the magnitudes of the corrections applied are clearly stated.

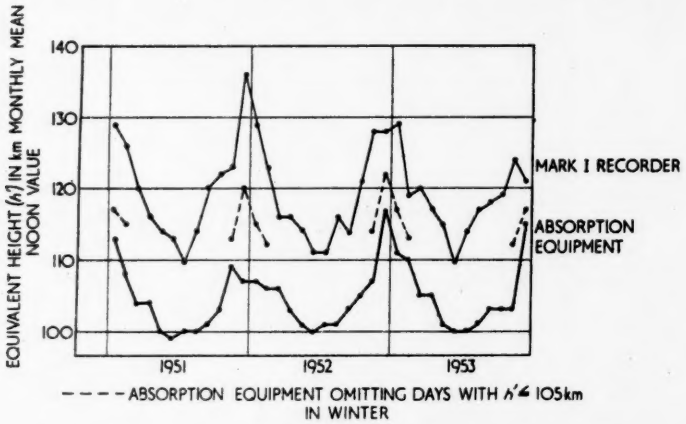

Fig. 8. Comparison of $h'E$ from the prototype recorder records with h' measured at 2·0 Mc/s (from routine data for Slough, England) with the absorption apparatus, showing a mean difference of 13 km between the heights measured on the two equipments (omitting heights <105 km in winter months).

6. CONCLUSIONS

We conclude that it is possible to correct the apparent heights obtained from a routine recorder, so that the equivalent height of E reflections can be measured with an accuracy of ± 2 km or better; and, since such corrections are not made in normal practice, that significant systematic errors are probably present in height and MUF measurements from ionospheric stations all over the world. The accuracy demanded by international standards, ± 10 km, may not in fact be reached unless these corrections are applied.

Acknowledgements—The authors wish to thank Messrs. W. R. PIGGOTT and R. W. MEADOWS of the Radio Research Station, Slough, for many helpful discussions and valuable suggestions, and Mr. A. M. HOWATSON (University of Edinburgh) for a number of useful comments. In particular, the experimental techniques used were based chiefly on suggestions by Mr. R. W. MEADOWS. One of us (A. J. L.) is indebted to the Director, Dr. R. L. SMITH-ROSE, for permission to participate in this work at the Radio Research Station.

This work was carried out as part of the programme of the Radio Research Board, and this paper is published by permission of the Director of Radio Research of the Department of Scientific and Industrial Research.

VOL. 8 1956

References

———	1948	C.C.I.R. Recommendation No. 6, C.C.I.R. Fifth Meeting, Stockholm, p. 23.
———	1953	C.C.I.R. Report No. 23, C.C.I.R. Seventh Plenary Assembly, London, **1**, 212.
Clarke C. and Shearman E. D. R.	1953	*Wireless Engr.* **30**, 211.
Naismith R.	1949	*U.R.S.I. Proceedings*, 251.
Naismith R. and Bailey R.	1951	*Proc. Inst. Elect. Engrs. Part III*, **28**, 271.
Piggott W. R.	1955	*Wireless Engr.* **32**, 164

OL.
8
956

Journal of Atmospheric and Terrestrial Physics, 1956, Vol. 8, pp. 318 to 330. Pergamon Press Ltd., London

A correlation treatment of fading signals

N. F. BARBER
Geophysics Division, D.S.I.R., Wellington, N.Z.

(*Received* 23 *November* 1955)

Abstract—The fading signals observed at spaced receivers are examined in terms of the complete correlogram. Two practical examples are discussed.

INTRODUCTION

THE fading signals observed at spaced receivers at the ground, when a radio signal has been reflected at the ionosphere, indicate a drifting and changing interference pattern due to a drifting and changing ionosphere. How best to deduce the ionospheric drift from the fading records has been much discussed. YERG (1955) has recently made use of the idea of the complete correlogram, and two records are discussed here by correlation methods that differ somewhat from previous approaches.

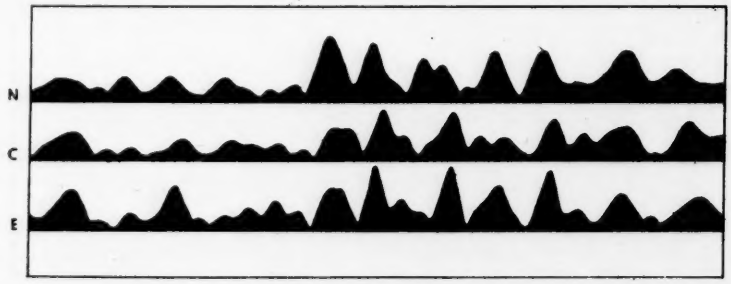

Fig. 1. Records of the variation of signal strength (modulus) at receivers 91 m north and east of a central receiver. Radio wavelength 120 m. Reflection occurred at the *E* layer. Time increases to the left. This sample covers 40 sec of a longer record lasting 100 sec.

PRACTICAL EXAMPLES

Fig. 1 shows a brief history of three fading signals from receivers sited 91 m north and east of a central one. It is part of a longer record lasting 100 sec. The curves in Fig. 2 are lag correlations calculated from the three traces. In Fig. 2(a) are the three autocorrelograms and in Fig. 2(b) are the three cross-correlograms.

Fig. 3 is a portion of another record from the same experiment. The calculated autocorrelograms are shown in Fig. 4(a) and the cross-correlograms in Fig. 4(b). These curves are based on a record lasting 12 min.

The records were provided by Mr. G. BURT of the Dominion Physical Laboratory. The correlograms were calculated using the punched-card machine at the Applied Mathematics Laboratory.

THEORETICAL APPROACH

The correlogram of a changing distribution is a function whose form and manner of change are a convenient summary of the general form and behaviour

VOL.
8
1956

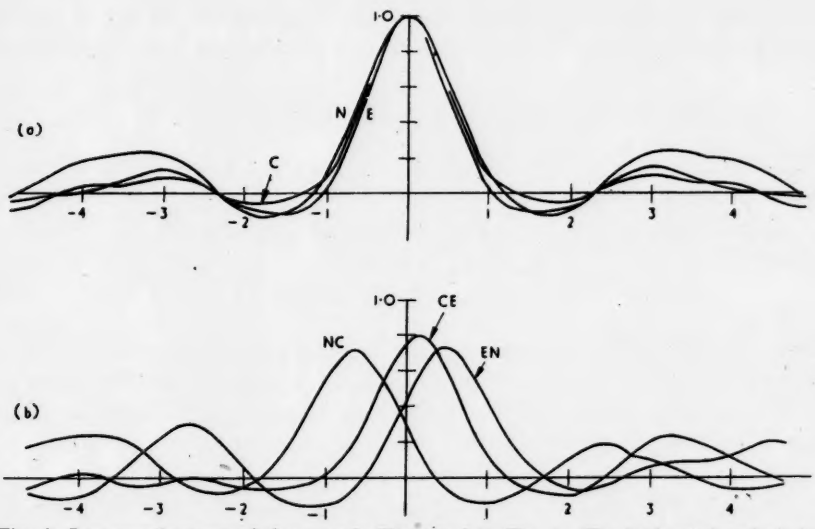

Fig. 2. Lag correlograms of the records illustrated in Fig. 1. The horizontal scale is in seconds of delay. The convention of sign is that delay is counted positive when events occur first on the first-named receiver of any pair. Curves (a) are autocorrelograms. Curves (b) are cross-correlograms.

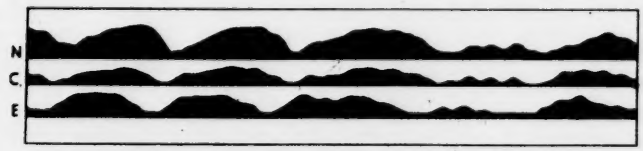

Fig. 3. A sample covering 60 sec of a record lasting 11 min.

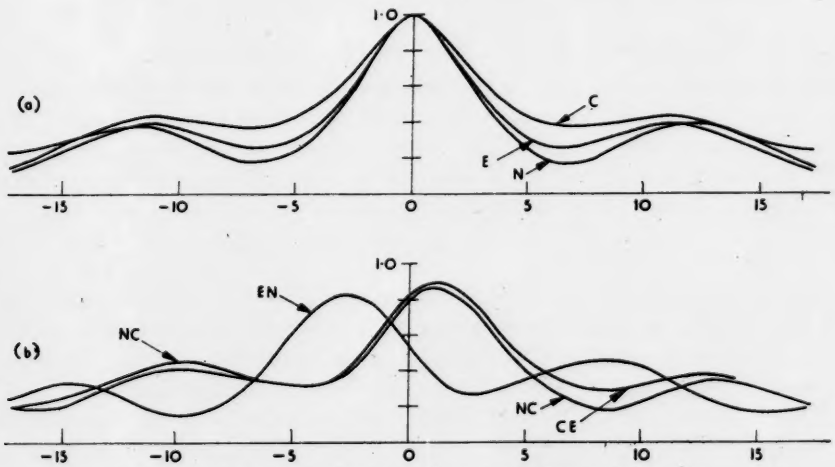

Fig. 4. Autocorrelograms (a), and cross-correlograms (b) of the long record illustrated in Fig. 3.

of the distribution. We write $R(x, y, t)$ for the complex amplitude of the radio signal at a position x, y on the ground and at a time t. Its correlogram is here defined as

$$\rho(X, Y, T) = \overline{R^*(x, y, t)\, R(x + X, y + Y, t + T)}$$

where the asterisk denotes the conjugate form and the bar denotes an average in all three variables x, y, and t.

The original function R may be regarded as the sum of sinusoids.

$$R(x, y, t) = \sum_{-\infty}^{l=+\infty} \sum_{-\infty}^{m=+\infty} \sum_{-\infty}^{\sigma=+\infty} a_{lm\sigma}\, e^{i(lx + my + \sigma t)}.$$

This is not a merely artificial expansion, for the radio wave reflected from a point in the ionosphere does approximately contribute a sinusoid to the interference pattern, so long as we confine attention to a small region, say a kilometre square. Using the expansion, the correlogram is found after some reduction to be

$$\rho(X, Y, T) = \sum_{-\infty}^{l=+\infty} \sum_{-\infty}^{m=+\infty} \sum_{-\infty}^{\sigma=+\infty} |a_{lm\sigma}|^2\, e^{i(lX + mY + \sigma T)}.$$

Thus the distribution R and its correlogram ρ are both made up of the same set of moving sinusoids, (l, m, σ).

If the original distribution R drifts bodily without changing its form, the correlogram will also drift with the same velocity without changing its form. If the distribution changes its detailed form with time, this is because its sinusoids have differing velocities. The correlogram, being composed of the same sinusoids, will also change its form, disintegrating or decaying as the delay T increases.

The calculated curves of Figs. 2 and 4 refer only to the fluctuating part of the recorded signal; that is, its departure from the mean value. Also, these curves are normalized so that the autocorrelograms have a maximum value that is unity. This does not affect the present conclusions.

THE MEASURABLE VALUES OF THE CORRELOGRAM

A pair of receivers at (x_1, y_1), (x_2, y_2) give a correlation that may be calculated for any delay T, but refers to space separations X, Y, equal to $x_2 - x_1$, $y_2 - y_1$. Thus the NC curve in Fig. 2(b) relates to the point 1 in the correlation plot of Fig. 5(b). Similarly, the CE and EN curves relate to the points 2 and 3 respectively. The correlogram always has a conjugate symmetry,

$$\rho(X, Y, T) = \rho^*(-X, -Y, -T)$$

and in the present examples is actually symmetrical because we are dealing with scalar values. Then the same curves also give the correlations at the image points $1'$, $2'$, $3'$, providing the sign of T is changed in these curves.

The autocorrelograms in Fig. 2(a) involve no space separation, and attach to the origin O of the correlation plot. The difference of the three curves is probably due to instrumental errors, and their scatter is an indication of what errors may be present in the other correlation curves. We shall adopt the mean of the three as being the value at O.

VOL. 8 1956

The correlation curves show how the correlation changes with the delay T. They are therefore the histories of the seven points in the correlogram. From these histories we attempt to estimate how the correlogram is behaving. Three methods will be used. All of them involve certain more or less plausible assumptions.

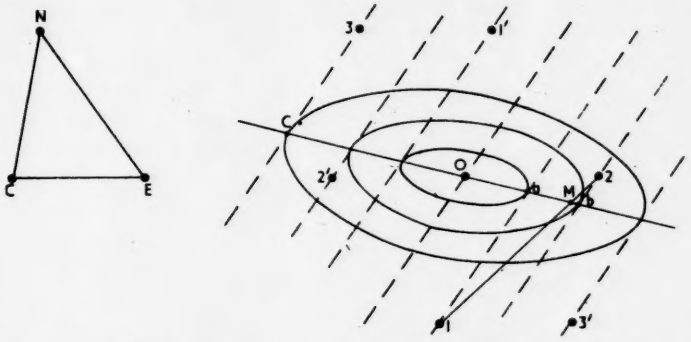

Fig. 5. A triangular array of receivers, N, C, and E, and the plot of their correlations. Correlations between the pairs NC, CE, and EN attach to points 1, 2, and 3 respectively, whose vector distances from O are the separations of the receivers. Autocorrelations attach to the origin O. The correlation curves in Fig. 2 or Fig. 4 are the histories of the correlation at these points. At the image-points 1′, 2′, and 3′, the histories are the same as at points 1, 2, and 3, but with the sign of the delay changed. For generality, the receivers are shown as a scalene triangle.

Assuming a Quadratic Form near the Origin

In these examples we are dealing with a real correlogram, and because of its symmetry it must be an even function of X, Y, and T. Near the origin, as Yerg points out, it may be treated as a quadratic. We shall write it

$$1 - \rho(X, Y, T) = A(X - 2uT)^2 + B(Y - 2vT)^2 + 2H(X - 2uT)(Y - 2vT) + KT^2$$

assuming the correlations to have been normalized so that the maximum in the autocorrelogram is unity. Then $2u$, $2v$ are the component velocities of drift of an elliptic correlogram. We infer an ionospheric drift with components u, v. The term KT^2 represents the decay due to turbulence or other causes.

It is proposed to determine the unknowns from six observations, and we shall take these to be the three correlations between the signals and their three rates of change of correlation, all measured at T zero. These are chosen because they could be found in practice without introducing any delay into the three signals. They might be obtained by watt-hour meters. The integrated product of two signals, when normalized, gives the correlation. The integrated product of one signal and the time differential of the other gives the rate of change of correlation. Thus, in general, the correlation at a delay T between signals $f_1(t)$ and $f_2(t)$, whose mean square values are σ_1^2, σ_2^2, is

$$\rho(T) = \overline{f_1(t) f_2(t + T)}/\sigma_1\sigma_2.$$

Then ρ and ρ' at zero T are given by

$$\rho(0) = \overline{f_1(t)f_2(t)}/\sigma_1\sigma_2$$

$$\rho'(0) \equiv \frac{d\rho}{dT}(0) = \overline{f_1(t)\frac{df_2}{dt}(t)}/\sigma_1\sigma_2.$$

If the receivers are at three corners of a square, their co-ordinates being $(0, h)$, $(0, 0)$, $(h, 0)$, the correlations between them refer to points on the correlogram whose X, Y co-ordinates are $(0, -h)$, $(h, 0)$, and $(-h, h)$. We shall distinguish values at these points by the suffixes 1, 2, and 3 respectively. It is found on substitution that five of the unknowns in the quadratic are given by

$$A = (1 - \rho_2)/h^2 \qquad B = (1 - \rho_1)/h^2$$

$$H = (1 + \rho_3 - \rho_2 - \rho_1)/2h^2$$

$$u = (H\rho_1' + B\rho_2')/4h(AB - H^2)$$

$$v = -(A\rho_1' + H\rho_2')/4h(AB - H^2)$$

The six observations are all independent of the decay coefficient K, and this cannot be found. But since they depend on only five unknowns, they fulfil a certain condition. It is

$$\rho_1' + \rho_2' + \rho_3' = 0$$

We may use this as a test. The quadratic analysis should only be used on observations that obey this rule.

The values of ρ and ρ' in the present examples have been determined from the ordinates and slopes of the curves in Figs. 2(b) and 4(b). They are listed in Table 1.

Table 1. The observed correlations and rates of change

Point		Receivers	ρ	ρ'
Fig. 2	1	NC	+0·28	−0·93
	2	CE	+0·76	+0·55
	3	EN	+0·44	+1·00
			Total	+0·62
Fig. 4	1	NC	+0·80	+0·12
	2	CE	+0·82	+0·12
	3	EN	+0·53	−0·17
			Total	+0·07

It will be seen that in neither of these examples do the rates of change have a zero total. The receivers are too far apart for the quadratic to be a good representation. The divergence from a quadratic should be greatest for the point whose

VOL. 8 1956

value of $(1 - \rho)$ is greatest. In fact, it can be seen that in both cases the zero rule could hold if the rate of change were increased at the point whose correlation is least. This is to be expected, for the actual correlogram is oscillatory, but the gradient of a quadratic continually increases.

Observations such as these would normally be rejected as unsuitable for quadratic analysis, but here we shall use them as illustrations. In the first example,

Table 2. The calculated coefficients of the quadratic correlograms

	u	v	Ah^2	Bh^2	Hh^2	α
Fig. 2	+11	+41	+0·24	+0·80	+0·24	−20°
Fig. 4	+12	−10	+0·18	+0·20	−0·06	+45°

the quadratic that fits the central part of the correlogram would lead to a larger value of ρ' and a somewhat smaller value of ρ than are recorded for point No. 1. To give a plausible interpretation of this example, these values will be amended to

$$\rho_1 = +0{\cdot}20 \qquad \rho_1' = -1{\cdot}55.$$

In the second example it is point No. 3 that requires amendment. We shall write the values at this point as

$$\rho_3 = 0{\cdot}50 \qquad \rho_3' = -0{\cdot}24.$$

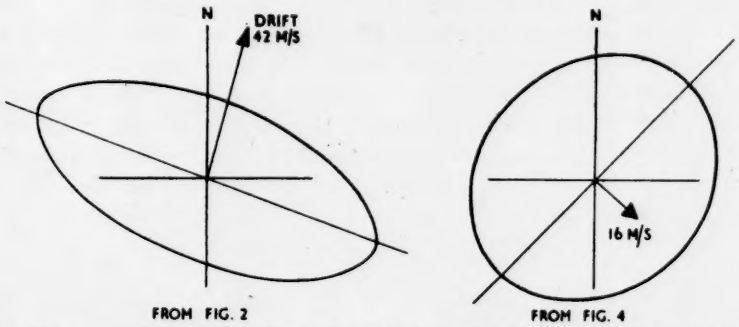

Fig. 6. The vector drift and the form of a typical contour of the correlogram in the two examples. These are found by quadratic analysis of the three correlations and their three rates of change, all measured at zero delay.

When we use these amended values to calculate the coefficients in the quadratic, we derive the values shown in Table 2. These findings have been summarized in Fig. 6, which shows in each case the form of a typical elliptic contour of the quadratic and shows also a vector representing the calculated ionospheric drift.

The figure also shows the diameter of the elliptic contour which is conjugate to the calculated direction of drift. This corresponds to the "line of maxima" which appears in the reconstructions that are attempted later. Its inclination α to the X axis is readily shown to be given by

$$\tan \alpha = \rho_2'/\rho_1'$$

and this value of α is listed in Table 2.

Assuming No Decay

If the interference pattern does not change appreciably in the space of a few seconds, we need make no special assumptions about the form of the correlogram. The correlogram will drift without change, and then the curves of Figs. 2 and 4 represent sections of the correlogram, taken through the seven points of Fig. 5(b) in a direction parallel to the drift.

If the drift were known, we could draw these section lines in the right direction, as illustrated in Fig. 5(b), and from the known velocity could convert the scale of T on each correlation curve into a scale of distance measured from the corresponding point. When the correlation values were entered upon these lines, it would be possible to draw contours to include them and so present a contour picture of the correlogram.

But if we do not know the drift, this construction can be done in an infinite number of ways, choosing different velocities and directions of drift. All the resulting pictures will be different, yet each will be an interpretation that is theoretically possible. The correlation treatment is not responsible for this ambiguity. Fading records can always be interpreted to mean a drift in any arbitrary direction and at any arbitrary speed so long as we are free to assume an interference pattern whose form is sufficiently specialized.* In practice we avoid assuming specialized forms. In the correlogram construction we must choose the drift which leads to the simplest picture. For instance, a correlogram with elliptic contours should be preferred to one with S-shaped contours.

If the contours of the correlogram are similar ellipses as pictures in Fig. 5(b), the maxima in the various sections occur where they are tangential to a contour, at a, b, and c. These maxima all lie on a diameter whose direction is conjugate to the direction of drift. Conversely, it seems reasonable to adopt, if possible, an interpretation in which the maxima are collinear. The condition that such an interpretation is possible is that the delays of the maxima in the three cross correlograms have a zero total.

$$T_{NC} + T_{CE} + T_{EN} = 0$$

This follows because in Fig. 5(b) the centroid of the points 1, 2, and 3 is the origin, since their vector co-ordinates are the three sides of the triangle of receivers. Then, if the maxima a, b, c lie on some diameter, the parallel distances $a1$, $b2$, $c3$ total zero, and these distances are proportional to the time delays.

This condition is fulfilled in the first example; the delays of the maxima in the curves of Fig. 2(b) are

$$T_{NC} = -0{\cdot}63, \qquad T_{CE} = +0.15, \qquad T_{EN} = +0{\cdot}48 \text{ sec}$$

The condition is not fulfilled in the second example, and we postpone its discussion till later.

The time-delays determine the line of the maxima. It is a diameter OM which divides the line 1, 2 externally in the ratio T_{NC}/T_{CE}. The delays also determine

* The radio interference pattern R and its correlogram ρ can contain no space periodicities less than a radio wavelength. This excludes some of the interpretations.

VOL. 8 1956

that component of the drift which is at right angles to the line of maxima. Indeed, it is this component velocity which is calculated when fading records are interpreted in the more usual way. The line must advance from 0 to 1 in the time T_{NC} by which the fading at the north receiver precedes the fading at the central receiver.

But we are still free to choose any value for the component of drift velocity

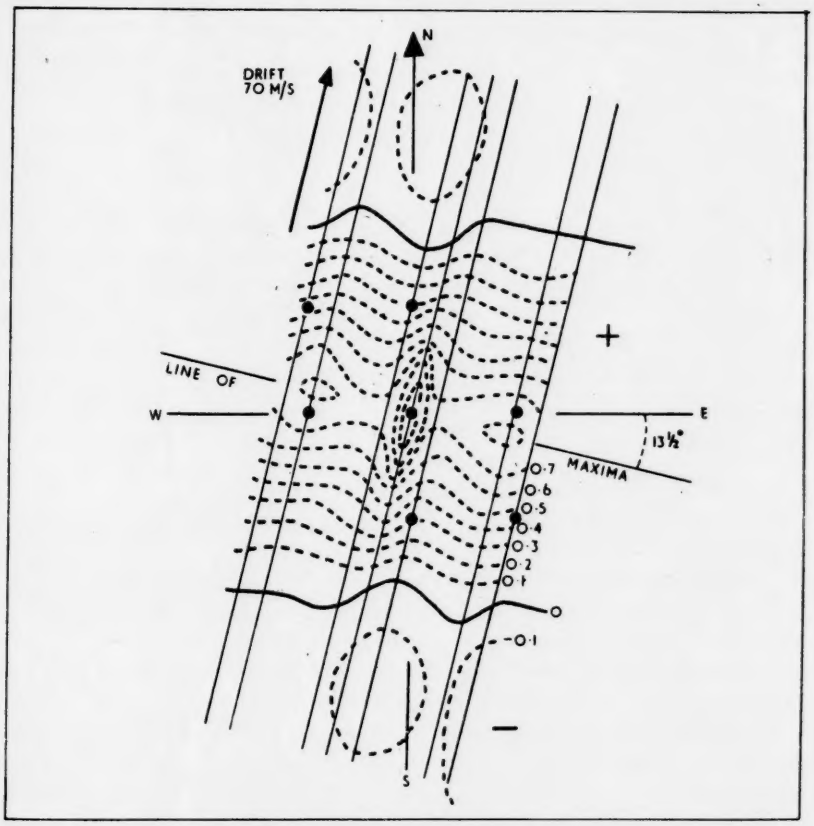

Fig. 7. An interpretation of the first example, Figs. 1 and 2, assuming no decay. The drift is assumed here to be at right angles to the line of maxima. This is the usual assumption, but it leads to a complicated correlogram because it brings a low correlation near to the origin.

parallel to the line of maxima, and of course each choice leads to a different interpretation for the form of the correlogram. We have to choose the simplest form. The two reconstructions in Figs. 7 and 8 illustrate this point. They are from the first example using the curves of Fig. 2.

In Fig. 7 the line of maxima was constructed from the delay-times and the drift was taken to be entirely at right angles to this line. The correlation values were transferred to sections through the seven points, and contours were drawn as shown. It is not a simple picture, because the section through point 1 falls nearest the origin and yet it shows the smallest peak correlation of any. This section

corresponds to the *NC* curve in Fig. 2(b). Fig. 8 is better, because the drift direction was chosen so that the section that falls nearest the origin is that through point 2, at which the peak correlation is greatest.

The velocities quoted in these figures are the ionospheric drift, that is half the velocity of drift of the radio interference pattern at the ground.

Briefly, the conclusion is that time-delays determine the direction and magnitude of only one rectangular component of the drift. The true line of drift is to be estimated from the resemblances between the fadings at the receivers. That pair

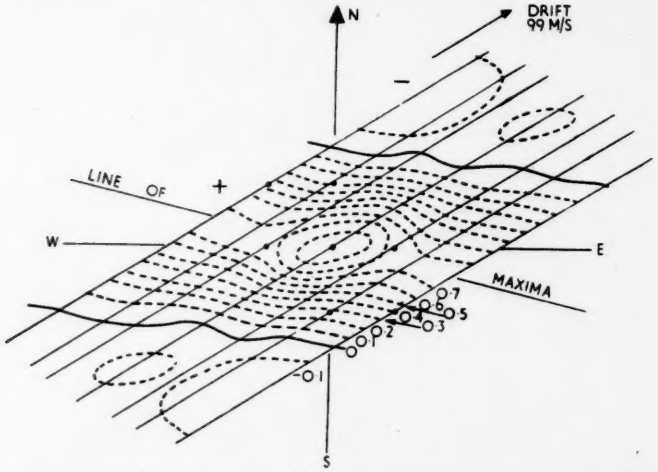

Fig. 8. An alternative interpretation to that in Fig. 7, the drift being taken to be at 45° to the line of maxima. Other plausible interpretations are possible, but they involve drifts at much smaller angles to the line of maxima and at high velocities, say 800 m/s.

of receivers whose fading is most alike, apart from a time-delay, are the pair of receivers most nearly in line with the true direction of drift.

Stated in this way, the conclusion seems almost obvious, but the next example shows that it is not always true.

Attempting to Assess a Decay

In the example of Fig. 4 we find that the time-delays of the peak correlations do not have a zero total. They are

$$T_{NC} = +1{\cdot}06, \qquad T_{CE} = +1{\cdot}13, \qquad T_{EN} = -2{\cdot}66 \text{ sec}$$

Apparently the central region of the correlogram has a skewed form.

On the assumption that the outer parts of the correlogram are less distorted, we may strike a median on each curve, lying midway between the subsidiary maxima. These medians are found to have time-delays,

$$T_{NC} = +1{\cdot}82, \qquad T_{CE} = +1{\cdot}64, \qquad T_{EN} = -3{\cdot}45 \text{ sec}$$

which total zero very nearly. It therefore seems appropriate to use them to

VOL. 8 1956

estimate a drift according to the methods of the previous section. The component of drift at right angles to the "line of medians" is found to be 19 m/s, directed nearly south-east. But the N and E receivers lie almost along this line, and their peak correlation is less than that of the other pairs. The inference would be that the true drift was at a considerable angle to the line of these two receivers. A reconstruction, not shown here, was made for a drift in a direction 30° north of east at a velocity of 109 m/s.

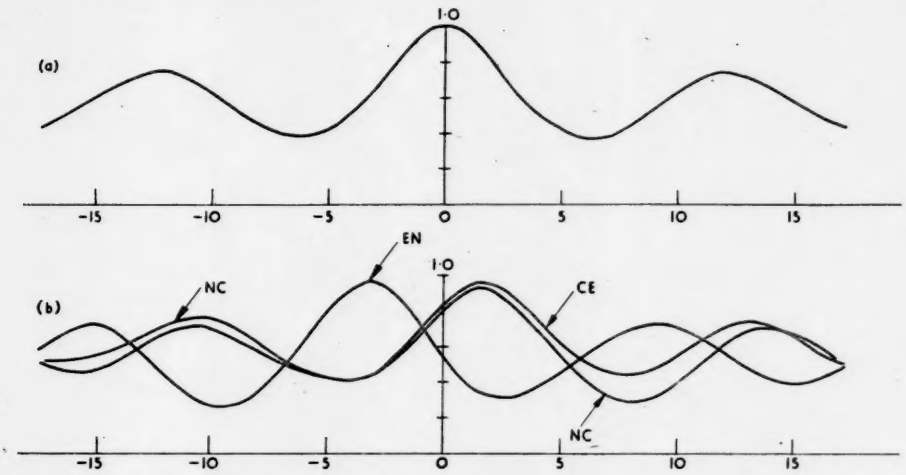

Fig. 9. The correlation curves of Fig. 4 multiplied by a factor $e^{+0\cdot055|T|}$. This aims to correct a decay in the correlogram. Curve (a) is the mean of the three autocorrelograms.

These arguments depend on the assumption that the interference pattern does not change its form, that the correlogram does not decay. But the curves themselves suggest that it does. The central maxima in the cross-correlograms of Fig. 4(b) do not lie midway between the secondary maxima: also the secondary maxima are unequal. In all cases the higher secondary maximum is that which occurs at the smaller delay.

An attempt was made to correct for a decay. The curves of Fig. 4 were all multiplied by the same factor

$$e^{+0\cdot055|T|}$$

and the revised curves are shown in Fig. 9. They are much more symmetrical. It is also noteworthy that the delay-times of the central maxima now have a zero total. They are now

$$T_{NC} = +1\cdot46, \qquad T_{CE} = 1\cdot64, \qquad T_{EN} = -3\cdot10 \text{ sec.}$$

A plausible reconstruction of the correlogram from these revised curves is shown in Fig. 10. The drift is at 21 m/s toward the south-east. This direction was preferred because in the corrected curves of Fig. 9 it is the north and east receivers which show the highest peak correlation.

When a decay is present it is evidently unsafe to judge the direction of drift from the degree of resemblance between the fading records.

It should be observed that the quadratic analysis in Fig. 6 gave the same direction of drift as that obtained in Fig. 10. The quadratic method is not affected by a decay in the correlogram, and this is one of its advantages.

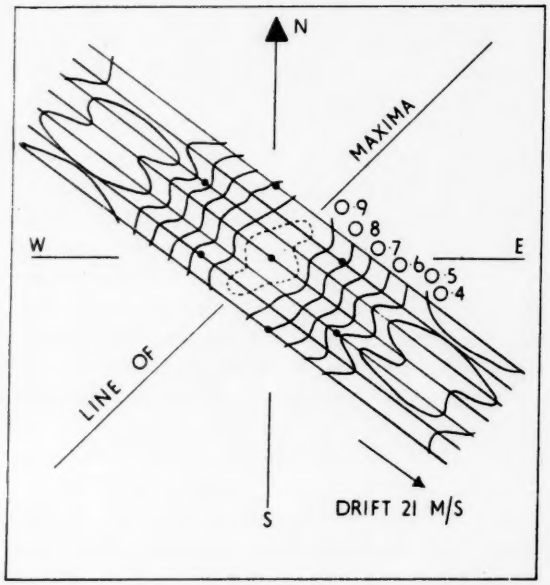

Fig. 10. A reconstruction of the correlogram from the curves of Fig. 9.

DISCUSSION

1. The form of the decay quoted in the last section is of interest. BANERJI (1955) has shown that the effect of random turbulence in the ionosphere would be to cause a decay in the correlogram, of the gaussian form

$$e^{-kT^2}$$

This form of decay was not adopted, because it could not account for the skewness of the correlogram or its asymmetry. Thus, a curve with a peak at T, is approximately $a \cos p(T - T_1)$ in that region. When multiplied by a small decay e^{-kT} the maximum of the curve shifts by an amount δT, where

$$\delta T_1 = 2kT_1/p^2.$$

Consequently, if three similar curves have peaks at T_1, T_2, and T_3 such that

$$T_1 + T_2 + T_3 = 0$$

this rule will still hold after the decay has been applied to all the curves; a gaussian

VOL. 8 1956

decay does not produce "skewness." Also, if a curve has three peaks of similar form that are equally spaced so that

$$T_1 - 2T_2 + T_3 = 0$$

this rule will also hold when the gaussian decay is imposed.

The assumption of a decay $e^{-k|T|}$ is justified by the simplicity it gives to the correlogram. The form of this decay is physically significant. It is the decay that would be expected if reflecting points were being created at random and were becoming weaker exponentially with time. It suggests that the fading in this example may have been due to meteor trails with an average life of $1/k$, or 18 sec.

2. Since a decay can so much affect the interpretation of the records, we may reconsider the first example. Though the time-lags have a zero total, a gaussian decay may be present, and it would invalidate the interpretation in Fig. 8.

The effect of a decay is always to reduce the apparent time-lags between the signals and to give a greater apparent velocity. It also reduces the correlation between the signals. The correlation tends to be least between those signals which have the greatest time-lag. We might therefore interpret this example as being due to an ionosphere drifting in the direction shown in Fig. 7; the decay would account for the low correlation observed between the N and C receivers. We would be prepared to find that the true drift was less than the 70 m/s that was calculated from the time-lags.

This example has already been examined by the quadratic method, with the result shown in Fig. 6(a). It does give a drift in the direction of Fig. 7, and shows a smaller velocity, 42 m/s. It is true that the data had to be amended in order to make them fit a quadratic, but other plausible amendments have been tried, and they do not lead to greatly different interpretations. The quadratic analysis gives a velocity between 40 and 50 m/s in a direction 10° to 15° east of north.

It seems probable, therefore, that a decay is present in the first example, and that the quadratic analysis gives the truest interpretation. In practice, we frequently find fading records in which those traces that have the greatest relative time-lag are least alike in their details. If we do not admit the possibility of a change in the details of the interference pattern, we have to suppose a high velocity of drift in the direction of those receivers whose outputs are most alike. If we admit that a decay may be present, we cannot judge the true direction by the similarity of the traces. We can only use the time-lags to estimate one rectangular component of the drift, and even this will be overestimated because of the decay.

3. It is very desirable to adopt some means of analysis that is not invalidated by a decay in the correlogram, that is by a change in the details of the drifting interference pattern. The quadratic method seems very suitable. It also appears to be practicable, since it calls for no time-delays to be introduced into the signals before finding the integrated products.

Conclusions

All the methods of analysis discussed here, except the quadratic method, are valid only in special conditions. There must be no decay in the correlogram, that

is no change in the form of the drifting pattern, or the space correlogram must be circular or perhaps elliptic.

There is little practical evidence of how much change can take place in the drifting pattern. Little is known in practice about the form the space correlogram may take, except that a circular form is improbable. It is very desirable to adopt a method of analysis that is independent of these unknown features. The quadratic method seems both suitable and practicable.

References

Banerji R. B. 1955 The autocorrelogram of randomly fading waves, *J. Atmosph. Terr. Phys.* **6**, 50–56

Yerg D. G. 1955 Notes on correlation methods for evaluating ionospheric winds from radio fading records, *J. Geophys. Res.* **60**, 173–185.

VOL.
8
1956

Journal of Atmospheric and Terrestrial Physics, 1956, Vol. 8, pp. 331 to 337. Pergamon Press Ltd., London

Sporadic echoes from the *E* region over Ahmedabad (23° 02′ N, 72° 38′ E)

K. M. KOTADIA
Physical Research Laboratory Ahmedabad, India

(*Received* 6 *January* 1956)

Abstract—In this paper, a study is made of the sporadic *E* echoes observed in the ionospheric *h′-f* records of Ahmedabad ($\Phi = 13{\cdot}6°$N). From the analysis of the data for 1953–1954, a sunspot minimum period, it was found that three types of sporadic, namely (i) *Esc* at 95–100 km, (ii) *Esn* at 105–125 km, and (iii) *Ess* at 115–125 km, occur in the *E* region. The overall behaviour of *Es* has been shown as being due to the combination of the characteristics of these three types. The sporadic ionization of type *Esc* has a maximum frequency of occurrence in the late evening hours, and has a thin structure. It is apparently evolved out of a downward drift of the residual ionization of the normal *E* layer. No correlation could be established with meteor activity. *Esn* shows a minimum in the afternoon and maximum in late-night hours before dawn. *Ess* is developed by the vertical downward movement of the *E2* layer.

1. INTRODUCTION

Es echoes of a transient or persistent nature are observed to occur at heights of 90–130 km above ground. Various attempts have been made to correlate *Es* echoes with the time of the day, season, magnetic disturbances, meteors, and thunderstorms (APPLETON *et al.*, 1937; BEST *et al.*, 1938; APPLETON and NAISMITH, 1940; HEY and STEWART, 1946). It is generally believed that *Es* occurs either in the form of discrete electron clouds or as a thin sheet embedded in the normal *E* layer. Sudden and temporary changes of ionization occurring below the level of normal *E* layer have also been reported (APPLETON and NAISMITH, 1947). The practical significance of high *Es* activity in low latitudes is that in long-distance communication it would be possible to communicate at frequencies greater than 25–30 Mc/s for about 40% of total time in summer, and at frequencies greater than 35–40 Mc/s for about 20% of total time.

Es strata are found to have different characteristics at different places. In this paper, the diurnal and seasonal variations of *Es* over Ahmedabad for the years 1953-1954 are analysed. It is found that there are different types of *Es*. The results are of interest because of the low latitude of the place and because of the fact that the observations were made during a period of minimum sunspot activity.

Data and method of analysis

The reflectivity of the sporadic *E* layer generally decreases with increasing frequency of the exploring radio wave, and the highest frequency, *fEs*, up to which reflection can be recorded, depends on the power of the transmitter, the directivity and gain of the antenna, and the sensitivity of the receiver. All these factors vary with the frequency. The recording equipment used at various places differs in one or more of these respects. So a quantitative comparison of results obtained at different stations is difficult; nevertheless, for a particular place, it is possible to study the relative diurnal and seasonal variations of the sporadic layer.

The data used in this study were obtained from the automatic ionospheric records of the Physical Research Laboratory, Ahmedabad. The frequency range is from 0·6 to 25 Mc/s, and this is swept in 5 min. The transmitter power varies

from 1750 watts at low frequencies to 250 watts at high frequencies. The co-ordinates of Ahmedabad are:

Geographic latitude 23° 02′ N, longitude 72° 38′ E
Geomagnetic latitude 13·6° N, magnetic dip 34° N.

The frequencies of occurrence of *Es* are expressed in the form of percentages of the total number of observations when *fEs* was greater than 3, 5, and 7 Mc/s. When *Es* occurrences are very frequent, the mean or median value of *fEs* can also be taken to indicate its characteristic variations. In finding the median value of *fEs*, only those hours at which observations were available were counted.

2. Diurnal and Seasonal Variations of *Es*

In the period February 1953 to December 1953, *Es* echoes (all types included) were recorded on 3036 occasions out of 5867, i.e. on 52% of occasions; and in 1954, on 4069 occasions out of a total of 7132, i.e. on 65% of occasions. The mean

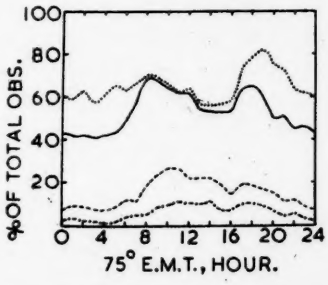

FIG. 1. Mean diurnal variation of sporadic *E*-layer occurrences in the year 1954. (. . . . .) all values of *fEs*; (————) *fEs* > 3 Mc/s; (— — — —) *fEs* > 5 Mc/s; (— . — . —) *fEs* > 7 Mc/s.

monthly relative sunspot numbers in the two years were 12 and 4·4 respectively. In Fig. 1 are shown the mean diurnal variations of the occurrence of *Es* with different limiting lower frequencies.

fEs is >3 Mc/s during most of the day hours, whereas the normal *E*-layer critical frequency during these hours varies from 2·2 to 3·3 Mc/s. In the curve for *fEs* > 3 Mc/s, two maxima are seen, one in the forenoon and the other near sunset, and two minima at 1400 and 0200. The midnight minimum is deeper than the afternoon one. In contrast to the above, the occurrences of *Es* with *fEs* > 5 and *fEs* > 7 Mc/s, indicate midday maxima falling down roughly symmetrically on both sides. Although the maximum frequency of reflections was generally higher during the day, some instances were recorded when *fEs* exceeded 10 Mc/s at night, but these were short-lived. Intense echoes, when they occurred during the day, were found to obstruct partially or wholly the upper layers; this was not so at night. Very often high-multiple and so-called *M* reflections from *Es* are observed at night, but they do not have a blanketing effect; while with *Es* echoes during day there is pronounced blanketing, and more than four multiples are rarely found. In summer, the frequency of *Es* with *fEs* > 5 Mc/s was about 40%, and those with *fEs* > 7 Mc/s about 20%. These were nearly twice the annual average and about seven times the winter average. Japanese stations show diurnal variations similar to those described above, whereas Canadian stations (near the auroral zone) show maxima round about midnight; Slough data show a midday maximum.

VOL. 8 1956

In midsummer *Es* occurs throughout day and night, and in midwinter during day mainly. The variation of median *fEs* which may be regarded as an index of the intensity of sporadic ionization is shown in Fig. 2 for June–July 1954 and for

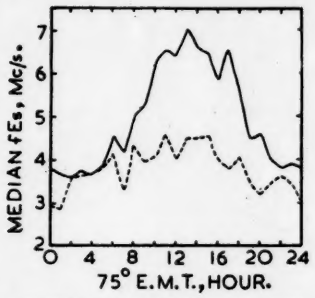

FIG. 2. Diurnal variation of median *fEs* in midsummer and midwinter. (————) June–July 1954; (— — — —) December 1953 to January 1954.

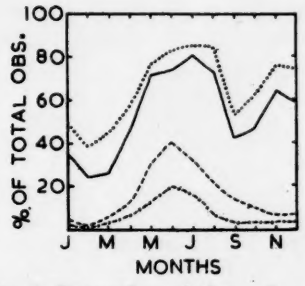

FIG. 3. Seasonal variation of sporadic *E*-layer occurrences. (. . . . .) all values of *fEs*; (————) *fEs* > 3 Mc/s; (— — — —) *fEs* > 5 Mc/s; (— . — . —) *fEs* > 7 Mc/s.

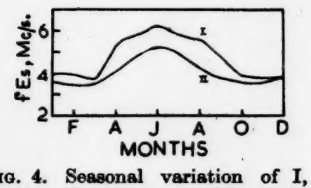

FIG. 4. Seasonal variation of I, noon median *fEs*; II, mean *fEs* of all hours. (April 1953 to March 1955).

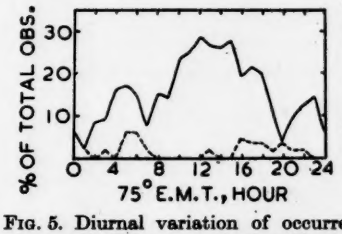

FIG. 5. Diurnal variation of occurrences of sporadic *E* layer producing blanketing effect in (————) June–July 1954 and (— — — —) December 1953 to January 1954.

December 1953 to January 1954. Both the curves show during daytime a variation similar to the daily normal *E*-layer critical frequencies, with the difference that daytime values in summer are much higher than those in winter; the night values approach each other. In summer, the maximum median *fEs* is 7·0 Mc/s as against 4·5 Mc/s in winter. Also, the variation in winter is not so smooth, as in summer. Four curves showing seasonal variations of *Es* for different limiting frequencies are drawn in Fig. 3. The upper two curves for low *fEs* show a second maximum in November, while the two lower curves with high *fEs* exhibit only one maximum in June. Such symmetrical curves are also obtained for *fEs* when the mean values for all the hours or noon median values are plotted (Fig. 4). These curves refer to the period April 1953 to March 1955.

The occurrence of blanketing effect by *Es* was studied, and the results are shown in Fig. 5. The curve for midsummer shows a prominent maximum during midday similar to that of *fEs* in Fig. 2.. Daytime blanketing effect in midwinter is infrequent, and it appears that winter *Es* is usually thin.

From the above discussion of the diurnal and seasonal variations of the intensity and frequency of occurrence of sporadic *E* layer as a whole, we conclude

that, superposed on an intense type of daytime ionization, there exists a weaker ionization which is more frequent near sunset in summer and in the late afternoon in winter. There is also a maximum near sunrise, which has to be explained. The h'-f records show *Es* reflections sometimes from a single height and sometimes from two or three heights simultaneously. The above results demand a closer analysis of the records. Results of such an analysis for the year 1954 are given in the following section.

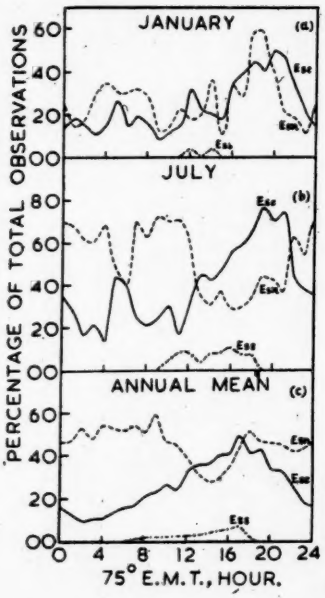

FIG. 7. Diurnal variation of occurrences of *Esc*, *Esn*, and *Ess*.
(a) January 1954, showing roughly similar variation of *Esc* and *Esn*.
(b) July 1954, showing almost complementary variations of *Esc* and *Esn*.
(c) Annual mean curves of the three types of sporadic for 1954.

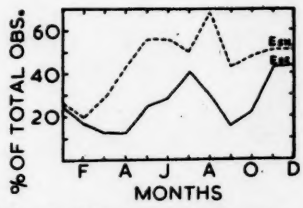

FIG. 8. Seasonal variation of occurrences of *Esc* and *Esn* layers in 1954.

3. THREE TYPES OF SPORADIC *E* LAYERS

In the above general treatment of *Es*, only the highest values of all *fEs*, recorded at each hour, were taken to study the variation. The height of the sporadic layer was not considered at all. (The CRPL F Series ionospheric data publication does not say anything about the height of *Es*.) Our analysis indicates that there are mainly three types of Sporadic *E*, (i) a type *Esc* which occurs at a constant height of 95–100 km, (ii) a type *Esn* which occurs embedded in the normal *E* but whose frequency maximum extends beyond f_0E, and (iii) a type *Ess* which descends in the afternoon from the level of *E2* to the normal *E* level in the evening.

(i) *Constant height type, or Esc*

This type of *Es* ionization occurs below the level of normal *E* layer at a height of 95–100 km. The reflected radio wave does not suffer any retardation, and no magneto-ionic splitting takes place. In other words, the reflection has the same apparent height at the low-frequency and high-frequency ends, which also means that this *Es* has a steep gradient. MCNICOL and GIPPS (1951) have called such a layer a "constant height type" of *Es* or *Esc*, and this term is also adopted here. *Esc* accounted for about 27% of the sporadic *E's* in 1954. Picture (a) in Fig. 6.

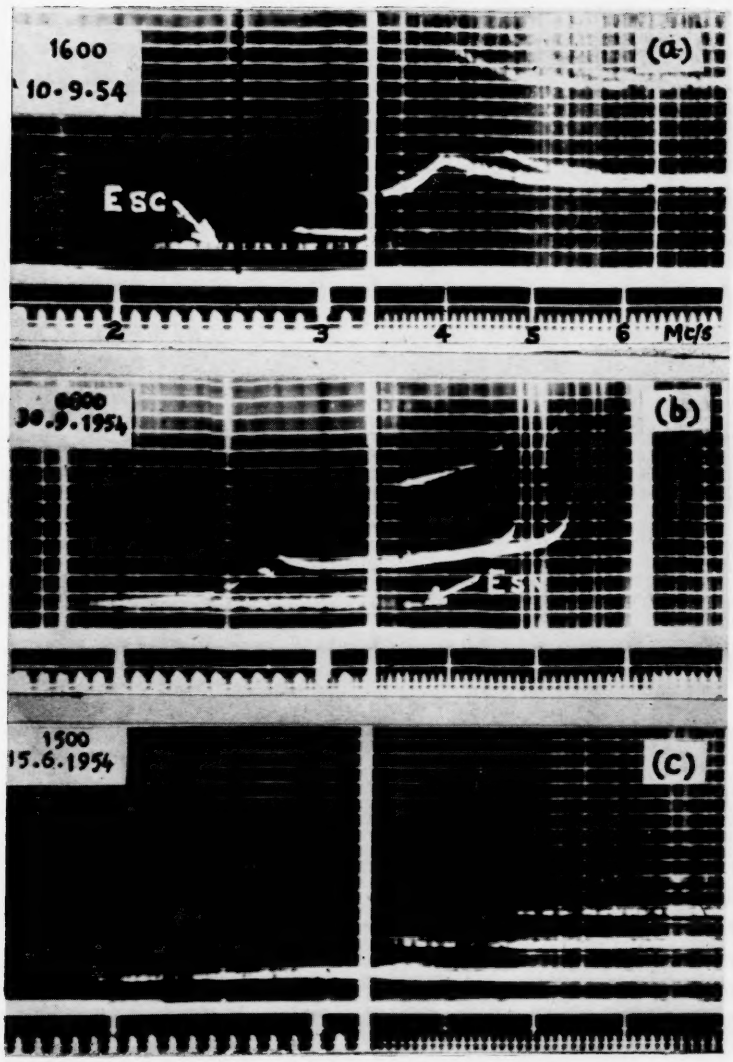

Fig. 6. Typical ionospheric h'-f records obtained at Ahmedabad. (a) Showing *Esc* at 100 km, (b) showing *Esn* at the level of normal *E* layer, (c) showing sporadic with blanketing effect.

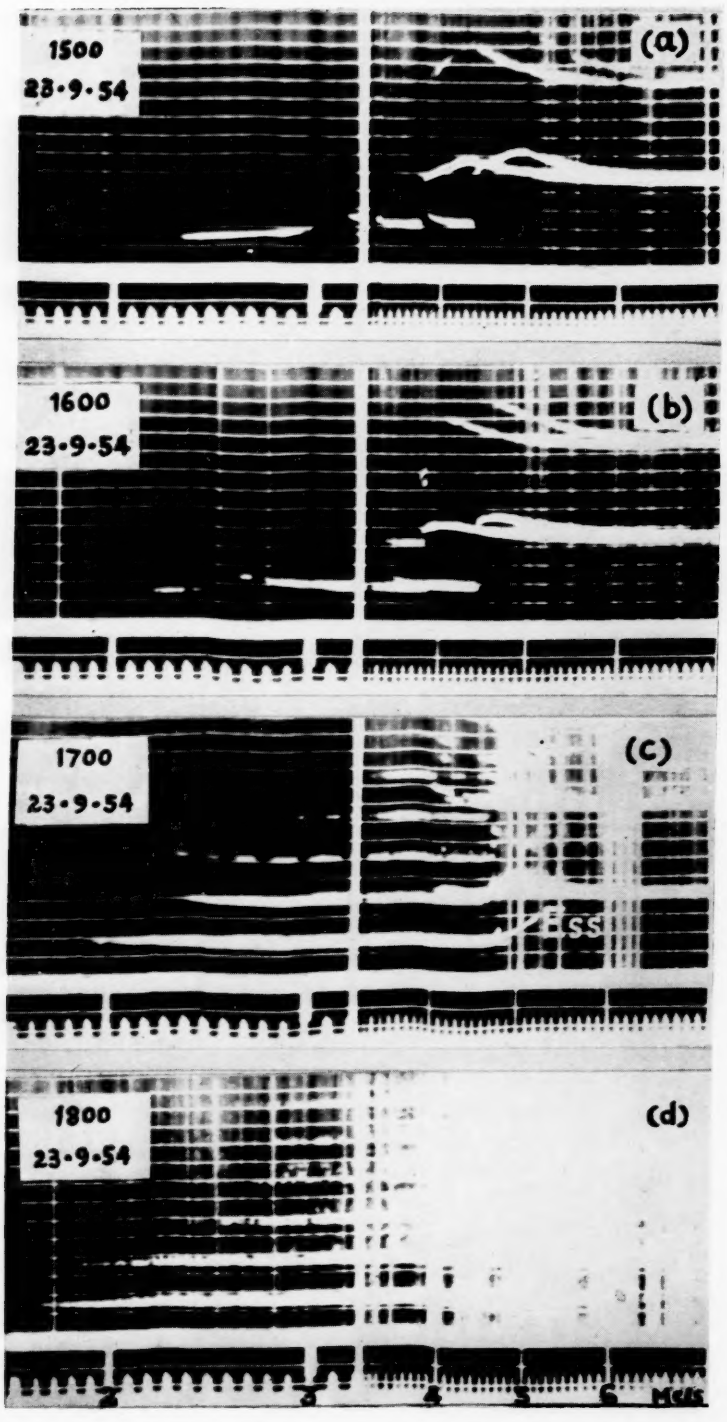

Fig. 9. Typical ionospheric h'-f records obtained at Ahmedabad, showing the sequence of the development of the *Ess* type of sporadic.

shows a typical record of *Esc*. The *h′-f* records in winter show weak *Esc* echoes and broken traces, but in summer this takes the form of intense ionization with unbroken traces and produces blanketing effect on some occasions. The strength of the echo decreases with increasing frequency, the layer becoming transparent at higher frequencies. *Esc* occurs most frequently at 1800–2000 (Fig. 7) in all the months except in winter, when it turns into a midday or afternoon phenomenon.

The seasonal variation of frequency of occurrence shows two maxima, one in summer and another in winter (Fig. 8). NAISMITH (1954) designates *Esc* as *Em* and attributes it to meteors, while RANGARAJAN (1954) calls *Esc* descriptively a patchy type of *Es*. The diurnal variation of *Esc* occurrence at Ahmedabad does not correspond to the variation reported by the above authors for Slough ($\Phi = 54°$ N) and Kodaikanal ($\Phi = 0{\cdot}6°$ N).

(ii) *Sporadic embedded in normal E or "Esn"*

This type of sporadic ionization is recorded as an extended *E* layer in *h′-f* record beyond its critical frequency, and normally its apparent height is the same as that of the *E* layer. We have called it "*Esn*," the '*n*' indicating that it is embedded

Table 1. Seasonal variation of *Esc*, *Esn*, and *Ess* in 1954

Month	% occurrences		
	Esc	*Esn*	*Ess*
Jan.	25	27	—
Feb.	17	20	—
Mar.	15	29	1
Apr.	13	43	1
May	25	56	(3)
June	29	57	(1)
July	41	50	(3)
Aug.	30	68	(1)
Sept.	16	43	2
Oct.	23	48	3
Nov.	43	51	3
Dec.	44	51	2

in the normal *E* layer. The height of *Esn* remains constant up to a certain frequency, after which it rises, but without magneto-ionic splitting (Fig. 6b). Its height rises after the normal *E* layer has disappeared, and varies from 105 km to 125 km, the ionization being sometimes split into two or more strata at night. The diurnal variation of *Esn* shows a minimum at 1400 (Fig. 7), and its frequency of occurrence increases after sunset, reaching a maximum in the late-night hours or near sunrise. From some records of simultaneous occurrences of *Esc* and *Esn*, it was found that *Esn* had more blanketing effect than *Esc* during daytime. The strength of *Esn* diminishes at night after the disappearance of daytime *E*. The seasonal variation of *Esn* shows one maximum in summer as against two maxima for *Esc* (Fig. 8), while the diurnal variations of the two are roughly complementary to each other.

Esn accounted for about 45% of the total observed sporadics in the year 1954. The figures for *Ess* in summer are placed within brackets (Table 1), because they are often merged in *Esn* and cannot be distinguished from them.

To investigate whether either *Esc* or *Esn* has any dependence on meteor activity and to find their distribution in each quarter of the day, the total number of occurrences of *Esc* and *Esn* for twenty-four hours were divided into four quarters and the percentage for each quarter calculated from the total number of occurrences and the total number of observations during the relevant quarter.

Table 2. Percentage occurrences of *Esc* and *Esn* in each quarter of the day for each month of 1954

Month	% occurrence of *Esc*				% occurrence of *Esn*			
	0000–0500	0600–1100	1200–1700	1800–2300	0000–0500	0600–1100	1200–1700	1800–2300
Jan.	17	14	28	39	25	24	24	35
Feb.	11	10	18	27	26	22	10	21
Mar.	8	12	17	24	43	29	11	37
Apr.	11	8	13	21	53	44	25	60
May	16	14	25	44	75	63	36	53
Jun.	22	17	25	55	65	67	45	49
Jul.	27	26	46	61	56	65	37	45
Aug.	6	16	45	52	74	88	54	55
Sept.	2	11	36	14	36	58	30	50
Oct.	8	17	57	9	35	54	45	59
Nov.	14	52	89	18	53	59	45	47
Dec.	10	59	72	33	52	57	53	44

It is well known that the frequency of meteors in the second half of the night (0000–0500) is twice that in the first half (1800–2300). If *Esc* (which NAISMITH calls *Em*) were due to meteors, it would show significant correspondence to meteor activity. The figures in Table 2 show that at least in the tropics, there is no marked correspondence either of *Esc* or *Esn* with meteors. Table 2 also shows that *Esc* is more an afternoon and premidnight phenomenon, while *Esn* tends to be a postmidnight and forenoon phenomenon.

(iii) *Sporadics of sequential type or "Ess"*

This type of sporadic ionization occurs mostly in the late afternoon. Very often the *E2* layer which appears at an apparent height of 150 km turns into a layer of intense ionization with sharp gradient and comes down to a height of 115 km, finally showing the same characteristics as *Esn* after sunset (pictures a, b, c, d, Fig. 9). This transformation of the *E2* layer takes place gradually and is called by MCNICOL and GIPPS "*Ess.*" It is characterized by the *h'-f* record emerging out and extending from the cusp of the critical frequency of the normal *E* layer, as was discussed by BEST, FARMER, and RATCLIFFE (1938). There is retardation only in the beginning of the trace. *Ess* behaves as sporadic from a height of 125 km down to 115 km, where it becomes sharply defined and invariably

VOL. 8 1956

produces a blanketing effect. In summer, this layer is so low that it cannot be distinguished from *Esn* (in Table 1, therefore, figures for *Ess* are put into brackets) and in such a case, f_0E is obscured (Fig. 6c).

The blanketing effect and its maintenance at constant height during observation is an indication of the fact that the sequence of change in the layer from 125 to 115 km is not due to the horizontal movement of an ion cloud coming up overhead, for then the blanketing effect will not be observed till the cloud comes overhead. The intensity of *Ess* and its merger with *Esn* in summer are responsible for the characteristic diurnal variation of median *fEs* and of $fEs > 5$ Mc/s and $fEs > 7$ Mc/s, as shown in Figs. 1 and 2. The frequency and intensity of occurrence of *Ess* are greatest in midsummer. *Ess* was observed on about 2·5% of the total number of observations.

4. Conclusions and Summary

We conclude that there are three types of sporadic *E* layers, and that the diurnal and seasonal variations of *Es* as a whole can be explained as being due to a combination of the behaviour of *Esc*, *Esn*, and *Ess*.

In this paper, a study is made of the sporadic *E* echoes observed in ionospheric *h′-f* records of Ahmedabad. From the analysis of the different types of the sporadic *E* layers, it is found that there is a weak type of sporadic ionization at a height of 95–100 km. The fact that this has a maximum frequency of occurrence in late evening hours suggests that it is often evolved by a downward drift of the residual ionization of the normal *E* layer or of the sporadics embedded in normal *E*.

The solar control of *Esn* is similar to that of the normal *E* layer. The weak *Esn* at night is probably the remnant of the daytime *E* layer.

The sequential or *Ess* type is developed by the vertical downward movement of the *E2* layer, its intensity increasing as it comes down to *Esn* level. *Ess* is only found during daytime and more often in afternoons.

Acknowledgements—The author has great pleasure in expressing his indebtedness to Professor K. R. Ramanathan for his valuable guidance and continued encouragement in preparing this paper. His thanks are also due to Dr. U. D. Desai and Mr. R. G. Rastogi for their assistance in the maintenance of the equipment. This work forms a part of the Radio Research programme of the Council of Scientific and Industrial Research.

References

Appleton E. V. and Naismith R.	1940	*Proc. Phys. Soc.* **52,** 402.
Appleton E. V., Naismith R., and Ingram L. J.	1937	*Phil. Trans.* **236,** 191.
Appleton E. V. and Naismith R.	1947	*Proc. Phys. Soc.* **59,** 461.
Best J. E., Farmer F. T., and Ratcliffe J. A.	1938	*Proc. Roy. Soc.* **A164,** 96.
Hey J. S. and Stewart G. S.	1946	*Nature* **159,** 119.
McNicol R. W. E. and Gipps G. de. V.	1951	*J. Geophys. Res.* **56,** 17.
Naismith R.	1954	*J. Atmosph. Terr. Phys.* **5,** 73.
Rangarajan S.	1954	*J. Geophys. Res.* **59,** 239.

Journal of Atmospheric and Terrestrial Physics, 1956, Vol. 8, pp. 338 to 344. Pergamon Press Ltd., London

On the propagation of whistling atmospherics

G. R. Ellis
Commonwealth Ionospheric Prediction Service, Hobart, Tasmania

(*Received* 3 *January* 1956)

Abstract—It is shown that the dispersion of whistling atmospherics propagated along the lines of force of the earth's magnetic field should be greatly dependent on the geomagnetic latitude of the observing point. The change in the magnetic-field intensity along a line of force produces an upper-frequency limit for whistler propagation which, at latitudes greater than 62°, should fall within the usually observed frequency region of 1–10 kc/s. Dispersion curves showing this critical frequency are given for geomagnetic latitudes 55°, 60°, and 65°.

1. Introduction

It has been shown by Storey (1953) that many of the observed properties of whistling atmospherics may be satisfactorily explained if they are propagated along the lines of force of the earth's magnetic field between the northern and southern hemispheres. Storey's analysis was based on a simplified magneto-ionic theory in which the quasi-longitudinal approximation for the refractive index equation was used, namely:

$$\mu^2 = 1 + \frac{X}{Y_L - 1} \tag{1}$$

together with the conditions

$$\frac{X}{Y} \gg 1, \quad Y_L \gg 1 \tag{2}$$

These equations result in an experimentally confirmed relation for the time-delay of the frequency components of a whistler,

$$t = Df^{-\frac{1}{2}} \tag{3}$$

The derivation of equation (3) depends greatly on the approximations (2), and a less simplified treatment without these approximations can lead to a completely different function of frequency for the time-delay. Situations where, in particular, the condition $Y_L \gg 1$ does not apply can easily be found by considering propagation paths which end at high geomagnetic latitudes, for frequencies in the range 1–10 kc/s. Under these circumstances, whistlers propagated along lines of force would be expected to have properties different from those observed at middle latitudes, for which Storey's theory provides an adequate description.

2. Notation

μ = refractive index
N = electron density
e = charge of electron
m = mass of electron
f = wave frequency
$X = f_0^2/f^2 = Ne^2/m\pi f^2$

VOL. 8 1956

$f_H = eH/2\pi mc$
H = geomagnetic-field intensity
$Y = f_H/f$
s = distance along a line of force
λ = geomagnetic latitude
R = distance from the centre of the earth, measured in units of the earth's radius.
D = dispersion
θ = propagation angle

3. Theoretical

If we assume a dipole field, then the least magnetic field intensity encountered along a line of force will occur in the magnetic equatorial plane. This value of the intensity, H_0, will determine an upper limiting frequency or critical frequency for whistler propagation at which $Y_L = 1$, that is $f_c = f_{H_0} \cos\theta$. Below the critical frequency the velocity of group propagation will at first increase with decreasing frequency, and the dispersion will be of opposite sign to that given by equation (3), which will apply as a limiting case when the frequency approaches zero.

(a) *Critical Frequency*

To calculate the variation of critical frequency with geomagnetic latitude, we need only the equations for the dipole field

$$R = R_0 \cos^2\lambda \tag{4}$$

$$H = 0{\cdot}31R^{-3}\cos\lambda(1 + 4\tan^2\lambda)^{\frac{1}{2}} \tag{5}$$

The subscript 0 is used for quantities measured in the geomagnetic equatorial plane. For longitudinal propagation ($\theta = 0$) we have

$$f_c = f_{H_0} = \frac{0{\cdot}31e\cos^6\lambda}{2\pi mc}. \tag{6}$$

This relationship is illustrated in Fig. 1. It can be seen that f_c is less than 10 kc/s for geomagnetic latitudes greater than 62°.

(b) *The Longitudinal Approximation*

For propagation not strictly longitudinal, f_c ($= f_{H_0}\cos\theta$) will be less than f_{H_0} which, in the absence of information about the direction of the wave-normal, may be considered to set an upper limit for the critical frequency. However, the error caused by assuming $f_c = f_{H_0}$ will not be great. This may be shown by an analysis of the way the refractive index changes along a line of force near the equatorial plane.

Let us assume that the electron density in the upper atmosphere is proportional to $\exp 2{\cdot}5/R$, as proposed by Dungey (1954). Then, if we take $\lambda \ll 1$, we can write

$$R \approx R_0(1 - \lambda^2)$$

and
$$X = X_0 \exp 2{\cdot}5\left(\frac{1}{R} - \frac{1}{R_0}\right)$$
$$\approx X_0 \exp \frac{2{\cdot}5\,\lambda^2}{1-\lambda^2}$$
$$\approx X_0 \qquad (7)$$

Also, we have, from equations (4) and (5),
$$Y = Y_0 \cos^{-5}\lambda(1 + 4\tan^2\lambda)^{\frac{1}{2}}$$
$$\approx Y_0(1 + 4{\cdot}5\lambda^2) \quad \text{if} \quad \lambda \ll 1. \qquad (8)$$

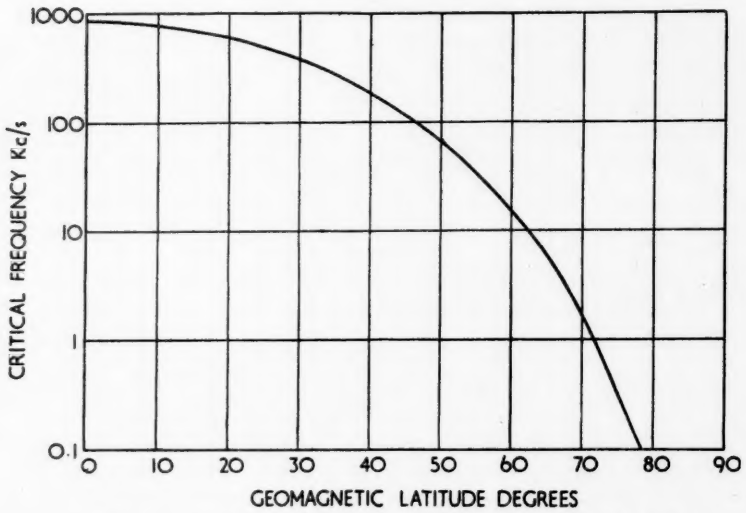

Fig. 1. Variation of critical frequency with geomagnetic latitude.

If we choose $f = f_{H_0}$, that is $Y_0 = 1$,
then for longitudinal propagation
$$\mu^2 \approx \frac{X}{Y-1}$$
$$\approx \frac{X_0}{4{\cdot}5\lambda^2} \quad \text{if} \quad X_0 \gg 1, \qquad \lambda \ll 1. \qquad (9)$$

It is obvious that changes in the longitudinal refractive index in these circumstances will be almost entirely due to changes in the field intensity. A similar situation exists for other directions of wave propagation. The medium may, therefore, be approximated to by one of uniform electron density with a varying magnetic field, and surfaces of equal refractive index will be perpendicular to the field direction. For large values of the refractive index, the directions of wave propagation will thus be confined to a narrow cone about the field direction.

VOL. 8 1956

This is illustrated by the typical refractive-index curves shown in Fig. 2. The possible directions of propagation are represented by those parts of the curves

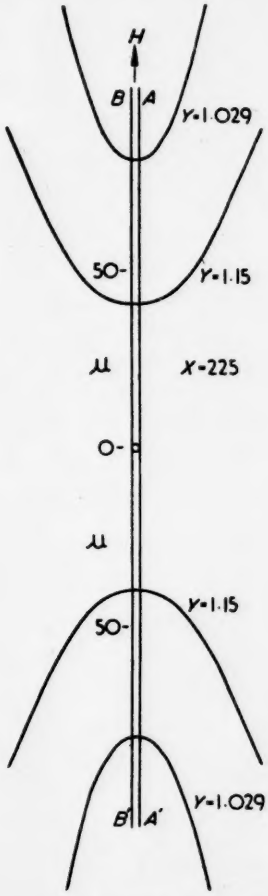

Fig. 2. Refractive index curves for a medium with uniform electron density and varying magnetic field.

between the parallel lines AA' and BB' which refer to angles of incidence of $\mp 90°$. The wave-normal direction in the medium is given by

$$\sin^2\theta \leqslant \frac{1}{\mu^2}$$

or

$$|\theta| \leqslant \lambda\sqrt{\frac{4{\cdot}5}{X_0}} \qquad X_0 \gg 1, \qquad \lambda \ll 1. \tag{10}$$

In investigating the propagation near the critical frequency in the vicinity of the equatorial plane, it is, therefore, sufficient to assume longitudinal propagation a medium of uniform electron density.

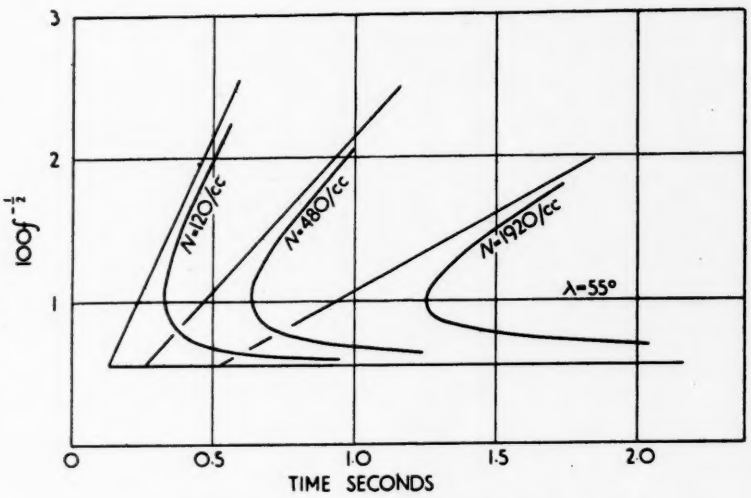

Fig. 3. Dispersion curves for geomagnetic latitude 55°.

VOL.
8
1956

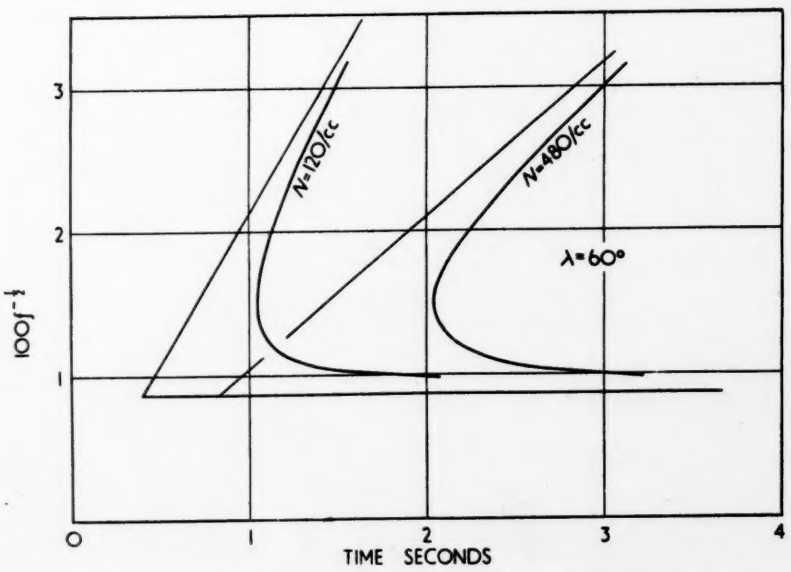

Fig. 4. Dispersion curves for geomagnetic latitude 60°.

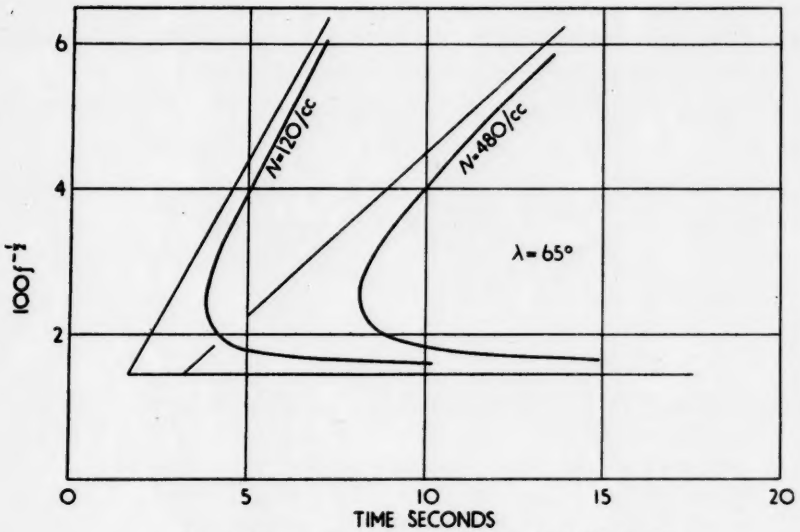

Fig. 5. Dispersion curves for geomagnetic latitude 65°.

OL.
8
956

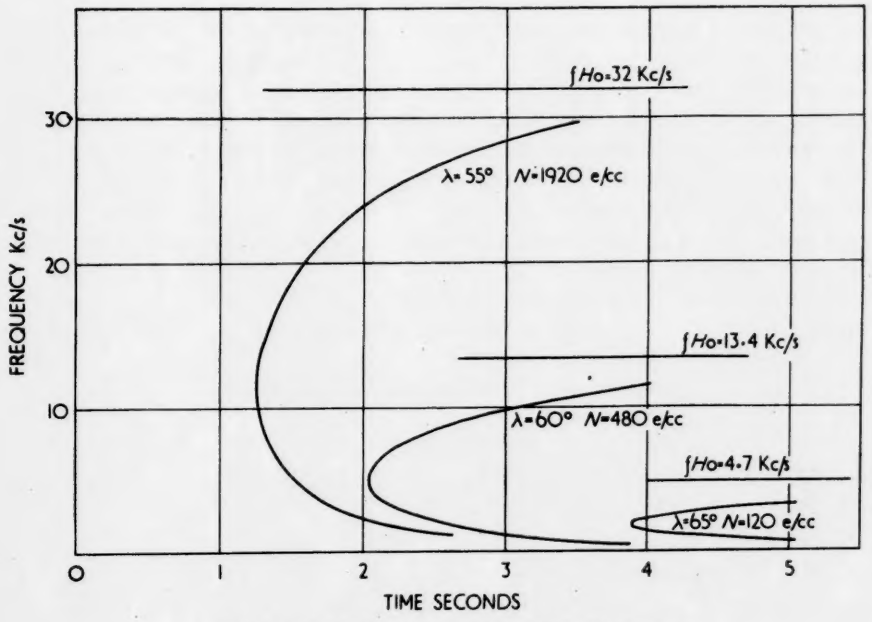

Fig. 6. Propagation times as functions of frequency.

(c) *Dispersion*

With longitudinal propagation, the dispersion can be calculated from the variation in group velocity along a line of force. We have, for the group refractive index

$$\mu' = \mu + f\frac{du}{df}$$

$$= \left(1 + \frac{X}{Y-1}\right)^{\frac{1}{2}} + \frac{X}{2}\frac{Y-2}{\left(Y-1\right)^{2}\left(1+\frac{X}{Y-1}\right)^{\frac{1}{2}}} \qquad (11)$$

and $$t = \int \frac{c}{\mu'}\, ds \qquad (12)$$

where $$ds = R_0 \cos^2\lambda(1 + 4\tan^2\lambda)^{\frac{1}{2}}\, d\lambda\,. \qquad (13)$$

Dispersion curves have been calculated from these equations for the geomagnetic latitudes of 55°, 60°, and 65°, assuming uniform electron densities sufficient to provide time-delays of the order of magnitude actually observed in whistlers. The curves are asymptotic at zero frequency to the function $t = Df^{-\frac{1}{2}}$ of STOREY, and at infinite time to the line $f = f_{H_0}$. They are illustrated in Figs. 3, 4, and 5. Fig. 6 shows the time of propagation plotted on a linear frequency scale. All curves are for propagation only once along a line of force.

VOL. 8 1956

4. DISCUSSION

The changes in dispersion associated with critical frequency should be observable in whistlers mainly between 60° and 65° geomagnetic latitude. Between these latitudes it could be expected that whistlers would have a note with a simultaneous rising and falling characteristic, while above 65° the frequency region for whistler occurrence should rapidly contract below 1 kc/s.

It may be that attenuation would prevent the high-frequency end of the whistler from being observable. However, if the assumptions which we have used here are valid, then the frequency range of whistlers should fall within the limits shown. These assumptions are:

(a) Whistlers are propagated along lines of force.

(b) The electron density at several earth radii can be considered to be essentially uniform.

(c) The earth's magnetic field can be treated as a dipole field.

REFERENCES

DUNGEY J. W. 1954 *Phys. Soc. Conference, Report on the Physics of the Ionosphere.*

STOREY L. R. O. 1953 *Phil. Trans.* **A246,** 908.

Journal of Atmospheric and Terrestrial Physics, 1956, Vol. 8, pp. 345 and 346. Pergamon Press Ltd., London

A photometric unit for the airglow and aurora

D. M. HUNTEN,* F. E. ROACH,† and J. W. CHAMBERLAIN‡

(*Received* 21 *January* 1956)

Abstract—It is suggested that the angular surface brightness B of these sources be measured in units of 10^6 quanta/cm² sec sterad. The number quoted should be $4\pi B$, and the unit of $4\pi B$ should be called the rayleigh. The advantages of this convention are pointed out and typical values of $4\pi B$ for the night and twilight airglow and the aurora are given.

RECENT discussions among the writers have shown that there is a need for agreement on a well-defined unit for photometry of the airglow and aurora. The definition should show clearly how the unit is to be found from observations, and the interpretation in terms of physical processes should be convenient. We believe that the proposal which follows is satisfactory in these regards.

The quantity actually measured is angular surface brightness B, which is most usefully expressed in such units as quanta/cm² sec sterad. However, the important quantity when the results are interpreted in terms of physical processes is usually volume emission rate, in quanta/cm³ sec. This emission rate cannot be found directly from surface-brightness measurements, but the rate of emission from a cm² column along the line of sight is ordinarily just $4\pi B$. This relation is true for any isotropic source with no self-absorption; for other sources $4\pi B$ gives a convenient starting-point for further correction. Consider a cylindrical column of cross-sectional area one cm² extending away from the photometer; the emission rate from a volume element of length dl at distance l is $\varepsilon(l)$ photons/cm³ sec. The element contributes to B an amount $dB = \varepsilon(l)\, dl/4\pi$. Integrating along the line of observation gives $4\pi B = \int_0^\infty \varepsilon(l)\, dl$ which is the emission rate from the whole column, as already stated.

Therefore, we propose that photometric measurements of the airglow and aurora be reported in terms of $4\pi B$, rather than the surface brightness B itself. Further, we suggest that $4\pi B$ be given the unit of "rayleigh" (symbol R), where B is in units of 10^6 quanta/cm² sec sterad. Hence 1 R = 10^6 quanta/cm² (column) sec. (The word "column" is often inserted into these units to convey the concept of an emission-rate from a column of unspecified length. As mentioned above, this interpretation of the observations would not be strictly correct in the event of self-absorption or non-isotropic emission, and the use of "column" in the units would then incorrectly imply a rate of emission within the column.) It should be emphasized that the rayleigh can be used as defined without any commitment as to its physical interpretation, even though it has been chosen to make interpretation convenient. Basically it is just the measured brightness multiplied by 4π.

* University of Saskatchewan, Saskatoon, Canada
† National Bureau of Standards, Boulder, Colorado, U.S.A.
‡ Yerkes Observatory, Williams Bay, Wisconsin, U.S.A.

The unit is of course named after the fourth Lord RAYLEIGH (R. J. STRUTT), who made the first absolute measurement of the intensity of the night airglow (1930). (It is his father, J. W. STRUTT, who is remembered for the theory of molecular scattering, among other things.) RAYLEIGH'S result for the zenith was $4\pi B = 1{\cdot}81 \times 10^8$ quanta/cm^2 (column) sec, or 181 rayleighs. The typical value in Table 1, found by photoelectric photometry, agrees very well with this old result of visual photometry.

Table 1. Typical values of $4\pi B$

Emission	Source	$4\pi B$	
[O I]-5577 Å	Night airglow, zenith	250 R	
	Aurora, I.B.C. I	1 kR	
	II	10 kR	
	III	100 kR	
	IV	1000 kR	
		summer	winter
NaI-5893 Å	Night airglow, zenith	70 R	300 R
	Twilight airglow, zenith	820 R	4300 R

A resolution making these proposals was presented by ROACH to Commission 22a of the International Astronomical Union at the ninth general assembly in September 1955. The present note is intended to clarify some ambiguities in the resolution as well as to amplify the ideas.

Measurements of the airglow have often been given in megaquanta/cm^2 (column) sec (for example, PETTIT, ROACH, ST. AMAND, and WILLIAMS, 1954). This unit is identical with the rayleigh. Some recent papers by HUNTEN (1955, 1956) have used a unit $Q(\lambda)$ equal to 10^7 quanta/cm^2 sec sterad. Multiplying numbers quoted in this unit by 40π or 126 transforms them into rayleighs. Some typical brightnesses are given in Table 1. Most of these data have been reported in the publications mentioned above. The scale for the auroral International Brightness Coefficients is a small modification of the one proposed by SEATON (1954), and has already been suggested as a standard (HUNTEN, 1955). It will be noted that the rayleigh is of convenient size for the airglow, and the kilorayleigh for the aurora.

REFERENCES

HUNTEN D. M. 1955 *J. Atmosph. Terr. Phys.* **7**, 141.

1956 Two papers read at the Belfast Conference on Aurora and Airglow, September 1955 (to be published by Pergamon Press).

PETTIT H. B., ROACH F. E., ST. AMAND P., and WILLIAMS D. R. 1954 *Ann. Géophys.* **10**, 326.

RAYLEIGH LORD 1930 *Proc. Roy. Soc.* **A129**, 458.

SEATON M. J. 1954 *J. Atmosph. Terr. Phys.* **4**, 285.

VOL. 8 1956

RESEARCH NOTES

Note on the variations of atmospheric ozone as a function of height*

(*Received* 13 *January* 1956)

In a recent issue of this journal, Paetzold (1955) discussed the annual variation of ozone at different levels of the atmosphere on the basis of ascents of recording ultra-violet balloon-spectrographs. In recent work at the Atmospheric Research Observatory (Epstein, Osterberg, and Adel, 1955), a new method, VODARO (Vertical Ozone Distributions from the Absorption and Radiation by Ozone) has been developed for determining ozone distributions from a ground station. The results of the first seven months of application of this method have been compared with those of Paetzold and show a remarkable similarity.

Paetzold demonstrated that, at levels from the surface to 20 km above his European location, the ozone densities were at a maximum in the spring and a minimum in the autumn, while at 20–25 km the minimum was shifted into the summer. Above 30 km the maximum occurred in the summer, and at 25–30 km there was no apparent seasonal change. The results obtained at ARO are shown in Fig. 1. The plotted points are monthly mean amounts for the several layers indicated. In all, they are based on a total of 124 distributions.

It should be noted that between the surface and 21·25 km, the same spring maximum is indicated here as was shown in Paetzold's results. Also, above 32·5 km there is a summer maximum, although it perhaps lags the European maximum by a month or two. The layer at 21·25–27·5 km is apparently in a transitional zone, for it shows traces of both the spring and summer maxima. It is noted that this transitional zone is lower than that over Europe (25–30 km).

The similarities between these results are all the more remarkable, considering the differences in both latitude (about 15°) and longitude (about 120°) between the two locations. They should lend credence to both Paetzold's explanation of the ozone economy, and the VODARO method.

A complete description of the VODARO method, including procedures and results, is being published as Scientific Report No. HA–7 under Contract No. AF19(122)–198.

Atmospheric Research Observatory,
Arizona State College,
Flagstaff, Arizona

Edward S. Epstein†
Charles Osterberg
Arthur Adel

References

Epstein E. S., Osterberg C., and Adel A. 1956 *Bull. Amer. Meteorol. Soc.* 37(1)
Paetzold H. K. 1955 *J. Atmosph. Terr. Phys.* **7**, 128

* This research has been sponsored in part by the Geophysics Research Directorate of the Air Force Cambridge Research Center, Air Research and Development Command, under Contract AF19(122)–198.

† 1st Lt., U.S.A.F., assigned to Geophysics Research Directorate, Air Force Cambridge Research Center, Air Research and Development Command, with duty station at Atmospheric Research Observatory.

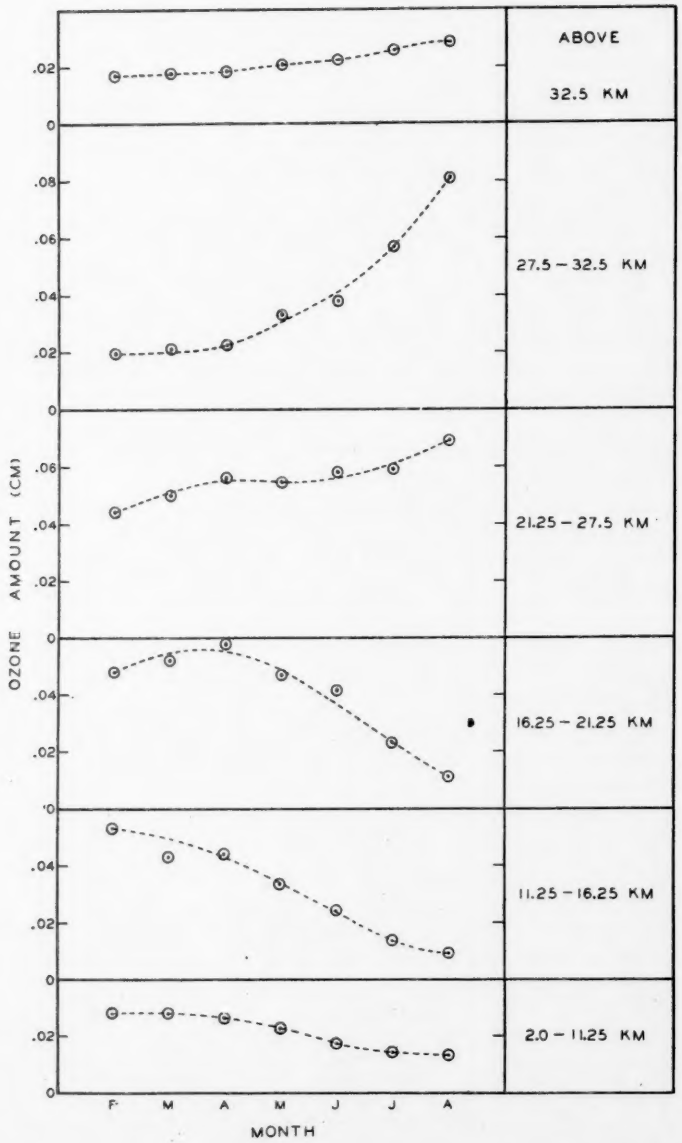

Fig. 1. The amounts of ozone in various layers of the atmosphere above Flagstaff, Arizona, February–August 1955.

VOL.
8
1956

The diurnal and annual motions of the north magnetic dip pole*

(*Received* 30 *January* 1956)

RECENTLY there has been a revival of interest in locating the position of the north magnetic dip pole. MADILL (1948) has described the work of the Dominion Observatory, and LINEHAN (1955) the work of the seaborne Dow expedition of 1954. In addition, three-component airborne magnetometers have been flown in the neighbourhood of the pole: the one of the Dominion Observatory in 1953, and the United States Naval Ordnance Laboratory vector airborne magnetometer described by SCHONSTEDT and IRONS (1955) in 1955.

This note is concerned with the uncertainties in determining the mean position of the pole at any given epoch from field determinations at any time. The observed position of the pole will not be that of the mean position at epoch, because of the local disturbance variations of extra-terrestrial origin, and because of the drift of the pole, produced by secular change of the geomagnetic field. However, no attempt is made to predict the path of the unperturbed pole.

Since 1948 a magnetic observatory has been operated at Resolute Bay, Cornwallis Island (lat. 74·7° N, long. 265·1° E), and since November 1953 variometers recording X, Y, and Z field components have been in operation. Absolute measurements have been made at intervals of two weeks for base-line determinations. The only comparable measurements in the neighbourhood of the dip pole known to the writers are those obtained at Amundsen's temporary observatory at Gjoahavn operated from November 1903 to May 1905 and situated about 130 miles from the estimated position of the pole in 1904. At Resolute Bay, from November 1953 to June 1955, X increased at an annual rate of 18 gammas, and Y increased at a rate of approximately 2 gammas/year. Earlier La Cour variometer records of declination have been used to infer that from October 1951 to August 1954, X increased at a constant rate estimated at about 19 gammas/year. Hence it seems reasonable to apply X, Y rates found for the twenty-month period to the five-year interval 1950.0 to 1955.0. Surveys in the Canadian Arctic in recent years described by MADILL (1948) have been reduced by HUTCHISON, and his unpublished charts for epoch 1950.0 show the regional field gradients at the pole in grid-north and grid-east magnetic components to be 7(.7) gammas/mile and 4(.2) gammas/mile respectively. To a good first approximation in the vicinity of the pole the grid-north isomagnetic contours run geographically N–S and the grid-east isomagnetic contours run geographically E–W. Furthermore there is good evidence from airborne flights and the surface geology of the area that there are no very severe anomalies in the regional gradients.

Because of the proximity of the two locations, the secular change at the pole cannot be very different from that at Resolute Bay, only 120 miles away. Assuming that secular change at the pole can be regarded over a small area in terms of a drift of the geomagnetic field, it can then be estimated that the pole drifted twenty-one miles north and three miles east during the period 1950–1955. The magnitude of the easterly drift is more uncertain than that of the northerly drift. In Fig. 1 a mean position for epoch 1955.0 is shown corresponding to a position 74° N, 100° W assumed for 1950.0. It is of interest to note that the present northerly drift agrees within 20% with the mean northerly drift for the last fifty years. During the first half of this century the drift has averaged 0·07 degrees of latitude north/year and 0·09 degrees of longitude west/year. These rates are less than

* Published by permission of the Acting Deputy Minister, Department of Mines and Technical Surveys, Ottawa, Ont.

half the northerly and the westerly motion in this longitude of the eccentric dipole considered by VESTINE (1953) and regarded by him as an indication of broad-scale features of the fluid motion of the core. However, if the position for the magnetic pole determined by Ross in 1831 is considered in relation to VESTINE's results, it seems likely that the result for the past fifty years is accidental, and that the core motions influencing the position of the dip pole are not related in any simple way to the broad-scale core motions

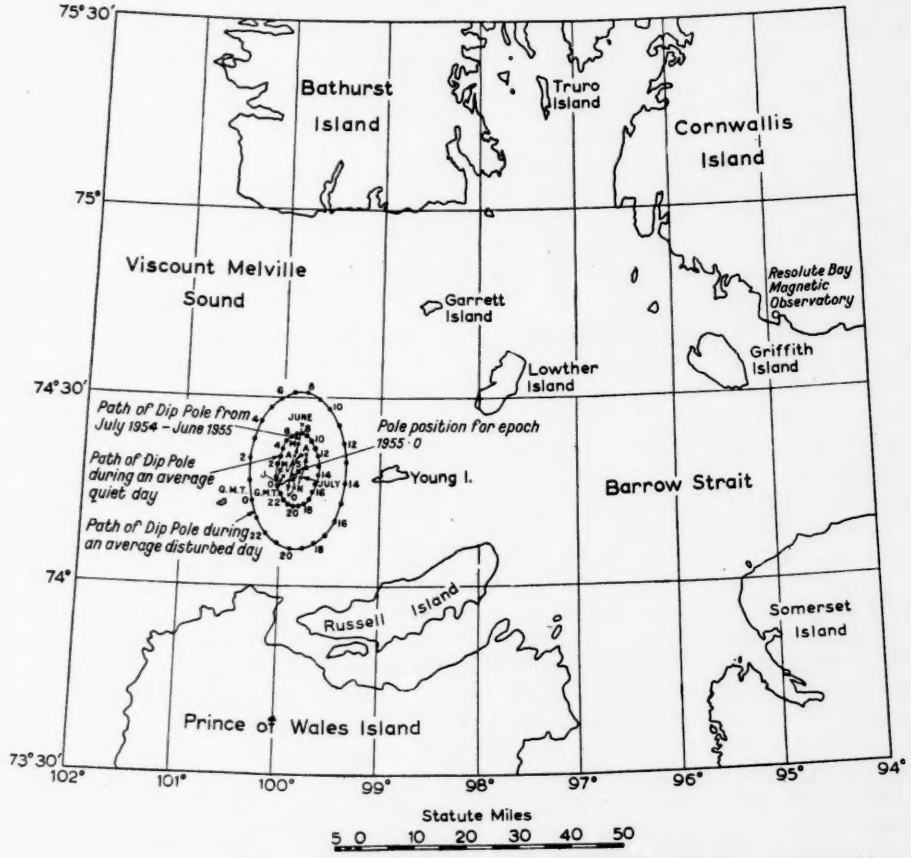

Fig. 1. Average diurnal paths of the north magnetic dip pole, and the mean monthly positions July 1954 to June 1955.

deduced by an analysis of the eccentric dipole at different epochs. Such a result would probably be expected of any feature of the earth's field which depends on higher harmonic terms modifying the picture of the eccentric dipole.

The average characteristics of the daily magnetic disturbance at Resolute Bay have been analysed, in another connection, for the period November 1953 to March 1955, and can be well represented by simple sine waves with 24-h periods. Higher harmonics have been shown not to be persistent in the statistical sense. Furthermore, the variations observed during local disturbed days can be accurately regarded as produced by an enhancement of the persistent polar-cap current system responsible for the quiet-day variations. The approximately elliptical paths shown in the figure represent the calculated

VOL. 8 1956

pole position during an average "local quiet" day and an average "local disturbed" day. The position at different hours is shown, and for convenience the paths are centred about the mean position 1955.0. The times are not corrected for the longitude difference between the two points, since this correction is less than the uncertainties in the mean phases, slight seasonal shifts in phase, etc.

The annual movement of the mean monthly position of the pole is also shown from July 1954 to June 1955. From March to August the motion is most rapidly to the north and during the autumnal equinox largely to the south. During the winter months the average motion is westerly. These changes correspond to the form of the mean monthly disturbance field over the polar cap, which will be described in another publication. The mean position of the annual track is not exactly the position shown for epoch 1955.0, since the latter position was based on a straight-line estimate of secular change, and the means in X and Y of the monthly values for this period of one year do not lie exactly on the best straight lines. The discrepancy, however, is less than one mile. Observations taken during severe storms can certainly displace the observed pole through 50–100 miles in the north–south direction and 25–50 miles in an east–west direction.

The estimates shown in the figure are known to be approximate only, but they do give a picture of the complicated nature of the track, produced by extra-terrestrial currents, of the observed pole, and give a semi-quantitative basis for the reduction of observations on the pole to epoch.

In contrast to these complicated motions, the secular variation field of internal origin is shown to be causing an approximately constant yearly drift of about four miles slightly east of north at the present time.

K. Whitham
E. I. Loomer

Dominion Observatory,
Ottawa, Ont., Canada

OL.
8
956

References

Linehan D.	1955	*Report of the Dow Expedition*, New York.
Madill R.	1948	*J. Arctic Inst. N. Amer.* **1,** 8.
Schonstedt E. O. and Irons H. R.	1955	*Trans. Amer. Geophys. Union* **36,** 25.
Vestine E. H.	1953	*J. Geophys. Res.* **58,** 127.

Book review

J. L. PAWSEY and R. N. BRACEWELL; **Radio Astronomy.** pp. x + 361. Figs. 150. Plates 23. International Monographs on Radio (General editors, Sir EDWARD APPLETON and R. L. SMITH-ROSE); Oxford, 55/-.

RECENT years have seen the phenomenal growth of radio-astronomy from a collection of odd observations by communication engineers to a subject which opens up wide new fields of astronomical knowledge. The spectrum of electromagnetic radiation available to observation has been dramatically increased, making possible the study of regions of the universe which were previously invisible or perhaps covered by obscuring clouds. The rapid growth of a very few radio-astronomical observatories, of which the Radio-physics Laboratory in Sydney is one of the most outstanding, is now being matched by an increasing interest on the part of many older observatories and other institutions, and correspondingly the need has become obvious for a comprehensive account of the new subject. Dr. PAWSEY and Dr. BRACEWELL are exceptionally well qualified for the task, since they have been for many years closely associated with radio-astronomy in Sydney and elsewhere.

The authors have faced the problem posed by the rapid development of radio-astronomy in the only possible way: they have dealt thoroughly with the groundwork both in its astronomical context and in its general technical principles, but they have imposed a limit on the experimental results by bringing them up to date in mid-1952, except for some small additions. The result is a well-considered balance between technical detail and basic physical principles, and between established results and suggestions of exciting new possibilities.

After a chapter on techniques, there are theoretical chapters on the behaviour of radio waves in ionized media, and on solar physics and astrophysics relevant to radio-astronomy. These chapters provide a very necessary introduction to the subject, since newcomers are usually grounded either in astronomy or radio physics, but rarely in both.

The sun was the first astronomical object to show clearly the power of the new radio methods, and here we find that the account which the authors present in the next chapter (written in 1952) largely corresponds to the situation of the present day. Recent advances such as the investigations of the dynamic spectra of solar radio bursts, of the distribution of radio brightness over the quiet sun at several wavelengths, and of the occultation of radio stars by the outer corona, are all included; only small additions would be needed to bring the survey up to 1955.

In the chapter on cosmic radio-waves we have necessarily a much more incomplete picture. The identification of several of the discrete sources had recently been established, and only a few more could now be added to the list, but the general picture of the galaxy as a radio emitter has considerably changed. No results of the work on H II emission could be included, for example, and only the preliminary results were available of the hydrogen-line investigations which have led to such a remarkable delineation of the spiral structure of the galaxy. In spite of this, the chapter stands as the best account available of the general field of cosmic radio research.

The remaining chapters are on radio-waves from the moon, extraterrestrial radio echoes, meteors, and ionospheric and atmospheric effects. An interesting series of plates is included; more would have been welcome.

The broad scope and the scholarly nature of this book are matched by the excellence of the printing by the Oxford University Press. A place will naturally be found for it in every observatory, but it is equally to be recommended for every physics library.

F. G. SMITH

VOL.
8
1956

OL.
8
956